UNIVERSIDAD DE SEVILLA
ESCUELA TÉCNICA SUPERIOR DE INGENIERÍA

DOCTORAL THESIS

ROBUST CONTROL STRATEGIES FOR A QUADROTOR HELICOPTER

An Underactuated Mechanical System

Guilherme Vianna Raffo

Seville
2011

UNIVERSIDAD DE SEVILLA
ESCUELA TÉCNICA SUPERIOR DE INGENIERÍA

DOCTORAL THESIS

ROBUST CONTROL STRATEGIES FOR A QUADROTOR HELICOPTER

An Underactuated Mechanical System

Thesis submitted to the Depto. de Ingeniería de Sistemas y Automática,
Escuela Técnica Superior de Ingeniería,
in partial fulfillment of the requirements for the degree of
Doctor of Philosophy
at the
Universidad de Sevilla.

By

Guilherme Vianna Raffo

Seville, March 2011

UNIVERSIDAD DE SEVILLA
ESCUELA TÉCNICA SUPERIOR DE INGENIERÍA

DOCTORAL THESIS

ROBUST CONTROL STRATEGIES FOR A QUADROTOR HELICOPTER

An Underactuated Mechanical System

Author: Guilherme Vianna Raffo
Advisors: Prof. Manuel G. Ortega Linares, Dr.
Prof. Francisco Rodríguez Rubio, Dr.

To Clarice

To my parents

Acknowledgments

The successful completion of this thesis is due to the effort, cooperation, support, understanding and dedication of many people.

First of all, I would like to thank my advisors Manolo Gil and Paco Rubio for the insightful discussions we had, their guidance in my studies at the Universidad de Sevilla and their support in my stay in Spain. It was a hard work, however, I think that Manolo Gil can agree with me, the patience and determination were the main propellers of this work. Thanks.

I am very grateful to the whole team that was and continues to work for the construction of our *QuadRotor* helicopter: Manolo Vargas, Rafa, Jesús and Ramón. I would like to especially thank Rafa for the sacrifice and the time spent, with which neither home I stopped talking about work. I would also like to express my thanks to the Grupo de Ingeniería de Automatización, Control y Robótica, especially to Manolo Lopez, Carlos Vivas, Luis Fernando and Guillermo.

Some of works presented, or at least initiated, in my PhD thesis have an enormous influence from different people, for what I would like to thank: José Ángel and Fabio for indispensable discussions about underactuated mechanical systems; I also wish to acknowledge Dani Limón for their encouragement to let me know the area of interval arithmetic and guaranteed estimation, as well as by the many conversations unrelated to work; I also appreciate the chance to be introduced to the field of numerical solutions of PDEs by Manolo Ruiz. My thankfulness to the Departamento de Ingeniería de Sistemas y Automática, and from those I have already mentioned, but not least, to Carlos Bordóns and Miguel Ángel R. for several de-stressful moments we spent playing paddle, to Fernando Dorado and Teo.

Moreover, I would like to thank to Ministry of Education and Science, MEC, by the doctorate grant that support me in Spain.

I would like to express my gratitude to Dr. Gilney Damm, Dr. Davide Raimondo and Dr. Rafael Morales for their stimulating reports recommending my PhD thesis to the European Doctorate degree.

During my stay in Seville I have met a lot of people, some of them became good friends. I would like to thank: Jörn, Maria, Antonio, Rafa, Vicente, Tito, Davide, Paco Duran, Paco Umbria, Isa, Filiberto, Rebeca, Pepe, Juanma, Rachad, João Paulo and Rafael, for their partnership, revisions and translations. I also wish to express my gratitude to Sergio, a good friend who, aside from his friendship,

provided me a clear knowledge and depth discussions on aeronautic and singular perturbations fields.

I am grateful to Julio Normey for his partnership, friendship and opportunities offered.

My deepest gratitude to my parents, Paulo and Ana, for having encouraged me to follow my choice, for having endured the distance, have been with me forever and for their love. Thanks to my brothers, Celo and Guto, and to my sisters, Dani and Paulinha, and my in-laws, Dessa, Leonardo and Vinicius, the support, help, talks, everything they did to bridge the gap. I would like to express an especial thanks to my niece Belinha and my godson Pedro for the funny moments we have gone through the computer. Thanks to all my family.

I would like to thank my beloved grandparents, Adalberto and Suzana, the encouragement and for talking to me almost every day during my first years in Spain, which made me feel a little less nostalgia. I would like to express my enormous gratitude to my grandfather, that support me even when I had to have supported him.

I would like to express my thanks to my in-laws who were always by my side. Thanks to Tinho, Mauricio, Carla, Nati, Guigue, Olinto and Beatriz, who every day sent me an email lift the mood.

I would like to render an especially thanks to Guto, Paulinha, Tina, Guigue, Antonio, Tito, Paco Umbria, Vicente and Isa, who made my thesis easier to read.

Last but the most important, I would like to dedicate this thesis to Cla, for her patience, understanding, dedication, friendship, partnership, endless encouragement, and to come to live very close to me. Thanks for these four years that we spent here together. Thanks for being part of this history.

Living to work or working to live?

The most important is to live working with pleasure.

Guilherme Vianna Raffo

Abstract of the Thesis submitted to the Depto. de Ingeniería de Sistemas y Automática, Escuela Técnica Superior de Ingeniería, in partial fulfillment of the requirements for the degree of Doctor of Philosophy at the Universidad de Sevilla.

Robust Control Strategies for a QuadRotor Helicopter An Underactuated Mechanical System

Guilherme Vianna Raffo

March / 2011

Advisors:	Prof. Manuel G. Ortega Linares, Dr.
	Prof. Francisco Rodríguez Rubio, Dr.
Area of Concentration:	Systems Engineering and Automation
Keywords:	Unmanned Aerial Vehicle, Underactuated Mechanical Systems, Modelling, Nonlinear $\mathscr{H}_\infty$ Control, Linear $\mathscr{H}_\infty$ Control, *Backstepping* Approach, Robust Control, Predictive Control, Path Tracking

This thesis deals with robust control strategies to solve the path tracking problem for an autonomous aerial vehicle. The UAV considered is a *QuadRotor* helicopter on a small scale, which is characterized by an underactuated mechanical system, i.e., they have fewer control inputs than degrees of freedom.

Normally, to design advanced control strategies an accuracy dynamic model of the system is necessary. Thus, in this thesis a proper dynamic model of the *QuadRotor* helicopter for control design purposes is formulated, keeping in mind a tradeoff between complexity and realism. The system is based on physical laws to obtain a model that represents the vehicle behavior in presence of several sources of uncertainties and to be suitable to the prototype used in this work.

Since the *QuadRotor* helicopter is an underactuated mechanical system, a common way to perform path tracking of UAV's is using cascade control strategies. Therefore, cascade structures are proposed to control two subsystems: the rotational one and the translational one. For the rotational subsystem a nonlinear state feedback $\mathscr{H}_\infty$ controller designed for mechanical systems is used, which provides

robustness in presence of exogenous disturbances, parametric uncertainties and unmodeled dynamics. To perform the path tracking for the *QuadRotor* helicopter three control techniques are used looking for a continuous performance improvement. First a linear state feedback $\mathscr{H}_\infty$ control law is applied assuring robustness properties. To enhance the guidance of the vehicle, an integral predictive controller based on the translational error model is designed given smoothness to the path tracking. After that, to enlarge the workspace of the translational motion, a control law based on an integral backstepping approach is performed using the nonlinear model of the helicopter.

Taking into account the underactuated configuration of the *QuadRotor* helicopter, two nonlinear $\mathscr{H}_\infty$ control strategies are proposed. First a control law is designed considering only a reduced system where is composed by the controlled degrees of freedom. This controller is applied to the helicopter in cascade with the previous predictive controller, where the nonlinear $\mathscr{H}_\infty$ controller is in a charge of the altitude and attitude motions, while the MPC controls the lateral and longitudinal movements. Other applications are also carried out using this controller, which are based on the inverted pendulum concept.

The cascade control strategies have an inconvenient. Although in the simulation results the whole closed loop presents a stable behavior, it is needed to be demonstrated. To avoid using cascade structures, a control strategy based on the nonlinear $\mathscr{H}_\infty$ technique applied to underactuated mechanical systems is performed. The goal is to obtain a control law that guarantees robustness for the path tracking problem of the *QuadRotor* helicopter without the necessity of cascade strategies nor state space augmentation. Additionally, an approach of the nonlinear $\mathscr{H}_\infty$ controller for mechanical systems is presented allowing to weight different dynamics of the system.

Another issue tackled is the robustness improvement of the nonlinear $\mathscr{H}_\infty$ controller designed for mechanical systems. This control law is computed taking into account that all uncertainties that affect the system are external disturbances. However, this hypothesis is not very realistic. Therefore, to counterattack this problem, a solution to robustify the nonlinear $\mathscr{H}_\infty$ control law is given, where an additional control signal is computed through the saturation function technique to cope with modeling errors.

Summarizing, this thesis presents a theoretic development of robust control strategies to solve the path tracking problem for unmanned aerial vehicles, focusing on underactuated mechanical systems.

Resumen de la Tesis presentada en el Depto. de Ingeniería de Sistemas y Automática, Escuela Técnica Superior de Ingeniería, como uno de los requisitos necesarios para la obtención del grado de Doctor en Ingeniería Industrial en la Universidad de Sevilla.

Estrategias de Control Robusto para un Helicóptero QuadRotor Un Sistema Mecánico Subactuado

Guilherme Vianna Raffo

Marzo / 2011

Directores:	Prof. Manuel G. Ortega Linares, Dr.
	Prof. Francisco Rodríguez Rubio, Dr.
Área de Concentración:	Ingeniería de Sistemas y Automática
Palabras-clave:	Vehículo Aéreo Autónomo, Sistemas Mecánicos Subactuados, Modelado, Control $\mathscr{H}_\infty$ No Lineal, Control $\mathscr{H}_\infty$ Lineal, *Backstepping*, Control Robusto, Control Predictivo, Seguimiento de Trayectorias

Esta tesis trata con estrategias de control robusto para resolver el problema de seguimiento de trayectorias para vehículos aéreos autónomos (en inglés conocidos como UAV's - *Unmanned Aerial Vehicles*). El UAV considerado es un helicóptero *QuadRotor* en escala reducida, que es caracterizado por un sistema mecánico subactuado, es decir, posee menos entradas de control que grados de libertad.

Normalmente, para el diseño de estrategias de control avanzado se necesita un modelo dinámico preciso del sistema. Siendo así, en esta tesis se obtiene un modelo dinámico adecuado del helicóptero *QuadRotor* con fines de diseño de control, teniendo en cuenta un equilibrio entre complejidad y realismo. El sistema se basa en leyes físicas para obtener un modelo que represente el comportamiento del vehículo en presencia de diversas fuentes de incertidumbres y que sea apropiado al prototipo utilizado en este trabajo.

Dado que el helicóptero *QuadRotor* es un sistema mecánico subactuado, una manera común para realizar el seguimiento de trayectorias de UAV's es utilizando estrategias de control en cascada. Por lo tanto, se proponen estructuras en

cascada para controlar dos subsistemas: el de rotación y el de traslación. Para el subsistema de rotación se diseña un controlador $\mathscr{H}_\infty$ no lineal con realimentación de estados para sistemas mecánicos, que proporciona robustez en presencia de perturbaciones exógenas, incertidumbres paramétricas y dinámicas no modeladas. Para realizar el seguimiento de trayectorias para el helicóptero *QuadRotor* se utilizan tres técnicas de control buscando una continua mejoría del desempeño. Primero se aplica una ley de control $\mathscr{H}_\infty$ lineal con realimentación de estados asegurando propiedades de robustez. Para mejorar la conducción del vehículo, se diseña un controlador predictivo con acción integral basado en el modelo del error de traslación, que proporciona suavidad al seguimiento de trayectorias. Por último, para ampliar el espacio de trabajo de los movimientos de traslación, se propone una ley de control basado en una técnica de *backstepping* con acción integral, utilizando el modelo no lineal del helicóptero.

Teniendo en cuenta el carácter subactuado del helicóptero *QuadRotor*, se proponen dos estrategias de control $\mathscr{H}_\infty$ no lineal. Primero se diseña una ley de control basada en un sistema reducido, donde solamente se consideran los grados de libertad controlados. Este controlador es aplicado en una estrategia en cascada al helicóptero con un controlador predictivo previo, donde el controlador $\mathscr{H}_\infty$ no lineal se encarga de los movimientos de altitud y orientación, mientras el MPC controla los movimientos laterales y longitudinales. Este controlador se ha empleado para controlar otras aplicaciones, las cuales están basadas en el concepto del péndulo invertido.

Las estrategias de control en cascada poseen un inconveniente: aunque en los resultados de simulación el sistema completo en bucle cerrado presente un comportamiento estable, se requiere que esto sea demostrable. Para evitar el uso de estructuras en cascada, se desarrolla una estrategia de control basada en técnicas de control $\mathscr{H}_\infty$ no lineal aplicadas a sistemas mecánicos subactuados. El objetivo es obtener una ley de control que garantice robustez para el problema de seguimiento de trayectorias del helicóptero *QuadRotor* sin la necesidad de estrategias en cascada ni de espacios de estado aumentado. Adicionalmente se presenta un enfoque del controlador $\mathscr{H}_\infty$ no lineal para sistemas mecánicos, permitiendo ponderar diferentes dinámicas del sistema.

Otra cuestión a ser abordada es la mejora de la robustez del controlador $\mathscr{H}_\infty$ no lineal diseñado para sistemas mecánicos. Esta ley de control es calculada teniendo en cuenta que todas las incertidumbres que afectan al sistema son perturbaciones externas. Sin embargo, esta hipótesis no es muy realista. Por lo tanto, para contrarestar este problema, se presenta una solución para robustificar la ley de control $\mathscr{H}_\infty$ no lineal, donde se calcula una señal de control adicional a través de la técnica de funciones de saturación para hacer frente a errores de modelado.

En resumen, esta tesis presenta un desarrollo teórico de estrategias de control robusto para resolver el problema de seguimiento de trayectorias de vehículos aéreos autónomos, centrándose en sistemas mecánicos subactuados.

Contents

List of Figures

List of Tables

Acronyms

CAS	Control Augmentation Systems
DOF	Degrees Of Freedom
Entire UActNL$\mathscr{H}_\infty$	Underactuated Nonlinear $\mathscr{H}_\infty$ Controller for the Entire System
E-SSPC	Error based State Space Predictive Controller
GDL	*Grados de Libertad*
GPC	Generalized Predictive Controller
GPS	Global Positioning System
HJ	Hamilton-Jacobi
HJB	Hamilton-Jacobi-Bellman
HJBI	Hamilton-Jacobi-Bellman-Isaacs
IADU	Integral Absolute Derivative of the control action
IMU	Inertial Measurement Unit
IntBS	Integral Backstepping Controller
ISE	Integral Square Error
L$\mathscr{H}_\infty$	State Feedback Linear $\mathscr{H}_\infty$ Controller
LMI	Linear Matrix Inequality
LPV	Linear Parameter Varying
LQR	Linear Quadratic Regulator
MEMS	MicroElectroMechanical Systems
MIMO	Multiple Input Multiple Output
MPC	Model Predictive Control
MPCxy	Model Predicitive Controller for the longitudinal and lateral movements
NCS	Networked Control System
NL$\mathscr{H}_\infty$	State Feedback Nonlinear $\mathscr{H}_\infty$ Controller
NL PD	Nonlinear Proportional - Derivative
NL PID	Nonlinear Proportional - Integral - Derivative
PD	Proportional - Derivative
PDE	Partial Differential Equation
PID	Proportional - Integral - Derivative
SAS	Stability Augmentation Systems
SISO	Single Input Single Output

UActNL$\mathscr{H}_\infty$	Underactuated Nonlinear $\mathscr{H}_\infty$ Controller for the Reduced System
UAV	Unmanned Aerial Vehicle
VTOL	Vertical Take-Off and Landing

Notation

Notation

a	italic lower case letters denote scalars
$\boldsymbol{a}$	boldface italic lower case letters denote vectors
$\boldsymbol{A}$	boldface italic upper case letters denote matrices

Symbols

$\mathbb{0}$	zero matrix with proper dimension
$\mathbb{1}$	identity matrix with proper dimension
k	number of sample
$\boldsymbol{x}$	vector with nth order, where x_i, $i = 1 \dots n$, $\boldsymbol{x} \in \Re^n$
$\boldsymbol{x}'$	transpose vector of $\boldsymbol{x}$
$\dot{\boldsymbol{x}}$	time-derivative of $\boldsymbol{x}$
$\widehat{\boldsymbol{x}}$	prediction of the state vector $\boldsymbol{x}$
$\boldsymbol{x_0}$	initial condition of $\boldsymbol{x}$
$\boldsymbol{x_r}$	reference vector of the variable $\boldsymbol{x}$
$\tilde{\boldsymbol{x}}$	error vector of the variable $\boldsymbol{x}$, $\tilde{\boldsymbol{x}} = \boldsymbol{x} - \boldsymbol{x_r}$

Model Notation

α_T	tilt angle of the rotors
b	thrust coefficient of the rotors
k_τ	drag coefficient of the propellers
l	distance between the rotors and the center of rotation
J_R	inertia moment of the motor around its rotation axis
Ω_i	angular velocity of ith rotor around its axis
g	acceleration due to the gravity
m	total mass of the helicopter
$\mathscr{B} = (\vec{x}_B, \vec{y}_B, \vec{z}_B)$	rotation body-fixed frame
$\mathscr{C} = (\vec{x}_C, \vec{y}_C, \vec{z}_C)$	frame with origin in the center of mass
$\mathscr{I} = (\vec{x}, \vec{y}, \vec{z})$	inertial frame
$\boldsymbol{r} = [r_x \; r_y \; r_z]'$	position of the center of mass with respect to the origin of the body-fixed frame expressed in the frame $\mathscr{B}$, ${}^{\mathscr{B}}\boldsymbol{r}$
${}^{i}\boldsymbol{p}_j$	point in the frame j expressed in the frame i
${}^{i}\boldsymbol{v}_j$	velocity of the point ${}^{j}\boldsymbol{p}_j$ expressed in the frame i

$\boldsymbol{v}_{\mathscr{B}}$	linear velocity of the rigid body expressed in the body-fixed frame
$\boldsymbol{v}_{\mathscr{I}}$	linear velocity of the rigid body expressed in the inertial frame
$\boldsymbol{R}_{\mathscr{I}}$	rotation matrix that describes the orientation of the body-fixed frame with respect to the inertial frame, i.e., ${}^{\mathscr{I}}\boldsymbol{R}_{\mathscr{B}}$
$\boldsymbol{R}_{\mathscr{B}}$	rotation matrix that describes the orientation of the inertial frame with respect to the body-frame frame, i.e., ${}^{\mathscr{B}}\boldsymbol{R}_{\mathscr{I}}$
$\boldsymbol{S}(.)$	skew-symmetric matrix
$\boldsymbol{\omega}$	absolute angular velocity vector of the helicopter expressed in the body-fixed frame
$\boldsymbol{W}_{\boldsymbol{\eta}}$	Euler matrix expressed in the body-fixed frame
T	total thrust applied to the body of the helicopter
f_i	force generated by the ith rotor
$\boldsymbol{f}_{\mathscr{B}}$	translational force vector applied to the vehicle
$\widehat{\boldsymbol{f}}$	translational control force vector applied to the vehicle
$\boldsymbol{f}_{\boldsymbol{\xi}}$	translational force vector applied to the vehicle expressed in the inertial frame
$\boldsymbol{f}_{\boldsymbol{\xi}_d}$	translational external disturbance vector applied to the system
$\boldsymbol{a}_{\boldsymbol{T}} = [a_x\ a_y\ a_z]'$	aerodynamic forces vector
$\mathscr{F}(\boldsymbol{q})$	generalized forces/torques vector
$\mathscr{L}(\boldsymbol{q},\dot{\boldsymbol{q}})$	Lagrangian function of the mechanical system
$\mathscr{K}(\boldsymbol{q},\dot{\boldsymbol{q}})$	system kinetic energy
$\mathscr{U}(\boldsymbol{q})$	system potential energy
$\boldsymbol{B}(\boldsymbol{q})$	force matrix (input coupling matrix)
$\boldsymbol{M}(\boldsymbol{q})$	inertia matrix
$\boldsymbol{C}(\boldsymbol{q},\dot{\boldsymbol{q}})$	Coriolis and centrifugal matrix
$\boldsymbol{G}(\boldsymbol{q})$	gravitational force vector
$\widehat{\boldsymbol{B}}$, $\widehat{\boldsymbol{M}}$, $\widehat{\boldsymbol{C}}$, $\widehat{\boldsymbol{G}}$	nominal matrices of the Euler-Lagrange model
$\boldsymbol{\Delta B}$, $\boldsymbol{\Delta M}$, $\boldsymbol{\Delta C}$, $\boldsymbol{\Delta G}$	parametric uncertainties of the dynamic matrices
$\boldsymbol{\delta}$	model uncertainty vector
m_{min}, m_{max}	lower and upper bounds of the inertia matrix
v_b	upper bound of the Coriolis and centrifugal forces
g_b	upper bound of the gravitational forces
$\boldsymbol{q}$	generalized coordinate vector of a mechanical system with $\boldsymbol{q} = [q_1, \cdots, q_n]'$
$\boldsymbol{q}_{\boldsymbol{a}} \in \Re^{n_a}$	*active* generalized coordinate vector
$\boldsymbol{q}_{\boldsymbol{c}} \in \Re^{n_c}$	*controlled* generalized coordinate vector

$\boldsymbol{q_x} \in \Re^{n_x}$	*external* generalized coordinate vector
$\boldsymbol{q_p} \in \Re^{n_p}$	*passive* generalized coordinate vector
$\boldsymbol{q_s} \in \Re^{n_s}$	*shape* generalized coordinate vector
$\boldsymbol{q_u} \in \Re^{n_u}$	*uncontrolled* generalized coordinate vector
$\mathbb{Q}$	n-dimensional configuration manifold
$\mathbb{U}$	m-dimensional actuation space
$\mathbb{D}$	q-dimensional disturbance space
$\boldsymbol{\Gamma}$	control action vector
$\boldsymbol{\Gamma_d}$	energy-bounded external disturbance vector
$\mathscr{J}(\boldsymbol{\eta})$	inertia matrix of the rotational subsystem
$\boldsymbol{J}$	moment of inertia tensor matrix
I_{xx}, I_{yy}, I_{zz}	moment of inertia about the principal axes, x, y, z
ϕ	roll angle
θ	pitch angle
ψ	yaw angle
$\boldsymbol{\eta}$	Euler-angles vector
$\boldsymbol{\xi}$	position of the origin of the rotation body-fixed frame of the helicopter, expressed in the inertial frame, ${}^{\mathscr{I}}\boldsymbol{\xi}$
$\rho(\boldsymbol{p})$	mass density at a point $\boldsymbol{p}$
τ_{drag}	aerodynamic force of propellers
τ_{M_i}	torsion effort generated by the ith electrical motor
$\boldsymbol{\tau_G}$	gyroscopic moment vector
τ_θ	pitching moment
τ_ϕ	rolling moment
τ_ψ	yawing moment
$\boldsymbol{\tau_a}$	control torque vector applied to the vehicle
$\boldsymbol{\tau_{\mathscr{B}}}$	torque vector applied to the vehicle expressed in the body-fixed frame
$\boldsymbol{\tau_\eta}$	torque vector applied to the vehicle expressed in the inertial frame
$\boldsymbol{\tau_{\eta_a}}$	control torque vector applied to the vehicle expressed in the inertial frame
$\boldsymbol{\tau_d}$	rotational external disturbance vector applied to the system
$\boldsymbol{\tau_{\eta_d}}$	rotational external disturbance vector applied to the system expressed in the inertial frame
$\boldsymbol{a_R} = \left[a_\phi\ a_\theta\ a_\psi\right]'$	aerodynamic moments vector
$\boldsymbol{a_r} = \left[a_p\ a_q\ a_r\right]'$	aerodynamic moments vector expressed in the body-fixed frame

Controllers Notation

$\boldsymbol{d}$	exogenous disturbance vector
$\boldsymbol{u}$	control effort vector
$\boldsymbol{\zeta}$	cost variable of the $\mathscr{H}_\infty$ problem
γ	attenuation level of the $\mathscr{H}_\infty$ problem
$J(\cdot)$	cost function (performance index)
$V(\boldsymbol{x},t)$	Lyapunov function
$H(\boldsymbol{x},\pi,t)$	Hamiltonian function
$H^*_\gamma(\boldsymbol{x},\boldsymbol{u}^*,\boldsymbol{d}^*,\boldsymbol{p}^*,t)$	optimal hamiltonian
$L(\boldsymbol{x},\boldsymbol{u},t)$	Lagrangian function
L_γ	parametrized soft-constrained cost function (associated performance index)
$\boldsymbol{p}$	co-state vector
$\boldsymbol{W}$	weighting matrix of the nonlinear $\mathscr{H}_\infty$ controller
$\boldsymbol{Q}$	state error weighting matrix
$\boldsymbol{R}$	control effort weighting matrix
$h(\boldsymbol{x},t)$	function of the state vector to be controlled by the nonlinear $\mathscr{H}_\infty$ controller
Δt	sampling time
$\sigma_{max}(\cdot)$	maximum singular value
$F(\boldsymbol{x_e})$	estimative vector of mechanical system
ω_{1i}	weighting of the speed error in the nonlinear $\mathscr{H}_\infty$ control
ω_{2i}	weighting of the position error in the nonlinear $\mathscr{H}_\infty$ control
ω_{3i}	weighting of the integral of the position error in the nonlinear $\mathscr{H}_\infty$ control
ω_{ui}	weighting of the control effort in the nonlinear $\mathscr{H}_\infty$ control
u_x	virtual input for the x-motion
u_x	virtual input for the y-motion
$\boldsymbol{u_\xi}$	definition of the virtual direction vector
$\boldsymbol{u^d_{\xi_{xy}}}$	desired virtual direction vector
$\boldsymbol{u^c_{\xi_{xy}}}$	virtual control input vector
$H_{\omega z}(s)$	transfer function between the input signal ω and the output signal z
$\|H_{\omega z}(s)\|_\infty$	$\mathscr{H}_\infty$-norm of the transfer function $H_{\omega z}(s)$
$\boldsymbol{C_\zeta}$, $\boldsymbol{D_{u\zeta}}$, $\boldsymbol{D_{d\zeta}}$	weighting matrices of the linear $\mathscr{H}_\infty$ controller
N_1	beginning of the prediction horizon
N_2	end of the prediction horizon

N_u	control horizon
N	prediction horizon
$\boldsymbol{P}$, $\boldsymbol{H}$	state prediction matrices
$\|\boldsymbol{x}\|^2_{\boldsymbol{Q}}$	2-norm of the variable $\boldsymbol{x}$ weighted by $\boldsymbol{Q}$, $\boldsymbol{x}'\boldsymbol{Q}\boldsymbol{x}$
$\hat{y}(k+j\|k)$	prediction of y in $k+j$ with the information in k
$\boldsymbol{C_1}$, $\boldsymbol{C_2}$, $\boldsymbol{K_\varphi}$	weighting matrices of the backstepping controllers
$\boldsymbol{T_M}$	normalization matrix
$\boldsymbol{v}$	control acceleration vector
$\boldsymbol{\Delta v}$	additional control signal computed through the saturation functions method
$\boldsymbol{E}(\boldsymbol{q})$	multiplicative uncertainty of the inertia matrix
$\boldsymbol{Q}_{max}$	upper bound of the reference acceleration

CHAPTER 1

Introduction

Contents

1.1 Motivation

The development of unmanned aerial vehicles (UAV's) has woken up great interest in the automatic control area in the last few decades. Many fields of control and robotics, such as fusion sensors, computer vision techniques, state estimators and control methodologies, have been exploited to improve the performance of these kinds of systems. UAV's have been used both in military and civil scopes, focusing on tasks as search and rescue, building exploration, security, inspection and aerial cinematography, as well as acrobatic maneuvers (Pallet and Ahmad, 1991). The UAV's are most useful, mainly, when these desired tasks are executed in dangerous and inaccessible environments.

Until recently, building a miniature and autonomous controlled aerial vehicle was a dream of many researchers, which were limited by restrictions imposed by the hitherto existing hardware. However, what truly enabled the successful construction of autonomous aerial vehicles was the technological advances in actuators and sensors on a small scale, the so-called MicroElectroMechanical Systems (MEMS), as well as energy storage and processing data.

Furthermore, the development of control systems for such vehicles is not trivial. UAV's have a high nonlinear and time-varying behavior and they are constantly affected by aerodynamic disturbances. In addition, they are usually subject to unmodeled dynamics and parametric uncertainties. This means that linear and monovariable classical control laws may have been a certain limitation in the aspect of their attraction basin, causing instability when the system is operating in conditions far from the equilibrium. Therefore, advanced control strategies are required to achieve good performance in autonomous flight or at least to help the piloting of the vehicle, with high maneuverability and robustness with respect to external disturbances.

Concerning this matter, it must be taken into account that due to the electromechanical design of aerial vehicles most of these systems are underactuated mechanical systems (i.e., they have fewer control inputs than degrees of freedom). Generally, the intentional electromechanical design results in a weight and cost reduction of the vehicle. However, underactuated systems bring a complexity and an increased challenge to the control area. Techniques developed for fully actuated robots cannot be directly applied to these kinds of mechanical systems, since most of the underactuated systems are not fully feedback linearizable and exhibit nonholonomic constraints (Fantoni and Lozano, 2002; Aguiar, 2002). Hence why, nonlinear modeling techniques and modern nonlinear control theory are usually employed to achieve autonomous flight with high performance and in specific flight conditions such as: hovering, landing / take-off, etc (Frazzoli et al., 2000; Isidori et al., 2003; Castillo et al., 2005b).

The objectives of a flight control system can be divided into three phases, depending on the autonomy of the system:

- *Stability Augmentation Systems* - SAS: The aim of these systems is to assist the piloting of the vehicle, where the SAS attempt to stabilize the system with a low-level control. This avoids that the pilot acts on the system based on its dynamic behavior. Since the vehicle is away from a certain equilibrium point, the dynamic behavior ceases to be intuitive to human reasoning.

- *Control Augmentation Systems* - CAS: These systems are in a hierarchical level above the SAS. Thus, in addition to stabilizing the vehicle, these systems must be able to provide improved responses to some references generated by the pilot, for example, the pitch angle tracking.

- *Autopilots*: possess an even higher control hierarchical level. They are fully automatic control systems that are able to exert certain types of maneuvers

autonomously, such as take-off, landing, or hovering at a determined altitude.

In the area of flight control, the most studied systems have been aircrafts and standard helicopters (i.e., helicopters with main and tail rotors). However, in the last years, UAV's in the *QuadRotor* configuration have been highlighted in a lot of works produced with it, which presents some advantageous features in comparison with the standard helicopter one, such as:

- The *QuadRotor* helicopter is lifted and propelled by four rotors, which makes it possible to reduce each individual rotor size and to maintain or to increase the total load capacity, when compared with a helicopter with one main rotor.
- These vehicles do not require mechanical linkages to act on propellers. This reduces the design, maintenance and cost of the vehicle (Hoffmann et al., 2007).
- The simplicity of the mechanical design, which provides motion control through direct drive of the rotors by varying their speeds. In a standard helicopter, the angular speed of the propellers is usually constant, where the movement is controlled varying the angle of attack of the blades (cyclic and collective). This requires transmission between the rotors, as well as accurately mechanical devices in order to change the cited angles.
- These helicopters are an interesting vehicle for use inside buildings due to the use of electrical motors instead of combustion ones, since they do not pollute the air with waste combustion.
- They are based on the VTOL (Vertical Take-Off and Landing) concept and it is usually used to develop control laws. The *QuadRotor* helicopter tries to reach a stable hovering and flight using the equilibrium forces produced by four rotors (Castillo et al., 2005b).
- The previous advantages added to its high maneuverability, allow take-offs and landings, as well as flight in tough environment.

The main drawback of this type of UAV is that it presents a weight and energy consumption augmentation due to the extra motors.

From the control point of view, the construction of this kind of miniature helicopter is far from simplifying the problem, rather the opposite happens. This is

because the torques and forces necessary to control the system are applied not only by aerodynamic effects, but also through the coupling effect that occurs between the dynamics of the rotors and the helicopter body. This coupling effect is due to the action-reaction principle originated in the acceleration and deceleration of the propellers (these effects do not occur in the control with constant speed propellers).

Despite of the coupling effects mentioned above, the absence of input coupling have some implications for the control design of the *QuadRotor* helicopter dynamics. Such decoupling arises from the assumption that the *QuadRotor* helicopter is in a coplanar configuration, i.e., the four propellers are parallel to each other, generating the force vector with elements only on the vertical axis. Therefore, if the controlled outputs are considered as the translational position and the yaw angle, a fully static feedback linearization of the *QuadRotor* helicopter model results in a singular matrix making the input-to-output decoupling be unfeasible. Thus, this control technique can not be used directly (Mistler et al., 2001). This fact jointly with the coupling between the dynamics of the rotors and the helicopter body, and also with the model uncertainties, especially in the high frequency range, makes the system even more complex to be controlled than a standard helicopter, at least, when using basic control techniques.

1.2 State of the Art

Many efforts have been made to control *QuadRotor*-based helicopters and several strategies have been developed to tackle with the path tracking problem for this type of system. Generally, two types of strategies are used to perform path tracking of the *QuadRotor* helicopter. On one hand, the most common structures are cascade control strategies, which use an inner control loop for the rotational subsystem, or in some cases for the actuated degrees of freedom, combined with an outer loop to control the translational movements. Control systems using this strategy can be found in Chen and Huzmezan (2003) and Bouabdallah and Siegwart (2007). On the other hand, some control structures use an augmented state-space (Mistler et al., 2001; Mokhtari et al., 2006b), where a double integrator is considered on the thrust, the altitude control input, which generates coupling between translational and rotational motion allowing using the feedback linearization technique.

In Mistler et al. (2001), a nonlinear model was proposed, presenting the helicopter kinematics and dynamics based on the Newton-Euler formalism. The aero-

dynamic forces and moments acting on this model were considered. To solve the path tracking problem, it was demonstrated that the desired outputs can not be decoupled using static feedback linearization, but it was solved using exact linearization techniques and noninteracting control via dynamic feedback.

In Bouabdallah et al. (2004a), a controller based on a Lyapunov control function was designed to perform the stabilization of the rotational subsystem, and, using the same control technique, the altitude control was implemented in cascade. In Bouabdallah et al. (2004b), the equations of motion of the *QuadRotor* helicopter were obtained through the Euler-Lagrange formulation, taking into account the rotor dynamics. Two control techniques were compared, a PID and a Linear Quadratic Regulator, where a linearized model was considered to design the PID controller. The development of the LQR was based on a time-variant model. In Castillo et al. (2005a, 2007) nonlinear controllers were designed to stabilize the *QuadRotor* based on Lyapunov analysis and nested saturation techniques. In Park et al. (2005) a compensation algorithm of the vehicle dynamics was used to control the system. In Lara et al. (2006) new results to compute the robustness margins of a control system for a *QuadRotor* helicopter using a multivariable PID to stabilize the vehicle position was presented. In Das et al. (2009b) a two-loop approach using input-output linearization to design a nonlinear controller was considered with a dynamic inversion inner-loop and an internal dynamics stabilization outer-loop. In Önkol and Efe (2009) four control approaches were compared to solve the path tracking problem, being them: PID control scheme, sliding model control, backstepping technique and feedback linearization.

In Mederreg et al. (2004) simulation results were presented using a backstepping control approach combined with a state estimator, while in Mahony and Hamel (2004) this technique was combined with a Lyapunov based control. In Bouabdallah and Siegwart (2005) the model was split up into two subsystems: the angular rotations and the linear translations. Backstepping and sliding-mode techniques were used to control the helicopter. In several works the backstepping technique was used to perform both path tracking and stabilization problems. Backstepping approaches applied to the *QuadRotor* helicopter are found in Madani and Benellegue (2006a,b); Madani and Benallegue (2007); Zemalache et al. (2007) and Guenard et al. (2008).

Although, several control strategies have been tested on the *QuadRotor* helicopter, most of them do not consider external disturbances on the six degrees of freedom, unmodeled dynamics and parametric uncertainty on the whole model. For example, in Bouabdallah and Siegwart (2005), Castillo et al. (2005a)

and Zemalache et al. (2007), the proposed controllers are not capable to reject sustained disturbances and in Mistler et al. (2001) just disturbances on the translational movements were considered.

However, in the last years researchers have begun to consider these effects at the control law design stage and, for example, robust sliding mode and backstepping approaches have also been developed, as well as disturbance observers. In Mokhtari et al. (2006b) a feedback linearization-based controller with a sliding mode observer was designed for the *QuadRotor* helicopter. An adaptive observer was added to the control system to estimate the effect of external disturbances. In Xu and Özgüner (2006) a sliding mode controller was synthesized, while Xu and Özgüner (2008) proposed an approach using sliding mode control for underactuated mechanical systems to stabilize a *QuadRotor* helicopter when 30% uncertainty is added in each parameter of the model. In Lee et al. (2009) a feedback linearization controller was compared with an adaptive sliding mode control using input augmentation to deal with the underactuated properties, parametric uncertainty and sensor noise. In Kim et al. (2010) a disturbance observer based controller using the dynamic model was proposed for robust hovering control, which is an internal loop compensator.

In Bouabdallah and Siegwart (2007) a backstepping approach using integral action was used to improve the *QuadRotor* helicopter path tracking performance when maintained winds disturb the whole system. In Das et al. (2009a) a backstepping approach was used to control the *QuadRotor* helicopter, by applying backstepping on the Lagrangian form of the dynamics. Besides, neural networks were introduced to estimate the aerodynamic components.

The use of integral action in the backstepping technique was first proposed by Kanellakopoulos and Krein (1993). The most common way to include integral action in this approach is to use parameter adaptation (Krstic et al., 1995). An analysis of different techniques using integral action in the backstepping approach was carried out by Skjetne and Fossen (2004), where another two methods that consist in the augmentation of the system dynamic with the integral state were presented.

In some papers the *QuadRotor* helicopter has also been controlled using a linear $\mathscr{H}_\infty$ controller based on linearized models. In Chen and Huzmezan (2003), a simplified nonlinear model of the UAV movements was presented. The path tracking problem was divided into two parts, the first one to achieve the angular rates and vertical velocity stabilization by a 2DOF linear $\mathscr{H}_\infty$ controller using the loop shaping technique. The same technique was used to control the longitudinal

and lateral velocities, the yaw angle and the height in the outer loop. In the second part a predictive control, based on a model including the inner loops and the helicopter dynamics, was designed to solve the path tracking problem. In Mokhtari et al. (2005, 2006a) a robust feedback linearization with a linear $\mathscr{H}_\infty$ controller was applied to deal with the path tracking problem with parameter uncertainties and external disturbances.

Additionally to the inertial control, the *QuadRotor* helicopter has also been controlled through artificial visual feedback. In Altug et al. (2002), a ground camera was used to estimate the helicopter position and orientation, while in Tournier et al. (2006) the estimation of the six degrees of freedom was obtained by an embedded camera on the helicopter using Moir'e patterns. In Altug et al. (2005) two cameras were used to estimate the six degrees of freedom pose of the helicopter. One of these cameras was embedded on the *QuadRotor*, while the other one was locatedinestabilizar on the ground. To perform an autonomous helicopter, two control methods were used, a backstepping controller and a model-based feedback linearizing controller. In Metni et al. (2005), a general mechanical dynamic model of the UAV was considered to perform hovering flight. The helicopter position and orientation were estimated using a visual servoing technique based on homography. By using this information, a control law designed through the backstepping approach forces the vehicles to track a prerecorded image sequences. The desired trajectory was obtained through an operator who previously teach it step by step, being compared the actual image and the desired one with a reference image through the homography matrices at each instant. The translational position vector was determined estimating the reference depth information using an adaptive control law.

Furthermore, there are two issues that are worth pointing out. On one hand, most of the above control applications assume that the computed control actions will never reach the saturation limits of the actuators, although in practice it is possible. For instance, when the UAV is far away from its destination, the generated control signals are normally higher than the admissible values. Moreover, the vehicles are composed of mechanical and electrical parts, which are also subject to physical constraints.

When on-line constraints must be considered, model predictive control (MPC) algorithms appear as an interesting choice. The objective of MPC is to compute a future control sequence in a defined horizon in such a way that the prediction of the plant output is driven close to the reference. This is accomplished by minimizing a multistage cost function with respect to the future control actions. To

perform that, the predicted output values are computed as a function of past values of inputs and outputs, and future control signals. Besides, an explicitly process model is used into the cost function, obtaining an expression whose minimization leads to the desired values. An analytical solution can be obtained for a quadratic cost function if the model is linear and there are no constraints; otherwise an iterative method of optimization should be implemented (Camacho and Bordons, 1998; Mayne et al., 2000; Rawlings and Mayne, 2009).

Moreover, the MPC formulation generates (implicitly) a non-smooth (discontinuous) control law. Given that trajectories are normally known and using an appropriate vehicle instrumentation to inform about position, orientation and movements, as well as with information from the environment where it is (e.g. using a GPS, digital maps, etc.), the predictive controller becomes even more suitable for this task. Apart from the fact that MPC guides the system smoothly, it presents an enhanced autonomy and can easily be extended to multivariable systems. One drawback, the high computational burden introduced by the MPC methodology may make impossible to perform real applications.

On the other hand, it is quite common to assume that all states are accessible by the controllers. Generally, it can result in difficulties for practical implementations. To avoid these practical problems, in some works state observers have been proposed to estimate the linear speed of a *QuadRotor* helicopter. In Benzemrane et al. (2007) a nonlinear adaptive estimator is proposed to improve robustness in the velocity estimation, when only the linear acceleration, the angles and the angular velocity are available for measurement. In Benzemrane et al. (2008) the speed estimation was observed through a Kalman filtering and an adaptive observer, being corroborated with exact and noisy acceleration measurements. At the same time, there are a large variety of sensors available that provide the necessary measurements. For instance, Euler angles and angular velocities can be obtained through Inertial Measurement Systems (IMU). Besides, if it is combined with GPS (or differential GPS) the linear position and linear velocity can also be measured. At this stage it is necessary to keep in mind the objectives of the application such as, for example, if the UAV must fly in an indoor or outdoor environment, or if the GPS accuracy is admissible. Other kinds of sensors can be also used to estimate the UAV position and attitude, like ultrasound systems in a structured environment (Roberts et al., 2007), vision systems (Altug et al., 2002; Metni et al., 2005; Tournier et al., 2006; Guenard et al., 2008) and 3D tracker system (POLHEMUS) (Castillo et al., 2005a; Guisser et al., 2006).

Apart from the above, in the last few years researches on the coordination

of multiple UAV's using the *QuadRotor* helicopter configuration have generated great interest, mainly in the robotics community. Some works in this field can be cited, such as Hoffmann et al. (2006); Bethke et al. (2007); Michael et al. (2010b,a).

In this thesis, the path tracking problem of a unique *QuadRotor* helicopter will be addressed, where the main objective is to enhance robustness of control strategies when the vehicle is flying in presence of external disturbances, unmodeled dynamics and parametric uncertainties.

1.2.1 Nonlinear $\mathscr{H}_\infty$ Control for Mechanical Systems

As it can be deduced from the presented above, many control strategies have been applied to the *QuadRotor* helicopter, but most of them do not consider parametric uncertainties nor external disturbances. However, UAV's are constantly affected by model uncertainties and wind gusts, which can easily destabilize the vehicle.

A proper selection to reject these disturbances is the nonlinear $\mathscr{H}_\infty$ control theory. The first efforts to extend the $\mathscr{H}_\infty$ control problem to nonlinear systems have been made in the 1980's. In Ball et al. (1987a,b) the nonlinear problem for discrete-time systems was formulated and using Volterra's Series acceptable solutions were found. The solution for nonlinear continuous-time systems was provided by van der Schaft in (van der Schaft, 1991) and (van der Schaft, 1992).

The aim of the $\mathscr{H}_\infty$ theory is to achieve a bounded ratio between the energy of the so-called error signals and the energy of the disturbance signals. In general, the nonlinear approach of this theory considers a Hamilton-Jacobi partial differential equation (HJ PDE), which replaces the Riccati equation in the case of the linear $\mathscr{H}_\infty$ control formulation. The solution of nonlinear $\mathscr{H}_\infty$ control can be obtained through two approaches, differential game theory (Doyle et al., 1989; Basar and Bernhard, 2008) and dissipative systems theory (van der Schaft, 2000). The main problem in the nonlinear case is the absence of a general method to solve this HJ PDE. Therefore, analytical solutions must be solved for each particular case.

Due to the difficult to obtain analytical solutions, some works propose numerical methods allowing integrate such equations, for example, Galerkin approximations, Taylor series (Beard et al., 1997; Beard and McLain, 1998; Beard et al., 1998; Hardt et al., 2000).

Since the main interest of this thesis is to work with mechanical systems models obtained via Euler-Lagrange formulation, solutions of the nonlinear $\mathscr{H}_\infty$

control can be found minimizing the forces that do work on the system, as was exposed in Johansson (1990). In this paper, the author proposed a solution for the nonlinear $\mathscr{H}_2$ optimal control problem of fully actuated mechanical systems. From this pioneering work, an enormous quantity of modifications have been done to formulate nonlinear $\mathscr{H}_2$, $\mathscr{H}_\infty$ and $\mathscr{H}_2/\mathscr{H}_\infty$ controllers for mechanical systems (Chen et al., 1994; Feng and Postlethwaite, 1994; Astolfi and Lanari, 1994; Kang, 1995; Chen et al., 1997; Postlethwaite and Bartoszewicz, 1998). In Sage et al. (1999) a survey about robust control of robot manipulators was presented, where a slight overview of nonlinear $\mathscr{H}_\infty$ control applied to mechanical systems can be found.

An explicit global parameterized solution to the state feedback $\mathscr{H}_\infty$ optimal control problem, formulated as a *min-max* game, was developed in Chen et al. (1994). This solution treats the particular case of fully actuated mechanical systems formulated via Euler-Lagrange equations by using the state tracking error equation proposed in Johansson (1990) and dynamic properties of mechanical systems. In the same year, Feng and Postlethwaite (1994) proposed a similar approach to the nonlinear state feedback $\mathscr{H}_\infty$ controller for robotic systems, where the cost variable considers the coupling between the controlled variables and the state feedback control law, which gives more degrees of freedom to the control design. Besides, a nonlinear $\mathscr{H}_\infty$ control law with an adaptive scheme was presented to enhance robustness of the whole system.

In Ortega et al. (2005) a strategy to control fully actuated mechanical systems considering the tracking error dynamic equation was proposed, where the integral of the error position is added to the error vector. In such strategy a nonlinear $\mathscr{H}_\infty$ control, formulated via game theory, was applied. This strategy provides, through an analytical solution, a time variant control law which is strongly model-dependent and it is similar to the results obtained with the feedback linearization procedures. Conditions to formulate the controller in the form of a nonlinear PID were established, where the control signal can be penalized, as well as the error signals, their integral and their derivative.

Some works using nonlinear $\mathscr{H}_2$, $\mathscr{H}_\infty$ and $\mathscr{H}_2/\mathscr{H}_\infty$ controllers have been published in the aeronautics area. In Yang and Chen (2001) the nonlinear $\mathscr{H}_\infty$ control theory was used to design a three-dimensional missile guidance law. In Chen et al. (2002) a tactical missiles pursuing maneuvering targets in three-dimensional space was solved by using a nonlinear $\mathscr{H}_\infty$ guidance law based on a fuzzy model. In Chen et al. (2003) an adaptive fuzzy mixed $\mathscr{H}_2/\mathscr{H}_\infty$ lateral control of nonlinear missile systems with uncertain disturbances was proposed. In López-Martínez et

al. (2007) a laboratory twin-rotor helicopter was controlled using a nonlinear $\mathscr{L}_2$ controller based on a reduced order model of the propellers.

1.2.2 Underactuated Mechanical Systems

As commented above, UAV's are typically underactuated mechanical systems, and the *QuadRotor* helicopter is no different, since it has six degrees of freedom and only four control actions, the four rotors. Underactuated mechanical systems appear in several applications such as aerospace and undersea robots, mobile systems, flexible systems, walking, brachiating and gymnastic robots. According to Olfati-Saber (2001), the underactuation property of underactuated systems is due to four reasons: dynamics of the system, by design for reduction of the cost or some practical purposes, actuator failure and imposed artificially to create complex low-order nonlinear systems for the purpose of gaining insight in control of high-order underactuated systems.

In the area of control of underactuated mechanical systems, an important contribution was presented in Spong (1994), where the authors used the partial feedback linearization proposed by Isidori (1989) to linearize the unactuated degrees of freedom.

Motion control of underactuated mechanical systems is frequently difficult due to the nonholonomics constraints on the acceleration generated by the underactuation, which results in the impossibility to regulate all degrees of freedom of the system at the same instant of time in a desired position. In Wichlund et al. (1995) control properties of the dynamics of underactuated vehicles (e.g. underwater vehicles, helicopters, airplanes, etc.) were studied. An interesting property of these kind of systems was stated, where says that underactuated mechanical systems with a gravitational field $\boldsymbol{G}(\boldsymbol{q})$ where the elements of $\boldsymbol{G}$ corresponding to the unactuated dynamics are zero, are not C^1 asymptotically stabilizable to a single equilibrium. Olfati-Saber (2001) rewritten this property stating that if the potential energy $\mathscr{U}(\boldsymbol{q})$ is independent of the *external* variable $\boldsymbol{q_x}$, i.e. $\partial \mathscr{U}(\boldsymbol{q_x}, \boldsymbol{q_s})/\partial \boldsymbol{q_x} = 0$, then $\boldsymbol{g_r} = 0$ (i.e. $\boldsymbol{g_r}$ is the gravitational term of the remaining subsystem) and the generalized momentum p_r is a conserved quantity. Therefore, the underactuated mechanical system is not controllable or stabilizable to any equilibrium points for initial conditions with $p_r(0) \neq 0$. The fact that the unactuated system is a simple Lagrangian system without any input forces means that the system must be controlled via its potential force that is parameterized by $\boldsymbol{q_s}$. Therefore, the *shape* vector $\boldsymbol{q_s}$ plays the role of the control input for the dynamics of the remaining sys-

tem. Besides, in Reyhanoglu et al. (1996, 1999) controllability and stabilizability properties of underactuated mechanical system with second-order nonholonomic constraints were derived. An interesting survey about underactuated mechanical systems can be found in Spong (1998).

Position tracking of underactuated mechanical systems has been performed in several publications using nonlinear $\mathscr{L}_2$ controllers. In Toussaint et al. (2000) an underactuated ship nonlinear model was controlled through a state feedback tracking $\mathscr{H}_\infty$ control law in presence of disturbances and noisy measurements of states. In Siqueira and Terra (2004a) a nonlinear $\mathscr{H}_\infty$ control for underactuated manipulators, as an extension of the one proposed by Chen et al. (1994), was presented. The same authors performed a comparison of the nonlinear $\mathscr{H}_\infty$ controller based on game theory with the one obtained through a quasi-linear parameter varying (LPV) representation in Siqueira and Terra (2004b), to control the position of underactuated manipulators. In this work, an $\mathscr{H}_\infty$ Markovian controller was also developed when the underactuated manipulator is subject to abrupt changes in configuration. In Siqueira et al. (2006) nonlinear controllers obtained via $\mathscr{H}_2$, $\mathscr{H}_\infty$, $\mathscr{H}_2/\mathscr{H}_\infty$ optimization problems using game theory were applied to underactuated manipulators through actuation redundancy. In He and Han (2008) an acceleration feedback control was proposed for both fully and under actuated nonlinear autonomous vehicles by using the $\mathscr{H}_\infty$ theory. Besides, simulations results for a helicopter trajectory tracking were presented.

1.3 Objectives

The main objective of this thesis is to contribute to the development and implementation of robust control strategies to solve the path tracking problem of autonomous aerial vehicles. The UAV to be used is a *QuadRotor* helicopter on a small scale, which is characterized by an underactuated mechanical system. Furthermore, the nonlinear $\mathscr{H}_\infty$ controller design for a class of underactuated mechanical systems is sought. Fig. 1.1 illustrates the flow chart used to develop this doctoral thesis.

Normally, to design advanced control strategies an accurate dynamic model of the system is necessary. Thus, the first objective formulated in this thesis is to obtain a proper dynamic model of the *QuadRotor* helicopter with control design purposes, taking in mind a tradeoff between complexity and realism. The system will be based on physical laws to obtain a model that represents the vehicle behavior in presence of several sources of uncertainties and to be suitable to the

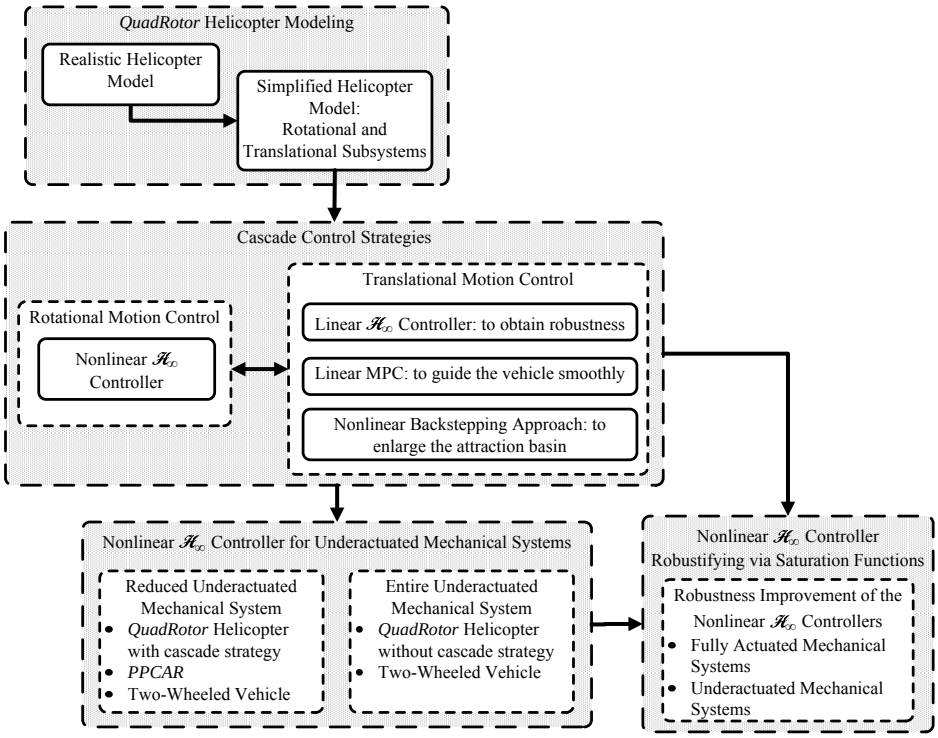

Figure 1.1: Flow chart of the thesis.

prototype used in this work.

Since the *QuadRotor* helicopter is an underactuated mechanical system, a common way to perform path tracking of UAV's is using cascade control strategies. Therefore, cascade structures are proposed to control two subsystems: the rotational and the translational. The control techniques used in each loop will be based on both nonlinear and linear $\mathscr{H}_\infty$ theory, backstepping approach and predictive control methodology. These techniques will be combined to perform a robust closed-loop control in presence of external disturbances, parametric uncertainties and unmodeled dynamics. A smooth path tracking is also required.

However, it must be emphasized that the cascade control strategies have an inconvenient. Although in the simulation results the whole closed loop presents a stable behavior, it is needed to be demonstrated. To avoid using cascade structures, a control strategy based on the nonlinear $\mathscr{H}_\infty$ technique applied to underactuated mechanical systems will be performed. The goal is to obtain a control law that guarantees robustness for the path tracking problem of the *QuadRotor* helicopter

without the necessity of cascade strategies. Additionally, an approach of the nonlinear $\mathscr{H}_\infty$ controller for mechanical systems will be presented allowing to weight different dynamics of the system.

Another issue to be tackled is the robustness improvement of the nonlinear $\mathscr{H}_\infty$ controller designed for mechanical systems. This control law is computed taking into account that all uncertainties that affect the system are external disturbances. However, this hypothesis is indeed not very realistic. Therefore, to counterattack this problem, a solution to robustify the nonlinear $\mathscr{H}_\infty$ control law will be given, where an additional control signal is computed through the saturation functions technique to cope with modeling errors.

In general, this thesis presents a theoretic development of robust control strategies to solve the path tracking problem for unmanned aerial vehicles, focusing on underactuated mechanical systems.

1.4 Outline

The thesis is organized as follows:

- **Chapter 2** presents the modeling of the *QuadRotor* helicopter. A description of the vehicle operation is provided, as well as static characteristics of the motor-propeller groups. The equations of motion of a UAV are obtained through two approaches: Euler-Lagrange and Newton-Euler. Parameters of the *QuadRotor* unmanned aerial vehicle used in this thesis are also provided. In this chapter some useful properties of mechanical systems are presented.

- **Chapter 3** deals with cascade control strategies to perform path tracking of the vehicle, which highlights the pursuit of continuous performance improvement. In this chapter the dynamic model is divided into two subsystems: the rotational and the translational. Three control structures are developed, being a state space feedback nonlinear $\mathscr{H}_\infty$ controller in charge for stabilizing the *QuadRotor* helicopter, while three techniques are applied to track the desired trajectory. First, a linear state feedback $\mathscr{H}_\infty$ controller based on the error model is computed using a synthesis method via LMIs, which ensures robustness properties. After that, a state-space predictive controller with integral action based on the time-variant error model is performed to follow smoothly the desired translational trajectory. The last

translational controller used is based on an integral backstepping approach improving robustness in presence of model uncertainties and enlarging the workspace of the translational motion when compared with the previous outer loop controllers. Simulation results are presented to corroborate the good features of the proposed control strategies.

- **Chapter 4** gives two novel nonlinear $\mathscr{H}_\infty$ controllers for underactuated mechanical systems. The first controller is based on a reduced model, where only the *controlled* degrees of freedom are considered. This controller is applied in a cascade control strategy to the *QuadRotor* helicopter, while is used to control the *passive* degrees of freedom of two vehicles based on the inverted pendulum concept. The second controller considers the entire dynamic of the underactuated mechanical systems allowing regulates the *controlled* degrees of freedom while the *remaining* ones are stabilized. The *QuadRotor* helicopter is controlled without the necessity of cascade strategies nor state-space augmentation. Experimental results are also obtained with a two-wheeled self-balanced vehicle.

- **Chapter 5** deals with a robustifying method of the nonlinear $\mathscr{H}_\infty$ controller designed for mechanical systems. A new analytical solution for the approach proposed in Ortega et al. (2005) is presented. This method is based on saturation functions technique. Preliminary simulation results with some of the controllers presented in Chapter 3 and Chapter 4 are carried out.

- **Chapter 6** summarizes the contributions and results presented in this thesis and suggests possible future research lines.

1.5 List of Publications

The following articles have been issued or submitted for publication during the elaboration of this thesis:

Book chapters:

1. (Raffo and Normey-Rico, 2011) G. V. Raffo and J. E. Normey-Rico. *Robótica Móvel, Ed. R. A. F. Romero, F. Osorio, E. Prestes and D. Wolf*, chapter *Controle de Robôs Móveis para Seguimento de Trajetórias*. Springer-Verlag, São Paulo, Brasil, 2011. Accepted for publication.

Journal papers:

1. (Raffo et al., 2011a) G. V. Raffo, M. G. Ortega, F. R. Rubio, *Path Tracking of a UAV via an Underactuated $\mathscr{H}_\infty$ Control Strategy*. European Journal of Control, 17(2), 2011. In press.

2. (Raffo et al., 2010d) G. V. Raffo, M. G. Ortega, F. R. Rubio, *Robust Backstepping/Nonlinear $\mathscr{H}_\infty$ control for path tracking of a quadRotor unmanned aerial vehicle*. IET Control Theory & Applications, 2010. Submitted for publication with preliminary review status: potentially publishable.

3. (Raffo et al., 2010c) G. V. Raffo, M. G. Ortega, F. R. Rubio, *An integral predictive/nonlinear $\mathscr{H}_\infty$ control structure for a quadrotor helicopter*. Automatica (Oxford), 46(1), p. 29-39, 2010.

4. (Raffo et al., 2009a) G. V. Raffo, G. K. Gomes, J. E. Normey-Rico, C. R. Kelber, and L. B. Becker. *A predictive controller for autonomous vehicle path tracking*. IEEE Transactions on Intelligent Transportation Systems, 10 (1):92–102, 2009.

5. (Raffo et al., 2009b) G. V. Raffo, J. E. Normey-Rico, F. R. Rubio, and C. R. Kelber. *Control predictivo en cascada de un vehículo autónomo*. Revista Iberoamericana de Informática y Automática (RIAI), 6(1):63–74, 2009.

Conference papers:

1. (Raffo et al., 2011b) G. V. Raffo, M. G. Ortega, F. R. Rubio, *Nonlinear $\mathscr{H}_\infty$ Controller for the Quad-Rotor Helicopter with Input Coupling*, Accepted to the 18th IFAC World Congress, IFAC'2011, Milan, Italy.

2. (Raffo et al., 2010b) G. V. Raffo, V. M. Madero, M. G. Ortega, *Un Controlador $\mathscr{H}_\infty$ No Lineal para Sistemas Mecánicos Subactuados con Acoplamiento en la Entrada - Una Aplicación a un Vehículo Auto-Balanceado con Dos Ruedas*, Actas de las XXXI Jornadas de Automática, 2010, Jaén, Spain.

3. (Raffo et al., 2010a) G. V. Raffo, V. M. Madero, M. G. Ortega, *An Application of the Underactuated Nonlinear $\mathscr{H}_\infty$ Controller to Two-Wheeled Self-Balanced Vehicles*. In Proc. of the 15th IEEE International Conference on Emerging Technologies and Factory Automation. ETFA'2010, Bilbao, Spain, September 2010.

4. (Raffo et al., 2009c) G. V. Raffo, M. G. Ortega, F. R. Rubio, *An Underactuated $\mathscr{H}_\infty$ Control Strategy for a QuadRotor Helicopter*. In Proc. of the European Control Conference 2009 - ECC2009, pages 3845-3850, Budapest, Hungary, August 2009.

5. (Raffo et al., 2008d) G. V. Raffo, M. G. Ortega, F. R. Rubio, *Plataforma de Pruebas para un Vehículo Aéreo No Tripulado Utilizando LabView*, 2008, Actas de las XXIX Jornadas de Automática, 2008, Tarragona, Spain.

6. (Raffo et al., 2008b) G. V. Raffo, M. G. Ortega, F. R. Rubio, *MPC with Nonlinear $\mathscr{H}_\infty$ Control for Path Tracking of a Quad-Rotor Helicopter*. In Proc. of the 17th IFAC World Congress 2008 - IFAC'08, pages 8564-8569, Seoul, Korea, July 2008.

7. (Raffo et al., 2008c) G. V. Raffo, M. G. Ortega, F. R. Rubio, *Robust $\mathscr{H}_\infty$ Control Strategy for a 6 DOF Quad-Rotor Helicopter*. In Proc. of the 8th Portuguese Conference on Automatic Control - CONTROLO'08, pages 402-407, Vila Real, Portugal, July 2008.

8. (Raffo et al., 2008a) G. V. Raffo, M. G. Ortega, F. R. Rubio, *Backstepping/Nonlinear $\mathscr{H}_\infty$ Control for Path Tracking of a QuadRotor Unmanned Aerial Vehicle*. In Proc. of the 2008 American Control Conference-ACC08, pages 3356-3361, Seattle, USA, June 2008.

9. (Raffo et al., 2007b) G. V. Raffo, M. G. Ortega, F. R. Rubio, *Nonlinear $\mathscr{H}_\infty$ Control Applied to the Personal Pendulum Car*. In Proc. of the European Control Conference. ECC'07, Kos, Greece, July 2007.

10. (Raffo et al., 2007a) G. V. Raffo, M. G. Ortega, F. R. Rubio, *Control Predictivo de la Dinámica de un Vehículo Autónomo*, 2007, Actas de las XXVIII Jornadas de Automática, 2007, Huelva, Spain.

11. (Raffo et al., 2006b) G. V. Raffo, M. G. Ortega, F. R. Rubio, *Control $\mathscr{H}_\infty$ Multivariable de un Modelo de Helicóptero*, 2006, Actas de las XXVII Jornadas de Automática, 2006. p. 854-859, Almería, Spain.

12. (Raffo et al., 2006a) G. V. Raffo, G. K. Gomes, J. E. Normey-Rico, L. B. Becker, and C. R. Kelber. *Seguimento de Trajetória de um Veículo Mini-Baja com CPBM*. Atas do XVI Congresso Brasileiro de Automática, Salvador, Brasil, 2006.

CHAPTER 2

QuadRotor Helicopter Modeling

Contents

2.1 Introduction

This chapter looks into the modeling of the *QuadRotor* autonomous aerial vehicle. The equations of motion are developed based on physical laws that describe the location of the mass center of the vehicle, using three position coordinates, and three Euler angles to specify the orientation of the body. Two approaches are used to obtain the dynamic equations that describe explicitly the relationship between force and motion. First the Euler-Lagrange formulation is described. Afterwards, an alternative description of the autonomous aerial vehicle is obtained using the Newton-Euler formulation.

The autonomous aerial vehicle used in this thesis is a miniature helicopter in a coplanar configuration of four rotors (*QuadRotor*), as illustrated in Fig. 2.1. In this figure, the forces generated by each propeller to produce motion can be also observed. The movement of the UAV results from changes on the lift force caused

by adjusting the velocities of each rotor. Longitudinal motions (i.e. pitch motions) are achieved varying the front and rear rotors velocity, which change the forces f_1 and f_3 (see Fig. 2.1), while lateral displacements (i.e. roll motions) are performed through the speed variation of the right and left propellers, which vary the forces f_2 and f_4. Yaw movements are obtained from the difference in the counter-torque between each pair of propellers, (f_1, f_3) and (f_2, f_4), i.e., accelerating the two clockwise turning rotors while decelerating the counter-clockwise turning rotors, and vice-versa. This movement is possible because the rotors 1 and 3 rotate in the opposite direction to the rotors 2 and 4. Finally, the total thrust T, which displaces the helicopter in the perpendicular plane with respect to the propellers, is obtained by the sum of the four forces generated by propellers.

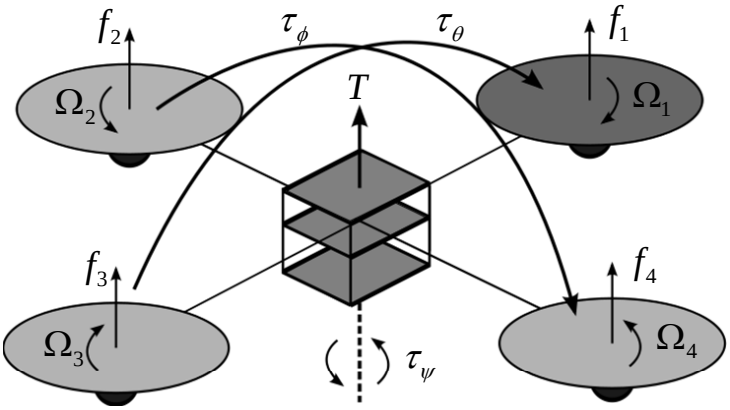

Figure 2.1: Operating diagram of the *QuadRotor* helicopter.

Therefore, the *applied* thrust, T, is given by (Castillo et al., 2005b):

$$T = \left(\sum_{i=1}^{4} f_i \right) = \left(\sum_{i=1}^{4} b\Omega_i^2 \right), \tag{2.1}$$

where f_i is the force generated by each rotor, Ω_i is the angular velocity of the ith rotor around its axis and b is the thrust coefficient of the rotors. Moreover, the *applied* torque vector on the three axes is given by:

$$\boldsymbol{\tau_a} = \begin{bmatrix} \tau_{\phi_a} \\ \tau_{\theta_a} \\ \tau_{\psi_a} \end{bmatrix} = \begin{bmatrix} (f_2 - f_4)\, l \\ (f_3 - f_1)\, l \\ \sum_{i=1}^{4} \tau_{M_i} \end{bmatrix}, \tag{2.2}$$

where l is the distance between the rotors and the center of rotation, and τ_{M_i} is the torsion effort generated by each electrical motor, considering the dynamic of each disc of the motor as an uncoupled system in the generalized variable Ω_i. The torsion effort of the motor is opposite to its aerodynamic force $\tau_{drag} = k_\tau \Omega_i^2$, where $k_\tau > 0$ is a constant. Thus, by using the Newton's second law, the torque generated by each rotor is given by (Castillo et al., 2005b):

$$J_R \dot{\Omega}_i = -\tau_{drag} + \tau_{M_i}\,, \tag{2.3}$$

and keeping the total thrust constant, that is, considering $\dot{\Omega}_i = 0$, it follows that:

$$\tau_{M_i} = \tau_{drag} = k_\tau \Omega_i^2\,. \tag{2.4}$$

Then, the equation of the *applied* torques (2.2) can be rewritten as follows:

$$\begin{bmatrix} \tau_{\phi_a} \\ \tau_{\theta_a} \\ \tau_{\psi_a} \end{bmatrix} = \begin{bmatrix} lb\left(\Omega_2^2 - \Omega_4^2\right) \\ lb\left(\Omega_3^2 - \Omega_1^2\right) \\ k_\tau\left(\Omega_1^2 + \Omega_3^2 - \Omega_2^2 - \Omega_4^2\right) \end{bmatrix}. \tag{2.5}$$

Additionally, this kind of system is a flight vehicle of lightweight structure and, therefore, gyroscopic effects resulting from the rotation of the rigid body and the four propellers should be included in the dynamic model (Bouabdallah et al., 2004b). Assuming each rotor as a rigid disc rotating around its vertical axis with an angular rate Ω_i, and that the rotation axis of the rotor rotates with the angular velocity of the reference frame, the gyroscopic moments due to the change in the orientation of the propeller plane are given by:

$$\boldsymbol{\tau_G} = -\sum_{i=1}^{4} J_R\left(\boldsymbol{\omega} \times \boldsymbol{e_3}\right) \cdot \Omega_i\,, \tag{2.6}$$

where J_R is the inertia moment of the motor around its rotation axis, $\boldsymbol{\omega}$ is the angular velocity of the helicopter, expressed in the body-fixed frame and $\boldsymbol{e_3} = [0 \quad 0 \quad 1]'$.[1] However, in this thesis the dynamic model of the system is obtained under the assumption that the vehicle is a rigid body in the space, subject to one main force (thrust) and three torques. This simplification implies that gyroscopic effects caused by the propellers will be considered as disturbances for the rotational control law.

Besides, this helicopter is an underactuated mechanical system with six de-

[1] The notation prime $'$ denotes transpose.

grees of freedom and only four control inputs, which increases the complexity and proposes an enormous challenge to the control area. Due to this difficulty, some assumptions are made to compute the model for control purposes. The ground effect is neglected and the helicopter airframe is assumed to be symmetric, which results in a moment of inertia tensor of the center of the body-fixed frame with just diagonal inertia terms.

Assuming these hypotheses, two approximations of the helicopter model are presented. First, a more realistic model is obtained by using the Steiner's parallel-axis theorem. This model considers that the axes passing through the center of mass are parallel to the axes of rotation of the body-fixed frame, and its origin is displaced by a position $\boldsymbol{r}$ from the origin of the same frame. This assumption results in a strongly-coupled dynamic model. To overcome that, a second model is proposed, where the center of mass and the body-fixed frame origin are assumed congruent, which leads to a decentralized dynamic model.

In what follows, the helicopter attitude is defined, which makes possible to obtain the helicopter kinematics of the translational and rotational motions. A brief explanation of the well-known Euler-Lagrange formulation is given, and based on that, the helicopter equations of motion are obtained. To complete this chapter, the equations of motion of the *QuadRotor* are presented by means of the Newton-Euler procedure.

2.2 Helicopter Attitude

Since the equations of motion depend on the attitude of the mechanical system, this section presents how to estimate the position and the orientation of the rigid body according to an inertial reference frame.

The helicopter, as a rigid body, is characterized by a frame linked to it, and with the origin at its center of rotation. Furthermore, assuming the center of mass is displaced by a position $\boldsymbol{r} = [r_x \quad r_y \quad r_z]'$ from the origin of the rotation body-fixed frame and expressed in this frame, three perpendicular axes passing through the center of mass and parallel to the body-fixed frame are considered ($\mathscr{C} = \{\vec{x}_C, \vec{y}_C, \vec{z}_C\}$). Let $\mathscr{B} = \{\vec{x}_B, \vec{y}_B, \vec{z}_B\}$ be the rotation body-fixed frame, where the $\vec{x}_B$ axis is the helicopter normal flight direction, $\vec{y}_B$ is orthogonal to $\vec{x}_B$ and negative to starboard in the horizontal plane, whereas $\vec{z}_B$ is oriented in ascendant sense and orthogonal to the plane $\vec{x}_B O \vec{y}_B$. The inertial frame $\mathscr{I} = \{\vec{x}, \vec{y}, \vec{z}\}$ is considered fixed with respect to the earth (see Fig. 2.2).

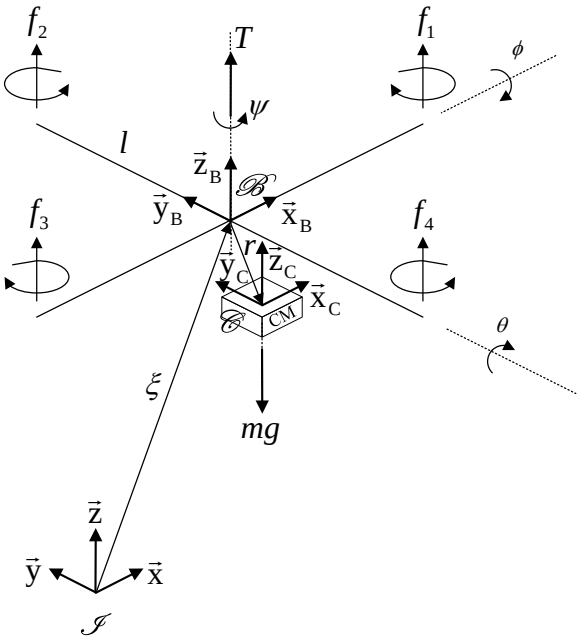

Figure 2.2: *QuadRotor* helicopter scheme.

To compute the coordinates of a point $\boldsymbol{p}$ rigidly attached to the frame $\mathscr{C}$ relative to the frame $\mathscr{I}$, with local coordinates ${}^{\mathscr{C}}\boldsymbol{p}$, the following equations must be composed:

$$ {}^{\mathscr{B}}\boldsymbol{p} = {}^{\mathscr{B}}\boldsymbol{R}_{\mathscr{C}}\,{}^{\mathscr{C}}\boldsymbol{p} + {}^{\mathscr{B}}\boldsymbol{r}, \tag{2.7} $$

$$ {}^{\mathscr{I}}\boldsymbol{p} = {}^{\mathscr{I}}\boldsymbol{R}_{\mathscr{B}}\,{}^{\mathscr{B}}\boldsymbol{p} + {}^{\mathscr{I}}\boldsymbol{\xi}, \tag{2.8} $$

resulting in:

$$ {}^{\mathscr{I}}\boldsymbol{p} = {}^{\mathscr{I}}\boldsymbol{R}_{\mathscr{B}}\,{}^{\mathscr{B}}\boldsymbol{R}_{\mathscr{C}}\,{}^{\mathscr{C}}\boldsymbol{p} + {}^{\mathscr{I}}\boldsymbol{R}_{\mathscr{B}}\,{}^{\mathscr{B}}\boldsymbol{r} + {}^{\mathscr{I}}\boldsymbol{\xi}, \tag{2.9} $$

where the rotation matrices ${}^{\mathscr{B}}\boldsymbol{R}_{\mathscr{C}}$ and ${}^{\mathscr{I}}\boldsymbol{R}_{\mathscr{B}}$ specify the orientations of frame $\mathscr{C}$ with respect to $\mathscr{B}$, and of this last one with respect to the frame $\mathscr{I}$, respectively. The vector ${}^{\mathscr{I}}\boldsymbol{\xi} = \boldsymbol{\xi} = [x \quad y \quad z]'$ represents the position of the origin of the rotation frame of the helicopter, expressed in the inertial frame $\mathscr{I}$. The vector ${}^{\mathscr{B}}\boldsymbol{r} = \boldsymbol{r}$, as commented above, describes the position of the center of mass, which is located at the origin of the frame $\mathscr{C}$, with respect to the origin of the frame $\mathscr{B}$.

As frames $\mathscr{C}$ and $\mathscr{B}$ are parallel, the rotation matrix ${}^{\mathscr{B}}\boldsymbol{R}_{\mathscr{C}}$ is equal to the identity matrix, which results in ${}^{\mathscr{I}}\boldsymbol{R}_{\mathscr{B}} = {}^{\mathscr{I}}\boldsymbol{R}_{\mathscr{C}}$. For the sake of notation simplicity, both rotation matrices ${}^{\mathscr{I}}\boldsymbol{R}_{\mathscr{B}}$ and ${}^{\mathscr{I}}\boldsymbol{R}_{\mathscr{C}}$ are defined as $\boldsymbol{R}_{\mathscr{I}}$. Therefore, equation

(2.9) can be written in a compact form:

$$^{\mathscr{I}}\boldsymbol{p} = \boldsymbol{R}_{\mathscr{I}}{}^{\mathscr{C}}\boldsymbol{p} + {}^{\mathscr{I}}\boldsymbol{d}_{\mathscr{C}}, \tag{2.10}$$

which describes the rigid motion between $^{\mathscr{I}}\boldsymbol{p}$ and $^{\mathscr{C}}\boldsymbol{p}$ (Spong et al., 2006). The vector from the origin of the frame $\mathscr{I}$ to the origin of the frame $\mathscr{C}$ is given by:

$$^{\mathscr{I}}\boldsymbol{d}_{\mathscr{C}} = \boldsymbol{R}_{\mathscr{I}}\boldsymbol{r} + \boldsymbol{\xi}, \tag{2.11}$$

and the vehicle orientation is given by the rotation matrix $\boldsymbol{R}_{\mathscr{I}} : \mathscr{B}, \mathscr{C} \rightarrow \mathscr{I}$, where $\boldsymbol{R}_{\mathscr{I}} \in SO(3)$ is an orthonormal rotation matrix.

The equation of the rigid motion (2.10) can be represented in a matrix form through the homogeneous transformation matrix as follows:

$$^{\mathscr{I}}\bar{\boldsymbol{p}} = \underbrace{\begin{bmatrix} \boldsymbol{R}_{\mathscr{I}} & {}^{\mathscr{I}}\boldsymbol{d}_{\mathscr{C}} \\ \mathbb{0}_{1\times n} & 1 \end{bmatrix}}_{\boldsymbol{H}_{\mathscr{I}}} \cdot {}^{\mathscr{C}}\bar{\boldsymbol{p}}, \tag{2.12}$$

where $^{\mathscr{C}}\bar{\boldsymbol{p}} = [x_C \quad y_C \quad z_C \quad 1]'$.

The rotational transformation of a UAV or, in broad terms, of a rigid body, can be parameterized through several methods such as: the Euler-angle representation, the quaternions representation, and the axis/angle representation (Spong et al., 2006). From twelve independent definitions of the Euler angles is possible to represent the relative orientation between two coordinate systems. The most common are the *x-convention* (rotation around z, x, z), the *y-convention* (rotation around z, y, z) and the *xyz-convention* (rotation around x, y, z). The last one, using intrinsic rotations, is usually found on aerospace applications, and it is named roll, pitch and yaw representation, also known as Tait-Bryan convention, Cardano convention, or nautical convention.

The rotation matrix can be obtained through three successive rotations around the axes of the body-fixed frame. In this thesis, the roll, pitch and yaw angles are used to describe the helicopter rotation in the three-dimensional Euclidean space with respect to the body-fixed frame. Thereby, the configuration of a rigid body rotation in the space is performed as follows (Murray et al., 1994):

1. *Rotation around $\vec{z}_B$ by ψ*: the first movement, assuming the inertial and the body-fixed frames coincide, is given by a rotation around the $\vec{z}_B$ axis from

the $\vec{z}$ axis by the *yaw* angle, ψ.

$$\begin{bmatrix} x'_B \\ y'_B \\ z'_B \end{bmatrix} = \begin{bmatrix} \cos\psi & \sin\psi & 0 \\ -\sin\psi & cos\psi & 0 \\ 0 & 0 & 1 \end{bmatrix} \begin{bmatrix} x \\ y \\ z \end{bmatrix} \tag{2.13}$$

2. Rotation around $\vec{y}_B$ by θ: the second movement is performed by a *pitch* motion around the $\vec{y}_B$ from the new $\vec{y}_B$ axis.

$$\begin{bmatrix} x''_B \\ y''_B \\ z''_B \end{bmatrix} = \begin{bmatrix} \cos\theta & 0 & -\sin\theta \\ 0 & 1 & 0 \\ \sin\theta & 0 & \cos\theta \end{bmatrix} \begin{bmatrix} x'_B \\ y'_B \\ z'_B \end{bmatrix} \tag{2.14}$$

3. *Rotation around $\vec{x}_B$ by ϕ*: the third movement is a rotation that corresponds to the *roll* angle, ϕ, it is carried out around the $\vec{x}_B$ axis from the new $\vec{x}_B$ to move the helicopter to the final position.

$$\begin{bmatrix} x_B \\ y_B \\ z_B \end{bmatrix} = \begin{bmatrix} 1 & 0 & 0 \\ 0 & \cos\phi & \sin\phi \\ 0 & -\sin\phi & \cos\phi \end{bmatrix} \begin{bmatrix} x''_B \\ y''_B \\ z''_B \end{bmatrix} \tag{2.15}$$

These angles are bounded as follows: roll angle, ϕ, by $(-\pi < \phi < \pi)$; pitch angle, θ, by $(-\pi/2 < \theta < \pi/2)$; and yaw angle, ψ, by $(-\pi < \psi < \pi)$.

From these three movements, the following rotation matrices that represent the orientation of the rigid body rotating around of each axis are defined:

$$\boldsymbol{R}(x_B,\phi) = \begin{bmatrix} 1 & 0 & 0 \\ 0 & \cos\phi & \sin\phi \\ 0 & -\sin\phi & \cos\phi \end{bmatrix}, \quad \boldsymbol{R}(y_B,\theta) = \begin{bmatrix} \cos\theta & 0 & -\sin\theta \\ 0 & 1 & 0 \\ \sin\theta & 0 & \cos\theta \end{bmatrix},$$

$$\boldsymbol{R}(z_B,\psi) = \begin{bmatrix} \cos\psi & \sin\psi & 0 \\ -\sin\psi & \cos\psi & 0 \\ 0 & 0 & 1 \end{bmatrix}.$$

Note that the rotations matrices $\boldsymbol{R}(x_B,\phi)$, $\boldsymbol{R}(y_B,\theta)$ and $\boldsymbol{R}(z_B,\psi)$ describe rotations starting from the inertial frame to the body-fixed one. Thus, the rotations from the body-fixed frame to the inertial one are given by: $\boldsymbol{R}(x,\phi) = \boldsymbol{R}(x_B,\phi)'$, $\boldsymbol{R}(y,\theta) = \boldsymbol{R}(y_B,\theta)'$ and $\boldsymbol{R}(z,\psi) = \boldsymbol{R}(z_B,\psi)'$

The following rotation matrix from $\mathscr{I}$ to $\mathscr{B}$ (it is the same one from $\mathscr{I}$ to $\mathscr{C}$),

named as Direction-Cosine Matrix, is obtained by:

$$\boldsymbol{R}_{\mathscr{B}} = {}^{\mathscr{B}}\boldsymbol{R}_{\mathscr{I}} = \boldsymbol{R}(x_B,\phi)\cdot\boldsymbol{R}(y_B,\theta)\cdot\boldsymbol{R}(z_B,\psi)$$

$$\boldsymbol{R}_{\mathscr{B}} = \begin{bmatrix} 1 & 0 & 0 \\ 0 & \cos\phi & \sin\phi \\ 0 & -\sin\phi & \cos\phi \end{bmatrix} \cdot \begin{bmatrix} \cos\theta & 0 & -\sin\theta \\ 0 & 1 & 0 \\ \sin\theta & 0 & \cos\theta \end{bmatrix} \cdot \begin{bmatrix} \cos\psi & \sin\psi & 0 \\ -\sin\psi & \cos\psi & 0 \\ 0 & 0 & 1 \end{bmatrix}$$

$$\boldsymbol{R}_{\mathscr{B}} = \begin{bmatrix} C\psi C\theta & S\psi C\theta & -S\theta \\ C\psi S\theta S\phi - S\psi C\phi & S\psi S\theta S\phi + C\psi C\phi & C\theta S\phi \\ C\psi S\theta C\phi + S\psi S\phi & S\psi S\theta C\phi - C\psi S\phi & C\theta C\phi \end{bmatrix},$$

where $C\cdot = \cos(\cdot)$ and $S\cdot = \sin(\cdot)$.

The rotation matrix that describes the orientation of the body-fixed frame with respect to the inertial frame $\mathscr{I}$ is the transpose matrix of $\boldsymbol{R}_{\mathscr{B}}$, due to its orthonormality property, and is given by:

$$\boldsymbol{R}_{\mathscr{I}} = \begin{bmatrix} C\psi C\theta & C\psi S\theta S\phi - S\psi C\phi & C\psi S\theta C\phi + S\psi S\phi \\ S\psi C\theta & S\psi S\theta S\phi + C\psi C\phi & S\psi S\theta C\phi - C\psi S\phi \\ -S\theta & C\theta S\phi & C\theta C\phi \end{bmatrix}. \tag{2.16}$$

2.3 Helicopter Kinematics

The kinematic equations of the rotational and translational movements are obtained by means of the rotation matrix (2.16) and the equation of rigid motion (2.10).

Since the frame $\mathscr{C}$ is attached to $\mathscr{B}$, the angular velocity of the frame $\mathscr{C}$ is the same as the angular velocity of the rotation body-fixed frame. Thus, the rotational kinematics can be obtained from the relationship between the rotation matrix (2.16) and its time derivative with a skew-symmetric matrix, which simplifies many of the computations involved (Craig, 1989; Spong et al., 2006).

Let $\boldsymbol{R} \in \Re^{n\times n}$ be an orthonormal matrix, where:

$$\boldsymbol{R}'\boldsymbol{R} = \mathbb{1}_{n\times n}\,. \tag{2.17}$$

Its time derivative is given by:

$$\dot{\boldsymbol{R}}'\boldsymbol{R} + \boldsymbol{R}'\dot{\boldsymbol{R}} = \mathbb{0}_{n\times n}\,. \tag{2.18}$$

By defining:

$$\boldsymbol{S} = \boldsymbol{R}'\dot{\boldsymbol{R}}, \tag{2.19}$$

from (2.18) it is obtained that:

$$\boldsymbol{S}' + \boldsymbol{S} = \mathbb{0}_{n\times n}, \tag{2.20}$$

where $\boldsymbol{S}$ is a skew-symmetric matrix. Multiplying both sides of equation (2.19) on the left by $\boldsymbol{R}$ and using the fact that $\boldsymbol{R}\boldsymbol{R}' = \mathbb{1}_{n\times n}$ produces:

$$\dot{\boldsymbol{R}} = \boldsymbol{R}\boldsymbol{S}. \tag{2.21}$$

Therefore, the kinematic equation used to determine the helicopter rotational motion, assuming the rotation matrix (2.16), is given by:

$$\dot{\boldsymbol{R}}_{\mathscr{I}} = \boldsymbol{R}_{\mathscr{I}} \cdot \boldsymbol{S}(\boldsymbol{\omega}), \tag{2.22}$$

where $\boldsymbol{\omega} = [p \quad q \quad r]'$ is the absolute angular velocity vector of the rigid body expressed in the rotation body-fixed frame (i.e., $\boldsymbol{\omega}$ is the angular velocity that corresponds to the derivative of ${}^{\mathscr{I}}\boldsymbol{R}_{\mathscr{B}}$, expressed in coordinates relative to the body-fixed frame $\mathscr{B}$), and $\boldsymbol{S}(\boldsymbol{\omega})$ ($\boldsymbol{S}(\boldsymbol{\omega})(\cdot) = \boldsymbol{\omega} \times \cdot$) is the following skew-symmetric matrix:

$$\boldsymbol{S}(\boldsymbol{\omega}) = \begin{bmatrix} 0 & -r & q \\ r & 0 & -p \\ -q & p & 0 \end{bmatrix}. \tag{2.23}$$

On the other hand, the angular velocity vector of the helicopter expressed in the inertial frame is given by:

$$\boldsymbol{\omega}_{\mathscr{I}} = \boldsymbol{R}_{\mathscr{I}}\boldsymbol{\omega}. \tag{2.24}$$

The relationship between the angular rates of the body-fixed frame and the time derivative of the Euler angles can be obtained from the equation (2.22) after some algebraic manipulations, or as follows:

$$\begin{bmatrix} p \\ q \\ r \end{bmatrix} = \begin{bmatrix} \dot{\phi} \\ 0 \\ 0 \end{bmatrix} + \boldsymbol{R}(x,\phi)^{-1} \begin{bmatrix} 0 \\ \dot{\theta} \\ 0 \end{bmatrix} + (\boldsymbol{R}(y,\theta)\boldsymbol{R}(x,\phi))^{-1} \begin{bmatrix} 0 \\ 0 \\ \dot{\psi} \end{bmatrix},$$

$$\boldsymbol{\omega} = \boldsymbol{W}_{\boldsymbol{\eta}}\dot{\boldsymbol{\eta}},$$

$$\begin{bmatrix} p \\ q \\ r \end{bmatrix} = \begin{bmatrix} 1 & 0 & -\sin\theta \\ 0 & \cos\phi & \sin\phi\cos\theta \\ 0 & -\sin\phi & \cos\phi\cos\theta \end{bmatrix} \begin{bmatrix} \dot{\phi} \\ \dot{\theta} \\ \dot{\psi} \end{bmatrix}, \tag{2.25}$$

where $\boldsymbol{\eta} = [\phi \quad \theta \quad \psi]'$, and $\boldsymbol{W}_{\boldsymbol{\eta}}$ is the Euler matrix.

The helicopter rotational motion is given by the angular rate components in the three axis: the roll angular rate (p), the pitch angular rate (q), and the yaw angular rate (r), around the $\vec{x}_B$, $\vec{y}_B$ and $\vec{z}_B$ axes, respectively. These rotational velocities occur due to the torques applied on the system linked to the helicopter structure, which are generated by external forces. These external forces define the different moments in the three axes: rolling moment (τ_{ϕ_a}), pitching moment (τ_{θ_a}), and yawing moment (τ_{ψ_a}) around the $\vec{x}_B$, $\vec{y}_B$ and $\vec{z}_B$ axes, respectively (Esteban, 2005).

The time derivative of the Euler angles is obtained through the inverted Euler matrix in (2.25), and can be posed by:

$$\dot{\boldsymbol{\eta}} = \boldsymbol{W}_{\boldsymbol{\eta}}^{-1}\boldsymbol{\omega}$$

$$\begin{bmatrix} \dot{\phi} \\ \dot{\theta} \\ \dot{\psi} \end{bmatrix} = \begin{bmatrix} 1 & \sin\phi\tan\theta & \cos\phi\tan\theta \\ 0 & \cos\phi & -\sin\phi \\ 0 & \sin\phi\sec\theta & \cos\phi\sec\theta \end{bmatrix} \begin{bmatrix} p \\ q \\ r \end{bmatrix}. \tag{2.26}$$

The time derivative of the Euler angles $\left(\dot{\phi}, \dot{\theta}, \dot{\psi}\right)$ is a discontinuous function. These time derivatives are different from the angular rates of the body-fixed frame (p, q, r), which can be physically measurable, for example, by means of gyroscopes. Generally, aerospace systems are equipped with Inertial Measurement Units (IMU's), that measure the angular rates and estimate the Euler angles (Bouabdallah et al., 2006).

The linear velocity of a point $\boldsymbol{p}$, that is rigidly attached to the frame $\mathscr{C}$ is obtained through the equation (2.10), where the velocity ${}^{\mathscr{I}}\dot{\boldsymbol{p}}$ is given by the product rule for differentiation as follows:

$${}^{\mathscr{I}}\dot{\boldsymbol{p}} = \dot{\boldsymbol{R}}_{\mathscr{I}}{}^{\mathscr{C}}\boldsymbol{p} + \boldsymbol{R}_{\mathscr{I}}{}^{\mathscr{C}}\dot{\boldsymbol{p}} + {}^{\mathscr{I}}\dot{\boldsymbol{d}}_{\mathscr{C}}, \tag{2.27}$$

where

$${}^{\mathscr{I}}\dot{\boldsymbol{d}}_{\mathscr{C}} = \dot{\boldsymbol{R}}_{\mathscr{I}}\boldsymbol{r} + \dot{\boldsymbol{\xi}}, \tag{2.28}$$

and as the point ${}^{\mathscr{C}}\boldsymbol{p}$ is assumed rigidly attached to the frame $\mathscr{C}$, its coordinates relative to the frame $\mathscr{C}$ do not change, giving ${}^{\mathscr{C}}\dot{\boldsymbol{p}} = 0$. Therefore, by substituting

the equations (2.22) and (2.28) into (2.27), the linear velocity is given by:

$$\begin{aligned} {}^{\mathscr{I}}\dot{\boldsymbol{p}} &= \boldsymbol{R}_{\mathscr{I}}\boldsymbol{S}(\boldsymbol{\omega})^{\mathscr{C}}\boldsymbol{p} + \boldsymbol{R}_{\mathscr{I}}\boldsymbol{S}(\boldsymbol{\omega})\boldsymbol{r} + \dot{\boldsymbol{\xi}} \\ &= \boldsymbol{R}_{\mathscr{I}}\boldsymbol{\omega} \times {}^{\mathscr{C}}\boldsymbol{p} + \boldsymbol{R}_{\mathscr{I}}\boldsymbol{\omega} \times \boldsymbol{r} + \dot{\boldsymbol{\xi}}\,, \end{aligned} \tag{2.29}$$

where $\boldsymbol{R}_{\mathscr{I}}\boldsymbol{\omega} \times {}^{\mathscr{C}}\boldsymbol{p}$ is the velocity of the point $\boldsymbol{p}$ with respect to the origin of the frame $\mathscr{C}$ expressed in the orientation of the frame $\mathscr{I}$, and the term $\boldsymbol{\omega} \times \boldsymbol{R}_{\mathscr{I}}\boldsymbol{r} + \dot{\boldsymbol{\xi}}$ is the rate at which the center of mass is moving. From now on, the linear velocity is defined by the simpler notation $\boldsymbol{v}_{\mathscr{I}} = {}^{\mathscr{I}}\dot{\boldsymbol{p}}$.

The linear velocity of the point $\boldsymbol{p}$ expressed in the frame $\mathscr{C}$ is obtained by:

$$\boldsymbol{v}_{\mathscr{C}} = \boldsymbol{R}'_{\mathscr{I}}\boldsymbol{v}_{\mathscr{I}} = \boldsymbol{R}_{\mathscr{B}}\boldsymbol{v}_{\mathscr{I}}\,, \tag{2.30}$$

where $\boldsymbol{v}_{\mathscr{I}} = [u_0 \quad v_0 \quad w_0]'$ and $\boldsymbol{v}_{\mathscr{C}} = [u_C \quad v_C \quad w_C]'$.

2.4 Euler-Lagrange Mechanical Systems

In this section, the forced Euler-Lagrange equations of mechanical systems are presented.

Simple mechanical systems can be described by their Lagrangian, which is the difference between the (positive semidefinite) kinetic energy and the potential energy:

$$\mathscr{L}(\boldsymbol{q}, \dot{\boldsymbol{q}}) = \mathscr{K}(\boldsymbol{q}, \dot{\boldsymbol{q}}) - \mathscr{U}(\boldsymbol{q}) = \frac{1}{2}\dot{\boldsymbol{q}}'\boldsymbol{M}(\boldsymbol{q})\dot{\boldsymbol{q}} - \mathscr{U}(\boldsymbol{q})\,, \tag{2.31}$$

where $\boldsymbol{q} \in \mathbb{Q}$ denotes the configuration vector of the system (i.e. the set of the so-called generalized coordinates) that belongs to an n-dimensional configuration manifold $\mathbb{Q}$, with n being the number of degrees of freedom of the system. $\mathscr{K}(\boldsymbol{q}, \dot{\boldsymbol{q}})$ is the system kinetic energy and $\mathscr{U}(\boldsymbol{q})$ is the potential energy, which here is related only to conservative forces such as the gravitational one.

$\boldsymbol{M}(\boldsymbol{q})$ is the inertia matrix which is a positive definite symmetric matrix. For a fixed value of the generalized coordinate $\boldsymbol{q}$, let $0 < \lambda_1(\boldsymbol{q}) \leq \ldots \leq \lambda_n(\boldsymbol{q})$ denote the n eigenvalues of $\boldsymbol{M}(\boldsymbol{q})$. These eigenvalues are positive as a consequence of the positive definiteness of $\boldsymbol{M}(\boldsymbol{q})$ (Spong et al., 2006). It results that:

$$\lambda_1(\boldsymbol{q})\mathbb{1}_{n\times n} \leq \boldsymbol{M}(\boldsymbol{q}) \leq \lambda_n(\boldsymbol{q})\mathbb{1}_{n\times n}\,. \tag{2.32}$$

If all joints are of revolution, the inertia matrix contains only terms involving sine and cosine functions and, hence, is bounded above and below as a function of the

generalized coordinates. For a more conservative result, constants can be find to provide uniform bounds in the inertia matrix, whose magnitudes can be bounded by unity:

$$\lambda_{min}\mathbb{1}_{n\times n} \leq \boldsymbol{M}(\boldsymbol{q}) \leq \lambda_{max}\mathbb{1}_{n\times n}\,, \tag{2.33}$$

with λ_{min} and λ_{max} scalars. The boundedness property of the inertia matrix can also be defined as (Lewis et al., 2004):

$$0 < m_{min} \leq \|\boldsymbol{M}(\boldsymbol{q})\| \leq m_{max} \quad \forall \quad \boldsymbol{q} \in \mathbb{Q}\,, \tag{2.34}$$

where any induced matrix norm can be used to define the positive scalars m_{min} and m_{max}.

Let $\boldsymbol{b_i}(\boldsymbol{q}) : \mathbb{Q} \to \Re^n$, $i = \{1,\ldots,m\}$ be an m vectors set of the external forces applied to the system. The Euler-Lagrange equation that describes this mechanical system is given by:

$$\frac{d}{dt}\left(\frac{\partial \mathscr{L}(\boldsymbol{q},\dot{\boldsymbol{q}})}{\partial \dot{\boldsymbol{q}}}\right) - \frac{\partial \mathscr{L}(\boldsymbol{q},\dot{\boldsymbol{q}})}{\partial \boldsymbol{q}} = \mathscr{F}(\boldsymbol{q})\,, \tag{2.35}$$

where $\mathscr{F}(\boldsymbol{q}) \in \Re^n$ is the generalized force/torque vector. By substituting (2.31) into (2.35), the following equation is obtained:

$$\frac{d}{dt}\left(\frac{\partial}{\partial \dot{\boldsymbol{q}}}\left(\frac{1}{2}\dot{\boldsymbol{q}}'\boldsymbol{M}(\boldsymbol{q})\dot{\boldsymbol{q}}\right)\right) - \left(\frac{\partial}{\partial \boldsymbol{q}}\left(\frac{1}{2}\dot{\boldsymbol{q}}'\boldsymbol{M}(\boldsymbol{q})\dot{\boldsymbol{q}}\right)\right) + \frac{\partial \mathscr{U}(\boldsymbol{q})}{\partial \boldsymbol{q}} = \boldsymbol{B}(\boldsymbol{q})\boldsymbol{\Gamma} + \boldsymbol{\Gamma_d}\,,$$

where $\boldsymbol{B}(\boldsymbol{q}) = [\boldsymbol{b_1}(\boldsymbol{q}),\ldots,\boldsymbol{b_m}(\boldsymbol{q})] \in \Re^{n\times m}$ is the input coupling matrix (also called external force matrix), $\boldsymbol{\Gamma} \in \mathbb{U}$ is the control action vector, being $\mathbb{U}$ the m-dimensional actuation space, and $\boldsymbol{\Gamma_d}$ represents the total effect of the modeling errors and energy-bounded external disturbances acting on the system.

Considering this expression, the equation of motion can be expressed by the following form (Kelly et al., 2005):

$$\boldsymbol{M}(\boldsymbol{q})\ddot{\boldsymbol{q}} + \dot{\boldsymbol{M}}(\boldsymbol{q})\dot{\boldsymbol{q}} - \frac{1}{2}\frac{\partial}{\partial \boldsymbol{q}}\left(\dot{\boldsymbol{q}}'\boldsymbol{M}(\boldsymbol{q})\dot{\boldsymbol{q}}\right) + \frac{\partial \mathscr{U}(\boldsymbol{q})}{\partial \boldsymbol{q}} = \boldsymbol{B}(\boldsymbol{q})\boldsymbol{\Gamma} + \boldsymbol{\Gamma_d}\,,$$

or, in a compact matrix form, as follows:

$$\boldsymbol{M}(\boldsymbol{q})\ddot{\boldsymbol{q}} + \boldsymbol{C}(\boldsymbol{q},\dot{\boldsymbol{q}})\dot{\boldsymbol{q}} + \boldsymbol{G}(\boldsymbol{q}) = \boldsymbol{B}(\boldsymbol{q})\boldsymbol{\Gamma} + \boldsymbol{\Gamma_d}\,, \tag{2.36}$$

where $\boldsymbol{C}(\boldsymbol{q},\dot{\boldsymbol{q}})\dot{\boldsymbol{q}}$ is the so-called Coriolis and centrifugal force vector and $\boldsymbol{G}(\boldsymbol{q})$ represents the gravitational force vector.

The Coriolis and centrifugal force matrix $\boldsymbol{C}(\boldsymbol{q},\dot{\boldsymbol{q}})$ is not unique, but the vector $\boldsymbol{C}(\boldsymbol{q},\dot{\boldsymbol{q}})\dot{\boldsymbol{q}}$ is indeed unique. For the sake of convenience, in the thesis this matrix is obtained through the well-known Christoffel Symbols (of the first kind), $c_{ijk}(\boldsymbol{q})$, defined as follows:

$$c_{ijk} := \frac{1}{2}\left\{\frac{\partial m_{kj}}{\partial q_i} + \frac{\partial m_{ki}}{\partial q_j} - \frac{\partial m_{ij}}{\partial q_k}\right\}, \tag{2.37}$$

and the (k,j)th element of the matrix $\boldsymbol{C}(\boldsymbol{q},\dot{\boldsymbol{q}})$ is given by:

$$\begin{aligned} c_{kj} &= \sum_{i=1}^{n} c_{ijk}(q)\dot{q}_i \\ &= \sum_{i=1}^{n} \frac{1}{2}\left\{\frac{\partial m_{kj}}{\partial q_i} + \frac{\partial m_{ki}}{\partial q_j} - \frac{\partial m_{ij}}{\partial q_k}\right\}\dot{q}_i\,. \end{aligned} \tag{2.38}$$

Furthermore, the equation (2.36) can be represented by the following recursive expression:

$$\sum_{j=1}^{n} m_{kj}(\boldsymbol{q})\ddot{q}_j + \sum_{i=1}^{n}\sum_{j=1}^{n} c_{ijk}(\boldsymbol{q})\dot{q}_i\dot{q}_j + g_k(\boldsymbol{q}) = e_k'\boldsymbol{B}(\boldsymbol{q})\boldsymbol{\Gamma} + \boldsymbol{\Gamma_d}\,, k = 1,\ldots,n\,, \tag{2.39}$$

where e_k is the kth standard basis in $\Re^n$, $g_k(\boldsymbol{q}) = \frac{\partial \mathscr{U}(\boldsymbol{q})}{\partial q_k}$.

The equations (2.39) have three types of terms. The first one involves the second derivative of the generalized coordinates. The second part involves quadratic terms in the first derivative of $\boldsymbol{q}$, where the coefficients may depend on $\boldsymbol{q}$. These latter terms are further classified into those involving a product of the type $\dot{q}_i^2$ and those involving a product of the type $\dot{q}_i\dot{q}_j$ where $i \neq j$. Terms of the type $\dot{q}_i^2$ are called centrifugal, while terms of the type $\dot{q}_i\dot{q}_j$ are called Coriolis terms. The third type of terms are those involving only $\boldsymbol{q}$ but not its derivative. This third type arises from differentiating the potential energy.

It is interesting to mention here some properties of the Coriolis and centrifugal force vector $\boldsymbol{C}(\boldsymbol{q},\dot{\boldsymbol{q}})\dot{\boldsymbol{q}}$, which helps at the control design stage and to perform the stability analysis, i.e.:

1. Property 1: $\boldsymbol{C}(\boldsymbol{q},\dot{\boldsymbol{q}})\dot{\boldsymbol{q}}$ is quadratic in $\dot{\boldsymbol{q}}$.
2. Property 2: $\|\boldsymbol{C}(\boldsymbol{q},\dot{\boldsymbol{q}})\dot{\boldsymbol{q}}\| \leq v_b\|\dot{\boldsymbol{q}}\|^2$.
3. Property 3: The matrix $\boldsymbol{C}(\boldsymbol{q},\dot{\boldsymbol{q}})$, obtained as in (2.38), is related to the inertia

matrix $\dot{\boldsymbol{M}}(\boldsymbol{q})$ by the expression (Kelly et al., 2005):

$$\boldsymbol{x}'\left(\frac{1}{2}\dot{\boldsymbol{M}}(\boldsymbol{q})-\boldsymbol{C}(\boldsymbol{q},\dot{\boldsymbol{q}})\right)\boldsymbol{x}=0 \quad \forall \boldsymbol{q},\dot{\boldsymbol{q}},\boldsymbol{x}\in\mathbb{Q}\,,$$

and consequently $\mathscr{N}(\boldsymbol{q},\dot{\boldsymbol{q}})=\dot{\boldsymbol{M}}(\boldsymbol{q})-2\boldsymbol{C}(\boldsymbol{q},\dot{\boldsymbol{q}})$ is a skew-symmetric matrix, and the following expression holds:

$$\dot{\boldsymbol{M}}(\boldsymbol{q})=\boldsymbol{C}(\boldsymbol{q},\dot{\boldsymbol{q}})+\boldsymbol{C}(\boldsymbol{q},\dot{\boldsymbol{q}})'\,.$$

This property states that the fictitious forces $\mathscr{N}(\boldsymbol{q},\dot{\boldsymbol{q}})\dot{\boldsymbol{q}}$ do no work in the mechanical system (Lewis et al., 2004).

Moreover, the gravity vector is also bounded, so that $\|\boldsymbol{G}(\boldsymbol{q})\|\leq g_b$.

2.4.1 Model Uncertainties

Since the equations of motion (2.36) represent the real system, the dynamic model can be divided in nominal and uncertain parts. Thus, the system can be rewritten as follows:

$$\widehat{\boldsymbol{M}}(\boldsymbol{q})\ddot{\boldsymbol{q}}+\widehat{\boldsymbol{C}}(\boldsymbol{q},\dot{\boldsymbol{q}})\dot{\boldsymbol{q}}+\widehat{\boldsymbol{G}}(\boldsymbol{q})=\widehat{\boldsymbol{B}}(\boldsymbol{q})\boldsymbol{\Gamma}+\boldsymbol{\delta}(\boldsymbol{q},\dot{\boldsymbol{q}},\ddot{\boldsymbol{q}},\boldsymbol{\Gamma}_{\boldsymbol{d}})\,, \tag{2.40}$$

where $\widehat{\boldsymbol{M}}(\boldsymbol{q})$, $\widehat{\boldsymbol{C}}(\boldsymbol{q},\dot{\boldsymbol{q}})$ and $\widehat{\boldsymbol{G}}(\boldsymbol{q})$ are the nominal matrices and vectors. The term $\boldsymbol{\delta}(\boldsymbol{q},\dot{\boldsymbol{q}},\ddot{\boldsymbol{q}},\boldsymbol{\Gamma}_{\boldsymbol{d}})$ considers the uncertainties of the model associated to an imperfect knowledge of the physical parameters that characterize the system, modeling errors, unmodeled dynamics of the actuators, sensors or structural mechanical vibrations, friction phenomena, electrical noise signals, computational errors and exogenous disturbances (Vivas, 2004). Besides, this term can be represented by additive uncertainties and partitioned into two terms as follows:

$$\boldsymbol{\delta}(\boldsymbol{q},\dot{\boldsymbol{q}},\ddot{\boldsymbol{q}},\boldsymbol{\Gamma}_{\boldsymbol{d}})=\boldsymbol{\Gamma}_{\boldsymbol{d}}+\boldsymbol{\Xi}(\boldsymbol{q},\dot{\boldsymbol{q}},\ddot{\boldsymbol{q}})\,, \tag{2.41}$$

where $\boldsymbol{\Gamma}_{\boldsymbol{d}}$ represents the unmodeled dynamics and energy-bounded external disturbances, as assumed before, while $\boldsymbol{\Xi}(\boldsymbol{q},\dot{\boldsymbol{q}},\ddot{\boldsymbol{q}})$ is a function of the parametric uncertainties of the system matrices and vectors.

From the equations of motion (2.36) and (2.40), the uncertain part of the dy-

namic model can be expressed in the following form:

$$\begin{aligned} \Delta \boldsymbol{M}(\boldsymbol{q}) &:= \widehat{\boldsymbol{M}}(\boldsymbol{q}) - \boldsymbol{M}(\boldsymbol{q}), \\ \Delta \boldsymbol{C}(\boldsymbol{q},\dot{\boldsymbol{q}}) &:= \widehat{\boldsymbol{C}}(\boldsymbol{q},\dot{\boldsymbol{q}}) - \boldsymbol{C}(\boldsymbol{q},\dot{\boldsymbol{q}}), \\ \Delta \boldsymbol{G}(\boldsymbol{q}) &:= \widehat{\boldsymbol{G}}(\boldsymbol{q}) - \boldsymbol{G}(\boldsymbol{q}), \end{aligned}$$

being $\Delta \boldsymbol{M}(\boldsymbol{q})$, $\Delta \boldsymbol{C}(\boldsymbol{q},\dot{\boldsymbol{q}})$ and $\Delta \boldsymbol{G}(\boldsymbol{q})$ the parametric uncertainties. Thus, function $\Xi(\boldsymbol{q},\dot{\boldsymbol{q}},\ddot{\boldsymbol{q}})$ is given by:

$$\Xi(\boldsymbol{q},\dot{\boldsymbol{q}},\ddot{\boldsymbol{q}}) = \Delta \boldsymbol{M}(\boldsymbol{q})\ddot{\boldsymbol{q}} + \Delta \boldsymbol{C}(\boldsymbol{q},\dot{\boldsymbol{q}})\dot{\boldsymbol{q}} + \Delta \boldsymbol{G}(\boldsymbol{q}). \tag{2.42}$$

In what follows, the equations of motion of the *QuadRotor* helicopter will be developed using the Euler-Lagrange formulation presented in this section.

2.5 Helicopter Model via Euler-Lagrange Formulation

The helicopter motion equations can be expressed by the Euler-Lagrange formalism based on the kinetic and potential energy concept:

$$\frac{d}{dt}\left(\frac{\partial \mathscr{L}(\boldsymbol{q},\dot{\boldsymbol{q}})}{\partial \dot{\boldsymbol{q}}}\right) - \frac{\partial \mathscr{L}(\boldsymbol{q},\dot{\boldsymbol{q}})}{\partial \boldsymbol{q}} = \begin{bmatrix} \boldsymbol{f}_{\xi} \\ \boldsymbol{\tau}_{\eta} \end{bmatrix}, \tag{2.43}$$

where $\boldsymbol{\tau}_{\eta} = \boldsymbol{\tau}_{\eta_a} + \boldsymbol{\delta}_{\eta}(\boldsymbol{q},\dot{\boldsymbol{q}},\ddot{\boldsymbol{q}},\boldsymbol{\tau}_{\eta_d}) \in \Re^3$ represents the total rolling, pitching and yawing moments expressed in the inertial reference frame, which join the applied torque vector $\boldsymbol{\tau}_{\eta_a}$ and the torques generated by the total effect of the modeling errors of the system and external disturbances. Recalling the equation (2.41), the uncertainty vector for the rotational motion is defined by:

$$\boldsymbol{\delta}_{\eta}(\boldsymbol{q},\dot{\boldsymbol{q}},\ddot{\boldsymbol{q}},\boldsymbol{\tau}_{\eta_d}) = \boldsymbol{\tau}_{\eta_d} + \Xi_{\eta}(\boldsymbol{q},\dot{\boldsymbol{q}},\ddot{\boldsymbol{q}}), \tag{2.44}$$

where $\boldsymbol{\tau}_{\eta_d} = \boldsymbol{a}_{\boldsymbol{R}} + \boldsymbol{\tau}_{\boldsymbol{G}_{\mathscr{I}}}$ represents the external disturbances, which, in this thesis, are assumed to be composed by the gyroscopic movements and the aerodynamic moment vector that affect the helicopter, both expressed in $\mathscr{I}$. The aerodynamic moment vector acting on the helicopter, $\boldsymbol{a}_{\boldsymbol{R}} = [a_{\phi} \quad a_{\theta} \quad a_{\psi}]'$, could be computed depending of the aerodynamic coefficients, air density and squared velocity of the helicopter with respect to the air. However, these moments are unknown in the presence of unpredictable winds and turbulence. Besides, the gyroscopic effects

are considered also unknown, because it is assumed, at the motion control design stage, that there are no access to the rotor speed. Consequently, these effects will be neglected for the control design and will be considered as external disturbances.

The translational force vector $\boldsymbol{f_\xi} = \boldsymbol{R}_{\mathscr{I}}\widehat{\boldsymbol{f}} + \boldsymbol{\delta_\xi}(\boldsymbol{q}, \dot{\boldsymbol{q}}, \ddot{\boldsymbol{q}}, \boldsymbol{f_{\xi_d}}) \in \Re^3$ is also divided into two parts: the first term, $\boldsymbol{R}_{\mathscr{I}}\widehat{\boldsymbol{f}} = \boldsymbol{R}_{\mathscr{I}_{\boldsymbol{e_3}}} T$, constitutes the applied force to the helicopter due to the main control input T in the $\vec{z}$ axis direction[2]. The second part, $\boldsymbol{\delta_\xi}(\boldsymbol{q}, \dot{\boldsymbol{q}}, \ddot{\boldsymbol{q}}, \boldsymbol{f_{\xi_d}})$, combines the parametric uncertainties with the external disturbances. For control design purposes, aerodynamic force vector, $\boldsymbol{f_{\xi_d}} = \boldsymbol{a_T} = [a_x \quad a_y \quad a_z]'$, whose components are in the $\vec{x}$, $\vec{y}$ and $\vec{z}$ axes respectively, are also assumed external disturbances. This force could be computed in the same way as in the case of aerodynamic moments.

The generalized coordinates of a rigid body evolutioning in a three-dimensional space can be written as follows:

$$\boldsymbol{q} = [\boldsymbol{\xi}' \quad \boldsymbol{\eta}']' \in \Re^6,$$

with $\boldsymbol{\xi} = [x \quad y \quad z]' \in \Re^3$ being the center of rotation position of the helicopter with respect to the inertial frame $\mathscr{I}$, and $\boldsymbol{\eta} = [\phi \quad \theta \quad \psi]' \in \Re^3$ represents the Euler angles described in Section 2.2.

To derive the equations of motion, first the kinetic and potential energy must be computed in terms of the generalized coordinates of the system. To start it, the inertial, the rotation body-fixed and the center of mass frames are invoked again (see Fig. 2.2).

First, the kinetic energy is developed considering the point $\boldsymbol{p}$ rigidly attached to the frame $\mathscr{C}$, with coordinates given by equation (2.10) expressed in the frame $\mathscr{I}$, and linear velocity vector also expressed in the inertial frame obtained by equation (2.29). Thus, let $\mathscr{K}$ be the kinetic energy at point $\boldsymbol{p}$ with respect to the frame $\mathscr{I}$, and let $d\mathscr{K}$ be the kinetic energy of a particle with differential mass dm in $\mathscr{C}$. The kinetic energy of the rigid body as a quadratic function of the first time derivative of the generalized coordinates is obtained by:

$$d\mathscr{K} = \frac{1}{2}\left(\boldsymbol{v}_{\mathscr{I}}{}' \cdot \boldsymbol{v}_{\mathscr{I}}\right) dm, \tag{2.45}$$

[2]The notation $\boldsymbol{e_3}$ represents the vector $\boldsymbol{e_3} = [0 \quad 0 \quad 1]'$. Thus, the therm $\boldsymbol{R}_{\mathscr{I}_{\boldsymbol{e_3}}}$ denotes the third column of the rotation matrix.

and the squared velocity is given by:

$$\begin{aligned}
\boldsymbol{v}_{\mathscr{I}}{}' \cdot \boldsymbol{v}_{\mathscr{I}} &= \left(\boldsymbol{R}_{\mathscr{I}}\boldsymbol{\omega} \times {}^{\mathscr{C}}\boldsymbol{p} + \boldsymbol{R}_{\mathscr{I}}\boldsymbol{\omega} \times \boldsymbol{r} + \dot{\boldsymbol{\xi}}\right)' \cdot \left(\boldsymbol{R}_{\mathscr{I}}\boldsymbol{\omega} \times {}^{\mathscr{C}}\boldsymbol{p} + \boldsymbol{R}_{\mathscr{I}}\boldsymbol{\omega} \times \boldsymbol{r} + \dot{\boldsymbol{\xi}}\right) \\
&= \dot{\boldsymbol{\xi}}'\dot{\boldsymbol{\xi}} + 2\dot{\boldsymbol{\xi}}'\boldsymbol{R}_{\mathscr{I}}\boldsymbol{\omega} \times {}^{\mathscr{C}}\boldsymbol{p} + 2\dot{\boldsymbol{\xi}}'\boldsymbol{R}_{\mathscr{I}}\boldsymbol{\omega} \times \boldsymbol{r} \\
&\quad + \left(\boldsymbol{R}_{\mathscr{I}}\boldsymbol{\omega} \times {}^{\mathscr{C}}\boldsymbol{p}\right)'\left(\boldsymbol{R}_{\mathscr{I}}\boldsymbol{\omega} \times {}^{\mathscr{C}}\boldsymbol{p}\right) + 2\left(\boldsymbol{R}_{\mathscr{I}}\boldsymbol{\omega} \times {}^{\mathscr{C}}\boldsymbol{p}\right)'\left(\boldsymbol{R}_{\mathscr{I}}\boldsymbol{\omega} \times {}^{\mathscr{C}}\boldsymbol{r}\right) \\
&\quad + \left(\boldsymbol{R}_{\mathscr{I}}\boldsymbol{\omega} \times \boldsymbol{r}\right)'\left(\boldsymbol{R}_{\mathscr{I}}\boldsymbol{\omega} \times \boldsymbol{r}\right).
\end{aligned}$$

By making use of the skew-symmetric matrix (2.22) and some of the cross product properties, the squared of the velocity is rearranged as follows:

$$\begin{aligned}
\boldsymbol{v}_{\mathscr{I}}{}' \cdot \boldsymbol{v}_{\mathscr{I}} &= \dot{\boldsymbol{\xi}}'\dot{\boldsymbol{\xi}} - 2\dot{\boldsymbol{\xi}}'\boldsymbol{R}_{\mathscr{I}}\boldsymbol{S}({}^{\mathscr{C}}\boldsymbol{p})\boldsymbol{\omega} - 2\dot{\boldsymbol{\xi}}'\boldsymbol{R}_{\mathscr{I}}\boldsymbol{S}(\boldsymbol{r})\boldsymbol{\omega} \\
&\quad + \boldsymbol{\omega}'\left(\boldsymbol{S}({}^{\mathscr{C}}\boldsymbol{p})'\boldsymbol{S}({}^{\mathscr{C}}\boldsymbol{p}) + 2\boldsymbol{S}({}^{\mathscr{C}}\boldsymbol{p})'\boldsymbol{S}(\boldsymbol{r}) + \boldsymbol{S}(\boldsymbol{r})'\boldsymbol{S}(\boldsymbol{r})\right)\boldsymbol{\omega}.
\end{aligned}$$

However, it is more suitable to write this expression in terms of the generalized coordinates. To perform that, the vector $\boldsymbol{\omega}$ is replaced by equation (2.25), which yields:

$$\begin{aligned}
\boldsymbol{v}_{\mathscr{I}}{}' \cdot \boldsymbol{v}_{\mathscr{I}} &= \dot{\boldsymbol{\xi}}'\dot{\boldsymbol{\xi}} - 2\dot{\boldsymbol{\xi}}'\boldsymbol{R}_{\mathscr{I}}\boldsymbol{S}({}^{\mathscr{C}}\boldsymbol{p})\boldsymbol{W}_{\boldsymbol{\eta}}\dot{\boldsymbol{\eta}} - 2\dot{\boldsymbol{\xi}}'\boldsymbol{R}_{\mathscr{I}}\boldsymbol{S}(\boldsymbol{r})\boldsymbol{W}_{\boldsymbol{\eta}}\dot{\boldsymbol{\eta}} \\
&\quad + \dot{\boldsymbol{\eta}}'\boldsymbol{W}_{\boldsymbol{\eta}}'\left(\boldsymbol{S}({}^{\mathscr{C}}\boldsymbol{p})'\boldsymbol{S}({}^{\mathscr{C}}\boldsymbol{p}) + 2\boldsymbol{S}({}^{\mathscr{C}}\boldsymbol{p})'\boldsymbol{S}(\boldsymbol{r}) + \boldsymbol{S}(\boldsymbol{r})'\boldsymbol{S}(\boldsymbol{r})\right)\boldsymbol{W}_{\boldsymbol{\eta}}\dot{\boldsymbol{\eta}}.
\end{aligned} \tag{2.46}$$

Therefore, solving the equation (2.45) with the squared velocity, the kinetic energy of the helicopter can be computed by the following expression:

$$\mathscr{K} = \frac{1}{2}\int \boldsymbol{v}_{\mathscr{I}}{}' \cdot \boldsymbol{v}_{\mathscr{I}} dm,$$

$$\begin{aligned}
\mathscr{K} &= \frac{1}{2}\int \dot{\boldsymbol{\xi}}'\dot{\boldsymbol{\xi}} dm - \int \dot{\boldsymbol{\xi}}'\boldsymbol{R}_{\mathscr{I}}\boldsymbol{S}({}^{\mathscr{C}}\boldsymbol{p})\boldsymbol{W}_{\boldsymbol{\eta}}\dot{\boldsymbol{\eta}} dm - \int \dot{\boldsymbol{\xi}}'\boldsymbol{R}_{\mathscr{I}}\boldsymbol{S}(\boldsymbol{r})\boldsymbol{W}_{\boldsymbol{\eta}}\dot{\boldsymbol{\eta}} dm \\
&\quad + \frac{1}{2}\int \dot{\boldsymbol{\eta}}'\boldsymbol{W}_{\boldsymbol{\eta}}'\left(\boldsymbol{S}({}^{\mathscr{C}}\boldsymbol{p})'\boldsymbol{S}({}^{\mathscr{C}}\boldsymbol{p}) + 2\boldsymbol{S}({}^{\mathscr{C}}\boldsymbol{p})'\boldsymbol{S}(\boldsymbol{r}) + \boldsymbol{S}(\boldsymbol{r})'\boldsymbol{S}(\boldsymbol{r})\right)\boldsymbol{W}_{\boldsymbol{\eta}}\dot{\boldsymbol{\eta}} dm.
\end{aligned}$$

By integrating the equation above, the second integral and the second term of

the fourth integral become null, and the kinetic energy results on:

$$\mathscr{K} = \frac{1}{2} m \dot{\boldsymbol{\xi}}' \dot{\boldsymbol{\xi}} - m \dot{\boldsymbol{\xi}}' \boldsymbol{R}_{\mathscr{I}} \boldsymbol{S}(\boldsymbol{r}) \boldsymbol{W}_{\boldsymbol{\eta}} \dot{\boldsymbol{\eta}} + \frac{1}{2} \dot{\boldsymbol{\eta}}' \mathscr{J}(\boldsymbol{\eta}) \dot{\boldsymbol{\eta}}, \tag{2.47}$$

or in the matrix form:

$$\mathscr{K} = \frac{1}{2} \begin{bmatrix} \dot{\boldsymbol{\xi}} \\ \dot{\boldsymbol{\eta}} \end{bmatrix}' \underbrace{\begin{bmatrix} m \mathbb{1}_{3\times 3} & -m \boldsymbol{R}_{\mathscr{I}} \boldsymbol{S}(\boldsymbol{r}) \boldsymbol{W}_{\boldsymbol{\eta}} \\ -m \boldsymbol{W}'_{\boldsymbol{\eta}} \boldsymbol{S}(\boldsymbol{r})' \boldsymbol{R}_{\mathscr{I}}' & \mathscr{J}(\boldsymbol{\eta}) \end{bmatrix}}_{\boldsymbol{M}(\boldsymbol{q})} \begin{bmatrix} \dot{\boldsymbol{\xi}} \\ \dot{\boldsymbol{\eta}} \end{bmatrix}, \tag{2.48}$$

where $\boldsymbol{M}(\boldsymbol{q})$ is the inertia matrix, and:

$$\mathscr{J}(\boldsymbol{\eta}) = \boldsymbol{W}'_{\boldsymbol{\eta}} \boldsymbol{J} \boldsymbol{W}_{\boldsymbol{\eta}}. \tag{2.49}$$

Assuming the helicopter as a continuous rigid body with mass density $\rho({}^{\mathscr{C}}\boldsymbol{p})$ at point $\boldsymbol{p}$ located at its center of mass and displaced by a position $\boldsymbol{r}$ from the rotation body-fixed frame, the mass of the helicopter is given by:

$$m = \int_V \rho({}^{\mathscr{C}}\boldsymbol{p}) dx_C \, dy_C \, dz_C, \tag{2.50}$$

where V denotes the volume of the body. By using this equation and the Steiner's parallel axis theorem, the moment of inertia tensor $\boldsymbol{J}$ is given by:

$$\begin{aligned} \boldsymbol{J} &= \int \left(\boldsymbol{S}({}^{\mathscr{C}}\boldsymbol{p})' \boldsymbol{S}({}^{\mathscr{C}}\boldsymbol{p}) + \boldsymbol{S}(\boldsymbol{r})' \boldsymbol{S}(\boldsymbol{r}) \right) dm \\ &= \int_V \left(\boldsymbol{S}({}^{\mathscr{C}}\boldsymbol{p})' \boldsymbol{S}({}^{\mathscr{C}}\boldsymbol{p}) + \boldsymbol{S}(\boldsymbol{r})' \boldsymbol{S}(\boldsymbol{r}) \right) dx_C \, dy_C \, dz_C \\ &= \boldsymbol{I} + m \boldsymbol{S}(\boldsymbol{r})' \boldsymbol{S}(\boldsymbol{r}), \end{aligned} \tag{2.51}$$

where:

$$\boldsymbol{I} = \begin{bmatrix} I_{xx} & I_{xy} & I_{xz} \\ I_{xy} & I_{yy} & I_{yz} \\ I_{xz} & I_{yz} & I_{zz} \end{bmatrix} = \int_V \begin{bmatrix} z_C^2 + y_C^2 & -x_C y_C & -x_C z_C \\ -x_C y_C & x_C^2 + z_C^2 & -z_C y_C \\ -x_C z_C & -z_C y_C & x_C^2 + y_C^2 \end{bmatrix} dx_C \, dy_C \, dz_C, \tag{2.52}$$

and

$$m \boldsymbol{S}(\boldsymbol{r})' \boldsymbol{S}(\boldsymbol{r}) = m \begin{bmatrix} r_z^2 + r_y^2 & -r_x r_y & -r_x r_z \\ -r_x r_y & r_x^2 + r_z^2 & -r_z r_y \\ -r_x r_z & -r_z r_y & r_x^2 + r_y^2 \end{bmatrix}. \tag{2.53}$$

To complete the Lagrangian, the potential energy term must be computed. In the case of the helicopter, the source of potential energy is the gravity. The potential energy of the helicopter can be computed by assuming the equation of the rigid motion (2.10) and is given by:

$$\begin{aligned} \mathscr{U} &= \int \boldsymbol{g}'^{\mathscr{I}} \boldsymbol{p} dm \\ &= m\boldsymbol{g}'^{\mathscr{I}} \boldsymbol{p}, \end{aligned} \tag{2.54}$$

where $\boldsymbol{g}$ is the vector of the direction of gravity expressed in the inertial frame, which in this case $\boldsymbol{g} = [0 \quad 0 \quad -g]'$. Thereby, the potential energy takes the following form:

$$\mathscr{U} = mg\left(-r_x \sin\theta + r_y \cos\theta \sin\phi + r_z \cos\theta \cos\phi + z\right). \tag{2.55}$$

Once, the kinetic and potential energy of the *QuadRotor* helicopter have been computed (see (2.48) and (2.55)), the Lagrangian (2.31) of the system can be written as follows:

$$\begin{aligned} \mathscr{L}(\boldsymbol{q}, \dot{\boldsymbol{q}}) &= \mathscr{K}(\boldsymbol{q}, \dot{\boldsymbol{q}}) - \mathscr{U}(\boldsymbol{q}) \\ &= \tfrac{1}{2}\dot{\boldsymbol{q}}' \boldsymbol{M}(\boldsymbol{q}) \dot{\boldsymbol{q}} - m\boldsymbol{g}'^{\mathscr{I}} \boldsymbol{p}. \end{aligned} \tag{2.56}$$

By solving the derivatives required by the Euler-Lagrange equations (2.35), the equations of motion, expressed in the form of the equation (2.40)[3], results in:

$$\boldsymbol{M}(\boldsymbol{q})\ddot{\boldsymbol{q}} + \boldsymbol{C}(\boldsymbol{q}, \dot{\boldsymbol{q}})\dot{\boldsymbol{q}} + \boldsymbol{G}(\boldsymbol{q}) = \boldsymbol{B}(\boldsymbol{q})\boldsymbol{\Gamma} + \boldsymbol{\delta}(\boldsymbol{q}, \dot{\boldsymbol{q}}, \ddot{\boldsymbol{q}}, \boldsymbol{\Gamma}_d)$$

$$\begin{bmatrix} m\mathbb{1}_{3\times 3} & -m\boldsymbol{R}_{\mathscr{I}}\boldsymbol{S}(\boldsymbol{r})\boldsymbol{W}_{\eta} \\ -m\boldsymbol{W}'_{\eta}\boldsymbol{S}(\boldsymbol{r})'\boldsymbol{R}_{\mathscr{I}}{}' & \mathscr{J}(\boldsymbol{\eta}) \end{bmatrix} \cdot \begin{bmatrix} \ddot{\boldsymbol{\xi}} \\ \ddot{\boldsymbol{\eta}} \end{bmatrix} + \begin{bmatrix} \boldsymbol{C}_{\xi\xi}(\boldsymbol{q}, \dot{\boldsymbol{q}}) & \boldsymbol{C}_{\xi\eta}(\boldsymbol{q}, \dot{\boldsymbol{q}}) \\ \boldsymbol{C}_{\eta\xi}(\boldsymbol{q}, \dot{\boldsymbol{q}}) & \boldsymbol{C}_{\eta\eta}(\boldsymbol{q}, \dot{\boldsymbol{q}}) \end{bmatrix} \cdot \begin{bmatrix} \dot{\boldsymbol{\xi}} \\ \dot{\boldsymbol{\eta}} \end{bmatrix}$$

$$+ \begin{bmatrix} \boldsymbol{G}_{\xi}(\boldsymbol{q}) \\ \boldsymbol{G}_{\eta}(\boldsymbol{q}) \end{bmatrix} = \begin{bmatrix} \boldsymbol{B}_{\xi}(\boldsymbol{q}) \\ \boldsymbol{B}_{\eta}(\boldsymbol{q}) \end{bmatrix} \cdot \begin{bmatrix} T \\ \boldsymbol{\tau}_{\eta_a} \end{bmatrix} + \begin{bmatrix} \boldsymbol{\delta}_{\xi}(\boldsymbol{q}, \dot{\boldsymbol{q}}, \ddot{\boldsymbol{q}}, f_{\xi_d}) \\ \boldsymbol{\delta}_{\eta}(\boldsymbol{q}, \dot{\boldsymbol{q}}, \ddot{\boldsymbol{q}}, \boldsymbol{\tau}_{\eta_d}) \end{bmatrix}. \tag{2.57}$$

where the elements of the Coriolis and centrifugal matrix can be computed by the Christoffel symbols using the equation (2.38). The gravitational vector has the

[3] For the sake of notation simplicity, the matrices and vectors of the nominal system will be presented without the argument $\hat{\cdot}$. Throughout the thesis, where necessary to make distinction with regard to this simplification, it will be observed.

following form:

$$\boldsymbol{G}(\boldsymbol{q}) = \begin{bmatrix} 0 \\ 0 \\ mg \\ -mg(-r_y \cos\theta\cos\phi + r_z \cos\theta \sin\phi) \\ -mg(r_x \cos\theta + r_y \sin\theta\sin\phi + r_z \sin\theta\cos\phi) \\ 0 \end{bmatrix}, \tag{2.58}$$

while the force matrix is given by:

$$\boldsymbol{B}(\boldsymbol{q}) = \begin{bmatrix} \boldsymbol{B}_{\boldsymbol{\xi}}(\boldsymbol{q}) \\ \cdots \\ \boldsymbol{B}_{\boldsymbol{\eta}}(\boldsymbol{q}) \end{bmatrix} = \begin{bmatrix} \boldsymbol{R}_{\mathscr{I}_{\boldsymbol{e_3}}} & \mathbb{O}_{3\times 3} \\ \cdots\cdots & \\ \mathbb{O}_{3\times 1} & \mathbb{1}_{3\times 3} \end{bmatrix}. \tag{2.59}$$

In summary, the equations of motion obtained in this section provide a strongly coupled dynamic model. This model will be used to emulate a real *QuadRotor* helicopter. In the following section this dynamic model is simplified and a decentralized model is achieved.

2.5.1 Simplified Equations of Motion of the Helicopter

In this section, the center of mass and the origin of the rotation body-fixed frame $\mathscr{B}$ are assumed congruent, which results in the vector $\boldsymbol{r} = 0$.

Consequently, the kinetic energy terms combining $\dot{\boldsymbol{\xi}}$ and $\dot{\boldsymbol{\eta}}$ in the the Lagrangian (2.56) disappear and, thus, the Euler-Lagrange equations can be divided into two interconnected dynamics, the translational and rotational subsystems. These simplified equations of motion compose a decentralized dynamic model, as it can be seen in Fig. 2.3.

Under this assumption, the equations of motion (2.57) can be rewritten as follows:

$$\begin{bmatrix} m\mathbb{1}_{3\times 3} & \mathbb{O}_{3\times 3} \\ \mathbb{O}_{3\times 3} & \mathscr{J}(\boldsymbol{\eta}) \end{bmatrix} \cdot \begin{bmatrix} \ddot{\boldsymbol{\xi}} \\ \ddot{\boldsymbol{\eta}} \end{bmatrix} + \begin{bmatrix} \mathbb{O}_{3\times 3} & \mathbb{O}_{3\times 3} \\ \mathbb{O}_{3\times 3} & \boldsymbol{C}_{\boldsymbol{\eta}\boldsymbol{\eta}}(\boldsymbol{q}, \dot{\boldsymbol{q}}) \end{bmatrix} \cdot \begin{bmatrix} \dot{\boldsymbol{\xi}} \\ \dot{\boldsymbol{\eta}} \end{bmatrix} + \begin{bmatrix} mg\boldsymbol{e_3} \\ \mathbb{O}_{3\times 3} \end{bmatrix}$$

$$= \begin{bmatrix} \boldsymbol{B}_{\boldsymbol{\xi}}(\boldsymbol{q}) \\ \boldsymbol{B}_{\boldsymbol{\eta}}(\boldsymbol{q}) \end{bmatrix} \cdot \begin{bmatrix} T \\ \boldsymbol{\tau}_{\boldsymbol{\eta}_a} \end{bmatrix} + \begin{bmatrix} \boldsymbol{\delta}_{\boldsymbol{\xi}}(\boldsymbol{q}, \dot{\boldsymbol{q}}, \ddot{\boldsymbol{q}}, \boldsymbol{f}_{\boldsymbol{\xi}_d}) \\ \boldsymbol{\delta}_{\boldsymbol{\eta}}(\boldsymbol{q}, \dot{\boldsymbol{q}}, \ddot{\boldsymbol{q}}, \boldsymbol{\tau}_{\boldsymbol{\eta}_d}) \end{bmatrix}, \tag{2.60}$$

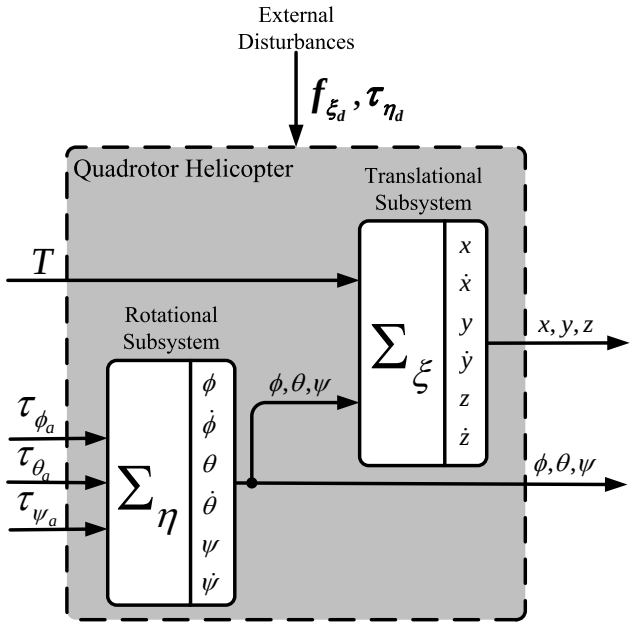

Figure 2.3: Dynamic system divided into two interconnected subsystems.

where, in this model, the inertia matrix of the rotational subsystem is given by $\mathscr{J}(\boldsymbol{\eta}) = \boldsymbol{W}_{\boldsymbol{\eta}}' \boldsymbol{I} \boldsymbol{W}_{\boldsymbol{\eta}}$. From now on, the Coriolis and centrifugal matrix of the rotational subsystem is defined by $\boldsymbol{C}_{\boldsymbol{\eta}\boldsymbol{\eta}}(\boldsymbol{q}, \dot{\boldsymbol{q}}) = \boldsymbol{C}(\boldsymbol{\eta}, \dot{\boldsymbol{\eta}})$.

The *translational movement* can be expressed by means of the state vector $\boldsymbol{\xi}$ by the following equations:

$$\begin{cases} \ddot{x} = \dfrac{1}{m}\left(\cos\psi \sin\theta \cos\phi + \sin\psi \sin\phi\right) T + \dfrac{\delta_{\xi_x}}{m} \\ \ddot{y} = \dfrac{1}{m}\left(\sin\psi \sin\theta \cos\phi - \cos\psi \sin\phi\right) T + \dfrac{\delta_{\xi_y}}{m} \\ \ddot{z} = -g + \dfrac{1}{m}\left(\cos\theta \cos\phi\right) T + \dfrac{\delta_{\xi_z}}{m} \end{cases} \tag{2.61}$$

The simplified rotational equations of motion in terms of $\boldsymbol{\eta}$ can be written as follows:

$$\mathscr{J}(\boldsymbol{\eta})\ddot{\boldsymbol{\eta}} + \boldsymbol{C}(\boldsymbol{\eta}, \dot{\boldsymbol{\eta}})\dot{\boldsymbol{\eta}} = \boldsymbol{\tau}_{\boldsymbol{\eta}}, \tag{2.62}$$

where:

$$\mathscr{J}(\boldsymbol{\eta}) = \begin{bmatrix} I_{xx} & 0 & -I_{xx}S\theta \\ 0 & I_{yy}C^2\phi + I_{zz}S^2\phi & (I_{yy} - I_{zz})\,C\phi S\phi C\theta \\ -I_{xx}S\theta & (I_{yy} - I_{zz})\,C\phi S\phi C\theta & I_{xx}S^2\theta + I_{yy}S^2\phi C^2\theta + I_{zz}C^2\phi C^2\theta \end{bmatrix}, \tag{2.63}$$

and

$$\boldsymbol{C}(\boldsymbol{\eta}, \dot{\boldsymbol{\eta}}) = \begin{bmatrix} c_{11} & c_{12} & c_{13} \\ c_{21} & c_{22} & c_{23} \\ c_{31} & c_{32} & c_{33} \end{bmatrix},$$

with:

$$\begin{aligned}
c_{11} &= 0 \\
c_{12} &= (I_{yy} - I_{zz})\left(\dot{\theta}C\phi S\phi + \tfrac{1}{2}\dot{\psi}S^2\phi C\theta\right) + \tfrac{1}{2}(I_{zz} - I_{yy})\,\dot{\psi}C^2\phi C\theta - \tfrac{1}{2}I_{xx}\dot{\psi}C\theta \\
c_{13} &= (I_{zz} - I_{yy})\,(\dot{\psi}C\phi S\phi C^2\theta + \tfrac{1}{2}\dot{\theta}C\theta C^2\phi) + \tfrac{1}{2}(I_{yy} - I_{zz})\,\dot{\theta}C\theta S^2\phi - \tfrac{1}{2}I_{xx}\dot{\theta}C\theta \\
c_{21} &= (I_{zz} - I_{yy})\left(\dot{\theta}C\phi S\phi + \tfrac{1}{2}\dot{\psi}S^2\phi C\theta\right) + \tfrac{1}{2}(I_{yy} - I_{zz})\,\dot{\psi}C^2\phi C\theta + \tfrac{1}{2}I_{xx}\dot{\psi}C\theta \\
c_{22} &= (I_{zz} - I_{yy})\,\dot{\phi}C\phi S\phi \\
c_{23} &= -I_{xx}\dot{\psi}S\theta C\theta + I_{yy}\dot{\psi}S^2\phi C\theta S\theta + I_{zz}\dot{\psi}C^2\phi S\theta C\theta + \tfrac{1}{2}(I_{yy} - I_{zz})\dot{\phi}C\theta C^2\phi \\
&\quad + \tfrac{1}{2}(I_{zz} - I_{yy})\dot{\phi}C\theta S^2\phi + \tfrac{1}{2}I_{xx}\dot{\phi}C\theta \\
c_{31} &= (I_{yy} - I_{zz})\,(\dot{\psi}C^2\theta S\phi C\phi + \tfrac{1}{2}\dot{\theta}C\theta C^2\phi) + \tfrac{1}{2}(I_{zz} - I_{yy})\,\dot{\theta}C\theta S^2\phi - \tfrac{1}{2}I_{xx}\dot{\theta}C\theta \\
c_{32} &= (I_{zz} - I_{yy})\left(\dot{\theta}C\phi S\phi S\theta + \tfrac{1}{2}\dot{\phi}S^2\phi C\theta\right) + \tfrac{1}{2}(I_{yy} - I_{zz})\,\dot{\phi}C^2\phi C\theta - \tfrac{1}{2}I_{xx}\dot{\phi}C\theta \\
&\quad + I_{xx}\dot{\psi}S\theta C\theta - I_{yy}\dot{\psi}S^2\phi S\theta C\theta - I_{zz}\dot{\psi}C^2\phi S\theta C\theta \\
c_{33} &= (I_{yy} - I_{zz})\,\dot{\phi}C\phi S\phi C^2\theta - I_{yy}\dot{\theta}S^2\phi C\theta S\theta - I_{zz}\dot{\theta}C^2\phi C\theta S\theta \\
&\quad + I_{xx}\dot{\theta}C\theta S\theta\,.
\end{aligned}$$

Therefore, the simplified mathematical model that describes the helicopter

rotational movement obtained from the Euler-Lagrange formalism is given by:

$$\ddot{\boldsymbol{\eta}} = \mathscr{J}(\boldsymbol{\eta})^{-1}\left(\boldsymbol{\tau}_{\boldsymbol{\eta}} - \boldsymbol{C}(\boldsymbol{\eta},\dot{\boldsymbol{\eta}})\dot{\boldsymbol{\eta}}\right). \tag{2.64}$$

These two interconnected subsystems will be used to design all control strategies presented in the thesis.

2.6 Helicopter Model via Newton-Euler Formulation

In this section the equations of motion of the *QuadRotor* helicopter are obtained via Newton-Euler formulation. This model is presented just as an alternative approach. Besides, this approach provides a clear understanding of the forces and torques applied to the vehicle, and from this a relationship between these forces and torques and the generalized forces and torques obtained from the Euler-Lagrange dynamic model are obtained. The basis theory of this formulation is omitted. For more details see the references therein the thesis.

The dynamic equations of a rigid body subject to external forces applied to the center of mass and expressed in the body-fixed frame can be obtained through the Newton-Euler approach using the relations (2.22) and (2.30) as follows:

$$\begin{bmatrix} m\mathbb{1}_{3\times3} & \mathbb{0}_{3\times3} \\ \mathbb{0}_{3\times3} & \boldsymbol{J} \end{bmatrix} \begin{bmatrix} \dot{\boldsymbol{v}}_{\mathscr{B}} \\ \dot{\boldsymbol{\omega}} \end{bmatrix} + \begin{bmatrix} \boldsymbol{\omega} \times m\boldsymbol{v}_{\mathscr{B}} \\ \boldsymbol{\omega} \times \boldsymbol{J}\boldsymbol{\omega} \end{bmatrix} = \begin{bmatrix} \boldsymbol{f}_{\mathscr{B}} \\ \boldsymbol{\tau}_{\mathscr{B}} \end{bmatrix}, \tag{2.65}$$

where $\boldsymbol{J} \in \Re^{3\times3}$ is the moment of inertia tensor obtained by equation (2.51), $\mathbb{1}_{3\times3} \in \Re^{3\times3}$ and $\mathbb{0}_{3\times3} \in \Re^{3\times3}$ are the identity and zeros matrices, respectively. $\boldsymbol{v}_{\mathscr{B}}$ is the linear velocity vector and $\boldsymbol{\omega}$ is the angular rate, both expressed in $\mathscr{B}$.

Considering the state vector $\begin{bmatrix} \boldsymbol{\xi} & \boldsymbol{v}_{\mathscr{I}} & \boldsymbol{\eta} & \boldsymbol{\omega} \end{bmatrix}'$, the helicopter dynamic model, assuming the center of mass at the origin of the frame $\mathscr{C}$, can be rewritten by:

$$\begin{cases} \dot{\boldsymbol{\xi}} = \boldsymbol{v}_{\mathscr{I}} - \boldsymbol{R}_{\mathscr{I}}\boldsymbol{\omega} \times \boldsymbol{r} \\ m\dot{\boldsymbol{v}}_{\mathscr{I}} = \boldsymbol{R}_{\mathscr{I}}\boldsymbol{f}_{\mathscr{B}} \\ \dot{\boldsymbol{R}}_{\mathscr{I}} = \boldsymbol{R}_{\mathscr{I}}\boldsymbol{S}(\boldsymbol{\omega}) \\ \boldsymbol{J}\dot{\boldsymbol{\omega}} = -\boldsymbol{\omega} \times \boldsymbol{J}\boldsymbol{\omega} + \boldsymbol{\tau}_{\mathscr{B}} \end{cases} \tag{2.66}$$

where the time derivative of the linear velocity $\boldsymbol{v}_{\mathscr{I}}$ (see equation (2.29)) with the center of mass at the origin of frame $\mathscr{C}$ (i.e. ${}^{\mathscr{C}}\boldsymbol{p} = 0$) is given by:

$$\dot{\boldsymbol{v}}_{\mathscr{I}} = \boldsymbol{R}_{\mathscr{I}}\boldsymbol{\omega} \times (\boldsymbol{\omega} \times \boldsymbol{r}) + \boldsymbol{R}_{\mathscr{I}}\dot{\boldsymbol{\omega}} \times \boldsymbol{r} + \ddot{\boldsymbol{\xi}}. \tag{2.67}$$

The forces and torques in which the helicopter is subject, $\boldsymbol{f}_{\mathscr{B}} \in \mathscr{B}$ and $\boldsymbol{\tau}_{\mathscr{B}} \in \mathscr{B}$, consist of: its weight, the aerodynamic force and moment vectors, the gyroscopic effects caused by the rotors, the applied thrust, and the torques generated by the four propellers. These forces and torques can be expressed by the following form:

$$\begin{cases} \boldsymbol{R}_{\mathscr{I}} \boldsymbol{f}_{\mathscr{B}} = -mg\boldsymbol{e}_3 + \boldsymbol{R}_{\mathscr{I}_{e_3}} T + \boldsymbol{f}_{\xi_d} \\ \boldsymbol{\tau}_{\mathscr{B}} = \boldsymbol{\tau}_a + \boldsymbol{a}_r + \boldsymbol{\tau}_G - \boldsymbol{r} \times (\widehat{\boldsymbol{f}} + \boldsymbol{R}_{\mathscr{I}}{}' \boldsymbol{f}_{\xi_d}) \end{cases} \tag{2.68}$$

where $\boldsymbol{\tau}_a$ is the applied torque vector defined by equation (2.2), $\boldsymbol{\tau}_G$ is the gyroscopic effect vector given by (2.6), and $\boldsymbol{a}_r = [a_p \quad a_q \quad a_r]'$ is the aerodynamic moment vector expressed in the body-fixed frame. Given that the aerodynamic moments and the gyroscopic effects are assumed to be external disturbances, they are considered as the vector $\boldsymbol{\tau}_d = \boldsymbol{a}_r + \boldsymbol{\tau}_G$. In this model, the parametric uncertainties are omitted.

By substituting the equations of forces and torques (2.68) into the dynamic model (2.66), these equations can be rewritten as follows:

$$\begin{cases} \dot{\boldsymbol{\xi}} = \boldsymbol{v}_{\mathscr{I}} - \boldsymbol{R}_{\mathscr{I}} \boldsymbol{\omega} \times \boldsymbol{r} \\ m\dot{\boldsymbol{v}}_{\mathscr{I}} = -mg\boldsymbol{e}_3 + \boldsymbol{R}_{\mathscr{I}_{e_3}} T + \boldsymbol{f}_{\xi_d} \\ \dot{\boldsymbol{R}}_{\mathscr{I}} = \boldsymbol{R}_{\mathscr{I}} \boldsymbol{S}(\boldsymbol{\omega}) \\ \boldsymbol{J}\dot{\boldsymbol{\omega}} = -\boldsymbol{\omega} \times \boldsymbol{J}\boldsymbol{\omega} + \boldsymbol{\tau}_a + \boldsymbol{\tau}_d - \boldsymbol{r} \times (\widehat{\boldsymbol{f}} + \boldsymbol{R}_{\mathscr{I}}{}' \boldsymbol{f}_{\xi_d}) \end{cases} \tag{2.69}$$

By replacing the linear acceleration (2.67) into the helicopter model (2.69), and after some algebraic manipulations, the following Newton-Euler equations of motion are obtained:

$$\begin{cases} \boldsymbol{R}_{\mathscr{I}_{e_3}} T + \boldsymbol{f}_{\xi_d} &= m\ddot{\boldsymbol{\xi}} - m\boldsymbol{R}_{\mathscr{I}} \boldsymbol{r} \times \dot{\boldsymbol{\omega}} - m\boldsymbol{R}_{\mathscr{I}} \boldsymbol{\omega} \times (\boldsymbol{r} \times \boldsymbol{\omega}) + mg\boldsymbol{e}_3 \\ \boldsymbol{\tau}_a + \boldsymbol{\tau}_d &= \boldsymbol{J}\dot{\boldsymbol{\omega}} - m\boldsymbol{r} \times (\boldsymbol{r} \times \dot{\boldsymbol{\omega}}) + m\boldsymbol{r} \times \boldsymbol{R}_{\mathscr{I}}{}' \ddot{\boldsymbol{\xi}} + \boldsymbol{\omega} \times \boldsymbol{J}\boldsymbol{\omega} \\ &\quad - m\boldsymbol{r} \times (\boldsymbol{\omega} \times (\boldsymbol{r} \times \boldsymbol{\omega})) + mg\boldsymbol{r} \times \boldsymbol{R}_{\mathscr{I}}{}' \boldsymbol{e}_3 \end{cases} \tag{2.70}$$

To obtain the Newton-Euler model (2.70) using the Euler angle parameterization and, consequently, expressed by the generalized coordinates $\boldsymbol{q} = [\boldsymbol{\xi}' \quad \boldsymbol{\eta}']'$, the equation (2.25) and its time derivative must be used together with the relation $\boldsymbol{\omega}\times = \boldsymbol{S}(\boldsymbol{\omega}) = \boldsymbol{R}_{\mathscr{I}}{}' \dot{\boldsymbol{R}}_{\mathscr{I}}$. These equations are obtained in an elementary way and by direct substitution. Thus, in this thesis it will not be developed. At the same time, it is interesting to mention here the relationship between the torques expressed in the body-fixed frame and in the inertial reference frame, that is:

$$\boldsymbol{\tau}_{\eta} = \boldsymbol{W}_{\eta}{}' \boldsymbol{\tau}_{\mathscr{B}}, \tag{2.71}$$

which leads to:

$$\begin{aligned} \boldsymbol{\tau}_{\eta_a} &= \boldsymbol{W}_{\eta}{}'\boldsymbol{\tau}_{\boldsymbol{a}}, \\ \boldsymbol{\tau}_{\eta_d} &= \boldsymbol{W}_{\eta}{}'\boldsymbol{\tau}_{\boldsymbol{d}}, \end{aligned}$$

As in the case of the helicopter model via Euler-Lagrange formulation, in this section the simplified model is also obtained. Considering the frames $\mathscr{C}$ and $\mathscr{B}$ congruent, the vector $\boldsymbol{r}$ is null, and, therefore, the equations (2.69) are rewritten as follows:

$$\begin{cases} \dot{\boldsymbol{\xi}} = \boldsymbol{v}_{\mathscr{I}} \\ m\dot{\boldsymbol{v}}_{\mathscr{I}} = -mg\boldsymbol{e}_3 + \boldsymbol{R}_{\mathscr{I}_{e_3}} T + \boldsymbol{f}_{\xi_d} \\ \dot{\boldsymbol{R}}_{\mathscr{I}} = \boldsymbol{R}_{\mathscr{I}} \boldsymbol{S}(\boldsymbol{\omega}) \\ \boldsymbol{I}\dot{\boldsymbol{\omega}} = -\boldsymbol{\omega} \times \boldsymbol{I}\boldsymbol{\omega} + \boldsymbol{\tau}_{\boldsymbol{a}} + \boldsymbol{\tau}_{\boldsymbol{d}} \end{cases} \tag{2.72}$$

By defining the following state vector:

$$\boldsymbol{\zeta} = [x \quad y \quad z \quad u_0 \quad v_0 \quad w_0 \quad \phi \quad \theta \quad \psi \quad p \quad q \quad r]^T, \tag{2.73}$$

the simplified model of the helicopter (2.72) can be presented in a state space form:

$$\dot{\boldsymbol{\zeta}} = \begin{cases} \dot{x} &= u_0 \\ \dot{y} &= v_0 \\ \dot{z} &= w_0 \\ \dot{u}_0 &= \frac{1}{m}(\cos\psi\sin\theta\cos\phi + \sin\psi\sin\phi)\cdot T + \frac{a_x}{m} \\ \dot{v}_0 &= \frac{1}{m}(\sin\psi\sin\theta\cos\phi - \cos\psi\sin\phi)\cdot T + \frac{a_y}{m} \\ \dot{w}_0 &= -g + \frac{1}{m}(\cos\theta\cos\phi)\cdot T + \frac{a_z}{m} \\ \dot{\phi} &= p + q\sin\phi\tan\theta + r\cos\phi\tan\theta \\ \dot{\theta} &= q\cos\phi - r\sin\phi \\ \dot{\psi} &= q\sin\phi\sec\theta + r\cos\phi\sec\theta \\ \dot{p} &= \frac{(I_{yy} - I_{zz})}{I_{xx}} qr + \frac{\tau_{a_p}}{I_{xx}} + \frac{\tau_{d_p}}{I_{xx}} \\ \dot{q} &= \frac{(I_{zz} - I_{xx})}{I_{yy}} pr + \frac{\tau_{a_q}}{I_{yy}} + \frac{\tau_{d_q}}{I_{yy}} \\ \dot{r} &= \frac{(I_{xx} - I_{yy})}{I_{zz}} pq + \frac{\tau_{a_r}}{I_{zz}} + \frac{\tau_{d_r}}{I_{zz}} \end{cases} \tag{2.74}$$

The equations of motion of the *QuadRotor* helicopter obtained via Newton-Euler procedure are not used to design the controllers in this thesis. However, many researchers make use of this approach, and some of their controllers used for results comparison have been designed by means of this model.

2.7 System Design Parameters

This section presents the parameters of a *QuadRotor* helicopter that is being designed in the Automation, Control and Robotic Group, Department of Systems Engineering and Automation at the University of Seville.

The design of the *QuadRotor* helicopter structure is based on the illustration presented in Fig. 2.1. The vehicle will be constituted of four brushless motors AXI 2217/16 Gold Line, which are able to provide a maximum thrust of 12.2 N per each motor-propeller group, assuming blades with dimension of $10'' \times 5''$. An Inertial Measurement Unit (IMU) MTi-G from Xsens will be used to measure the linear accelerations, Euler angles and angular rates. An infrared sensor is considered to estimate the altitude, while to obtain the translational displacement, an on-board visual sensor is being implemented. These data will be treated in an embedded computer based on the PC-104 platform, which will be in charge of guiding the vehicle autonomously.

By previous analysis, some values of the model parameters have already been estimated, whose will be used to carry out all the simulation results in this thesis, and are shown in Table 2.1.

2.8 Conclusions

In this chapter the modeling of the *QuadRotor* helicopter has been presented. The models developed here have been obtained taking into account the control design purposes.

A more realistic modeling has been performed considering the center of mass displaced of the helicopter center of rotation, which generates coupling between the translational and rotational movements. From this coupled model, a simplified and decentralized model has been obtained, which will be used to design the control strategies presented in this work.

The equations of motion have been computed through two approaches, the Euler-Lagrange and the Newton-Euler formulations, allowing a wide range of control structures to be chosen.

Table 2.1: *QuadRotor* helicopter model parameters.

Parameter Description	**Parameter**	**Value**
Mass of the *QuadRotor* helicopter	m	$2.24\ kg$
Distance between the mass center and the rotors	l	$0.332\ m$
Thrust coefficient of the rotors	b	$9.5e-6\ Ns^2$
Drag coefficient of the rotors	k_τ	$1.7e-7\ Nms^2$
Gravitational acceleration	g	$9.81\ m/s^2$
Moment of inertia around the x-axis	I_{xx}	$0.0363\ Kg.m^2$
Moment of inertia around the y-axis	I_{yy}	$0.0363\ Kg.m^2$
Moment of inertia around the z-axis	I_{zz}	$0.0615\ Kg.m^2$
Position of the center of mass in x from the body-fixed frame	r_x	$-0.00069\ m$
Position of the center of mass in y from the body-fixed frame	r_y	$-0.0014\ m$
Position of the center of mass in z from the body-fixed frame	r_z	$-0.0311\ m$

CHAPTER 3

Cascade Control Strategies

Contents

3.1 Introduction

This chapter deals with cascade control strategies to solve the path tracking problem for the *QuadRotor* helicopter. By combining specific control techniques, the continuous performance improvement of the whole closed-loop system is obtained. The development of this chapter is based on previous published works: in Raffo et al. (2008a) a control law based on a standard backstepping approach for translational movements and a fully actuated nonlinear $\mathscr{H}_\infty$ controller to stabilize the helicopter were combined to perform path tracking in the presence of aerodynamic moment disturbances and parametric uncertainties; in Raffo et al. (2008b) the same nonlinear $\mathscr{H}_\infty$ controller presented in Raffo et al. (2008a) was used to stabilize the UAV, while a predictive controller was employed to control

the translational motion and to provide a smooth path tracking through its predictive features. However, both these strategies are only able to reject sustained disturbances applied to the rotational motion.

Therefore, the main objective is to design controllers that provide certain required performances during the *QuadRotor* flight, as null tracking error and robustness in presence of sustained external disturbances affecting the six degrees of freedom, parametric uncertainties and unmodeled dynamics. The proposed control strategies are based on the simplified equations of motion (2.60), which are represented by the decentralized structure of the *QuadRotor* helicopter in Fig. 2.3. On one hand, translational controllers are obtained based on the translational movement given by equations (2.61), while, on the other hand, rotational controllers are computed based on the rotational equations of motion (2.62). The overall scheme of the control strategies is depicted in Fig. 3.1.

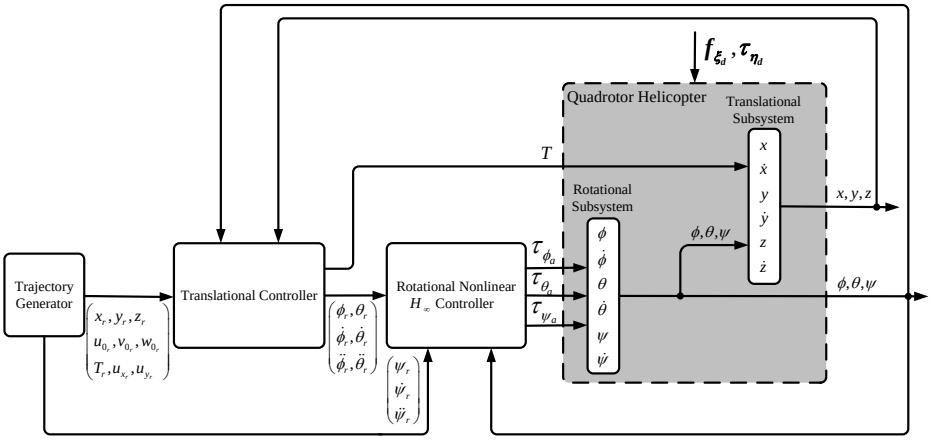

Figure 3.1: The decentralized structure of the *QuadRotor* helicopter.

Firstly, the reference trajectory for the translational movements is provided off-line by the *Trajectory Generator* block. The computation of this trajectory is based on a virtual reference vehicle whose model is the same as the *QuadRotor* simplified one for the translational motion. Thereby, starting from a desired route for the translational movements, x_r, y_r, and z_r, and their derivatives, the reference control inputs T_r, u_{x_r} and u_{y_r}, are computed. The reference yaw angle is defined separately. This trajectory is generated under the following assumptions: there are no external disturbances acting on the virtual vehicle; and the attitude of the virtual vehicle is assumed stabilized.

For the inner-loop control, a nonlinear $\mathscr{H}_\infty$ controller for the rotational subsystem is used to perform the *QuadRotor* helicopter stabilization. The angular position and velocity are controlled in this loop, being the torques applied on the three axis, $\boldsymbol{\tau_{\eta_a}} = [\tau_{\phi_a}\ \tau_{\theta_a}\ \tau_{\psi_a}]'$, the manipulated variables. To obtain null steady-state error in presence of sustained external disturbances, the integral of the angular position error is considered. Due to the cascade structure of this strategy and taking into account the closed-loop performance achieved by the nonlinear $\mathscr{H}_\infty$ inner-loop controller, the Euler angles can be considered as time-varying parameters on the design of the translational controllers.

To design the controllers for the outer loop, i.e. for the translational movement, three control methodologies are proposed: linear $\mathscr{H}_\infty$ control, model predictive control, and backstepping approach. The translational motion control is performed in two stages. In the first one, the helicopter height, z, is controlled and the total thrust, T, is the manipulated signal. In the second stage, the reference of pitch and roll angles (θ_r and ϕ_r, respectively) are generated through two virtual inputs, computed to follow the desired xy movement. In this step, the control variable T is used as a time-varying parameter.

The first technique discussed to design the outer-loop controller is a linear state feedback $\mathscr{H}_\infty$ controller based on the error model, in which the integral of the translational position error into the state vector is included. The aim of combining this technique with the nonlinear $\mathscr{H}_\infty$ inner-loop controller is to guarantee robustness of the whole system in presence of sustained disturbances acting on the six degrees of freedom of the *QuadRotor* helicopter, and uncertainty parameters. To design the linear $\mathscr{H}_\infty$ controller, a synthesis methods via LMIs (Linear Matrix Inequalities) is used. This control strategy was presented in Raffo et al. (2008c).

As a second outer-loop control, a model-based predictive controller (MPC) is proposed to control the *QuadRotor* translational movements, using the references provided by the trajectory generator. The main idea is to combine the advantages of the predictive control methodology to follow a predefined trajectory in a smooth way, with the capacity of the nonlinear $\mathscr{H}_\infty$ theory to cope with unknown disturbances. To carry out these objectives, a state-space predictive controller with integral action based on the time variant error model is used to track the reference trajectory, which is an improvement of the controller presented in Raffo et al. (2009a). The integral action is also considered on the position error into the state vector in order to achieve null steady-state error when sustained disturbances are acting on xyz-motions. This control structure was published in Raffo et al. (2010c).

Lastly, an integral backstepping approach is used to design the *QuadRotor* translational motion controller, which, combined with the nonlinear $\mathscr{H}_\infty$ inner-loop controller, are performed to reach a robust flight of the *QuadRotor* helicopter in presence of unmodeled dynamics, parametric uncertainties and sustained disturbances on the six degrees of freedom. This control structure provides an enlarged workspace of the translational movement when compared with other strategies proposed in this chapter. In the translational controller design, the integral backstepping procedure is performed considering the integral term in its second step. This controller guarantees stability and convergence of the tracking error for a generic plant when a maintained disturbance affects the system and the reference signal is time-varying. This cascade control strategy was presented in Raffo et al. (2010d).

The development of these controllers is analyzed in the following sections.

3.2 Simulation Protocol

This section presents the procedure used to carry out the simulation results of the proposed control strategies throughout the thesis. It is described at this point of the manuscript in order to elaborate a simulation protocol that provides the same test conditions for the controllers, allowing comparisons between them.

The proposed control strategies will be tested by simulation in order to corroborate the effectiveness to solve the path tracking problem when sustained disturbances affect the whole system. The performance obtained by the control strategies will be checked considering the more accurate model (2.57) as well as saturated control inputs, which emulates a real *QuadRotor* helicopter. As presented in Chapter 2, this model considers that the axes of rotation of the body-fixed frame are parallel to the axes passing through the center of mass, and its origin is displaced by a position $\boldsymbol{r}$ to the center of mass, resulting in crossed inertia terms in the moment of inertia tensor. Moreover, this assumption results in a strongly-coupled dynamic model, with crossed terms in the inertia matrix and in the Coriolis and centrifugal matrix between $\boldsymbol{\xi}$ and $\boldsymbol{\eta}$, and in the gravitational force vector. Taking into account that the simplified model derived in Section 2.5.1 will be used just for control synthesis purposes, structural uncertainties are present because that model considers a moment of inertia tensor with only diagonal inertia terms.

In addition, an amount of $\pm 40\%$ in the uncertainty of the elements of the moment of inertia tensor and the mass will also be considered to test the robustness

provided by the control strategies with respect to parametric uncertainty. Finally, sustained disturbances affecting all the degrees of freedom will be applied in different instants of time to check the disturbance rejection capability of the proposed controllers. The values of the nominal model parameters used for simulations are the same shown in Table 2.1.

Furthermore, simulations comparing the control structures developed in this chapter with the one of Bouabdallah and Siegwart (2007) (IntBS) will be performed in order to show the improvement obtained with the proposed strategies. The control strategy presented in Bouabdallah and Siegwart (2007) proposes an integral backstepping approach, which uses the integral term in the first step of the procedure. It has been chosen for the comparison analysis because it is able to present similar performance results, as well as to reject sustained disturbances.

Assuming that the *QuadRotor* helicopter needs, under ideal conditions, a thrust value of about $T \approx 21.97$N to perform hovering flight, the following persistent light gusts of wind are considered as external disturbances on the aerodynamic forces and moments:

$$\begin{array}{rcl} a_x = 1\text{N} & \text{at} & t = 5\text{s}, \\ a_\phi = 2\text{Nm} & \text{at} & t = 10\text{s}, \\ a_y = 1\text{N} & \text{at} & t = 15\text{s}, \\ a_\theta = 2\text{Nm} & \text{at} & t = 20\text{s}, \\ a_z = 1\text{N} & \text{at} & t = 25\text{s}, \\ a_\psi = 2\text{Nm} & \text{at} & t = 30\text{s}. \end{array}$$

Two reference trajectories will be used to evaluate the control strategies. The first reference path used is a circle evolving in the $\Re^3$ Cartesian space defined by:

$$x_r = \frac{1}{2}\cos\left(\frac{\pi t}{20}\right) m,\ \ y_r = \frac{1}{2}\sin\left(\frac{\pi t}{20}\right) m,\ \ z_r = 3 - 2\cos\left(\frac{\pi t}{20}\right) m,\ \ \psi_r = \frac{\pi}{4}\, rad\,.$$

For this trajectory, the initial conditions of the helicopter coordinates are $\boldsymbol{\xi_0} = [0 \quad 0 \quad 0]'$m and $\boldsymbol{\eta_0} = [0 \quad 0 \quad 0.5]'$rad. Fig 3.2 illustrates the first reference trajectory.

A second simulation collection will be carried out with a reference trajectory made up of a set of several kinds of stretches (see Fig. 3.3), starting from $x_{r_0} = 0.5\ m$, $y_{r_0} = 0.0\ m$, $z_{r_0} = 1.0\ m$ and $\psi_{r_0} = \pi/3\ rad$. The helicopter began tracking this trajectory in the following initial conditions of position and orientation: $\boldsymbol{\xi_0} = [0 \quad 0.5 \quad 0.5]'\ m$ and $\boldsymbol{\eta_0} = [0 \quad 0 \quad 0.5]'\ rad$. In these simulations, results attained by the control strategies are compared with the ones achieved by the

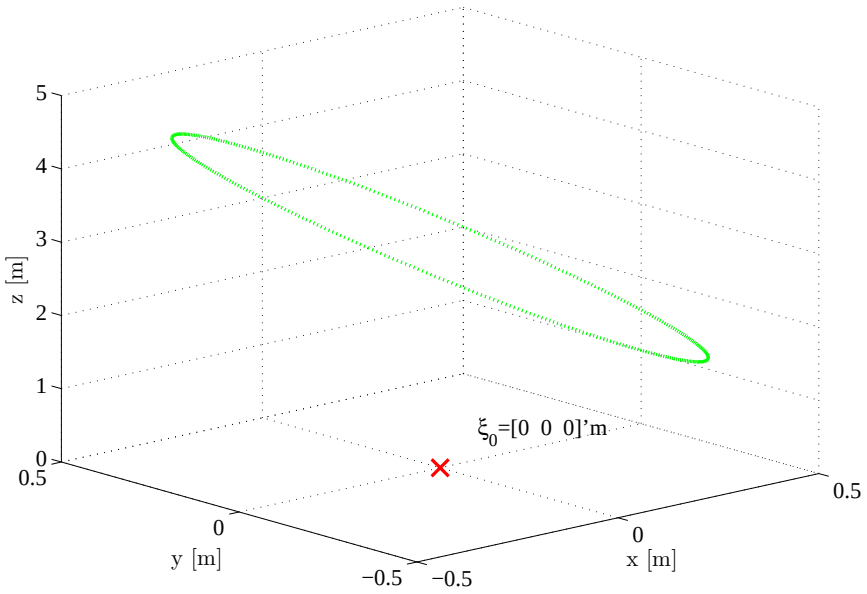

Figure 3.2: Circular reference path.

integral backstepping controller proposed by Bouabdallah and Siegwart (2007). The parameters for all the control structures are synthesized to obtain a smooth reference tracking, with a quick disturbance rejection and a small transient error.

Moreover, in order to make a quantitative comparison of the results attained by the control strategies, some performance indexes will be computed. On one hand, the Integral Square Error (ISE) performance indexes obtained from the simulation results are presented. On the other hand, the Integral Absolute Derivative control signal (IADU) index will be computed for all control signals in all control strategies. This performance index is indeed very appropriate to check the control signals' smoothness.

3.3 Rotational Subsystem Controllers

In this section the rotational subsystem control law to achieve robustness in the presence of sustained disturbances, parametric and structural uncertainties is developed. The approach used to perform is based on the nonlinear $\mathscr{H}_\infty$ theory.

The nonlinear $\mathscr{H}_\infty$ approach used in this chapter consists in an adaptation of

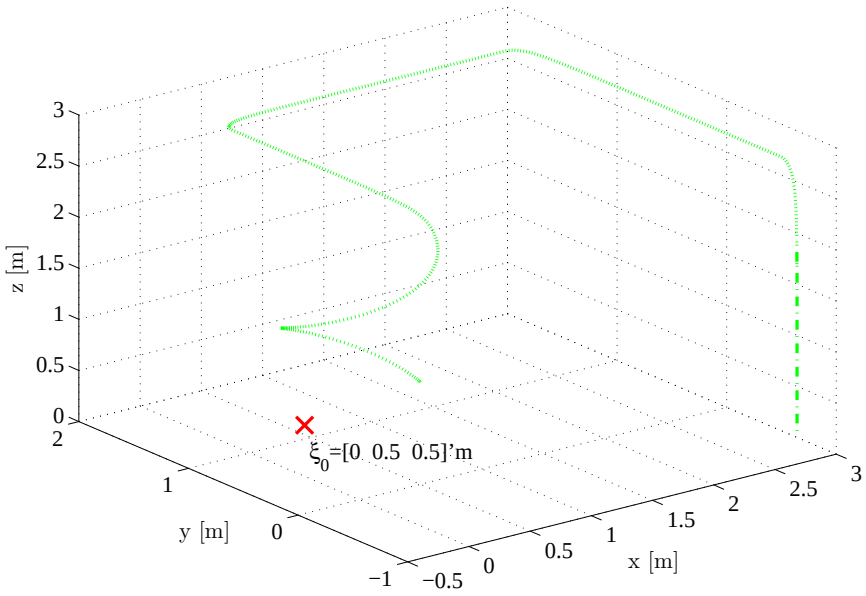

Figure 3.3: Assorted reference path.

a previous work, presented in Ortega et al. (2005), formulated via game theory, to control mechanical systems considering the tracking error dynamic equation. This strategy provides, through an analytical solution, a time variant control law which is strongly model-dependent and it is similar to the results obtained with the feedback linearization procedures.

In what follows the nonlinear $\mathscr{H}_\infty$ control theory and its formulation via game theory for the state feedback case is presented. Finally, the nonlinear state feedback $\mathscr{H}_\infty$ control for the rotational subsystem is developed.

The preliminary definitions about the nonlinear $\mathscr{H}_\infty$ control theory and differential game theory made in this chapter will be needed to formulate the underactuated nonlinear $\mathscr{H}_\infty$ controllers in Chapter 4.

3.3.1 Nonlinear $\mathscr{H}_\infty$ Control

A good choice to deal with unknown disturbances affecting a nonlinear system is the nonlinear $\mathscr{H}_\infty$ control theory. The goal of this control theory is to achieve a bounded ratio between the energy of the so-called error signals and the energy of the disturbance signals. One advantage of the nonlinear $\mathscr{H}_\infty$ controller when

compared with the linear approach is related with the attraction basin, which is enlarged by the nonlinear approach.

The solution of the nonlinear $\mathscr{H}_\infty$ control problem for nonlinear continuous systems has been provided by van der Schaft in van der Schaft (1991) and van der Schaft (1992), which uses the $\mathscr{L}_2$-gain as an extension of the $\mathscr{H}_\infty$-norm for linear systems, as will be seen in Section 3.4.1. The definition of $\mathscr{H}_\infty$-norm when treated in the time domain can be interpreted as the induced 2-norm or $\mathscr{L}_2$-norm of a system, which is the relationship between the energy (2-norm) of its output signals and the energy (2-norm) of its input ones. This definition can be used in both nonlinear and linear systems. In a general approach, the problem leads to a Hamilton-Jacobi (HJ) equation, which is a first order, nonlinear partial differential equation (PDE) for a function $S(\boldsymbol{q_1},\ldots,\boldsymbol{q_n},t)$ called Hamilton's principal function. However, the main problem in this approach is the absence of a general method to solve this HJ PDE.

In the next section, the nonlinear $\mathscr{H}_\infty$ problem is formulated, and its solution using differential game theory is presented. After that, as will be seen throughout this section, the controller design for mechanical system models using Euler-Lagrange equations is carried out by a direct method.

3.3.1.1 Nonlinear $\mathscr{H}_\infty$ Control Theory - General Approach

Considering a nonlinear dynamic system Σ in the following form:

$$\Sigma : \begin{cases} \dot{\boldsymbol{x}} &= a(\boldsymbol{x},\boldsymbol{u},\boldsymbol{d},t) \\ \boldsymbol{\zeta} &= h(\boldsymbol{x},\boldsymbol{u},\boldsymbol{d},t) \\ \boldsymbol{y} &= c(\boldsymbol{x},\boldsymbol{u},\boldsymbol{d},t) \end{cases} \tag{3.1}$$

where $\boldsymbol{x} \in \Re^n$ represents the system state vector, $\boldsymbol{u} \in \Re^m$ is the control input vector, $\boldsymbol{d} \in \Re^q$ represents the exogenous disturbance vector acting on the system, $\boldsymbol{y} \in \Re^p$ is the measurable signal vector and $\boldsymbol{\zeta} \in \Re^r$ is the cost variable associated with the optimization problem, whose energy is a behavior index.

In this way, the nonlinear $\mathscr{H}_\infty$ control problem consists in calculating an admissible controller:

$$K(x_k,\boldsymbol{y}) : \boldsymbol{y}(\cdot) \longmapsto \boldsymbol{u}(\cdot)\,,$$

with x_k being its states, and such that the resulting closed-loop is stable and verifies the attenuation relationship in $\mathscr{L}_2$-norm between the energy of the cost vector $\boldsymbol{\zeta}$ and the energy of the disturbance signal vector $\boldsymbol{d}$, i.e. in the channel $\boldsymbol{d} \longmapsto \boldsymbol{\zeta}$,

given by:

$$J_\infty = \frac{1}{2}\int_0^T \|\boldsymbol{\zeta}(t)\|_2^2 dt - \frac{1}{2}\gamma^2 \int_0^T \|\boldsymbol{d}(t)\|_2^2 dt \leq 0 \quad \forall T\,, \tag{3.2}$$

where the level attenuation achieved is called γ, and $\|\boldsymbol{\zeta}(t)\|_2^2$ and $\|\boldsymbol{d}(t)\|_2^2$ represent the power (instantaneous energy) supplied to the system of the cost variable vector and of the disturbances, respectively:

$$\|\boldsymbol{\zeta}(t)\|_2^2 = \boldsymbol{\zeta}(t)'\boldsymbol{\zeta}(t) = \sum_{i=1}^{r} |\zeta_i(t)|^2\,, \tag{3.3}$$

$$\|\boldsymbol{d}(t)\|_2^2 = \boldsymbol{d}(t)'\boldsymbol{d}(t) = \sum_{i=1}^{q} |d_i(t)|^2\,. \tag{3.4}$$

Thus, this is an optimization problem. The objective consists in formulating a stabilizing control law that minimizes the $\mathscr{L}_2$-gain (see Definition 3.1) of the application of the nonlinear input-output $\boldsymbol{d} \longmapsto \boldsymbol{\zeta}$, for the worst admissible disturbance acting on the system.

Definition 3.1 ((van der Schaft, 2000) $\mathscr{L}_2$-Gain)**.** *A dynamic system* Σ *has* $\mathscr{L}_2$*-gain* $\leq \gamma$ *if it is dissipative with respect to the supply rate* $s(\boldsymbol{d},\boldsymbol{\zeta}) = \frac{1}{2}\gamma^2\|\boldsymbol{d}(t)\|_2^2 - \frac{1}{2}\|\boldsymbol{\zeta}(t)\|_2^2$*. The* $\mathscr{L}_2$*-gain of* Σ *is defined as* $\gamma(\Sigma) = \inf\{\gamma | \Sigma \text{ has } \mathscr{L}_2 - gain \leq \gamma\}$*.* Σ *is said to have* $\mathscr{L}_2$*-gain* $< \gamma$ *if there exists* $\gamma^* < \gamma$ *such that* Σ *has* $\mathscr{L}_2$*-gain* $\leq \gamma^*$*.*

The relationship of the disturbance attenuation allows to catch in a simple way the performance idea for nonlinear systems. So that, if the cost variable $\boldsymbol{\zeta}$ is formulated as a weighting function of the control effort $\boldsymbol{u}$ versus the tracking error, it will determine to some extent the requirements of performance to the problem.

As the performance idea can be captured by the attenuation relation (3.2), other point is the closed-loop stability for the $\mathscr{H}_\infty$ control structure. Thus, the controlled system is weakly internally stable, if for Σ starting in the initial state $\boldsymbol{x_0}$ and the disturbances $\boldsymbol{d}(t) \in \mathscr{L}_2$, all the signals, $\boldsymbol{u}(\cdot)$, $\boldsymbol{y}(\cdot)$ and $\boldsymbol{\zeta}(\cdot)$ as well as $\boldsymbol{x}(\cdot)$ converge to zero when $t \to \infty$. On the other hand, the closed-loop system is internally stable, if it is weakly internally stable and additionally the controller supports an internal representation such that its state tends to zero when $t \to \infty$ (Helton and James, 1999).

The solution of nonlinear $\mathscr{H}_\infty$ control can be obtained through two approaches, differential game theory (Doyle et al., 1989; Basar and Bernhard, 2008) and dissipative systems theory (van der Schaft, 2000). However, for the sake of sim-

plicity, in this thesis only the first one will be used. Furthermore, in this chapter only the state feedback control approach will be exposed, since for the applications used in this thesis, an accessible state vector will be assumed .

Before exposing the differential game formulation to solve the nonlinear $\mathscr{H}_\infty$ problem, in order to clarity, a brief explanation about dynamic programming will be given.

3.3.1.2 Dynamic Programming

Firstly, to introduce the dynamic programming approach used in this thesis, the optimal control problem must be formulated. Thus, considering an unperturbed time-varying nonlinear system expressed as follows:

$$\dot{\boldsymbol{x}} = a(\boldsymbol{x}, \boldsymbol{u}, t)\,, \tag{3.5}$$

where the variables are the same as in system (3.1), the optimal control problem can be posed as follows:

Computing the control variable $\boldsymbol{u}(t)$ that must be applied to the system (3.5) over the time interval $[t_0, t_f]$, so that in its evolution the following continuous-time cost functional is minimized:

$$J = \phi(\boldsymbol{x}(t_f), t_f) + \int_{t_0}^{t_f} L(\boldsymbol{x}(t), \boldsymbol{u}(t), t)dt\,, \tag{3.6}$$

where t is the independent variable, t_0 is the initial time and t_f is the terminal time. The terms $\phi(\boldsymbol{x}(t_f), t_f)$ and $L(\boldsymbol{x}(t), \boldsymbol{u}(t), t)$ are the so-called terminal cost and Lagrangian, respectively. It is also assumed an initial condition $\boldsymbol{x}(t_0) = \boldsymbol{x_0}$ with t_0 constant and t_f probably variable. Of all the control signals $\boldsymbol{u}(t) \in \mathbb{U}$ that can be applied to the system during the time interval $[t_0, t_f]$, there will exist a $\boldsymbol{u}^*(t)$ such that:

$$J(\boldsymbol{u}^*(t)) \leq J(\boldsymbol{u}(t)) \quad \forall \boldsymbol{u}(t) \in \mathbb{U}\,, \tag{3.7}$$

where the signal $\boldsymbol{u}^*(t)$ is called the optimal control signal. (Bhattacharyya et al., 2009; Aracil and Gordillo, 2004)

In some problems it is interesting to obtain an expression that allows to compute the input signal value $\boldsymbol{u}$ as a function of the states $\boldsymbol{x}$, which is a feedback solution and is called the optimal control law, $\boldsymbol{u}^*(\boldsymbol{x}, t)$.

The optimal control signal can be achieved using Pontryagin's maximum principle, through the variational calculus, or by solving the Hamilton-Jacobi-Bellman

(HJB) equation, through dynamic programming (Sontag, 1998). However, in this thesis only dynamic programming will be treated.

Therefore, dynamic programming can be used to approximate the solution of the optimal control problem making use of the Bellman's Principle of Optimality, which can be summarized as follows:

Given an optimal trajectory between the initial time, t_0, and an intermediate time, t, the optimal trajectory between t_0 and a terminal time $t_f > t$ can be found concatenating the initial optimal trajectory to the computed one between t and t_f for the system starting at $\boldsymbol{x}(t)$ with $\boldsymbol{u}(t)$ at time t, which are the terminal states and control signals of the previous computed trajectory between t_0 and t.

Then, to perform that, the optimal cost-to-go function (also called the value function) concept is introduced as follows:

$$V(\boldsymbol{x},t) = J^*(\boldsymbol{x},t) = \min_{u(\cdot)} \left\{ \phi(\boldsymbol{x}(t_f),t_f) + \int_{t_0}^{t_f} L(\boldsymbol{x}(t),\boldsymbol{u}(t),t)dt \right\}, \tag{3.8}$$

where $J^*(\boldsymbol{x},t)$ is the best possible value of the cost functional J when the system covers the optimal trajectory from the state $(\boldsymbol{x},t)$.

If J^* is assumed continuously differentiable as a function of $\boldsymbol{x}$ and t, the Bellman's Principle of Optimality can be applied as follows:

- Assuming that the system has an initial state $\boldsymbol{x_0}$ at t_0 and evolutioning during Δt with a control action $\boldsymbol{u}$.
- For $t_0 + \Delta t$ the state is $\boldsymbol{x}'$.
- If from $\boldsymbol{x}'$ the state evolves according to an optimal trajectory to the final instant t_f, the cumulative cost in this track will be $J^*(\boldsymbol{x}', t_0 + \Delta t)$.
- $\boldsymbol{x}' \approx \boldsymbol{x} + a(\boldsymbol{x},\boldsymbol{u},t)\Delta t$ for $\Delta t \to 0$.
- The cost associated to the evolution from the state $\boldsymbol{x_0}$ at t_0 to the end point through $\boldsymbol{x}'$ at $t_0 + \Delta t$ is

$$J'(\boldsymbol{x},t) = J^*(\boldsymbol{x}', t_0 + \Delta t) + L(\boldsymbol{x},\boldsymbol{u},t)\Delta t\,.$$

Since $J^*(\boldsymbol{x},t) \leq J'(\boldsymbol{x},t)$, and whereas $J^*(\boldsymbol{x},t)$ is, by hypothesis, the minimum

with respect to the optimal trajectory, that is:

$$\begin{aligned} J^*(\boldsymbol{x},t) &= \min_{\boldsymbol{u}(\cdot)} \{J^*(\boldsymbol{x}',t+\Delta t)+L(\boldsymbol{x},\boldsymbol{u},t)\Delta t\} \\ &= \min_{\boldsymbol{u}(\cdot)} \{J^*(\boldsymbol{x}+a(\boldsymbol{x},\boldsymbol{u}(t),t)\Delta t,t+\Delta t)+L(\boldsymbol{x},\boldsymbol{u},t)\Delta t\} \\ &= \min_{\boldsymbol{u}(\cdot)} \left\{ J^*(\boldsymbol{x},t)+\frac{\partial J^*}{\partial \boldsymbol{x}}a(\boldsymbol{x},\boldsymbol{u},t)\Delta t+\frac{\partial J^*}{\partial t}\Delta t+L(\boldsymbol{x},\boldsymbol{u},t)\Delta t \right\}, \end{aligned}$$

for Δt small enough, it results in:

$$\frac{\partial J^*}{\partial t}\Delta t = -\min_{\boldsymbol{u}(\cdot)} \left\{ \frac{\partial J^*}{\partial \boldsymbol{x}}a(\boldsymbol{x},\boldsymbol{u},t)\Delta t+L(\boldsymbol{x},\boldsymbol{u},t)\Delta t \right\}.$$

Besides, by assuming $\Delta t \to 0$, the following expression is obtained:

$$\frac{\partial J^*}{\partial t} = -\min_{\boldsymbol{u}(\cdot)} \left\{ \frac{\partial J^*}{\partial \boldsymbol{x}}a(\boldsymbol{x},\boldsymbol{u},t)+L(\boldsymbol{x},\boldsymbol{u},t) \right\}, \tag{3.9}$$

which is the so-called Hamilton-Jacobi-Bellman equation, with the boundary condition $J^*(\boldsymbol{x},t_f)=\phi(\boldsymbol{x},t_f)$ where the values of $\boldsymbol{x}$ verify $\varphi(\boldsymbol{x},t_f)=0$. This equation can be seen as an extension of the Hamilton-Jacobi equation used in classical mechanics.

To solve this optimization problem, two stages are necessary. First, the cost function is minimized, which yields to:

$$\boldsymbol{u}^*(\boldsymbol{x},t) = arg\min_{\boldsymbol{u}\in\mathbb{U}} \left\{ \frac{\partial J^*}{\partial \boldsymbol{x}}a(\boldsymbol{x},\boldsymbol{u},t)+L(\boldsymbol{x},\boldsymbol{u},t) \right\},$$

or in a compact form:

$$\boldsymbol{u}^*(\boldsymbol{x},t) = \pi\left(\frac{\partial J^*}{\partial \boldsymbol{x}},\boldsymbol{x},t\right). \tag{3.10}$$

After that, this optimal control law is substituted in (3.9) and the following nonlinear PDE must be solved:

$$\frac{\partial J^*}{\partial t}+\frac{\partial J^*}{\partial \boldsymbol{x}}a(\boldsymbol{x},\pi,t)+L(\boldsymbol{x},\pi,t)=0. \tag{3.11}$$

If there exist a differentiable smooth solution, J^*, for this PDE, the optimal control law is computed obtaining the gradient of the value function J^* and substituting it in (3.10).

Moreover, by using the Hamiltonian notation:

$$H(\boldsymbol{x},\pi,t) = \frac{\partial J^*}{\partial \boldsymbol{x}} a(\boldsymbol{x},\pi,t) + L(\boldsymbol{x},\pi,t)\,,$$

equation (3.11) can be rewritten as follows:

$$H(\boldsymbol{x},\pi,t) + \frac{\partial J^*}{\partial t} = 0\,,$$

which is the so-called Hamilton-Jacobi (HJ) equation.

The main problem associated with the dynamic programming approach of the optimal control is to find explicits solution to the HJB equation. There are two research lines: one of them tries to formulate the solution using numerical methods, while the other one tries to find explicits solution for particular systems with a determined structure.

3.3.1.3 Nonlinear State Feedback $\mathscr{H}_\infty$ Control via Game Theory

This section presents the nonlinear state feedback $\mathscr{H}_\infty$ control law, assuming accessible states. The suboptimal nonlinear controller approach is described, where an attenuation level γ must be assumed *a priori*.

The nonlinear $\mathscr{H}_\infty$ problem can be formulated through the differential game theory, which is based on the observation that the frequency formulation of the $\mathscr{H}_\infty$ linear problem is equivalent to the *min-max* optimization problem in the time domain. So that, by adopting its realization in the game theory framework as a two-player zero-sum differential game, it can be assumed that one player manipulates the control action $\boldsymbol{u}$, whose objective is to guide the dynamic evolution of the system minimizing a cost function, and the other player plays the role of the disturbances acting on the system, whose goals is to maximize the performance index. The game consists in computing the control action $\boldsymbol{u}$ that minimizes the performance index for the worst of all possible disturbances acting on the system, maintaining the closed-loop stability.

Therefore, by considering the disturbed nonlinear time-varying system given by:

$$\dot{\boldsymbol{x}} = a(\boldsymbol{x},\boldsymbol{u},\boldsymbol{d},t)\,, \tag{3.12}$$

where the variables are the same as in system (3.1), the $\mathscr{H}_\infty$ (*min-max*) problem is

to compute the control input $\boldsymbol{u}^*(t)$ that minimizes the following cost functional:

$$J = \phi(\boldsymbol{x}(t_f), t_f) + \int_{t_0}^{t_f} L(\boldsymbol{x}(t), \boldsymbol{u}(t), t)dt\,, \tag{3.13}$$

where the disturbances try to maximize the following associated performance index:

$$\begin{aligned} L_\gamma &= \frac{1}{2}L(\boldsymbol{x}(t), \boldsymbol{u}(t)) - \frac{1}{2}\gamma^2\|\boldsymbol{d}(t)\|^2 \\ &= \frac{1}{2}\|\boldsymbol{\zeta}(t)\|^2 - \frac{1}{2}\gamma^2\|\boldsymbol{d}(t)\|^2\,, \end{aligned} \tag{3.14}$$

which is a so-called *parametrized soft-constrained* cost function (Basar and Bernhard, 2008).

The solution of this problem can be formulated through a Hamiltonian formulation:

$$H_\gamma(\boldsymbol{x}, \boldsymbol{u}, \boldsymbol{d}, \boldsymbol{p}, t) = L_\gamma(\boldsymbol{x}, \boldsymbol{u}, \boldsymbol{d}, t) + \boldsymbol{p}'a(\boldsymbol{x}, \boldsymbol{u}, \boldsymbol{d}, t)\,, \tag{3.15}$$

with $\boldsymbol{p}$ being the co-state vector . The problem has a (pure-strategy) saddle point solution if there exist $\boldsymbol{u}^* \in \mathbb{U}$ and $\boldsymbol{d}^* \in \mathbb{D}$, such that it satisfies the so-called *pair of saddle point inequalities*:

$$H_\gamma(\boldsymbol{x}, \boldsymbol{u}^*, \boldsymbol{d}, \boldsymbol{p}, t) \leq H_\gamma(\boldsymbol{x}, \boldsymbol{u}^*, \boldsymbol{d}^*, \boldsymbol{p}, t) \leq H_\gamma(\boldsymbol{x}, \boldsymbol{u}, \boldsymbol{d}^*, \boldsymbol{p}, t) \quad \forall \boldsymbol{u} \in \mathbb{U}, \boldsymbol{d} \in \mathbb{D}\,, \tag{3.16}$$

where $\mathbb{U}$ and $\mathbb{D}$ are the domains where the control input and the disturbances are defined, respectively, and it is verified that:

$$\min_{\boldsymbol{u}} \max_{\boldsymbol{d}} H_\gamma(\boldsymbol{x}, \boldsymbol{u}, \boldsymbol{d}, \boldsymbol{p}, t) = \max_{\boldsymbol{d}} \min_{\boldsymbol{u}} H_\gamma(\boldsymbol{x}, \boldsymbol{u}, \boldsymbol{d}, \boldsymbol{p}, t)\,.$$

If this saddle point exists, the optimal values for $\boldsymbol{u}$ and $\boldsymbol{d}$ are given by:

$$\boldsymbol{u}^*(t) = arg\min_{\boldsymbol{u}} \left(\max_{\boldsymbol{d}} H_\gamma(\boldsymbol{x}, \boldsymbol{u}, \boldsymbol{d}, \boldsymbol{p}, t) \right)\,,$$

and

$$\boldsymbol{d}^*(t) = arg\max_{\boldsymbol{d}} \left(\min_{\boldsymbol{u}} H_\gamma(\boldsymbol{x}, \boldsymbol{u}, \boldsymbol{d}, \boldsymbol{p}, t) \right)\,.$$

It is also possible to demonstrate that whether the optimal cost function $J^* : \Re^n \times \Re \to \Re$ is continuously differentiable (see Section 3.3.1.2), so that, the

saddle point condition can be written as follows:

$$\begin{aligned}\frac{\partial J^*}{\partial t}(\boldsymbol{x},t) &= -\max_{\boldsymbol{d}}\min_{\boldsymbol{u}} H_\gamma(\boldsymbol{x},\boldsymbol{u},\boldsymbol{d},\frac{\partial J^*}{\partial \boldsymbol{x}}(\boldsymbol{x},t),t)\\ &= -\min_{\boldsymbol{u}}\max_{\boldsymbol{d}} H_\gamma(\boldsymbol{x},\boldsymbol{u},\boldsymbol{d},\frac{\partial J^*}{\partial \boldsymbol{x}}(\boldsymbol{x},t),t)\\ &= -H^*_\gamma(\boldsymbol{x},\boldsymbol{u}^*,\boldsymbol{d}^*,\frac{\partial J^*}{\partial \boldsymbol{x}}(\boldsymbol{x},t),t)\,,\end{aligned} \tag{3.17}$$

where the pair $(\boldsymbol{u}^*,\boldsymbol{d}^*)$ constitutes a saddle point solution of the proposed problem. This PDE is the so-called Hamilton-Jacobi-Bellman-Isaacs (HJBI) equation (also named Hamilton-Jacobi-Isaacs equation or only Isaacs equation, in honor of Rufus Isaacs, the first one who studies differential games and who proposed this equation in the early 1950s), which is a generalization of the HJB PDE that provides a sufficient condition in optimal control, as discussed in the previous section (Basar and Bernhard, 2008).

Instead of this equality, the more general HJBI inequality is obtained by replacing "=" with "≤" as follows:

$$\begin{aligned}\frac{\partial J^*}{\partial t}(\boldsymbol{x},t) &\leq -\max_{\boldsymbol{d}}\min_{\boldsymbol{u}} H_\gamma(\boldsymbol{x},\boldsymbol{u},\boldsymbol{d},\frac{\partial J^*}{\partial \boldsymbol{x}}(\boldsymbol{x},t),t)\\ &\leq -\min_{\boldsymbol{u}}\max_{\boldsymbol{d}} H_\gamma(\boldsymbol{x},\boldsymbol{u},\boldsymbol{d},\frac{\partial J^*}{\partial \boldsymbol{x}}(\boldsymbol{x},t),t)\\ &\leq -H^*_\gamma(\boldsymbol{x},\boldsymbol{u}^*,\boldsymbol{d}^*,\frac{\partial J^*}{\partial \boldsymbol{x}}(\boldsymbol{x},t),t)\,.\end{aligned} \tag{3.18}$$

To solve the optimization problem and to obtain the expressions of the optimal control $\boldsymbol{u}^*$ and the worst-case disturbance $\boldsymbol{d}^*$, the equation (3.17) must be differentiated with respect to $\boldsymbol{u}$ and $\boldsymbol{d}$ and equalized to zero, that is:

$$\frac{\partial H_\gamma(\boldsymbol{x},\boldsymbol{u},\boldsymbol{d},\boldsymbol{p},t)}{\partial \boldsymbol{u}} = 0\,, \tag{3.19}$$

$$\frac{\partial H_\gamma(\boldsymbol{x},\boldsymbol{u},\boldsymbol{d},\boldsymbol{p},t)}{\partial \boldsymbol{d}} = 0\,. \tag{3.20}$$

Once the optimal control law and worst-case disturbances are obtained, and assuming that the HJBI equation admits a solution, denoted J^*, which is continu-

ously differentiable in both arguments, they must be replaced in (3.17), and the following HJ equation is obtained:

$$\frac{\partial J^*}{\partial t}(\boldsymbol{x},t)+H^*_\gamma(\boldsymbol{x},\boldsymbol{u}^*(\boldsymbol{x},\frac{\partial J^*}{\partial \boldsymbol{x}},t),\boldsymbol{d}^*(\boldsymbol{x},\frac{\partial J^*}{\partial \boldsymbol{x}},t),\frac{\partial J^*}{\partial \boldsymbol{x}},t)=0\,. \tag{3.21}$$

Therefore, the state feedback $\mathscr{H}_\infty$ control is reduced to compute a function $J^*\geq 0$ that satisfies the HJ equation (3.21), where H^*_γ is the optimal Hamiltonian. If there exists this value function, the control law:

$$\boldsymbol{u}^*(\boldsymbol{x},\frac{\partial J^*}{\partial \boldsymbol{x}},t)\,, \tag{3.22}$$

will guarantee that the closed-loop system given by (3.12) and (3.22) will have $\mathscr{L}_2$-gain (from $\boldsymbol{d}$ to $\boldsymbol{\zeta}$) less than γ.

In what follows, the nonlinear $\mathscr{H}_\infty$ controller with state feedback for affine nonlinear systems is presented.

Affine nonlinear input-state system

Consider the following nth order affine and smooth nonlinear input-state dynamic system Σ:

$$\Sigma:\left\{\begin{array}{rcl}\dot{\boldsymbol{x}} &=& f(\boldsymbol{x},t)+g(\boldsymbol{x},t)\boldsymbol{u}+k(\boldsymbol{x},t)\boldsymbol{d}\\ \boldsymbol{\zeta} &=& \boldsymbol{W}\left[\begin{array}{c}h(\boldsymbol{x},t)\\ \boldsymbol{u}\end{array}\right]\end{array}\right. \tag{3.23}$$

which is affected by unknown disturbances and the involved variables are the same as (3.1). As it has been exposed in Section 3.3.1.3, the desired performance of the system can be defined using the cost variable $\boldsymbol{\zeta}\in\Re^{(s+m)}$, with $r=s+m$, where $h(\boldsymbol{x},\boldsymbol{t})\in\Re^s$ represents a function of the state vector to be controlled and $\boldsymbol{W}\in\Re^{(s+m)\times(s+m)}$ is a weighting matrix. Moreover, it is assumed that: $f(\boldsymbol{x_0},t)=0$, $h(\boldsymbol{x_0},t)=0\;\forall t\geq 0$, with sufficient conditions: $\boldsymbol{x_0}$ is an equilibrium point of the system (in the absence disturbances), and the functions $f(\boldsymbol{x},t)$, $g(\boldsymbol{x},t)$, $k(\boldsymbol{x},t)$ and $h(\boldsymbol{x},t)$ are smooth functions.

Therefore, if the states $\boldsymbol{x}$ are assumed to be available for measurement, then the optimal $\mathscr{H}_\infty$ problem can be posed as follows (van der Schaft, 1992):

Theorem 3.3.1. *Find the smallest value $\gamma^*\geq 0$, such that, for any $\gamma\geq\gamma^*$ there exists a state feedback $\boldsymbol{u}=\boldsymbol{u}(\boldsymbol{x},t)$, $\boldsymbol{u}(\boldsymbol{x_0},t)=0\;\forall t\geq 0$, such that the $\mathscr{L}_2$ gain from*

$\boldsymbol{d}(t)$ to $\boldsymbol{\zeta}(t)$ is less than or equal to γ, that is:

$$\int_0^T \|\boldsymbol{\zeta}(t)\|_2^2 dt \leq \gamma^2 \int_0^T \|\boldsymbol{d}(t)\|_2^2 dt \,. \tag{3.24}$$

The internal term of the integral expression on the left-hand side of inequality (3.24) can be written as:

$$\|\boldsymbol{\zeta}(t)\|_2^2 = \boldsymbol{\zeta}(t)'\boldsymbol{\zeta}(t) = \left[\begin{array}{cc} h(\boldsymbol{x},t) & \boldsymbol{u}' \end{array}\right] \boldsymbol{W}'\boldsymbol{W} \left[\begin{array}{c} h(\boldsymbol{x},t) \\ \boldsymbol{u} \end{array}\right],$$

and the symmetric positive definite matrix $\boldsymbol{W}'\boldsymbol{W}$ can be partitioned as follows:

$$\boldsymbol{W}'\boldsymbol{W} = \left[\begin{array}{cc} \boldsymbol{Q} & \boldsymbol{S} \\ \boldsymbol{S}' & \boldsymbol{R} \end{array}\right]. \tag{3.25}$$

Matrices $\boldsymbol{Q}$ and $\boldsymbol{R}$ are symmetric positive definite and the fact that $\boldsymbol{W}'\boldsymbol{W} > \mathbb{0}$ guarantees that $\boldsymbol{Q} - \boldsymbol{S}\boldsymbol{R}^{-1}\boldsymbol{S}' > \mathbb{0}$, where $\mathbb{0}$ is the nth order zero matrix.

In this case, the associated performance index (3.14) is expressed by:

$$L_\gamma = \frac{1}{2}\|\boldsymbol{\zeta}(t)\|_2^2 - \frac{1}{2}\gamma^2\|\boldsymbol{d}(t)\|_2^2 = \frac{1}{2}\left\|\boldsymbol{W}\left[\begin{array}{c} h(\boldsymbol{x},t) \\ \boldsymbol{u}(t) \end{array}\right]\right\|_2^2 - \frac{1}{2}\gamma^2\|\boldsymbol{d}(t)\|_2^2. \tag{3.26}$$

By substituting this equation in (3.15), the following expression is obtained:

$$\begin{aligned} H_\gamma(\boldsymbol{x},\boldsymbol{u},\boldsymbol{d},\boldsymbol{p},t) &= \boldsymbol{p}'(f(\boldsymbol{x},t) + g(\boldsymbol{x},t)\boldsymbol{u} + k(\boldsymbol{x},t)\boldsymbol{d}) - \frac{1}{2}\gamma^2\|\boldsymbol{d}(t)\|_2^2 \\ &\quad + \frac{1}{2}\left\|\boldsymbol{W}\left[\begin{array}{c} h(\boldsymbol{x},t) \\ \boldsymbol{u}(t) \end{array}\right]\right\|_2^2 \\ &= \boldsymbol{p}'(f(\boldsymbol{x},t) + g(\boldsymbol{x},t)\boldsymbol{u} + k(\boldsymbol{x},t)\boldsymbol{d}) - \frac{1}{2}\gamma^2\boldsymbol{d}(t)'\boldsymbol{d}(t) \\ &\quad + \frac{1}{2}h(\boldsymbol{x},t)'\boldsymbol{Q}h(\boldsymbol{x},t) + h(\boldsymbol{x},t)'\boldsymbol{S}\boldsymbol{u}(\boldsymbol{x},t) + \frac{1}{2}\boldsymbol{u}(t)'\boldsymbol{R}\boldsymbol{u}(t). \end{aligned} \tag{3.27}$$

Therefore, the nonlinear $\mathscr{H}_\infty$ problem admits a solution if there exists a smooth differentiable function $V(\boldsymbol{x},t)$, with $V(\boldsymbol{x}_\mathbf{0},t) \equiv 0$ for $t \geq 0$, such that the following

min-max problem is verified:

$$\begin{aligned}\frac{\partial V(\boldsymbol{x},t)}{\partial t} &= -\max_{\boldsymbol{d}}\min_{\boldsymbol{u}}\left(\frac{\partial V}{\partial \boldsymbol{x}}(f(\boldsymbol{x},t)+g(\boldsymbol{x},t)\boldsymbol{u}+k(\boldsymbol{x},t)\boldsymbol{d})+L_\gamma(\boldsymbol{x},\boldsymbol{u},t)\right)\\ &= -\max_{\boldsymbol{d}}\min_{\boldsymbol{u}}\left(\frac{\partial V}{\partial \boldsymbol{x}}(f(\boldsymbol{x},t)+g(\boldsymbol{x},t)\boldsymbol{u}+k(\boldsymbol{x},t)\boldsymbol{d})-\frac{1}{2}\gamma^2\boldsymbol{d}(t)'\boldsymbol{d}(t)\right.\\ &\quad\left.+\frac{1}{2}h(\boldsymbol{x},t)'\boldsymbol{Q}h(\boldsymbol{x},t)+h(\boldsymbol{x},t)'\boldsymbol{S}\boldsymbol{u}(\boldsymbol{x},t)+\frac{1}{2}\boldsymbol{u}(t)'\boldsymbol{R}\boldsymbol{u}(t)\right),\end{aligned} \tag{3.28}$$

which is the already mentioned HJBI equation. The co-state vector $\boldsymbol{p}$ is the gradient $\frac{\partial V}{\partial \boldsymbol{x}}$. Under these assumptions, the solution of the nonlinear $\mathscr{H}_\infty$ state feedback problem can be formulated as follows:

$$\boldsymbol{u}^*(t) = arg\min_{\boldsymbol{u}}\left(\max_{\boldsymbol{d}}\left(\frac{\partial V}{\partial \boldsymbol{x}}(f(\boldsymbol{x},t)+g(\boldsymbol{x},t)\boldsymbol{u}+k(\boldsymbol{x},t)\boldsymbol{d})+L_\gamma(\boldsymbol{x},\boldsymbol{u},t)\right)\right),$$

$$\boldsymbol{d}^*(t) = arg\max_{\boldsymbol{d}}\left(\min_{\boldsymbol{u}}\left(\frac{\partial V}{\partial \boldsymbol{x}}(f(\boldsymbol{x},t)+g(\boldsymbol{x},t)\boldsymbol{u}+k(\boldsymbol{x},t)\boldsymbol{d})+L_\gamma(\boldsymbol{x},\boldsymbol{u},t)\right)\right).$$

For the particular case wherein the index (3.13) is equivalent to consider $L(\boldsymbol{x},\boldsymbol{u},t) = \boldsymbol{\zeta}'\boldsymbol{\zeta}$ presenting a square functional dependence in $\boldsymbol{u}$, the *min-max* problem supports a unique and explicit solution. Thus, taking the first derivatives over $\boldsymbol{u}$ and $\boldsymbol{d}$ for the expression to be optimized in (3.28) and by equaling it to zero, the saddle point is founded as follows:

$$\frac{\partial H_\gamma(\boldsymbol{x},\boldsymbol{u},\boldsymbol{d},\boldsymbol{p},t)}{\partial \boldsymbol{d}} = \frac{\partial' V}{\partial \boldsymbol{x}}k(\boldsymbol{x},t)-\gamma^2\boldsymbol{d}(t)' = 0, \tag{3.29}$$

$$\frac{\partial H_\gamma(\boldsymbol{x},\boldsymbol{u},\boldsymbol{d},\boldsymbol{p},t)}{\partial \boldsymbol{u}} = \frac{\partial' V}{\partial \boldsymbol{x}}g(\boldsymbol{x},t)+h(\boldsymbol{x},t)'\boldsymbol{S}+\boldsymbol{u}(t)'\boldsymbol{R} = 0, \tag{3.30}$$

where the worst-case of the admissible disturbances is given by:

$$\boldsymbol{d}^*(\boldsymbol{x},t) = \frac{1}{\gamma^2}k(\boldsymbol{x},t)'\frac{\partial V}{\partial \boldsymbol{x}}, \tag{3.31}$$

while the optimal state feedback control law is derived as follows:

$$\boldsymbol{u}^*(\boldsymbol{x},t) = -\boldsymbol{R}^{-1}\left(h(\boldsymbol{x})'\boldsymbol{S}+g'(\boldsymbol{x},t)\frac{\partial V(\boldsymbol{x},t)}{\partial \boldsymbol{x}}\right). \tag{3.32}$$

As commented before, the point $(\boldsymbol{d}^*(\boldsymbol{x},t),\boldsymbol{u}^*(\boldsymbol{x},t))$ is a saddle point in the Hamiltonian function $H_\gamma(\boldsymbol{x},\boldsymbol{u},\boldsymbol{d},\boldsymbol{p},t)$. However, in the particular case of affine systems, the following inequalities:

$$H_\gamma(\boldsymbol{x},\boldsymbol{u}^*,\boldsymbol{d},\boldsymbol{p},t) \leq H_\gamma(\boldsymbol{x},\boldsymbol{u}^*,\boldsymbol{d}^*,\boldsymbol{p},t) \leq H_\gamma(\boldsymbol{x},\boldsymbol{u},\boldsymbol{d}^*,\boldsymbol{p},t) \quad \forall \boldsymbol{d},\boldsymbol{u} \text{ and } \boldsymbol{x}, \tag{3.33}$$

results more restrictive than the exposed ones in (3.16). This implies that $\boldsymbol{d}^*$ may be considered as the worst-case disturbance while $\boldsymbol{u}^*$ may be considered as the optimal control for any possible disturbance.

By substituting equations (3.31) and (3.32) in (3.28), the following HJ inequality is obtained (van der Schaft, 2000):

$$\begin{aligned} &\frac{\partial V}{\partial t} + \frac{\partial' V}{\partial \boldsymbol{x}} f(\boldsymbol{x},t) + \frac{1}{2}\frac{\partial' V}{\partial \boldsymbol{x}}\left[\frac{1}{\gamma^2}k(\boldsymbol{x},t)k'(\boldsymbol{x},t) - g(\boldsymbol{x},t)\boldsymbol{R}^{-1}g'(\boldsymbol{x},t)\right]\frac{\partial V}{\partial \boldsymbol{x}} \\ &\qquad - \frac{\partial' V}{\partial \boldsymbol{x}} g(\boldsymbol{x},t)\boldsymbol{R}^{-1}\boldsymbol{S}'h(\boldsymbol{x}) + \frac{1}{2}h'(\boldsymbol{x})\left(\boldsymbol{Q} - \boldsymbol{S}\boldsymbol{R}^{-1}\boldsymbol{S}'\right)h(\boldsymbol{x}) \leq 0, \end{aligned} \tag{3.34}$$

for each $\gamma > \sqrt{\sigma_{\max}(\boldsymbol{R})} \geq 0$, where $\sigma_{\max}$ stands for the maximum singular value.

Therefore, the computation of state feedback control law for nonlinear affine input-state systems can be achieved by means of the following theorem:

Theorem 3.3.2. *Let $\gamma > 0$ be a level attenuation value. If there exists a differentiable scalar function $V(\boldsymbol{x},t) \geq 0$ that satisfies the Hamilton-Jacobi equation (3.34), then the closed-loop system corresponding to the system (3.23) with the control law (3.32) is stable and has $\mathscr{L}_2$-gain (in the channel $\boldsymbol{d} \mapsto \boldsymbol{\zeta}$) less than or equal to γ.*

Proof:

Despite of this theorem is well known in the literature (see van der Schaft (2000)), a brief explanation of it will be given in this demonstration.

By considering the HJBI equation (3.28) with the worst-case of the admissible disturbances, $\boldsymbol{d}^*$, and the optimal feedback control law $\boldsymbol{u}^*$, (3.28) can be rewritten as follows:

$$\begin{aligned} &\frac{\partial V(\boldsymbol{x},t)}{\partial t} + \frac{\partial V(\boldsymbol{x},t)}{\partial \boldsymbol{x}}(f(\boldsymbol{x},t) + g(\boldsymbol{x},t)\boldsymbol{u} + k(\boldsymbol{x},t)\boldsymbol{d}) - \frac{1}{2}\gamma^2\boldsymbol{d}^*(t)'\boldsymbol{d}^*(t) \\ &\qquad + \frac{1}{2}h(\boldsymbol{x},t)'\boldsymbol{Q}h(\boldsymbol{x},t) + h(\boldsymbol{x},t)'\boldsymbol{S}\boldsymbol{u}^*(t) + \frac{1}{2}\boldsymbol{u}^*(t)'\boldsymbol{R}\boldsymbol{u}^*(t) \leq 0, \end{aligned}$$

or equivalently:

$$\frac{\partial V(\boldsymbol{x},t)}{\partial t}+\frac{\partial V(\boldsymbol{x},t)}{\partial \boldsymbol{x}}(f(\boldsymbol{x},t)+g(\boldsymbol{x},t)\boldsymbol{u}+k(\boldsymbol{x},t)\boldsymbol{d})\leq -\frac{1}{2}\left\|\boldsymbol{\zeta}^*(t)\right\|_2^2+\frac{1}{2}\gamma^2\left\|\boldsymbol{d}^*(t)\right\|_2^2. \tag{3.35}$$

From this expression and considering $V(\boldsymbol{x},t)$ as a Lyapunov function, the stability of the closed-loop system, given by (3.23) and (3.32), is easily demonstrated by taking the time derivative of $V(\boldsymbol{x},t)$ as follows:

$$\dot{V}(\boldsymbol{x},t)=-\frac{1}{2}\left\|\boldsymbol{\zeta}^*(t)\right\|_2^2+\frac{1}{2}\gamma^2\left\|\boldsymbol{d}^*(t)\right\|_2^2,$$

and, therefore, the system is uniformly bounded. If there are no disturbances acting on the system, $\boldsymbol{d}(t)=0$, $\dot{V}(\boldsymbol{x},t)=-\frac{1}{2}\left\|\boldsymbol{\zeta}^*(t)\right\|_2^2\leq 0$, which guarantees the uniform asymptotic stability of the closed-loop system.

Moreover, this expression shows that the scalar function $V(\boldsymbol{x},t)\geq 0$ is a storage function with supply rate $\frac{1}{2}\gamma^2\left\|\boldsymbol{d}^*(t)\right\|_2^2-\frac{1}{2}\left\|\boldsymbol{\zeta}^*(t)\right\|_2^2$ ($\mathscr{L}_2$-gain), for the closed-loop system corresponding to the system (3.23) with the control law (3.32).

■

3.3.2 Nonlinear $\mathscr{H}_\infty$ control for the rotational subsystem

In this section, the nonlinear state feedback $\mathscr{H}_\infty$ approach presented previously is used to control Euler-Lagrange mechanical systems, which results in a known and direct method to solve the HJ equation.

The rotational movement dynamic model (2.62), obtained from the Euler-Lagrange formalism, is used in order to develop the nonlinear $\mathscr{H}_\infty$ controller:

$$\mathscr{J}(\boldsymbol{\eta})\ddot{\boldsymbol{\eta}}+\boldsymbol{C}(\boldsymbol{\eta},\dot{\boldsymbol{\eta}})\dot{\boldsymbol{\eta}}=\boldsymbol{\tau}_{\boldsymbol{\eta}},$$

where $\boldsymbol{\tau}_{\boldsymbol{\eta}}$ joins the control torques and external disturbances, and is redefined as:

$$\boldsymbol{\tau}_{\boldsymbol{\eta}}=\boldsymbol{\tau}_{\boldsymbol{\eta}_a}+\boldsymbol{\delta}_{\boldsymbol{\eta}}\left(\boldsymbol{\eta},\dot{\boldsymbol{\eta}},\ddot{\boldsymbol{\eta}},\boldsymbol{\tau}_{\boldsymbol{\eta}_d}\right),$$

with $\boldsymbol{\tau}_{\boldsymbol{\eta}_a}$ being the applied torque vector with respect to the roll, pitch and yaw moments, and $\boldsymbol{\delta}_{\boldsymbol{\eta}}$ representing the total effect of system modeling errors and external disturbances.

In this section, a state-space description of the error dynamics of the Euler-Lagrange mechanical system, focusing on the rotational equations of motion, is

used. This representation was presented originally by Johansson (1990), and modified by Ortega (2001). As it is well known, for a mechanical system to follow a desired trajectory it is necessary to compute the applied torques. If the position, velocity and acceleration references of the rotational DOF are defined by $\boldsymbol{\eta_r}$, $\dot{\boldsymbol{\eta}}_{\boldsymbol{r}}$ and $\ddot{\boldsymbol{\eta}}_{\boldsymbol{r}} \in \Re^n$, respectively, which are provided by a trajectory generator or by an outer-loop controller and assumed to be within the physical and kinematic limits of the control object, it is possible to obtain their errors at each instant of time as follows:

$$\begin{aligned}
\dddot{\tilde{\boldsymbol{\eta}}} &= \ddot{\boldsymbol{\eta}} - \ddot{\boldsymbol{\eta}}_{\boldsymbol{r}}\,, \\
\ddot{\tilde{\boldsymbol{\eta}}} &= \dot{\boldsymbol{\eta}} - \dot{\boldsymbol{\eta}}_{\boldsymbol{r}}\,, \\
\tilde{\boldsymbol{\eta}} &= \boldsymbol{\eta} - \boldsymbol{\eta}_{\boldsymbol{r}}\,, \\
\int_0^t \tilde{\boldsymbol{\eta}}\,dt &= \int_0^t (\boldsymbol{\eta} - \boldsymbol{\eta}_{\boldsymbol{r}})\,dt\,.
\end{aligned}$$

Thus, as a first step to synthesize the control law, the tracking error vector is defined as follows:

$$\boldsymbol{x_\eta} = \begin{bmatrix} \ddot{\tilde{\boldsymbol{\eta}}} \\ \dot{\tilde{\boldsymbol{\eta}}} \\ \int \tilde{\boldsymbol{\eta}}\,dt \end{bmatrix}. \tag{3.36}$$

Note that an integral term has been included in the error vector. This term will allow the achievement of a null steady-state error when persistent disturbances are acting on the system (Ortega et al., 2005).

Thereby, by using the tracking error vector (3.36) and equation (2.64), the error dynamics of the rotational subsystem can be written in a state-space form:

$$\dot{\boldsymbol{x}}_{\boldsymbol{\eta}} = \overline{f}(\boldsymbol{x_\eta}, t) + \overline{g_0}(\boldsymbol{\eta}, \dot{\boldsymbol{\eta}}, \ddot{\boldsymbol{\eta}}_{\boldsymbol{r}}, \dot{\boldsymbol{\eta}}_{\boldsymbol{r}}) + \overline{g}(\boldsymbol{x_\eta}, t)\boldsymbol{\tau}_{\boldsymbol{\eta_a}} + \overline{k}(\boldsymbol{x_\eta}, t)\boldsymbol{\delta_\eta}\,, \tag{3.37}$$

where

$$\overline{f}(\boldsymbol{x_\eta}, t) = \begin{bmatrix} -\mathscr{J}(\boldsymbol{\eta})^{-1}\boldsymbol{C}(\boldsymbol{\eta}, \dot{\boldsymbol{\eta}}) & \mathbb{0} & \mathbb{0} \\ \mathbb{1} & \mathbb{0} & \mathbb{0} \\ \mathbb{0} & \mathbb{1} & \mathbb{0} \end{bmatrix} \boldsymbol{x_\eta}\,,$$

$$\overline{g_0}(\boldsymbol{\eta}, \dot{\boldsymbol{\eta}}, \ddot{\boldsymbol{\eta}}_{\boldsymbol{r}}, \dot{\boldsymbol{\eta}}_{\boldsymbol{r}}) = \begin{bmatrix} -\mathscr{J}(\boldsymbol{\eta})^{-1}(\mathscr{J}(\boldsymbol{\eta})\ddot{\boldsymbol{\eta}}_{\boldsymbol{r}} + \boldsymbol{C}(\boldsymbol{\eta}, \dot{\boldsymbol{\eta}})\dot{\boldsymbol{\eta}}_{\boldsymbol{r}}) \\ \mathbb{0} \\ \mathbb{0} \end{bmatrix},$$

$$\overline{g}(\boldsymbol{x_\eta}, t) = \overline{k}(\boldsymbol{x_\eta}, t) = \begin{bmatrix} \mathscr{J}(\boldsymbol{\eta})^{-1} \\ \mathbb{0} \\ \mathbb{0} \end{bmatrix},$$

with $\mathbb{1} \in \Re^{n\times n}$ being the identity matrix and $\mathbb{0} \in \Re^{n\times n}$ the zero matrix.

Note that there are no gravitational and frictional terms in this equation, since the simplified rotational equations of motion, which are being used in this section, are not affected by these forces. However, in a more generalized representation (see Johansson (1990); Ortega (2001); Vivas (2004)), these forces compound the function $\overline{g_0}(\cdot)$.

As a second step to synthesize the control law, the following state transformation is defined:

$$z = \begin{bmatrix} z_1 \\ z_2 \\ z_3 \end{bmatrix} = \boldsymbol{T_o} \boldsymbol{x_\eta} = \begin{bmatrix} \boldsymbol{T_1} & \boldsymbol{T_2} & \boldsymbol{T_3} \\ \mathbb{0} & \mathbb{1} & \mathbb{1} \\ \mathbb{0} & \mathbb{0} & \mathbb{1} \end{bmatrix} \begin{bmatrix} \dot{\tilde{\boldsymbol{\eta}}} \\ \tilde{\boldsymbol{\eta}} \\ \int \tilde{\boldsymbol{\eta}} dt \end{bmatrix}, \tag{3.38}$$

where $\boldsymbol{T_1}$, $\boldsymbol{T_2}$ and $\boldsymbol{T_3} \in \Re^{n\times n}$ are arbitrary constant matrices, and $\boldsymbol{T_1}$ must be invertible and, besides, $\boldsymbol{T_1} = \rho\mathbb{1}$, where ρ is a positive scalar.

Despite of this state-space transformation, a change of variables over the control action and disturbances must be considered. To perform that, an optimization strategy must also be defined. Thus, as exposed in Johansson (1990), a natural aim is to minimize the error vector with a minimum of applied torque and energy consumption. However, it makes no sense to include in the optimizing index the components of the generalized forces that change the potential energy of the system, as gravitational forces, since the increment of potential energy is given by the trajectory and it cannot be changed by any control strategy (Vivas, 2004). Besides, as a standard result from Lagrangian mechanics, the term $\mathscr{N}(\boldsymbol{\eta}, \dot{\boldsymbol{\eta}})\dot{\boldsymbol{\eta}}$ represents a workless force of the system (see property 3 in Section 2.4), being also not necessary to consider it in the optimizing index. Therefore, a natural choice of generalized forces and applied torques to be included in an optimization strategy that affect the kinetic energy, $\boldsymbol{\tau_\kappa}$, are:

$$\boldsymbol{\tau_\kappa} = \mathscr{J}(\boldsymbol{\eta})\ddot{\boldsymbol{\eta}} + \frac{1}{2}\dot{\mathscr{J}}(\boldsymbol{\eta}, \dot{\boldsymbol{\eta}})\dot{\boldsymbol{\eta}},$$

where:

$$\boldsymbol{\tau_\kappa} = \boldsymbol{\tau_\eta} - \frac{\partial \mathscr{U}}{\partial \boldsymbol{\eta}}.$$

Thus, to minimize the necessary forces/torques for the worst case of all possible disturbances acting on the system, a change of variables in the control action

and disturbances is defined as follows:

$$\begin{aligned} \boldsymbol{u}+\boldsymbol{d} &= \left[\begin{array}{cc} \mathscr{J}(\boldsymbol{\eta}) & \frac{1}{2}\dot{\mathscr{J}}(\boldsymbol{\eta},\dot{\boldsymbol{\eta}}) \end{array}\right]\left[\begin{array}{c} \dot{\boldsymbol{z}}_1 \\ \boldsymbol{z}_1 \end{array}\right] \\ \boldsymbol{u}+\boldsymbol{d} &= \mathscr{J}(\boldsymbol{\eta})\boldsymbol{T}\dot{\boldsymbol{x}}_{\boldsymbol{\eta}}+\boldsymbol{C}(\boldsymbol{\eta},\dot{\boldsymbol{\eta}})\boldsymbol{T}\boldsymbol{x}_{\boldsymbol{\eta}}\,, \end{aligned} \tag{3.39}$$

where matrix $\boldsymbol{T}$ can be partitioned as follows:

$$\boldsymbol{T} = \left[\begin{array}{ccc} \boldsymbol{T}_1 & \boldsymbol{T}_2 & \boldsymbol{T}_3 \end{array}\right].$$

By expanding this transformation, which includes the reference trajectories, the forces and torques affecting kinetic energy and the state-space transformation (3.38), the equation (3.37) can be rewritten as follows:

$$\dot{\boldsymbol{x}}_{\boldsymbol{\eta}} = f(\boldsymbol{x}_{\boldsymbol{\eta}},t)+g(\boldsymbol{x}_{\boldsymbol{\eta}},t)\boldsymbol{u}+k(\boldsymbol{x}_{\boldsymbol{\eta}},t)\boldsymbol{d}\,, \tag{3.40}$$

$$f(\boldsymbol{x}_{\boldsymbol{\eta}},t) = \boldsymbol{T}_o^{-1}\left[\begin{array}{ccc} -\mathscr{J}(\boldsymbol{\eta})^{-1}\boldsymbol{C}(\boldsymbol{\eta},\dot{\boldsymbol{\eta}}) & \mathbb{0} & \mathbb{0} \\ \boldsymbol{T}_1^{-1} & \mathbb{1}-\boldsymbol{T}_1^{-1}\boldsymbol{T}_2 & -\mathbb{1}+\boldsymbol{T}_1^{-1}(\boldsymbol{T}_2-\boldsymbol{T}_3) \\ \mathbb{0} & \mathbb{1} & -\mathbb{1} \end{array}\right]\boldsymbol{T}_o\boldsymbol{x}_{\boldsymbol{\eta}}\,,$$

$$g(\boldsymbol{x}_{\boldsymbol{\eta}},t) = k(\boldsymbol{x}_{\boldsymbol{\eta}},t) = \boldsymbol{T}_o^{-1}\left[\begin{array}{c} \mathscr{J}(\boldsymbol{\eta})^{-1} \\ \mathbb{0} \\ \mathbb{0} \end{array}\right].$$

Without loss of generality, equaling equations (3.37) and (3.40), the external disturbance vector $\boldsymbol{d}$ and the control action $\boldsymbol{u}$ are obtained by:

$$\boldsymbol{d} = \mathscr{J}(\boldsymbol{\eta})\boldsymbol{T}_1\mathscr{J}^{-1}(\boldsymbol{\eta})\boldsymbol{\delta}_{\boldsymbol{\eta}}\,, \tag{3.41}$$

$$\boldsymbol{u} = \boldsymbol{T}_1(-\boldsymbol{F}(\boldsymbol{x}_e)+\boldsymbol{\tau}_{\boldsymbol{\eta}_a})\,, \tag{3.42}$$

with

$$\begin{aligned} F(\boldsymbol{x}_e) &= \mathscr{J}(\boldsymbol{\eta})(\ddot{\boldsymbol{\eta}}_r-\boldsymbol{T}_1^{-1}\boldsymbol{T}_2\dot{\tilde{\boldsymbol{\eta}}}-\boldsymbol{T}_1^{-1}\boldsymbol{T}_3\tilde{\boldsymbol{\eta}}) \\ &+ \boldsymbol{C}(\boldsymbol{\eta},\dot{\boldsymbol{\eta}})(\dot{\boldsymbol{\eta}}_r-\boldsymbol{T}_1^{-1}\boldsymbol{T}_2\tilde{\boldsymbol{\eta}}-\boldsymbol{T}_1^{-1}\boldsymbol{T}_3\int\tilde{\boldsymbol{\eta}}dt)\,. \end{aligned}$$

Equation (3.40) represents the *dynamic equation of the system error*. It is a nonlinear matrix equation due to the time-varying matrices $\mathscr{J}(\boldsymbol{\eta})$ and $\boldsymbol{C}(\boldsymbol{\eta},\dot{\boldsymbol{\eta}})$, and affine in the actuation and disturbances. Note that explicit functional dependence of time in this equation is due to the implicit presence of trajectory reference, which is time-varying. Moreover, Coriolis and centrifugal matrix, $\boldsymbol{C}(\boldsymbol{\eta},\dot{\boldsymbol{\eta}})$, must

be obtained by using the Christoffel Symbols presented in Section 2.4, which guarantees the skew-symmetric matrix $\mathscr{N}(\boldsymbol{\eta},\dot{\boldsymbol{\eta}}) = \mathscr{J}(\boldsymbol{\eta}) - 2\boldsymbol{C}(\boldsymbol{\eta},\dot{\boldsymbol{\eta}})$. This property is very useful to demonstrate stability of the controller.

The relationship between the applied torque, $\boldsymbol{\tau}_{\eta_a}$, and the control input, $\boldsymbol{u}$, is given by equation (3.42). So that, by isolating $\boldsymbol{\tau}_{\eta_a}$ and considering $\boldsymbol{T}_1 = \rho\mathbb{1}$, the following control law is obtained for the rotational subsystem:

$$\begin{aligned}\boldsymbol{\tau}_{\eta_a} &= \mathscr{J}(\boldsymbol{\eta})\ddot{\boldsymbol{\eta}}_r + \boldsymbol{C}(\boldsymbol{\eta},\dot{\boldsymbol{\eta}})\dot{\boldsymbol{\eta}} - \boldsymbol{T}_1^{-1}\mathscr{J}(\boldsymbol{\eta})\left(\boldsymbol{T}_2\dot{\tilde{\boldsymbol{\eta}}} + \boldsymbol{T}_3\tilde{\boldsymbol{\eta}}\right) \\ &\quad -\boldsymbol{T}_1^{-1}\boldsymbol{C}(\boldsymbol{\eta},\dot{\boldsymbol{\eta}})\boldsymbol{T}\boldsymbol{x}_{\boldsymbol{\eta}} + \boldsymbol{T}_1^{-1}\boldsymbol{u}.\end{aligned} \tag{3.43}$$

It is interesting to note that equation (3.43) adopts a similar structure of a linearizing feedback control law with a nonlinear term in the control acceleration, which can be expressed in a clearer manner as follows:

$$\boldsymbol{\tau}_{\eta_a} = \mathscr{J}(\boldsymbol{\eta})\ddot{\boldsymbol{\eta}} + \boldsymbol{C}(\boldsymbol{\eta},\dot{\boldsymbol{\eta}})\dot{\boldsymbol{\eta}},$$

with

$$\ddot{\boldsymbol{\eta}} = \ddot{\boldsymbol{\eta}}_r - \boldsymbol{T}_1^{-1}\mathscr{J}(\boldsymbol{\eta})\left(\boldsymbol{T}_2\dot{\tilde{\boldsymbol{\eta}}} + \boldsymbol{T}_3\tilde{\boldsymbol{\eta}}\right) - \boldsymbol{T}_1^{-1}\boldsymbol{C}(\boldsymbol{\eta},\dot{\boldsymbol{\eta}})\boldsymbol{T}\boldsymbol{x}_{\boldsymbol{\eta}} + \boldsymbol{T}_1^{-1}\boldsymbol{u}. \tag{3.44}$$

By arranging this equation, it is possible to write this control law in terms just of the error vector and its time derivative, which is given by:

$$\boldsymbol{\tau}_{\eta_a} = \mathscr{J}(\boldsymbol{\eta})\ddot{\boldsymbol{\eta}} + \boldsymbol{C}(\boldsymbol{\eta},\dot{\boldsymbol{\eta}})\dot{\boldsymbol{\eta}} + \boldsymbol{G}(\boldsymbol{\eta}) - \boldsymbol{T}_1^{-1}\left(\mathscr{J}(\boldsymbol{\eta})\boldsymbol{T}\dot{\boldsymbol{x}}_{\boldsymbol{\eta}} + \boldsymbol{C}(\boldsymbol{\eta},\dot{\boldsymbol{\eta}})\boldsymbol{T}\boldsymbol{x}_{\boldsymbol{\eta}}\right) + \boldsymbol{T}_1^{-1}\boldsymbol{u}. \tag{3.45}$$

However, it can be pointed out that, the previous control law might not seem a well posed system, since it depends on accelerations of the generalized coordinates. Thereby, to avoid misunderstanding, equation (3.43) will be used throughout this section.

The control law can be split up into three different parts: the first one consists of the first two terms of that equation, which are designed in order to compensate the system dynamics (2.62). The second part consists of two terms including the error vector $\boldsymbol{x}_{\boldsymbol{\eta}}$ and its derivative, $\dot{\boldsymbol{x}}_{\boldsymbol{\eta}}$. Assuming $\boldsymbol{\delta}_{\boldsymbol{\eta}} \equiv \boldsymbol{0}$, these two terms of the control law enable perfect tracking, which means that they represent the *essential control* effort needed to perform the task. Finally, the third part includes a vector $\boldsymbol{u}$, which represents the *additional control* effort needed for disturbance rejection.

Therefore, equation (3.40) considering the *additional control* input vector $\boldsymbol{u}$

is used to apply the nonlinear $\mathscr{H}_\infty$ theoretical results presented in Section 3.3.1.3. This *additional control* signal provides $\mathscr{H}_\infty$ robustness and represents a state feedback. Taking into account this nonlinear equation, the nonlinear $\mathscr{H}_\infty$ control problem can be posed as follows:

"Find a control law $\boldsymbol{u}(t)$ such that the ratio between the energy of the cost variable $\boldsymbol{\zeta} = \boldsymbol{W}\left[h'(\boldsymbol{x_\eta})\ \boldsymbol{u}'\right]'$ and the energy of the disturbance signals $\boldsymbol{d}$ is less than a given attenuation level γ".

Taking into account the definition of the error vector, $\boldsymbol{x_\eta}$, and the definition of the cost variable, $\boldsymbol{\zeta}$, the following structures are considered for matrices $\boldsymbol{Q}$ and $\boldsymbol{S}$ in (3.25):

$$\boldsymbol{Q} = \begin{bmatrix} \boldsymbol{Q_1} & \boldsymbol{Q_{12}} & \boldsymbol{Q_{13}} \\ \boldsymbol{Q_{12}} & \boldsymbol{Q_2} & \boldsymbol{Q_{23}} \\ \boldsymbol{Q_{13}} & \boldsymbol{Q_{23}} & \boldsymbol{Q_3} \end{bmatrix}, \quad \boldsymbol{S} = \begin{bmatrix} \boldsymbol{S_1} \\ \boldsymbol{S_2} \\ \boldsymbol{S_3} \end{bmatrix}.$$

As stated in Section 3.3.1.3, the solution of the HJBI equation depends on the choice of the cost variable, $\boldsymbol{\zeta}$, and particularly on the selection of function $h(\boldsymbol{x_\eta})$ (see (3.23)). In this section, this function is taken to be equal to the error vector. That is, $h(\boldsymbol{x_\eta}) = \boldsymbol{x_\eta}$. Once this function has been selected, computing the *additional control* effort, $\boldsymbol{u}$, will require finding the Lyapunov function, $V(\boldsymbol{x_\eta}, t)$, to the HJ equation posed in the previous section (see (3.34)).

The following theorem will help to do this.

Theorem 3.3.3. *Let $V(\boldsymbol{x_\eta}, t)$ be the scalar function:*

$$V(\boldsymbol{x_\eta}, t) = \frac{1}{2}\boldsymbol{x_\eta'}\boldsymbol{T_o'}\begin{bmatrix} \mathscr{J}(\boldsymbol{\eta}) & \mathbb{0} & \mathbb{0} \\ \mathbb{0} & \boldsymbol{Y} & \boldsymbol{X}-\boldsymbol{Y} \\ \mathbb{0} & \boldsymbol{X}-\boldsymbol{Y} & \boldsymbol{Z}+\boldsymbol{Y} \end{bmatrix}\boldsymbol{T_o}\boldsymbol{x_\eta}, \tag{3.46}$$

where $\boldsymbol{X}$, $\boldsymbol{Y}$ and $\boldsymbol{Z} \in \Re^{n\times n}$ are constant, symmetric, and positive definite matrices such that $\boldsymbol{Z}-\boldsymbol{X}\boldsymbol{Y}^{-1}\boldsymbol{X}+2\boldsymbol{X} > \mathbb{0}$, and $\boldsymbol{T_o}$ is as defined in (3.38). Let $\boldsymbol{T}$ be the matrix appearing in (3.39). If these matrices verify the following equation:

$$\begin{bmatrix} \mathbb{0} & \boldsymbol{Y} & \boldsymbol{X} \\ \boldsymbol{Y} & 2\boldsymbol{X} & \boldsymbol{Z}+2\boldsymbol{X} \\ \boldsymbol{X} & \boldsymbol{Z}+2\boldsymbol{X} & \mathbb{0} \end{bmatrix} + \boldsymbol{Q} + \frac{1}{\gamma^2}\boldsymbol{T}'\boldsymbol{T} - \left(\boldsymbol{S}'+\boldsymbol{T}\right)'\boldsymbol{R}^{-1}\left(\boldsymbol{S}'+\boldsymbol{T}\right) = \mathbb{0}, \tag{3.47}$$

then, function $V(\boldsymbol{x_\eta}, t)$ constitutes a solution to the HJBI, for a sufficiently high value of γ.

Proof: The proof of this theorem is obtained following the steps presented

in Ortega et al. (2005). ■

Once the matrix $\boldsymbol{T} = \begin{bmatrix} \boldsymbol{T_1} & \boldsymbol{T_2} & \boldsymbol{T_3} \end{bmatrix}$ is computed by solving some Riccati algebraic equations, by substituting $V(\boldsymbol{x_\eta}, t)$ in (3.32), the *additional control* effort $\boldsymbol{u}^*$ is given by

$$\boldsymbol{u}^* = -\boldsymbol{R}^{-1}\left(\boldsymbol{S}' + \boldsymbol{T}\right)\boldsymbol{x_\eta}\,, \tag{3.48}$$

which corresponds to the $\mathscr{H}_\infty$ suboptimal control law according to $\mathscr{L}_2$-gain criteria, from the disturbances $\boldsymbol{d}$ to the cost variable $\boldsymbol{\zeta} = \boldsymbol{W}[\boldsymbol{x}' \quad \boldsymbol{u}']'$, for an attenuation level γ previously selected.

Finally, if the *additional control* effort (3.48) is replaced into (3.43) under the assumption that $\boldsymbol{d} = 0$, and after some manipulations, the control law can be written as:

$$\boldsymbol{\tau}^*_{\boldsymbol{\eta_a}} = \mathscr{J}(\boldsymbol{\eta})\ddot{\boldsymbol{\eta}}_r + \boldsymbol{C}(\boldsymbol{\eta}, \dot{\boldsymbol{\eta}})\dot{\boldsymbol{\eta}} - \mathscr{J}(\boldsymbol{\eta})\left(\boldsymbol{K_D}\dot{\tilde{\boldsymbol{\eta}}} + \boldsymbol{K_P}\tilde{\boldsymbol{\eta}} + \boldsymbol{K_I}\int \tilde{\boldsymbol{\eta}}\,dt\right), \tag{3.49}$$

where

$$\begin{aligned}
\boldsymbol{K_D} &= \boldsymbol{T_1}^{-1}\left(\boldsymbol{T_2} + \mathscr{J}(\boldsymbol{\eta})^{-1}\boldsymbol{C}(\boldsymbol{\eta}, \dot{\boldsymbol{\eta}})\boldsymbol{T_1} + \mathscr{J}(\boldsymbol{\eta})^{-1}\boldsymbol{R}^{-1}\left(\boldsymbol{S_1}' + \boldsymbol{T_1}\right)\right), \\
\boldsymbol{K_P} &= \boldsymbol{T_1}^{-1}\left(\boldsymbol{T_3} + \mathscr{J}(\boldsymbol{\eta})^{-1}\boldsymbol{C}(\boldsymbol{\eta}, \dot{\boldsymbol{\eta}})\boldsymbol{T_2} + \mathscr{J}(\boldsymbol{\eta})^{-1}\boldsymbol{R}^{-1}\left(\boldsymbol{S_2}' + \boldsymbol{T_2}\right)\right), \\
\boldsymbol{K_I} &= \boldsymbol{T_1}^{-1}\left(\mathscr{J}(\boldsymbol{\eta})^{-1}\boldsymbol{C}(\boldsymbol{\eta}, \dot{\boldsymbol{\eta}})\boldsymbol{T_3} + \mathscr{J}(\boldsymbol{\eta})^{-1}\boldsymbol{R}^{-1}\left(\boldsymbol{S_3}' + \boldsymbol{T_3}\right)\right).
\end{aligned} \tag{3.50}$$

Taking into account that these matrices multiply the time derivative of the position error vector, the position error vector itself and its integral, this controller can be interpreted as a PID control law. However, its coefficients are nonlinear, since its values depends on the positions and velocities of the degrees of freedom, which vary with time.

A particular case can be obtained when the components of the weighting compound $\boldsymbol{W}'\boldsymbol{W}$ verify:

$$\begin{gathered}
\boldsymbol{Q_1} = {\omega_1}^2\mathbb{1}, \quad \boldsymbol{Q_2} = {\omega_2}^2\mathbb{1}, \quad \boldsymbol{Q_3} = {\omega_3}^2\mathbb{1}, \quad \boldsymbol{R} = {\omega_u}^2\mathbb{1}, \\
\boldsymbol{Q_{12}} = \boldsymbol{Q_{13}} = \boldsymbol{Q_{23}} = \mathbb{0}, \quad \boldsymbol{S_1} = \boldsymbol{S_2} = \boldsymbol{S_3} = \mathbb{0}.
\end{gathered} \tag{3.51}$$

where ω_1, ω_2 and ω_3 are scalars that weight the time derivative of the error, the error itself and its integral, respectively, and ω_u weights the incremental control actions.

In this case, the following analytical expressions for the gain matrices have

been obtained:

$$\begin{aligned}
\boldsymbol{K_D} &= \frac{\sqrt{{\omega_2}^2 + 2\omega_1\omega_3}}{\omega_1}\mathbb{1} + \mathscr{J}(\boldsymbol{\eta})^{-1}\left(\boldsymbol{C}(\boldsymbol{\eta},\dot{\boldsymbol{\eta}}) + \frac{1}{{\omega_u}^2}\mathbb{1}\right), \\
\boldsymbol{K_P} &= \frac{\omega_3}{\omega_1}\mathbb{1} + \frac{\sqrt{{\omega_2}^2 + 2\omega_1\omega_3}}{\omega_1}\mathscr{J}(\boldsymbol{\eta})^{-1}\left(\boldsymbol{C}(\boldsymbol{\eta},\dot{\boldsymbol{\eta}}) + \frac{1}{{\omega_u}^2}\mathbb{1}\right), \\
\boldsymbol{K_I} &= \frac{\omega_3}{\omega_1}\mathscr{J}(\boldsymbol{\eta})^{-1}\left(\boldsymbol{C}(\boldsymbol{\eta},\dot{\boldsymbol{\eta}}) + \frac{1}{{\omega_u}^2}\mathbb{1}\right).
\end{aligned} \tag{3.52}$$

where the parameters ω_1, ω_2, ω_3 and ω_u can be tuned by a systematic procedure keeping in mind a linear PID control action interpretation.

These expressions have an important property: they do not depend on the parameter γ. So, an algebraic expression for computing the general optimal solution for this particular case can be obtained.

3.4 Translational Subsystem Controllers

In this section control laws able to solve the path tracking problem by translational movements are proposed. Linear $\mathscr{H}_\infty$, model predictive control and backstepping techniques are used to design a control law in such way that the subsystem is forced to track the reference trajectory.

The controllers for translational subsystem are performed in two phases. The first one controls the height through the input T, whereas the second one makes use of this signal as a time variant parameter in the linear xy-motion to compute two virtual control inputs, u_x^c and u_y^c.

For the controller design, the system (2.61) can be written in a state-space form as $\dot{\overline{\boldsymbol{\xi}}}(t) = f\left(\overline{\boldsymbol{\xi}}(t), \boldsymbol{u_\xi}(t), \boldsymbol{\delta_\xi}(t)\right)$, where $\overline{\boldsymbol{\xi}}(t) = [x(t)\ u_0(t)\ y(t)\ v_0(t)\ z(t)\ w_0(t)]'$ stands for the state-space vector of the system, where $u_0(t)$, $v_0(t)$, and $w_0(t)$ are the components of the linear velocity of the vehicle mass center expressed in the inertial frame (see equation. (2.29)). Variable $\boldsymbol{u_\xi}(t) = [T(t)\ u_x(t)\ u_y(t)]'$ is the control input vector, and $\boldsymbol{\delta_\xi}(t) = [\delta_{\xi_x}(t)\ \delta_{\xi_y}(t)\ \delta_{\xi_z}(t)]'$ is the unknown disturbance vector defined in Section 2.5.

From (2.61) and the new state-space vector, the system dynamic equation for

control design purpose can be written in the following form[1]:

$$\dot{\bar{\boldsymbol{\xi}}}(t) = f\left(\bar{\boldsymbol{\xi}}(t), \boldsymbol{u}_{\boldsymbol{\xi}}(t), \boldsymbol{\delta}_{\boldsymbol{\xi}}(t)\right) = \begin{bmatrix} u_0(t) \\ u_x(t)\dfrac{T(t)}{m} + \dfrac{\delta_{\xi_x}(t)}{m} \\ v_0(t) \\ u_y(t)\dfrac{T(t)}{m} + \dfrac{\delta_{\xi_y}(t)}{m} \\ w_0(t) \\ -g + (\cos\phi(t)\cos\theta(t))\dfrac{T(t)}{m} + \dfrac{\delta_{\xi_z}(t)}{m} \end{bmatrix}, \tag{3.53}$$

with:

$$\begin{aligned} u_x(t) &\triangleq \cos\psi(t)\sin\theta(t)\cos\phi(t) + \sin\psi(t)\sin\phi(t) \\ u_y(t) &\triangleq \sin\psi(t)\sin\theta(t)\cos\phi(t) - \cos\psi(t)\sin\phi(t) \end{aligned}, \tag{3.54}$$

Furthermore, system (3.53) shows that the movement through the x and y axes depends on the control input T. In fact, T is the designed total thrust magnitude to obtain the desired linear movement, while u_x and u_y can be considered as the directions of T that cause the movement through the x and y axes, respectively.

Therefore, equations (3.54) are a definition of the system to be controlled, and through the virtual inputs, u_x and u_y, the necessary values of ϕ and θ to guide the helicopter in the xy plane could be computed. However, these values cannot be set directly since these angles are two of the outputs of the rotational subsystem; being the nonlinear $\mathscr{H}_\infty$ inner-loop in charge of carrying out this task. On the other hand, assuming the error vector definition (3.36), equations (3.54) can be written as follows:

$$\begin{aligned} u_x(t) &\triangleq \cos(\psi)\sin(\tilde{\theta}+\theta_r)\cos(\tilde{\phi}+\phi_r) + \sin(\psi)\sin(\tilde{\phi}+\phi_r) \\ u_y(t) &\triangleq \sin(\psi)\sin(\tilde{\theta}+\theta_r)\cos(\tilde{\phi}+\phi_r) - \cos(\psi)\sin(\tilde{\phi}+\phi_r) \end{aligned}, \tag{3.55}$$

Moreover, because of the cascade structure of the strategy proposed in this chapter (see Fig. 3.1), and considering the closed-loop performance achieved by the inner-loop controller, the Euler angles error can be considered at the origin for the outer-loop controller design. Besides, it can be pointed out that the yaw angle, ψ, is assumed measurable for the computation of the desired magnitudes θ_r and ϕ_r. For this reason, the variable ψ_r has not been considered in equation

[1] The term $\cos\phi(t)\cos\theta(t)$ can be considered the direction of the thrust, T, that causes altitude motion. However, since it is not a control signal, the variable u_z is not used in the model, as it happens with the control actions u_x and u_y.

(3.55). In consequence of these assumptions, the desired virtual direction vector, $\boldsymbol{u}^{\boldsymbol{d}}_{\boldsymbol{\xi}_{xy}} = [u_x^d \; u_y^d]'$, to follow the path reference in the xy plane, is defined as follows:

$$\begin{aligned} u_x^d(t) &= \cos\psi(t)\sin\theta_r(t)\cos\phi_r(t) + \sin\psi(t)\sin\phi_r(t) \\ u_y^d(t) &= \sin\psi(t)\sin\theta_r(t)\cos\phi_r(t) - \cos\psi(t)\sin\phi_r(t) \end{aligned}, \tag{3.56}$$

which is used to obtain the roll and pitch reference angles.

In the next sections the controllers proposed for the outer loop of the cascade control strategy, presented in Fig. 3.1, are developed.

3.4.1 Linear $\mathscr{H}_\infty$ Control

The aim of this section is to obtain a robust path tracking, where a linear state feedback $\mathscr{H}_\infty$ controller via LMI formulation is used to control the *QuadRotor* translational movements. This controller combined with the nonlinear $\mathscr{H}_\infty$ one for the rotational motion, presented in Section 3.3.2, will provide a robust control strategy, which will be able to deal with sustained external disturbances affecting the six degrees of freedom of UAV.

In what follows, a brief introduction about the linear $\mathscr{H}_\infty$ control is given, followed by its state feedback formulation via LMIs.

3.4.1.1 Linear $\mathscr{H}_\infty$ Control Theory

The diagram block, presented in Fig 3.4, can be used to describe many practice controllers. The control design can be formulated like a $\mathscr{H}_\infty$ optimization problem. In this diagram block, $\boldsymbol{P}(s)$ is the generalized process, $\boldsymbol{K}(s)$ is the controller, $\boldsymbol{u}$ are the control signals, $\boldsymbol{y}$ the measured variables, $\boldsymbol{d}$ the exogenous signals and $\boldsymbol{\zeta}$ are the cost variables.

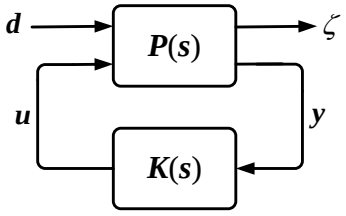

Figure 3.4: General control problem formulation.

The $\mathscr{H}_\infty$-norm of a stable scalar transfer function $H_{d\boldsymbol{\zeta}}(s)$ can be defined as the maximum magnitude of its frequency response, i.e., the peak value of the maximum singular value of the frequency response in the multivariable case. For SISO (Single-Input-Single-Output) systems, Bode diagram can be used to obtain the peak value of the system over all frequencies. On the other hand, for MIMO (Multiply-Input-Multiply-Output) systems, the module idea cannot be applied and it must be substituted by the spectral norm of a transfer matrix, where the frequency response can be obtained by the singular value decomposition approach. Thus, for SISO systems, the $\mathscr{H}_\infty$-norm can be described as the maximum peak magnitude, M_p, of the frequency response, which is the highest gain that the system is able to offer to the input signal:

$$\left\|H_{d\zeta}(s)\right\|_\infty = \max_\omega \left|H_{d\zeta}(j\omega)\right| = M_p\,, \tag{3.57}$$

and for MIMO systems:

$$\left\|H_{d\boldsymbol{\zeta}}(s)\right\|_\infty = \sup_\omega \bar{\sigma}\left\{H_{d\boldsymbol{\zeta}}(j\omega)\right\}. \tag{3.58}$$

As commented before, the $\mathscr{H}_\infty$-norm of a system represents the highest gain of its frequency response and, it can also be interpreted like the highest gain in energy terms that the system is capable of providing for the input signal. This interpretation is quite useful and provides an alternative definition for the $\mathscr{H}_\infty$-norm. By the Parseval's theorem, it holds:

$$\|\boldsymbol{d}(t)\|_2^2 = \frac{1}{2\pi}\int_0^\infty \boldsymbol{D}(j\omega)^*\cdot\boldsymbol{D}(j\omega)d\omega, \quad \|\boldsymbol{\zeta}(t)\|_2^2 = \frac{1}{2\pi}\int_0^\infty \boldsymbol{Z}(j\omega)^*\cdot\boldsymbol{Z}(j\omega)d\omega\,,$$

where $\boldsymbol{D}(j\omega)$, $\boldsymbol{Z}(j\omega)$ are the Fourier transforms of the signals $\boldsymbol{d}(t)$ and $\boldsymbol{\zeta}(t)$, respectively. Since $\boldsymbol{Z}(j\omega) = H_{d\boldsymbol{\zeta}}(j\omega)\boldsymbol{D}(j\omega)$, it yields:

$$\begin{aligned}
\|\boldsymbol{\zeta}(t)\|_2^2 &= \frac{1}{2\pi}\int_0^\infty \boldsymbol{D}(j\omega)^*\cdot H_{d\boldsymbol{\zeta}}(j\omega)^*\cdot H_{d\boldsymbol{\zeta}}(j\omega)\cdot\boldsymbol{D}(j\omega)d\omega \\
&\leq \frac{1}{2\pi}\int_0^\infty \left(\bar{\sigma}\left\{H_{d\boldsymbol{\zeta}}(j\omega)\right\}\right)^2 \boldsymbol{D}(j\omega)^*\cdot\boldsymbol{D}(j\omega)d\omega \\
&\leq \left(\sup_\omega \bar{\sigma}\left\{H_{d\boldsymbol{\zeta}}(j\omega)\right\}\right)^2 \frac{1}{2\pi}\int_0^\infty \boldsymbol{D}(j\omega)^*\cdot\boldsymbol{D}(j\omega)d\omega\,.
\end{aligned} \tag{3.59}$$

This expression can be written in the following form:

$$\|\boldsymbol{\zeta}(t)\|_2 \leq \left\|H_{\boldsymbol{d}\boldsymbol{\zeta}}(s)\right\|_\infty \|\boldsymbol{d}(t)\|_2 .$$

If the input signal $\boldsymbol{D}(j\omega)$ is properly chosen, it is possible to obtain the equality $\|\boldsymbol{\zeta}(t)\|_2 = \left\|H_{\boldsymbol{d}\boldsymbol{\zeta}}(s)\right\|_\infty \|\boldsymbol{d}(t)\|_2$. From this relationship, it can define the version of the $\mathscr{H}_\infty$-norm in the time domain as follows (Skogestad and Postlethwaite, 2005):

$$\left\|H_{\boldsymbol{d}\boldsymbol{\zeta}}(s)\right\|_\infty = \sup_{\boldsymbol{d}\neq 0} \frac{\|\boldsymbol{\zeta}(t)\|_2}{\|\boldsymbol{d}(t)\|_2} . \tag{3.60}$$

The optimal $\mathscr{H}_\infty$ control problem, in this configuration, consists in computing the controller that minimizes the level attenuation γ between the energy of the cost variable $\boldsymbol{\zeta}$ and the energy of the exogenous signal vector $\boldsymbol{d}$. This optimal problem is not solved yet, but the solution for the suboptimal problem exists (Ortega and Rubio, 2004), where a quite common idea consists in determining numerically an upper bound γ for $\|H_{\boldsymbol{d}\boldsymbol{\zeta}}(s)\|_\infty$ using the definition (3.60), that is, a positive scalar is looked for such that:

$$\left\|H_{\boldsymbol{d}\boldsymbol{\zeta}}(s)\right\|_\infty < \gamma . \tag{3.61}$$

However, this fact limits to deal with suboptimal controllers, since to obtain optimal $\mathscr{H}_\infty$ controllers is a hard task, and in practice, despite of these controllers can present undesirable properties, the computation can lead to numerical problems (Sánchez-Peña and Sznaier, 1998).

Thus, for the suboptimal $\mathscr{H}_\infty$ problem, the level attenuation γ can be computed as the $\mathscr{H}_\infty$-norm of the closed-loop transfer matrix from $\boldsymbol{d}$ to $\boldsymbol{\zeta}$, $H_{\boldsymbol{d}\boldsymbol{\zeta}}(s)$, looking for the minimum value through an iterative process (Ortega et al., 2006). This problem can be solved by different manners, as, for example, via Riccati's equation, Hamiltonian matrix or by LMIs (Skogestad and Postlethwaite, 2005).

In what follows the suboptimal $\mathscr{H}_\infty$ problem is solved using LMIs.

3.4.1.2 Linear State Feedback $\mathscr{H}_\infty$ control via LMIs

Consider the following uncertain linear system:

$$\Sigma : \begin{cases} \dot{\boldsymbol{x}}(t) &= \boldsymbol{A}(\boldsymbol{\delta})\boldsymbol{x}(t) + \boldsymbol{B_u}(\boldsymbol{\delta})\boldsymbol{u}(t) + \boldsymbol{B_d}(\boldsymbol{\delta})\boldsymbol{d}(t) \\ \boldsymbol{\zeta}(t) &= \boldsymbol{C_\zeta}(\boldsymbol{\delta})\boldsymbol{x}(t) + \boldsymbol{D_{u\zeta}}(\boldsymbol{\delta})\boldsymbol{u}(t) + \boldsymbol{D_{d\zeta}}(\boldsymbol{\delta})\boldsymbol{d}(t) \\ \boldsymbol{u}(t) &= \boldsymbol{K}\boldsymbol{x}(t) \qquad \boldsymbol{\delta} \in \boldsymbol{\Delta} \end{cases} \tag{3.62}$$

where $\boldsymbol{x}(t) \in \Re^n$ is the state, $\boldsymbol{u}(t) \in \Re^m$ is the control input, $\boldsymbol{d} \in \Re^q$ is any exogenous input, including disturbances, measurement noise, etc., $\boldsymbol{A}$, $\boldsymbol{B_u}$ and $\boldsymbol{B_d}$ are matrices with suitable dimensions, $\boldsymbol{C_\zeta}$, $\boldsymbol{D_{u\zeta}}$ and $\boldsymbol{D_{d\zeta}}$ are weighting matrices and $\boldsymbol{K}$ is a controller gain matrix to be determined. $\boldsymbol{\delta} \in \Re^l$ is the parameter uncertainty vector and $\boldsymbol{\Delta} = Co\{\boldsymbol{v_1}, \ldots, \boldsymbol{v_{2^q}}\}$ is a polytope with known vertices $\boldsymbol{v_i}$. Matrices $\boldsymbol{A}(\boldsymbol{\delta})$, $\boldsymbol{B_u}(\boldsymbol{\delta})$, $\boldsymbol{B_d}(\boldsymbol{\delta})$, $\boldsymbol{C_\zeta}(\boldsymbol{\delta})$, $\boldsymbol{D_{u\zeta}}(\boldsymbol{\delta})$, $\boldsymbol{D_{d\zeta}}(\boldsymbol{\delta})$ are affine functions in $\boldsymbol{\delta}$.

The closed-loop system (3.62) is given by:

$$\Sigma_{CL} : \begin{cases} \dot{\boldsymbol{x}}(t) &= (\boldsymbol{A}(\boldsymbol{\delta}) + \boldsymbol{B_u}(\boldsymbol{\delta})\boldsymbol{K})\boldsymbol{x}(t) + \boldsymbol{B_d}(\boldsymbol{\delta})\boldsymbol{d}(t) \\ \boldsymbol{\zeta}(t) &= (\boldsymbol{C_\zeta}(\boldsymbol{\delta}) + \boldsymbol{D_{u\zeta}}(\boldsymbol{\delta})\boldsymbol{K})\boldsymbol{x}(t) + \boldsymbol{D_{d\zeta}}(\boldsymbol{\delta})\boldsymbol{d}(t) \end{cases} \tag{3.63}$$

To perform the synthesis of a state feedback $\mathscr{H}_\infty$ controller via LMIs, the $\mathscr{H}_\infty$-norm is rewritten in the following form:

$$\left\| H_{\boldsymbol{d\zeta}}(s) \right\|_\infty = \sup_{\boldsymbol{d} \neq 0} \frac{\|\boldsymbol{\zeta}(t)\|_2}{\|\boldsymbol{d}(t)\|_2} = \sup_{\boldsymbol{d} \neq 0} \sqrt{\int_0^\infty \frac{\boldsymbol{\zeta}(t)'\boldsymbol{\zeta}(t)}{\boldsymbol{d}(t)'\boldsymbol{d}(t)} dt} < \gamma \,, \tag{3.64}$$

which, as in the nonlinear case, can be expressed as follows:

$$\int_0^\infty \boldsymbol{\zeta}(t)'\boldsymbol{\zeta}(t) dt < \gamma^2 \int_0^\infty \boldsymbol{d}(t)'\boldsymbol{d}(t) dt \,. \tag{3.65}$$

For a stable exponentially system with null initial conditions, one can consider the problem of determining a Lyapunov function $V(\boldsymbol{x}) = \boldsymbol{x}(t)'\boldsymbol{P}\boldsymbol{x}(t)$, where $\boldsymbol{P}$ is a symmetric positive definite matrix, such that:

$$\dot{V}(\boldsymbol{x}) + \boldsymbol{\zeta}(t)'\boldsymbol{\zeta}(t) - \gamma^2 \boldsymbol{d}(t)'\boldsymbol{d}(t) < 0 \,, \tag{3.66}$$

where $\dot{V}(\boldsymbol{x})$ is the time derivative of $V(\boldsymbol{x})$ for all trajectories of the system. If $V(\boldsymbol{x})$ is found and satisfy the condition (3.66), then it satisfies (3.64) and therefore (3.65). The main interest of the previous condition is that it can be expressed as a LMI.

Thus, by using (3.66), by putting the system (3.63) in this formulation, and through the Schur complement and some variable changes, the $\mathscr{H}_\infty$-norm of the

system (3.63) is given by the following optimization problem:

$$\min_{\boldsymbol{Q},\boldsymbol{Y}} \gamma : \begin{cases} \boldsymbol{Q} > \mathbb{0}, \\ \begin{bmatrix} \boldsymbol{A}(\boldsymbol{\delta})\boldsymbol{Q} + \boldsymbol{Q}\boldsymbol{A}(\boldsymbol{\delta})' + \boldsymbol{B_u}(\boldsymbol{\delta})\boldsymbol{Y} + \boldsymbol{Y}'\boldsymbol{B_u}(\boldsymbol{\delta})' & * & * \\ \boldsymbol{B_d}(\boldsymbol{\delta})' & -\gamma \mathbb{1}_{n_z} & * \\ \boldsymbol{C_\zeta}(\boldsymbol{\delta})\boldsymbol{Q} + \boldsymbol{D_{d\zeta}}(\boldsymbol{\delta})\boldsymbol{Y} & \boldsymbol{D_{d\zeta}}(\boldsymbol{\delta}) & -\gamma \mathbb{1}_{n_z} \end{bmatrix} < \mathbb{0} \end{cases} \tag{3.67}$$

where $*$ represents the terms that can be inferred by symmetry. Besides, due to the convexity, the previous LMIs are equivalent to the 2^q LMIs set:

$$\min_{\boldsymbol{Q},\boldsymbol{Y}} \gamma : \begin{cases} \boldsymbol{Q} > \mathbb{0}, \\ \begin{bmatrix} \boldsymbol{A}(\boldsymbol{v_1})\boldsymbol{Q} + \boldsymbol{Q}\boldsymbol{A}(\boldsymbol{v_1})' + \boldsymbol{B_u}(\boldsymbol{v_1})\boldsymbol{Y} + \boldsymbol{Y}'\boldsymbol{B_u}(\boldsymbol{v_1})' & * & * \\ \boldsymbol{B_d}(\boldsymbol{v_1})' & -\gamma \mathbb{1}_{n_z} & * \\ \boldsymbol{C_\zeta}(\boldsymbol{v_1})\boldsymbol{Q} + \boldsymbol{D_{d\zeta}}(\boldsymbol{v_1})\boldsymbol{Y} & \boldsymbol{D_{d\zeta}}(\boldsymbol{v_1}) & -\gamma \mathbb{1}_{n_z} \end{bmatrix} < \mathbb{0} \\ \vdots \\ \begin{bmatrix} \boldsymbol{A}(\boldsymbol{v}_{2^q})\boldsymbol{Q} + \boldsymbol{Q}\boldsymbol{A}(\boldsymbol{v}_{2^q})' + \boldsymbol{B_u}(\boldsymbol{v}_{2^q})\boldsymbol{Y} + \boldsymbol{Y}'\boldsymbol{B_u}(\boldsymbol{v}_{2^q})' & * & * \\ \boldsymbol{B_d}(\boldsymbol{v}_{2^q})' & -\gamma \mathbb{1}_{n_z} & * \\ \boldsymbol{C_\zeta}(\boldsymbol{v}_{2^q})\boldsymbol{Q} + \boldsymbol{D_{d\zeta}}(\boldsymbol{v}_{2^q})\boldsymbol{Y} & \boldsymbol{D_{d\zeta}}(\boldsymbol{v}_{2^q}) & -\gamma \mathbb{1}_{n_z} \end{bmatrix} < \mathbb{0} \end{cases} \tag{3.68}$$

obtained by (3.67) with $\boldsymbol{\delta} = \boldsymbol{v_i}$ for $i = 1, \ldots, 2^q$, where $\boldsymbol{v_i}$ are the vertices of the polytope $\boldsymbol{\Delta}$.

The previous result is summarized in the following theorem:

Theorem 3.4.1. *Consider the linear system (3.62). Assuming that matrices $\boldsymbol{Q} = \boldsymbol{Q}'$, $\boldsymbol{Y}$, with proper dimensions, and the scalar γ are the solution of the optimization problem defined in (3.68).*

Thus, the system (3.63) with $\boldsymbol{K} = \boldsymbol{Y}\boldsymbol{Q}^{-1}$ is asymptotically stable and the $\mathscr{H}_\infty$-norm of the closed-loop system satisfy $\|H_{\boldsymbol{d\zeta}}(s)\|_\infty \leq \sqrt{\gamma}$.

3.4.1.3 Linear $\mathscr{H}_\infty$ Control for the Translational Subsystem

The linear state feedback $\mathscr{H}_\infty$ controller approach presented above is designed to control the altitude and the lateral-longitudinal motions. In the altitude controller, ϕ and θ angles are considered as uncertain parameters, while the xy motion control law is computed for an uncertainty thrust, which in both controllers the uncertain parameters are confined into polytopes with known vertices. The reference of pitch and roll angles are defined through the two virtual inputs computed to follow the desired xy movement, whereas the yaw angle reference is given by the trajectory generator.

The objective of this approach is to guarantee that the UAV follows a previ-

ously defined reference trajectory minimizing the displacement error, even when sustained disturbances are acting on the system. However, due to the fact that the target coordinates vary in time, a virtual reference vehicle with the same *Quad-Rotor* helicopter mathematical model (3.53) is defined on the desired track, that is:

$$\dot{\bar{\boldsymbol{\xi}}}_{\boldsymbol{r}}(t) = f\left(\bar{\boldsymbol{\xi}}_{\boldsymbol{r}}(t), \boldsymbol{u}_{\boldsymbol{\xi r}}(t), \boldsymbol{\delta}_{\boldsymbol{\xi}_r}(t)\right) \tag{3.69}$$

$$\dot{\bar{\boldsymbol{\xi}}}_{\boldsymbol{r}}(t) = f\left(\bar{\boldsymbol{\xi}}_{\boldsymbol{r}}(t), \boldsymbol{u}_{\boldsymbol{\xi r}}(t), \boldsymbol{\delta}_{\boldsymbol{\xi}_r}(t)\right) = \begin{bmatrix} u_{0_r}(t) \\ u_{x_r}(t)\dfrac{T_r(t)}{m} \\ v_{0_r}(t) \\ u_{y_r}(t)\dfrac{T_r(t)}{m} \\ w_{0_r}(t) \\ -g + (\cos\theta(t)\cos\phi(t))\dfrac{T_r(t)}{m} \end{bmatrix},$$

where $\bar{\boldsymbol{\xi}}_{\boldsymbol{r}}(t) = [x_r(t)\ u_{0_r}(t)\ y_r(t)\ v_{0_r}(t)\ z_r(t)\ w_{0_r}(t)]'$ and $\boldsymbol{u}_{\boldsymbol{\xi r}}(t) = [T_r\ u_{x_r}\ u_{y_r}]'$ are the reference states and the control inputs, respectively. Null external disturbances, $\boldsymbol{\delta}_{\boldsymbol{\xi r}}(t) = [0\,0\,0]'$, are assumed in the virtual reference vehicle. This virtual reference vehicle is used to obtain the reference control inputs for translational movements under the assumption that the helicopter attitude has been stabilized by the inner-loop controller. Therefore, for the case of the *QuadRotor* helicopter, the reference values are given by:

$$T_r(t) = m \cdot (\ddot{z}_r(t) + g), \quad u_{x_r}(t) = \frac{\ddot{x}_r(t) \cdot m}{T_r(t)}, \quad u_{y_r}(t) = \frac{\ddot{y}_r(t) \cdot m}{T_r(t)}\,.$$

where the input control $T_r(t)$ is considered as a time-varying parameter for the reference x and y motions.

By subtracting the virtual reference vehicle (3.69) from the system (3.53), the proposed translational error model is given by:

$$\dot{\tilde{\bar{\boldsymbol{\xi}}}}(t) = \boldsymbol{A}(t) \cdot \tilde{\bar{\boldsymbol{\xi}}}(t) + \boldsymbol{B_u}(t) \cdot \tilde{\boldsymbol{u}}_{\boldsymbol{\xi}}(t) + \boldsymbol{B_d}(t) \cdot \boldsymbol{\delta}_{\boldsymbol{\xi}}(t)\,. \tag{3.70}$$

where $\tilde{\bar{\boldsymbol{\xi}}}(t) = \bar{\boldsymbol{\xi}}(t) - \bar{\boldsymbol{\xi}}_{\boldsymbol{r}}(t)$ represents the error vector, and $\tilde{\boldsymbol{u}}_{\boldsymbol{\xi}}(t) = \boldsymbol{u}_{\boldsymbol{\xi}}(t) - \boldsymbol{u}_{\boldsymbol{\xi r}}(t)$ is the control input error. Matrices $\boldsymbol{A}(t)$, $\boldsymbol{B_u}(t)$ and $\boldsymbol{B_d}(t)$ are the Jacobians of the system (3.53) in relation to $\bar{\boldsymbol{\xi}}(t)$, $\boldsymbol{u}_{\boldsymbol{\xi}}(t)$ and $\boldsymbol{\delta}_{\boldsymbol{\xi}}(t)$, respectively, computed around

the operating point $\left(\bar{\boldsymbol{\xi}}_{\boldsymbol{r}}(t), \boldsymbol{u}_{\boldsymbol{\xi}\boldsymbol{r}}(t), \boldsymbol{\delta}_{\boldsymbol{\xi}\boldsymbol{r}}(t)\right)$, and are given by:

$$\boldsymbol{A}(t) = \left.\frac{\partial f(\bar{\boldsymbol{\xi}}(t), \boldsymbol{u}_{\boldsymbol{\xi}}(t), \boldsymbol{\delta}_{\boldsymbol{\xi}}(t))}{\partial \bar{\boldsymbol{\xi}}(t)}\right|_{\substack{\bar{\xi}=\bar{\xi}_r \\ u_\xi = u_{\xi_r} \\ \delta_\xi = 0}}, \quad \boldsymbol{B}_{\boldsymbol{u}}(t) = \left.\frac{\partial f(\bar{\boldsymbol{\xi}}(t), \boldsymbol{u}_{\boldsymbol{\xi}}(t), \boldsymbol{\delta}_{\boldsymbol{\xi}}(t))}{\partial \boldsymbol{u}_{\boldsymbol{\xi}}(t)}\right|_{\substack{\bar{\xi}=\bar{\xi}_r \\ u_\xi = u_{\xi_r} \\ \delta_\xi = 0}}$$

$$\boldsymbol{B}_{\boldsymbol{d}}(t) = \left.\frac{\partial f(\bar{\boldsymbol{\xi}}(t), \boldsymbol{u}_{\boldsymbol{\xi}}(t), \boldsymbol{d}_{\boldsymbol{\xi}}(t))}{\partial \boldsymbol{\delta}_{\boldsymbol{\xi}}(t)}\right|_{\substack{\bar{\xi}=\bar{\xi}_r \\ u_\xi = u_{\xi_r} \\ \delta_\xi = 0}} .$$

On the other hand, by using the error model (3.70) for the control design via state feedback, it would not be possible to reject sustained external disturbance. Therefore, to take it into account, the integral of the position error term has been included in the error vector to perform an appropriate path tracking. Hence, the following augmented error vector is considered:

$$\boldsymbol{x}_{\boldsymbol{\xi}}(t) = \begin{bmatrix} \tilde{x}(t) \\ \tilde{u}_0(t) \\ \int \tilde{x}(t)dt \\ \tilde{y}(t) \\ \tilde{v}_0(t) \\ \int \tilde{y}(t)dt \\ \tilde{z}(t) \\ \tilde{w}_0(t) \\ \int \tilde{z}(t)dt \end{bmatrix} = \begin{bmatrix} x(t) - x_r(t) \\ u_0(t) - u_{0_r}(t) \\ \int (x(t) - x_r(t))dt \\ y(t) - y_r(t) \\ v_0(t) - v_{0_r}(t) \\ \int (y(t) - y_r(t))dt \\ z(t) - z_r(t) \\ w_0(t) - w_{0_r}(t) \\ \int (z(t) - z_r(t))dt \end{bmatrix} . \tag{3.71}$$

Thus, the error model (3.70), considering the augmented state vector $\boldsymbol{x}_{\boldsymbol{\xi}}(t)$ and external disturbance vector $\boldsymbol{\delta}_{\boldsymbol{\xi}}(t)$, is rewritten as follows:

$$\dot{\boldsymbol{x}}_{\boldsymbol{\xi}}(t) = \overline{\boldsymbol{A}}(t) \cdot \boldsymbol{x}_{\boldsymbol{\xi}}(t) + \overline{\boldsymbol{B}}_{\boldsymbol{u}}(t) \cdot \widetilde{\boldsymbol{u}}_{\boldsymbol{\xi}}(t) + \overline{\boldsymbol{B}}_{\boldsymbol{d}}(t) \cdot \boldsymbol{\delta}_{\boldsymbol{\xi}}(t) . \tag{3.72}$$

Since the error model (3.72) does not present any coupling between the states, it can be split up into two subsystems: the height error and the xy-motion error.

Therefore, these two subsystems can be expressed in the following form:

$$\dot{\boldsymbol{x}}_{\boldsymbol{\xi}_z}(t) = \overline{\boldsymbol{A}}_z \cdot \boldsymbol{x}_{\boldsymbol{\xi}_z}(t) + \overline{\boldsymbol{B}}_{\boldsymbol{u}_z}(t) \cdot \widetilde{T}(t) + \overline{\boldsymbol{B}}_{\boldsymbol{d}_z} \cdot \boldsymbol{\delta}_{\boldsymbol{\xi}_z}(t), \tag{3.73}$$

$$\dot{\boldsymbol{x}}_{\boldsymbol{\xi}_{xy}}(t) = \overline{\boldsymbol{A}}_{\boldsymbol{xy}} \cdot \boldsymbol{x}_{\boldsymbol{\xi}_{xy}}(t) + \overline{\boldsymbol{B}}_{\boldsymbol{u}_{xy}}(t) \cdot \widetilde{\boldsymbol{u}}_{\boldsymbol{\xi}_{xy}}(t) + \overline{\boldsymbol{B}}_{\boldsymbol{d}_{xy}} \cdot \boldsymbol{\delta}_{\boldsymbol{\xi}_{xy}}(t), \tag{3.74}$$

where matrices $\overline{\boldsymbol{A}}$, $\overline{\boldsymbol{B}}_{\boldsymbol{u}}$ and $\overline{\boldsymbol{B}}_{\boldsymbol{d}}$ for each subsystem are the following:

$$\overline{\boldsymbol{A}}_{\boldsymbol{z}} = \begin{bmatrix} 0 & 1 & 0 \\ 0 & 0 & 0 \\ 1 & 0 & 0 \end{bmatrix}, \quad \overline{\boldsymbol{B}}_{\boldsymbol{u}_z}(\boldsymbol{\delta}_{\boldsymbol{z}}(t)) = \begin{bmatrix} 0 \\ \frac{1}{m}\cos\theta(t)\cos\phi(t) \\ 0 \end{bmatrix}, \quad \overline{\boldsymbol{B}}_{\boldsymbol{d}_z} = \begin{bmatrix} 0 \\ \frac{1}{m} \\ 0 \end{bmatrix}, \tag{3.75}$$

$$\overline{\boldsymbol{A}}_{\boldsymbol{xy}} = \begin{bmatrix} 0 & 1 & 0 & 0 & 0 & 0 \\ 0 & 0 & 0 & 0 & 0 & 0 \\ 1 & 0 & 0 & 0 & 0 & 0 \\ 0 & 0 & 0 & 0 & 1 & 0 \\ 0 & 0 & 0 & 0 & 0 & 0 \\ 0 & 0 & 0 & 1 & 0 & 0 \end{bmatrix},$$

$$\overline{\boldsymbol{B}}_{\boldsymbol{u}_{xy}}(\boldsymbol{\delta}_{\boldsymbol{xy}}(t)) = \begin{bmatrix} 0 & 0 \\ \frac{1}{m}T(t) & 0 \\ 0 & 0 \\ 0 & 0 \\ 0 & \frac{1}{m}T(t) \\ 0 & 0 \end{bmatrix}, \quad \overline{\boldsymbol{B}}_{\boldsymbol{d}_{xy}} = \begin{bmatrix} 0 & 0 \\ \frac{1}{m} & 0 \\ 0 & 0 \\ 0 & 0 \\ 0 & \frac{1}{m} \\ 0 & 0 \end{bmatrix}, \tag{3.76}$$

where $\boldsymbol{\delta}_{\boldsymbol{z}}(t) = [\phi(t)\ \theta(t)]'$ and $\boldsymbol{\delta}_{\boldsymbol{xy}}(t) = T(t)$ consist in the uncertain parameter vector for each subsystem.

In the first step of the translational control design, the height controller is carried out. In this application, the values of uncertain parameters are considered inside of a compact set defined by $\boldsymbol{\delta}_{\boldsymbol{z}}(t) \in [-60^\circ, 60^\circ] \times [-60^\circ, 60^\circ]$. Thus, the closed-loop system from the disturbances $\boldsymbol{\delta}_{\boldsymbol{\xi}_z}(t)$ to the so called *cost variable* $\boldsymbol{\zeta}_{\boldsymbol{z}}(t)$ can be written as follows:

$$\begin{cases} \dot{\boldsymbol{x}}_{\boldsymbol{\xi}_z}(t) = \left(\overline{\boldsymbol{A}}_z + \overline{\boldsymbol{B}}_{\boldsymbol{u}_z}(\boldsymbol{\delta}_z(t))\boldsymbol{K}_z\right)\boldsymbol{x}_{\boldsymbol{\xi}_z}(t) + \overline{\boldsymbol{B}}_{\boldsymbol{d}_z}(t) \cdot \boldsymbol{\delta}_{\boldsymbol{\xi}_z}(t) \\ \boldsymbol{\zeta}_z = \left(\boldsymbol{C}_{\zeta_z} + \boldsymbol{D}_{u\zeta_z}\boldsymbol{K}_z\right)\boldsymbol{x}_{\boldsymbol{\xi}_z}(t) + \boldsymbol{D}_{d\zeta_z}\boldsymbol{\delta}_{\boldsymbol{\xi}_z}(t) \end{cases} \tag{3.77}$$

with:

$$\widetilde{T}(t) = \boldsymbol{K}_z \boldsymbol{x}_{\boldsymbol{\xi}_z}(t),$$

being the resulting feedback control law, and $\boldsymbol{C}_{\zeta_z}$, $\boldsymbol{D}_{u\zeta_z}$, and $\boldsymbol{D}_{d\zeta_z}$ the weighting matrices to design $\boldsymbol{K}_z$.

Therefore, from the subsystem (3.73) and using the $\mathscr{H}_\infty$ control design via state feedback for uncertain linear systems through LMIs presented in Section 3.4.1.2, the control law for the height is computed in a robust way. The gain matrix $\boldsymbol{K}_z$ is given by $\boldsymbol{K}_z = \boldsymbol{Y}\boldsymbol{Q}^{-1}$.

Once the error control signal $\widetilde{T}(t)$ has been computed, the control signal $T(t) = \widetilde{T}(t) + T_r(t)$ can be calculated.

The value of $\boldsymbol{\delta}_{xy}(t) = T(t) \in [10 \quad 30]$ Newtons has been considered for the computing of the virtual control law of movements in the xy-plane, assuming the nominal thrust value of $T(t) = mg \approx 22$Newtons . This is the value necessary to get a hovering flight.

The matrix $\boldsymbol{K}_{xy}$ can be computed with the same procedure used for the height control, which yields (Álamo et al., 2006):

$$\boldsymbol{K}_{xy} = \boldsymbol{Y}\boldsymbol{Q}^{-1} .$$

Hence, the error control signals $\tilde{\boldsymbol{u}}_{\boldsymbol{\xi}_{xy}}(t) = [\tilde{u}_x(t) \quad \tilde{u}_y(t)]'$ are obtained by:

$$\widetilde{\boldsymbol{u}}_{\boldsymbol{\xi}_{xy}} = \boldsymbol{K}_{xy}\boldsymbol{x}_{\boldsymbol{\xi}_{xy}}(t) . \tag{3.78}$$

Taking into account this control law, the virtual control inputs are computed as follows:

$$\boldsymbol{u}^{\boldsymbol{c}}_{\boldsymbol{\xi}_{xy}}(t) = \widetilde{\boldsymbol{u}}_{\boldsymbol{\xi}_{xy}}(t) + \boldsymbol{u}_{\boldsymbol{\xi}_{xy_r}}(t) . \tag{3.79}$$

Thus, replacing the desired virtual input control, $\boldsymbol{u}^{\boldsymbol{d}}_{\boldsymbol{\xi}_{xy}}$, with the computed control signal (3.79), the roll and pitch reference angles, ϕ_r and θ_r respectively, are derived using equation (3.56). These references are used by the nonlinear $\mathscr{H}_\infty$ controller to stabilize the rotational subsystem of the helicopter.

The next section presents some simulation results combining the linear $\mathscr{H}_\infty$ controller designed in this section with the nonlinear $\mathscr{H}_\infty$ controller synthesized for the rotational motion of the *QuadRotor* helicopter.

3.4.1.4 Simulation Results

Simulations combining the translational linear $\mathscr{H}_\infty$ controller presented above with the nonlinear $\mathscr{H}_\infty$ one for the rotational subsystem, discussed on Section

3.3.2, have been performed making use of the first trajectory reference described in Section 3.2.

The altitude and lateral-longitudinal control laws have been computed by means of the *Linear Matrix Inequalities Toolbox* provided by MATLAB, with the following values of the weighting matrices:

$$\boldsymbol{C}_{\zeta_z} = \begin{bmatrix} 2 & 0 & 0 \\ 0 & 1 & 0 \\ 0 & 0 & 3 \end{bmatrix}, \quad \boldsymbol{D}_{u\zeta_z} = \begin{bmatrix} 0 \\ 0.5 \\ 0.1 \end{bmatrix}, \quad \boldsymbol{D}_{d\zeta_z} = \begin{bmatrix} 0 \\ 1 \\ 1.5 \end{bmatrix},$$

$$\boldsymbol{C}_{\zeta_{xy}}(\delta(t)) = \begin{bmatrix} 2 & 0 & 0 & 0 & 0 & 0 \\ 0 & 0.5 & 0 & 0 & 0 & 0 \\ 0 & 0 & 3.5 & 0 & 0 & 0 \\ 0 & 0 & 0 & 2 & 0 & 0 \\ 0 & 0 & 0 & 0 & 0.5 & 0 \\ 0 & 0 & 0 & 0 & 0 & 3.5 \end{bmatrix},$$

$$\boldsymbol{D}_{u\zeta_{xy}}(\delta(t)) = \begin{bmatrix} 0 & 0 \\ 5 & 0 \\ 2 & 0 \\ 0 & 0 \\ 0 & 5 \\ 0 & 2 \end{bmatrix}, \quad \boldsymbol{C}_{d\zeta_{xy}}(\delta(t)) = \begin{bmatrix} 0 & 0 \\ 1 & 0 \\ 1 & 0 \\ 0 & 0 \\ 0 & 1 \\ 0 & 1 \end{bmatrix}.$$

The minimum value achieved of the attenuation level for the altitude controller was $\gamma_z = 1.8060$, while for the xy-motion controller was $\gamma_{xy} = 1.4175$. The following matrices have been obtained:

$$\mathbf{K_z} = [-48.1799 \quad -46.7945 \quad -34.7074],$$

$$\mathbf{K_{xy}} = \begin{bmatrix} -2.3144 & -1.0567 & -2.0393 & 0 & 0 & 0 \\ 0 & 0 & 0 & -2.3144 & -1.0567 & -2.0393 \end{bmatrix},$$

The nonlinear $\mathscr{H}_\infty$ controller gains were tuned with the following values: $\omega_1 = 0.1$, $\omega_2 = 5$, $\omega_3 = 9$, and $\omega_u = 0.5$.

Figs. 3.5 to 3.9 show the simulation results of the path tracking for the *Quad-Rotor* helicopter. These results illustrate the robust performance provided by the controllers in the case of parametric uncertainty in the inertia and mass terms, and structural uncertainty due to the displacement of the mass center. Moreover, the proposed control strategy was able to reject all the sustained disturbances that

affect the whole system.

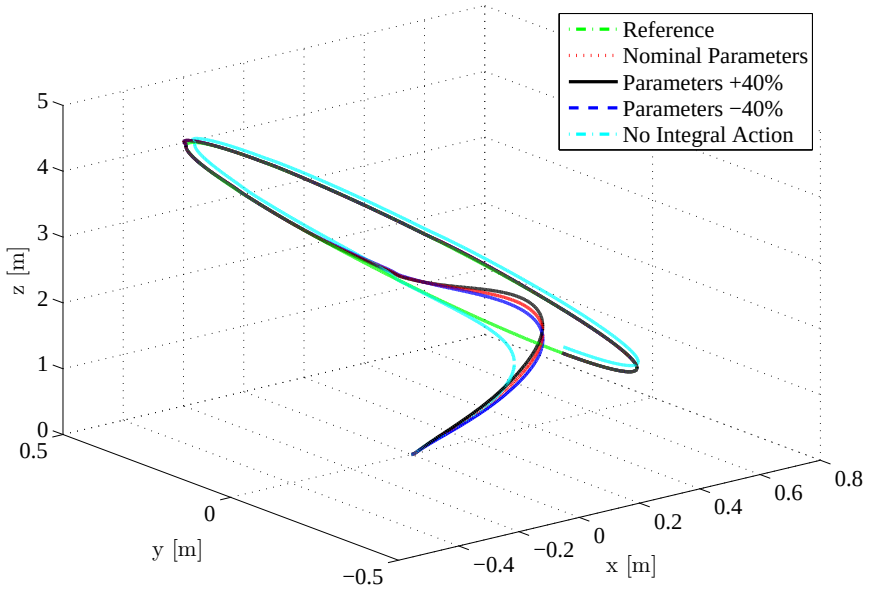

Figure 3.5: Path tracking.

Figs. 3.6 and 3.7 illustrate the time evolution of the translational motion and its error. The control strategy guided the vehicle smoothly. Moreover, the controllers provided null steady-state error in both translational and rotational motions. An additional simulation collection has been presented to show the improvement achieved with the use of the integral action in the control laws. It can be observed that when the weight of the integral action was settled null, the control strategy was not able to reject the sustained disturbances.

In Figs. 3.8 and 3.9 are presented the temporal response of the Euler angles and their errors. It can be noted that the inner-loop controller controls the rotational movements quickly, which guarantees the cascade strategy assumption made before.

In this section a robust control strategy to solve the path tracking problem for a *QuadRotor* helicopter has been presented. A robust control based on the nonlinear $\mathscr{H}_\infty$ theory has been used for the stabilization of the rotation subsystem of the helicopter, while a linear $\mathscr{H}_\infty$ controller has been designed to perform path tracking in the Euclidean space. Besides, the $\mathscr{H}_\infty$ controllers robustness has been checked under uncertainty in the mass and inertia terms and in presence of

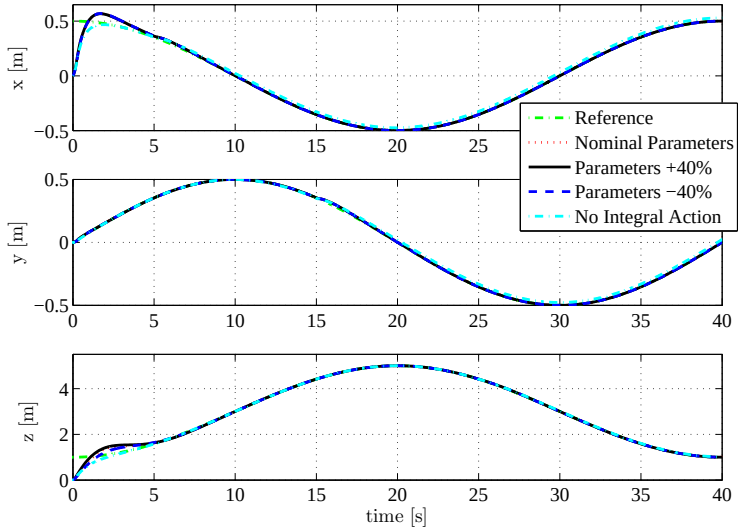

Figure 3.6: Position (x, y, z).

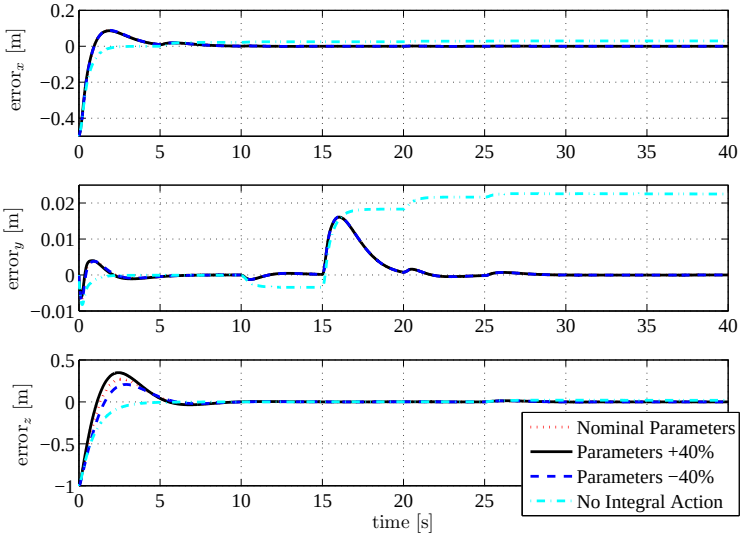

Figure 3.7: Position error (x, y, z).

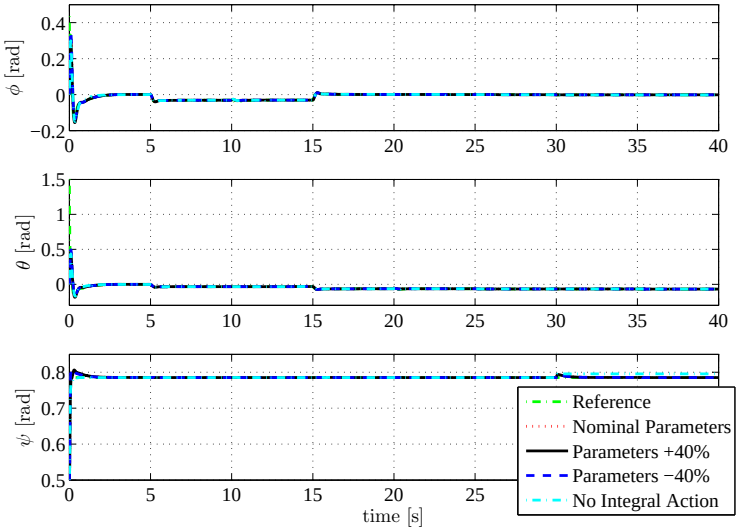

Figure 3.8: Orientation (ϕ, θ, ψ).

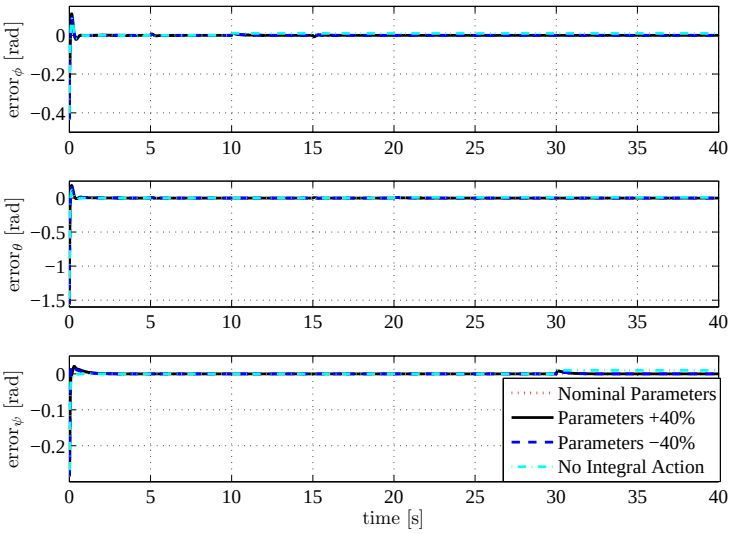

Figure 3.9: Orientation error (ϕ, θ, ψ).

persistent aerodynamic forces and moments.

3.4.2 Model Predictive Control

In this section, a linear predictive controller based on the translational subsystem model (3.53) is proposed to solve the path tracking problem for the *QuadRotor* helicopter, which is used in the cascade control structure described at the beginning of this chapter. As in the control strategy presented in the previous section, the nonlinear $\mathscr{H}_\infty$ controller, presented in Section 3.3.2, is used to stabilize the system through the rotational movements. This control strategy was presented firstly in Raffo et al. (2008b), but in that work, the control strategy was only able to reject sustained disturbances acting on the rotational subsystem. To improve the performance, the integral of the translational position error has been included into the error vector, which makes possible to consider sustained external disturbances on the six degrees of freedom. This work has been published in Raffo et al. (2010c).

The predictive control, used to perform the path tracking for the *QuadRotor* helicopter, makes use of a linear state-space MPC strategy based on the error model. As commented before, two controllers are synthesized for the translational subsystem: one for the altitude, and other for the *xy*-motion.

In what follows, a brief explanation about the state space MPC method is given and, after that, the controllers are presented.

3.4.2.1 Linear State Space Predictive Control

By considering a known reference in any future instant of the trajectory, it is possible, by means of successive linearization along the reference trajectory, to obtain a linear and time varying model of the system. Thus, assuming that all states are accessible, the time varying and discrete state space model used by the algorithm to obtain the predictions is given by:

$$\boldsymbol{x}(k+1) = \boldsymbol{A}(k) \cdot \boldsymbol{x}(k) + \boldsymbol{B}(k) \cdot \boldsymbol{u}(k)\,. \tag{3.80}$$

Therefore, considering this system, the prediction horizon, N_2, and the control horizon, N_u, the system's state predictions $\widehat{\boldsymbol{x}}(k+j|k)$[2] are described as follows

[2]The notation $(k+j|k)$ means prediction in $k+j$ with the information in k.

(Rossiter, 2003):

$$\widehat{\boldsymbol{x}} = \boldsymbol{P}(k|k) \cdot \boldsymbol{x}(k|k) + \boldsymbol{H}(k|k) \cdot \widehat{\boldsymbol{u}} \,, \tag{3.81}$$

with

$$\widehat{\boldsymbol{x}} \triangleq \begin{bmatrix} \boldsymbol{x}(k+1|k) \\ \boldsymbol{x}(k+2|k) \\ \vdots \\ \boldsymbol{x}(k+N_2-1|k) \\ \boldsymbol{x}(k+N_2|k) \end{bmatrix}, \quad \widehat{\boldsymbol{u}} \triangleq \begin{bmatrix} \boldsymbol{u}(k|k) \\ \boldsymbol{u}(k+1|k) \\ \vdots \\ \boldsymbol{u}(k+N_u-2|k) \\ \boldsymbol{u}(k+N_u-1|k) \end{bmatrix}.$$

The matrices $\boldsymbol{P}(k|k)$ and $\boldsymbol{H}(k|k)$, when $N_2 = N_u$, can be written in the following form:

$$\boldsymbol{P}(k|k) \triangleq \begin{bmatrix} \boldsymbol{A}(k|k) \\ \boldsymbol{A}(k|k)\boldsymbol{A}(k+1|k) \\ \vdots \\ \alpha(k,0,2) \\ \alpha(k,0,1) \end{bmatrix},$$

$$\boldsymbol{H}(k|k) \triangleq \begin{bmatrix} \boldsymbol{B}(k|k) & 0 & \cdots & 0 \\ \boldsymbol{A}(k+1|k)\cdot\boldsymbol{B}(k|k) & \boldsymbol{B}(k+1|k) & \cdots & 0 \\ \vdots & \vdots & \ddots & \vdots \\ \alpha(k,1,2)\cdot\boldsymbol{B}(k|k) & \alpha(k,2,2)\cdot\boldsymbol{B}(k+1|k) & \cdots & 0 \\ \alpha(k,1,1)\cdot\boldsymbol{B}(k|k) & \alpha(k,2,1)\cdot\boldsymbol{B}(k+1|k) & \cdots & \boldsymbol{B}(k+N_u-1|k) \end{bmatrix}$$

where $\alpha(k,j,l)$ is defined by:

$$\alpha(k,j,l) \triangleq \prod_{i=j}^{N_2-l} \boldsymbol{A}(k+i|k) \,. \tag{3.82}$$

When the prediction horizon is higher than the control one ($N_2 > N_u$), matrix $\boldsymbol{H}(k|k) \in \Re^{N_2 \times N_u}$ must be rewritten, where the terms of the remaining columns are added to the terms of the last column (N_u-th column), that is, column terms of $N_u + 1$ until $N_u = N_2$.

These prediction equations do not consider the disturbance model in an explicit form. However, an integral action can be included in the model to guarantee null error in steady state by the following form:

$$\widehat{\boldsymbol{u}} = -\boldsymbol{K}(\widehat{\boldsymbol{x}} - \widehat{\boldsymbol{x}}_{\boldsymbol{r}}) + \widehat{\boldsymbol{u}}_{\boldsymbol{r}} \,, \tag{3.83}$$

where $\widehat{\boldsymbol{x}}_{\boldsymbol{r}}$ and $\widehat{\boldsymbol{u}}_{\boldsymbol{r}}$ are, respectively, the reference values of the states and control computed off-line, and are defined as follows:

$$\widehat{\boldsymbol{x}}_{\boldsymbol{r}} \triangleq \begin{bmatrix} \boldsymbol{x_r}(k+1|k) \\ \boldsymbol{x_r}(k+2|k) \\ \vdots \\ \boldsymbol{x_r}(k+N_2-1|k) \\ \boldsymbol{x_r}(k+N_2|k) \end{bmatrix}, \quad \widehat{\boldsymbol{u}}_{\boldsymbol{r}} \triangleq \begin{bmatrix} \boldsymbol{u_r}(k|k) \\ \boldsymbol{u_r}(k+1|k) \\ \vdots \\ \boldsymbol{u_r}(k+N_u-2|k) \\ \boldsymbol{u_r}(k+N_u-1|k) \end{bmatrix}.$$

By using the prediction equation (3.81) and considering that the reference states and the reference control signals are known, it can be ensured that the minimum of the following cost function, in a quadratic norm shape:

$$\begin{aligned} J &= \sum_{j=1}^{N_2} \|\widehat{\boldsymbol{x}}(k+j|k) - \widehat{\boldsymbol{x}}_{\boldsymbol{r}}(k+j|k)\|^2_{\boldsymbol{Q}} + \sum_{j=0}^{N_u-1} \|\widehat{\boldsymbol{u}}(k+j|k) - \widehat{\boldsymbol{u}}_{\boldsymbol{r}}(k+j|k)\|^2_{\boldsymbol{R}} \\ &\quad + \Omega\left(\widehat{\boldsymbol{x}}(k+\boldsymbol{N_2}|k) - \widehat{\boldsymbol{x}}_{\boldsymbol{r}}(k+\boldsymbol{N_2}|k)\right). \end{aligned} \tag{3.84}$$

is consistent with zero tracking error (Rossiter, 2003). $\boldsymbol{Q}$ and $\boldsymbol{R}$ are diagonal positive definite weighting matrices, and Ω is the terminal state cost defined by:

$$\Omega\left(\widehat{\boldsymbol{x}}(k+\boldsymbol{N_2}|k) - \widehat{\boldsymbol{x}}_{\boldsymbol{r}}(k+\boldsymbol{N_2}|k)\right) =$$

$$\left[\widehat{\boldsymbol{x}}(k+\boldsymbol{N_2}|k) - \widehat{\boldsymbol{x}}_{\boldsymbol{r}}(k+\boldsymbol{N_2}|k)\right]' \boldsymbol{S} \left[\widehat{\boldsymbol{x}}(k+\boldsymbol{N_2}|k) - \widehat{\boldsymbol{x}}_{\boldsymbol{r}}(k+\boldsymbol{N_2}|k)\right]$$

, with $\boldsymbol{S} \geq 0$.

The cost function (3.84) can be optimized by the following form:

$$\begin{aligned} \min_{\widehat{\boldsymbol{u}}} J &= \left[\widehat{\boldsymbol{x}} - \widehat{\boldsymbol{x}}_{\boldsymbol{r}}\right]' \boldsymbol{Q} \left[\widehat{\boldsymbol{x}} - \widehat{\boldsymbol{x}}_{\boldsymbol{r}}\right] + \left[\widehat{\boldsymbol{u}} - \widehat{\boldsymbol{u}}_{\boldsymbol{r}}\right]' \boldsymbol{R} \left[\widehat{\boldsymbol{u}} - \widehat{\boldsymbol{u}}_{\boldsymbol{r}}\right] \\ &\quad + \Omega\left(\widehat{\boldsymbol{x}}(k+\boldsymbol{N_2}|k) - \widehat{\boldsymbol{x}}_{\boldsymbol{r}}(k+\boldsymbol{N_2}|k)\right). \end{aligned} \tag{3.85}$$

which penalizes deviations from the steady-state value. This fact differs from the GPC (Generalized Predictive Control) cost function, because optimizes the distance from the inputs to the steady-state value, instead of the control input incremental.

Asymptotic stability is guaranteed for the cost function (3.85) if the trajectory reference is constant and no constraints are considered (see Rawlings and Mayne (2009)). However, if the path to be followed varies on time, only asymptotic

convergence can be guaranteed.

In the absence of constraints on the states and on the control signals, the control law can be obtained in an algebraic form, by minimizing the cost function (3.85), which turns out to be a state feedback, given by:

$$\widehat{\boldsymbol{u}} = \left[\boldsymbol{H}' \cdot \boldsymbol{Q} \cdot \boldsymbol{H} + \boldsymbol{R}\right]^{-1} \cdot \left[\boldsymbol{H}' \cdot \boldsymbol{Q} \cdot (\widehat{\boldsymbol{x}}_{\boldsymbol{r}} - \boldsymbol{P} \cdot \boldsymbol{x}(k)) + \boldsymbol{R} \cdot \widehat{\boldsymbol{u}}_{\boldsymbol{r}}\right] . \tag{3.86}$$

Due to the receding horizon property of the MPC, only $\boldsymbol{u}(k)$ is needed at each instant k (Camacho and Bordons, 1998).

This predictive control algorithm is used in the next section to design two controllers for the translational motion based on the discrete version of the error model obtained in Section 3.4.1.3.

3.4.2.2 Error based State Space Predictive Controller (E-SSPC) For Path Tracking

The objective of this approach is to obtain a linear control law that leads dynamically the error between a real vehicle and a virtual reference one to zero. So that, a linear state-space MPC strategy based on the error model is performed.

Since the aerodynamic forces are assumed as external disturbances, they are not considered at the control design stage. Thus, by using Euler's method (e.g., $\dot{\tilde{x}}(t) = \frac{\tilde{x}[(k+1)\Delta t] - \tilde{x}(k\Delta t)}{\Delta t}$), the system (3.72) is discretized and the following model is obtained:

$$\boldsymbol{x}_{\boldsymbol{\xi}}(k+1) = \bar{\boldsymbol{A}} \cdot \boldsymbol{x}_{\boldsymbol{\xi}}(k) + \bar{\boldsymbol{B}}(k) \cdot \widetilde{\boldsymbol{u}}_{\boldsymbol{\xi}}(k) . \tag{3.87}$$

which is time-varying and linear.

As performed for the linear $\mathscr{H}_\infty$ controller, to compute the predictive controller based on the error model (3.87), this system can be split up into two subsystems taking into account that the translational dynamics depend only on the thrust, T: the height error and the xy motions error. Thus, matrices $\bar{\boldsymbol{A}}$ and $\bar{\boldsymbol{B}}$ for each subsystem are written in the discrete-time domain as follows:

$$\bar{\boldsymbol{A}}_{\boldsymbol{z}} = \begin{bmatrix} 1 & \Delta t & 0 \\ 0 & 1 & 0 \\ \Delta t & 0 & 1 \end{bmatrix} , \bar{\boldsymbol{B}}_{\boldsymbol{z}}(k) = \begin{bmatrix} 0 \\ \frac{\Delta t}{m} \cos\theta(k) \cos\phi(k) \\ 0 \end{bmatrix} , \tag{3.88}$$

$$\bar{\boldsymbol{A}}_{\boldsymbol{xy}} = \begin{bmatrix} 1 & \Delta t & 0 & 0 & 0 & 0 \\ 0 & 1 & 0 & 0 & 0 & 0 \\ \Delta t & 0 & 1 & 0 & 0 & 0 \\ 0 & 0 & 0 & 1 & \Delta t & 0 \\ 0 & 0 & 0 & 0 & 1 & 0 \\ 0 & 0 & 0 & \Delta t & 0 & 1 \end{bmatrix}, \bar{\boldsymbol{B}}_{\boldsymbol{xy}}(k) = \begin{bmatrix} 0 & 0 \\ \frac{\Delta t}{m} T(k) & 0 \\ 0 & 0 \\ 0 & 0 \\ 0 & \frac{\Delta t}{m} T(k) \\ 0 & 0 \end{bmatrix}, \quad (3.89)$$

where Δt is the sampling time, which has been chosen sufficiently small to capture all translational motion error dynamic and high enough to consider the rotational closed-loop dynamics in steady state. As the control signal is updated only at $t_k = k\Delta t$ instants of time, being k the number of sample, these sequences are denoted by the simplified form $\boldsymbol{x}_{\boldsymbol{\xi}}(k) = \boldsymbol{x}_{\boldsymbol{\xi}}(k\Delta t)$ and $\widetilde{\boldsymbol{u}}_{\boldsymbol{\xi}}(k) = \widetilde{\boldsymbol{u}}_{\boldsymbol{\xi}}(k\Delta t)$.

Based on this analysis, the path tracking problem for a UAV can be understood as:

Find the control inputs in a bounded group of possible values that drive the state variables in (3.87) from an initial position $\boldsymbol{x}_{\boldsymbol{\xi}_0}$ to the origin (Sun, 2005)*, i.e.:*

$$\lim_{t \to \infty} \boldsymbol{x}_{\boldsymbol{\xi}} = 0.$$

Therefore, from the height and longitudinal-lateral error models the control laws can be designed in such a way that the system is forced to track the reference trajectory. The first law computes the control input T in such a way that the following cost function is minimized:

$$\begin{aligned} J_z = &\left[\widehat{\boldsymbol{x}}_{\boldsymbol{\xi}_z} - \widehat{\boldsymbol{x}}_{\boldsymbol{\xi}_{zr}}\right]' \boldsymbol{Q}_z \left[\widehat{\boldsymbol{x}}_{\boldsymbol{\xi}_z} - \widehat{\boldsymbol{x}}_{\boldsymbol{\xi}_{zr}}\right] + \left[\widehat{\widetilde{\boldsymbol{u}}}_{\boldsymbol{\xi}_z} - \widehat{\widetilde{\boldsymbol{u}}}_{\boldsymbol{\xi}_{zr}}\right]' \boldsymbol{R}_z \left[\widehat{\widetilde{\boldsymbol{u}}}_{\boldsymbol{\xi}_z} - \widehat{\widetilde{\boldsymbol{u}}}_{\boldsymbol{\xi}_{zr}}\right] \\ &+ \Omega \left(\widehat{\boldsymbol{x}}_{\boldsymbol{\xi}_z}(k + \boldsymbol{N}_{2_z}|k) - \widehat{\boldsymbol{x}}_{\boldsymbol{\xi}_{zr}}(k + \boldsymbol{N}_{2_z}|k)\right). \end{aligned} \quad (3.90)$$

The height reference vectors are:

$$\widehat{\boldsymbol{x}}_{\boldsymbol{\xi}_{zr}} \triangleq \begin{bmatrix} \boldsymbol{x}_{\boldsymbol{\xi}_{zr}}(k+1|k) - \boldsymbol{x}_{\boldsymbol{\xi}_{zr}}(k|k) \\ \boldsymbol{x}_{\boldsymbol{\xi}_{zr}}(k+2|k) - \boldsymbol{x}_{\boldsymbol{\xi}_{zr}}(k|k) \\ \vdots \\ \boldsymbol{x}_{\boldsymbol{\xi}_{zr}}(k + \boldsymbol{N}_{2_z} - 1|k) - \boldsymbol{x}_{\boldsymbol{\xi}_{zr}}(k|k) \\ \boldsymbol{x}_{\boldsymbol{\xi}_{zr}}(k + \boldsymbol{N}_{2_z}|k) - \boldsymbol{x}_{\boldsymbol{\xi}_{zr}}(k|k) \end{bmatrix},$$

$$\widehat{\widetilde{\boldsymbol{u}}}_{\boldsymbol{\xi}_{z_r}} \triangleq \begin{bmatrix} T_r(k|k) - T_r(k-1|k) \\ T_r(k+1|k) - T_r(k-1|k) \\ \vdots \\ T_r(k+\boldsymbol{N}_{\boldsymbol{u}_z} - 2|k) - T_r(k-1|k) \\ T_r(k+\boldsymbol{N}_{\boldsymbol{u}_z} - 1|k) - T_r(k-1|k) \end{bmatrix}.$$

The system's state predictions (3.81), for the altitude subsystem, are computed using the linear time-varying state-space model of the vehicle (3.87) with (3.88), obtaining:

$$\widehat{\boldsymbol{x}}_{\boldsymbol{\xi}_z} = \boldsymbol{P}_{\boldsymbol{z}}(k|k) \cdot \boldsymbol{x}_{\boldsymbol{\xi}_z}(k|k) + \boldsymbol{H}_{\boldsymbol{z}}(k|k) \cdot \widehat{\widetilde{\boldsymbol{u}}}_{\boldsymbol{\xi}_z}, \tag{3.91}$$

where $\widetilde{u}_{\xi_z}(k|k) = T(k) - T_r(k)$, and $\boldsymbol{x}_{\boldsymbol{\xi}_z}(k)$ is the height state error vector. As only matrix $\bar{\boldsymbol{B}}_{\boldsymbol{z}}$ is time-varying, matrices $\boldsymbol{P}_{\boldsymbol{z}}$ and $\boldsymbol{H}_{\boldsymbol{z}}$ can be rewritten as follows:

$$\boldsymbol{P}_z \triangleq \begin{bmatrix} \bar{\boldsymbol{A}}_z \\ \bar{\boldsymbol{A}}_z^2 \\ \vdots \\ \bar{\boldsymbol{A}}_z^{(N_2-1)} \\ \bar{\boldsymbol{A}}_z^{N_2} \end{bmatrix}, \tag{3.92}$$

$$\boldsymbol{H}_{\boldsymbol{z}}(k|k) \triangleq$$

$$\begin{bmatrix} \bar{\boldsymbol{B}}_z(k|k) & 0 & 0 & \cdots & 0 \\ \bar{\boldsymbol{A}}_z\bar{\boldsymbol{B}}_z(k|k) & \bar{\boldsymbol{B}}_z(k+1|k) & 0 & \cdots & 0 \\ \bar{\boldsymbol{A}}_z^2\bar{\boldsymbol{B}}_z(k|k) & \bar{\boldsymbol{A}}_z\bar{\boldsymbol{B}}_z(k+1|k) & \bar{\boldsymbol{B}}_z(k+2|k) & \cdots & 0 \\ \vdots & \vdots & \vdots & \ddots & \vdots \\ \bar{\boldsymbol{A}}_z^{(N_2-1)}\bar{\boldsymbol{B}}_z(k|k) & \bar{\boldsymbol{A}}_z^{(N_2-2)}\bar{\boldsymbol{B}}_z(k+1|k) & \bar{\boldsymbol{A}}_z^{(N_2-3)}\bar{\boldsymbol{B}}_z(k+2|k) & \cdots & \bar{\boldsymbol{A}}_z^{(N_2-N_u)}\bar{\boldsymbol{B}}_z(k+N_u-1|k) + \boldsymbol{\beta}(k,j) \end{bmatrix} \tag{3.93}$$

with $\boldsymbol{\beta}(k,j)$ given by:

$$\boldsymbol{\beta}(k,j) = \begin{cases} \mathbb{0} & \text{if } N_u = N_2 \\ \sum_{j=1}^{N_2-N_u} \bar{\boldsymbol{A}}^{(N_2-(N_u+j))}\bar{\boldsymbol{B}}(k+(N_u+j)-1) & \text{if } N_u < N_2 \end{cases} \tag{3.94}$$

By minimizing the equation (3.90) in the case where no constraints are con-

sidered, the control law can be obtained by:

$$\widehat{\widetilde{\boldsymbol{u}}}_{\xi_z} = \left[\boldsymbol{H}_z'\boldsymbol{Q}_z\boldsymbol{H}_z + \boldsymbol{R}_z\right]^{-1} \cdot \left[\boldsymbol{H}_z'\boldsymbol{Q}_z\left(\widehat{\boldsymbol{x}}_{\xi_{z_r}} - \boldsymbol{P}_z\boldsymbol{x}_{\xi_z}(k)\right) + \boldsymbol{R}_z\widehat{\widetilde{\boldsymbol{u}}}_{\xi_{z_r}}\right] . \tag{3.95}$$

As commented before, from the computed sequence of control actions, only $\widetilde{u}_{\xi_z}(k|k)$ is needed at each instant k (Camacho and Bordons, 1998; Rossiter, 2003; Rawlings and Mayne, 2009; Mayne et al., 2000). Thus, the following control signal is applied to the helicopter: $T(k) = \widetilde{u}_{\xi_z}(k|k) + T_r(k)$.

The second control law computes the x and y motion control inputs. If the same previous procedure is carried out using the error model (3.87) with (3.89), the following control signal is obtained:

$$\widehat{\widetilde{\boldsymbol{u}}}_{\xi_{xy}} = \left[\boldsymbol{H}_{xy}'\boldsymbol{Q}_{xy}\boldsymbol{H}_{xy} + \boldsymbol{R}_{xy}\right]^{-1} \cdot \left[\boldsymbol{H}_{xy}'\boldsymbol{Q}_{xy}\left(\widehat{\boldsymbol{x}}_{\xi_{xy_r}} - \boldsymbol{P}_{xy}\boldsymbol{x}_{\xi_{xy}}(k)\right) + \boldsymbol{R}_{xy}\widehat{\widetilde{\boldsymbol{u}}}_{\xi_{xy_r}}\right] , \tag{3.96}$$

where $\widetilde{\boldsymbol{u}}_{\xi_{xy}}(k|k) = [\tilde{u}_x(k|k) \quad \tilde{u}_y(k|k)]'$ and, in the same way as in equation (3.79):

$$\boldsymbol{u}^c_{\xi_{xy}}(k) = \widetilde{\boldsymbol{u}}_{\xi_{xy}}(k|k) + \boldsymbol{u}_{\xi_{xy_r}}(k) \tag{3.97}$$

$$\begin{bmatrix} u^c_x(k) \\ u^c_y(k) \end{bmatrix} = \begin{bmatrix} \tilde{u}_x(k|k) \\ \tilde{u}_y(k|k) \end{bmatrix} + \begin{bmatrix} u_{x_r}(k) \\ u_{y_r}(k) \end{bmatrix} . \tag{3.98}$$

The reference vectors of the error states, $\widehat{\boldsymbol{x}}_{\xi_{xy_r}}$, and the error control inputs, $\widehat{\widetilde{\boldsymbol{u}}}_{\xi_{xy_r}}$, are obtained by the same way as the one of the height controller case.

Thereby, substituting the desired virtual input value from the computed one obtained with equation (3.98), the roll and pitch reference angles, ϕ_r and θ_r respectively, are derived using equation (3.56). These references are necessary for the helicopter inner-loop controller.

3.4.2.3 Simulation Results

As performed on Section 3.4.1.3, the nonlinear $\mathscr{H}_\infty$ controller, designed to stabilize the helicopter, is combined with the proposed error based state-space controller. The first reference path presented in the simulation protocol is also used in this section to corroborate the effectiveness of the control strategy.

The E-SSPC parameters were adjusted as follows:

$$\boldsymbol{N}_{\boldsymbol{2}_z} = \boldsymbol{N}_{\boldsymbol{u}_z} = 3\boldsymbol{I}_{n_z},\ \boldsymbol{Q}_z = \mathrm{diag}(2, 0.8, 15),\ R_z = 0.03\,,$$

$$\boldsymbol{N}_{\boldsymbol{2}_{xy}} = \boldsymbol{N}_{\boldsymbol{u}_{xy}} = 10\boldsymbol{I}_{n_{xy}},$$

$$\boldsymbol{Q}_{xy} = \mathrm{diag}(26, 35, 20, 26, 35, 20),\ \boldsymbol{R}_{xy} = \mathrm{diag}(150, 150)\,.$$

The nonlinear $\mathscr{H}_\infty$ controller gains were tuned with the following values: $\omega_1 = 0.1$, $\omega_2 = 5$, $\omega_3 = 9$ and $\omega_u = 0.5$.

Figs. 3.10 to 3.14 show the simulation results of the path tracking of this reference trajectory. The way in which the helicopter follows the reference for different vehicle parameters is presented in Figs. 3.10 (in the 3D space) and 3.11.

It can be seen how, starting from an initial position far from the reference, the proposed control strategy is able to make the vehicle to follow the reference trajectory. In addition, the vehicle trajectory in the case of no integral action considered in the control strategy, is also presented in this figure. It can be clearly observed that, in this last case, the vehicle leaves the trajectory of reference when a disturbance is introduced, and it never reaches the reference again.

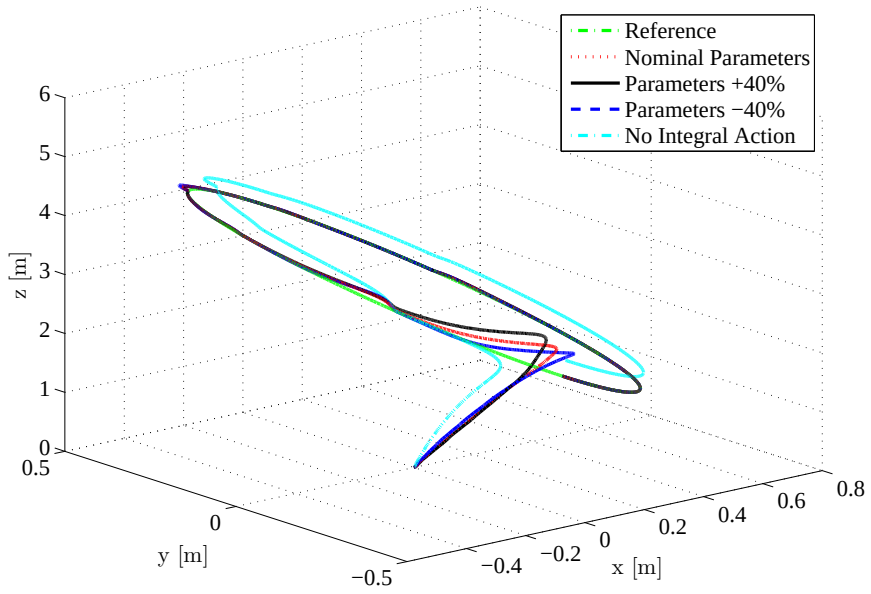

Figure 3.10: Path tracking.

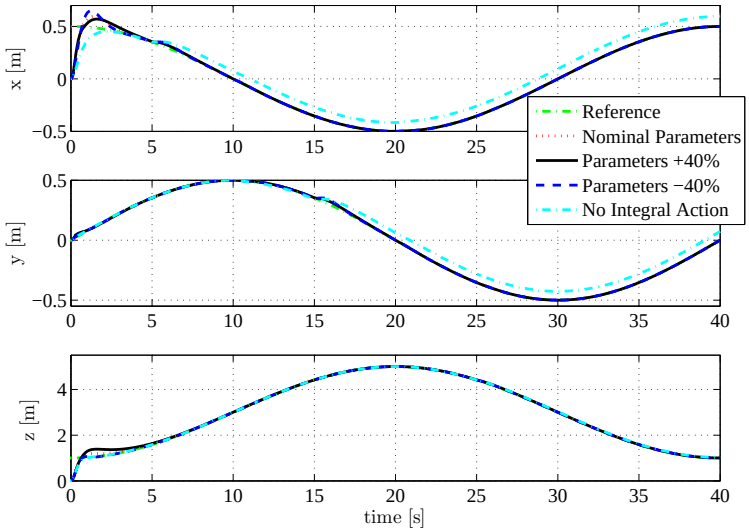

Figure 3.11: Position (x, y, z).

Fig. 3.12 shows the translational coordinates errors. It can be seen that null steady-state error is achieved for all coordinates, even if structural uncertainty is considered in the vehicle. Besides, this figure also shows that a null steady-state error is not obtained in case that no integral action is included in the controller synthesis.

The way the inner nonlinear $\mathscr{H}_\infty$ controller makes the vehicle tracking its rotational references is presented in Figs. 3.13 and 3.14. It can be observed how much highly-coupled the system is, since each degree of freedom is affected by the disturbances applied to the whole helicopter. The first figure shows how the references generated by the (E-SSPC) translational controller, i.e. ϕ_r and θ_r, vary in its attainment of an appropriate performance in the translational loop. As an emphasis, Fig. 3.14 corroborates the fact that null steady-state error is also achieved for the inner-loop variables, unless in the case of no integral action is considered by the inner-loop controller.

In this section, an integral and robust nonlinear $\mathscr{H}_\infty$ control strategy to solve the path tracking problem for a *QuadRotor* helicopter has been presented. This proposed control strategy has also been corroborated under consideration of external disturbances acting on all degrees of freedom, parametric and structural uncertainties. The predictive controller used for the translational movements has provided a good and smooth performance in the reference tracking.

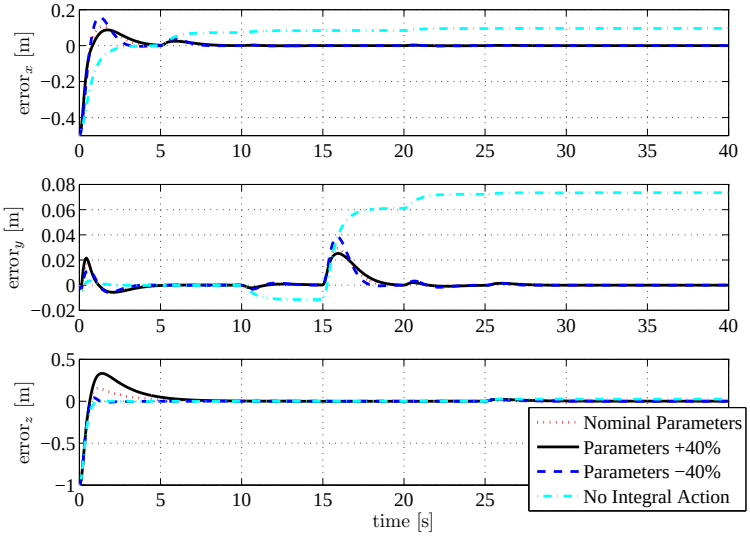

Figure 3.12: Position error (x, y, z).

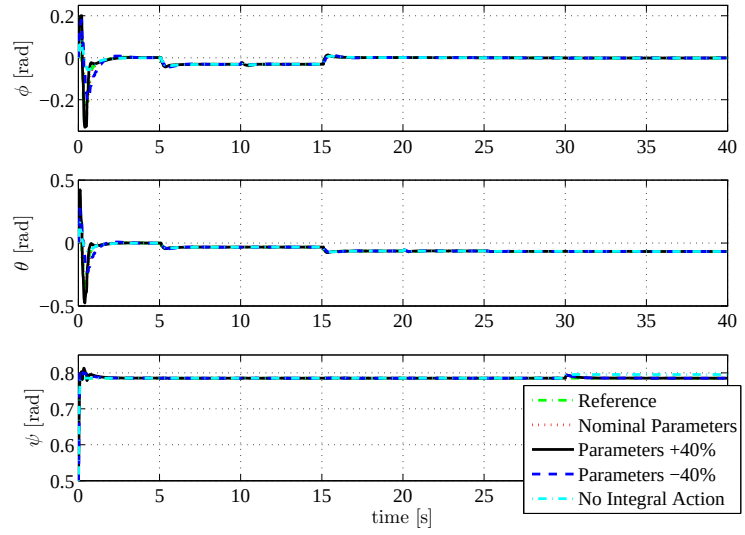

Figure 3.13: Orientation (ϕ, θ, ψ).

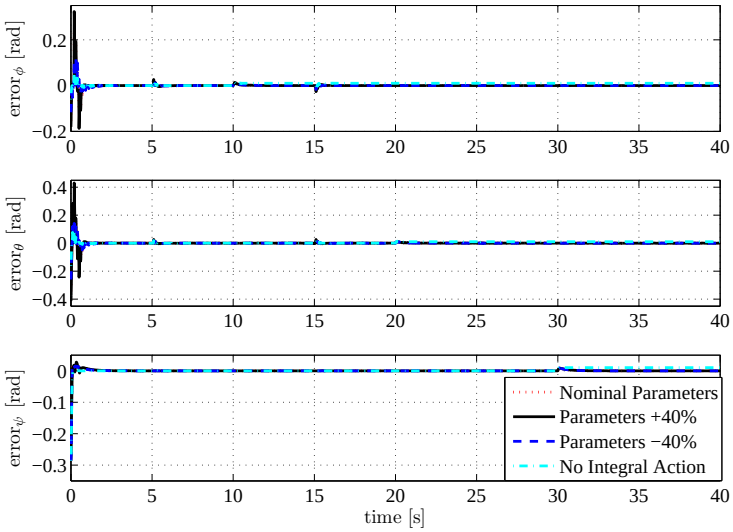

Figure 3.14: Orientation error (ϕ, θ, ψ).

3.4.3 Backstepping Control Approach

In this section, a backstepping approach is presented to solve the path tracking problem for the *QuadRotor* helicopter, controlling the translational motion. As in the two translational controllers described before, the *xyz*-motion is divided in the altitude and lateral-longitudinal subsystems. The second one makes use of the control signal, T, as a time-varying parameter, which is generated by the altitude controller. An advantageous of the controller exposed in this section when compared with the linear $\mathscr{H}_\infty$ controller and the MPC is that, now, it does not depend on the linearized error model, since it makes use of the translational subsystem (3.53).

The control strategy combining the backstepping control, for the translational movements, with the nonlinear $\mathscr{H}_\infty$ one, for stabilization, applied to the *QuadRotor* helicopter, was published in Raffo et al. (2008a). However, this control strategy was able to treat only with maintained winds affecting the stabilization loop. But a helicopter can be subject to external disturbances like wind gusts or, in the worst case, sustained winds in all degrees of freedom. Hence why, a modification in the standard backstepping methodology is introduced to deal with these kind of disturbances, where the integral action is considered. The control strategy considering the integral action of position error in both backstepping and

nonlinear $\mathscr{H}_\infty$ controllers was presented in Raffo et al. (2010d). As well known, the inclusion of the integral action allows to remove constant steady-state offsets in closed-loop, besides to enable the path tracking in presence of sustained disturbances, unmodeled dynamics and parameters deviations (Skjetne and Fossen, 2004).

The use of integral action in the backstepping technique was first proposed by Kanellakopoulos and Krein (1993). The most common way to include integral action in this approach is to use parameter adaptation (Krstic et al., 1995). An analysis of different techniques using integral action in the backstepping approach was carried out by Skjetne and Fossen (2004), where another two methods that consist in the augmentation of the system dynamic with the integral state were presented.

In the following, the backstepping formulation is presented, which is used to generate the altitude and lateral-longitudinal control laws.

3.4.3.1 Backstepping control with integral action for path tracking

Consider a nonlinear system given by:

$$\begin{cases} \dot{\boldsymbol{x}}_1 = f_1(\boldsymbol{x}_1) + g_1(\boldsymbol{x}_1)\boldsymbol{x}_2 \\ \dot{\boldsymbol{x}}_2 = f_2(\boldsymbol{x}_1, \boldsymbol{x}_2) + g_2(\boldsymbol{x}_1, \boldsymbol{x}_2)\boldsymbol{u} + \boldsymbol{d} \end{cases}, \tag{3.99}$$

where $\boldsymbol{x}_1$ and $\boldsymbol{x}_2$ are the state vectors, $\boldsymbol{u}$ is the control input vector, $\boldsymbol{d}$ is an unknown sustained disturbance vector and the functions f_1, f_2, g_1 and g_2 are smooth. Moreover, g_1 and g_2 are nonsingular for all $\boldsymbol{x}_1$, $\boldsymbol{x}_2$, and all variables are of the same dimension.

First of all, the backstepping state transformation is considered:

$$\begin{aligned} \widetilde{\boldsymbol{x}}_1 &= \boldsymbol{x}_1 - \boldsymbol{x}_r(t)\,, \\ \widetilde{\boldsymbol{x}}_2 &= \boldsymbol{x}_2 - \boldsymbol{\alpha}(\widetilde{\boldsymbol{x}}_1, t)\,, \end{aligned} \tag{3.100}$$

where $\boldsymbol{\alpha}(\widetilde{\boldsymbol{x}}_1, t)$ is a virtual control and $\boldsymbol{x}_r(t)$ is a reference signal. The goal of this approach is to solve the tracking problem $lim_{t\to\infty}\widetilde{\boldsymbol{x}}_1(t) = 0$.

The integral term $\boldsymbol{\vartheta}(t) = \int_0^t \widetilde{\boldsymbol{x}}_2(\tau)d\tau$ is considered in the second step of the backstepping approach. As commented in Skjetne and Fossen (2004), this method guarantees convergence for constant or time-varying reference signals, what might not be guaranteed for a generic plant when the integral action is added in the first step of this control design.

Then, for the plant (3.99), the system for the first step is given by:

$$\dot{\widetilde{\boldsymbol{x}}}_{\boldsymbol{1}} = f_1(\widetilde{\boldsymbol{x}}_{\boldsymbol{1}} + \boldsymbol{x_r}(t)) + g_1(\widetilde{\boldsymbol{x}}_{\boldsymbol{1}} + \boldsymbol{x_r}(t))\widetilde{\boldsymbol{x}}_{\boldsymbol{2}} + g_1(\widetilde{\boldsymbol{x}}_{\boldsymbol{2}} + \boldsymbol{x_r}(t))\boldsymbol{\alpha}(\widetilde{\boldsymbol{x}}_{\boldsymbol{1}}, t) - \dot{\boldsymbol{x}}_{\boldsymbol{r}}(t)\,. \quad (3.101)$$

Using the Lyapunov theorem under the consideration of $V_1(\widetilde{\boldsymbol{x}}_{\boldsymbol{1}}, t)$ is positive definite and its time derivative is negative semidefinite, the first Lyapunov function is chosen as:

$$V_1(\widetilde{\boldsymbol{x}}_{\boldsymbol{1}}, t) = \frac{1}{2}\widetilde{\boldsymbol{x}}_{\boldsymbol{1}}'\widetilde{\boldsymbol{x}}_{\boldsymbol{1}}\,. \quad (3.102)$$

Its time derivative becomes:

$$\dot{V}_1(\widetilde{\boldsymbol{x}}_{\boldsymbol{1}}, t) = \widetilde{\boldsymbol{x}}_{\boldsymbol{1}}'\dot{\widetilde{\boldsymbol{x}}}_{\boldsymbol{1}}\,. \quad (3.103)$$

The virtual control, $\boldsymbol{\alpha}(\widetilde{\boldsymbol{x}}_{\boldsymbol{1}}, t)$, is defined as follows:

$$\boldsymbol{\alpha}(\widetilde{\boldsymbol{x}}_{\boldsymbol{1}}, t) = g_1(\widetilde{\boldsymbol{x}}_{\boldsymbol{1}} + \boldsymbol{x_r}(t))^{-1}[-f_1(\widetilde{\boldsymbol{x}}_{\boldsymbol{1}} + \boldsymbol{x_r}(t)) - \boldsymbol{C_1}\widetilde{\boldsymbol{x}}_{\boldsymbol{1}} + \dot{\boldsymbol{x}}_{\boldsymbol{r}}(t)]\,, \quad (3.104)$$

where $\boldsymbol{C_1} = \boldsymbol{C_1}' > 0$.

Thus, the time derivative of the Lyapunov function can be written as:

$$\dot{V}_1(\widetilde{\boldsymbol{x}}_{\boldsymbol{1}}, t) = -\widetilde{\boldsymbol{x}}_{\boldsymbol{1}}'\boldsymbol{C_1}\widetilde{\boldsymbol{x}}_{\boldsymbol{1}} + \widetilde{\boldsymbol{x}}_{\boldsymbol{1}}' g_1(\widetilde{\boldsymbol{x}}_{\boldsymbol{1}} + \boldsymbol{x_r}(t))\widetilde{\boldsymbol{x}}_{\boldsymbol{2}}\,, \quad (3.105)$$

allowing to proceed the control design, which for $\widetilde{\boldsymbol{x}}_{\boldsymbol{2}} = 0$ it is negative definite.

In the second step the integral action is introduced and the following system is considered:

$$\begin{cases} \dot{\boldsymbol{\vartheta}} &= \widetilde{\boldsymbol{x}}_{\boldsymbol{2}} \\ \dot{\widetilde{\boldsymbol{x}}}_{\boldsymbol{2}} &= f_2(\widetilde{\boldsymbol{x}}_{\boldsymbol{1}} + \boldsymbol{x_r}(t), \widetilde{\boldsymbol{x}}_{\boldsymbol{2}} + \boldsymbol{\alpha}(\widetilde{\boldsymbol{x}}_{\boldsymbol{1}}, t)) + g_2(\widetilde{\boldsymbol{x}}_{\boldsymbol{1}} + \boldsymbol{x_r}(t), \widetilde{\boldsymbol{x}}_{\boldsymbol{2}} \\ & \quad + \boldsymbol{\alpha}(\widetilde{\boldsymbol{x}}_{\boldsymbol{1}}, t))\boldsymbol{u} - \dot{\boldsymbol{\alpha}}(\widetilde{\boldsymbol{x}}_{\boldsymbol{1}}, t) + \boldsymbol{d} \end{cases} \quad (3.106)$$

where (from now on the arguments of the system functions will be omitted):

$$\dot{\boldsymbol{\alpha}}(\widetilde{\boldsymbol{x}}_{\boldsymbol{1}}, t) = \frac{\partial \boldsymbol{\alpha}}{\partial \widetilde{\boldsymbol{x}}_{\boldsymbol{1}}}\dot{\widetilde{\boldsymbol{x}}}_{\boldsymbol{1}} + \frac{\partial \boldsymbol{\alpha}}{\partial t}\,, \quad (3.107)$$

$$\frac{\partial \boldsymbol{\alpha}}{\partial \widetilde{\boldsymbol{x}}_{\boldsymbol{1}}} = g_1^{-1}[-g_1(-f_1 - \boldsymbol{C_1}\widetilde{\boldsymbol{x}}_{\boldsymbol{1}} + \dot{\boldsymbol{x}}_{\boldsymbol{r}}(t))D_{(\widetilde{\boldsymbol{x}}_{\boldsymbol{1}} + \boldsymbol{x_r}(t))}g_1 - D_{(\widetilde{\boldsymbol{x}}_{\boldsymbol{1}} + \boldsymbol{x_r}(t))}f_1 - \boldsymbol{C_1}]\,,$$

$$\frac{\partial \boldsymbol{\alpha}}{\partial t} = g_1^{-1}\left[(-f_1 - \boldsymbol{C_1}\widetilde{\boldsymbol{x}}_{\boldsymbol{1}} + \dot{\boldsymbol{x}}_{\boldsymbol{r}}(t))D_{(\widetilde{\boldsymbol{x}}_{\boldsymbol{1}}+\boldsymbol{x}_{\boldsymbol{r}}(t))}g_1\dot{\boldsymbol{x}}_{\boldsymbol{r}}(t) - D_{(\widetilde{\boldsymbol{x}}_{\boldsymbol{1}}+\boldsymbol{x}_{\boldsymbol{r}}(t))}f_1\dot{\boldsymbol{x}}_{\boldsymbol{r}}(t) + \ddot{\boldsymbol{x}}_{\boldsymbol{r}}(t)\right].$$

A second Lyapunov function is chosen as:

$$V_2(\boldsymbol{\vartheta}, \widetilde{\boldsymbol{x}}_{\boldsymbol{1}}, \widetilde{\boldsymbol{x}}_{\boldsymbol{2}}, t) = V_1 + \frac{1}{2}\boldsymbol{\vartheta}'\boldsymbol{K}_{\boldsymbol{\vartheta}}\boldsymbol{\vartheta} + \frac{1}{2}\widetilde{\boldsymbol{x}}_{\boldsymbol{2}}'\widetilde{\boldsymbol{x}}_{\boldsymbol{2}}, \tag{3.108}$$

where $\boldsymbol{K}_{\boldsymbol{\vartheta}} = \boldsymbol{K}_{\boldsymbol{\vartheta}}{}' > 0$, and its time derivative is given by:

$$\begin{aligned}\dot{V}_2(\boldsymbol{\vartheta}, \widetilde{\boldsymbol{x}}_{\boldsymbol{1}}, \widetilde{\boldsymbol{x}}_{\boldsymbol{1}}, t) &= \dot{V}_1(\widetilde{\boldsymbol{x}}_{\boldsymbol{1}}, t) + \boldsymbol{\vartheta}'\boldsymbol{K}_{\boldsymbol{\vartheta}}\dot{\boldsymbol{\vartheta}} + \widetilde{\boldsymbol{x}}_{\boldsymbol{2}}'\dot{\widetilde{\boldsymbol{x}}}_{\boldsymbol{2}} \\ &= -\widetilde{\boldsymbol{x}}_{\boldsymbol{1}}'\boldsymbol{C_1}\widetilde{\boldsymbol{x}}_{\boldsymbol{1}} + \widetilde{\boldsymbol{x}}_{\boldsymbol{1}}'g_1\widetilde{\boldsymbol{x}}_{\boldsymbol{2}} + \boldsymbol{\vartheta}'\boldsymbol{K}_{\boldsymbol{\vartheta}}\widetilde{\boldsymbol{x}}_{\boldsymbol{2}} + \widetilde{\boldsymbol{x}}_{\boldsymbol{2}}'[f_2 + g_2\boldsymbol{u} - \dot{\boldsymbol{\alpha}}(\widetilde{\boldsymbol{x}}_{\boldsymbol{1}}, t) + \boldsymbol{d}].\end{aligned} \tag{3.109}$$

The computed control law, $\boldsymbol{u}$, is defined as follows:

$$\boldsymbol{u} = g_2^{-1}\left[-f_2 + \dot{\boldsymbol{\alpha}}(\widetilde{\boldsymbol{x}}_{\boldsymbol{1}}, t) - g_1'\widetilde{\boldsymbol{x}}_{\boldsymbol{2}} - \boldsymbol{K}_{\boldsymbol{\vartheta}}\boldsymbol{\vartheta} - \boldsymbol{C_2}\widetilde{\boldsymbol{x}}_{\boldsymbol{2}}\right], \tag{3.110}$$

with $\boldsymbol{C_2} = \boldsymbol{C_2'} > 0$.

From this control law gives:

$$\dot{V}_2(\boldsymbol{\vartheta}, \widetilde{\boldsymbol{x}}_{\boldsymbol{1}}, \widetilde{\boldsymbol{x}}_{\boldsymbol{2}}, t) = -\widetilde{\boldsymbol{x}}_{\boldsymbol{1}}'\boldsymbol{C_1}\widetilde{\boldsymbol{x}}_{\boldsymbol{1}} - \widetilde{\boldsymbol{x}}_{\boldsymbol{2}}'\boldsymbol{C_2}\widetilde{\boldsymbol{x}}_{\boldsymbol{2}} + \widetilde{\boldsymbol{x}}_{\boldsymbol{2}}'\boldsymbol{d}. \tag{3.111}$$

The control law (3.110) can be written in terms of a nonlinear PID with a feedforward action control law as follows:

$$\boldsymbol{u} = -\boldsymbol{K_I}\boldsymbol{\vartheta} - \boldsymbol{K_P}[\boldsymbol{x_1} - \boldsymbol{x_r}(t)] - \boldsymbol{K_D}[\boldsymbol{x_2} - g_1^{-1}(\dot{\boldsymbol{x}}_{\boldsymbol{r}}(t) - f_1)] + \boldsymbol{F_F}, \tag{3.112}$$

where:

$$\begin{aligned}\boldsymbol{K_I} &= g_2^{-1}\boldsymbol{K}_{\boldsymbol{\vartheta}}, \\ \boldsymbol{K_P} &= g_2^{-1}(g_1' + \boldsymbol{C_2}g_1^{-1}\boldsymbol{C_1}), \\ \boldsymbol{K_D} &= g_2^{-1}\boldsymbol{C_2}, \\ \boldsymbol{F_F} &= g_2^{-1}[-f_2 + \dot{\boldsymbol{\alpha}}(\widetilde{\boldsymbol{x}}_{\boldsymbol{1}}, t)],\end{aligned} \tag{3.113}$$

Altitude Control

To design the altitude controller the two last equations of the system (3.53) with the unknown disturbance term $\delta_{\xi_z} \neq 0$ are considered. Besides, due to the *Quad-Rotor* helicopter cascade structure (see Fig. 3.1), the Euler angles are supposed as time-varying parameters.

The first step considers the backstepping state transformation :

$$\begin{aligned} \tilde{x}_{1_z} &= z - z_r(t)\,, \\ \tilde{x}_{2_z} &= w_0 - \alpha_z(\tilde{x}_1, t)\,, \end{aligned} \tag{3.114}$$

where the integral term is $\vartheta_z(t) = \int_0^t \tilde{x}_{2_z}(\tau)d\tau$, and the virtual control, $\alpha_1(\tilde{x}_{1_z}, t)$, is obtained from equation (3.104) for the altitude system as follows:

$$\alpha_z(\tilde{x}_{1_z}, t) = -c_{1_z}\tilde{x}_{1_z} + w_{0_r}(t)\,.$$

Then, the system based on backstepping approach for altitude control is given by:

$$\left\{ \begin{array}{rcl} \dot{\tilde{x}}_{1_z} & = & \tilde{x}_{2_z} + \alpha_z(\tilde{x}_{1_z}, t) \\ \dot{\vartheta}_z & = & \tilde{x}_{2_z} \\ \dot{\tilde{x}}_{2_z} & = & -g + (\cos\phi\cos\theta)\dfrac{T}{m} + \dfrac{\delta_{\xi_z}}{m} - \dot{\alpha}_z(\tilde{x}_{1_z}, t) \end{array} \right. \tag{3.115}$$

where the thrust T, computed through the backstepping approach, is defined as follows:

$$T = \frac{m}{\cos\phi\cos\theta}\left[-k_{\vartheta_z}\vartheta_z - (1 + c_{2_z}c_{1_z})(z - z_r) - (c_{1_z} + c_{2_z})(w_0 - w_{0_r}) + g + \dot{w}_{0_r}\right]. \tag{3.116}$$

Longitudinal and lateral movement control

To compute u_x^c and u_y^c the same backstepping approach is used and the following backstepping transformation is considered:

$$\begin{aligned} \widetilde{\boldsymbol{x}}_{\mathbf{1}_{xy}} &= \boldsymbol{x}_{\mathbf{1}_{xy}} - \boldsymbol{x}_{\boldsymbol{r}_{xy}}(t)\,, \\ \widetilde{\boldsymbol{x}}_{\mathbf{2}_{xy}} &= \boldsymbol{x}_{\mathbf{2}_{xy}} - \boldsymbol{\alpha}_{\boldsymbol{xy}}(\widetilde{\boldsymbol{x}}_{\mathbf{1}_{xy}}, t)\,, \end{aligned} \tag{3.117}$$

where:

$$\boldsymbol{x}_{\mathbf{1}_{xy}} = \begin{bmatrix} x \\ y \end{bmatrix}, \quad \boldsymbol{x}_{\mathbf{2}_{xy}} = \begin{bmatrix} u_0 \\ v_0 \end{bmatrix}, \quad \boldsymbol{\vartheta}_{\boldsymbol{xy}} = \begin{bmatrix} \int_0^t \widetilde{x}_{2_x}(\tau)d\tau \\ \int_0^t \widetilde{x}_{2_y}(\tau)d\tau \end{bmatrix},$$

and the virtual control, $\boldsymbol{\alpha}_{\boldsymbol{xy}}(\widetilde{\boldsymbol{x}}_{\mathbf{1}_{xy}}, t) = [\alpha_x(\widetilde{x}_{1_x}, t) \quad \alpha_y(\widetilde{x}_{1_y}, t)]'$, is obtained from equation (3.104).

Therefore, the control law is given by:

$$\begin{bmatrix} u_x^c \\ u_y^c \end{bmatrix} = \frac{m}{T}\left[-\boldsymbol{K}_{\boldsymbol{\vartheta}_{xy}}\boldsymbol{\vartheta}_{xy} - \left(\mathbb{1} + \boldsymbol{C}_{\boldsymbol{2}_{xy}}\boldsymbol{C}_{\boldsymbol{1}_{xy}}\right)\left(\boldsymbol{x}_{\boldsymbol{1}_{xy}} - \boldsymbol{x}_{\boldsymbol{d}_{xy}}\right) - \right. \\ \left. -\left(\boldsymbol{C}_{\boldsymbol{2}_{xy}} + \boldsymbol{C}_{\boldsymbol{1}_{xy}}\right)\left(\boldsymbol{x}_{\boldsymbol{2}_{xy}} - \dot{\boldsymbol{x}}_{\boldsymbol{d}_{xy}}\right) + \ddot{\boldsymbol{x}}_{\boldsymbol{d}_{xy}}\right], \tag{3.118}$$

where T is assumed non-zero and:

$$\boldsymbol{C}_{\boldsymbol{1}_{xy}} = \begin{bmatrix} c_{1_x} & 0 \\ 0 & c_{1_y} \end{bmatrix}, \quad \boldsymbol{C}_{\boldsymbol{2}_{xy}} = \begin{bmatrix} c_{2_x} & 0 \\ 0 & c_{2_y} \end{bmatrix}, \quad \boldsymbol{K}_{\boldsymbol{\vartheta}_{xy}} = \begin{bmatrix} k_{\vartheta_x} & 0 \\ 0 & k_{\vartheta_y} \end{bmatrix}.$$

Taking into account that the control virtual inputs u_x^c and u_y^c have been obtained to track the path reference in the xy plane, the reference values of ϕ and θ can be computed by the same way used in the previous translational controllers. Thus, by making the control virtual inputs equal to the desired values, $\boldsymbol{u}_{\boldsymbol{xy}}^{\boldsymbol{c}} = \boldsymbol{u}_{\boldsymbol{xy}}^{\boldsymbol{d}}$, the reference of the roll and pitch angles, ϕ_r and θ_r respectively, are derived using equation (3.54). These references are passed to the helicopter rotational loop.

3.4.3.2 Simulation results

The proposed control strategy, using an integral backstepping controller in cascade with a nonlinear $\mathscr{H}_\infty$ controller, has been tested by simulation in order to corroborate the effectiveness to solve the path tracking problem when sustained disturbances affect the whole system. Simulations have been performed again taking into account the simulation protocol presented in Section 3.2.

For the translational motion, the parameters were adjusted as follows: $c_{1_x} = c_{1_y} = 6$, $c_{1_z} = 7$, $c_{2_x} = c_{2_y} = c_{2_z} = 3.5$, $k_{\vartheta_x} = k_{\vartheta_y} = 7$, $k_{\vartheta_z} = 12$. The nonlinear $\mathscr{H}_\infty$ controller gains were tuned with the following values: $\omega_1 = 0.1$, $\omega_2 = 5$, $\omega_3 = 9$ and $\omega_u = 0.5$.

The first reference path used is a circle evolving in the $\Re^3$ Cartesian space.

Figs. 3.15 to 3.18 show the simulation results of the path tracking for the first reference trajectory. They illustrate how, starting from an initial position far from the reference, the proposed control strategy is able to make the *QuadRotor* helicopter follow the reference trajectory.

Figs. 3.16 and 3.17 show the translational coordinates motion. It can be seen that null steady-state error is achieved for all coordinates, even if structural uncertainty and different model parameter values are considered in the vehicle.

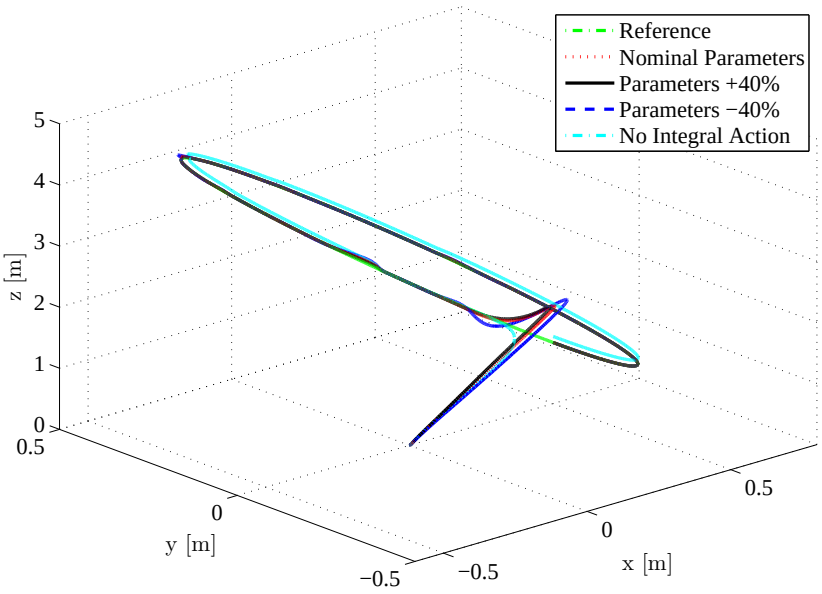

Figure 3.15: Path tracking.

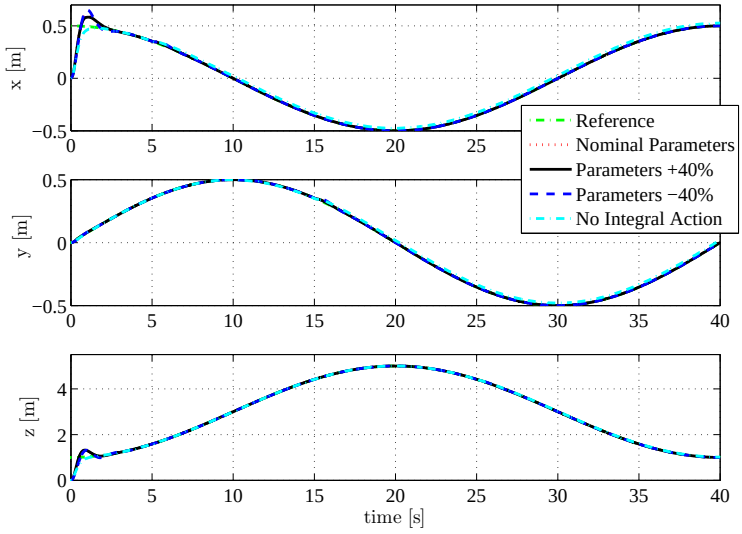

Figure 3.16: Position (x, y, z).

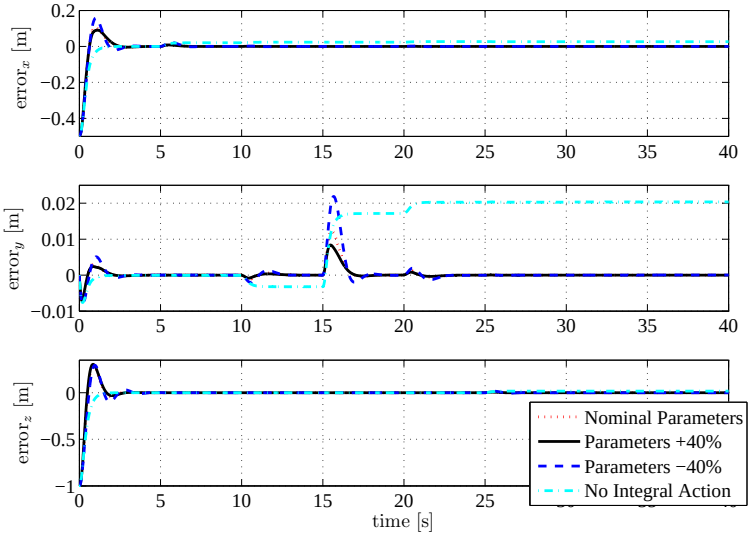

Figure 3.17: Position error (x, y, z).

Besides, the translational controller provides to the *QuadRotor* helicopter a fast and smooth recovery to the reference trajectory when external disturbances affect it.

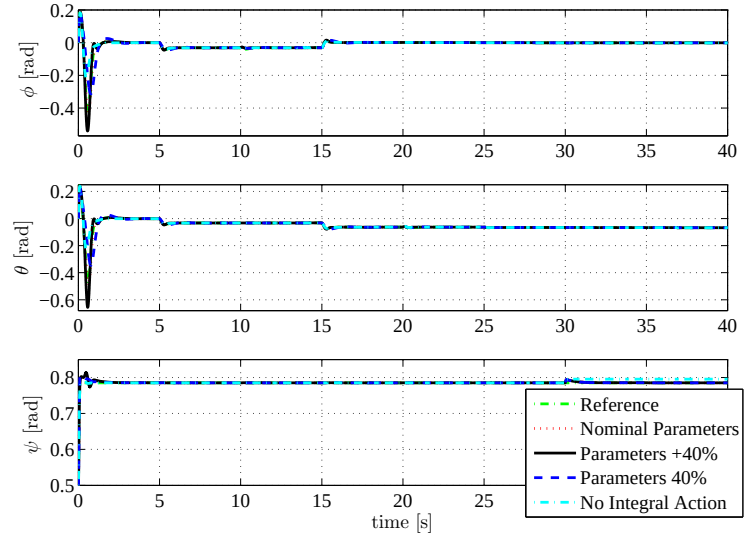

Figure 3.18: Orientation (ϕ, θ, ψ).

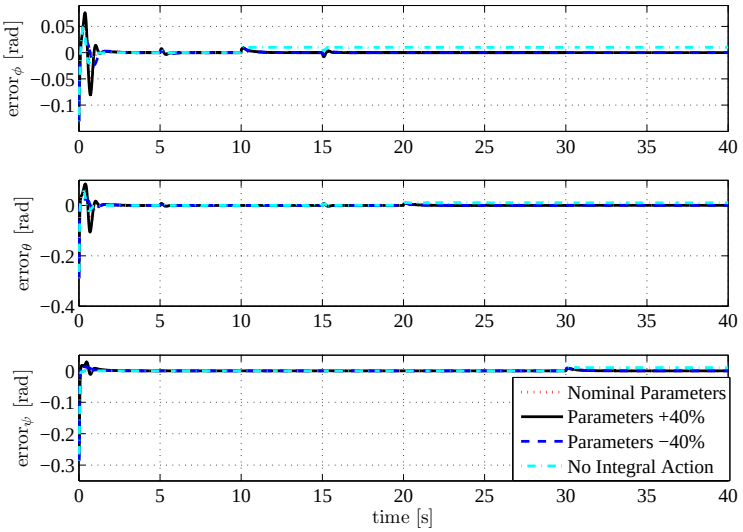

Figure 3.19: Orientation error (ϕ, θ, ψ).

The behavior produced by the nonlinear $\mathscr{H}_\infty$ control law in the rotational motion is showed in Figs. 3.18 and 3.19. It can be observed how that controller reacts when the helicopter is disturbed on the six degrees of freedom. When disturbances affect the translational motion, the rotational controller counter-attack them so quick that its damages are minimum for the inner loop. The first two graphs show how the references generated by the integral backstepping controller (translational motion loop), i.e, ϕ_r and θ_r, varies in its attainment of an appropriate performance in the translational loop. It is due to the system coupling.

In this section a robust control strategy to solve the path tracking problem for a *QuadRotor* helicopter has been presented. The proposed control strategy combines an integral backstepping approach to control the translational movements with a nonlinear $\mathscr{H}_\infty$ controller designated to stabilize the helicopter. This control structure has been designed in consideration of external disturbances, like aerodynamic forces and moments, acting on all degrees of freedom.

3.5 Comparative Simulation Results

This section presents comparison results between the proposed control strategies described in this chapter, where each one will be named as follows, considering the same order that they have appeared in the chapter: L$\mathscr{H}_\infty$-NL$\mathscr{H}_\infty$, MPC-NL$\mathscr{H}_\infty$

and IntBS-NL$\mathscr{H}_\infty$. In addition, simulations comparing these control structures with the one of Bouabdallah and Siegwart (2007) (IntBS) have been performed in order to show the improvements obtained by the proposed strategies. This work proposes an integral backstepping control strategy, which uses the integral term in the first step of the procedure. It has been chosen for the comparison analysis because it is able to present similar performance results, as well as to reject sustained disturbances.

A simulation collection has been carried out with a reference trajectory made up of a set of several kinds of stretches, as commented in Section 3.2. An amount of $+40\%$ of uncertainty in the elements of the mass and the moment of inertia tensor has been considered. The parameters for all control structures have been adjusted to obtain a smooth reference tracking, with a quick disturbance rejection, when it is possible, and a small transient error. The backstepping parameters for the translational controller used in IntBS structure are the same of the integral bascktepping controller presented in Section 3.4.3, while its parameters for the rotational controller have been synthesized to produce a similar behaviour of the nonlinear $\mathscr{H}_\infty$ rotational controller. The simulation results are depicted in Figs. 3.20 to 3.25.

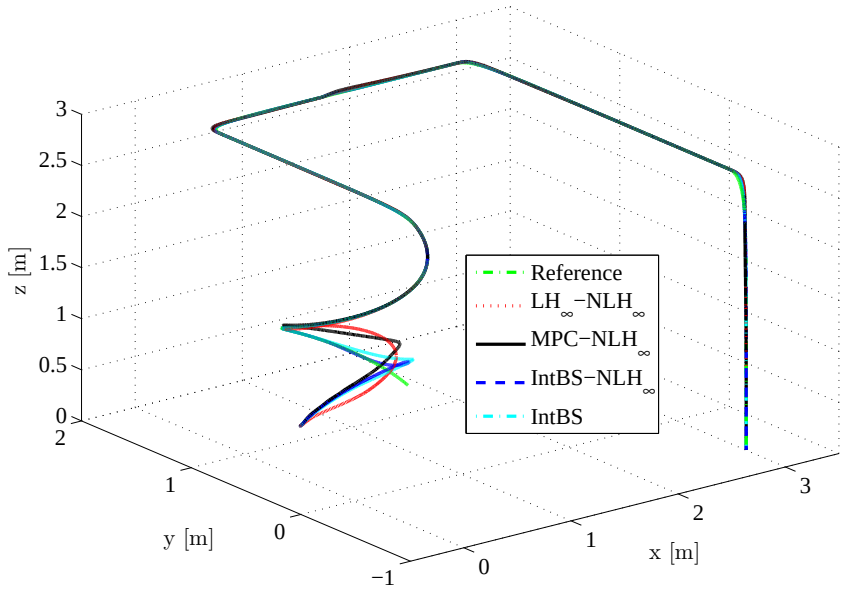

Figure 3.20: Path tracking.

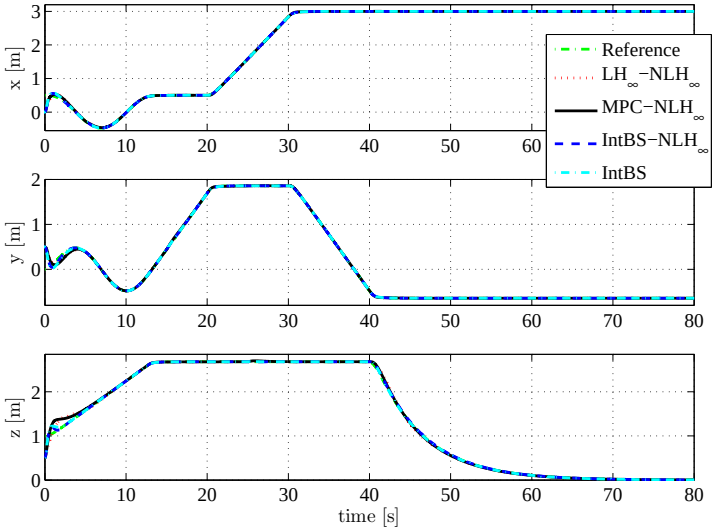

Figure 3.21: Position (x, y, z).

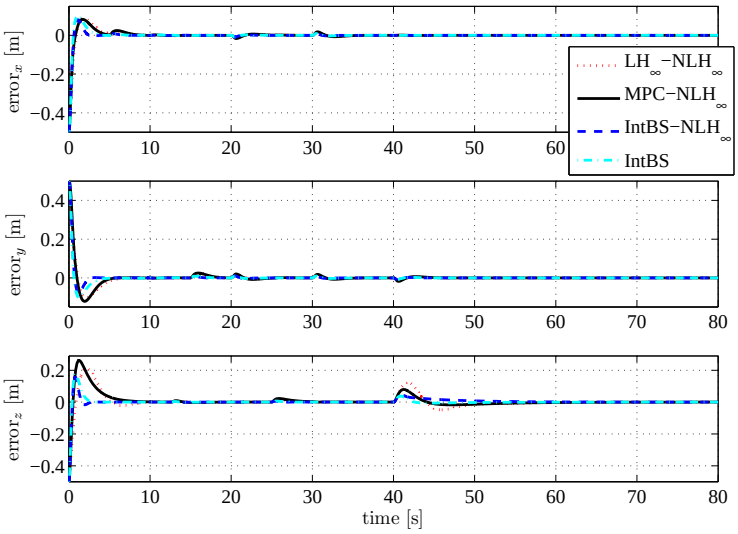

Figure 3.22: Position error (x, y, z).

These figures show that all control strategies present a robust path tracking when abrupt changes of references and sustained disturbances are applied on the whole *QuadRotor* helicopter degrees of freedom. Despite of the faster time response of the translational controllers of both IntBS-NL$\mathscr{H}_\infty$ and IntBS control strategies, it can be clearly observed in Fig. 3.22 that the translational motion response, in the case of the IntBS, converges slower to the reference than the proposed IntBS-NL$\mathscr{H}_\infty$ control strategy. As commented in Skjetne and Fossen (2004), increasing the positive feedbacks gains k_{ϑ_i}, c_{1_i} and c_{2_i} will eventually give stability and convergence, for the backstepping procedure with the integral term in the first step, when $g_1(x_1)$ is constant (see Eq. (3.99)), which is the case for the *QuadRotor* helicopter model. On the other hand, both L$\mathscr{H}_\infty$-NL$\mathscr{H}_\infty$ and MPC-NL$\mathscr{H}_\infty$ control strategies have been provide smoother translational movements.

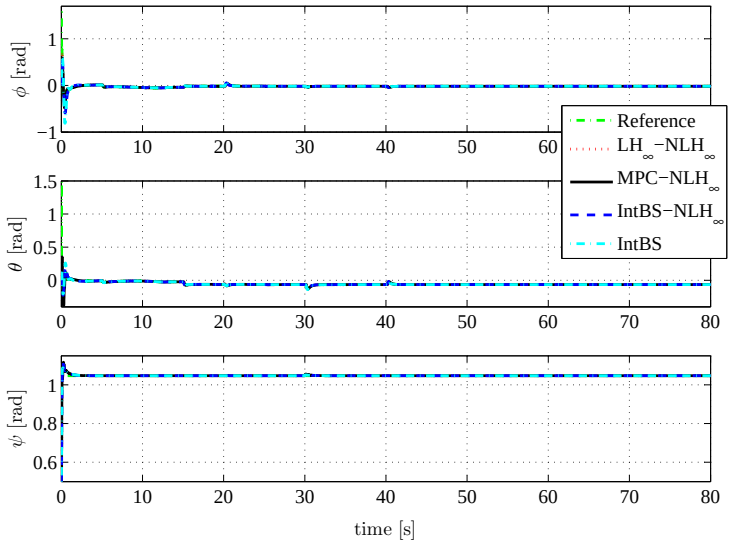

Figure 3.23: Orientation (ϕ, θ, ψ).

In order to make a quantitative comparison of the results attained by these four control strategies, some performance indexes have been computed.

On one hand, the Integral Square Error (ISE) performance indexes obtained from the simulation results are presented in Table 3.1. It can be observed that the performance is improved by the Integral MPC/Nonlinear $\mathscr{H}_\infty$ and Integral Backstepping/Nonlinear $\mathscr{H}_\infty$ control strategies for all states. The difference expressed through the ISE index between these two control strategies can be decreased by an exhaustive adjustment of the controller parameters. These index values cor-

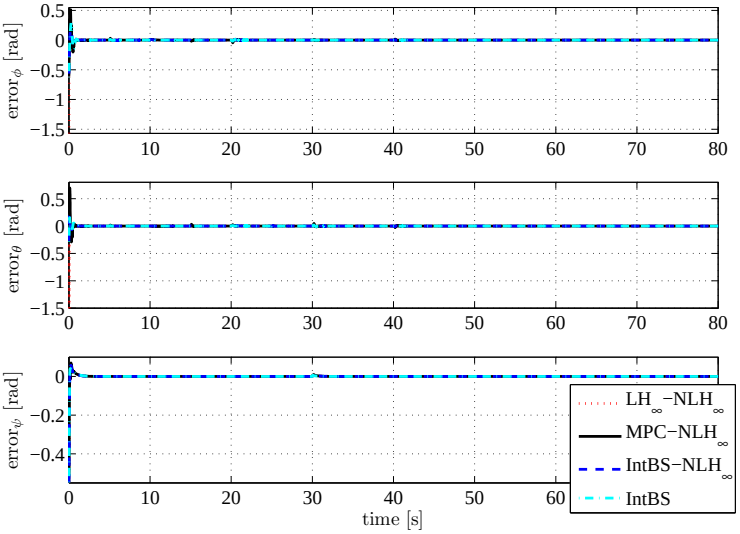

Figure 3.24: Orientation error(ϕ, θ, ψ).

roborate the results presented in Figs. 3.22 and 3.23. On the other hand, it can be observed that, apart from the good performance attained with the L$\mathscr{H}_\infty$-NL $\mathscr{H}_\infty$ control strategy, this control structure have presented the worst ISE index of this comparison analysis. The performance for this control strategy can be improved adjusting its control parameters. However, the linear $\mathscr{H}_\infty$ controller does not present an intuitive adjustment of the parameters when compared with the other ones presented in this chapter, which needs an exhaustive tuning process.

Although higher overshoots in the x and y error responses presented at the beginning of the trajectory for the results obtained with the integral MPC-NL$\mathscr{H}_\infty$ control strategy (see Fig. 3.22), the accumulated error along the path is less than the error achieved by the L$\mathscr{H}_\infty$-NL $\mathscr{H}_\infty$ and IntBS control strategies.

Furthermore, the Integral Absolute Derivative control signal (IADU) index has been computed for all control signals in the four control strategies (depicted in Fig. 3.25). As it is well-known, the use of integral action in a controller allows to obtain null steady-error, however, the control action turns more aggressive. In Table 3.2, when the L$\mathscr{H}_\infty$-NL$\mathscr{H}_\infty$ control strategy is compared with the other structures, it can be observed why this strategy has been obtained higher accumulative errors along the trajectory. This strategy has presented a smooth control signal. However, it is noted that despite of some smoother signals presented by the others strategies, only the IntBs-NL$\mathscr{H}_\infty$ strategy has successfully achieved the

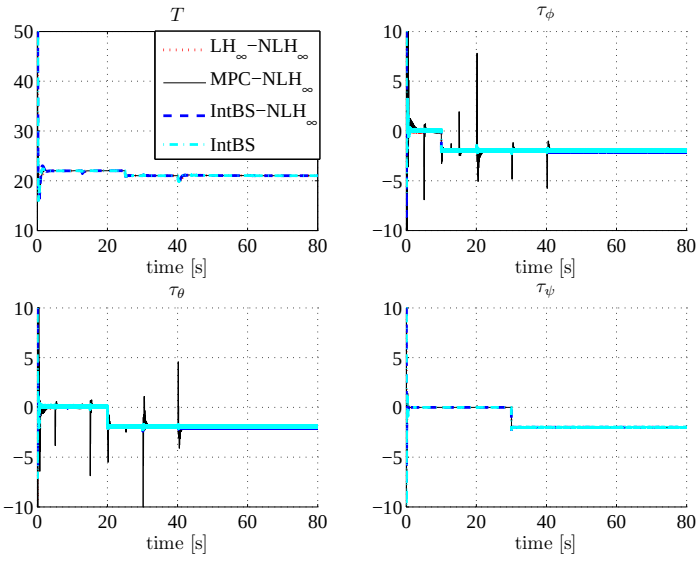

Figure 3.25: Control inputs $(U_1, \tau_{\phi_a}, \tau_{\theta_a}, \tau_{\psi_a})$.

Table 3.1: ISE Index Performance Analysis.

States [Unit Symbol]	**L$\mathscr{H}_\infty$-NL$\mathscr{H}_\infty$**	**MPC-NL$\mathscr{H}_\infty$**	**IntBs-NL$\mathscr{H}_\infty$**	**IntBs**
$x\ [m^2 \cdot s]$	18.9776	12.5464	12.7508	25.2893
$y\ [m^2 \cdot s]$	22.0242	18.3501	14.6774	29.8017
$z\ [m^2 \cdot s]$	31.6255	18.1153	12.3788	25.3689
$\phi\ [rad^2 \cdot s]$	61.5304	7.6366	5.7640	15.7457
$\theta\ [rad^2 \cdot s]$	20.4235	5.4915	1.1897	2.4403
$\psi\ [rad^2 \cdot s]$	8.9350	4.7319	5.5054	6.8851

control objectives, where it has presented the smaller errors along of the trajectory and a faster response than the other ones with very smooth control signals. Moreover, when all the proposed control strategies are compared with the IntBS one, the IADU index values are very similar for the control input T, but for the rotational loop, the proposed controllers have provided smoother control signals.

Table 3.2: IADU Index Performance Analysis.

Control Signals [Unit Symbol]	**L$\mathscr{H}_\infty$-NL$\mathscr{H}_\infty$**	**MPC-NL$\mathscr{H}_\infty$**	**IntBS-NL$\mathscr{H}_\infty$**	**IntBS**
$T\ [N]$	36.7681	40.2395	48.4741	51.9268
$\tau_{\phi_a}\ [N \cdot m]$	297.6354	463.0468	254.6423	1609.7
$\tau_{\theta_a}\ [N \cdot m]$	307.6367	431.3856	261.4491	1645.7
$\tau_{\psi_a}\ [N \cdot m]$	31.1399	56.9412	32.3249	56.2156

3.6 Conclusions

In this chapter three robust control strategies to solve the path tracking problem for a *QuadRotor* helicopter have been proposed. All of them were designed in consideration of external disturbances like aerodynamic forces and moments acting on the six degrees of freedom of the *QuadRotor* helicopter.

A robust control based on nonlinear $\mathscr{H}_\infty$ theory has been developed for the stabilization of the rotational subsystem of the helicopter, which is able to reject sustained disturbances due to the use of the integral action in the state vector. This controller has been combined with three translational controllers.

First, a linear $\mathscr{H}_\infty$ controller has been designed to perform path tracking in the Euclidean space, which is robust in presence of uncertainties of mass and inertia terms. After that, a state-space predictive controller for the translational movements has been proposed for the outer loop, which achieves a good and smooth performance in the reference tracking. In both controllers, to reject sustained disturbances affecting the translational motion, the integral of the position error has been considered in the error model used by these control laws. Lastly, a translational controller has been designed by an integral backstepping procedure, using the integral term in its second step. This controller guarantees stability and convergence of the tracking error for a generic plant when a maintained disturbance affects the system and the reference signal is time-varying. A comparison with other integral backstepping controller using the integral term in the first step has been provided, and it has confirmed the improvement of the approach used in this chapter.

The robustness, the smoothness and the predictive features of the proposed control strategies have been corroborated by simulations, where parametric and structural uncertainties, and unmodeled dynamics, besides sustained disturbances,

have been taken into account.

The results have presented an excellent tracking for different classes of trajectories, and have illustrated the robust performance provided by the nonlinear $\mathscr{H}_\infty$ inner controller in the case of parametric uncertainties in the inertia terms. Moreover, the use of integral action in the inner and outer loop controllers has provided the capability to deal with sustained disturbances when all degrees of freedom are affected by this kind of perturbation in different moments of time.

Finally, to show the improvements achieved by the proposed control strategies, a comparative analysis among the proposed ones and other recent controller has been carried out by means of the ISE and IADU performance indexes.

CHAPTER 4

Underactuated Nonlinear $\mathscr{H}_\infty$ Control

Contents

4.1 Introduction

In this chapter, control laws for underactuated mechanical systems are proposed, where the main goal is to develop controllers to solve the path tracking problem of the *QuadRotor* helicopter considering the overall behavior in the nonlinear $\mathscr{H}_\infty$ controller design. Moreover, a control structure is presented without the necessity of cascade strategies. In addition, other applications are also considered to corroborate the effectiveness of the proposed control strategies.

Control design for underactuated mechanical systems is a big challenge in automatic control area. Furthermore, despite the considerable effort to minimizing system errors, this problem is considerably increased due to uncertainties, that

are usually present and may have significant effects. The sources of uncertainties can be unmodeled dynamics, exogenous disturbances, parameter estimation errors and noise. Thus, apart from the difficulty of controlling underactuated mechanical systems because they have fewer control inputs than degrees of freedom, an additional question is whether the proposed control law possesses desirable rejection properties even without assuming perfect models.

As discussed in Chapter 3, a usual approach to deal with system imperfections on the control design stage is the $\mathscr{H}_\infty$ control theory (van der Schaft, 2000), whose aim is to achieve a bounded ratio between the energy of the cost variable and the energy of external disturbance signals. In general, the nonlinear approach of this theory considers a Hamilton-Jacobi partial differential equation. As commented before, the main problem in this approach is the lack of a general method to solve this HJ PDE. Hence, solutions have to be found for each particular case. As seen in Section 3.3.1.3, by applying game theory to formulate the nonlinear $\mathscr{H}_\infty$ control, a constant gain, similar to the results obtained with feedback linearization procedures, is provided by an analytical solution. An explicit global parameterized solution to this problem, formulated as a *min-max* game, was developed in Chen et al. (1994) for the particular case of fully actuated mechanical systems formulated via Euler-Lagrange equations by using the state tracking error equation proposed in Johansson (1990). This controller was modified in Feng and Postlethwaite (1994) given more degrees of freedom to the control design and, *a posteriori*, these works were improved in Ortega et al. (2005), being this last one discussed in Section 3.3.2.

In Siqueira and Terra (2004b) a nonlinear $\mathscr{H}_\infty$ control for underactuated manipulators, as an extension of the one proposed by Chen et al. (1994), was presented. Nonetheless, this result presents some important restrictions, such as the assumption of null-average disturbances and an exact robot model. In Raffo et al. (2007b), this controller, considering underactuated mechanical systems, was modified taking into account the error vector with the integral term proposed in Ortega et al. (2005), which allows to reject persistent disturbances. This controller and its variations are a contribution of this work.

In this chapter, this controller has been applied to the *QuadRotor* helicopter (Raffo et al., 2009c, 2011a), apart from others two different underactuated systems, an inverted pendulum on a cart (Raffo et al., 2007b) and a two-wheeled self-balanced vehicle (Raffo et al., 2010a). The difference between the self-balanced vehicle and the inverted pendulum on a cart lies in the fact that, in the first system, the axle of the motors is at the same time the pivot axis of the pendulum, whereas

in the second one, the pendulum goes freely around the pivot axis. These characteristics results that the inverted pendulum on a cart has noninteracting input control, while the two-wheeled vehicle has input coupling.

Since this control law design considers only the dynamics of *controlled* DOF into the error state vector, the *remaining* ones must be assumed to have stable zero dynamics, or they must be controlled in an outer loop. As the standard *QuadRotor* configuration is constituted by four coplanar propellers (see Fig. 2.1), it is not static feedback exact linearizable for the desired controlled outputs, x, y, z and ψ, i.e., the translational and yaw angle positions. If the desired controlled outputs are chosen as the Euler angles and the altitude, the problem remains in the xy-motion, which is unstable. In the literature there are two approaches to solve these problems: on one hand, if the outputs are chosen as in the first case, it is possible to use an augmented state vector with a double integrator of the thrust (the translational control input). This makes that the system with the controlled outputs x, y, z and ψ be realizable. Hence, the system becomes exact linearizable with a dynamic feedback controller (for more details see Mistler et al. (2001)). On the other hand, if the desired controlled outputs are chosen as in the second case, an outer-loop controller is needed to ensure the stability of the whole system. This second approach is the selected one to develop some control strategies in this thesis (as can be seen in Chapter 3, and in the first control strategy presented in this chapter, with both outer and inner loop state vector changed, which has been published in Raffo et al. (2009c), and in an augmented version in Raffo et al. (2010d)). The controller proposed in this chapter considers the overall dynamic behavior in order to control the helicopter attitude and altitude. This fact implies that translational and rotational motion control are not considered separately, being their couplings do not treated like external disturbances. Therefore, this approach constitutes a clear advantage with respect to the control strategies proposed in Chapter 3.

As stated in Chen et al. (1994), the standard formulation of the nonlinear $\mathscr{H}_\infty$ control for Euler-Lagrange mechanical systems used, for example, in Feng and Postlethwaite (1994), Siqueira and Terra (2004b) and Ortega et al. (2005), presents a limitation in the way to weigh the cost variable. For its appropriate formulation, some weighting matrices must be considered like positive real scalars multiplied by the identity matrix. In this work, a way to design the nonlinear $\mathscr{H}_\infty$ control for mechanical systems is proposed, allowing to weight different dynamics through various values, and represents another contribution of this thesis. In this chapter, only two dynamics are considered. The procedure for weighting more dynamics can be obtained through a natural way, but at the cost of more dynamics

are considered, more Riccati's equations must be solved.

Moreover, to overcome cascade control strategies for the *QuadRotor* helicopter, or an augmented state space, a nonlinear $\mathscr{H}_\infty$ controller for a class of underactuated mechanical systems with input coupling is also proposed. This approach considers the dynamics of the *non-controlled* degrees of freedom (i.e. the *remaining* DOF) in the cost variable allowing to maintain these coordinates stabilized. More precisely, to reach this behavior, the time-derivative of their positions is considered in the error vector, which ensures that the speed error of the *remaining* DOF tends to zero when the positions are given by their coupling with the *controlled* DOF. This controller, combined with the possibility to weight different DOF, constitutes one of the main contribution of this thesis. This control law is also applied to the two-wheeled self-balanced vehicle, with the same controller structure but with a slight change in the control objective raised to the *QuadRotor* helicopter.

The chapter begins presenting the underactuated mechanical control system representation used to design the nonlinear $\mathscr{H}_\infty$ controllers, followed by their development. Simulation and experimental results are showed for the *QuadRotor* helicopter and other applications.

4.2 Underactuated Mechanical Systems

In agreement with the Euler-Lagrange mechanical system (2.40) presented in Chapter 2:

$$\boldsymbol{M}(\boldsymbol{q})\ddot{\boldsymbol{q}}+\boldsymbol{C}(\boldsymbol{q},\dot{\boldsymbol{q}})\dot{\boldsymbol{q}}+\boldsymbol{G}(\boldsymbol{q})=\boldsymbol{B}(\boldsymbol{q})\boldsymbol{\Gamma}+\boldsymbol{\delta}(\boldsymbol{q},\dot{\boldsymbol{q}},\ddot{\boldsymbol{q}},\boldsymbol{\Gamma}_{\boldsymbol{d}}),$$

it is possible to classify mechanical systems with respect to their actuation degree, that is, the difference between the number of configuration variables, $\boldsymbol{q}\in\mathbb{Q}$, and control inputs, $\boldsymbol{\Gamma}\in\mathbb{U}$, being $\mathbb{Q}$ the n-dimensional configuration space and $\mathbb{U}$ the m-dimensional actuation space. Therefore, the following definitions are stated (Olfati-Saber, 2001; Gómez-Stern, 2002; Acosta, 2004; Vivas, 2004):

Definition 4.1. ***Fully actuated mechanical systems*** *are those systems where* $m=rank(\boldsymbol{B}(\boldsymbol{q}))=n$*, that is,* $\boldsymbol{B}(\boldsymbol{q})$ *is invertible. In these systems, the number of available control actions is the same than the dimension of the system configuration space. Besides, they are feedback exact linearizable, i.e., they do not present zero dynamics.*

Definition 4.2. ***Underactuated mechanical systems*** *are those systems where* $m=$

rank$(\boldsymbol{B}(\boldsymbol{q})) < n$*, which means that they have fewer control actions than the dimension of the configuration space. Thus, due to the impossibility to act in the whole configuration space, some limitations appear with respect to the kind of performance which is possible to reach in closed-loop. Besides, it is not possible to apply fully feedback exact linearization of underactuated systems.*

Regarding underactuated mechanical systems, in general, the dynamic equations of these kind of systems with n DOF can be partitioned into two components: one corresponding to the *uncontrolled* (also called *remaining*) *generalized coordinates*, $\boldsymbol{q_u} \in \Re^{n_u}$, and the other to the *controlled* ones, $\boldsymbol{q_c} \in \Re^{n_c}$. Furthermore, it is well-known that no more than m degrees of freedom can be controlled (i.e. regulated at an operation point) at each moment by the external generalized forces/torques (Siqueira and Terra, 2004a). Therefore, the m DOF to be controlled should be grouped in the vector $\boldsymbol{q_c} \in \Re^m$, while the *uncontrolled* generalized coordinates should be grouped in the vector $\boldsymbol{q_u} \in \Re^{n-n_c}$, where $n_c = m$ and $n_u = n - n_c$. However, the partition of underactuated systems also depends on the system structure, being these systems as well classified by the presence or lack of any input coupling due to the force matrix $\boldsymbol{B}(\boldsymbol{q})$, and by the actuated or unactuated *shape* variables. *Shape variables* are those that appear in the inertia matrix of a system. In the case that an underactuated system is flat (i.e. has constant inertia matrix), *shape variables* are called those that appear in the force matrix $\boldsymbol{B}(\boldsymbol{q})$. If a configuration variable q_j does not appear in the inertia matrix, i.e. $\partial \boldsymbol{M}(\boldsymbol{q})/\partial q_j = 0$, it is called an *external variable* (Olfati-Saber, 2001). Thus, underactuated systems can also be labeled with respect to the type of variable, for example, *passive-active* (*unactuated-actuated*), *shape-external* and/or *controlled-stabilized*. A list sorting underactuated systems can be found in Olfati-Saber (2001).

In the *passive-active* configuration, for the particular case where $\boldsymbol{B}(\boldsymbol{q}) = [\mathbb{0} \quad \mathbb{1}_m]'$, that means the system with noninteracting input, the *passive* subsystem can be expressed without loss of generality in the form $\vartheta(\boldsymbol{q}, \dot{\boldsymbol{q}}, \ddot{\boldsymbol{q}}) = 0$. This is a highly nonlinear second-order dynamic equation and includes dynamics of the *active* subsystem. In this case, $\boldsymbol{q_p} \in \Re^{n_p}$, where $n_p = n - m$, is the *passive* coordinate vector and $\boldsymbol{q_a} \in \Re^{n_a}$, with $n_a = m$, is the *active* one. Moreover, as commented before, the application of feedback linearization techniques to underactuated systems is not always direct. However, in Spong (1996) is showed that the system for this special case can be partially linearized by an invertible change of variable on the control. Nevertheless, after partial linearization, *unactuated* subsystem still remains as a nonlinear system that is coupled with the linearized

actuated subsystem through both the new control input and other nonlinear terms (Olfati-Saber, 2001).

Accordingly, for the particular case where there are noninteracting inputs, there exist three possibilities to form the vector $\boldsymbol{q_c}$ (Siqueira, 2004):

1. $\boldsymbol{q_c}$ contains only *active* DOF, when $n_a \geq n_p$.
2. $\boldsymbol{q_c}$ contains only *passive* DOF, when $n_p = n_a$.
3. $\boldsymbol{q_c}$ contains both *passive* and *active* DOF, when $n_p < n_a$.

Furthermore, as in Olfati-Saber (2001), underactuated systems with noninteracting inputs can be classified according the *shape* variables: i) with fully-actuated *shape* variables, ii) with unactuated *shape* variables, and iii) with partially-actuated *shape* variables.

Thus, assuming that the Euler-Lagrange equations of motion (2.40), again given by:

$$\boldsymbol{M}(\boldsymbol{q})\ddot{\boldsymbol{q}} + \boldsymbol{C}(\boldsymbol{q},\dot{\boldsymbol{q}})\dot{\boldsymbol{q}} + \boldsymbol{G}(\boldsymbol{q}) = \boldsymbol{B}(\boldsymbol{q})\boldsymbol{\Gamma} + \boldsymbol{\delta}(\boldsymbol{q},\dot{\boldsymbol{q}},\ddot{\boldsymbol{q}},\boldsymbol{\Gamma_d}),$$

represent an underactuated mechanical system with the same vectors and matrices defined in Section 2.4, for the suitable partition between *uncontrolled* and *controlled* DOF, the system (2.40) can be written as follows:

$$\begin{bmatrix} \boldsymbol{M_{uu}}(\boldsymbol{q}) & \boldsymbol{M_{uc}}(\boldsymbol{q}) \\ \boldsymbol{M_{cu}}(\boldsymbol{q}) & \boldsymbol{M_{cc}}(\boldsymbol{q}) \end{bmatrix} \begin{bmatrix} \ddot{\boldsymbol{q}}_{\boldsymbol{u}} \\ \ddot{\boldsymbol{q}}_{\boldsymbol{c}} \end{bmatrix} + \begin{bmatrix} \boldsymbol{C_{uu}}(\boldsymbol{q},\dot{\boldsymbol{q}}) & \boldsymbol{C_{uc}}(\boldsymbol{q},\dot{\boldsymbol{q}}) \\ \boldsymbol{C_{cu}}(\boldsymbol{q},\dot{\boldsymbol{q}}) & \boldsymbol{C_{cc}}(\boldsymbol{q},\dot{\boldsymbol{q}}) \end{bmatrix} \begin{bmatrix} \dot{\boldsymbol{q}}_{\boldsymbol{u}} \\ \dot{\boldsymbol{q}}_{\boldsymbol{c}} \end{bmatrix} + \begin{bmatrix} \boldsymbol{G_u}(\boldsymbol{q}) \\ \boldsymbol{G_c}(\boldsymbol{q}) \end{bmatrix} = \begin{bmatrix} \boldsymbol{B_u}(\boldsymbol{q}) \\ \boldsymbol{B_c}(\boldsymbol{q}) \end{bmatrix} \boldsymbol{\Gamma} + \begin{bmatrix} \boldsymbol{\delta_u} \\ \boldsymbol{\delta_c} \end{bmatrix}, \tag{4.1}$$

where

$$\begin{aligned} \boldsymbol{\delta_u} &= -(\boldsymbol{\Delta M_{uc}}(\boldsymbol{q})\ddot{\boldsymbol{q}}_{\boldsymbol{c}} + \boldsymbol{\Delta M_{uu}}(\boldsymbol{q})\ddot{\boldsymbol{q}}_{\boldsymbol{u}} + \boldsymbol{\Delta C_{uc}}(\boldsymbol{q},\dot{\boldsymbol{q}})\dot{\boldsymbol{q}}_{\boldsymbol{c}} \\ &\quad + \boldsymbol{\Delta C_{uu}}(\boldsymbol{q},\dot{\boldsymbol{q}})\dot{\boldsymbol{q}}_{\boldsymbol{u}} + \boldsymbol{\Delta G_u}(\boldsymbol{q}) - \boldsymbol{\Gamma}_{\boldsymbol{d_u}}), \\ \boldsymbol{\delta_c} &= -(\boldsymbol{\Delta M_{cc}}(\boldsymbol{q})\ddot{\boldsymbol{q}}_{\boldsymbol{c}} + \boldsymbol{\Delta M_{cu}}(\boldsymbol{q})\ddot{\boldsymbol{q}}_{\boldsymbol{u}} + \boldsymbol{\Delta C_{cc}}(\boldsymbol{q},\dot{\boldsymbol{q}})\dot{\boldsymbol{q}}_{\boldsymbol{c}} \\ &\quad + \boldsymbol{\Delta C_{cu}}(\boldsymbol{q},\dot{\boldsymbol{q}})\dot{\boldsymbol{q}}_{\boldsymbol{u}} + \boldsymbol{\Delta G_c}(\boldsymbol{q}) - \boldsymbol{\Gamma}_{\boldsymbol{d_c}}). \end{aligned}$$

The forces/torques in the *controlled* and *uncontrolled* DOF are defined by $\boldsymbol{\Gamma_c} = \boldsymbol{B_c}(\boldsymbol{q})\boldsymbol{\Gamma} \in \Re^{n_c}$ and $\boldsymbol{\Gamma_u} = \boldsymbol{B_u}(\boldsymbol{q})\boldsymbol{\Gamma} \in \Re^{n_u}$, respectively. $\boldsymbol{\delta_c}$ and $\boldsymbol{\delta_u}$ represent

the total effect of the parametric uncertainties (matrices expressed by $\boldsymbol{\Delta}\bullet$) and energy-bounded external disturbances on the *controlled* and *uncontrolled* DOF, $\boldsymbol{\Gamma}_{\boldsymbol{d_c}}$ and $\boldsymbol{\Gamma}_{\boldsymbol{d_u}}$, respectively. For the particular case where there are noninteracting input, if the option chosen to control is 1), $\boldsymbol{\Gamma_c} = \boldsymbol{\Gamma_a}$; if the option is 2), $\boldsymbol{\Gamma_c} = \mathbb{0}$; and if the option is 3), $\boldsymbol{\Gamma_c} = [\boldsymbol{\Gamma}_{\boldsymbol{a_c}} \quad \mathbb{0}]'$, being $\boldsymbol{\Gamma}_{\boldsymbol{a_c}}$ the forces/torques in the *active* DOF being controlled.

Without loss of generality, if there is input coupling, regarding the partition of matrix $\boldsymbol{B}(\boldsymbol{q})$:

$$\boldsymbol{B}(\boldsymbol{q}) = \begin{bmatrix} \boldsymbol{B_u}(\boldsymbol{q}) \\ \boldsymbol{B_c}(\boldsymbol{q}) \end{bmatrix}, \tag{4.2}$$

$\boldsymbol{B_c}(\boldsymbol{q})$ must be an invertible $m \times m$ matrix and, from the input coupling, it follows that $\boldsymbol{B_u}(\boldsymbol{q}) \neq 0$ for all $\boldsymbol{q}$ (Olfati-Saber, 2001). If the *controlled* degrees of freedom vector is chosen the same as the *active* one, it is obvious that $\boldsymbol{B_c}(\boldsymbol{q}) = \boldsymbol{B_a}(\boldsymbol{q})$ is an invertible $n_a \times n_a$ matrix.

In what follows, two representations of the dynamics of underactuated mechanical systems are presented. In the first one, the reduced underactuated system is used to obtain the dynamic equation of the system error for the *controlled* degrees of freedom. In the second representation of the system, the entire dynamic model is considered to obtain the equations of the system error, where both dynamics of *controlled* and *uncontrolled* DOF are included in the tracking error vector. In this formulation, the objective is, at least, to obtain the stabilization of the *uncontrolled* DOF at an equilibrium point.

Reduced Underactuated Mechanical System

Taking into account this partition, it is possible to reduce the order of the underactuated system to be controlled. Therefore, from the second row of (4.1), and the definition of $\boldsymbol{\Gamma_c} = \boldsymbol{B_c}(\boldsymbol{q})\boldsymbol{\Gamma}$:

$$\boldsymbol{M_{cc}}(\boldsymbol{q})\ddot{\boldsymbol{q}}_{\boldsymbol{c}} + \boldsymbol{M_{cu}}(\boldsymbol{q})\ddot{\boldsymbol{q}}_{\boldsymbol{u}} + \boldsymbol{C_{cc}}(\boldsymbol{q},\dot{\boldsymbol{q}})\dot{\boldsymbol{q}}_{\boldsymbol{c}} + \boldsymbol{C_{cu}}(\boldsymbol{q},\dot{\boldsymbol{q}})\dot{\boldsymbol{q}}_{\boldsymbol{u}} + \boldsymbol{G_c}(\boldsymbol{q}) = \boldsymbol{\Gamma_c} + \boldsymbol{\delta_c}, \tag{4.3}$$

the *controlled* degrees of freedom acceleration can be isolated, yielding:

$$\ddot{\boldsymbol{q}}_{\boldsymbol{c}} = -\boldsymbol{M}_{\boldsymbol{cc}}^{-1}(\boldsymbol{q})(\boldsymbol{C_{cc}}(\boldsymbol{q},\dot{\boldsymbol{q}})\dot{\boldsymbol{q}}_{\boldsymbol{c}} + \boldsymbol{G_c}(\boldsymbol{q}) - \bar{\boldsymbol{\Gamma}} - \boldsymbol{\delta_c}), \tag{4.4}$$

where $\bar{\boldsymbol{\Gamma}} = \boldsymbol{\Gamma_c} - \boldsymbol{M_{cu}}(\boldsymbol{q})\ddot{\boldsymbol{q}}_{\boldsymbol{u}} - \boldsymbol{C_{cu}}(\boldsymbol{q},\dot{\boldsymbol{q}})\dot{\boldsymbol{q}}_{\boldsymbol{u}}$.

By defining the tracking error vector of the *controlled* DOF as follows:

$$\boldsymbol{x_c} = \begin{bmatrix} \dot{\tilde{\boldsymbol{q}}}_{\boldsymbol{c}} \\ \tilde{\boldsymbol{q}}_{\boldsymbol{c}} \\ \int \tilde{\boldsymbol{q}}_{\boldsymbol{c}} dt \end{bmatrix} = \begin{bmatrix} \dot{\boldsymbol{q}}_{\boldsymbol{c}} - \dot{\boldsymbol{q}}_{\boldsymbol{c_r}} \\ \boldsymbol{q}_{\boldsymbol{c}} - \boldsymbol{q}_{\boldsymbol{c_r}} \\ \int \left(\boldsymbol{q}_{\boldsymbol{c}} - \boldsymbol{q}_{\boldsymbol{c_r}} \right) dt \end{bmatrix}, \tag{4.5}$$

equation (4.4) with respect to the reference trajectory can be written in the state space form as follows:

$$\dot{\boldsymbol{x}}_{\boldsymbol{c}} = \overline{f}(\boldsymbol{x_c}, \boldsymbol{q_u}, t) + \overline{g_0}(\boldsymbol{q}, \dot{\boldsymbol{q}}, \ddot{\boldsymbol{q}}_{\boldsymbol{c_r}}, \dot{\boldsymbol{q}}_{\boldsymbol{c_r}}) + \overline{g}(\boldsymbol{x_c}, \boldsymbol{q_u}, t)\bar{\boldsymbol{\Gamma}} + \overline{k}(\boldsymbol{x_c}, \boldsymbol{q_u}, t)\boldsymbol{\delta_c}, \tag{4.6}$$

with

$$\overline{f}(\boldsymbol{x_c}, \boldsymbol{q_u}, t) = \begin{bmatrix} -\boldsymbol{M}_{\boldsymbol{cc}}^{-1}(\boldsymbol{q})\boldsymbol{C}_{\boldsymbol{cc}}(\boldsymbol{q}, \dot{\boldsymbol{q}}) & \mathbb{0} & \mathbb{0} \\ \mathbb{1} & \mathbb{0} & \mathbb{0} \\ \mathbb{0} & \mathbb{1} & \mathrm{O} \end{bmatrix} \boldsymbol{x_c},$$

$$\overline{g_0}(\boldsymbol{q}, \dot{\boldsymbol{q}}, \ddot{\boldsymbol{q}}_{\boldsymbol{c_r}}, \dot{\boldsymbol{q}}_{\boldsymbol{c_r}}) = \begin{bmatrix} -\boldsymbol{M}_{\boldsymbol{cc}}^{-1}(\boldsymbol{q})(\boldsymbol{M}_{\boldsymbol{cc}}(\boldsymbol{q})\ddot{\boldsymbol{q}}_{\boldsymbol{c_r}} + \boldsymbol{C}_{\boldsymbol{cc}}(\boldsymbol{q}, \dot{\boldsymbol{q}})\dot{\boldsymbol{q}}_{\boldsymbol{c_r}} + \boldsymbol{G}_{\boldsymbol{c}}(\boldsymbol{q})) \\ \mathbb{0} \\ \mathbb{0} \end{bmatrix},$$

$$\overline{g}(\boldsymbol{x_c}, \boldsymbol{q_u}, t) = \overline{k}(\boldsymbol{x_c}, \boldsymbol{q_u}, t) = \begin{bmatrix} \boldsymbol{M}_{\boldsymbol{cc}}^{-1}(\boldsymbol{q}) \\ \mathbb{0} \\ \mathbb{0} \end{bmatrix},$$

where $\boldsymbol{q}_{\boldsymbol{c_r}}$, $\dot{\boldsymbol{q}}_{\boldsymbol{c_r}}$ and $\ddot{\boldsymbol{q}}_{\boldsymbol{c_r}} \in \Re^{n_c}$ are the desired trajectory of the *controlled* DOF, and the corresponding velocity and acceleration, respectively. $\mathbb{1}$ is the identity matrix and $\mathbb{0}$ the zero matrix, both of n_c-th order. Note that an integral term has been included in the error vector, as in (3.36). This term will allow the achievement of a null steady-state error when persistent disturbances are acting on the *controlled* subsystem.

By using the state space equations (4.6) to design a control law for the *controlled* subsystem, the *remaining* ones must be assumed to have stable zero dynamics, or to be controlled by an outer loop controller. In the next section, a nonlinear $\mathscr{H}_\infty$ control design will be presented for this subsystem. This controller is applied to the *QuadRotor* helicopter in a cascade strategy, to the inverted pendulum on a cart and to the two-wheeled self-balanced vehicle.

Entire Underactuated Mechanical System

On the other hand, if the system to be controlled does not present a stable zero dynamic, or because the cascade control can introduce stability problems to the whole system, it must be guaranteed that the *remaining* (*uncontrolled*) degrees of freedom will be stabilized. To perform that, the partitioned system (4.1) is taken into account again, assuming that the inertia matrix presents cross terms between the *controlled* and *uncontrolled* DOF. This system can be normalized to obtain a block diagonal inertia matrix through the following form:

$$\overline{\boldsymbol{M}}(\boldsymbol{q})\ddot{\boldsymbol{q}}+\overline{\boldsymbol{C}}(\boldsymbol{q},\dot{\boldsymbol{q}})\dot{\boldsymbol{q}}+\overline{\boldsymbol{G}}(\boldsymbol{q})=\overline{\boldsymbol{\Gamma}}(\boldsymbol{q})+\overline{\boldsymbol{\delta}}\,, \tag{4.7}$$

$$\begin{bmatrix} \boldsymbol{M}_{su}(\boldsymbol{q}) & \mathbb{0} \\ \mathbb{0} & \boldsymbol{M}_{rc}(\boldsymbol{q}) \end{bmatrix}\begin{bmatrix} \ddot{\boldsymbol{q}}_u \\ \ddot{\boldsymbol{q}}_c \end{bmatrix}+\begin{bmatrix} \boldsymbol{C}_{su}(\boldsymbol{q},\dot{\boldsymbol{q}}) & \boldsymbol{C}_{sc}(\boldsymbol{q},\dot{\boldsymbol{q}}) \\ \boldsymbol{C}_{ru}(\boldsymbol{q},\dot{\boldsymbol{q}}) & \boldsymbol{C}_{rc}(\boldsymbol{q},\dot{\boldsymbol{q}}) \end{bmatrix}\begin{bmatrix} \dot{\boldsymbol{q}}_u \\ \dot{\boldsymbol{q}}_c \end{bmatrix} + \begin{bmatrix} \boldsymbol{G}_{su}(\boldsymbol{q}) \\ \boldsymbol{G}_{rc}(\boldsymbol{q}) \end{bmatrix}=\begin{bmatrix} \boldsymbol{\Gamma}_{su}(\boldsymbol{q}) \\ \boldsymbol{\Gamma}_{rc}(\boldsymbol{q}) \end{bmatrix}+\begin{bmatrix} \boldsymbol{\delta}_{su} \\ \boldsymbol{\delta}_{rc} \end{bmatrix}, \tag{4.8}$$

where the subscripts $\boldsymbol{s}$ and $\boldsymbol{r}$ denote stabilized and regulated subsystem, respectively, and:

$$\begin{aligned} \overline{\boldsymbol{\Gamma}}(\boldsymbol{q}) &= \boldsymbol{T}_{\boldsymbol{M}}(\boldsymbol{q})\boldsymbol{B}(\boldsymbol{q})\boldsymbol{\Gamma}, \\ \overline{\boldsymbol{\delta}}(\boldsymbol{q}) &= \boldsymbol{T}_{\boldsymbol{M}}(\boldsymbol{q})\boldsymbol{\delta}(\boldsymbol{q},\dot{\boldsymbol{q}},\ddot{\boldsymbol{q}},\boldsymbol{\Gamma}_d), \\ \overline{\boldsymbol{M}}(\boldsymbol{q}) &= \boldsymbol{T}_{\boldsymbol{M}}(\boldsymbol{q})\boldsymbol{M}(\boldsymbol{q}), \\ \overline{\boldsymbol{C}}(\boldsymbol{q},\dot{\boldsymbol{q}}) &= \boldsymbol{T}_{\boldsymbol{M}}(\boldsymbol{q})\boldsymbol{C}(\boldsymbol{q},\dot{\boldsymbol{q}}), \\ \overline{\boldsymbol{G}}(\boldsymbol{q}) &= \boldsymbol{T}_{\boldsymbol{M}}(\boldsymbol{q})\boldsymbol{G}(\boldsymbol{q}), \end{aligned}$$

with $\overline{\boldsymbol{M}}(\boldsymbol{q})$ symmetric and positive definite. This normalized system will be referred throughout the chapter as the *entire* underactuated mechanical system.

The normalization matrix $\boldsymbol{T}_{\boldsymbol{M}}$ is easily obtained when only two dynamics are considered, as follows: i) by isolating $\ddot{\boldsymbol{q}}_u$ in the first row of (4.1), ii) replacing it in the second one, iii) making the same procedure with $\ddot{\boldsymbol{q}}_c$ in the second row of (4.1) and, iv) substituting it in the first one, yielding:

$$\boldsymbol{T}_{\boldsymbol{M}}(\boldsymbol{q})=\begin{bmatrix} \mathbb{1} & -\boldsymbol{M}_{uc}(\boldsymbol{q})\boldsymbol{M}_{cc}^{-1}(\boldsymbol{q}) \\ -\boldsymbol{M}_{cu}(\boldsymbol{q})\boldsymbol{M}_{uu}^{-1}(\boldsymbol{q}) & \mathbb{1} \end{bmatrix}.$$

To partition the mechanical system in more than two dynamics and diagonalize the inertia matrix, the normalization matrix can be obtained following the steps:

1. Compute the inverse of the inertia matrix $\boldsymbol{M}^{-1}(\boldsymbol{q})$.

2. From $\boldsymbol{M}^{-1}(\boldsymbol{q})$, the matrix $\overline{\boldsymbol{M}}^{-1}(\boldsymbol{q})$ is given by:

$$\overline{\boldsymbol{M}}^{-1}(\boldsymbol{q}) = \text{diag}(\boldsymbol{M}^{-1}(\boldsymbol{q}))\,.$$

3. By inverting $\overline{\boldsymbol{M}}^{-1}(\boldsymbol{q})$, the diagonalized inertia matrix is obtained, $\overline{\boldsymbol{M}}(\boldsymbol{q})$.

4. Finally, the normalization matrix is computed as follows:

$$\boldsymbol{T}_{\boldsymbol{M}}(\boldsymbol{q}) = \overline{\boldsymbol{M}}(\boldsymbol{q})\boldsymbol{M}^{-1}(\boldsymbol{q})\,.$$

This system normalization will allow to weigh different dynamics through different weighting parameters due to the diagonal structure of the inertia matrix, as will be seen in Sections 4.3.1 and 4.4. Therefore, it will enable to consider the time-derivative of the *remaining* DOF in the tracking error vector.

As the control objective, proposed here for the underactuated mechanical system under input coupling, is to perform a reference tracking of the *controlled* DOF, $\boldsymbol{q}_{\boldsymbol{c}}$, while the *remaining* ones, $\boldsymbol{q}_{\boldsymbol{u}}$, or at least their velocities are maintained stabilized (it depends on the control objective for each system, more details are given in Section 4.4 and its applications), the dynamics of the *uncontrolled* degrees of freedom are considered into the error vector. It leads the tracking error vector to be defined as follows:

$$\boldsymbol{x} = \begin{bmatrix} \dot{\tilde{\boldsymbol{q}}}_{\boldsymbol{u}} \\ \dot{\tilde{\boldsymbol{q}}}_{\boldsymbol{c}} \\ \tilde{\boldsymbol{q}}_{\boldsymbol{c}} \\ \int \tilde{\boldsymbol{q}}_{\boldsymbol{c}} dt \end{bmatrix} = \begin{bmatrix} \dot{\boldsymbol{q}}_{\boldsymbol{u}} - \dot{\boldsymbol{q}}_{\boldsymbol{u}_r} \\ \dot{\boldsymbol{q}}_{\boldsymbol{c}} - \dot{\boldsymbol{q}}_{\boldsymbol{c}_r} \\ \boldsymbol{q}_{\boldsymbol{c}} - \boldsymbol{q}_{\boldsymbol{c}_r} \\ \int \left(\boldsymbol{q}_{\boldsymbol{c}} - \boldsymbol{q}_{\boldsymbol{c}_r}\right) dt \end{bmatrix}. \tag{4.9}$$

By considering the proposed error vector, equation (4.8) can be rewritten with respect to the desired trajectory in the state space form:

$$\dot{\boldsymbol{x}} = \overline{f}(\boldsymbol{x}, \boldsymbol{q}_{\boldsymbol{u}}, t) + \overline{g_0}(\boldsymbol{q}, \dot{\boldsymbol{q}}, \ddot{\boldsymbol{q}}_{\boldsymbol{r}}, \dot{\boldsymbol{q}}_{\boldsymbol{r}}) + \overline{g}(\boldsymbol{x}, \boldsymbol{q}_{\boldsymbol{u}}, t)\overline{\boldsymbol{\Gamma}} + \overline{k}(\boldsymbol{x}, \boldsymbol{q}_{\boldsymbol{u}}, t)\overline{\boldsymbol{\delta}}\,, \tag{4.10}$$

where

$$\overline{f}(\boldsymbol{x},\boldsymbol{q_u},t) = \begin{bmatrix} -\boldsymbol{M_{su}^{-1}}(\boldsymbol{q})\boldsymbol{C_{su}}(\boldsymbol{q},\dot{\boldsymbol{q}}) & -\boldsymbol{M_{su}^{-1}}(\boldsymbol{q})\boldsymbol{C_{sc}}(\boldsymbol{q},\dot{\boldsymbol{q}}) & \mathbb{0} & \mathbb{0} \\ -\boldsymbol{M_{rc}^{-1}}(\boldsymbol{q})\boldsymbol{C_{ru}}(\boldsymbol{q},\dot{\boldsymbol{q}}) & -\boldsymbol{M_{rc}^{-1}}(\boldsymbol{q})\boldsymbol{C_{rc}}(\boldsymbol{q},\dot{\boldsymbol{q}}) & \mathbb{0} & \mathbb{0} \\ \mathbb{0} & \mathbb{1} & \mathbb{0} & \mathbb{0} \\ \mathbb{0} & \mathbb{0} & \mathbb{1} & \mathbb{0} \end{bmatrix} \boldsymbol{x},$$

$$\overline{g_0}(\boldsymbol{q},\dot{\boldsymbol{q}},\ddot{\boldsymbol{q}}_{\boldsymbol{r}},\dot{\boldsymbol{q}}_{\boldsymbol{r}}) = \begin{bmatrix} -\boldsymbol{M_{su}^{-1}}(\boldsymbol{q})(\boldsymbol{M_{su}}(\boldsymbol{q})\ddot{\boldsymbol{q}}_{\boldsymbol{u_r}} + \boldsymbol{C_{su}}(\boldsymbol{q},\dot{\boldsymbol{q}})\dot{\boldsymbol{q}}_{\boldsymbol{u_r}} + \boldsymbol{C_{sc}}(\boldsymbol{q},\dot{\boldsymbol{q}})\dot{\boldsymbol{q}}_{\boldsymbol{c_r}} + \boldsymbol{G_{su}}(\boldsymbol{q})) \\ -\boldsymbol{M_{rc}^{-1}}(\boldsymbol{q})(\boldsymbol{M_{rc}}(\boldsymbol{q})\ddot{\boldsymbol{q}}_{\boldsymbol{c_r}} + \boldsymbol{C_{ru}}(\boldsymbol{q},\dot{\boldsymbol{q}})\dot{\boldsymbol{q}}_{\boldsymbol{u_r}} + \boldsymbol{C_{rc}}(\boldsymbol{q},\dot{\boldsymbol{q}})\dot{\boldsymbol{q}}_{\boldsymbol{c_r}} + \boldsymbol{G_{rc}}(\boldsymbol{q})) \\ \mathbb{0} \\ \mathbb{0} \end{bmatrix},$$

$$\overline{g}(\boldsymbol{x},\boldsymbol{q_u},t) = \overline{k}(\boldsymbol{x},\boldsymbol{q_u},t) = \begin{bmatrix} \boldsymbol{M_{su}^{-1}}(\boldsymbol{q}) & \mathbb{0} \\ \mathbb{0} & \boldsymbol{M_{rc}^{-1}}(\boldsymbol{q}) \\ \mathbb{0} & \mathbb{0} \\ \mathbb{0} & \mathbb{0} \end{bmatrix},$$

being $\boldsymbol{q_r}$, $\dot{\boldsymbol{q}}_{\boldsymbol{r}}$ and $\ddot{\boldsymbol{q}}_{\boldsymbol{r}} \in \Re^n$ the desired trajectory and the corresponding velocity and acceleration, respectively. Matrices $\mathbb{1}$ and $\mathbb{0}$ represent the identity and zero matrices, respectively, both with proper dimensions.

In the following sections, nonlinear $\mathscr{H}_\infty$ controllers for the *reduced* and *entire* underactuated systems will be developed.

4.3 Underactuated Nonlinear $\mathscr{H}_\infty$ Control of the Reduced Subsystem

In this section, a nonlinear $\mathscr{H}_\infty$ controller, designed for the reduced underactuated mechanical system to achieve robustness in presence of sustained disturbances and parametric uncertainty, is developed. The control law is based on the error dynamic equation of the *controlled* DOF (4.6). As stated before, the advantage of this method is based on the knowledge of all underactuated system behavior at the moment to compute the control signals, and not solely considering the remaining behavior of the coordinates as external disturbances.

Firstly, the methodology proposed in Siqueira and Terra (2004a) is improved in this thesis by extending the work introduced in Ortega et al. (2005) for fully actuated mechanical systems, to underactuated ones. The proposed controller

is able to cope with persistent disturbances acting on underactuated mechanical systems. Furthermore, the work presented in Siqueira and Terra (2004a) develops a strategy in which *passive* degrees of freedom are controlled by *active* ones, with a local passive redundancy. In this way, the control strategy is applied in two phases: first the *passive* coordinates are driven to the set-points via dynamic coupling with the *active* ones, and then, are locked; and in the second control phase, the *active* coordinates are controlled.

The objective in this section is to develop a controller where only the first control phase is considered for the system, that is, only the *controlled* degrees of freedom are guided, assuming that the *uncontrolled* degrees of freedom can not be locked. Moreover, as commented at the beginning of the chapter, in order to the whole closed-loop system be stable, it must be assumed that either the *remaining* DOF have stable zero dynamics, or their dynamics must be controlled by an outer loop controller if they are unstable.

Thus, as a previous step to synthesize the underactuated nonlinear $\mathscr{H}_\infty$ controller, a state transformation similar to (3.38) is used:

$$z = \begin{bmatrix} z_1 \\ z_2 \\ z_3 \end{bmatrix} = \boldsymbol{T_o x_c} = \begin{bmatrix} \boldsymbol{T_1} & \boldsymbol{T_2} & \boldsymbol{T_3} \\ \mathbb{0} & \mathbb{1} & \mathbb{1} \\ \mathbb{0} & \mathbb{0} & \mathbb{1} \end{bmatrix} \begin{bmatrix} \dot{\tilde{\boldsymbol{q}}}_{\boldsymbol{c}} \\ \tilde{\boldsymbol{q}}_{\boldsymbol{c}} \\ \int \tilde{\boldsymbol{q}}_{\boldsymbol{c}} dt \end{bmatrix}, \tag{4.11}$$

with $\boldsymbol{T_1} = \rho\mathbb{1}$, where ρ is a positive scalar and $\mathbb{1} \in \Re^{n_c \times n_c}$ is the identity matrix. As discussed in Section 3.3.2, and taking into account the assumptions about the choice of generalized forces and torques to be included in the optimization strategy, the following change of variables over the control action and disturbances is also considered:

$$\boldsymbol{u} + \boldsymbol{d} = \boldsymbol{M_{cc}}(\boldsymbol{q})\boldsymbol{T}\dot{\boldsymbol{x}}_{\boldsymbol{c}} + \boldsymbol{C_{cc}}(\boldsymbol{q}, \dot{\boldsymbol{q}})\boldsymbol{T}\boldsymbol{x_c}\,. \tag{4.12}$$

where $\boldsymbol{T} = [\boldsymbol{T_1} \quad \boldsymbol{T_2} \quad \boldsymbol{T_3}]$.

By expanding this transformation, the following state space equation is obtained:

$$\dot{\boldsymbol{x}}_{\boldsymbol{c}} = f(\boldsymbol{x_c}, \boldsymbol{q_u}, t) + g(\boldsymbol{x_c}, \boldsymbol{q_u}, t)\boldsymbol{u} + k(\boldsymbol{x_c}, \boldsymbol{q_u}, t)\boldsymbol{d}\,, \tag{4.13}$$

$$f(\boldsymbol{x_c}, \boldsymbol{q_u}, t) = \boldsymbol{T_o}^{-1} \begin{bmatrix} -\boldsymbol{M_{cc}}^{-1}(\boldsymbol{q})\boldsymbol{C_{cc}}(\boldsymbol{q}, \dot{\boldsymbol{q}}) & \mathbb{0} & \mathbb{0} \\ \boldsymbol{T_1}^{-1} & \mathbb{1} - \boldsymbol{T_1}^{-1}\boldsymbol{T_2} & -\mathbb{1} + \boldsymbol{T_1}^{-1}(\boldsymbol{T_2} - \boldsymbol{T_3}) \\ \mathbb{0} & \mathbb{1} & -\mathbb{1} \end{bmatrix} \boldsymbol{T_o x_c}\,,$$

$$g(\boldsymbol{x_c},\boldsymbol{q_u},t) = k(\boldsymbol{x_c},t) = \boldsymbol{T_o}^{-1}\begin{bmatrix} \boldsymbol{M_{cc}}^{-1}(\boldsymbol{q}) \\ \mathbb{0} \\ \mathbb{0} \end{bmatrix},$$

which represents the *dynamic equation of the system error*.

By comparing equations (4.13) and (4.6), results that $\boldsymbol{d} = \rho \mathbb{1} \boldsymbol{\delta_c} \in \Re^{n_c}$ is the external disturbance vector and $\boldsymbol{u} = \boldsymbol{T_1}(-\boldsymbol{F}(\boldsymbol{x_e}) + \bar{\boldsymbol{\Gamma}})$ is the *additional control* effort, with:

$$\begin{aligned} F(\boldsymbol{x_e}) \;\; = \;\; & \boldsymbol{M_{cc}}(\boldsymbol{q})\left(\ddot{\boldsymbol{q}}_{\boldsymbol{c_r}} - \boldsymbol{T_1}^{-1}\boldsymbol{T_2}\dot{\tilde{\boldsymbol{q}}}_{\boldsymbol{c}} - \boldsymbol{T_1}^{-1}\boldsymbol{T_3}\tilde{\boldsymbol{q}}_{\boldsymbol{c}}\right) \\ & + \boldsymbol{C_{cc}}(\boldsymbol{q},\dot{\boldsymbol{q}})\left(\dot{\boldsymbol{q}}_{\boldsymbol{c_r}} - \boldsymbol{T_1}^{-1}\boldsymbol{T_2}\tilde{\boldsymbol{q}}_{\boldsymbol{c}} - \boldsymbol{T_1}^{-1}\boldsymbol{T_3}\int \tilde{\boldsymbol{q}}_{\boldsymbol{c}} dt\right) + \boldsymbol{G_c}(\boldsymbol{q}). \end{aligned}$$

Thus, the control input vector for the *controlled* DOF is given by:

$$\bar{\boldsymbol{\Gamma}} = \boldsymbol{M_{cc}}(\boldsymbol{q})\ddot{\boldsymbol{q}}_{\boldsymbol{c}} + \boldsymbol{C_{cc}}(\boldsymbol{q},\dot{\boldsymbol{q}})\dot{\boldsymbol{q}}_{\boldsymbol{c}} + \boldsymbol{G_c}(\boldsymbol{q}) - \boldsymbol{T_1}^{-1}\left(\boldsymbol{M_{cc}}\boldsymbol{T}\dot{\boldsymbol{x}}_{\boldsymbol{c}} + \boldsymbol{C_{cc}}\boldsymbol{T}\boldsymbol{x_c}\right) + \boldsymbol{T_1}^{-1}\boldsymbol{u}. \tag{4.14}$$

It can be pointed out that, despite the preceding control law might not seem a well posed system, it will be shown afterwards that the computed forces/torques does not rely on DOF accelerations, but on their references. In this way, the *control acceleration* $\ddot{\boldsymbol{q}}_{\boldsymbol{c}}$, computed in equation (4.17), will be replaced into (4.14) which makes it a well posed equation.

Therefore, equation (4.13) considering the *additional control* input vector $\boldsymbol{u}$, which is into the standard form of the nonlinear $\mathscr{H}_\infty$ problem, is used to apply the nonlinear $\mathscr{H}_\infty$ theoretical results presented in Sections 3.3.1.3 and 3.3.2. The same procedure, used in those sections to obtain the nonlinear $\mathscr{H}_\infty$ controller for Euler-Lagrange mechanical systems, is also applied here to compute the control law for the *controlled* subsystem. Thus, this procedure has been omitted in order to avoid unnecessary explanation.

As stated in Section 3.3.1.3, the solution of the HJ equation depends on the choice of the cost variable, $\boldsymbol{\zeta}$, and particularly on the selection of function $h(\boldsymbol{x_c})$. In this section, this function is taken to be equal to the error vector, that is, $h(\boldsymbol{x_c}) = \boldsymbol{x_c}$. Once this function has been selected, computing the *additional control* effort, $\boldsymbol{u}$, will require finding the solution to the HJ equation (3.34), which, in this case, may depend on the *remaining* DOF like a time varying parameter, i.e. $V(\boldsymbol{x_c},\boldsymbol{q_u},t)$. This dependence on $\boldsymbol{q_u}$ occurs if some *uncontrolled* DOF is a *shape* variable and it appears in the terms of the inertia matrix with respect to the *controlled* DOF,

that is, $\boldsymbol{M_{cc}(q)}$ (see the system (4.1)). For the controller proposed in this section, the following candidate Lyapunov function is chosen:

$$V(\boldsymbol{x_c}, \boldsymbol{q_u}, t) = \frac{1}{2}\boldsymbol{x_c'T_o'}\begin{bmatrix} \boldsymbol{M_{cc}(q)} & \mathbb{0} & \mathbb{0} \\ \mathbb{0} & \boldsymbol{Y} & \boldsymbol{X-Y} \\ \mathbb{0} & \boldsymbol{X-Y} & \boldsymbol{Z+Y} \end{bmatrix}\boldsymbol{T_o x_c}, \tag{4.15}$$

where $\boldsymbol{X}$, $\boldsymbol{Y}$ and $\boldsymbol{Z} \in \Re^{n_c \times n_c}$ are constant, symmetric, and positive definite matrices such that $\boldsymbol{Z - XY^{-1}X + 2X} > \mathbb{0}$, and $\boldsymbol{T_o}$ is as defined in (4.11). Besides, $\boldsymbol{M_{cc}(q)}$ is a symmetric positive definite matrix, being $\frac{1}{2}\boldsymbol{\dot{M}_{cc}(q) - C_{cc}(q,\dot{q})}$ a skew-symmetric matrix. Using this Lyapunov function, the Theorem 3.3.3 follows.

As exposed before, once matrix $\boldsymbol{T}$ is computed by solving some Riccati algebraic equations, by substituting $V(\boldsymbol{x_c}, \boldsymbol{q_u}, t)$ into the optimal state feedback *additional control* effort (3.32), the *additional control* effort $\boldsymbol{u^*}$ corresponding to the $\mathscr{H}_\infty$ optimal index γ is given by:

$$\boldsymbol{u^* = -R^{-1}\left(S' + T\right)x_c}. \tag{4.16}$$

Finally, if the *additional control* effort (4.16) is replaced into (4.12) under the assumption that $\boldsymbol{d} = 0$, and after some manipulations, the *control acceleration* for the *controlled* subsystem can be obtained as follows:

$$\boldsymbol{\ddot{q}_c = \ddot{q}_c^d - K_D\dot{\tilde{q}}_c - K_P\tilde{q}_c - K_I}\int \boldsymbol{\tilde{q}_c}dt, \tag{4.17}$$

where

$$\begin{aligned}
\boldsymbol{K_D} &= \boldsymbol{T_1^{-1}\left(T_2 + M_{cc}^{-1}(q)C_{cc}(q,\dot{q})T_1 + M_{cc}^{-1}(q)R^{-1}\left(S_1' + T_1\right)\right)}, \\
\boldsymbol{K_P} &= \boldsymbol{T_1^{-1}\left(T_3 + M_{cc}^{-1}(q)C_{cc}(q,\dot{q})T_2 + M_{cc}^{-1}(q)R^{-1}\left(S_2' + T_2\right)\right)}, \\
\boldsymbol{K_I} &= \boldsymbol{-T_1^{-1}\left(M_{cc}^{-1}(q)C_{cc}(q,\dot{q})T_3 + M_{cc}^{-1}(q)R^{-1}\left(S_3' + T_3\right)\right)}.
\end{aligned}$$

A particular case can be obtained when the components of weighting compound $\boldsymbol{W'W}$ verify:

$$\boldsymbol{Q} = \begin{bmatrix} \omega_1^2\mathbb{1} & \mathbb{0} & \mathbb{0} \\ \mathbb{0} & \omega_2^2\mathbb{1} & \mathbb{0} \\ \mathbb{0} & \mathbb{0} & \omega_3^2\mathbb{1} \end{bmatrix}, \quad \boldsymbol{S} = \begin{bmatrix} \mathbb{0} \\ \mathbb{0} \\ \mathbb{0} \end{bmatrix}, \quad \boldsymbol{R} = \omega_u^2\mathbb{1}. \tag{4.18}$$

In this case, the following analytical expressions for the gain matrices have been obtained:

$$\begin{aligned}
\boldsymbol{K_D} &= \frac{\sqrt{\omega_2^2+2\omega_1\omega_3}}{\omega_1}\mathbb{1}+\boldsymbol{M_{cc}^{-1}}(\boldsymbol{q})\left(\boldsymbol{C_{cc}}(\boldsymbol{q},\dot{\boldsymbol{q}})+\frac{1}{\omega_u^2}\mathbb{1}\right),\\
\boldsymbol{K_P} &= \frac{\omega_3}{\omega_1}\mathbb{1}+\frac{\sqrt{\omega_2^2+2\omega_1\omega_3}}{\omega_1}\boldsymbol{M_{cc}^{-1}}(\boldsymbol{q})\left(\boldsymbol{C_{cc}}(\boldsymbol{q},\dot{\boldsymbol{q}})+\frac{1}{\omega_u^2}\mathbb{1}\right),\\
\boldsymbol{K_I} &= \frac{\omega_3}{\omega_1}\boldsymbol{M_{cc}^{-1}}(\boldsymbol{q})\left(\boldsymbol{C_{cc}}(\boldsymbol{q},\dot{\boldsymbol{q}})+\frac{1}{\omega_u^2}\mathbb{1}\right),
\end{aligned} \tag{4.19}$$

where the parameters ω_1, ω_2, ω_3 and ω_u are tuned by a systematic procedure taking in mind a linear PID control action interpretation (see López-Martínez et al. (2007)).

Equation (4.17) gives the *controlled* degrees of freedom acceleration required to track the desired reference. The forces/torques applied to the underactuated mechanical system can be computed using this *control acceleration*, which does not depend on the acceleration of the *controlled* DOF, but on their reference acceleration as pointed out before. Thereby, if the underactuated mechanical system has noninteracting inputs, equation (4.1), considering $\boldsymbol{\delta}=0$, can be written as follows (Siqueira and Terra, 2004a):

$$\begin{bmatrix} \boldsymbol{M_{au}}(\boldsymbol{q}) & \boldsymbol{M_{ac}}(\boldsymbol{q}) \\ \boldsymbol{M_{pu}}(\boldsymbol{q}) & \boldsymbol{M_{pc}}(\boldsymbol{q}) \end{bmatrix}\begin{bmatrix} \ddot{\boldsymbol{q}}_{\boldsymbol{u}} \\ \ddot{\boldsymbol{q}}_{\boldsymbol{c}} \end{bmatrix}+\begin{bmatrix} \boldsymbol{C_{au}}(\boldsymbol{q},\dot{\boldsymbol{q}}) & \boldsymbol{C_{ac}}(\boldsymbol{q},\dot{\boldsymbol{q}}) \\ \boldsymbol{C_{pu}}(\boldsymbol{q},\dot{\boldsymbol{q}}) & \boldsymbol{C_{pc}}(\boldsymbol{q},\dot{\boldsymbol{q}}) \end{bmatrix}\begin{bmatrix} \dot{\boldsymbol{q}}_{\boldsymbol{u}} \\ \dot{\boldsymbol{q}}_{\boldsymbol{c}} \end{bmatrix}+\begin{bmatrix} \boldsymbol{G_a}(\boldsymbol{q}) \\ \boldsymbol{G_p}(\boldsymbol{q}) \end{bmatrix}=\begin{bmatrix} \boldsymbol{\Gamma_a}(\boldsymbol{q}) \\ \mathbb{0} \end{bmatrix}, \tag{4.20}$$

where the subscripts $\boldsymbol{a}$ and $\boldsymbol{p}$ denote *active* and *passive*, respectively. Thus, the forces/torques in the *active* DOF can be obtained by isolating vector $\ddot{\boldsymbol{q}}_{\boldsymbol{u}}$ in the second row of (4.20) and replacing it in the first one, as follows:

$$\boldsymbol{\Gamma_a}=\boldsymbol{M_o}(\boldsymbol{q})\ddot{\boldsymbol{q}}_{\boldsymbol{c}}+\boldsymbol{C_o}(\boldsymbol{q},\dot{\boldsymbol{q}})\dot{\boldsymbol{q}}_{\boldsymbol{c}}+\boldsymbol{E_o}(\boldsymbol{q},\dot{\boldsymbol{q}})\dot{\boldsymbol{q}}_{\boldsymbol{u}}+\boldsymbol{G_o}(\boldsymbol{q}), \tag{4.21}$$

where:

$$\begin{aligned}
\boldsymbol{M}_o(\boldsymbol{q}) &= \boldsymbol{M}_{ac}(\boldsymbol{q}) - \boldsymbol{M}_{au}(\boldsymbol{q})\boldsymbol{M}_{pu}^{-1}(\boldsymbol{q})\boldsymbol{M}_{pc}(\boldsymbol{q}),\\
\boldsymbol{C}_o(\boldsymbol{q},\dot{\boldsymbol{q}}) &= \boldsymbol{C}_{ac}(\boldsymbol{q},\dot{\boldsymbol{q}}) - \boldsymbol{M}_{au}(\boldsymbol{q})\boldsymbol{M}_{pu}^{-1}(\boldsymbol{q})\boldsymbol{C}_{pc}(\boldsymbol{q},\dot{\boldsymbol{q}}),\\
\boldsymbol{E}_o(\boldsymbol{q},\dot{\boldsymbol{q}}) &= \boldsymbol{C}_{au}(\boldsymbol{q},\dot{\boldsymbol{q}}) - \boldsymbol{M}_{au}(\boldsymbol{q})\boldsymbol{M}_{pu}^{-1}(\boldsymbol{q})\boldsymbol{C}_{pu}(\boldsymbol{q},\dot{\boldsymbol{q}}),\\
\boldsymbol{G}_o(\boldsymbol{q}) &= \boldsymbol{G}_a(\boldsymbol{q}) - \boldsymbol{M}_{au}(\boldsymbol{q})\boldsymbol{M}_{pu}^{-1}(\boldsymbol{q})\boldsymbol{G}_p(\boldsymbol{q}).
\end{aligned}$$

On the other hand, if the underactuated mechanical system presents input coupling, it is not suitable to use the *passive/active* (*unactuated/actuated*) notation, since all degrees of freedom are directly affected by the control input vector. Then, for the sake of clarity, the *uncontrolled/controlled* nomenclature is maintained, and the applied force/torque vector is obtained by isolating the vector $\ddot{\boldsymbol{q}}_{\boldsymbol{u}}$ in the first row of (4.1) and replacing it in the second one, as follows:

$$\boldsymbol{\Gamma} = \boldsymbol{B}_o^{-1}(\boldsymbol{q})\left[\boldsymbol{M}_o(\boldsymbol{q})\ddot{\boldsymbol{q}}_{\boldsymbol{c}} + \boldsymbol{C}_o(\boldsymbol{q},\dot{\boldsymbol{q}})\dot{\boldsymbol{q}}_{\boldsymbol{c}} + \boldsymbol{E}_o(\boldsymbol{q},\dot{\boldsymbol{q}})\dot{\boldsymbol{q}}_{\boldsymbol{u}} + \boldsymbol{G}_o(\boldsymbol{q})\right], \tag{4.22}$$

where:

$$\begin{aligned}
\boldsymbol{B}_o(\boldsymbol{q}) &= \boldsymbol{B}_c(\boldsymbol{q}) - \boldsymbol{M}_{cu}(\boldsymbol{q})\boldsymbol{M}_{uu}^{-1}(\boldsymbol{q})\boldsymbol{B}_u(\boldsymbol{q}),\\
\boldsymbol{M}_o(\boldsymbol{q}) &= \boldsymbol{M}_{cc}(\boldsymbol{q}) - \boldsymbol{M}_{cu}(\boldsymbol{q})\boldsymbol{M}_{uu}^{-1}(\boldsymbol{q})\boldsymbol{M}_{uc}(\boldsymbol{q}),\\
\boldsymbol{C}_o(\boldsymbol{q},\dot{\boldsymbol{q}}) &= \boldsymbol{C}_{cc}(\boldsymbol{q},\dot{\boldsymbol{q}}) - \boldsymbol{M}_{cu}(\boldsymbol{q})\boldsymbol{M}_{uu}^{-1}(\boldsymbol{q})\boldsymbol{C}_{uc}(\boldsymbol{q},\dot{\boldsymbol{q}}),\\
\boldsymbol{E}_o(\boldsymbol{q},\dot{\boldsymbol{q}}) &= \boldsymbol{C}_{cu}(\boldsymbol{q},\dot{\boldsymbol{q}}) - \boldsymbol{M}_{cu}(\boldsymbol{q})\boldsymbol{M}_{uu}^{-1}(\boldsymbol{q})\boldsymbol{C}_{uu}(\boldsymbol{q},\dot{\boldsymbol{q}}),\\
\boldsymbol{G}_o(\boldsymbol{q}) &= \boldsymbol{G}_c(\boldsymbol{q}) - \boldsymbol{M}_{cu}(\boldsymbol{q})\boldsymbol{M}_{uu}^{-1}(\boldsymbol{q})\boldsymbol{G}_u(\boldsymbol{q}).
\end{aligned}$$

The proposed control law guarantees that all equilibrium points in the *controlled* workspace are globally asymptotically stable for the *controlled* subsystem if the *remaining* degrees of freedom are stable or converge asymptotically to the path to be followed. Therefore, the attraction basin in the outer-inner closed-loop is enlarged or reduced by modifying the gains parameters.

It should be pointed out that the first step of the controller proposed in Siqueira and Terra (2004a) can be considered as a particular case of the previous control law, which is obtained if parameter ω_3 is set to a null value.

4.3.1 A Generalization Approach of the Weighting Matrices

In this section, the nonlinear $\mathscr{H}_\infty$ controller presented previously will be generalized giving more flexibility to tune the control law, allowing to weight different dynamics of the system. This is an improvement of nonlinear $\mathscr{H}_\infty$ controllers applied to mechanical systems when compared with the ones proposed by Chen et al. (1994), Feng and Postlethwaite (1994), Siqueira and Terra (2004b) and Ortega et al. (2005).

The controller developed here is based on the reduced model of the *controlled* subsystem, and on the diagonalization method discussed in Section 4.2. Therefore, consider the reduced system (4.1), which is presented again:

$$\boldsymbol{M}_{cc}(\boldsymbol{q})\ddot{\boldsymbol{q}}_c + \boldsymbol{C}_{cc}(\boldsymbol{q},\dot{\boldsymbol{q}})\dot{\boldsymbol{q}}_c + + \boldsymbol{G}_c(\boldsymbol{q}) = \bar{\boldsymbol{\Gamma}} + \boldsymbol{\delta}_c\,, \tag{4.23}$$

and partitioned in two different dynamics by the diagonalization of the inertia matrix $\boldsymbol{M}_{cc}(\boldsymbol{q})$. Hence, a normalized *controlled* subsystem can be obtained by the same way performed with the system (4.7):

$$\overline{\boldsymbol{M}}_{cc}(\boldsymbol{q})\ddot{\boldsymbol{q}}_c + \overline{\boldsymbol{C}}_{cc}(\boldsymbol{q},\dot{\boldsymbol{q}})\dot{\boldsymbol{q}}_c + \overline{\boldsymbol{G}}_c(\boldsymbol{q}) = \overline{\boldsymbol{\Gamma}}_c(\boldsymbol{q}) + \overline{\boldsymbol{\delta}}_c\,, \tag{4.24}$$

with the following form:

$$\begin{bmatrix} \boldsymbol{M}_{c1}(\boldsymbol{q}) & \mathbb{0} \\ \mathbb{0} & \boldsymbol{M}_{c2}(\boldsymbol{q}) \end{bmatrix} \begin{bmatrix} \ddot{\boldsymbol{q}}_{c1} \\ \ddot{\boldsymbol{q}}_{c2} \end{bmatrix} + \begin{bmatrix} \boldsymbol{C}_{c1_1}(\boldsymbol{q},\dot{\boldsymbol{q}}) & \boldsymbol{C}_{c1_2}(\boldsymbol{q},\dot{\boldsymbol{q}}) \\ \boldsymbol{C}_{c2_1}(\boldsymbol{q},\dot{\boldsymbol{q}}) & \boldsymbol{C}_{c2_2}(\boldsymbol{q},\dot{\boldsymbol{q}}) \end{bmatrix} \begin{bmatrix} \dot{\boldsymbol{q}}_{c1} \\ \dot{\boldsymbol{q}}_{c2} \end{bmatrix} + \begin{bmatrix} \boldsymbol{G}_{c1}(\boldsymbol{q}) \\ \boldsymbol{G}_{c2}(\boldsymbol{q}) \end{bmatrix} = \begin{bmatrix} \boldsymbol{\Gamma}_{c1}(\boldsymbol{q}) \\ \boldsymbol{\Gamma}_{c2}(\boldsymbol{q}) \end{bmatrix} + \begin{bmatrix} \boldsymbol{\delta}_{c1} \\ \boldsymbol{\delta}_{c2} \end{bmatrix}, \tag{4.25}$$

where:

$$\begin{aligned} \overline{\boldsymbol{\Gamma}}_c(\boldsymbol{q}) &= \boldsymbol{T}_{\boldsymbol{M}}(\boldsymbol{q})\bar{\boldsymbol{\Gamma}}, \\ \overline{\boldsymbol{\delta}}(\boldsymbol{q})(\boldsymbol{q}) &= \boldsymbol{T}_{\boldsymbol{M}}(\boldsymbol{q})\boldsymbol{\delta}_c(\boldsymbol{q},\dot{\boldsymbol{q}},\ddot{\boldsymbol{q}},\boldsymbol{\Gamma}_d)\,, \\ \overline{\boldsymbol{M}}_{cc}(\boldsymbol{q}) &= \boldsymbol{T}_{\boldsymbol{M}}(\boldsymbol{q})\boldsymbol{M}_{cc}(\boldsymbol{q})\,, \\ \overline{\boldsymbol{C}}_{cc}(\boldsymbol{q},\dot{\boldsymbol{q}}) &= \boldsymbol{T}_{\boldsymbol{M}}(\boldsymbol{q})\boldsymbol{C}_{cc}(\boldsymbol{q},\dot{\boldsymbol{q}})\,, \\ \overline{\boldsymbol{G}}_c(\boldsymbol{q}) &= \boldsymbol{T}_{\boldsymbol{M}}(\boldsymbol{q})\boldsymbol{G}_c(\boldsymbol{q})\,, \end{aligned}$$

and the normalization matrix $\boldsymbol{T_M}$ is obtained as follows:

$$\boldsymbol{T_M}(\boldsymbol{q}) = \begin{bmatrix} \mathbb{1} & -\boldsymbol{M}_{c_{12}}(\boldsymbol{q})\boldsymbol{M}_{c_{22}}^{-1}(\boldsymbol{q}) \\ -\boldsymbol{M}_{c_{21}}(\boldsymbol{q})\boldsymbol{M}_{c_{11}}^{-1}(\boldsymbol{q}) & \mathbb{1} \end{bmatrix}.$$

By redefining the tracking error of the *controlled* DOF, results in:

$$\boldsymbol{x_c} = \begin{bmatrix} \dot{\tilde{\boldsymbol{q}}}_{c1} \\ \dot{\tilde{\boldsymbol{q}}}_{c2} \\ \tilde{\boldsymbol{q}}_{c1} \\ \tilde{\boldsymbol{q}}_{c2} \\ \int \tilde{\boldsymbol{q}}_{c1} dt \\ \int \tilde{\boldsymbol{q}}_{c2} dt \end{bmatrix} = \begin{bmatrix} \dot{\boldsymbol{q}}_{c1} - \dot{\boldsymbol{q}}_{c1_r} \\ \dot{\boldsymbol{q}}_{c2} - \dot{\boldsymbol{q}}_{c2_r} \\ \boldsymbol{q}_{c1} - \boldsymbol{q}_{c1_r} \\ \boldsymbol{q}_{c2} - \boldsymbol{q}_{c2_r} \\ \int \left(\boldsymbol{q}_{c1} - \boldsymbol{q}_{c1_r}\right) dt \\ \int \left(\boldsymbol{q}_{c2} - \boldsymbol{q}_{c2_r}\right) dt \end{bmatrix}, \tag{4.26}$$

The equation (4.6) in the state space form is rewritten as follows:

$$\dot{\boldsymbol{x}}_{\boldsymbol{c}} = \overline{f}(\boldsymbol{x_c}, \boldsymbol{q_u}, t) + \overline{g_0}(\boldsymbol{q}, \dot{\boldsymbol{q}}, \ddot{\boldsymbol{q}}_{\boldsymbol{c_r}}, \dot{\boldsymbol{q}}_{\boldsymbol{c_r}}) + \overline{g}(\boldsymbol{x_c}, \boldsymbol{q_u}, t)\overline{\boldsymbol{\Gamma}}_{\boldsymbol{c}} + \overline{k}(\boldsymbol{x_c}, \boldsymbol{q_u}, t)\overline{\boldsymbol{\delta}}_{\boldsymbol{c}}\,, \tag{4.27}$$

where

$$\overline{f}\,(\boldsymbol{x}, \boldsymbol{q_u}, t) = \begin{bmatrix} -\boldsymbol{M}_{\boldsymbol{c1}}^{-1}\boldsymbol{C}_{\boldsymbol{c1_1}} & -\boldsymbol{M}_{\boldsymbol{c1}}^{-1}\boldsymbol{C}_{\boldsymbol{c1_2}} & \mathbb{0} & \mathbb{0} & \mathbb{0} & \mathbb{0} \\ -\boldsymbol{M}_{\boldsymbol{c2}}^{-1}\boldsymbol{C}_{\boldsymbol{c2_1}} & -\boldsymbol{M}_{\boldsymbol{c2}}^{-1}\boldsymbol{C}_{\boldsymbol{c2_2}} & \mathbb{0} & \mathbb{0} & \mathbb{0} & \mathbb{0} \\ \mathbb{1} & \mathbb{0} & \mathbb{0} & \mathbb{0} & \mathbb{0} & \mathbb{0} \\ \mathbb{0} & \mathbb{1} & \mathbb{0} & \mathbb{0} & \mathbb{0} & \mathbb{0} \\ \mathbb{0} & \mathbb{0} & \mathbb{1} & \mathbb{0} & \mathbb{0} & \mathbb{0} \\ \mathbb{0} & \mathbb{0} & \mathbb{0} & \mathbb{1} & \mathbb{0} & \mathbb{0} \end{bmatrix} \boldsymbol{x_c}\,,$$

$$\overline{g_0}(\boldsymbol{q}, \dot{\boldsymbol{q}}, \ddot{\boldsymbol{q}}_{\boldsymbol{r}}, \dot{\boldsymbol{q}}_{\boldsymbol{r}}) = \begin{bmatrix} -\boldsymbol{M}_{\boldsymbol{c1}}^{-1}(\boldsymbol{M}_{\boldsymbol{c1}}\ddot{\boldsymbol{q}}_{\boldsymbol{c1_r}} + \boldsymbol{C}_{\boldsymbol{c1_1}}\dot{\boldsymbol{q}}_{\boldsymbol{c1_r}} + \boldsymbol{C}_{\boldsymbol{c1_2}}\dot{\boldsymbol{q}}_{\boldsymbol{c2_r}} + \boldsymbol{G}_{\boldsymbol{c1}} \\ -\boldsymbol{M}_{\boldsymbol{c2}}^{-1}(\boldsymbol{M}_{\boldsymbol{c1}}\ddot{\boldsymbol{q}}_{\boldsymbol{c1_r}} + \boldsymbol{C}_{\boldsymbol{c2_1}}\dot{\boldsymbol{q}}_{\boldsymbol{c1_r}} + \boldsymbol{C}_{\boldsymbol{c2_2}}\dot{\boldsymbol{q}}_{\boldsymbol{c2_r}} + \boldsymbol{G}_{\boldsymbol{c2}} \\ \mathbb{0} \\ \mathbb{0} \\ \mathbb{0} \\ \mathbb{0} \end{bmatrix},$$

$$\overline{g}(\boldsymbol{x_c},\boldsymbol{q_u},t)=\overline{k}(\boldsymbol{x_c},\boldsymbol{q_u},t)=\begin{bmatrix}\boldsymbol{M_{c1}^{-1}} & \mathbb{0}\\ \mathbb{0} & \boldsymbol{M_{c2}^{-1}}\\ \mathbb{0} & \mathbb{0}\\ \mathbb{0} & \mathbb{0}\\ \mathbb{0} & \mathbb{0}\\ \mathbb{0} & \mathbb{0}\end{bmatrix},$$

being $\boldsymbol{q_{c1_r}}$ and $\boldsymbol{q_{c2_r}}$, $\dot{\boldsymbol{q}}_{\boldsymbol{c1_r}}$ and $\dot{\boldsymbol{q}}_{\boldsymbol{c2_r}}$, and $\ddot{\boldsymbol{q}}_{\boldsymbol{c1_r}}$ and $\ddot{\boldsymbol{q}}_{\boldsymbol{c2_r}}$ the desired trajectories and the corresponding velocities and accelerations of the *controlled* dynamics, respectively.

Therefore, from the state transformation (4.11), an augmented one is also used:

$$z=\begin{bmatrix}z_1\\z_2\\z_3\\z_4\\z_5\\z_6\end{bmatrix}=\boldsymbol{T_o x_c}=\begin{bmatrix}\boldsymbol{T_{11}} & \mathbb{0} & \boldsymbol{T_{13}} & \mathbb{0} & \boldsymbol{T_{15}} & \mathbb{0}\\ \mathbb{0} & \boldsymbol{T_{22}} & \mathbb{0} & \boldsymbol{T_{24}} & \mathbb{0} & \boldsymbol{T_{26}}\\ \mathbb{0} & \mathbb{0} & \mathbb{1} & \mathbb{0} & \mathbb{1} & \mathbb{0}\\ \mathbb{0} & \mathbb{0} & \mathbb{0} & \mathbb{1} & \mathbb{0} & \mathbb{1}\\ \mathbb{0} & \mathbb{0} & \mathbb{0} & \mathbb{0} & \mathbb{1} & \mathbb{0}\\ \mathbb{0} & \mathbb{0} & \mathbb{0} & \mathbb{0} & \mathbb{0} & \mathbb{1}\end{bmatrix}\begin{bmatrix}\dot{\tilde{\boldsymbol{q}}}_{\boldsymbol{c1}}\\ \dot{\tilde{\boldsymbol{q}}}_{\boldsymbol{c2}}\\ \tilde{\boldsymbol{q}}_{\boldsymbol{c1}}\\ \tilde{\boldsymbol{q}}_{\boldsymbol{c2}}\\ \int\tilde{\boldsymbol{q}}_{\boldsymbol{c1}}dt\\ \int\tilde{\boldsymbol{q}}_{\boldsymbol{c2}}dt\end{bmatrix},\tag{4.28}$$

with $\boldsymbol{T_{11}}=\rho\mathbb{1}$ and $\boldsymbol{T_{22}}=\mu\mathbb{1}$, being ρ and μ positive scalars and $\mathbb{1}$ the identity matrix with suitable dimension. For this case, where two different dynamics are considered, equation (4.12) is rewritten considering the transformation matrix $\boldsymbol{T_M}$:

$$\overline{\boldsymbol{u}}+\overline{\boldsymbol{d}}=\boldsymbol{T_M}(\boldsymbol{q})\,(\boldsymbol{u}+\boldsymbol{d})\,,\tag{4.29}$$

where, by considering the normalized system, it is given by:

$$\overline{\boldsymbol{u}}+\overline{\boldsymbol{d}}=\overline{\boldsymbol{M}}_{\boldsymbol{cc}}(\boldsymbol{q})\boldsymbol{T}\dot{\boldsymbol{x}}_{\boldsymbol{c}}+\overline{\boldsymbol{C}}_{\boldsymbol{cc}}(\boldsymbol{q},\dot{\boldsymbol{q}})\boldsymbol{T}\boldsymbol{x_c}\,,\tag{4.30}$$

$$\begin{bmatrix}\boldsymbol{u_{c1}}+\boldsymbol{d_{c1}}\\ \boldsymbol{u_{c2}}+\boldsymbol{d_{c1}}\end{bmatrix}=\begin{bmatrix}\boldsymbol{M_{c1}} & \mathbb{0} & \boldsymbol{C_{c1_1}} & \boldsymbol{C_{c1_2}}\\ \mathbb{0} & \boldsymbol{M_{c2}} & \boldsymbol{C_{c2_1}} & \boldsymbol{C_{c1_2}}\end{bmatrix}\begin{bmatrix}\dot{z}_1\\ \dot{z}_2\\ z_1\\ z_2\end{bmatrix}\tag{4.31}$$

$$=\begin{bmatrix}\boldsymbol{M_{c1}}(\boldsymbol{T_{11}}\ddot{\tilde{\boldsymbol{q}}}_{\boldsymbol{c1}}+\boldsymbol{T_{13}}\dot{\tilde{\boldsymbol{q}}}_{\boldsymbol{c1}}+\boldsymbol{T_{15}}\tilde{\boldsymbol{q}}_{\boldsymbol{c1}}) & + & \boldsymbol{C_{c1_1}}(\boldsymbol{T_{11}}\dot{\tilde{\boldsymbol{q}}}_{\boldsymbol{c1}}+\boldsymbol{T_{13}}\tilde{\boldsymbol{q}}_{\boldsymbol{c1}}+\boldsymbol{T_{15}}\int\tilde{\boldsymbol{q}}_{\boldsymbol{c1}})\\ & & +\boldsymbol{C_{c1_2}}(\boldsymbol{T_{22}}\dot{\tilde{\boldsymbol{q}}}_{\boldsymbol{c2}}+\boldsymbol{T_{24}}\tilde{\boldsymbol{q}}_{\boldsymbol{c2}}+\boldsymbol{T_{26}}\int\tilde{\boldsymbol{q}}_{\boldsymbol{c2}})\\ \boldsymbol{M_{c2}}(\boldsymbol{T_{22}}\ddot{\tilde{\boldsymbol{q}}}_{\boldsymbol{c2}}+\boldsymbol{T_{24}}\dot{\tilde{\boldsymbol{q}}}_{\boldsymbol{c2}}+\boldsymbol{T_{24}}\tilde{\boldsymbol{q}}_{\boldsymbol{c2}}) & + & \boldsymbol{C_{c2_1}}(\boldsymbol{T_{11}}\dot{\tilde{\boldsymbol{q}}}_{\boldsymbol{c1}}+\boldsymbol{T_{13}}\tilde{\boldsymbol{q}}_{\boldsymbol{c1}}+\boldsymbol{T_{15}}\int\tilde{\boldsymbol{q}}_{\boldsymbol{c1}})\\ & & +\boldsymbol{C_{c2_2}}(\boldsymbol{T_{22}}\dot{\tilde{\boldsymbol{q}}}_{\boldsymbol{c2}}+\boldsymbol{T_{24}}\tilde{\boldsymbol{q}}_{\boldsymbol{c2}}+\boldsymbol{T_{26}}\int\tilde{\boldsymbol{q}}_{\boldsymbol{c2}})\end{bmatrix},$$

where matrix $\boldsymbol{T}$ can be partitioned as follows:

$$\boldsymbol{T} = \begin{bmatrix} \boldsymbol{T_{11}} & \mathbb{0} & \boldsymbol{T_{13}} & \mathbb{0} & \boldsymbol{T_{15}} & \mathbb{0} \\ \mathbb{0} & \boldsymbol{T_{22}} & \mathbb{0} & \boldsymbol{T_{24}} & \mathbb{0} & \boldsymbol{T_{26}} \end{bmatrix}. \tag{4.32}$$

Therefore, the *dynamic equation of the system error* (4.13) for the partitioned *controlled* subsystem can be expressed in the following state space form:

$$\dot{\boldsymbol{x}}_{\boldsymbol{c}} = f(\boldsymbol{x}_{\boldsymbol{c}}, \boldsymbol{q}_{\boldsymbol{u}}, t) + g(\boldsymbol{x}_{\boldsymbol{c}}, \boldsymbol{q}_{\boldsymbol{u}}, t)\overline{\boldsymbol{u}} + k(\boldsymbol{x}_{\boldsymbol{c}}, \boldsymbol{q}_{\boldsymbol{r}}, t)\overline{\boldsymbol{d}}\,, \tag{4.33}$$

$$f(\boldsymbol{x}_{\boldsymbol{c}}, \boldsymbol{q}_{\boldsymbol{u}}, t) =$$

$$\boldsymbol{T}_{\boldsymbol{o}}^{-1} \begin{bmatrix} -\boldsymbol{M}_{\boldsymbol{c1}}^{-1}\boldsymbol{C}_{\boldsymbol{c1_1}} & -\boldsymbol{M}_{\boldsymbol{c1}}^{-1}\boldsymbol{C}_{\boldsymbol{c1_2}} & \mathbb{0} & \mathbb{0} & \mathbb{0} & \mathbb{0} \\ -\boldsymbol{M}_{\boldsymbol{c2}}^{-1}\boldsymbol{C}_{\boldsymbol{c2_1}} & -\boldsymbol{M}_{\boldsymbol{c2}}^{-1}\boldsymbol{C}_{\boldsymbol{c2_2}} & \mathbb{0} & \mathbb{0} & \mathbb{0} & \mathbb{0} \\ \boldsymbol{T}_{\boldsymbol{11}}^{-1} & \mathbb{0} & \boldsymbol{a_{33}} & \mathbb{0} & \boldsymbol{a_{35}} & \mathbb{0} \\ \mathbb{0} & \boldsymbol{T}_{\boldsymbol{22}}^{-1} & \mathbb{0} & \boldsymbol{a_{44}} & \mathbb{0} & \boldsymbol{a_{46}} \\ \mathbb{0} & \mathbb{0} & \mathbb{1} & \mathbb{0} & -\mathbb{1} & \mathbb{0} \\ \mathbb{0} & \mathbb{0} & \mathbb{0} & \mathbb{1} & \mathbb{0} & -\mathbb{1} \end{bmatrix} \boldsymbol{T}_{\boldsymbol{o}}\boldsymbol{x}_{\boldsymbol{c}}\,,$$

$$g(\boldsymbol{x}_{\boldsymbol{c}}, \boldsymbol{q}_{\boldsymbol{u}}, t) = k(\boldsymbol{x}_{\boldsymbol{c}}, \boldsymbol{q}_{\boldsymbol{u}}, t) = \boldsymbol{T}_{\boldsymbol{o}}^{-1} \begin{bmatrix} \boldsymbol{M}_{\boldsymbol{c1}}^{-1} & \mathbb{0} \\ \mathbb{0} & \boldsymbol{M}_{\boldsymbol{c2}}^{-1} \\ \mathbb{0} & \mathbb{0} \\ \mathbb{0} & \mathbb{0} \\ \mathbb{0} & \mathbb{0} \\ \mathbb{0} & \mathbb{0} \end{bmatrix},$$

where:

$$\begin{aligned} \boldsymbol{a_{33}} &= \mathbb{1} - \boldsymbol{T}_{\boldsymbol{11}}^{-1}\boldsymbol{T_{13}}\,, \\ \boldsymbol{a_{35}} &= -\mathbb{1} + \boldsymbol{T}_{\boldsymbol{11}}^{-1}(\boldsymbol{T_{13}} - \boldsymbol{T_{15}})\,, \\ \boldsymbol{a_{44}} &= \mathbb{1} - \boldsymbol{T}_{\boldsymbol{22}}^{-1}\boldsymbol{T_{24}}\,, \\ \boldsymbol{a_{46}} &= -\mathbb{1} + \boldsymbol{T}_{\boldsymbol{22}}^{-1}(\boldsymbol{T_{24}} - \boldsymbol{T_{26}})\,. \end{aligned}$$

By comparing equations (4.27) and (4.33), the transformed external disturbance vector $\overline{\boldsymbol{d}}$ and the control input $\overline{\boldsymbol{u}}$ are obtained:

$$\overline{\boldsymbol{d}} = \overline{\boldsymbol{M}}_{\boldsymbol{cc}}(\boldsymbol{q})\boldsymbol{T}_{\boldsymbol{c}}\overline{\boldsymbol{M}}_{\boldsymbol{cc}}^{-1}(\boldsymbol{q})\overline{\boldsymbol{\delta}}_{\boldsymbol{c}}\,, \tag{4.34}$$

$$\overline{\boldsymbol{u}} = \boldsymbol{T}_{\boldsymbol{c}}\left(-\boldsymbol{F}(\boldsymbol{x}_{\boldsymbol{e}}) + \overline{\boldsymbol{\Gamma}}_{\boldsymbol{c}}\right), \tag{4.35}$$

where:

$$\boldsymbol{T_c} = \begin{bmatrix} \boldsymbol{T_{11}} & \mathbb{0} \\ \mathbb{0} & \boldsymbol{T_{22}} \end{bmatrix},$$

and:

$$\begin{aligned} F(\boldsymbol{x_{e_1}}) &= \boldsymbol{M_{c1}}(\boldsymbol{q})\left(\ddot{\boldsymbol{q}}_{c1_r} - \boldsymbol{T_{11}^{-1}}\boldsymbol{T_{13}}\dot{\tilde{\boldsymbol{q}}}_{c1} - \boldsymbol{T_{11}^{-1}}\boldsymbol{T_{15}}\tilde{\boldsymbol{q}}_{c1}\right) + \boldsymbol{G_{c1}}(\boldsymbol{q}) \\ &\quad + \boldsymbol{C_{c1_2}}(\boldsymbol{q},\dot{\boldsymbol{q}})\left(\dot{\tilde{\boldsymbol{q}}}_{c2} + \dot{\boldsymbol{q}}_{c2_r} - \boldsymbol{T_{11}^{-1}}\boldsymbol{T_{22}}\dot{\tilde{\boldsymbol{q}}}_{c2} - \boldsymbol{T_{11}^{-1}}\boldsymbol{T_{24}}\tilde{\boldsymbol{q}}_{c2} - \boldsymbol{T_{11}^{-1}}\boldsymbol{T_{26}}\int \tilde{q}_{c2}\right) \\ &\quad + \boldsymbol{C_{c1_1}}(\boldsymbol{q},\dot{\boldsymbol{q}})\left(\dot{\boldsymbol{q}}_{c1_r} - \boldsymbol{T_{11}^{-1}}\boldsymbol{T_{13}}\tilde{\boldsymbol{q}}_{c1} - \boldsymbol{T_{11}^{-1}}\boldsymbol{T_{15}}\int \tilde{\boldsymbol{q}}_{c1}\right), \\ F(\boldsymbol{x_{e_2}}) &= \boldsymbol{M_{c1}}(\boldsymbol{q})\left(\ddot{\boldsymbol{q}}_{c2_r} - \boldsymbol{T_{22}^{-1}}\boldsymbol{T_{24}}\dot{\tilde{\boldsymbol{q}}}_{c2} - \boldsymbol{T_{22}^{-1}}\boldsymbol{T_{26}}\tilde{\boldsymbol{q}}_{c2}\right) + \boldsymbol{G_{c2}}(\boldsymbol{q}) \\ &\quad + \boldsymbol{C_{c2_1}}(\boldsymbol{q},\dot{\boldsymbol{q}})\left(\dot{\tilde{\boldsymbol{q}}}_{c1} + \dot{\boldsymbol{q}}_{c1_r} - \boldsymbol{T_{22}^{-1}}\boldsymbol{T_{11}}\dot{\tilde{\boldsymbol{q}}}_{c1} - \boldsymbol{T_{22}^{-1}}\boldsymbol{T_{13}}\tilde{\boldsymbol{q}}_{c1} - \boldsymbol{T_{22}^{-1}}\boldsymbol{T_{15}}\int \tilde{\boldsymbol{q}}_{c1}\right) \\ &\quad + \boldsymbol{C_{c2_2}}(\boldsymbol{q},\dot{\boldsymbol{q}})\left(\dot{\boldsymbol{q}}_{c2_r} - \boldsymbol{T_{22}^{-1}}\boldsymbol{T_{24}}\tilde{\boldsymbol{q}}_{c2} - \boldsymbol{T_{22}^{-1}}\boldsymbol{T_{26}}\int \tilde{\boldsymbol{q}}_{c2}\right). \end{aligned}$$

Note that from the definition of matrix $\boldsymbol{T_c}$ and since $\overline{\boldsymbol{M}}_{\boldsymbol{cc}}$ is a block diagonal matrix, both velocities of the dynamics 1 and 2 can be weighted independently. As mentioned before, the more dynamics are considered different, the more weighting blocks of the the diagonal matrix $\boldsymbol{T_c}$ form.

Therefore, the control input vector (4.14) is computed now for the normalized *controlled* subsystem, and is given by:

$$\overline{\boldsymbol{\Gamma}}_{\boldsymbol{c}} = \overline{\boldsymbol{M}}_{\boldsymbol{cc}}(\boldsymbol{q})\ddot{\boldsymbol{q}}_{\boldsymbol{c}} + \overline{\boldsymbol{C}}_{\boldsymbol{cc}}(\boldsymbol{q},\dot{\boldsymbol{q}})\dot{\boldsymbol{q}}_{\boldsymbol{c}} + \overline{\boldsymbol{G}}_{\boldsymbol{c}}(\boldsymbol{q}) - \boldsymbol{T_c^{-1}}\left(\overline{\boldsymbol{M}}_{\boldsymbol{cc}}\boldsymbol{T}\dot{\boldsymbol{x}}_{\boldsymbol{c}} + \overline{\boldsymbol{C}}_{\boldsymbol{cc}}\boldsymbol{T}\boldsymbol{x}_{\boldsymbol{c}}\right) + \boldsymbol{T_c^{-1}}\overline{\boldsymbol{u}}. \tag{4.36}$$

Since the controller developed in this section is a generalization of the one presented before, the same assumptions about the cost variable $\boldsymbol{\zeta}$ are considered here. Thus, from the symmetric positive definite matrix $\boldsymbol{W}'\boldsymbol{W}$ defined as in (3.25), and the definition of the error vector, $\boldsymbol{x_c}$, matrices $\boldsymbol{Q} \in \Re^{(3n_c \times 3n_c)}$, $\boldsymbol{S} \in \Re^{(3n_c \times m)}$ and $\boldsymbol{R} \in \Re^{(m \times m)}$ are structured as follows:

$$\boldsymbol{Q} = \begin{bmatrix} \boldsymbol{Q_1} & \boldsymbol{Q_{12}} & \boldsymbol{Q_{13}} & \boldsymbol{Q_{14}} & \boldsymbol{Q_{15}} & \boldsymbol{Q_{16}} \\ \boldsymbol{Q_{12}} & \boldsymbol{Q_2} & \boldsymbol{Q_{23}} & \boldsymbol{Q_{24}} & \boldsymbol{Q_{25}} & \boldsymbol{Q_{26}} \\ \boldsymbol{Q_{13}} & \boldsymbol{Q_{23}} & \boldsymbol{Q_3} & \boldsymbol{Q_{34}} & \boldsymbol{Q_{35}} & \boldsymbol{Q_{36}} \\ \boldsymbol{Q_{14}} & \boldsymbol{Q_{24}} & \boldsymbol{Q_{34}} & \boldsymbol{Q_4} & \boldsymbol{Q_{45}} & \boldsymbol{Q_{46}} \\ \boldsymbol{Q_{15}} & \boldsymbol{Q_{25}} & \boldsymbol{Q_{35}} & \boldsymbol{Q_{45}} & \boldsymbol{Q_5} & \boldsymbol{Q_{56}} \\ \boldsymbol{Q_{16}} & \boldsymbol{Q_{26}} & \boldsymbol{Q_{36}} & \boldsymbol{Q_{46}} & \boldsymbol{Q_{56}} & \boldsymbol{Q_6} \end{bmatrix}, \quad \boldsymbol{S} = \begin{bmatrix} \boldsymbol{S_{11}} & \boldsymbol{S_{12}} \\ \boldsymbol{S_{21}} & \boldsymbol{S_{22}} \\ \boldsymbol{S_{31}} & \boldsymbol{S_{32}} \\ \boldsymbol{S_{41}} & \boldsymbol{S_{42}} \\ \boldsymbol{S_{51}} & \boldsymbol{S_{52}} \\ \boldsymbol{S_{61}} & \boldsymbol{S_{62}} \end{bmatrix},$$

$$\boldsymbol{R} = \begin{bmatrix} \boldsymbol{R_{c1}} & \mathbb{0} \\ \mathbb{0} & \boldsymbol{R_{c2}} \end{bmatrix},$$

where $\boldsymbol{R_{c1}} \in \Re^{n_{c1} \times n_{c1}}$ and $\boldsymbol{R_{c2}} \in \Re^{n_{c2} \times n_{c2}}$. Note that $\boldsymbol{R}$ is chosen as a block diagonal matrix, which will allow to weight separately the control effort in both dynamics of *controlled* DOF.

Therefore, under these assumptions, the *value function* (4.15), $V(\boldsymbol{x_c}, \boldsymbol{q_u}, t)$, is rewritten in an expanded form:

$$V(\boldsymbol{x_c}, \boldsymbol{q_u}, t) = \frac{1}{2} \boldsymbol{x_c'} \boldsymbol{T_o'} \begin{bmatrix} \boldsymbol{M_{c_{11}}} & \boldsymbol{M_{c_{12}}} & \mathbb{0} & \mathbb{0} & \mathbb{0} & \mathbb{0} \\ \boldsymbol{M_{c_{21}}} & \boldsymbol{M_{c_{22}}} & \mathbb{0} & \mathbb{0} & \mathbb{0} & \mathbb{0} \\ \mathbb{0} & \mathbb{0} & \boldsymbol{K_{11}} & \boldsymbol{K_{12}} & \boldsymbol{K_{13}} & \boldsymbol{K_{14}} \\ \mathbb{0} & \mathbb{0} & \boldsymbol{K_{12}'} & \boldsymbol{K_{22}} & \boldsymbol{K_{23}} & \boldsymbol{K_{24}} \\ \mathbb{0} & \mathbb{0} & \boldsymbol{K_{13}'} & \boldsymbol{K_{23}'} & \boldsymbol{K_{33}} & \boldsymbol{K_{34}} \\ \mathbb{0} & \mathbb{0} & \boldsymbol{K_{14}'} & \boldsymbol{K_{24}'} & \boldsymbol{K_{34}'} & \boldsymbol{K_{44}} \end{bmatrix} \boldsymbol{T_o} \boldsymbol{x_c}, \quad (4.37)$$

where $\boldsymbol{M_{c_{11}}}$, $\boldsymbol{M_{c_{12}}}$, $\boldsymbol{M_{c_{21}}}$ and $\boldsymbol{M_{c_{22}}}$ form the inertia matrix of the *controlled* subsystem, $\boldsymbol{T_o}$ and $\boldsymbol{T}$ are the matrices defined in (4.28) and (4.32), respectively, and $\boldsymbol{K_{ij}}$ are constant and symmetric matrices. Furthermore, $\boldsymbol{K_{ii}} > \mathbb{0}$ with $i = 1, \ldots, 4$, such that:

$$\begin{bmatrix} \boldsymbol{K_{11}} & \boldsymbol{K_{12}} \\ \boldsymbol{K_{21}} & \boldsymbol{K_{22}} \end{bmatrix} > \mathbb{0},$$

$$\begin{bmatrix} \boldsymbol{K_{33}} & \boldsymbol{K_{34}} \\ \boldsymbol{K_{43}} & \boldsymbol{K_{44}} \end{bmatrix} > \mathbb{0},$$

$$\begin{bmatrix} \boldsymbol{K_{11}} & \boldsymbol{K_{12}} \\ \boldsymbol{K_{21}} & \boldsymbol{K_{22}} \end{bmatrix} - \begin{bmatrix} \boldsymbol{K_{13}} & \boldsymbol{K_{14}} \\ \boldsymbol{K_{23}} & \boldsymbol{K_{24}} \end{bmatrix} \begin{bmatrix} \boldsymbol{K_{33}} & \boldsymbol{K_{34}} \\ \boldsymbol{K_{43}} & \boldsymbol{K_{44}} \end{bmatrix}^{-1} \begin{bmatrix} \boldsymbol{K_{31}} & \boldsymbol{K_{32}} \\ \boldsymbol{K_{41}} & \boldsymbol{K_{42}} \end{bmatrix} > \mathbb{0}.$$

If these matrices verify the following equation:

$$\begin{bmatrix} \mathbb{0} & \mathbb{0} & \boldsymbol{K_{11}} & \boldsymbol{K_{12}} & \boldsymbol{K_{11}} + \boldsymbol{K_{13}} & \boldsymbol{K_{12}} + \boldsymbol{K_{14}} \\ * & \mathbb{0} & \boldsymbol{K_{12}} & \boldsymbol{K_{22}} & \boldsymbol{K_{12}} + \boldsymbol{K_{23}} & \boldsymbol{K_{22}} + \boldsymbol{K_{24}} \\ * & * & 2\boldsymbol{K_{11}} + 2\boldsymbol{K_{13}} & 2\boldsymbol{K_{12}} + \boldsymbol{K_{14}} + \boldsymbol{K_{23}} & \boldsymbol{K_{11}} + 2\boldsymbol{K_{13}} + \boldsymbol{K_{33}} & \boldsymbol{K_{12}} + \boldsymbol{K_{23}} + \boldsymbol{K_{14}} + \boldsymbol{K_{34}} \\ * & * & * & 2\boldsymbol{K_{22}} + 2\boldsymbol{K_{24}} & \boldsymbol{K_{12}} + \boldsymbol{K_{23}} + \boldsymbol{K_{14}} + \boldsymbol{K_{34}} & \boldsymbol{K_{22}} + 2\boldsymbol{K_{34}} + \boldsymbol{K_{44}} \\ * & * & * & * & \mathbb{0} & \mathbb{0} \\ * & * & * & * & * & \mathbb{0} \end{bmatrix} +$$

$$+\boldsymbol{Q} + \frac{1}{\gamma^2} \boldsymbol{T'} \boldsymbol{T} - \left(\boldsymbol{S'} + \boldsymbol{T}\right)' \boldsymbol{R}^{-1} \left(\boldsymbol{S'} + \boldsymbol{T}\right) = \mathbb{0}, \quad (4.38)$$

function $V(\boldsymbol{x_c}, \boldsymbol{q_u}, t)$ constitutes a solution to the HJ equation (3.34), for a sufficiently high value of γ. The symbol $*$ represents terms that can be inferred by

symmetry.

The algorithm for obtaining matrix $\boldsymbol{T}$ is the following:

1. Compute $\boldsymbol{T}_{11}$, $\boldsymbol{T}_{22}$, $\boldsymbol{T}_{15}$ and $\boldsymbol{T}_{26}$ by solving the following Riccati algebraic equations:

$$\boldsymbol{Q}_1 + \frac{1}{\gamma^2}\boldsymbol{T}'_{11}\boldsymbol{T}_{11} - \left(\boldsymbol{S}'_{11} + \boldsymbol{T}_{11}\right)' \boldsymbol{R}_{c1}^{-1}\left(\boldsymbol{S}'_{11} + \boldsymbol{T}_{11}\right) - \boldsymbol{S}_{12}\boldsymbol{R}_{c2}^{-1}\boldsymbol{S}'_{12} = \mathbb{0} \tag{4.39}$$

$$\boldsymbol{Q}_2 + \frac{1}{\gamma^2}\boldsymbol{T}'_{22}\boldsymbol{T}_{22} - \left(\boldsymbol{S}'_{22} + \boldsymbol{T}_{22}\right)' \boldsymbol{R}_{c2}^{-1}\left(\boldsymbol{S}'_{22} + \boldsymbol{T}_{22}\right) - \boldsymbol{S}_{21}\boldsymbol{R}_{u}^{-1}\boldsymbol{S}'_{21} = \mathbb{0} \tag{4.40}$$

$$\boldsymbol{Q}_5 + \frac{1}{\gamma^2}\boldsymbol{T}'_{15}\boldsymbol{T}_{15} - \left(\boldsymbol{S}'_{51} + \boldsymbol{T}_{15}\right)' \boldsymbol{R}_{c1}^{-1}\left(\boldsymbol{S}'_{51} + \boldsymbol{T}_{15}\right) - \boldsymbol{S}_{52}\boldsymbol{R}_{c2}^{-1}\boldsymbol{S}'_{52} = \mathbb{0} \tag{4.41}$$

$$\boldsymbol{Q}_6 + \frac{1}{\gamma^2}\boldsymbol{T}'_{26}\boldsymbol{T}_{26} - \left(\boldsymbol{S}'_{62} + \boldsymbol{T}_{26}\right)' \boldsymbol{R}_{c2}^{-1}\left(\boldsymbol{S}'_{62} + \boldsymbol{T}_{26}\right) - \boldsymbol{S}_{61}\boldsymbol{R}_{c1}^{-1}\boldsymbol{S}'_{41} = \mathbb{0} \tag{4.42}$$

2. Compute matrices $\boldsymbol{K}_{11} + \boldsymbol{K}_{13}$ and $\boldsymbol{K}_{11} + \boldsymbol{K}_{13}$ through the following equations:

$$\begin{aligned}\boldsymbol{K}_{11} + \boldsymbol{K}_{13} + \boldsymbol{Q}_{15} + \tfrac{1}{\gamma^2}\boldsymbol{T}'_{11}\boldsymbol{T}_{15} - \left(\boldsymbol{S}'_{11} + \boldsymbol{T}_{11}\right)' \boldsymbol{R}_{c1}^{-1}\left(\boldsymbol{S}'_{51} + \boldsymbol{T}_{15}\right) \\ -\boldsymbol{S}_{12}\boldsymbol{R}_{c2}^{-1}\boldsymbol{S}'_{52} = \mathbb{0}\end{aligned} \tag{4.43}$$

$$\begin{aligned}\boldsymbol{K}_{22} + \boldsymbol{K}_{24} + \boldsymbol{Q}_{26} + \tfrac{1}{\gamma^2}\boldsymbol{T}'_{22}\boldsymbol{T}_{26} - \left(\boldsymbol{S}'_{22} + \boldsymbol{T}_{22}\right)' \boldsymbol{R}_{c2}^{-1}\left(\boldsymbol{S}'_{62} + \boldsymbol{T}_{26}\right) \\ -\boldsymbol{S}_{21}\boldsymbol{R}_{c1}^{-1}\boldsymbol{S}'_{61} = \mathbb{0}\end{aligned} \tag{4.44}$$

3. Compute $\boldsymbol{T}_{13}$ and $\boldsymbol{T}_{24}$ by solving the following Riccati algebraic equations:

$$\begin{aligned}2(\boldsymbol{K}_{11} + \boldsymbol{K}_{13}) + \boldsymbol{Q}_3 + \tfrac{1}{\gamma^2}\boldsymbol{T}'_{13}\boldsymbol{T}_{13} - \left(\boldsymbol{S}'_{31} + \boldsymbol{T}_{13}\right)' \boldsymbol{R}_{c1}^{-1}\left(\boldsymbol{S}'_{31} + \boldsymbol{T}_{13}\right) \\ -\boldsymbol{S}_{32}\boldsymbol{R}_{c2}^{-1}\boldsymbol{S}'_{32} = \mathbb{0}\end{aligned} \tag{4.45}$$

$$\begin{aligned}2(\boldsymbol{K}_{22} + \boldsymbol{K}_{24}) + \boldsymbol{Q}_{34} + \tfrac{1}{\gamma^2}\boldsymbol{T}'_{24}\boldsymbol{T}_{24} - \left(\boldsymbol{S}'_{42} + \boldsymbol{T}_{24}\right)' \boldsymbol{R}_{c2}^{-1}\left(\boldsymbol{S}'_{42} + \boldsymbol{T}_{24}\right) \\ -\boldsymbol{S}_{41}\boldsymbol{R}_{c1}^{-1}\boldsymbol{S}'_{41} = \mathbb{0}\end{aligned} \tag{4.46}$$

Once matrix $\boldsymbol{T}$ is computed, from the optimal state feedback control law (3.32), the *additional control* effort $\overline{\boldsymbol{u}}^*$ corresponding to the $\mathscr{H}_\infty$ optimal index

γ is given by

$$\overline{\boldsymbol{u}}^* = -\boldsymbol{T}_{\boldsymbol{M}}\boldsymbol{R}^{-1}\left(\boldsymbol{S}' + \boldsymbol{T}\right)\boldsymbol{x}_{\boldsymbol{c}}\,. \tag{4.47}$$

Finally, if the *additional control* effort (4.47) is replaced into (4.30) under the assumption that $\overline{\boldsymbol{d}} = 0$, and after some manipulations, the *control acceleration* can be obtained as follows:

$$\ddot{\boldsymbol{q}}_{\boldsymbol{c}} = \ddot{\boldsymbol{q}}_{\boldsymbol{c}}^{\boldsymbol{d}} - \boldsymbol{K}_{\boldsymbol{Dc}}\dot{\tilde{\boldsymbol{q}}}_{\boldsymbol{c}} - \boldsymbol{K}_{\boldsymbol{Pc}}\tilde{\boldsymbol{q}}_{\boldsymbol{c}} - \boldsymbol{K}_{\boldsymbol{Ic}}\int \tilde{\boldsymbol{q}}_{\boldsymbol{c}}dt\,, \tag{4.48}$$

with

$$\boldsymbol{K}_{\boldsymbol{Dc}} = \begin{bmatrix} \boldsymbol{K}_{\boldsymbol{Dc}_{11}} & \boldsymbol{K}_{\boldsymbol{Dc}_{12}} \\ \boldsymbol{K}_{\boldsymbol{Dc}_{21}} & \boldsymbol{K}_{\boldsymbol{Dc}_{22}} \end{bmatrix}, \boldsymbol{K}_{\boldsymbol{Pc}} = \begin{bmatrix} \boldsymbol{K}_{\boldsymbol{Pc}_{11}} & \boldsymbol{K}_{\boldsymbol{Pc}_{12}} \\ \boldsymbol{K}_{\boldsymbol{Pc}_{21}} & \boldsymbol{K}_{\boldsymbol{Pc}_{22}} \end{bmatrix}, \boldsymbol{K}_{\boldsymbol{Dc}} = \begin{bmatrix} \boldsymbol{K}_{\boldsymbol{Ic}_{11}} & \boldsymbol{K}_{\boldsymbol{Ic}_{12}} \\ \boldsymbol{K}_{\boldsymbol{Ic}_{21}} & \boldsymbol{K}_{\boldsymbol{Ic}_{22}} \end{bmatrix},$$

where

$$\begin{aligned}
\boldsymbol{K}_{\boldsymbol{Dc}_{11}} &= \boldsymbol{T}_{11}^{-1}\boldsymbol{M}_{c1}^{-1}\left(\boldsymbol{C}_{c1_1}\boldsymbol{T}_{11} + \boldsymbol{R}_{c1}^{-1}(\boldsymbol{S}'_{11} + \boldsymbol{T}_{11}) - \boldsymbol{M}_{c_{12}}\boldsymbol{M}_{c_{22}}^{-1}\boldsymbol{R}_{c2}^{-1}\boldsymbol{S}'_{12}\right) + \boldsymbol{T}_{11}^{-1}\boldsymbol{T}_{13} \\
\boldsymbol{K}_{\boldsymbol{Dc}_{12}} &= \boldsymbol{T}_{11}^{-1}\boldsymbol{M}_{c1}^{-1}\left(\boldsymbol{C}_{c1_2}\boldsymbol{T}_{22} + \boldsymbol{R}_{c1}^{-1}\boldsymbol{S}'_{21} - \boldsymbol{M}_{c_{12}}\boldsymbol{M}_{c_{22}}^{-1}\boldsymbol{R}_{c2}^{-1}(\boldsymbol{S}'_{22} + \boldsymbol{T}_{22})\right) \\
\boldsymbol{K}_{\boldsymbol{Pc}_{11}} &= \boldsymbol{T}_{11}^{-1}\boldsymbol{M}_{c1}^{-1}\left(\boldsymbol{C}_{c1_1}\boldsymbol{T}_{13} + \boldsymbol{R}_{c1}^{-1}(\boldsymbol{S}'_{31} + \boldsymbol{T}_{13}) - \boldsymbol{M}_{c_{12}}\boldsymbol{M}_{c_{22}}^{-1}\boldsymbol{R}_{c2}^{-1}\boldsymbol{S}'_{32}\right) + \boldsymbol{T}_{11}^{-1}\boldsymbol{T}_{15} \\
\boldsymbol{K}_{\boldsymbol{Pc}_{12}} &= \boldsymbol{T}_{11}^{-1}\boldsymbol{M}_{c1}^{-1}\left(\boldsymbol{C}_{c1_2}\boldsymbol{T}_{24} + \boldsymbol{R}_{c1}^{-1}\boldsymbol{S}'_{41} - \boldsymbol{M}_{c_{12}}\boldsymbol{M}_{c_{22}}^{-1}\boldsymbol{R}_{c2}^{-1}(\boldsymbol{S}'_{42} + \boldsymbol{T}_{24})\right) \\
\boldsymbol{K}_{\boldsymbol{Ic}_{11}} &= \boldsymbol{T}_{11}^{-1}\boldsymbol{M}_{c1}^{-1}\left(\boldsymbol{C}_{c1_1}\boldsymbol{T}_{15} + \boldsymbol{R}_{c1}^{-1}(\boldsymbol{S}'_{51} + \boldsymbol{T}_{15}) - \boldsymbol{M}_{c_{12}}\boldsymbol{M}_{c_{22}}^{-1}\boldsymbol{R}_{c2}^{-1}\boldsymbol{S}'_{52}\right) \\
\boldsymbol{K}_{\boldsymbol{Ic}_{12}} &= \boldsymbol{T}_{11}^{-1}\boldsymbol{M}_{c1}^{-1}\left(\boldsymbol{C}_{c1_2}\boldsymbol{T}_{26} + \boldsymbol{R}_{c1}^{-1}\boldsymbol{S}'_{61} - \boldsymbol{M}_{c_{12}}\boldsymbol{M}_{c_{22}}^{-1}\boldsymbol{R}_{c2}^{-1}(\boldsymbol{S}'_{62} + \boldsymbol{T}_{26})\right) \\
\boldsymbol{K}_{\boldsymbol{Dc}_{21}} &= \boldsymbol{T}_{22}^{-1}\boldsymbol{M}_{c2}^{-1}\left(\boldsymbol{C}_{c2_1}\boldsymbol{T}_{11} + \boldsymbol{R}_{c2}^{-1}\boldsymbol{S}'_{12} - \boldsymbol{M}_{c_{21}}\boldsymbol{M}_{c_{11}}^{-1}\boldsymbol{R}_{c1}^{-1}(\boldsymbol{S}'_{11} + \boldsymbol{T}_{11})\right) \\
\boldsymbol{K}_{\boldsymbol{Dc}_{22}} &= \boldsymbol{T}_{22}^{-1}\boldsymbol{M}_{c2}^{-1}\left(\boldsymbol{C}_{c2_2}\boldsymbol{T}_{22} + \boldsymbol{R}_{c2}^{-1}(\boldsymbol{S}'_{22} + \boldsymbol{T}_{22}) - \boldsymbol{M}_{c_{21}}\boldsymbol{M}_{c_{11}}^{-1}\boldsymbol{R}_{c1}^{-1}\boldsymbol{S}'_{21}\right) + \boldsymbol{T}_{22}^{-1}\boldsymbol{T}_{24} \\
\boldsymbol{K}_{\boldsymbol{Pc}_{21}} &= \boldsymbol{T}_{22}^{-1}\boldsymbol{M}_{c2}^{-1}\left(\boldsymbol{C}_{c2_1}\boldsymbol{T}_{13} + \boldsymbol{R}_{c2}^{-1}\boldsymbol{S}'_{32} - \boldsymbol{M}_{c_{21}}\boldsymbol{M}_{c_{11}}^{-1}\boldsymbol{R}_{c1}^{-1}(\boldsymbol{S}'_{31} + \boldsymbol{T}_{13})\right) \\
\boldsymbol{K}_{\boldsymbol{Pc}_{22}} &= \boldsymbol{T}_{22}^{-1}\boldsymbol{M}_{c2}^{-1}\left(\boldsymbol{C}_{c2_2}\boldsymbol{T}_{24} + \boldsymbol{R}_{c2}^{-1}(\boldsymbol{S}'_{42} + \boldsymbol{T}_{24}) - \boldsymbol{M}_{c_{21}}\boldsymbol{M}_{c_{11}}^{-1}\boldsymbol{R}_{c1}^{-1}\boldsymbol{S}'_{41}\right) + \boldsymbol{T}_{22}^{-1}\boldsymbol{T}_{26} \\
\boldsymbol{K}_{\boldsymbol{Ic}_{21}} &= \boldsymbol{T}_{22}^{-1}\boldsymbol{M}_{c2}^{-1}\left(\boldsymbol{C}_{c2_1}\boldsymbol{T}_{15} + \boldsymbol{R}_{c2}^{-1}\boldsymbol{S}'_{52} - \boldsymbol{M}_{c_{21}}\boldsymbol{M}_{c_{11}}^{-1}\boldsymbol{R}_{c1}^{-1}(\boldsymbol{S}'_{51} + \boldsymbol{T}_{15})\right) \\
\boldsymbol{K}_{\boldsymbol{Ic}_{22}} &= \boldsymbol{T}_{22}^{-1}\boldsymbol{M}_{c2}^{-1}\left(\boldsymbol{C}_{c2_2}\boldsymbol{T}_{26} + \boldsymbol{R}_{c2}^{-1}(\boldsymbol{S}'_{62} + \boldsymbol{T}_{26}) - \boldsymbol{M}_{c_{21}}\boldsymbol{M}_{c_{11}}^{-1}\boldsymbol{R}_{c1}^{-1}\boldsymbol{S}'_{61}\right).
\end{aligned} \tag{4.49}$$

Note that for the generic case, the more dynamics are considered, the more Riccati's equations must be solved.

As in the nonlinear $\mathscr{H}_\infty$ controller discussed before, a particular case can also be obtained when the elements of the weighting compound $\boldsymbol{W}'\boldsymbol{W}$ verify:

$$\boldsymbol{Q} = \begin{bmatrix} \omega_{11}^2\mathbb{1} & \mathbb{0} & \mathbb{0} & \mathbb{0} & \mathbb{0} & \mathbb{0} \\ \mathbb{0} & \omega_{12}^2\mathbb{1} & \mathbb{0} & \mathbb{0} & \mathbb{0} & \mathbb{0} \\ \mathbb{0} & \mathbb{0} & \omega_{21}^2\mathbb{1} & \mathbb{0} & \mathbb{0} & \mathbb{0} \\ \mathbb{0} & \mathbb{0} & \mathbb{0} & \omega_{22}^2\mathbb{1} & \mathbb{0} & \mathbb{0} \\ \mathbb{0} & \mathbb{0} & \mathbb{0} & \mathbb{0} & \omega_{31}^2\mathbb{1} & \mathbb{0} \\ \mathbb{0} & \mathbb{0} & \mathbb{0} & \mathbb{0} & \mathbb{0} & \omega_{32}^2\mathbb{1} \end{bmatrix}, \boldsymbol{S} = \begin{bmatrix} \mathbb{0} & \mathbb{0} \\ \mathbb{0} & \mathbb{0} \\ \mathbb{0} & \mathbb{0} \\ \mathbb{0} & \mathbb{0} \\ \mathbb{0} & \mathbb{0} \\ \mathbb{0} & \mathbb{0} \end{bmatrix},$$

$$\boldsymbol{R} = \begin{bmatrix} \omega_{u1}^2\mathbb{1} & \mathbb{0} \\ \mathbb{0} & \omega_{u2}^2\mathbb{1} \end{bmatrix}.$$

In this case, matrices $\boldsymbol{T_{11}}$, $\boldsymbol{T_{13}}$, $\boldsymbol{T_{15}}$, $\boldsymbol{T_{22}}$, $\boldsymbol{T_{24}}$ and $\boldsymbol{T_{26}}$ can be defined as follows:

$$\boldsymbol{T_{11}} = \rho\mathbb{1}, \quad \boldsymbol{T_{11}} = \beta\mathbb{1}, \quad \boldsymbol{T_{11}} = \alpha\mathbb{1},$$

$$\boldsymbol{T_{22}} = \nu\mathbb{1}, \quad \boldsymbol{T_{23}} = \mu\mathbb{1}, \quad \boldsymbol{T_{24}} = \lambda\mathbb{1},$$

where ρ, β, α, ν, μ and λ can be computed, using the Riccati's equations presented before, as follows:

1. Compute ρ, ν, α and λ with equations (4.39), (4.40), (4.41) and (4.42), respectively:

$$\rho = \frac{\gamma\omega_{u1}\omega_{11}}{\sqrt{\gamma^2 - \omega_{u1}^2}},$$

$$\nu = \frac{\gamma\omega_{u2}\omega_{12}}{\sqrt{\gamma^2 - \omega_{u2}^2}},$$

$$\alpha = \frac{\gamma\omega_{u1}\omega_{31}}{\sqrt{\gamma^2 - \omega_{u1}^2}},$$

$$\lambda = \frac{\gamma\omega_{u2}\omega_{32}}{\sqrt{\gamma^2 - \omega_{u2}^2}}.$$

2. Compute $\boldsymbol{K_{11}}+\boldsymbol{K_{13}}$ and $\boldsymbol{K_{22}}+\boldsymbol{K_{24}}$ using (4.43) and (4.44):

$$\boldsymbol{K_{11}}+\boldsymbol{K_{13}} = -\rho\alpha\left(\frac{\mathbb{1}}{\gamma^2}-\frac{\mathbb{1}}{\omega_{u1}^2}\right),$$

$$\boldsymbol{K_{22}}+\boldsymbol{K_{24}} = -\nu\lambda\left(\frac{\mathbb{1}}{\gamma^2}-\frac{\mathbb{1}}{\omega_{u2}^2}\right).$$

3. Compute β and μ with (4.45) and (4.46):

$$\beta = \frac{\gamma\omega_{u1}\sqrt{\omega_{21}^2+2\omega_{11}\omega_{31}}}{\sqrt{\gamma^2-\omega_{u1}^2}},$$

$$\mu = \frac{\gamma\omega_{u2}\sqrt{\omega_{22}^2+2\omega_{12}\omega_{32}}}{\sqrt{\gamma^2-\omega_{u2}^2}}.$$

Therefore, the analytical equations (4.49) for the gain matrices can be expressed for the particular case as follows:

$$\boldsymbol{K_{Dc_{11}}} = \frac{\sqrt{\omega_{21}^2+2\omega_{11}\omega_{31}}}{\omega_{11}}\mathbb{1}+\boldsymbol{M_{c1}^{-1}}\left(\boldsymbol{C_{c1_1}}+\frac{1}{\omega_{u1}^2}\mathbb{1}\right),$$

$$\boldsymbol{K_{Dc_{12}}} = \boldsymbol{M_{c1}^{-1}}\left(\boldsymbol{C_{c1_2}}-\boldsymbol{M_{c_{12}}}\boldsymbol{M_{c_{22}}^{-1}}\frac{1}{\omega_{u2}^2}\right)\frac{\omega_{u2}\omega_{12}}{\sqrt{\gamma^2-\omega_{u2}^2}}\frac{\sqrt{\gamma^2-\omega_{u1}^2}}{\omega_{u1}\omega_{11}},$$

$$\boldsymbol{K_{Pc_{11}}} = \frac{\omega_{31}}{\omega_{11}}\mathbb{1}+\frac{\sqrt{\omega_{21}^2+2\omega_{11}\omega_{31}}}{\omega_{11}}\boldsymbol{M_{c1}^{-1}}\left(\boldsymbol{C_{c1_1}}+\frac{1}{\omega_{u1}^2}\mathbb{1}\right),$$

$$\boldsymbol{K_{Pc_{12}}} = \boldsymbol{M_{c1}^{-1}}\left(\boldsymbol{C_{c1_2}}-\boldsymbol{M_{c_{12}}}\boldsymbol{M_{c_{22}}^{-1}}\frac{1}{\omega_{u2}^2}\right)\frac{\omega_{u2}\sqrt{\omega_{22}^2+2\omega_{12}\omega_{32}}}{\sqrt{\gamma^2-\omega_{u2}^2}}\frac{\sqrt{\gamma^2-\omega_{u1}^2}}{\omega_{u1}\omega_{11}},$$

$$\boldsymbol{K_{Ic_{11}}} = \frac{\omega_{31}}{\omega_{11}}\boldsymbol{M_{c1}^{-1}}\left(\boldsymbol{C_{c1_1}}+\frac{1}{\omega_{u1}^2}\mathbb{1}\right),$$

$$
\begin{aligned}
\boldsymbol{K}_{\boldsymbol{Ic}_{12}} &= \boldsymbol{M}_{\boldsymbol{c1}}^{-1}\left(\boldsymbol{C}_{\boldsymbol{c1}_2}-\boldsymbol{M}_{\boldsymbol{c}_{12}}\boldsymbol{M}_{\boldsymbol{c}_{22}}^{-1}\frac{1}{\omega_{u2}^2}\right)\frac{\omega_{u2}\omega_{32}}{\sqrt{\gamma^2-\omega_{u2}^2}}\frac{\sqrt{\gamma^2-\omega_{u1}^2}}{\omega_{u1}\omega_{11}},\\
\boldsymbol{K}_{\boldsymbol{Dc}_{21}} &= \boldsymbol{M}_{\boldsymbol{c2}}^{-1}\left(\boldsymbol{C}_{\boldsymbol{c2}_1}-\boldsymbol{M}_{\boldsymbol{c}_{21}}\boldsymbol{M}_{\boldsymbol{c}_{11}}^{-1}\frac{1}{\omega_{u1}^2}\right)\frac{\omega_{u1}\omega_{11}}{\sqrt{\gamma^2-\omega_{u1}^2}}\frac{\sqrt{\gamma^2-\omega_{u2}^2}}{\omega_{u2}\omega_{12}},\\
\boldsymbol{K}_{\boldsymbol{Dc}_{22}} &= \frac{\sqrt{\omega_{22}^2+2\omega_{12}\omega_{32}}}{\omega_{12}}\mathbb{1}+\boldsymbol{M}_{\boldsymbol{c2}}^{-1}\left(\boldsymbol{C}_{\boldsymbol{c2}_2}+\frac{1}{\omega_{u2}^2}\mathbb{1}\right),\\
\boldsymbol{K}_{\boldsymbol{Pc}_{21}} &= \boldsymbol{M}_{\boldsymbol{c2}}^{-1}\left(\boldsymbol{C}_{\boldsymbol{c2}_1}-\boldsymbol{M}_{\boldsymbol{c}_{21}}\boldsymbol{M}_{\boldsymbol{c}_{11}}^{-1}\frac{1}{\omega_{u1}^2}\right)\frac{\omega_{u1}\sqrt{\omega_{21}^2+2\omega_{11}\omega_{31}}}{\sqrt{\gamma^2-\omega_{u1}^2}}\frac{\sqrt{\gamma^2-\omega_{u2}^2}}{\omega_{u2}\omega_{12}},\\
\boldsymbol{K}_{\boldsymbol{Pc}_{22}} &= \frac{\omega_{32}}{\omega_{12}}\mathbb{1}+\frac{\sqrt{\omega_{22}^2+2\omega_{12}\omega_{32}}}{\omega_{12}}\boldsymbol{M}_{\boldsymbol{c2}}^{-1}\left(\boldsymbol{C}_{\boldsymbol{c2}_2}+\frac{1}{\omega_{u2}^2}\mathbb{1}\right),\\
\boldsymbol{K}_{\boldsymbol{Ic}_{21}} &= \boldsymbol{M}_{\boldsymbol{c2}}^{-1}\left(\boldsymbol{C}_{\boldsymbol{c2}_1}-\boldsymbol{M}_{\boldsymbol{c}_{21}}\boldsymbol{M}_{\boldsymbol{c}_{11}}^{-1}\frac{1}{\omega_{u1}^2}\right)\frac{\omega_{u1}\omega_{31}}{\sqrt{\gamma^2-\omega_{u1}^2}}\frac{\sqrt{\gamma^2-\omega_{u2}^2}}{\omega_{u2}\omega_{12}},\\
\boldsymbol{K}_{\boldsymbol{Ic}_{22}} &= \frac{\omega_{32}}{\omega_{12}}\boldsymbol{M}_{\boldsymbol{c2}}^{-1}\left(\boldsymbol{C}_{\boldsymbol{c2}_2}+\frac{1}{\omega_{u2}^2}\mathbb{1}\right),
\end{aligned}
\tag{4.50}
$$

where ω_{1_i} are the weighting parameters of the time-derivative of the position error of the i-dynamics, ω_{2_i} are the weighting values of position error and ω_{3_i} are the weighting of its integral. The weighting parameters of the *additional control* effort for the i-dynamics are ω_{u_i}.

4.3.2 Application to the QuadRotor Helicopter

The control strategy used in this section is based on the idea presented in Fig. 4.1, which is composed by an outer-inner control structure. The applied techniques were designed to guide the vehicle in the presence of parametric and structural uncertainties, as well as sustained disturbances, that may affect all the degrees of

freedom of the helicopter.

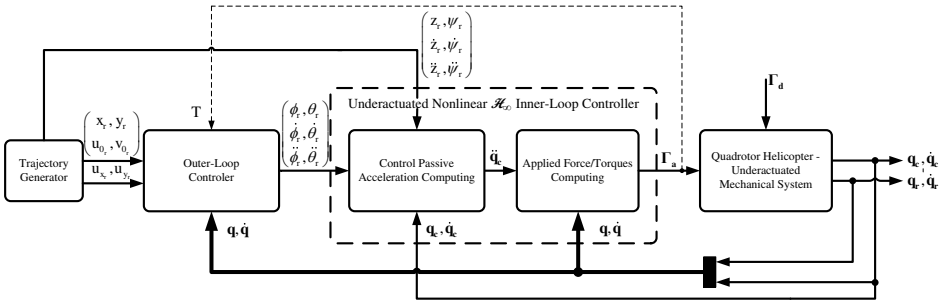

Figure 4.1: Nonlinear $\mathscr{H}_\infty$ control block diagram for the underactuated *QuadRotor* helicopter with an outer-loop controller. (Thick and thin lines mean full and partial data vectors, respectively. Dashed line means a single data)

The path to be followed in the $\Re^3$ Cartesian space is generated beforehand by the *Trajectory Generator* block. To compute the reference trajectory, a virtual reference vehicle, with the same *QuadRotor* mathematical model defined in Section 2.5.1, is used. However, the trajectory is generated under the assumption that there are no external disturbances affecting the system, and its attitude is in steady-state. Firstly, considering that the vehicle is hovering, the desired altitude, z_r, its time derivatives, $\dot{z}_r$, and the desired thrust, T_r, are computed using the model (2.61). These altitude references, jointly with the desired yaw angle, ψ_r, and its time derivatives, $\dot{\psi}_r$, are supplied by the *Trajectory Generator* block to the inner-loop controller through a feedforward action. The yaw reference angle is defined separately. In a second step, making use of the computed reference thrust, T_r, the same block generates the xy reference trajectory, being these reference positions, x_r and y_r, their speeds and the virtual control references, u_{x_r} and u_{y_r} (see definition in Section 3.4.1.3), provided to the outer-loop controller.

Keeping in mind that the *QuadRotor* helicopter is an underactuated mechanical system, the nonlinear $\mathscr{H}_\infty$ controller presented before is used in the inner-loop control law. The synthesized controller considers the overall dynamic behavior in order to control the helicopter attitude and altitude, where $\boldsymbol{q_u} = [x \quad y]'$ and $\boldsymbol{q_c} = [z \quad \phi \quad \theta \quad \psi]'$ are the *uncontrolled* and *controlled* generalized coordinates, respectively. This fact implies that the translational and rotational motion control are not considered separately, being that their coupling are not treated like external disturbances. Therefore, this approach has a clear advantage with respect to the control strategies proposed in Chapter 3 and other ones presented in the

literature (e.g. Bouabdallah and Siegwart (2007)). Besides, note that the chosen *controlled* vector results in the case 1) where $\boldsymbol{q_c} = \boldsymbol{q_a}$. The force/torque vector for the *uncontrolled* and *controlled* subsystems are defined by $\boldsymbol{\Gamma_u} = [0 \quad 0]'$ and $\boldsymbol{\Gamma_c} = [T \quad \tau_{\phi_a} \quad \tau_{\theta_a} \quad \tau_{\psi_a}]'$, respectively.

Thus, taking into account the partition of the underactuated system (4.1), the *QuadRotor* dynamic equations (2.61) and (2.62) can be written in the following form:

$$\begin{bmatrix} \boldsymbol{M_{uu}}(\boldsymbol{q}) & \boldsymbol{M_{uc}}(\boldsymbol{q}) \\ \boldsymbol{M_{cu}}(\boldsymbol{q}) & \boldsymbol{M_{cc}}(\boldsymbol{q}) \end{bmatrix} \begin{bmatrix} \ddot{\boldsymbol{q}}_{\boldsymbol{u}} \\ \ddot{\boldsymbol{q}}_{\boldsymbol{c}} \end{bmatrix} + \begin{bmatrix} \boldsymbol{C_{uu}}(\boldsymbol{q},\dot{\boldsymbol{q}}) & \boldsymbol{C_{uc}}(\boldsymbol{q},\dot{\boldsymbol{q}}) \\ \boldsymbol{C_{cu}}(\boldsymbol{q},\dot{\boldsymbol{q}}) & \boldsymbol{C_{cc}}(\boldsymbol{q},\dot{\boldsymbol{q}}) \end{bmatrix} \begin{bmatrix} \dot{\boldsymbol{q}}_{\boldsymbol{u}} \\ \dot{\boldsymbol{q}}_{\boldsymbol{c}} \end{bmatrix} + \begin{bmatrix} \boldsymbol{G_u}(\boldsymbol{q}) \\ \boldsymbol{G_c}(\boldsymbol{q}) \end{bmatrix}$$

$$= \begin{bmatrix} \boldsymbol{\Gamma_u} + \boldsymbol{\delta_p} \\ \boldsymbol{\Gamma_c} + \boldsymbol{\delta_a} \end{bmatrix},$$

where

$$\boldsymbol{M_{uu}} = \begin{bmatrix} mC\psi C\theta & mS\psi C\theta \\ m(C\psi S\theta S\phi - S\psi C\phi) & m(S\psi S\theta S\phi + C\psi C\phi) \end{bmatrix},$$

$$\boldsymbol{M_{uc}} = \begin{bmatrix} -mS\theta & \mathbb{O}_{1\times 3} \\ mC\theta S\phi & \mathbb{O}_{1\times 3} \end{bmatrix},$$

$$\boldsymbol{M_{cu}} = \begin{bmatrix} m(C\psi S\theta C\phi + S\psi S\phi) & m(S\psi S\theta C\phi - C\psi S\phi) \\ \mathbb{O}_{3\times 1} & \mathbb{O}_{3\times 1} \end{bmatrix},$$

$$\boldsymbol{M_{cc}} = \begin{bmatrix} mC\theta C\phi & \mathbb{O}_{1\times 3} \\ \mathbb{O}_{3\times 1} & \boldsymbol{M}(\boldsymbol{\eta}) \end{bmatrix},$$

$$\boldsymbol{C_{uu}} = \mathbb{O}_{2\times 2}\,,\ \boldsymbol{C_{uc}} = \mathbb{O}_{2\times 4}\,,\ \boldsymbol{C_{cu}} = \mathbb{O}_{4\times 2}\,,$$

$$\boldsymbol{C_{cc}} = \begin{bmatrix} 0 & \mathbb{O}_{1\times 3} \\ \mathbb{O}_{3\times 1} & \boldsymbol{C}(\boldsymbol{\eta},\dot{\boldsymbol{\eta}}) \end{bmatrix},$$

$$\boldsymbol{G_u} = \begin{bmatrix} -mgS\theta \\ mgC\theta S\phi \end{bmatrix},\ \boldsymbol{G_c} = \begin{bmatrix} mgC\theta C\phi \\ \mathbb{O}_{3\times 1} \end{bmatrix}.$$

As described above, the control law presented in this section also includes the integral of both altitude and angular position errors in the state vector (see equation (4.6)) in order to obtain null steady-state error in presence of sustained disturbances. Moreover, the proposed generalization approach is implemented, where the vector of *controlled* degrees of freedom, $\boldsymbol{q_c}$, is divided in two dynam-

ics, the altitude, $\boldsymbol{q_{c1}} = z$, and the Euler angles, $\boldsymbol{q_{c2}} = \boldsymbol{\eta}$. This is justified by the rotational subsystem have a faster dynamic than the altitude one, which can be appreciated by the magnitudes of the moment of inertia. The underactuated nonlinear $\mathscr{H}_\infty$ controller is split up into two parts:

1. First the *controlled* coordinate accelerations (4.48) required to track the desired reference are computed using the nonlinear gain matrices $\boldsymbol{K_{Dc}}$, $\boldsymbol{K_{Pc}}$ and $\boldsymbol{K_{Ic}}$, given by (4.50). These matrices depend on the partitioned model of the *QuadRotor* helicopter presented above;

2. In a second step, these values are considered to generate the forces and torques applied to the *QuadRotor* helicopter, by substituting them in the equation (4.21).

In the *Outer-Loop Controller* block, the integral predictive controller, presented in Section 3.4.2.2, is executed to determine the desired roll, ϕ_r, and pitch, θ_r, angles for the inner-loop controller. Thus, only the controller for the x and y motions is used (see equations (3.96) and (3.97)). This outer-loop controller provides a smooth path tracking due to the fact that the MPC formulation allows the use of previously known references for the control law calculation.

As the control input T is computed by the inner-loop controller, which has a faster settling time than the outer one, for the outer-loop controller synthesis, this control action is considered as a time variant parameter to the x and y motions in (3.53). That is, between each outer-loop sampling time, the inner-loop controlled variables are considered in steady-state.

Taking into account the cascade structure of this strategy and considering the performance attained by the inner-loop controller, the *QuadRotor* helicopter is assumed stabilized at the desired height. Therefore, for the design of the outer-loop controller, the thrust, T, and the Euler angles can be considered as time-varying parameters, and in steady-state between two outer-loop sampling time. Moreover, the attraction basin in the inner closed-loop is enlarged or reduced by modifying the gains parameters. The estimated attraction basin can be augmented by modifying the relation of gains between the inner-loop controller and outer-loop one, which guarantees convergence.

Simulations have been performed in order to test the proposed control strategy when the *QuadRotor* helicopter executes a path tracking. The performance obtained by this strategy have been checked considering the assumptions made in the *Simulation Protocol*, in Section 3.2.

The MPC parameters were adjusted with the same values used in Chapter 3, while the nonlinear $\mathscr{H}_\infty$ controller gains were tuned with the following values: $\omega_{11} = 0.8$, $\omega_{21} = 10$, $\omega_{31} = 15$ and $\omega_{u1} = 0.7$, $\omega_{12} = 0.1$, $\omega_{22} = 5$, $\omega_{32} = 9$, $\omega_{u2} = 0.5$ and $\gamma = 10$. In addition, a simulation without considering the integral term was performed in order to show the improvement obtained with this action on both inner and outer-loop control. The simulation results are illustrated in Figs. 4.2 to 4.7.

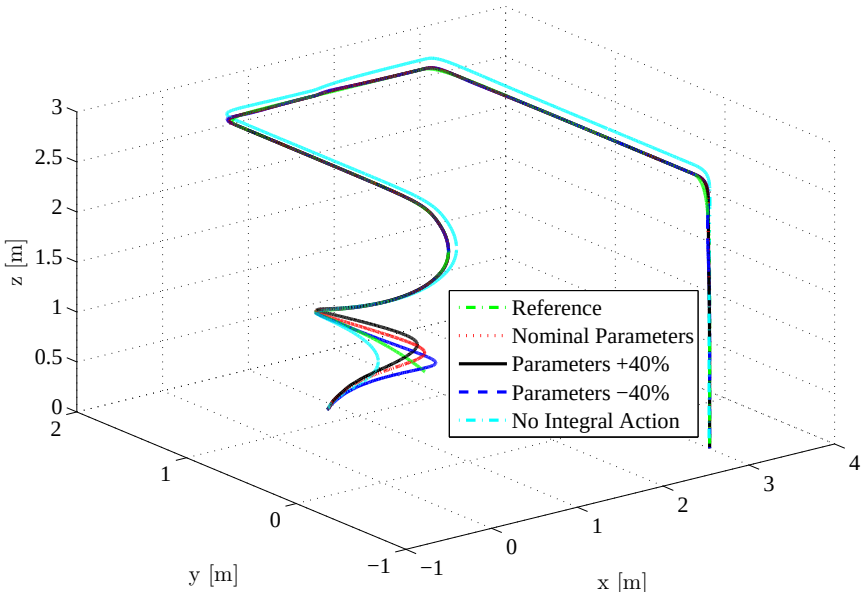

Figure 4.2: Path tracking.

These figures indicate an expected reference tracking performance even if external disturbances, originated by aerodynamic forces and moments, are considered. These results illustrate the robust behavior provided by the outer-inner control structure in the case of both parametric and structural uncertainty.

The smooth reference tracking provided by the MPC can be observed through the time evolution of the translational position and its error showed in Figs. 4.3 and 4.4, respectively. This fact is clearly visible at the beginning of the trajectory where the vehicle is far from the reference. This is due to the fact that the predictive controller considers the future reference in the computation of the control signal so as to predict a path that would result in a softer displacement. Moreover, the integral action features of the MPC controller can be easily observed in Fig. 4.4. This integral action makes it possible to obtain null error in the path tracking

when sustained disturbances affect the xy motion of the helicopter.

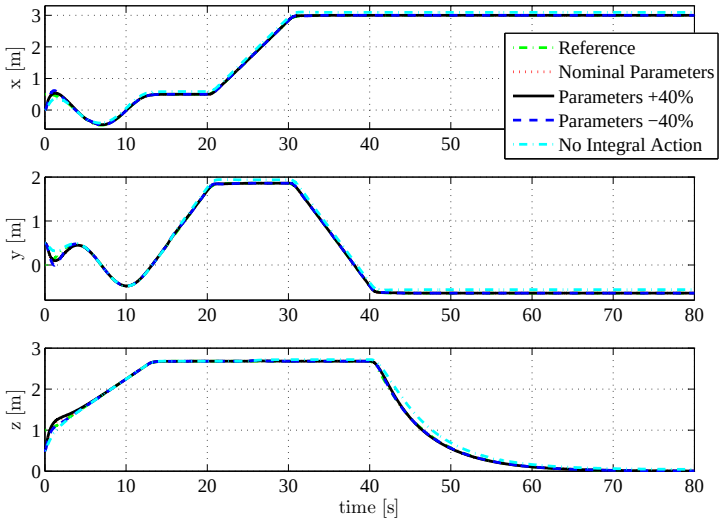

Figure 4.3: Position (x, y, z).

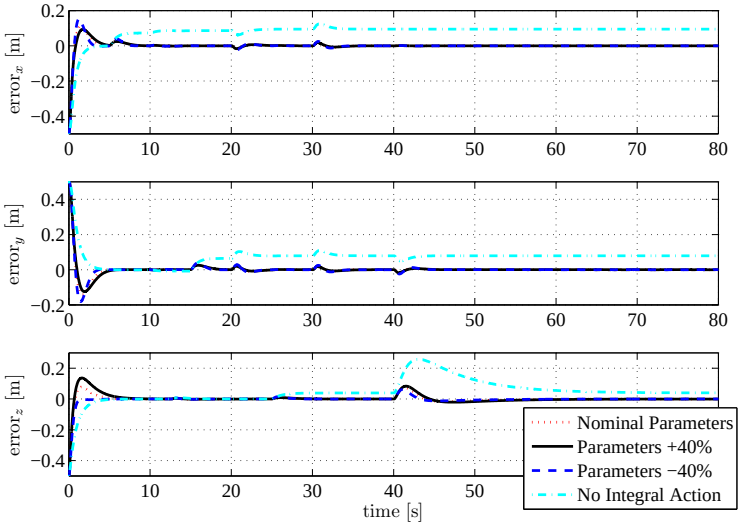

Figure 4.4: Position error (x, y, z).

An additional simulation considering the integral action weighting of the inner and outer loop equal to zero is also plotted in the graphs. This simulation

shows the deterioration in the tracking performance when this action is not taken into account, since the inner and outer-loop controllers are not able to reject the sustained disturbances acting on the helicopter.

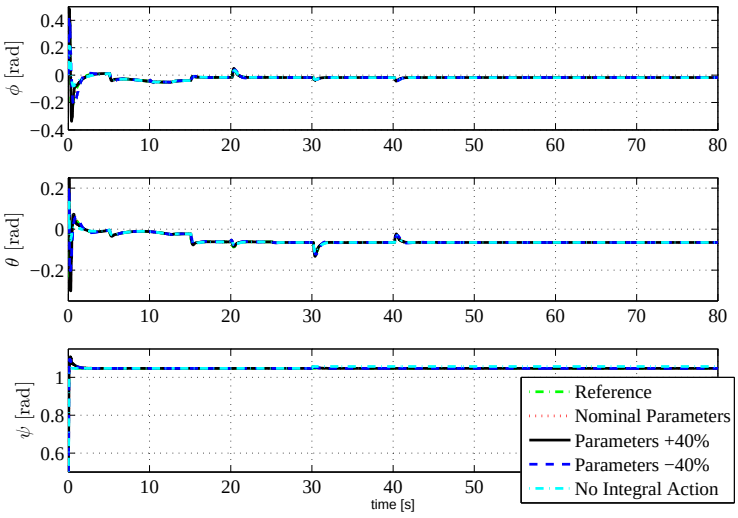

Figure 4.5: Orientation (ϕ, θ, ψ).

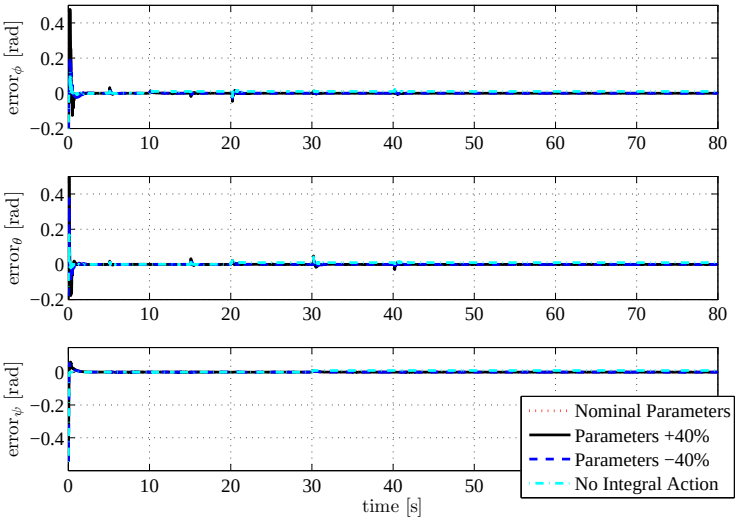

Figure 4.6: Orientation error (ϕ, θ, ψ).

Figs. 4.5 and 4.6 illustrate the Euler angles evolution. In these graphs the Euler angles steady-state error can also be observed in the trajectory where the integral action weighting is equal to zero. In this case, apart from the fact that the inner loop loses performance, it is interesting to note that the outer-loop controller tries to compensate for the lack of integral action by increasing ϕ and θ reference angles.

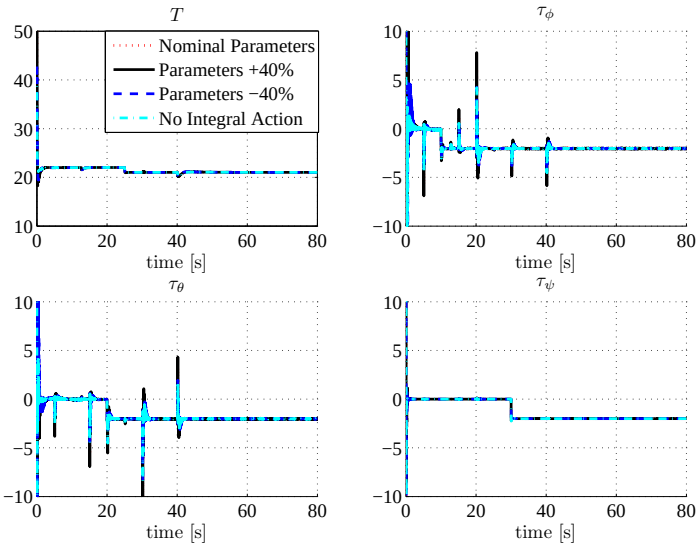

Figure 4.7: Control actions $(T, \tau_\phi, \tau_\theta, \tau_\psi)$.

In Fig. 4.7, the control actions computed by the proposed controllers to solve the path tracking problem for the *QuadRotor* helicopter are presented.

These figures show that the control strategies present a robust path tracking when parametric uncertainties and sustained disturbances are applied to the system. In order to make a quantitative comparison of the results obtained by this control strategy with the proposed one in Section 3.4.2.2, the Integral Square Error (ISE) performance indexes, presented in Table 4.1, have been computed again from the simulation results showed in Figs. 4.2 to 4.6. Results obtained considering the *QuadRotor* helicopter model (2.61-2.62) with nominal parameters have presented very similar ISE performance indexes. However, when an amount of $+40\%$ in the uncertainty of parameters of the moment of inertia tensor and the mass has been considered, a large improvement has been achieved with respect to the variables controlled by the proposed nonlinear $\mathscr{H}_\infty$ controller in this section.

This improvement, in the presence of parametric uncertainties, are due to the underactuated nonlinear $\mathscr{H}_\infty$ robustness properties. It computes the applied control inputs taking into account the *non-controlled* DOF, that is, the uncertainty on the mass that affects the *xy* motion is also counterattacked by the inner-loop controller. Meanwhile, with the controller proposed in the previous chapter, this effect is only considered as an unknown external disturbance.

Table 4.1: ISE Index Performance Analysis.

States [ISE Unit Symbol]	**MPCxy-UActNL$\mathscr{H}_\infty$**	**MPC-NL$\mathscr{H}_\infty$**
$x\ [m^2 \cdot s]$	12.8514	12.5464
$y\ [m^2 \cdot s]$	17.5974	18.3501
$z\ [m^2 \cdot s]$	13.4216	18.1153
$\phi\ [rad^2 \cdot s]$	4.8036	7.6366
$\theta\ [rad^2 \cdot s]$	2.7511	5.4915
$\psi\ [rad^2 \cdot s]$	4.8859	4.7319

As made in the chapter before, the Integral Absolute Derivative control signal (IADU) index has been computed for all control signals in both control strategies. As presented in Figs. 4.7 and 3.25, the difference between the control signals generated by both controllers are practically unnoticed. However, through the IADU index is possible to assess the improvement of the controller proposed in this section, which provides smoothness to the path tracking through the control signals. The results obtained from the simulation are presented in Table 4.2.

Table 4.2: IADU Index Performance Analysis.

Control Signals [IADU Unit Symbol]	**MPCxy-UActNL$\mathscr{H}_\infty$**	**MPC-NL$\mathscr{H}_\infty$**
$T\ [N]$	50.7787	40.2395
$\tau_{\phi_a}\ [N \cdot m]$	446.7466	463.0468
$\tau_{\theta_a}\ [N \cdot m]$	402.9134	431.3856
$\tau_{\psi_a}\ [N \cdot m]$	49.4207	56.9412

4.3.3 Other Applications

The nonlinear $\mathscr{H}_\infty$ controller for underactuated mechanical systems developed in this section has also been applied to vehicles based on the inverted pendulum

concept. This kind of vehicle is a typical case of underactuated mechanical system, since it is usually composed by two degrees of freedom and only one control input. Besides, the inverted pendulum on its many variations is one of the most important benchmark in the automatic control area, which can be found through the Furuta pendulum (Aström and Furuta, 2000; Acosta et al., 2002), the pendulum on a cart (Mazenc and Bowong, 2003; Gordillo and Aracil, 2008) and the pendulum on a two-wheeled vehicle (Pathak et al., 2005; Madero et al., 2010).

Pendulum on a two-wheeled vehicle or two-wheeled self-balanced vehicles have been made popular by the vehicle called Segway. Moreover, this kind of system has attractive properties of interest for the academic field. Commercial vehicles limit their workspace to a small area around the static upper vertical position due to safety maneuver constraints. In order to maintain these features even when the workspace is enlarged, robustness properties must be taken into account at the control design stage.

As commented before, an inverted pendulum on a cart and a two-wheeled self-balanced vehicle are used to corroborate the effectiveness of the proposed controller. The difference between these inverted pendulum systems lies in the fact that, in the first system, the pendulum goes freely around the pivot point, whereas in the second one the axle of the motors is at the same time the pivot point of the pendulum.

In what follows, simulation and experimental results are presented for these two systems.

4.3.3.1 Inverted Pendulum on a Cart

The system considered in this section is modeled through the inverted pendulum on a cart idea, that is, the pendulum is assumed goes freely around the pivot point. The modeling has been performed focusing on the vehicle named as *PPCar*, which stands for *Personal Pendulum Car* (Fiacchini et al., 2006). Basically, the system consists of an inverted pendulum on a two-wheeled vehicle for human transportation, where the pendulum is actually the person riding the vehicle. The forward movement is caused by the rider's inclination with respect to the equilibrium position. A scheme of the vehicle is depicted in Fig. 4.8.

A dynamic model of the system can be derived from Euler-Lagrange formula-

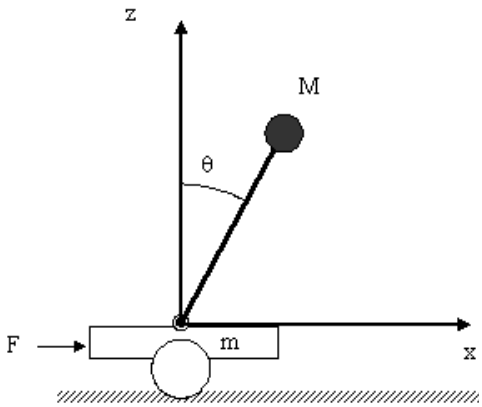

Figure 4.8: Scheme of an inverted pendulum on a cart.

tion. For this particular system, the following nominal model has been considered:

$$\begin{bmatrix} M+m & Ml\cos(\theta) \\ Ml\cos(\theta) & Ml^2 \end{bmatrix} \begin{bmatrix} \ddot{x} \\ \ddot{\theta} \end{bmatrix} + \begin{bmatrix} 0 & -Ml\sin(\theta)\dot{\theta} \\ 0 & 0 \end{bmatrix} \begin{bmatrix} \dot{x} \\ \dot{\theta} \end{bmatrix} + \begin{bmatrix} 0 \\ -Mgl\sin(\theta) \end{bmatrix} = \begin{bmatrix} F \\ 0 \end{bmatrix} + \begin{bmatrix} \delta_x \\ \delta_\theta \end{bmatrix}, \tag{4.51}$$

where m and M are the masses of the cart and pendulum, respectively, l is the distance of the center of mass of the pendulum from the vehicle platform and g is the gravity acceleration. The generalized coordinate vector is defined as $\boldsymbol{q} = [x \quad \theta]'$, where x is the displacement position and θ is the pendulum angular position. The control variable is the force, F, applied through the wheels. δ_x and δ_θ are the uncertainties of the system acting on x and θ, respectively.

Taking into account the partition for underactuated mechanical systems (4.1), and by selecting the *controlled* degree of freedom as $q_c = \theta$ and the *uncontrolled* one as $q_u = x$, the relationship between the applied force, F, and the *control acceleration*, $\ddot{\theta}$, for the *controlled* degree of freedom on the actuated subsystem (in the absence of disturbances), is obtained through (4.21) resulting in:

$$F = \left[Ml\cos(\theta) - \frac{(M+m)\,l}{\cos(\theta)} \right] \ddot{\theta} - Ml\sin(\theta)\,\dot{\theta}^2 - \frac{(M+m)\,g\sin(\theta)}{\cos(\theta)}. \tag{4.52}$$

This expression relates the dynamics of the angular position of the pendulum with the force applied to the cart. Although neither the variable x nor its derivat-

ive appear in (4.52), it is important to keep in mind that, in this application, the velocity of the vehicle, $\dot{x}(t)$, must be bounded. It means that the velocity must be stabilized at an equilibrium point with null acceleration, i.e. $\ddot{x}(t) = 0$. This equilibrium point will be given by the coupling between the dynamic of θ and x in closed-loop.

The model parameters, used in this work, has been taken from Fiacchini et al. (2006), wherein these parameters were identified. Table 4.3 shows the nominal parameters.

Table 4.3: *PPCar* model parameters.

Parameter Description	**Parameter**	**Value**
Mass of the cart	m	35 kg
Mass of the pendulum	M	80 kg
Height of the center of mass	l	1 m
Gravity acceleration	g	9.8 m/s^2

Some simulation experiments on the *PPCar* model have been carried out to evaluate the performance of the proposed controller. Besides, comparison results with the nonlinear $\mathscr{H}_\infty$ controller developed in Siqueira et al. (2006) has also been presented. These controllers will be referred in what follows as NL PID and NL PD, respectively.

Simulation results have been obtained considering the reference angular position $\theta_r = 0°$. The initial angular position of the vehicle is $\theta = -10°$, with null initial angular speed and acceleration.

In order to check the performance of the controllers, an uncertainty in the parameter M has been considered simulating the conductor mass variation. A range of the mass driver between 40kg and 120kg has been estimated. Additionally, in order to introduce some disturbances to the system, a sudden variation in θ of 15° is applied in the time interval of $t = [10.10 \quad 10.15]$ s, as well as a persistent external torque of -100 Nm at $t = 20$ s.

For the controller design a diagonal $\boldsymbol{W}'\boldsymbol{W}$ weighting matrix has been considered, and the nonlinear $\mathscr{H}_\infty$ gains (4.19) have been used to compute the desired *controlled* degree of freedom acceleration (4.17). Table 4.4 shows the values for the weights for the *PPCar*.

Fig. 4.9a and 4.9b present the simulation results obtained for different con-

Table 4.4: Weights for the *PPCar's* controller.

Signal	Weight parameter	NL PD	NL PID
Speed error $\dot{\tilde{q}}_p$	ω_1	0.5	0.5
Position error $\tilde{q}_p$	ω_2	1	1
Error integral $\int \tilde{q}_p dt$	ω_3	-	1.5
Control effort u	ω_u	0.012	0.012

ductor mass values, with the nonlinear $\mathscr{H}_\infty$ controller proposed in this section and when the parameter ω_3 is settled equal to zero. It can be observed that the controller is robust against parametric variations, even when the integral action is not considered. However, it can be seen that when the integral weight is settled to zero, the controller is not able to reject persistent disturbance, since the angular position can not remain in the reference position. Besides the linear velocity does not reach a constant value as it tends to infinity. Therefore, considering the integral term in the error state vector, this control law rejects sustained disturbances applied to the system, keeping the position error null at steady-state, and maintaining the velocity of the cart bounded.

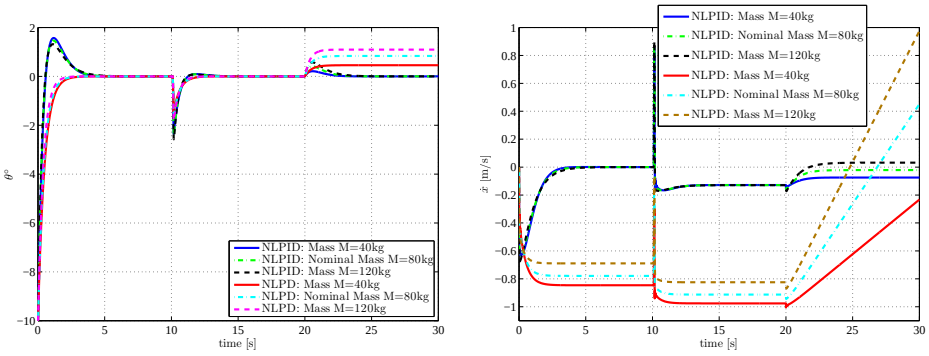

(a) Angular position of the *PPCar*.

(b) Linear velocity of the *PPCar*.

Figure 4.9: Simulation results with the underactuated nonlinear $\mathscr{H}_\infty$ controller applied to the PPCar.

4.3.3.2 Two-Wheeled Self-Balanced Vehicle

In this section, the preceding nonlinear $\mathscr{H}_\infty$ controller, designed for the reduced underactuated mechanical system, is applied to a real two-wheeled self-balanced vehicle in order to achieve robustness in presence of sustained disturbances and unmodeled dynamics. As discussed previously, the main difference between the inverted pendulum on a cart used in the above section and the vehicle used here is due to the coupling of the pendulum and the base of the vehicle. In this case, the pendulum is fixed rigidly to the axle of the motors, presenting an input coupling. Thus, the external torque applied by the motors produces effects of the same value on wheels and pendulum but with opposite direction.

The system constituted by the vehicle consists of two parts or subsystems. On the one hand, the two motors, the electronic control devices and other auxiliary devices are fixed to the frame to compose the pendulum. On the other hand, the wheels are fixed to the axle of the motors, constituting the second subsystem. Fig. 4.10b shows a schematic diagram of the vehicle and gives an outline of the hardware. The vehicle is composed of an aluminum framework with an inverted T-shape, with two motors fixed on its lower section, which axles are at the same time the ones for the two wheels. Two boxes are shown, where the electronics and sensors needed to implement the control of the system (microcontroller board, motor controller, wireless transmitter, batteries and Inertial Measurement Unit (IMU)) are placed to be properly protected. The vehicle is illustrated in Fig. 4.10a.

(a) General view of the vehicle.

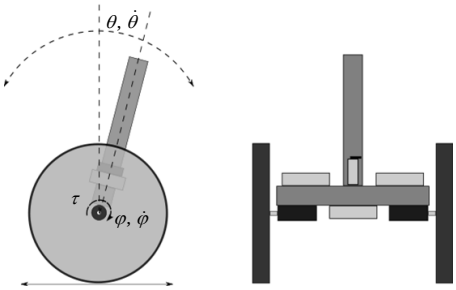

(b) Diagram of the two-wheeled vehicle.

Figure 4.10: Two-wheeled self-balanced vehicle description.

From Fig. 4.10b the following system variables can be defined: θ, the inclination angle or deviation between the pendulum and vertical line; $\dot{\theta}$, the angular

rate of the pendulum; φ, the angular position of the axle of the motors; $\dot{\varphi}$, the respective angular rate; and τ, the torque applied by the motors. Accordingly, the *controlled* and *uncontrolled* degrees of freedom are chosen as $q_c = \theta$ and $q_u = \varphi$.

In order to simplify the model of the vehicle, it can be assumed the mass of the entire pendulum set (frame, motors and other elements) to be a punctual mass located on the center of mass of the physical pendulum. Thus, the pendulum has a mass m separated by a distance l from the axle, where there are two wheels fixed with radius r and mass M_r.

By using the Lagrangian of the dynamical system and the Euler-Lagrange approach for non-conservative forces, the equations of motion for the system can be written in the underactuated mechanical system representation under input coupling (4.1) as follows (Madero et al., 2010):

$$\begin{bmatrix} (M_r+m)\,r^2+I_r & mlr\cos\theta \\ mlr\cos\theta & ml^2+I_p \end{bmatrix} \begin{bmatrix} \ddot{\varphi} \\ \ddot{\theta} \end{bmatrix} + \begin{bmatrix} 0 & -mlr\dot{\theta}\sin\theta \\ 0 & 0 \end{bmatrix} \begin{bmatrix} \dot{\varphi} \\ \dot{\theta} \end{bmatrix} + \begin{bmatrix} 0 \\ -mgl\sin\theta \end{bmatrix} = \begin{bmatrix} -k\dot{\varphi} \\ k\dot{\varphi} \end{bmatrix} + \begin{bmatrix} 1 \\ -1 \end{bmatrix} \tau + \begin{bmatrix} \delta_\varphi \\ \delta_\theta \end{bmatrix}, \tag{4.53}$$

where g is the gravity acceleration, k is a constant that represents the static friction of the motor and I_p and I_r are the inertia of the pendulum and the wheel, respectively. Note that, in comparison with the model (4.1), a vector including the friction forces has also been considered. The design of the control law is based on the model of the vehicle (4.53), whose parameters have been experimentally identified. The main parameters that characterize the model are listed in Table 4.5.

Table 4.5: Two-wheeled self-balanced vehicle model parameters.

Parameter Description	Parameter	Value
Mass of the pendulum	m	3.75 kg
Mass of the two wheels	M_r	2.75 kg
Height of the center of gravity	l	0.1435 m
Radius of the wheels	r	0.25 m
Inertia of the pendulum	I_p	$0.201\ \text{kg}\cdot\text{m}^2$
Inertia of the wheel	I_r	$0.0421\ \text{kg}\cdot\text{m}^2$
Static friction constant of the motor	k	$0.00215\ \text{N}\cdot\text{m/rad/s}$

Therefore, by using the *control acceleration* (4.17) with the applied torque (4.22) and considering the friction forces, the following control law is obtained:

$$\boldsymbol{\tau} = \boldsymbol{B_o}^{-1}(\boldsymbol{q}) \left[\boldsymbol{M_o}(\boldsymbol{q})\ddot{\boldsymbol{\theta}} + \boldsymbol{C_o}(\boldsymbol{q},\dot{\boldsymbol{q}})\dot{\boldsymbol{\theta}} + \boldsymbol{E_o}(\boldsymbol{q},\dot{\boldsymbol{q}})\dot{\boldsymbol{\varphi}} + \boldsymbol{G_o}(\boldsymbol{q}) + \boldsymbol{K_o}(\boldsymbol{q},\dot{\boldsymbol{q}}) \right] ,$$

where:

$$\boldsymbol{B_o}(\boldsymbol{q}) = -(1 + \frac{mlr\cos\theta}{(M_r+m)r^2+I_r}) , \quad \boldsymbol{M_o}(\boldsymbol{q}) = ml^2 + Ip - \frac{m^2l^2r^2\cos^2\theta}{(M_r+m)r^2+I_r} ,$$

$$\boldsymbol{C_o}(\boldsymbol{q},\dot{\boldsymbol{q}}) = \frac{m^2l^2r^2\cos\theta\sin\theta\,\dot{\theta}}{(M_r+m)r^2+I_r} , \quad \boldsymbol{E_o}(\boldsymbol{q},\dot{\boldsymbol{q}}) = 0 ,$$

$$\boldsymbol{G_o}(\boldsymbol{q}) = -mgl\sin\theta , \quad \boldsymbol{K_o}(\boldsymbol{q},\dot{\boldsymbol{q}}) = -\left(1 - \frac{mlr\cos\theta}{(M_r+m)r^2+I_r}\right) k\dot{\varphi} .$$

The designed control law has been implemented on an embedded microcontroller board. This board is based on a ATmega128 microcontroller (8-bit AVR microcontroller with 128Kb in-system programmable flash and up to 16 Mhz internal clock). The torque calculated by the control law is applied to the motors by using two Maxon EPOS24/5 motor controller boards. Each board receives the current value through a serial connection, and applies it to the corresponding motor. This motor controller boards can be driven up to 120Watts. The vehicle uses two Maxon RE30, 60W brushed motors, with a nominal voltage of 12V. These motors are equipped with encoder and planetary gearhead (reduction of 66:1), which allows the set to provide a torque up to 4Nm. The angle of inclination and the angular rate of the vehicle are obtained using the 3DM-GX1 IMU from MicroStrain. Electronics and auxiliary elements for the vehicle are located near the axle and in a way that the effective center of mass is lowered. During the experiments, all the data can be reported to a PC via a bluetooth-serial connection.

Two experiments have been carried out to evaluate the performance of the designed controller. The values of the nonlinear $\mathscr{H}_\infty$ weights, defined in (4.18), for the two-wheeled self-balanced vehicle have been adjusted as follows:

$$\omega_1 = 2.5 , \quad \omega_2 = 1.5 , \quad \omega_3 = 18.0 , \quad \omega_u = 1.05 .$$

The first experimental result has been obtained with the two-wheeled vehicle at an initial condition of the inclination angle $\theta \approx -25^\circ$, as shown in Fig. 4.11a. This figure illustrates that the vehicle is quickly stabilized by the proposed con-

troller around the upper vertical position. It can be observed in Fig. 4.11a small oscillations around the equilibrium point, which is caused by the noise that affects the measures obtained from IMU.

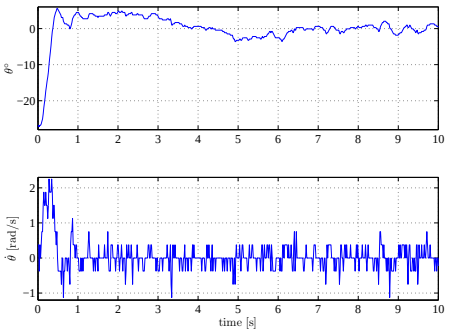

(a) Two-wheeled vehicle angular position, θ, and angular rate, $\dot{\theta}$.

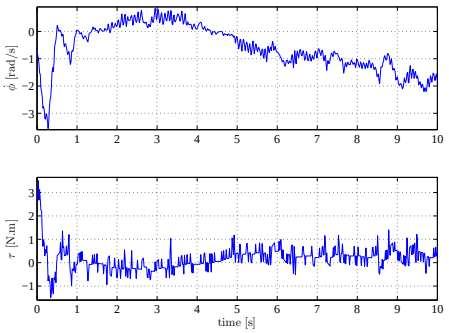

(b) Motors axle angular rate, $\dot{\varphi}$, and the applied torque, τ.

Figure 4.11: First experimental results with the two-wheeled self-balanced vehicle.

In a second experiment, the vehicle has been subjected to heavier conditions to corroborate the robustness of the controller when it is under the influence of external disturbances. Furthermore, the vehicle has been initialized at the horizontal position, which verifies the good features of the nonlinear controller to deal with angular positions far away from the upper vertical position.

The obtained experimental results are presented in Figs. 4.12. As shown in Fig. 4.12a, through the angular position graph, the nonlinear $\mathscr{H}_\infty$ controller is able to drive the two-wheeled vehicle from an initial condition about $\approx -80^\circ$ to the upper vertical position with a small response time and maintain it stabilized around the operating point. Moreover, it can be observed that the controller is able to reject external disturbances applied to the system, keeping the angular position and the angular rate around zero at steady-state.

Fig. 4.12b shows the temporal response of the motors axle angular rate, $\dot{\varphi}$, and the applied torque, τ. As can be observed in that angular rate graph, the velocity of the motors tends to a constant value because the controller does not consider this state as a controlled variable. However, due to the integral action, it is possible to keep the angular rate of the motors axle constant and bounded. This behavior can be interpreted as a disturbance caused by the driver, in the case of the

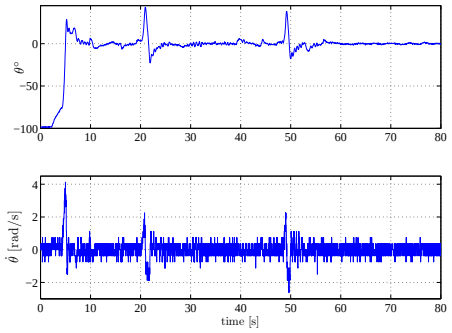

(a) Two-wheeled vehicle angular position, θ, and angular rate, $\dot{\theta}$.

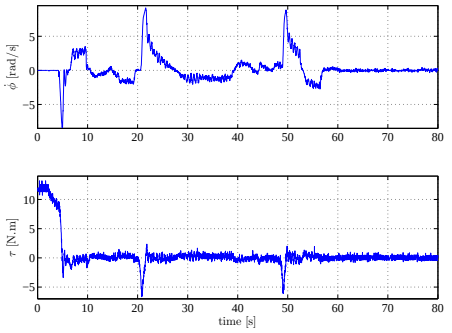

(b) Motors axle angular rate, $\dot{\varphi}$, and the applied torque, τ.

Figure 4.12: Second experimental results with the two-wheeled self-balanced vehicle.

Segway, to move forward/backward with constant speed. It can also be observed in Fig. 4.12b the smooth input control signal, τ, generated by the nonlinear $\mathscr{H}_\infty$ controller.

4.4 Underactuated Nonlinear $\mathscr{H}_\infty$ Control of the Entire System

This section deals with the design of a nonlinear $\mathscr{H}_\infty$ controller for a class of underactuated mechanical systems with input coupling. The main difference between this controller and the proposed in the previous section remains on the presence of the time-derivative of the *remaining* degrees of freedom position in the error state vector (see (4.9)).

As commented at the beginning of the chapter, the control objective in this section is to regulate the *controlled* degrees of freedom at a desired operating point, while the *remaining* ones are driven to steady state, i.e., the *non-controlled* DOF are maintained stabilized (static equilibrium), or at least their velocities (mechanical equilibrium). Thus, the proposed controller considers the whole dynamic of the system into its structure, which ensures that the whole dynamic of the system is stable in closed-loop, avoiding the use of cascade strategies, an augmented state space nor the necessity that the *remaining* DOF must be stable. Furthermore, this control law allows to achieve robustness in presence of sustained disturbances,

unmodeled dynamics, and parametric and structural uncertainties acting on the whole system.

This controller is obtained taking into account the diagonalization of the inertia matrix allowing, as presented in Section 4.3.1, a flexibility to weigh different dynamics of the system. The controller developed in this section constitutes one of the main contributions of this thesis.

To design the nonlinear $\mathscr{H}_\infty$ controller, the normalized system (4.8) is considered. As performed in others control design procedures presented in this thesis, in a previous step, the following state transformation is used:

$$z = \begin{bmatrix} z_1 \\ z_2 \\ z_3 \\ z_4 \end{bmatrix} = \boldsymbol{T}_o \boldsymbol{x} = \begin{bmatrix} \boldsymbol{T}_{11} & \mathbb{0} & \mathbb{0} & \mathbb{0} \\ \mathbb{0} & \boldsymbol{T}_{22} & \boldsymbol{T}_{23} & \boldsymbol{T}_{24} \\ \mathbb{0} & \mathbb{0} & \mathbb{1} & \mathbb{1} \\ \mathbb{0} & \mathbb{0} & \mathbb{0} & \mathbb{1} \end{bmatrix} \begin{bmatrix} \dot{\tilde{\boldsymbol{q}}}_u \\ \dot{\tilde{\boldsymbol{q}}}_c \\ \tilde{\boldsymbol{q}}_c \\ \int \tilde{\boldsymbol{q}}_c dt \end{bmatrix}, \tag{4.54}$$

with $\boldsymbol{T}_{11} = \rho\mathbb{1}$ and $\boldsymbol{T}_{22} = \nu\mathbb{1}$, where ρ and ν are positive scalars. Note that this state transformation is a particular case of the one showed in Section 4.3.1, where $\boldsymbol{T}_{13}$ and $\boldsymbol{T}_{15}$ are disregarded. This is due to the control constraints found when the whole underactuated system is controlled by a centralized controller, i.e., only m degrees of freedom can be regulated at an operation point, while the *remaining* one can only be stabilized.

Apart from this state-space transformation, to minimize the necessary forces and torques for the worst case of all possible disturbances acting on the system, the following change of variables over the control action and disturbances is considered:

$$\overline{\boldsymbol{u}} + \overline{\boldsymbol{d}} = \begin{bmatrix} \overline{\boldsymbol{M}} & \overline{\boldsymbol{C}} \end{bmatrix} \begin{bmatrix} \dot{z}_1 \\ \dot{z}_2 \\ z_1 \\ z_2 \end{bmatrix}, \tag{4.55}$$

which, in an expanded form, is given by:

$$\begin{bmatrix} \boldsymbol{u}_{su} + \boldsymbol{d}_{su} \\ \boldsymbol{u}_{rc} + \boldsymbol{d}_{rc} \end{bmatrix} = \begin{bmatrix} \boldsymbol{M}_{su} & \mathbb{0} & \boldsymbol{C}_{su} & \boldsymbol{C}_{sc} \\ \mathbb{0} & \boldsymbol{M}_{rc} & \boldsymbol{C}_{ru} & \boldsymbol{C}_{rc} \end{bmatrix} \begin{bmatrix} \dot{z}_1 \\ \dot{z}_2 \\ z_1 \\ z_2 \end{bmatrix} =$$

$$\begin{bmatrix} \boldsymbol{M}_{su}\boldsymbol{T}_{11}\ddot{\tilde{\boldsymbol{q}}}_u + \boldsymbol{C}_{su}\boldsymbol{T}_{11}\dot{\tilde{\boldsymbol{q}}}_u + \boldsymbol{C}_{sc}\left(\boldsymbol{T}_{22}\dot{\tilde{\boldsymbol{q}}}_c + \boldsymbol{T}_{23}\tilde{\boldsymbol{q}}_c + \boldsymbol{T}_{24}\int \tilde{\boldsymbol{q}}_c\right) \\ \boldsymbol{M}_{rc}\left(\boldsymbol{T}_{22}\ddot{\tilde{\boldsymbol{q}}}_c + \boldsymbol{T}_{23}\dot{\tilde{\boldsymbol{q}}}_c + \boldsymbol{T}_{24}\tilde{\boldsymbol{q}}_c\right) + \boldsymbol{C}_{ru}\boldsymbol{T}_{11}\dot{\tilde{\boldsymbol{q}}}_u + \boldsymbol{C}_{rc}\left(\boldsymbol{T}_{22}\dot{\tilde{\boldsymbol{q}}}_c + \boldsymbol{T}_{23}\tilde{\boldsymbol{q}}_c + \boldsymbol{T}_{24}\int \tilde{\boldsymbol{q}}_c\right) \end{bmatrix},$$

It can also be written in terms of the error vector and its derivative:

$$\overline{\boldsymbol{u}}+\overline{\boldsymbol{d}}=\overline{\boldsymbol{M}}(\boldsymbol{q})\boldsymbol{T}\dot{\boldsymbol{x}}+\overline{\boldsymbol{C}}(\boldsymbol{q},\dot{\boldsymbol{q}})\boldsymbol{T}\boldsymbol{x}, \tag{4.56}$$

where matrix $\boldsymbol{T}$ can be partitioned as follows:

$$\boldsymbol{T}=\begin{bmatrix} \boldsymbol{T}_{11} & \mathbb{0} & \mathbb{0} & \mathbb{0} \\ \mathbb{0} & \boldsymbol{T}_{22} & \boldsymbol{T}_{23} & \boldsymbol{T}_{24} \end{bmatrix}, \tag{4.57}$$

and

$$\overline{\boldsymbol{u}}+\overline{\boldsymbol{d}}=\boldsymbol{T}_{\boldsymbol{M}}(\boldsymbol{q})\left(\boldsymbol{u}+\boldsymbol{d}\right). \tag{4.58}$$

Equation (4.56) can be expressed in the state space form, which includes reference trajectories, forces and torques affecting kinetic energy and the state-space transformation (4.54):

$$\dot{\boldsymbol{x}}=f(\boldsymbol{x},\boldsymbol{q}_{\boldsymbol{u}},t)+g(\boldsymbol{x},\boldsymbol{q}_{\boldsymbol{u}},t)\overline{\boldsymbol{u}}+k(\boldsymbol{x},\boldsymbol{q}_{\boldsymbol{r}},t)\overline{\boldsymbol{d}}\,, \tag{4.59}$$

$$f\left(\boldsymbol{x},\boldsymbol{q}_{\boldsymbol{u}},t\right)= \boldsymbol{T}_{\boldsymbol{o}}^{-1}\begin{bmatrix} -\boldsymbol{M}_{\boldsymbol{su}}^{-1}\boldsymbol{C}_{\boldsymbol{su}} & -\boldsymbol{M}_{\boldsymbol{su}}^{-1}\boldsymbol{C}_{\boldsymbol{sc}} & \mathbb{0} & \mathbb{0} \\ -\boldsymbol{M}_{\boldsymbol{rc}}^{-1}\boldsymbol{C}_{\boldsymbol{ru}} & -\boldsymbol{M}_{\boldsymbol{rc}}^{-1}\boldsymbol{C}_{\boldsymbol{rc}} & \mathbb{0} & \mathbb{0} \\ \mathbb{0} & \boldsymbol{T}_{22}^{-1} & \mathbb{1}-\boldsymbol{T}_{22}^{-1}\boldsymbol{T}_{23} & -\mathbb{1}+\boldsymbol{T}_{22}^{-1}(\boldsymbol{T}_{23}-\boldsymbol{T}_{24}) \\ \mathbb{0} & \mathbb{0} & \mathbb{1} & -\mathbb{1} \end{bmatrix}\boldsymbol{T}_{\boldsymbol{o}}\boldsymbol{x}\,,$$

$$g\left(\boldsymbol{x},\boldsymbol{q}_{\boldsymbol{u}},t\right)=k\left(\boldsymbol{x},\boldsymbol{q}_{\boldsymbol{u}},t\right)=\boldsymbol{T}_{\boldsymbol{o}}^{-1}\begin{bmatrix} \boldsymbol{M}_{\boldsymbol{su}}^{-1} & \mathbb{0} \\ \mathbb{0} & \boldsymbol{M}_{\boldsymbol{rc}}^{-1} \\ \mathbb{0} & \mathbb{0} \\ \mathbb{0} & \mathbb{0} \end{bmatrix},$$

which represents the *dynamic equation of the system error*.

As performed in the controller designed before, by comparing equations (4.10) and (4.59), the transformed external disturbance vector $\overline{\boldsymbol{d}}$ and the control input $\overline{\boldsymbol{u}}$ are obtained as follows:

$$\overline{\boldsymbol{d}}=\overline{\boldsymbol{M}}(\boldsymbol{q})\boldsymbol{T}_{\boldsymbol{c}}\overline{\boldsymbol{M}}^{-1}(\boldsymbol{q})\overline{\boldsymbol{\delta}}, \tag{4.60}$$

$$\overline{\boldsymbol{u}}=\boldsymbol{T}_{\boldsymbol{c}}\left(-\boldsymbol{F}(\boldsymbol{x}_{\boldsymbol{e}})+\overline{\boldsymbol{\Gamma}}\right), \tag{4.61}$$

where:

$$\boldsymbol{T}_{\boldsymbol{c}}=\begin{bmatrix} \boldsymbol{T}_{11} & \mathbb{0} \\ \mathbb{0} & \boldsymbol{T}_{22} \end{bmatrix},$$

and:

$$\begin{aligned} F(\boldsymbol{x}_{e_s}) &= \boldsymbol{M}_{su}(\boldsymbol{q})\ddot{\boldsymbol{q}}_{u_r} + \boldsymbol{C}_{su}(\boldsymbol{q},\dot{\boldsymbol{q}})\dot{\boldsymbol{q}}_{u_r} + \boldsymbol{G}_{su}(\boldsymbol{q}) \\ &\quad + \boldsymbol{C}_{sc}(\boldsymbol{q},\dot{\boldsymbol{q}})\left(\dot{\tilde{\boldsymbol{q}}}_c + \dot{\boldsymbol{q}}_{c_r} - \boldsymbol{T}_{11}^{-1}\boldsymbol{T}_{22}\dot{\tilde{\boldsymbol{q}}}_c - \boldsymbol{T}_{11}^{-1}\boldsymbol{T}_{23}\tilde{\boldsymbol{q}}_c - \boldsymbol{T}_{11}^{-1}\boldsymbol{T}_{24}\int\tilde{\boldsymbol{q}}_c\right), \end{aligned}$$

$$\begin{aligned} F(\boldsymbol{x}_{e_r}) &= \boldsymbol{M}_{rc}(\boldsymbol{q})\left(\ddot{\boldsymbol{q}}_{c_r} - \boldsymbol{T}_{22}^{-1}\boldsymbol{T}_{23}\dot{\tilde{\boldsymbol{q}}}_c - \boldsymbol{T}_{22}^{-1}\boldsymbol{T}_{24}\tilde{\boldsymbol{q}}_c\right) + \boldsymbol{G}_{rc}(\boldsymbol{q}) \\ &\quad + \boldsymbol{C}_{ru}(\boldsymbol{q},\dot{\boldsymbol{q}})\left(\dot{\tilde{\boldsymbol{q}}}_u + \dot{\boldsymbol{q}}_{u_r} - \boldsymbol{T}_{22}^{-1}\boldsymbol{T}_{11}\dot{\tilde{\boldsymbol{q}}}_u\right) \\ &\quad + \boldsymbol{C}_{rc}(\boldsymbol{q},\dot{\boldsymbol{q}})\left(\dot{\boldsymbol{q}}_{c_r} - \boldsymbol{T}_{22}^{-1}\boldsymbol{T}_{23}\tilde{\boldsymbol{q}}_c - \boldsymbol{T}_{22}^{-1}\boldsymbol{T}_{24}\int\tilde{\boldsymbol{q}}_c\right). \end{aligned}$$

Note that from the definition of matrix $\boldsymbol{T}_c$ and since $\overline{\boldsymbol{M}}$ is a block diagonal matrix, both velocities of the *non-controlled* and *controlled* DOF can be weighted independently, which is an important improvement of this control design when compared to similar approaches found in the literature (Siqueira and Terra, 2004b; Ortega et al., 2005). As mentioned before, the more dynamics are considered different, the more weighting blocks of the diagonal matrix $\boldsymbol{T}_c$ form.

The relationship between the transformed force/torque vector, $\overline{\boldsymbol{\Gamma}}$, and the *additional control* effort, $\overline{\boldsymbol{u}}$, is given by equation (4.61). Then, by isolating $\overline{\boldsymbol{\Gamma}}$, the following transformed control law is obtained:

$$\overline{\boldsymbol{\Gamma}} = \overline{\boldsymbol{M}}(\boldsymbol{q})\ddot{\boldsymbol{q}} + \overline{\boldsymbol{C}}(\boldsymbol{q},\dot{\boldsymbol{q}})\dot{\boldsymbol{q}} + \overline{\boldsymbol{G}}(\boldsymbol{q}) - \boldsymbol{T}_c^{-1}\left(\overline{\boldsymbol{M}}(\boldsymbol{q})\boldsymbol{T}\dot{\boldsymbol{x}} + \overline{\boldsymbol{C}}(\boldsymbol{q},\dot{\boldsymbol{q}})\boldsymbol{T}\boldsymbol{x}\right) + \boldsymbol{T}_c^{-1}\overline{\boldsymbol{u}}, \quad (4.62)$$

which is arranged in terms of the error vector and its time derivative.

As in the nonlinear $\mathscr{H}_\infty$ controller presented in Section 3.3.2, this control law can also be divided into three different parts, presenting the same configuration discussed previously.

Consider the nonlinear equation (4.59) and the following cost variable:

$$\boldsymbol{\zeta} = \boldsymbol{W}\begin{bmatrix} h(\boldsymbol{x}) \\ \boldsymbol{u} \end{bmatrix}, \quad (4.63)$$

where, in this case, $h(\boldsymbol{x}) \in \Re^{n_u+3n_c}$ represents a function of the vector of the states to be controlled and stabilized, $\boldsymbol{W} \in \Re^{(3n_c+n_u+n)\times(3n_c+n_u+n)}$ is a weighting matrix, and $\boldsymbol{u}$ is the control signal without the transformation $\boldsymbol{T}_M$. In this case, the nonlinear $\mathscr{H}_\infty$ control problem for the entire underactuated mechanical system can be

posed as follows:

Theorem 4.4.1. *Find the smallest value $\gamma^* \geq 0$ such that for any $\gamma \geq \gamma^*$ exists an* additional control *effort $\boldsymbol{u} = \boldsymbol{u}(\boldsymbol{x}, \boldsymbol{q_u}, t)$, such that the $\mathscr{L}_2$ gain from the disturbance signals $\boldsymbol{d}$ to the cost variable $\boldsymbol{\zeta} = \boldsymbol{W}\,[h'(\boldsymbol{x})\ \boldsymbol{u}']'$ is less than or equal to a given attenuation level γ, that is:*

$$\int_0^T \|\boldsymbol{\zeta}\|_2^2 dt \leq \gamma^2 \int_0^T \|\boldsymbol{d}\|_2^2 dt\ . \tag{4.64}$$

This theorem is quite similar to the one presented in Section 3.3.1.3 (see Theorem 3.3.1). The *additional control* effort, $\boldsymbol{u} = \boldsymbol{u}(\boldsymbol{x}, \boldsymbol{q_u}, t)$, also depends on the *non-controlled* generalized coordinates, and not only on the error vector $\boldsymbol{x}$.

From the symmetric positive definite matrix $\boldsymbol{W'W}$ defined as in (3.25), and the definition of the error vector, $\boldsymbol{x}$, matrices $\boldsymbol{Q} \in \Re^{(n_u+3n_c \times n_u+3n_c)}$, $\boldsymbol{S} \in \Re^{(n_u+3n_c \times n)}$ and $\boldsymbol{R} \in \Re^{(n \times n)}$ are structured as follows:

$$\boldsymbol{Q} = \begin{bmatrix} \boldsymbol{Q_1} & \boldsymbol{Q_{12}} & \boldsymbol{Q_{13}} & \boldsymbol{Q_{14}} \\ \boldsymbol{Q_{12}} & \boldsymbol{Q_2} & \boldsymbol{Q_{23}} & \boldsymbol{Q_{24}} \\ \boldsymbol{Q_{13}} & \boldsymbol{Q_{23}} & \boldsymbol{Q_3} & \boldsymbol{Q_{34}} \\ \boldsymbol{Q_{14}} & \boldsymbol{Q_{24}} & \boldsymbol{Q_{34}} & \boldsymbol{Q_4} \end{bmatrix}, \quad \boldsymbol{S} = \begin{bmatrix} \boldsymbol{S_{11}} & \boldsymbol{S_{12}} \\ \boldsymbol{S_{21}} & \boldsymbol{S_{22}} \\ \boldsymbol{S_{31}} & \boldsymbol{S_{32}} \\ \boldsymbol{S_{41}} & \boldsymbol{S_{42}} \end{bmatrix}, \quad \boldsymbol{R} = \begin{bmatrix} \boldsymbol{R_u} & \mathbb{0} \\ \mathbb{0} & \boldsymbol{R_c} \end{bmatrix},$$

where $\boldsymbol{R_r} \in \Re^{n_u \times n_u}$ and $\boldsymbol{R_c} \in \Re^{n_c \times n_c}$. Note that $\boldsymbol{R}$ is chosen as a block diagonal matrix, which will allow to weight separately the control effort in both *non-controlled* and *controlled* DOF.

As stated before, the solution of the optimization problem depends on the choice of the cost variable, $\boldsymbol{\zeta}$, and particularly on the selection of function $h(\boldsymbol{x})$. In the same way that the previous nonlinear $\mathscr{H}_\infty$ controllers designed in this thesis, in this section, the function $h(\boldsymbol{x})$ is taken to be equal to the error vector, that is, $h(\boldsymbol{x}) = \boldsymbol{x}$. Thus, taking into account the cost variable (4.63) and from the associated performance index (3.26), shown again for the sake of clarity:

$$L_\gamma = \frac{1}{2}\|\boldsymbol{\zeta}\|_2^2 - \frac{1}{2}\gamma^2\|\boldsymbol{d}\|_2^2 = \frac{1}{2}\left\|\boldsymbol{W}\begin{bmatrix} \boldsymbol{x} \\ \boldsymbol{u} \end{bmatrix}\right\|_2^2 - \frac{1}{2}\gamma^2\|\boldsymbol{d}\|_2^2,$$

the Hamiltonian of optimization is defined as follows:

$$H_\gamma\left(\boldsymbol{x}, \boldsymbol{q_u}, \boldsymbol{u}, \boldsymbol{d}, \frac{\partial V(\boldsymbol{x}, \boldsymbol{q_u}, t)}{\partial \boldsymbol{x}}, \frac{\partial V(\boldsymbol{x}, \boldsymbol{q_u}, t)}{\partial \boldsymbol{q_u}}, t\right) = \frac{\partial' V}{\partial \boldsymbol{x}}\dot{\boldsymbol{x}} + \frac{\partial' V}{\partial \boldsymbol{q_u}}\dot{\boldsymbol{q}}_{\boldsymbol{u}} + L_\gamma. \tag{4.65}$$

Therefore, the nonlinear $\mathscr{H}_\infty$ problem admits a solution if there exists a value

function $V(\boldsymbol{x},\boldsymbol{q_u},t)$,with $\boldsymbol{x_0}=0$ and $V(\boldsymbol{x_0},\boldsymbol{q_{u_0}},t)\equiv 0$ for $t\geq 0$, that satisfies the following HJBI equation:

$$\begin{aligned}
\frac{\partial V}{\partial t} &= -\max_{\boldsymbol{d}}\min_{\boldsymbol{u}}\left(\frac{\partial' V}{\partial \boldsymbol{x}}\dot{\boldsymbol{x}}+\frac{\partial' V}{\partial \boldsymbol{q_u}}\dot{\boldsymbol{q}}_{\boldsymbol{u}}+L_\gamma\right)\\
&= -\max_{\boldsymbol{d}}\min_{\boldsymbol{u}}\left(\frac{\partial' V}{\partial \boldsymbol{x}}(f(\boldsymbol{x},\boldsymbol{q_u},t)+g(\boldsymbol{x},\boldsymbol{q_u},t)\overline{\boldsymbol{u}}+k(\boldsymbol{x},\boldsymbol{q_u},t)\overline{\boldsymbol{d}})\right.\\
&\quad \left.+\frac{\partial' V}{\partial \boldsymbol{q_u}}\dot{\boldsymbol{q}}_{\boldsymbol{u}}-\frac{1}{2}\gamma^2\boldsymbol{d}(t)'\boldsymbol{d}(t)+\frac{1}{2}\boldsymbol{x}'\boldsymbol{Q}\boldsymbol{x}+\boldsymbol{x}'\boldsymbol{S}\boldsymbol{u}(\boldsymbol{x},t)+\frac{1}{2}\boldsymbol{u}(t)'\boldsymbol{R}\boldsymbol{u}(t)\right)\\
&= -\max_{\boldsymbol{d}}\min_{\boldsymbol{u}}\left(\frac{\partial' V}{\partial \boldsymbol{x}}(f(\boldsymbol{x},\boldsymbol{q_u},t)+g(\boldsymbol{x},\boldsymbol{q_u},t)\boldsymbol{T_M}\boldsymbol{u}+k(\boldsymbol{x},\boldsymbol{q_u},t)\boldsymbol{T_M}\boldsymbol{d})\right.\\
&\quad \left.+\frac{\partial' V}{\partial \boldsymbol{q_u}}\dot{\boldsymbol{q}}_{\boldsymbol{u}}-\frac{1}{2}\gamma^2\boldsymbol{d}(t)'\boldsymbol{d}(t)+\frac{1}{2}\boldsymbol{x}'\boldsymbol{Q}\boldsymbol{x}+\boldsymbol{x}'\boldsymbol{S}\boldsymbol{u}(\boldsymbol{x},t)+\frac{1}{2}\boldsymbol{u}(t)'\boldsymbol{R}\boldsymbol{u}(t)\right).
\end{aligned} \tag{4.66}$$

Under these assumptions, the solution of the nonlinear state feedback $\mathscr{H}_\infty$ problem for underactuated systems can be reformulated following the same steps presented in Section 3.3.1.3, where:

$$\boldsymbol{u}^*(t)=arg\min_{\boldsymbol{u}}\left(\max_{\boldsymbol{d}}\left(\frac{\partial' V(\boldsymbol{x},\boldsymbol{q_u},t)}{\partial \boldsymbol{x}}\dot{\boldsymbol{x}}+\frac{\partial V(\boldsymbol{x},\boldsymbol{q_u},t)}{\partial \boldsymbol{q_u}}\dot{\boldsymbol{q}}_{\boldsymbol{u}}+L_\gamma\right)\right),$$

$$\boldsymbol{d}^*(t)=arg\max_{\boldsymbol{d}}\left(\min_{\boldsymbol{u}}\left(\frac{\partial' V(\boldsymbol{x},\boldsymbol{q_u},t)}{\partial \boldsymbol{x}}\dot{\boldsymbol{x}}+\frac{\partial V(\boldsymbol{x},\boldsymbol{q_u},t)}{\partial \boldsymbol{q_u}}\dot{\boldsymbol{q}}_{\boldsymbol{u}}+L_\gamma\right)\right),$$

which results for the particular case, where the performance index presents a square functional dependence in $\boldsymbol{u}$, in an explicit solution for the *min-max* problem as in (3.31) and (3.32). Thus, the worst-case of the admissible disturbances and the optimal state feedback control law are computed as follows:

$$\boldsymbol{d}^*(\boldsymbol{x},\boldsymbol{q_u},t)=\frac{1}{\gamma^2}\boldsymbol{T}'_{\boldsymbol{M}}k(\boldsymbol{x},t)'\frac{\partial V}{\partial \boldsymbol{x}}, \tag{4.67}$$

$$\boldsymbol{u}^*(\boldsymbol{x},\boldsymbol{q_u},t)=-\boldsymbol{R}^{-1}\left(\boldsymbol{x}'\boldsymbol{S}+\boldsymbol{T}'_{\boldsymbol{M}}g'(\boldsymbol{x},t)\frac{\partial V}{\partial \boldsymbol{x}}\right). \tag{4.68}$$

By replacing equations (4.67) and (4.68) in (4.66), the following HJ equation

is obtained:

$$\frac{\partial V}{\partial t}+\frac{\partial' V}{\partial \boldsymbol{x}}f(\boldsymbol{x},\boldsymbol{q_u},t)+\frac{\partial' V}{\partial \boldsymbol{q_u}}\dot{\boldsymbol{q}}_{\boldsymbol{u}}+\frac{1}{2}\frac{\partial' V}{\partial \boldsymbol{x}}\left[\frac{1}{\gamma^2}k(\boldsymbol{x},\boldsymbol{q_u},t)\boldsymbol{T_M}\boldsymbol{T}'_{\boldsymbol{M}}k'(\boldsymbol{x},\boldsymbol{q_u},t)\right.$$

$$\left.-g(\boldsymbol{x},\boldsymbol{q_u},t)\boldsymbol{T_M}\boldsymbol{R}^{-1}\boldsymbol{T}'_{\boldsymbol{M}}g'(\boldsymbol{x},\boldsymbol{q_u},t)\right]\frac{\partial V}{\partial \boldsymbol{x}}-\frac{\partial' V}{\partial \boldsymbol{x}}g(\boldsymbol{x},\boldsymbol{q_u},t)\boldsymbol{T_M}\boldsymbol{R}^{-1}\boldsymbol{S}'\boldsymbol{x}$$

$$+\frac{1}{2}\boldsymbol{x}'\left(\boldsymbol{Q}-\boldsymbol{S}\boldsymbol{R}^{-1}\boldsymbol{S}'\right)\boldsymbol{x}=0\,, \tag{4.69}$$

for each $\gamma>\sqrt{\sigma_{\max}(\boldsymbol{R})}\geq 0$, where $\sigma_{\max}$ stands for the maximum singular value. Then, the computation of the control effort, $\boldsymbol{u}$, will require to find the solution, $V(\boldsymbol{x},\boldsymbol{q_u},t)$, to the HJ equation (4.69). Through the following theorem, a solution is proposed:

Theorem 4.4.2. *Let $V(\boldsymbol{x},\boldsymbol{q_u},t)$ be the parameterized scalar function:*

$$V(\boldsymbol{x},\boldsymbol{q_u},t)=\frac{1}{2}\boldsymbol{x}'\boldsymbol{T}'_{\boldsymbol{o}}\begin{bmatrix}\boldsymbol{M_{uu}} & \boldsymbol{M_{uc}} & \mathbb{0} & \mathbb{0}\\ \boldsymbol{M_{cu}} & \boldsymbol{M_{cc}} & \mathbb{0} & \mathbb{0}\\ \mathbb{0} & \mathbb{0} & \boldsymbol{Y} & \boldsymbol{X}-\boldsymbol{Y}\\ \mathbb{0} & \mathbb{0} & \boldsymbol{X}-\boldsymbol{Y} & \boldsymbol{Z}+\boldsymbol{Y}\end{bmatrix}\boldsymbol{T_o}\boldsymbol{x}\,, \tag{4.70}$$

where $\boldsymbol{M_{uu}}$, $\boldsymbol{M_{uc}}$, $\boldsymbol{M_{cu}}$ and $\boldsymbol{M_{cc}}$ form the inertia matrix of the system, and $\boldsymbol{X}$, $\boldsymbol{Y}$ and $\boldsymbol{Z}\in\Re^{n_c\times n_c}$ are constant and symmetric matrices. Besides, $\boldsymbol{Y}>\mathbb{0}$ and $\boldsymbol{Z}+\boldsymbol{Y}>\mathbb{0}$ such that $\boldsymbol{Z}-\boldsymbol{X}\boldsymbol{Y}^{-1}\boldsymbol{X}+2\boldsymbol{X}>\mathbb{0}$. $\boldsymbol{T_o}$ is defined in (4.54) and $\boldsymbol{T}$ is the matrix appearing in (4.62). If these matrices verify the following equation:

$$\begin{bmatrix}\mathbb{0} & \mathbb{0} & \mathbb{0} & \mathbb{0}\\ \mathbb{0} & \mathbb{0} & \boldsymbol{Y} & \boldsymbol{X}\\ \mathbb{0} & \boldsymbol{Y} & 2\boldsymbol{X} & \boldsymbol{Z}+2\boldsymbol{X}\\ \mathbb{0} & \boldsymbol{X} & \boldsymbol{Z}+2\boldsymbol{X} & \mathbb{0}\end{bmatrix}+\boldsymbol{Q}+\frac{1}{\gamma^2}\boldsymbol{T}'\boldsymbol{T}-\left(\boldsymbol{S}'+\boldsymbol{T}\right)'\boldsymbol{R}^{-1}\left(\boldsymbol{S}'+\boldsymbol{T}\right)=\mathbb{0}\,, \tag{4.71}$$

then, function $V(\boldsymbol{x},\boldsymbol{q_u},t)$ constitutes a solution to the HJ equation (4.69), for a sufficiently high value of γ.

Proof:

Firstly, it is necessary to show that the scalar function $V(\boldsymbol{x},\boldsymbol{q_u},t)$ is positive definite. Thus, under the assumption that $\boldsymbol{Y}>\mathbb{0}$ and $\boldsymbol{Z}+\boldsymbol{Y}>\mathbb{0}$ and through the

Schur complement of $\boldsymbol{Y}$, the following inequality is checked:

$$\boldsymbol{Z}+\boldsymbol{Y}-(\boldsymbol{X}-\boldsymbol{Y})'\boldsymbol{Y}^{-1}(\boldsymbol{X}-\boldsymbol{Y})>\mathbb{0}$$

$$\boldsymbol{Z}-\boldsymbol{X}\boldsymbol{Y}^{-1}\boldsymbol{X}+2\boldsymbol{X}>\mathbb{0}\,.$$

And since the inertia matrix:

$$\boldsymbol{M}(\boldsymbol{q})=\begin{bmatrix}\boldsymbol{M}_{\boldsymbol{uu}}(\boldsymbol{q}) & \boldsymbol{M}_{\boldsymbol{uc}}(\boldsymbol{q})\\ \boldsymbol{M}_{\boldsymbol{cu}}(\boldsymbol{q}) & \boldsymbol{M}_{\boldsymbol{cc}}(\boldsymbol{q})\end{bmatrix},$$

is symmetric positive definite, the theorem assumption is verified, i.e.:

$$\begin{bmatrix}\boldsymbol{M}(\boldsymbol{q}) & \mathbb{0} & \mathbb{0}\\ & \mathbb{0} & \mathbb{0}\\ \mathbb{0}\quad\mathbb{0} & \boldsymbol{Y} & \boldsymbol{X}-\boldsymbol{Y}\\ \mathbb{0}\quad\mathbb{0} & \boldsymbol{X}-\boldsymbol{Y} & \boldsymbol{Z}+\boldsymbol{Y}\end{bmatrix}>\mathbb{0}\,.$$

Next, the hypothesis that the scalar function $V(\boldsymbol{x},\boldsymbol{q_u},t)$ constitutes a solution of Hamilton-Jacobi equation is proven. First, to verify that $V(\boldsymbol{x},\boldsymbol{q_u},t)$ is a function of $\boldsymbol{x}$, $\boldsymbol{q_u}$, and t, $\boldsymbol{M}(\boldsymbol{q})$ must also be function of them. Thus, the inertia matrix can be written as follows:

$$\boldsymbol{M}(\boldsymbol{q})=\boldsymbol{M}(\boldsymbol{q_c},\boldsymbol{q_u})=\boldsymbol{M}(\tilde{\boldsymbol{q}}_{\boldsymbol{c}}+\boldsymbol{q}_{\boldsymbol{c_r}}(t),\boldsymbol{q_u})=\boldsymbol{M}(\boldsymbol{x},\boldsymbol{q_u},t)\,,$$

which is a function of the error vector, $\boldsymbol{x}$, the *uncontrolled* degrees of freedom position, $\boldsymbol{q_u}$, considered as a time varying parameter, and time, t. The time derivative of the inertia matrix is given by:

$$\begin{aligned}\frac{d\boldsymbol{M}(\boldsymbol{q})}{dt} &= \frac{d\boldsymbol{M}(\tilde{\boldsymbol{q}}_{\boldsymbol{c}}+\boldsymbol{q}_{\boldsymbol{c_r}}(t),\boldsymbol{q_u})}{dt}\\ &= \sum_{k=1}^{n_c}\frac{\partial'\boldsymbol{M}(\boldsymbol{q})}{\partial\tilde{\boldsymbol{q}}_{\boldsymbol{c}}^{\boldsymbol{k}}}\dot{\tilde{\boldsymbol{q}}}_{\boldsymbol{c}}^{\boldsymbol{k}}+\sum_{k=1}^{n_c}\frac{\partial'\boldsymbol{M}(\boldsymbol{q})}{\partial\boldsymbol{q}_{\boldsymbol{c_r}}^{\boldsymbol{k}}}\dot{\boldsymbol{q}}_{\boldsymbol{c_r}}^{\boldsymbol{k}}+\sum_{k=1}^{n_u}\frac{\partial'\boldsymbol{M}(\boldsymbol{q})}{\partial\boldsymbol{q}_{\boldsymbol{u}}^{\boldsymbol{k}}}\dot{\boldsymbol{q}}_{\boldsymbol{u}}^{\boldsymbol{k}}\,,\end{aligned}$$

and, as $\boldsymbol{q}_{\boldsymbol{c_r}}(t)$ is only a function of time, the partial derivative of $\boldsymbol{M}(\boldsymbol{q})$ with respect to t is obtained as follows:

$$\frac{\partial\boldsymbol{M}(\boldsymbol{q})}{\partial t}=\frac{\partial\boldsymbol{M}(\tilde{\boldsymbol{x}},\boldsymbol{q_u},t)}{\partial t}=\sum_{k=1}^{n_c}\frac{\partial'\boldsymbol{M}(\boldsymbol{q})}{\partial\boldsymbol{q}_{\boldsymbol{c}}^{\boldsymbol{k}}}\dot{\boldsymbol{q}}_{\boldsymbol{c_r}}^{\boldsymbol{k}}\,.$$

Therefore, disregarding the functional dependence, partial derivatives of V are

solved separately in what follows, in order to verify that V is a solution to the HJ equation (4.69).

- The partial derivative of $V(\boldsymbol{x},\boldsymbol{q_u},t)$ with respect to time is:

$$\begin{aligned}\frac{\partial V}{\partial t} &= \frac{1}{2}\boldsymbol{x}'\boldsymbol{T}_{\boldsymbol{o}}'\begin{bmatrix}\dfrac{\partial \boldsymbol{M}}{\partial t} & \mathbb{0} & \mathbb{0}\\ \mathbb{0}\ \ \mathbb{0} & \mathbb{0} & \mathbb{0}\\ \mathbb{0}\ \ \mathbb{0} & \mathbb{0} & \mathbb{0}\end{bmatrix}\boldsymbol{T}_{\boldsymbol{o}}\boldsymbol{x}\\ &= \frac{1}{2}\boldsymbol{x}'\boldsymbol{T}_{\boldsymbol{o}}'\begin{bmatrix}\sum_{k=1}^{n_c}\dfrac{\partial' \boldsymbol{M}}{\partial \boldsymbol{q}_{\boldsymbol{c}^k}}\dot{\boldsymbol{q}}_{\boldsymbol{c}_r^k} & \mathbb{0} & \mathbb{0}\\ \mathbb{0}\ \ \mathbb{0} & \mathbb{0} & \mathbb{0}\\ \mathbb{0}\ \ \mathbb{0} & \mathbb{0} & \mathbb{0}\end{bmatrix}\boldsymbol{T}_{\boldsymbol{o}}\boldsymbol{x}.\end{aligned} \tag{4.72}$$

- The gradient of $V(\boldsymbol{x},\boldsymbol{q_u},t)$ with respect to the error vector, $\boldsymbol{x}$, is given by:

$$\begin{aligned}\frac{\partial' V}{\partial \boldsymbol{x}} &= \boldsymbol{x}'\boldsymbol{T}_{\boldsymbol{o}}'\begin{bmatrix}\boldsymbol{M} & \mathbb{0} & \mathbb{0}\\ & \mathbb{0} & \mathbb{0}\\ \mathbb{0}\ \ \mathbb{0} & \boldsymbol{Y} & \boldsymbol{X}-\boldsymbol{Y}\\ \mathbb{0}\ \ \mathbb{0} & \boldsymbol{X}-\boldsymbol{Y} & \boldsymbol{Z}+\boldsymbol{Y}\end{bmatrix}\boldsymbol{T}_{\boldsymbol{o}}\\ &+\frac{1}{2}\boldsymbol{x}'\boldsymbol{T}_{\boldsymbol{o}}'\frac{\partial'}{\partial \boldsymbol{x}}\left(\underbrace{\begin{bmatrix}\boldsymbol{M} & \mathbb{0} & \mathbb{0}\\ & \mathbb{0} & \mathbb{0}\\ \mathbb{0}\ \ \mathbb{0} & \boldsymbol{Y} & \boldsymbol{X}-\boldsymbol{Y}\\ \mathbb{0}\ \ \mathbb{0} & \boldsymbol{X}-\boldsymbol{Y} & \boldsymbol{Z}+\boldsymbol{Y}\end{bmatrix}}_{w}\right)\boldsymbol{T}_{\boldsymbol{o}}\boldsymbol{x},\end{aligned} \tag{4.73}$$

where:

$$\frac{\partial' w}{\partial \boldsymbol{x}} = \left(\frac{\partial' w}{\partial \dot{\tilde{\boldsymbol{q}}}_{\boldsymbol{u}}}, \frac{\partial' w}{\partial \dot{\tilde{\boldsymbol{q}}}_{\boldsymbol{c}}}, \frac{\partial' w}{\partial \tilde{\boldsymbol{q}}_{\boldsymbol{c}}}, \frac{\partial' w}{\partial \int \tilde{\boldsymbol{q}}_{\boldsymbol{c}}}\right) = \left(\mathbb{0}, \mathbb{0}, \frac{\partial' w}{\partial \tilde{\boldsymbol{q}}_{\boldsymbol{c}}}, \mathbb{0}\right), \tag{4.74}$$

with the zero matrices, $\mathbb{0}$, in the last expression, of dimension $n_u+3n_c \times n_u+3n_c$. Then, the unique term that is needed to be computed is:

$$\frac{\partial' w}{\partial \tilde{\boldsymbol{q}}_{\boldsymbol{c}}} = \left(\begin{bmatrix}\dfrac{\partial' \boldsymbol{M}}{\partial \tilde{\boldsymbol{q}}_{\boldsymbol{c}_1}} & \mathbb{0} & \mathbb{0}\\ \mathbb{0}\ \ \mathbb{0} & \mathbb{0} & \mathbb{0}\\ \mathbb{0}\ \ \mathbb{0} & \mathbb{0} & \mathbb{0}\end{bmatrix}, \cdots, \begin{bmatrix}\dfrac{\partial' \boldsymbol{M}}{\partial \tilde{\boldsymbol{q}}_{\boldsymbol{c}_{n_c}}} & \mathbb{0} & \mathbb{0}\\ \mathbb{0}\ \ \mathbb{0} & \mathbb{0} & \mathbb{0}\\ \mathbb{0}\ \ \mathbb{0} & \mathbb{0} & \mathbb{0}\end{bmatrix}\right).$$

Thus, the equation (4.73) can be written as follows:

$$\frac{\partial' V}{\partial \boldsymbol{x}} = \boldsymbol{x}' \boldsymbol{T}_{\boldsymbol{o}}' \begin{bmatrix} \boldsymbol{M} & & \mathbb{0} & \mathbb{0} \\ & & \mathbb{0} & \mathbb{0} \\ \mathbb{0} & \mathbb{0} & \boldsymbol{Y} & \boldsymbol{X}-\boldsymbol{Y} \\ \mathbb{0} & \mathbb{0} & \boldsymbol{X}-\boldsymbol{Y} & \boldsymbol{Z}+\boldsymbol{Y} \end{bmatrix} \boldsymbol{T}_{\boldsymbol{o}} + \frac{1}{2}\left[\mathbb{0}_{1\times n_u}, \mathbb{0}_{1\times n_c}, \boldsymbol{\Omega}, \mathbb{0}_{1\times n_c}\right], \tag{4.75}$$

where $\boldsymbol{\Omega} \in \Re^{1\times n_c}$:

$$\boldsymbol{\Omega} = \boldsymbol{x}' \boldsymbol{T}_{\boldsymbol{o}}' \frac{\partial' w}{\partial \tilde{\boldsymbol{q}}_{\boldsymbol{c}}} \boldsymbol{T}_{\boldsymbol{o}} \boldsymbol{x}.$$

Therefore, multiplying (4.75) by $\dot{\boldsymbol{x}}$ given by (4.59) results in:

$$\begin{aligned} \frac{\partial' V}{\partial \boldsymbol{x}} \dot{\boldsymbol{x}} = & \\ &= \left(\boldsymbol{x}' \boldsymbol{T}_{\boldsymbol{o}}' \begin{bmatrix} \boldsymbol{M} & & \mathbb{0} & \mathbb{0} \\ & & \mathbb{0} & \mathbb{0} \\ \mathbb{0} & \mathbb{0} & \boldsymbol{Y} & \boldsymbol{X}-\boldsymbol{Y} \\ \mathbb{0} & \mathbb{0} & \boldsymbol{X}-\boldsymbol{Y} & \boldsymbol{Z}+\boldsymbol{Y} \end{bmatrix} \boldsymbol{T}_{\boldsymbol{o}} + \frac{1}{2}\left[\mathbb{0}_{1\times n_u}, \mathbb{0}_{1\times n_c}, \boldsymbol{\Omega}, \mathbb{0}_{1\times n_c}\right] \right) \cdot \dot{\boldsymbol{x}} \\ &= \frac{\partial' V}{\partial \boldsymbol{x}} \left(f + g\bar{\boldsymbol{u}} + k\bar{\boldsymbol{d}} \right) \\ &= \frac{\partial' V}{\partial \boldsymbol{x}} f + \frac{\partial' V}{\partial \boldsymbol{x}} \left(g\bar{\boldsymbol{u}} + k\bar{\boldsymbol{d}} \right). \end{aligned} \tag{4.76}$$

Moreover, it is easy to verify that:

$$\left[\mathbb{0}_{1\times n_u}, \mathbb{0}_{1\times n_c}, \boldsymbol{\Omega}, \mathbb{0}_{1\times n_c}\right] \cdot \left(g\bar{\boldsymbol{u}} + k\bar{\boldsymbol{d}} \right) = 0,$$

and consequently, the second part of (4.76) is given by:

$$\frac{\partial' V}{\partial \boldsymbol{x}} \left(g\bar{\boldsymbol{u}} + k\bar{\boldsymbol{d}} \right) =$$

$$= \boldsymbol{x}' \boldsymbol{T}_{\boldsymbol{o}}' \begin{bmatrix} \boldsymbol{M} & & \mathbb{0} & \mathbb{0} \\ & & \mathbb{0} & \mathbb{0} \\ \mathbb{0} & \mathbb{0} & \boldsymbol{Y} & \boldsymbol{X}-\boldsymbol{Y} \\ \mathbb{0} & \mathbb{0} & \boldsymbol{X}-\boldsymbol{Y} & \boldsymbol{Z}+\boldsymbol{Y} \end{bmatrix} \cdot \boldsymbol{T}_{\boldsymbol{o}} \boldsymbol{T}_{\boldsymbol{o}}^{-1} \cdot \begin{bmatrix} \boldsymbol{M}_{\boldsymbol{su}}^{-1} & \mathbb{0} \\ \mathbb{0} & \boldsymbol{M}_{\boldsymbol{rc}}^{-1} \\ \mathbb{0} & \mathbb{0} \\ \mathbb{0} & \mathbb{0} \end{bmatrix} \left(\bar{\boldsymbol{u}} + \bar{\boldsymbol{d}} \right)$$

$$
\begin{aligned}
&= \boldsymbol{x}'\boldsymbol{T}_o' \begin{bmatrix} \boldsymbol{M} & & \mathbb{0} & \mathbb{0} \\ & & \mathbb{0} & \mathbb{0} \\ \mathbb{0} & \mathbb{0} & \boldsymbol{Y} & \boldsymbol{X}-\boldsymbol{Y} \\ \mathbb{0} & \mathbb{0} & \boldsymbol{X}-\boldsymbol{Y} & \boldsymbol{Z}+\boldsymbol{Y} \end{bmatrix} \cdot \begin{bmatrix} \bar{\boldsymbol{M}}^{-1} & & & \\ & & \mathbb{0} & \mathbb{0} \\ & & \mathbb{0} & \mathbb{0} \end{bmatrix} \boldsymbol{T}_{\boldsymbol{M}}(\boldsymbol{u}+\boldsymbol{d}) \\
&= \boldsymbol{x}'\boldsymbol{T}_o' \begin{bmatrix} \boldsymbol{M} & & \mathbb{0} & \mathbb{0} \\ & & \mathbb{0} & \mathbb{0} \\ \mathbb{0} & \mathbb{0} & \boldsymbol{Y} & \boldsymbol{X}-\boldsymbol{Y} \\ \mathbb{0} & \mathbb{0} & \boldsymbol{X}-\boldsymbol{Y} & \boldsymbol{Z}+\boldsymbol{Y} \end{bmatrix} \cdot \begin{bmatrix} \boldsymbol{M}^{-1} & & & \\ & & \mathbb{0} & \mathbb{0} \\ & & \mathbb{0} & \mathbb{0} \end{bmatrix} (\boldsymbol{u}+\boldsymbol{d}) \\
&= \boldsymbol{x}'\boldsymbol{T}'\boldsymbol{u}+\boldsymbol{x}'\boldsymbol{T}'\boldsymbol{d}\,,
\end{aligned}
\tag{4.77}
$$

with $\boldsymbol{T}$ defined in (4.57).

The first part of (4.76) is computed as follows:

$$
\begin{aligned}
&\frac{\partial' V}{\partial \boldsymbol{x}} f = \\
&= \left(\boldsymbol{x}'\boldsymbol{T}_o' \begin{bmatrix} \boldsymbol{M} & & \mathbb{0} & \mathbb{0} \\ & & \mathbb{0} & \mathbb{0} \\ \mathbb{0} & \mathbb{0} & \boldsymbol{Y} & \boldsymbol{X}-\boldsymbol{Y} \\ \mathbb{0} & \mathbb{0} & \boldsymbol{X}-\boldsymbol{Y} & \boldsymbol{Z}+\boldsymbol{Y} \end{bmatrix} \boldsymbol{T}_o + \frac{1}{2}[\mathbb{0}_{1\times n_u}, \mathbb{0}_{1\times n_c}, \boldsymbol{\Omega}, \mathbb{0}_{1\times n_c}] \right) f \\
&= \boldsymbol{x}'\boldsymbol{T}_o' \begin{bmatrix} \boldsymbol{M} & & \mathbb{0} & \mathbb{0} \\ & & \mathbb{0} & \mathbb{0} \\ \mathbb{0} & \mathbb{0} & \boldsymbol{Y} & \boldsymbol{X}-\boldsymbol{Y} \\ \mathbb{0} & \mathbb{0} & \boldsymbol{X}-\boldsymbol{Y} & \boldsymbol{Z}+\boldsymbol{Y} \end{bmatrix} \boldsymbol{T}_o \times \\
&\quad \boldsymbol{T}_o^{-1} \begin{bmatrix} -\bar{\boldsymbol{M}}^{-1}\bar{\boldsymbol{C}} & \mathbb{0} & \mathbb{0} \\ & \mathbb{0} & \mathbb{0} \\ \mathbb{0} \quad \boldsymbol{T}_{22}^{-1} & \mathbb{1}-\boldsymbol{T}_{22}^{-1}\boldsymbol{T}_{23} & -\mathbb{1}+\boldsymbol{T}_{22}^{-1}(\boldsymbol{T}_{23}-\boldsymbol{T}_{24}) \\ \mathbb{0} \quad \mathbb{0} & \mathbb{1} & -\mathbb{1} \end{bmatrix} \boldsymbol{T}_o \boldsymbol{x} \\
&\quad + \frac{1}{2}[\mathbb{0}_{1\times n_u}, \mathbb{0}_{1\times n_c}, \boldsymbol{\Omega}, \mathbb{0}_{1\times n_c}] \cdot f
\end{aligned}
$$

$$= \boldsymbol{x}'\boldsymbol{T}_o' \begin{bmatrix} \boldsymbol{M} & & \mathbb{0} & \mathbb{0} \\ & & \mathbb{0} & \mathbb{0} \\ \mathbb{0} & \mathbb{0} & \boldsymbol{Y} & \boldsymbol{X}-\boldsymbol{Y} \\ \mathbb{0} & \mathbb{0} & \boldsymbol{X}-\boldsymbol{Y} & \boldsymbol{Z}+\boldsymbol{Y} \end{bmatrix} \times$$

$$\begin{bmatrix} -\boldsymbol{M}^{-1}\boldsymbol{C} & & \mathbb{0} & \mathbb{0} \\ & & \mathbb{0} & \mathbb{0} \\ \mathbb{0} & \boldsymbol{T}_{22}^{-1} & \mathbb{1}-\boldsymbol{T}_{22}^{-1}\boldsymbol{T}_{23} & -\mathbb{1}+\boldsymbol{T}_{22}^{-1}(\boldsymbol{T}_{23}-\boldsymbol{T}_{24}) \\ \mathbb{0} & \mathbb{0} & \mathbb{1} & -\mathbb{1} \end{bmatrix} \boldsymbol{T}_o\boldsymbol{x}$$

$$+\frac{1}{2}[\mathbb{0}_{1\times n_u}, \mathbb{0}_{1\times n_c}, \boldsymbol{\Omega}, \mathbb{0}_{1\times n_c}]\cdot f + [\mathbb{0}_{1\times n_u}, \mathbb{0}_{1\times n_c}, \boldsymbol{\Omega}, \mathbb{0}_{1\times n_c}]\cdot\left(g\bar{\boldsymbol{u}}+k\bar{\boldsymbol{d}}\right)$$

$$= \boldsymbol{x}'\boldsymbol{T}_o' \begin{bmatrix} & -\boldsymbol{C} & \mathbb{0} & \mathbb{0} \\ & & \mathbb{0} & \mathbb{0} \\ \mathbb{0} & \boldsymbol{Y}\boldsymbol{T}_{22}^{-1} & -\boldsymbol{Y}\boldsymbol{T}_{22}^{-1}\boldsymbol{T}_{23}+\boldsymbol{X} & \boldsymbol{Y}\boldsymbol{T}_{22}^{-1}(\boldsymbol{T}_{23}-\boldsymbol{T}_{24})-\boldsymbol{X} \\ \mathbb{0} & (\boldsymbol{X}-\boldsymbol{Y})\boldsymbol{T}_{22}^{-1} & \boldsymbol{X}+\boldsymbol{Z} & -\boldsymbol{X}(\mathbb{1}+\boldsymbol{T}_{22}^{-1}(\boldsymbol{T}_{24}+\boldsymbol{T}_{23})) \\ & & -(\boldsymbol{X}-\boldsymbol{Y})\boldsymbol{T}_{22}^{-1}\boldsymbol{T}_{23} & +\boldsymbol{Y}\boldsymbol{T}_{22}^{-1}(\boldsymbol{T}_{24}+\boldsymbol{T}_{23})-\boldsymbol{Z} \end{bmatrix} \boldsymbol{T}_o\boldsymbol{x}$$

$$+\frac{1}{2}[\mathbb{0}_{1\times n_u}, \mathbb{0}_{1\times n_c}, \boldsymbol{\Omega}, \mathbb{0}_{1\times n_c}]\cdot\dot{\boldsymbol{x}}.$$

Using the property 3 presented in Section 2.4, the last expression can be written as follows:

$$\frac{\partial' V}{\partial \boldsymbol{x}} f = \boldsymbol{x}'\boldsymbol{T}_o' \begin{bmatrix} -\frac{1}{2}(\dot{\boldsymbol{M}}-\mathscr{N}) & & \mathbb{0} & \mathbb{0} \\ & & \mathbb{0} & \mathbb{0} \\ \mathbb{0} & \boldsymbol{Y}\boldsymbol{T}_{22}^{-1} & -\boldsymbol{Y}\boldsymbol{T}_{22}^{-1}\boldsymbol{T}_{23}+\boldsymbol{X} & \boldsymbol{Y}\boldsymbol{T}_{22}^{-1}(\boldsymbol{T}_{23}-\boldsymbol{T}_{24})-\boldsymbol{X} \\ \mathbb{0} & (\boldsymbol{X}-\boldsymbol{Y})\boldsymbol{T}_{22}^{-1} & \boldsymbol{X}+\boldsymbol{Z} & -\boldsymbol{X}(\mathbb{1}+\boldsymbol{T}_{22}^{-1}(\boldsymbol{T}_{24}+\boldsymbol{T}_{23})) \\ & & -(\boldsymbol{X}-\boldsymbol{Y})\boldsymbol{T}_{22}^{-1}\boldsymbol{T}_{23} & +\boldsymbol{Y}\boldsymbol{T}_{22}^{-1}(\boldsymbol{T}_{24}+\boldsymbol{T}_{23})-\boldsymbol{Z} \end{bmatrix} \boldsymbol{T}_o\boldsymbol{x}$$

$$+\frac{1}{2}[\mathbb{0}_{1\times n_u}, \mathbb{0}_{1\times n_c}, \boldsymbol{\Omega}, \mathbb{0}_{1\times n_c}]\cdot\dot{\boldsymbol{x}}, \tag{4.78}$$

with:

$$\frac{1}{2}\left[\mathbb{O}_{1\times n_u},\mathbb{O}_{1\times n_c},\boldsymbol{\Omega},\mathbb{O}_{1\times n_c}\right]\cdot\dot{\boldsymbol{x}}=\frac{1}{2}\left[\mathbb{O}_{1\times n_u},\mathbb{O}_{1\times n_c},\boldsymbol{\Omega},\mathbb{O}_{1\times n_c}\right]\cdot\begin{bmatrix}\ddot{\boldsymbol{q}}_{\boldsymbol{u}}\\ \ddot{\boldsymbol{q}}_{\boldsymbol{c}}\\ \dot{\tilde{\boldsymbol{q}}}_{\boldsymbol{c}}\\ \tilde{\boldsymbol{q}}_{\boldsymbol{c}}\end{bmatrix}$$

$$=\frac{1}{2}\boldsymbol{\Omega}\dot{\tilde{\boldsymbol{q}}}_{\boldsymbol{c}}=\frac{1}{2}\boldsymbol{x}'\boldsymbol{T}_{\boldsymbol{o}}'\begin{bmatrix}\sum_{k=1}^{n_c}\frac{\partial'\boldsymbol{M}}{\partial\boldsymbol{q}_{\boldsymbol{c}^k}}(\dot{\boldsymbol{q}}_{\boldsymbol{c}^k}-\dot{\boldsymbol{q}}_{\boldsymbol{c}_r^k}) & \mathbb{O} & \mathbb{O}\\ \mathbb{O} & \mathbb{O} & \mathbb{O} & \mathbb{O}\\ \mathbb{O} & \mathbb{O} & \mathbb{O} & \mathbb{O}\end{bmatrix}\boldsymbol{T}_{\boldsymbol{o}}\boldsymbol{x}.$$

- The gradient of $V(\boldsymbol{x},\boldsymbol{q}_{\boldsymbol{u}},t)$ with respect to the *non-controlled* DOF, $\boldsymbol{q}_{\boldsymbol{u}}$, is given by:

$$\frac{\partial' V}{\partial\boldsymbol{q}_{\boldsymbol{u}}}=\frac{1}{2}\boldsymbol{x}'\boldsymbol{T}_{\boldsymbol{o}}'\begin{bmatrix}\sum_{k=1}^{n_u}\frac{\partial'\boldsymbol{M}}{\partial\boldsymbol{q}_{\boldsymbol{u}^k}} & \mathbb{O} & \mathbb{O}\\ \mathbb{O} & \mathbb{O} & \mathbb{O}\\ \mathbb{O} & \mathbb{O} & \mathbb{O}\end{bmatrix}\boldsymbol{T}_{\boldsymbol{o}}\boldsymbol{x},$$

which gives:

$$\frac{\partial' V}{\partial\boldsymbol{q}_{\boldsymbol{u}}}\dot{\boldsymbol{q}}_{\boldsymbol{u}}=\frac{1}{2}\boldsymbol{x}'\boldsymbol{T}_{\boldsymbol{o}}'\begin{bmatrix}\sum_{k=1}^{n_u}\frac{\partial'\boldsymbol{M}}{\partial\boldsymbol{q}_{\boldsymbol{u}^k}}\dot{\boldsymbol{q}}_{\boldsymbol{u}^k} & \mathbb{O} & \mathbb{O}\\ \mathbb{O} & \mathbb{O} & \mathbb{O}\\ \mathbb{O} & \mathbb{O} & \mathbb{O}\end{bmatrix}\boldsymbol{T}_{\boldsymbol{o}}\boldsymbol{x}. \tag{4.79}$$

Therefore, the time derivative of equation $V(\boldsymbol{x}, \boldsymbol{q_u}, t)$ is obtained as follows:

$$
\begin{aligned}
\dot{V} &= \frac{\partial V}{\partial t} + \frac{\partial' V}{\partial \boldsymbol{x}}\dot{\boldsymbol{x}} + \frac{\partial' V}{\partial \boldsymbol{q_u}}\dot{\boldsymbol{q}}_{\boldsymbol{u}} \\
&= \frac{1}{2}\boldsymbol{x}'\boldsymbol{T}_{\boldsymbol{o}}' \begin{bmatrix} \sum_{k=1}^{n_c} \frac{\partial' \boldsymbol{M}}{\partial \boldsymbol{q}_{\boldsymbol{c}^k}} \dot{\boldsymbol{q}}_{\boldsymbol{c}_r^k} & \mathbb{0} & \mathbb{0} \\ \mathbb{0} & \mathbb{0} & \mathbb{0} \\ \mathbb{0} & \mathbb{0} & \mathbb{0} \end{bmatrix} \boldsymbol{T}_{\boldsymbol{o}}\boldsymbol{x} + \boldsymbol{x}'\boldsymbol{T}'\boldsymbol{u} + \boldsymbol{x}'\boldsymbol{T}'\boldsymbol{d} \\
&\quad + \boldsymbol{x}'\boldsymbol{T}_{\boldsymbol{o}}' \begin{bmatrix} -\frac{1}{2}(\dot{\boldsymbol{M}} - \mathscr{N}) & \mathbb{0} & \mathbb{0} \\ & \mathbb{0} & \mathbb{0} \\ \mathbb{0} \quad \boldsymbol{Y}\boldsymbol{T}_{\boldsymbol{22}}^{-1} & -\boldsymbol{Y}\boldsymbol{T}_{\boldsymbol{22}}^{-1}\boldsymbol{T}_{\boldsymbol{23}} + \boldsymbol{X} & \boldsymbol{Y}\boldsymbol{T}_{\boldsymbol{22}}^{-1}(\boldsymbol{T}_{\boldsymbol{23}} - \boldsymbol{T}_{\boldsymbol{24}}) - \boldsymbol{X} \\ \mathbb{0} \quad (\boldsymbol{X} - \boldsymbol{Y})\boldsymbol{T}_{\boldsymbol{22}}^{-1} & \boldsymbol{X} + \boldsymbol{Z} & -\boldsymbol{X}(\mathbb{1} + \boldsymbol{T}_{\boldsymbol{22}}^{-1}(\boldsymbol{T}_{\boldsymbol{24}} + \boldsymbol{T}_{\boldsymbol{23}})) \\ & -(\boldsymbol{X} - \boldsymbol{Y})\boldsymbol{T}_{\boldsymbol{22}}^{-1}\boldsymbol{T}_{\boldsymbol{23}} & +\boldsymbol{Y}\boldsymbol{T}_{\boldsymbol{22}}^{-1}(\boldsymbol{T}_{\boldsymbol{24}} + \boldsymbol{T}_{\boldsymbol{23}}) - \boldsymbol{Z} \end{bmatrix} \boldsymbol{T}_{\boldsymbol{o}}\boldsymbol{x} \\
&\quad + \frac{1}{2}\boldsymbol{x}'\boldsymbol{T}_{\boldsymbol{o}}' \begin{bmatrix} \sum_{k=1}^{n_c} \frac{\partial' \boldsymbol{M}}{\partial \boldsymbol{q}_{\boldsymbol{c}^k}} (\dot{\boldsymbol{q}}_{\boldsymbol{c}^k} - \dot{\boldsymbol{q}}_{\boldsymbol{c}_r^k}) & \mathbb{0} & \mathbb{0} \\ \mathbb{0} \quad \mathbb{0} & \mathbb{0} & \mathbb{0} \\ \mathbb{0} \quad \mathbb{0} & \mathbb{0} & \mathbb{0} \end{bmatrix} \boldsymbol{T}_{\boldsymbol{o}}\boldsymbol{x} \\
&\quad + \frac{1}{2}\boldsymbol{x}'\boldsymbol{T}_{\boldsymbol{o}}' \begin{bmatrix} \sum_{k=1}^{n_u} \frac{\partial' \boldsymbol{M}}{\partial \boldsymbol{q}_{\boldsymbol{u}^k}} \dot{\boldsymbol{q}}_{\boldsymbol{u}^k} & \mathbb{0} & \mathbb{0} \\ \mathbb{0} \quad \mathbb{0} & \mathbb{0} & \mathbb{0} \\ \mathbb{0} \quad \mathbb{0} & \mathbb{0} & \mathbb{0} \end{bmatrix} \boldsymbol{T}_{\boldsymbol{o}}\boldsymbol{x} \\
&= \boldsymbol{x}'\boldsymbol{T}'\boldsymbol{u} + \boldsymbol{x}'\boldsymbol{T}'\boldsymbol{d} + \frac{1}{2}\boldsymbol{x}'\boldsymbol{T}_{\boldsymbol{o}}' \begin{bmatrix} \dot{\boldsymbol{M}} & \mathbb{0} & \mathbb{0} \\ & \mathbb{0} & \mathbb{0} \\ \mathbb{0} \quad \mathbb{0} & \mathbb{0} & \mathbb{0} \\ \mathbb{0} \quad \mathbb{0} & \mathbb{0} & \mathbb{0} \end{bmatrix} \boldsymbol{T}_{\boldsymbol{o}}\boldsymbol{x} \\
&\quad + \boldsymbol{x}'\boldsymbol{T}_{\boldsymbol{o}}' \begin{bmatrix} -\frac{1}{2}(\dot{\boldsymbol{M}} - \mathscr{N}) & \mathbb{0} & \mathbb{0} \\ & \mathbb{0} & \mathbb{0} \\ \mathbb{0} \quad \boldsymbol{Y}\boldsymbol{T}_{\boldsymbol{22}}^{-1} & -\boldsymbol{Y}\boldsymbol{T}_{\boldsymbol{22}}^{-1}\boldsymbol{T}_{\boldsymbol{23}} + \boldsymbol{X} & \boldsymbol{Y}\boldsymbol{T}_{\boldsymbol{22}}^{-1}(\boldsymbol{T}_{\boldsymbol{23}} - \boldsymbol{T}_{\boldsymbol{24}}) - \boldsymbol{X} \\ \mathbb{0} \quad (\boldsymbol{X} - \boldsymbol{Y})\boldsymbol{T}_{\boldsymbol{22}}^{-1} & \boldsymbol{X} + \boldsymbol{Z} & -\boldsymbol{X}(\mathbb{1} + \boldsymbol{T}_{\boldsymbol{22}}^{-1}(\boldsymbol{T}_{\boldsymbol{24}} + \boldsymbol{T}_{\boldsymbol{23}})) \\ & -(\boldsymbol{X} - \boldsymbol{Y})\boldsymbol{T}_{\boldsymbol{22}}^{-1}\boldsymbol{T}_{\boldsymbol{23}} & +\boldsymbol{Y}\boldsymbol{T}_{\boldsymbol{22}}^{-1}(\boldsymbol{T}_{\boldsymbol{24}} + \boldsymbol{T}_{\boldsymbol{23}}) - \boldsymbol{Z} \end{bmatrix} \boldsymbol{T}_{\boldsymbol{o}}\boldsymbol{x}
\end{aligned}
$$

$$\dot{V} = \boldsymbol{x}'\boldsymbol{T}'\boldsymbol{u}+\boldsymbol{x}'\boldsymbol{T}'\boldsymbol{d}$$

$$+\boldsymbol{x}'\boldsymbol{T}_o'\begin{bmatrix} & \frac{1}{2}\mathscr{N} & \mathbb{0} & \mathbb{0} \\ & & \mathbb{0} & \mathbb{0} \\ \mathbb{0} & \boldsymbol{Y}\boldsymbol{T}_{22}^{-1} & -\boldsymbol{Y}\boldsymbol{T}_{22}^{-1}\boldsymbol{T}_{23}+\boldsymbol{X} & \boldsymbol{Y}\boldsymbol{T}_{22}^{-1}(\boldsymbol{T}_{23}-\boldsymbol{T}_{24})-\boldsymbol{X} \\ \mathbb{0} & (\boldsymbol{X}-\boldsymbol{Y})\boldsymbol{T}_{22}^{-1} & \boldsymbol{X}+\boldsymbol{Z} & -\boldsymbol{X}(\mathbb{1}+\boldsymbol{T}_{22}^{-1}(\boldsymbol{T}_{24}+\boldsymbol{T}_{23})) \\ & & -(\boldsymbol{X}-\boldsymbol{Y})\boldsymbol{T}_{22}^{-1}\boldsymbol{T}_{23} & +\boldsymbol{Y}\boldsymbol{T}_{22}^{-1}(\boldsymbol{T}_{24}+\boldsymbol{T}_{23})-\boldsymbol{Z} \end{bmatrix}\boldsymbol{T}_o\boldsymbol{x}\,.$$

Taking into account that matrix $\mathscr{N}$ is skew-symmetric and due to the particular structure of $\boldsymbol{T}_o$, the following equality is verified:

$$\boldsymbol{x}'\boldsymbol{T}_o'\begin{bmatrix} \frac{1}{2}\mathscr{N} & & \mathbb{0} & \mathbb{0} \\ & & \mathbb{0} & \mathbb{0} \\ \mathbb{0} & \mathbb{0} & \mathbb{0} & \mathbb{0} \\ \mathbb{0} & \mathbb{0} & \mathbb{0} & \mathbb{0} \end{bmatrix}\boldsymbol{T}_o\boldsymbol{x} = 0\,.$$

Thus, substituting this expression in the preceding equation yields to:

$$\begin{aligned}\dot{V} &= \boldsymbol{x}'\boldsymbol{T}'\boldsymbol{u}+\boldsymbol{x}'\boldsymbol{T}'\boldsymbol{d} \\ &+\boldsymbol{x}'\boldsymbol{T}_o'\begin{bmatrix} \mathbb{0} & \mathbb{0} & \mathbb{0} & \mathbb{0} \\ \mathbb{0} & \mathbb{0} & \mathbb{0} & \mathbb{0} \\ \mathbb{0} & \boldsymbol{Y}\boldsymbol{T}_{22}^{-1} & -\boldsymbol{Y}\boldsymbol{T}_{22}^{-1}\boldsymbol{T}_{23}+\boldsymbol{X} & \boldsymbol{Y}\boldsymbol{T}_{22}^{-1}(\boldsymbol{T}_{23}-\boldsymbol{T}_{24})-\boldsymbol{X} \\ \mathbb{0} & (\boldsymbol{X}-\boldsymbol{Y})\boldsymbol{T}_{22}^{-1} & \boldsymbol{X}+\boldsymbol{Z} & -\boldsymbol{X}(\mathbb{1}+\boldsymbol{T}_{22}^{-1}(\boldsymbol{T}_{24}+\boldsymbol{T}_{23})) \\ & & -(\boldsymbol{X}-\boldsymbol{Y})\boldsymbol{T}_{22}^{-1}\boldsymbol{T}_{23} & +\boldsymbol{Y}\boldsymbol{T}_{22}^{-1}(\boldsymbol{T}_{24}+\boldsymbol{T}_{23})-\boldsymbol{Z} \end{bmatrix}\boldsymbol{T}_o\boldsymbol{x} \\ &= \boldsymbol{x}'\boldsymbol{T}'\boldsymbol{u}+\boldsymbol{x}'\boldsymbol{T}'\boldsymbol{d}+\boldsymbol{x}'\begin{bmatrix} \mathbb{0} & \mathbb{0} & \mathbb{0} & \mathbb{0} \\ \mathbb{0} & \mathbb{0} & \mathbb{0} & \mathbb{0} \\ \mathbb{0} & \boldsymbol{Y} & \boldsymbol{X} & \mathbb{0} \\ \mathbb{0} & \boldsymbol{X} & 2\boldsymbol{X}+\boldsymbol{Z} & \mathbb{0} \end{bmatrix}\boldsymbol{x} \\ &= \boldsymbol{x}'\boldsymbol{T}'\boldsymbol{u}+\boldsymbol{x}'\boldsymbol{T}'\boldsymbol{d}+\frac{1}{2}\boldsymbol{x}'\left(\begin{bmatrix} \mathbb{0} & \mathbb{0} & \mathbb{0} & \mathbb{0} \\ \mathbb{0} & \mathbb{0} & \mathbb{0} & \mathbb{0} \\ \mathbb{0} & \boldsymbol{Y} & \boldsymbol{X} & \mathbb{0} \\ \mathbb{0} & \boldsymbol{X} & 2\boldsymbol{X}+\boldsymbol{Z} & \mathbb{0} \end{bmatrix}+\begin{bmatrix} \mathbb{0} & \mathbb{0} & \mathbb{0} & \mathbb{0} \\ \mathbb{0} & \mathbb{0} & \boldsymbol{Y} & \boldsymbol{X} \\ \mathbb{0} & \mathbb{0} & \boldsymbol{X} & 2\boldsymbol{X}+\boldsymbol{Z} \\ \mathbb{0} & \mathbb{0} & \mathbb{0} & \mathbb{0} \end{bmatrix}\right)\boldsymbol{x} \\ &= \boldsymbol{x}'\boldsymbol{T}'\boldsymbol{u}+\boldsymbol{x}'\boldsymbol{T}'\boldsymbol{d}+\frac{1}{2}\boldsymbol{x}'\begin{bmatrix} \mathbb{0} & \mathbb{0} & \mathbb{0} & \mathbb{0} \\ \mathbb{0} & \mathbb{0} & \boldsymbol{Y} & \boldsymbol{X} \\ \mathbb{0} & \boldsymbol{Y} & 2\boldsymbol{X} & 2\boldsymbol{X}+\boldsymbol{Z} \\ \mathbb{0} & \boldsymbol{X} & 2\boldsymbol{X}+\boldsymbol{Z} & \mathbb{0} \end{bmatrix}\boldsymbol{x}\,. \end{aligned} \tag{4.80}$$

By replacing the gradient of V with respect to $\boldsymbol{x}$ into (4.67) and (4.68), the worst-case of the admissible disturbances $\boldsymbol{d}^*$, and the optimal control effort $\boldsymbol{u}^*$ to the candidate value function are obtained as follows:

$$\boldsymbol{d}^* = \frac{1}{\gamma^2}\boldsymbol{T}\boldsymbol{x}, \tag{4.81}$$

$$\boldsymbol{u}^* = -\boldsymbol{R}^{-1}\left(\boldsymbol{S}' + \boldsymbol{T}\right)\boldsymbol{x}, \tag{4.82}$$

which are substituted into (4.80):

$$\dot{V} = -\boldsymbol{x}'\boldsymbol{T}'\boldsymbol{R}^{-1}\left(\boldsymbol{S}' + \boldsymbol{T}\right)\boldsymbol{x} + \frac{1}{\gamma^2}\boldsymbol{x}'\boldsymbol{T}'\boldsymbol{T}\boldsymbol{x} + \frac{1}{2}\boldsymbol{x}'\begin{bmatrix} \mathbb{0} & \mathbb{0} & \mathbb{0} & \mathbb{0} \\ \mathbb{0} & \mathbb{0} & \boldsymbol{Y} & \boldsymbol{X} \\ \mathbb{0} & \boldsymbol{Y} & 2\boldsymbol{X} & 2\boldsymbol{X}+\boldsymbol{Z} \\ \mathbb{0} & \boldsymbol{X} & 2\boldsymbol{X}+\boldsymbol{Z} & \mathbb{0} \end{bmatrix}\boldsymbol{x}. \tag{4.83}$$

Applying $\boldsymbol{u}^*$ and $\boldsymbol{d}^*$ to the associated performance index (3.26) gives:

$$L_\gamma = \frac{1}{2}\boldsymbol{x}'\left(\boldsymbol{Q} - \boldsymbol{S}\boldsymbol{R}^1\boldsymbol{S}' + \boldsymbol{T}'\boldsymbol{R}^1\boldsymbol{T} - \frac{1}{\gamma^2}\boldsymbol{T}'\boldsymbol{T}\right)\boldsymbol{x}. \tag{4.84}$$

Thus, the HJ equation (4.69) is satisfied for $\boldsymbol{u} = \boldsymbol{u}^*$ and $\boldsymbol{d} = \boldsymbol{d}^*$ if:

$$\frac{\partial V}{\partial t} + H_\gamma\left(\boldsymbol{x}, \boldsymbol{q}_{\boldsymbol{u}}, \boldsymbol{u}^*, \boldsymbol{d}^*, \frac{\partial V(\boldsymbol{x}, \boldsymbol{q}_{\boldsymbol{u}})}{\partial \boldsymbol{x}}, \frac{\partial V(\boldsymbol{x}, \boldsymbol{q}_{\boldsymbol{u}}, t)}{\partial \boldsymbol{q}_{\boldsymbol{u}}}, t\right) =$$

$$= \frac{\partial V}{\partial t} + \frac{\partial' V(\boldsymbol{x}, \boldsymbol{q}_{\boldsymbol{u}}, t)}{\partial \boldsymbol{x}}\dot{\boldsymbol{x}} + \frac{\partial V(\boldsymbol{x}, \boldsymbol{q}_{\boldsymbol{u}}, t)}{\partial \boldsymbol{q}_{\boldsymbol{u}}}\dot{\boldsymbol{q}}_{\boldsymbol{u}} + L_\gamma$$

$$= \frac{1}{2}\boldsymbol{x}'\left(\begin{bmatrix} \mathbb{0} & \mathbb{0} & \mathbb{0} & \mathbb{0} \\ \mathbb{0} & \mathbb{0} & \boldsymbol{Y} & \boldsymbol{X} \\ \mathbb{0} & \boldsymbol{Y} & 2\boldsymbol{X} & \boldsymbol{Z}+2\boldsymbol{X} \\ \mathbb{0} & \boldsymbol{X} & \boldsymbol{Z}+2\boldsymbol{X} & \mathbb{0} \end{bmatrix} + \boldsymbol{Q} + \frac{1}{\gamma^2}\boldsymbol{T}'\boldsymbol{T} - \left(\boldsymbol{S}' + \boldsymbol{T}\right)'\boldsymbol{R}^{-1}\left(\boldsymbol{S}' + \boldsymbol{T}\right)\right)\boldsymbol{x}$$

$$= 0.$$

Thus, $V(\boldsymbol{x}, \boldsymbol{q}_{\boldsymbol{u}}, t)$ is a solution to the Hamilton-Jacobi equation (4.69) for $\boldsymbol{u} = \boldsymbol{u}^*$ and $\boldsymbol{d} = \boldsymbol{d}^*$, which proves Theorem 4.4.2.

■

The algorithm to obtain the matrix $\boldsymbol{T}$ is the following:

1. Compute $\boldsymbol{T}_{11}$, $\boldsymbol{T}_{22}$ and $\boldsymbol{T}_{24}$ by solving the following Riccati algebraic equations:

$$\boldsymbol{Q}_1 + \frac{1}{\gamma^2}\boldsymbol{T}'_{11}\boldsymbol{T}_{11} - \left(\boldsymbol{S}'_{11} + \boldsymbol{T}_{11}\right)'\boldsymbol{R}_u^{-1}\left(\boldsymbol{S}'_{11} + \boldsymbol{T}_{11}\right) - \boldsymbol{S}_{12}\boldsymbol{R}_c^{-1}\boldsymbol{S}'_{12} = \mathbb{0}, \tag{4.85}$$

$$\boldsymbol{Q}_2 + \frac{1}{\gamma^2}\boldsymbol{T}'_{22}\boldsymbol{T}_{22} - \left(\boldsymbol{S}'_{22} + \boldsymbol{T}_{22}\right)'\boldsymbol{R}_c^{-1}\left(\boldsymbol{S}'_{22} + \boldsymbol{T}_{22}\right) - \boldsymbol{S}_{21}\boldsymbol{R}_u^{-1}\boldsymbol{S}'_{21} = \mathbb{0}, \tag{4.86}$$

$$\boldsymbol{Q}_4 + \frac{1}{\gamma^2}\boldsymbol{T}'_{24}\boldsymbol{T}_{24} - \left(\boldsymbol{S}'_{42} + \boldsymbol{T}_{24}\right)'\boldsymbol{R}_c^{-1}\left(\boldsymbol{S}'_{42} + \boldsymbol{T}_{24}\right) - \boldsymbol{S}_{41}\boldsymbol{R}_u^{-1}\boldsymbol{S}'_{41} = \mathbb{0}. \tag{4.87}$$

2. Compute matrix $\boldsymbol{X}$ through the following equation:

$$\boldsymbol{X} + \boldsymbol{Q}_{24} + \frac{1}{\gamma^2}\boldsymbol{T}'_{22}\boldsymbol{T}_{24} - \left(\boldsymbol{S}'_{22} + \boldsymbol{T}_{22}\right)'\boldsymbol{R}_c^{-1}\left(\boldsymbol{S}'_{42} + \boldsymbol{T}_{24}\right) - \boldsymbol{S}_{21}\boldsymbol{R}_u^{-1}\boldsymbol{S}'_{41} = \mathbb{0}. \tag{4.88}$$

3. Compute $\boldsymbol{T}_{23}$ by solving the following Riccati algebraic equation:

$$2\boldsymbol{X} + \boldsymbol{Q}_3 + \frac{1}{\gamma^2}\boldsymbol{T}'_{23}\boldsymbol{T}_{23} - \left(\boldsymbol{S}'_{32} + \boldsymbol{T}_{23}\right)'\boldsymbol{R}_c^{-1}\left(\boldsymbol{S}'_{32} + \boldsymbol{T}_{23}\right) - \boldsymbol{S}_{31}\boldsymbol{R}_u^{-1}\boldsymbol{S}'_{31} = \mathbb{0}. \tag{4.89}$$

Once matrix $\boldsymbol{T}$ is computed and from the optimal state feedback control law (4.82), *additional control* effort $\overline{\boldsymbol{u}}^*$ corresponding to the $\mathscr{H}_\infty$ optimal index γ is given by

$$\overline{\boldsymbol{u}}^* = -\boldsymbol{T}_{\boldsymbol{M}}\boldsymbol{R}^{-1}\left(\boldsymbol{S}' + \boldsymbol{T}\right)\boldsymbol{x}. \tag{4.90}$$

Finally, if the *additional control* effort (4.90) is replaced into (4.56) under the assumption that $\overline{\boldsymbol{d}} = 0$, and after some manipulations, the *control acceleration* can be obtained as follows:

$$\ddot{\boldsymbol{q}} = \ddot{\boldsymbol{q}}^{\boldsymbol{d}} - \boldsymbol{K}_{\boldsymbol{D}}\dot{\tilde{\boldsymbol{q}}} - \boldsymbol{K}_{\boldsymbol{P}}\tilde{\boldsymbol{q}} - \boldsymbol{K}_{\boldsymbol{I}}\int \tilde{\boldsymbol{q}}dt, \tag{4.91}$$

with

$$\boldsymbol{K}_{\boldsymbol{D}} = \begin{bmatrix} \boldsymbol{K}_{D_{su}} & \boldsymbol{K}_{D_{sc}} \\ \boldsymbol{K}_{D_{ru}} & \boldsymbol{K}_{D_{rc}} \end{bmatrix}, \quad \boldsymbol{K}_{\boldsymbol{P}} = \begin{bmatrix} \mathbb{0} & \boldsymbol{K}_{P_{sc}} \\ \mathbb{0} & \boldsymbol{K}_{P_{rc}} \end{bmatrix}, \quad \boldsymbol{K}_{\boldsymbol{I}} = \begin{bmatrix} \mathbb{0} & \boldsymbol{K}_{I_{sc}} \\ \mathbb{0} & \boldsymbol{K}_{I_{rc}} \end{bmatrix},$$

where

$$\begin{aligned}
\boldsymbol{K}_{\boldsymbol{D}_{su}} &= \boldsymbol{T}_{\boldsymbol{11}}^{-1}\boldsymbol{M}_{su}^{-1}\left(\boldsymbol{C}_{su}\boldsymbol{T}_{11}+\boldsymbol{R}_u^{-1}(\boldsymbol{S}'_{11}+\boldsymbol{T}_{11})-\boldsymbol{M}_{uc}\boldsymbol{M}_{cc}^{-1}\boldsymbol{R}_c^{-1}\boldsymbol{S}'_{12}\right),\\
\boldsymbol{K}_{\boldsymbol{D}_{sc}} &= \boldsymbol{T}_{\boldsymbol{11}}^{-1}\boldsymbol{M}_{su}^{-1}\left(\boldsymbol{C}_{sc}\boldsymbol{T}_{22}+\boldsymbol{R}_u^{-1}\boldsymbol{S}'_{21}-\boldsymbol{M}_{uc}\boldsymbol{M}_{cc}^{-1}\boldsymbol{R}_c^{-1}(\boldsymbol{S}'_{22}+\boldsymbol{T}_{22})\right),\\
\boldsymbol{K}_{\boldsymbol{P}_{sc}} &= \boldsymbol{T}_{\boldsymbol{11}}^{-1}\boldsymbol{M}_{su}^{-1}\left(\boldsymbol{C}_{sc}\boldsymbol{T}_{23}+\boldsymbol{R}_u^{-1}\boldsymbol{S}'_{31}-\boldsymbol{M}_{uc}\boldsymbol{M}_{cc}^{-1}\boldsymbol{R}_c^{-1}(\boldsymbol{S}'_{32}+\boldsymbol{T}_{23})\right),\\
\boldsymbol{K}_{\boldsymbol{I}_{sc}} &= \boldsymbol{T}_{\boldsymbol{11}}^{-1}\boldsymbol{M}_{su}^{-1}\left(\boldsymbol{C}_{sc}\boldsymbol{T}_{24}+\boldsymbol{R}_u^{-1}\boldsymbol{S}'_{41}-\boldsymbol{M}_{uc}\boldsymbol{M}_{cc}^{-1}\boldsymbol{R}_c^{-1}(\boldsymbol{S}'_{42}+\boldsymbol{T}_{24})\right),\\
\boldsymbol{K}_{\boldsymbol{D}_{ru}} &= \boldsymbol{T}_{\boldsymbol{22}}^{-1}\boldsymbol{M}_{rc}^{-1}\left(\boldsymbol{C}_{ru}\boldsymbol{T}_{11}+\boldsymbol{R}_c^{-1}\boldsymbol{S}'_{12}-\boldsymbol{M}_{cu}\boldsymbol{M}_{uu}^{-1}\boldsymbol{R}_u^{-1}(\boldsymbol{S}'_{11}+\boldsymbol{T}_{11})\right),\\
\boldsymbol{K}_{\boldsymbol{D}_{rc}} &= \boldsymbol{T}_{\boldsymbol{22}}^{-1}\boldsymbol{M}_{rc}^{-1}\left(\boldsymbol{C}_{rc}\boldsymbol{T}_{22}+\boldsymbol{R}_c^{-1}(\boldsymbol{S}'_{22}+\boldsymbol{T}_{22})-\boldsymbol{M}_{cu}\boldsymbol{M}_{uu}^{-1}\boldsymbol{R}_u^{-1}\boldsymbol{S}'_{21}\right)+\boldsymbol{T}_{\boldsymbol{22}}^{-1}\boldsymbol{T}_{\boldsymbol{23}},\\
\boldsymbol{K}_{\boldsymbol{P}_{rc}} &= \boldsymbol{T}_{\boldsymbol{22}}^{-1}\boldsymbol{M}_{rc}^{-1}\left(\boldsymbol{C}_{rc}\boldsymbol{T}_{23}+\boldsymbol{R}_c^{-1}(\boldsymbol{S}'_{32}+\boldsymbol{T}_{23})-\boldsymbol{M}_{cu}\boldsymbol{M}_{uu}^{-1}\boldsymbol{R}_u^{-1}\boldsymbol{S}'_{31}\right)+\boldsymbol{T}_{\boldsymbol{22}}^{-1}\boldsymbol{T}_{\boldsymbol{24}},\\
\boldsymbol{K}_{\boldsymbol{I}_{rc}} &= \boldsymbol{T}_{\boldsymbol{22}}^{-1}\boldsymbol{M}_{rc}^{-1}\left(\boldsymbol{C}_{rc}\boldsymbol{T}_{24}+\boldsymbol{R}_c^{-1}(\boldsymbol{S}'_{42}+\boldsymbol{T}_{23})-\boldsymbol{M}_{cu}\boldsymbol{M}_{uu}^{-1}\boldsymbol{R}_u^{-1}\boldsymbol{S}'_{41}\right).
\end{aligned} \tag{4.92}$$

As in the nonlinear $\mathscr{H}_\infty$ controllers discussed along the thesis, a particular case can also be obtained when the elements of the weighting compound $\boldsymbol{W}'\boldsymbol{W}$ verify:

$$\boldsymbol{Q}=\begin{bmatrix}\omega_{1s}^2\mathbb{1} & \mathbb{0} & \mathbb{0} & \mathbb{0}\\ \mathbb{0} & \omega_{1c}^2\mathbb{1} & \mathbb{0} & \mathbb{0}\\ \mathbb{0} & \mathbb{0} & \omega_{2c}^2\mathbb{1} & \mathbb{0}\\ \mathbb{0} & \mathbb{0} & \mathbb{0} & \omega_{3c}^2\mathbb{1}\end{bmatrix},\ \boldsymbol{S}=\begin{bmatrix}\mathbb{0} & \mathbb{0}\\ \mathbb{0} & \mathbb{0}\\ \mathbb{0} & \mathbb{0}\\ \mathbb{0} & \mathbb{0}\end{bmatrix},\ \boldsymbol{R}=\begin{bmatrix}\omega_{us}^2\mathbb{1} & \mathbb{0}\\ \mathbb{0} & \omega_{uc}^2\mathbb{1}\end{bmatrix}.$$

In this case, matrices $\boldsymbol{T}_{\boldsymbol{11}}$, $\boldsymbol{T}_{\boldsymbol{22}}$, $\boldsymbol{T}_{\boldsymbol{23}}$ and $\boldsymbol{T}_{\boldsymbol{24}}$ can be defined as follows:

$$\boldsymbol{T}_{\boldsymbol{11}}=\rho\mathbb{1},\quad \boldsymbol{T}_{\boldsymbol{22}}=\nu\mathbb{1},\quad \boldsymbol{T}_{\boldsymbol{23}}=\mu\mathbb{1},\quad \boldsymbol{T}_{\boldsymbol{24}}=\lambda\mathbb{1},$$

where ρ, ν, μ and λ can be computed, using the Riccati's equations presented before, as follows:

1. Compute ρ, ν and λ with equations (4.85), (4.86) and (4.87), respectively:

$$\rho=\frac{\gamma\omega_{us}\omega_{1s}}{\sqrt{\gamma^2-\omega_{us}^2}},$$

$$\nu=\frac{\gamma\omega_{uc}\omega_{1c}}{\sqrt{\gamma^2-\omega_{uc}^2}},$$

$$\rho = \frac{\gamma \omega_{uc} \omega_{3c}}{\sqrt{\gamma^2 - \omega_{uc}^2}}.$$

2. Compute $\boldsymbol{X}$ using (4.88):

$$\boldsymbol{X} = -\rho\lambda \left(\frac{\mathbb{1}}{\gamma^2} - \frac{\mathbb{1}}{\omega_{uc}} \right).$$

3. Compute μ with (4.89):

$$\mu = \frac{\gamma \omega_{uc} \sqrt{\omega_{2c}^2 + 2\omega_{1c}\omega_{3c}}}{\sqrt{\gamma^2 - \omega_{uc}^2}}.$$

Therefore, the analytical equations (4.92) for the gain matrices can be expressed for the particular case as follows:

$$\begin{aligned}
\boldsymbol{K}_{\boldsymbol{D}_{su}} &= \boldsymbol{M}_{\boldsymbol{su}}^{-1} \left(\boldsymbol{C}_{\boldsymbol{su}} + \frac{1}{\omega_{us}^2} \mathbb{1} \right), \\
\boldsymbol{K}_{\boldsymbol{D}_{sc}} &= \boldsymbol{M}_{\boldsymbol{su}}^{-1} \left(\boldsymbol{C}_{\boldsymbol{sc}} - \boldsymbol{M}_{\boldsymbol{uc}} \boldsymbol{M}_{\boldsymbol{cc}}^{-1} \frac{1}{\omega_{uc}^2} \right) \frac{\omega_{uc}\omega_{1c}}{\sqrt{\gamma^2 - \omega_{uc}^2}} \frac{\sqrt{\gamma^2 - \omega_{us}^2}}{\omega_{us}\omega_{1s}}, \\
\boldsymbol{K}_{\boldsymbol{P}_{sc}} &= \boldsymbol{M}_{\boldsymbol{su}}^{-1} \left(\boldsymbol{C}_{\boldsymbol{sc}} - \boldsymbol{M}_{\boldsymbol{uc}} \boldsymbol{M}_{\boldsymbol{cc}}^{-1} \frac{1}{\omega_{uc}^2} \right) \frac{\omega_{uc}\sqrt{\omega_{2c}^2 + 2\omega_{1c}\omega_{3c}}}{\sqrt{\gamma^2 - \omega_{uc}^2}} \frac{\sqrt{\gamma^2 - \omega_{us}^2}}{\omega_{us}\omega_{1s}}, \\
\boldsymbol{K}_{\boldsymbol{I}_{sc}} &= \boldsymbol{M}_{\boldsymbol{su}}^{-1} \left(\boldsymbol{C}_{\boldsymbol{sc}} - \boldsymbol{M}_{\boldsymbol{uc}} \boldsymbol{M}_{\boldsymbol{cc}}^{-1} \frac{1}{\omega_{uc}^2} \right) \frac{\omega_{uc}\omega_{3c}}{\sqrt{\gamma^2 - \omega_{uc}^2}} \frac{\sqrt{\gamma^2 - \omega_{us}^2}}{\omega_{us}\omega_{1s}}, \\
\boldsymbol{K}_{\boldsymbol{D}_{ru}} &= \boldsymbol{M}_{\boldsymbol{rc}}^{-1} \left(\boldsymbol{C}_{\boldsymbol{ru}} - \boldsymbol{M}_{\boldsymbol{cu}} \boldsymbol{M}_{\boldsymbol{uu}}^{-1} \frac{1}{\omega_{us}^2} \right) \frac{\omega_{us}\omega_{1s}}{\sqrt{\gamma^2 - \omega_{us}^2}} \frac{\sqrt{\gamma^2 - \omega_{uc}^2}}{\omega_{uc}\omega_{1c}}, \\
\boldsymbol{K}_{\boldsymbol{D}_{rc}} &= \frac{\sqrt{\omega_{2c}^2 + 2\omega_{1c}\omega_{3c}}}{\omega_{1c}} \mathbb{1} + \boldsymbol{M}_{\boldsymbol{rc}}^{-1} \left(\boldsymbol{C}_{\boldsymbol{rc}} + \frac{1}{\omega_{uc}^2} \mathbb{1} \right),
\end{aligned}$$

$$\boldsymbol{K}_{\boldsymbol{P}_{\boldsymbol{rc}}} = \frac{\sqrt{\omega_{2c}^2 + 2\omega_{1c}\omega_{3c}}}{\omega_{1c}} \boldsymbol{M}_{\boldsymbol{rc}}^{-1} \left(\boldsymbol{C}_{\boldsymbol{rc}} + \frac{1}{\omega_{uc}^2} \mathbb{1} \right) + \frac{\omega_{3c}}{\omega_{1c}} \mathbb{1},$$

$$\boldsymbol{K}_{\boldsymbol{I}_{\boldsymbol{rc}}} = \boldsymbol{M}_{\boldsymbol{rc}}^{-1} \left(\boldsymbol{C}_{\boldsymbol{rc}} + \frac{1}{\omega_{uc}^2} \mathbb{1} \right) \frac{\omega_{3c}}{\omega_{1c}} \mathbb{1},$$

where ω_{1s} and ω_{1c} are the weighting parameters of the time-derivative of the position error of the *non-controlled* and *controlled* DOF, respectively; ω_{2c} and ω_{3c} are the weighting values of position error and its integral of the *controlled* DOF, respectively; and the weighting of the *additional control* effort for the *non-controlled* and *controlled* degrees of freedom are ω_{us} and ω_{uc}.

Equation (4.91) gives the necessary acceleration of the DOF to track the reference trajectory. Therefore, the transformed forces/torques for the underactuated mechanical system with input coupling can be computed substituting this *control acceleration* in (4.7).

4.4.1 Application to the QuadRotor Helicopter

As stated at the introduction of this chapter, the objective of this section is to synthesize a controller to perform path tracking for the *QuadRotor* helicopter without the necessity of dealing with an augmented state-space, nor any cascade control strategy. Therefore, the desired controlled outputs are chosen as $\boldsymbol{q}_{\boldsymbol{c}} = [\psi \quad x \quad y \quad z]'$, while the *remaining* DOF are $\boldsymbol{q}_{\boldsymbol{u}} = [\phi \quad \theta]'$. However, as demonstrated in Mistler et al. (2001), the helicopter dynamic model given by the translational subsystem (2.61) and the rotational one (2.62) is not static feedback exact linearizable. Thus, to overcome that, a change on the mechanical structure of the *QuadRotor* helicopter is proposed. It is interesting to note that this mechanical change affect only the model used to design the controller, which is robust enough to deal with this uncertainty with respect to the model of the *QuadRotor* (2.57) used to emulate it. The mechanical change consists in *tilting the rotors toward the origin of the body-fixed frame of a certain angle* α_T, which makes it possible to choose the x and y positions like the controlled variables. This tilt, proposed in this section, provides a certain coupling between longitudinal and lateral motions with the roll and pitch movements, yielding the input coupling submatrix $\boldsymbol{B}_{\boldsymbol{c}}(\boldsymbol{q})$ become a column full rank matrix. Thus, the proposed nonlinear $\mathscr{H}_\infty$ controller, for the entire underactuated mechanical systems with input coupling, can be synthesized to solve the path tracking problem of this modified *QuadRotor* helicopter.

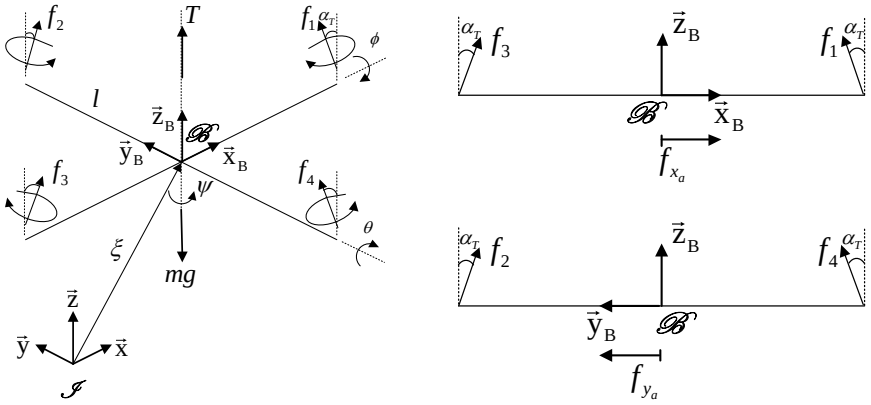

(a) General view. (b) Lateral view.

Figure 4.13: *QuadRotor* helicopter scheme.

Fig. 4.13 illustrates the four propellers tilted toward the origin of the body-fixed frame of the same angle α_T. Therefore, the components of the propeller forces projected on $\vec{x}_B$ and $\vec{y}_B$, and the applied thrust, T, (i.e. the propeller forces projected on $\vec{z}_B$) are given by:

$$\boldsymbol{f_a} = \begin{bmatrix} f_{x_a} \\ f_{y_a} \\ f_{z_a} \end{bmatrix} = \begin{bmatrix} \sin(\alpha_T)(f_3 - f_1) \\ \sin(\alpha_T)(f_4 - f_2) \\ \left(\sum_{i=1}^{4} \cos(\alpha_T) f_i\right) \end{bmatrix} = \begin{bmatrix} \sin(\alpha_T) b \left(\Omega_3^2 - \Omega_1^2\right) \\ \sin(\alpha_T) b \left(\Omega_4^2 - \Omega_2^2\right) \\ \left(\sum_{i=1}^{4} \cos(\alpha_T) b \Omega_i^2\right) \end{bmatrix}, \quad (4.93)$$

where the subscript a means *applied* and, as commented in Chapter 2, f_i is the force generated by the ith rotor, Ω_i is the angular velocity of the ith rotor around its axis and b is the thrust coefficient of the rotors.

The applied torque vector on the three body-fixed axes is given by:

$$\begin{aligned} \boldsymbol{\tau_a} &= \begin{bmatrix} \tau_{\phi_a} \\ \tau_{\theta_a} \\ \tau_{\psi_a} \end{bmatrix} = \begin{bmatrix} (f_2 - f_4)\, l \cos(\alpha_T) \\ (f_3 - f_1)\, l \cos(\alpha_T) \\ \sum_{i=1}^{4} \tau_{M_i} \cos(\alpha_T) \end{bmatrix} \\ &= \begin{bmatrix} lb \cos(\alpha_T) \left(\Omega_2^2 - \Omega_4^2\right) \\ lb \cos(\alpha_T) \left(\Omega_3^2 - \Omega_1^2\right) \\ k_\tau \cos(\alpha_T) \left(\Omega_1^2 + \Omega_3^2 - \Omega_2^2 - \Omega_4^2\right) \end{bmatrix}, \end{aligned} \quad (4.94)$$

where l is the distance between the rotors and the center of rotation, $k_\tau > 0$ is the drag constant of the propellers, and τ_{M_i} is the torsion effort generated by each electrical motor considering the dynamic of each disc of the motor as an uncoupled system in the generalized variable Ω_i.

Taking into account the simplified equations of motion of the helicopter described in Section 2.5.1, and assuming the squared of the four angular velocities of the rotors, $\boldsymbol{u_M} = [\Omega_1^2 \quad \Omega_2^2 \quad \Omega_3^2 \quad \Omega_4^2]'$, as the applied control signals, the dynamic model (2.60) is rewritten, with an appropriated reordering of the system, as follows:

$$\boldsymbol{M}(\boldsymbol{q})\ddot{\boldsymbol{q}} + \boldsymbol{C}(\boldsymbol{q},\dot{\boldsymbol{q}})\dot{\boldsymbol{q}} + \boldsymbol{G}(\boldsymbol{q}) = \boldsymbol{B}(\boldsymbol{q})\boldsymbol{\Gamma} + \boldsymbol{\delta}(\boldsymbol{q},\dot{\boldsymbol{q}},\ddot{\boldsymbol{q}},\boldsymbol{\Gamma_d}),$$

which yields to:

$$\begin{aligned}
&\boldsymbol{M}(\boldsymbol{q})\ddot{\boldsymbol{q}} + \boldsymbol{C}(\boldsymbol{q},\dot{\boldsymbol{q}})\dot{\boldsymbol{q}} + \boldsymbol{G}(\boldsymbol{q}) = \boldsymbol{B}_{\mathscr{J}}(\boldsymbol{q})\boldsymbol{u_M} + \boldsymbol{\delta}(\boldsymbol{q},\dot{\boldsymbol{q}},\ddot{\boldsymbol{q}},\boldsymbol{\Gamma_d}) \\
&\begin{bmatrix} \mathscr{J}(\boldsymbol{\eta}) & \mathbb{0} \\ \mathbb{0} & m\mathbb{1} \end{bmatrix} \begin{bmatrix} \ddot{\boldsymbol{\eta}} \\ \ddot{\boldsymbol{\xi}} \end{bmatrix} + \begin{bmatrix} \boldsymbol{C}_{\boldsymbol{\eta}\boldsymbol{\eta}}(\boldsymbol{q},\dot{\boldsymbol{q}}) & \mathbb{0} \\ \mathbb{0} & \mathbb{0} \end{bmatrix} \begin{bmatrix} \dot{\boldsymbol{\eta}} \\ \dot{\boldsymbol{\xi}} \end{bmatrix} + \begin{bmatrix} \mathbb{0} \\ mg\boldsymbol{e_3} \end{bmatrix} \\
&\qquad = \begin{bmatrix} \boldsymbol{B}_{\mathscr{J}_{\boldsymbol{\eta}}}(\boldsymbol{q}) \\ \boldsymbol{B}_{\mathscr{J}_{\boldsymbol{\xi}}}(\boldsymbol{q}) \end{bmatrix} \boldsymbol{u_M} + \begin{bmatrix} \boldsymbol{\delta}_{\boldsymbol{\eta}}(\boldsymbol{q},\dot{\boldsymbol{q}},\ddot{\boldsymbol{q}},\boldsymbol{\tau}_{\boldsymbol{\eta_d}}) \\ \boldsymbol{\delta}_{\boldsymbol{\xi}}(\boldsymbol{q},\dot{\boldsymbol{q}},\ddot{\boldsymbol{q}},\boldsymbol{f}_{\boldsymbol{\xi_d}}) \end{bmatrix},
\end{aligned} \tag{4.95}$$

where $\boldsymbol{B}_{\mathscr{J}}(\boldsymbol{q})$ is the input coupling matrix that transforms the input signals (the squared of the angular velocities of the rotors) represented in the body-fixed frame to the forces and torques represented in the inertial reference frame. This matrix is obtained by the following form:

$$\boldsymbol{B}(\boldsymbol{q})\boldsymbol{\Gamma} = \boldsymbol{B}_{\mathscr{J}}(\boldsymbol{q})\boldsymbol{u_M} = \boldsymbol{B}(\boldsymbol{q})\boldsymbol{B_M}\boldsymbol{u_M}, \tag{4.96}$$

$$\boldsymbol{B}_{\mathscr{J}}(\boldsymbol{q})\boldsymbol{u_M} =$$

$$= \begin{bmatrix} \boldsymbol{W}'_{\boldsymbol{\eta}} & \mathbb{0} \\ \mathbb{0} & \boldsymbol{R}_{\mathscr{J}} \end{bmatrix} \begin{bmatrix} 0 & lb\cos(\alpha_T) & 0 & -lb\cos(\alpha_T) \\ -lb\cos(\alpha_T) & 0 & lb\cos(\alpha_T) & 0 \\ k_\tau\cos(\alpha_T) & -k_\tau\cos(\alpha_T) & k_\tau\cos(\alpha_T) & -k_\tau\cos(\alpha_T) \\ -b\sin(\alpha_T) & 0 & b\sin(\alpha_T) & 0 \\ 0 & -b\sin(\alpha_T) & 0 & b\sin(\alpha_T) \\ b\cos(\alpha_T) & b\cos(\alpha_T) & b\cos(\alpha_T) & b\cos(\alpha_T) \end{bmatrix} \begin{bmatrix} \Omega_1^2 \\ \Omega_2^2 \\ \Omega_3^2 \\ \Omega_4^2 \end{bmatrix},$$

where $\boldsymbol{B}(\boldsymbol{q})$ is the force matrix and $rank(\boldsymbol{B}_{\mathscr{J}}(\boldsymbol{q})) = n_a < n$, being n_a the number of actuators available in the system.

The main objective of the proposed *QuadRotor* helicopter control strategy is to regulate the *controlled* DOF, $\boldsymbol{q_c} = [\psi \quad x \quad y \quad z]'$, at a desired operation point that changes with time, i.e., to perform path tracking, while the *remaining* DOF, $\boldsymbol{q_u} = [\phi \quad \theta]'$, are maintained stable. It is obvious that for a stable flight, it is necessary that the derivatives of the Euler angles must be null. Since the yaw angle is one of the *controlled* DOF, it is regulated at a desired point with a desired velocity, which is selected equal to zero in this case. On the other hand, since the roll and pitch angles compose the *remaining* dynamics, through the proposed controller, is only possible to stabilize it. Thus, for the *QuadRotor* helicopter application, $\dot{\boldsymbol{q}}_{\boldsymbol{u_r}}$ is null. Moreover, the same assumptions considered in previous sections to generate the translational trajectory reference in the *Trajectory Generator* block are used here. The diagram block representing this control strategy is showed in Fig. 4.14.

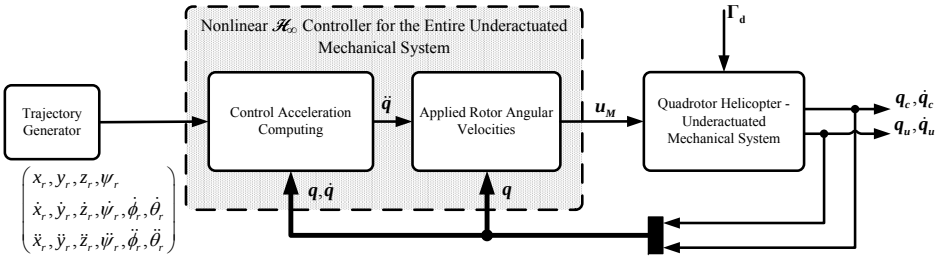

Figure 4.14: Control strategy for the *QuadRotor* helicopter using the nonlinear $\mathscr{H}_\infty$ controller for the entire underactuated mechanical system.

Therefore, by considering the *QuadRotor* helicopter model (4.95) and the partitioned description of underactuated mechanical systems (4.8), the nonlinear $\mathscr{H}_\infty$ controller, proposed in this section, is performed calculating the *control acceleration* (4.91). By substituting that equation into (4.7), the transformed forces/torques are computed. Thus, undoing the system transformation through the inverse of $\boldsymbol{T_M}(\boldsymbol{q})$, resulting in the forces and torques necessary to follow the desired trajectory, the squared velocities of the rotors can be computed as follows:

$$\boldsymbol{u_M} = \boldsymbol{B}_{\mathscr{I}}(\boldsymbol{q})^{\#}\boldsymbol{T_M}(\boldsymbol{q})^{-1}\overline{\boldsymbol{\Gamma}}, \tag{4.97}$$

where # means the pseudo inverse operator of a matrix.

Simulations have been carried out in order to corroborate the performance provided by the proposed controller when the *QuadRotor* helicopter tracks some trajectory. The simulations have been executed considering the procedure de-

scribed in Section 3.2. The tilt angle of the rotors has been designed as $\alpha_T = 5°$.

The nonlinear $\mathscr{H}_\infty$ controller gains were tuned with the following values: $\omega_{1s} = 1.5$, $\omega_{1c} = 1.2$, $\omega_{2c} = 0.5$, $\omega_{3c} = 15.0$, $\omega_{us} = 1.5$, $\omega_{uc} = 0.5$ and $\gamma = 2.0$.

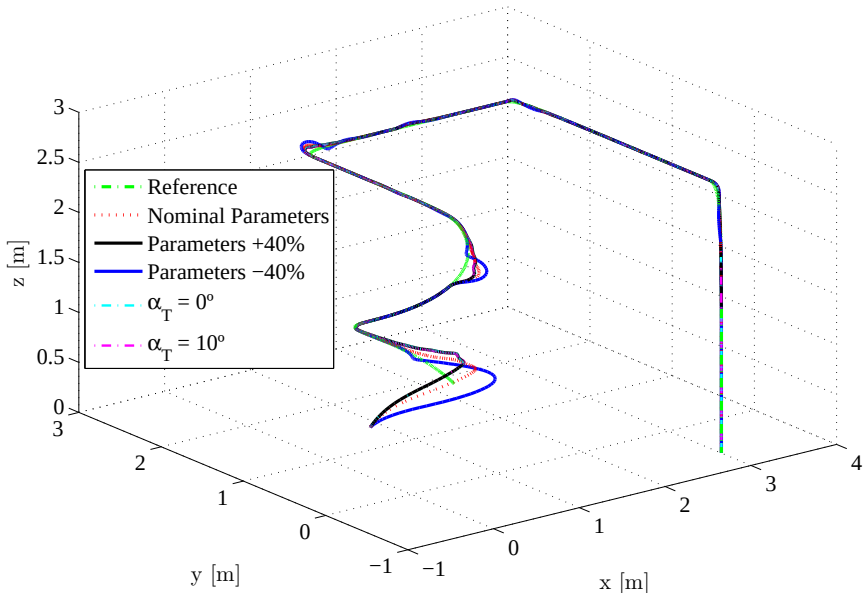

Figure 4.15: Path tracking.

Figs. 4.15 to 4.20 illustrate a good performance of the *QuadRotor* helicopter to perform path tracking when sustained disturbances, and structural and parametric uncertainties are considered, which confirm the robustness provided by the proposed controller. Fig. 4.16 shows that the *controlled* DOF achieve null steady state error when aerodynamic forces and moments are acting on the whole system; this is due to the inclusion of an integral term in the error vector. Moreover, it can be observed in Fig. 4.18 that the *remaining* DOF are maintained stable, which verify the use of their velocities in the objective vector.

Additional simulations have also been performed assuming the emulated helicopter with $\alpha_T = 0°$ and $\alpha_T = 10°$, and also $+40\%$ of parametric uncertainty, while for the controller design, $\alpha_T = 5°$ has been used. It results in an uncertainty of the input coupling matrix, which the nonlinear $\mathscr{H}_\infty$ control law designed in this section was able to deal with these kind of disturbances. On the other hand, it must be noted that if the tilt angle, α_T, is null, the *QuadRotor* helicopter model lost controllability, since its dynamics with respect to the natural choice of

the controlled DOF, $\boldsymbol{q_c} = [\psi \quad x \quad y \quad z]'$, result to be differentially flat. However, simulations considering $\alpha_T = 0$ have been carried out, and the proposed controller was able to tackle with that solving the path tracking problem.

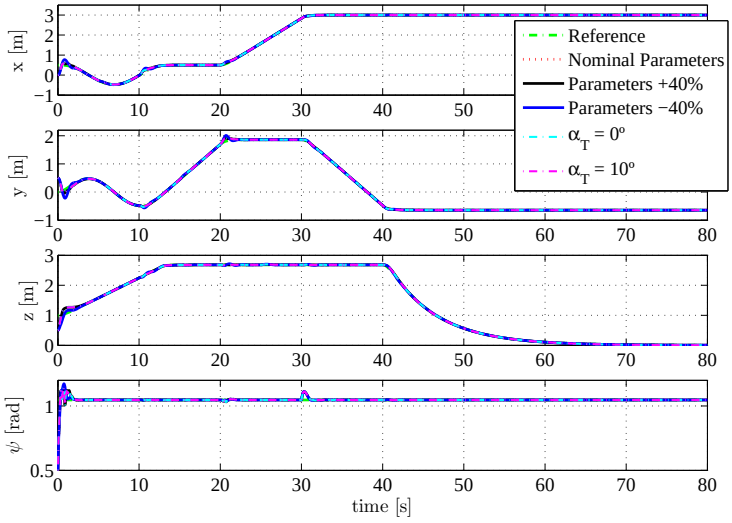

Figure 4.16: Position of the *controlled* DOF (x, y, z, ψ).

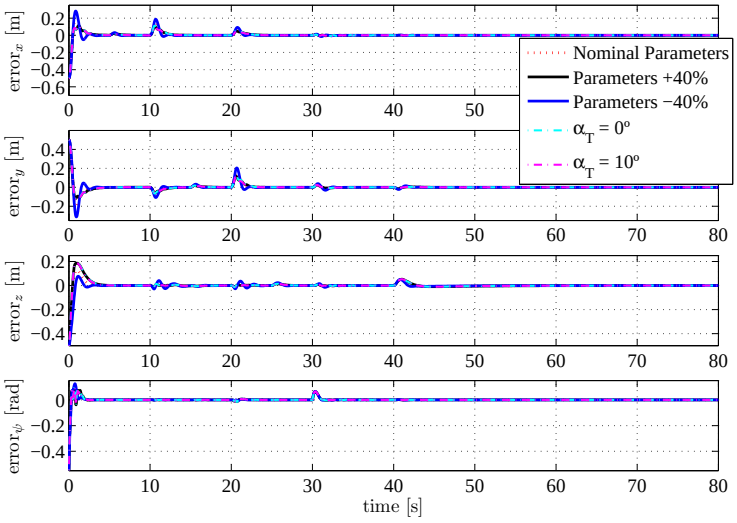

Figure 4.17: Position error of the *controlled* DOF (x, y, z, ψ).

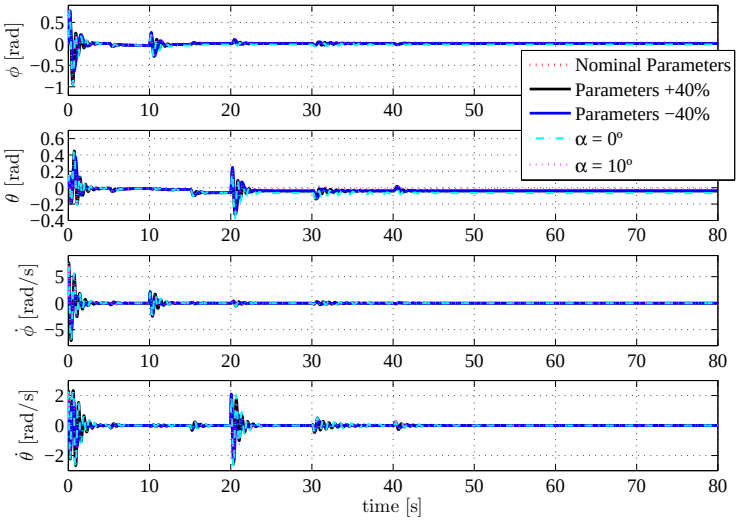

Figure 4.18: Position and velocity of the *remaining* DOF $(\phi, \theta, \dot{\phi}, \dot{\theta})$.

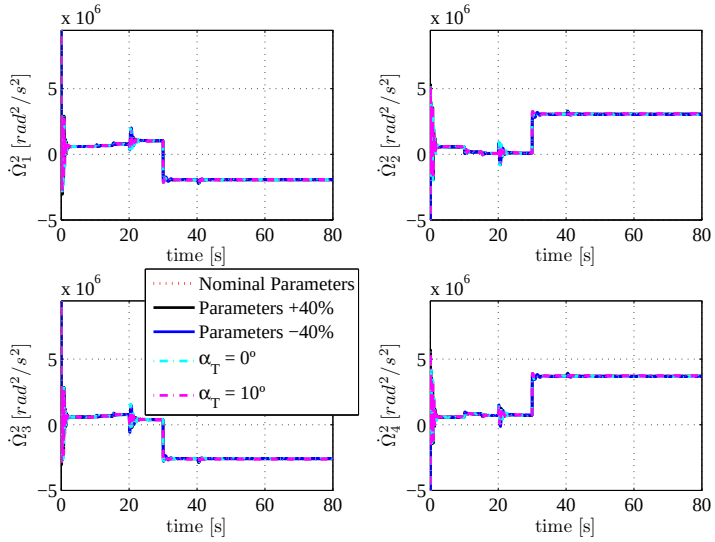

Figure 4.19: Squared Angular velocities of the rotors.

In Fig. 4.19 the squared angular velocities of the rotors are presented. They have different values in hovering because it is considered a displacement, of a distance $\boldsymbol{r}$, from the origin of the body-fixed frame to the center of mass in the emulated *QuadRotor* helicopter model. Moreover, Fig. 4.20 presents the applied

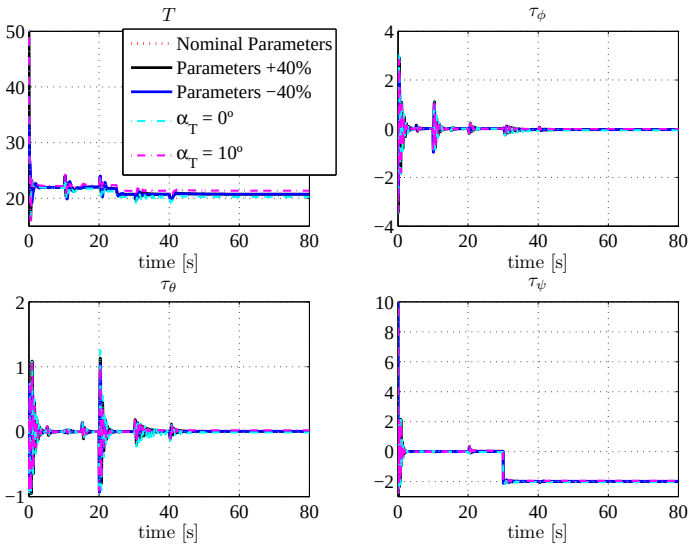

Figure 4.20: Control actions (T, τ_ϕ τ_θ τ_ψ).

thrust and torques to the helicopter in order to make a comparison with the control signals generated by the others control strategies presented in this thesis. It can be observed that the torques and force computed by the proposed control law are smoother than the other ones, mainly the pitching and rolling moments, which are calculated to perform the *xy*-motion. Again, the ISE and IADU indexes are used to confirm the obtained results. In Tables 4.6 and 4.7 such indexes are presented. The ISE index is computed only for the *controlled* DOF. It can be noticed that the accumulative error of the *controlled* DOF are considerably decreased in comparison with the ISE indexes obtained previously for the other control strategies. Besides, this controller has provided smoother pitch and roll control torques, while the applied yaw torque and thrust are similar or bigger in comparison with the obtained ones by the others controllers. However, by analyzing the performance improvement and the smoothness of the control signals, the much better performance attained by the nonlinear $\mathscr{H}_\infty$ control for the entire underactuated mechanical systems is corroborated.

4.4.2 Case study: Two-Wheeled Self-Balanced Vehicle

In this section, the nonlinear $\mathscr{H}_\infty$ controller considering the entire underactuated mechanical system is used to control the two-wheeled self-balanced vehicle de-

Table 4.6: ISE Index Performance Analysis.

States [Unit Symbol]	**Entire UActNL$\mathscr{H}_\infty$**	**IntBs-NL$\mathscr{H}_\infty$**	**MPCxy-UActNL$\mathscr{H}_\infty$**
$x\ [m^2 \cdot s]$	5.8763	12.7508	12.8514
$y\ [m^2 \cdot s]$	6.4108	14.6774	17.5974
$z\ [m^2 \cdot s]$	6.1900	12.3788	13.4216
$\psi\ [rad^2 \cdot s]$	4.4252	5.5054	4.8859

Table 4.7: IADU Index Performance Analysis.

Control Signals [Unit Symbol]	**Entire UActNL$\mathscr{H}_\infty$**	**IntBS-NL$\mathscr{H}_\infty$**	**MPCxy-UActNL$\mathscr{H}_\infty$**
$T\ [N]$	80.3479	48.4741	50.7787
$\tau_{\phi_a}\ [N \cdot m]$	38.3891	254.6423	446.7466
$\tau_{\theta_a}\ [N \cdot m]$	25.8533	261.4491	402.9134
$\tau_{\psi_a}\ [N \cdot m]$	54.8557	32.3249	49.4207

scribed in Section 4.3.3.2. Compared with the control objective stated for the *QuadRotor* helicopter, there is a slight change in the control purposes desired to the two-wheeled vehicle. Despite that, the controller structure is maintained. The control objective raised here is to ensure that the inclination angle of the pendulum is stabilized around an equilibrium point, while the angular velocity of the wheel, $\dot{\varphi}$, can be regulated in a desired reference value. The operation points of the pendulum can be $\theta_{eq} = n\pi$ with $n = 0, 1, 2, \ldots$. However, only the upper vertical position is desired. Note that, there is no interest in control the angular position of the wheel around some of its operation point, that are infinite.

Therefore, taking into account the two-wheeled self balanced vehicle model (4.53) and considering the same partition of this underactuated mechanical system carried out in Section 4.3.3.2, where $q_c = \theta$ and $q_u = \varphi$, the dynamic model of the system can be written using the diagonalized form (4.8) and adding the friction force vector.

For this application, the weighting of the integral action will be considered null, which is the same to consider the error vector (4.9) as follows:

$$\boldsymbol{x} = \begin{bmatrix} \dot{\tilde{\boldsymbol{q}}}_{\boldsymbol{u}} \\ \dot{\tilde{\boldsymbol{q}}}_{\boldsymbol{c}} \\ \tilde{\boldsymbol{q}}_{\boldsymbol{c}} \end{bmatrix}. \tag{4.98}$$

Assuming the control objective proposed for this system, it can be expressed by:

$$\boldsymbol{x} = \begin{bmatrix} \dot{\boldsymbol{q}}_{\boldsymbol{u}} - \dot{\boldsymbol{q}}_{\boldsymbol{u}_r} \\ \dot{\boldsymbol{q}}_{\boldsymbol{c}} \\ \boldsymbol{q}_{\boldsymbol{c}} \end{bmatrix} .$$

Thus, the nonlinear $\mathscr{H}_\infty$ controller proposed in this section is performed by calculating the *control acceleration* (4.91). By substituting that equation in (4.7), considering the friction force vector, the transformed torques are computed. By the definition of $\boldsymbol{\Gamma}_{\boldsymbol{su}}(\boldsymbol{q})$, $\boldsymbol{\Gamma}_{\boldsymbol{rc}}(\boldsymbol{q})$, $\boldsymbol{\Gamma}_{\boldsymbol{u}} = \boldsymbol{B}_{\boldsymbol{u}}\boldsymbol{\tau}$ and $\boldsymbol{\Gamma}_{\boldsymbol{c}} = \boldsymbol{B}_{\boldsymbol{c}}\boldsymbol{\tau}$, the applied torque $\boldsymbol{\tau}$ can be obtained as follows:

$$\boldsymbol{\tau} = \boldsymbol{B}_{\boldsymbol{c}}^{-1}\left(\mathbb{1}_{n_c \times n_c} - \boldsymbol{M}_{\boldsymbol{cu}}\boldsymbol{M}_{\boldsymbol{uu}}^{-1}\boldsymbol{M}_{\boldsymbol{uc}}\boldsymbol{M}_{\boldsymbol{cc}}^{-1}\right)^{-1}\left(\boldsymbol{\Gamma}_{\boldsymbol{rc}} + \boldsymbol{M}_{\boldsymbol{cu}}\boldsymbol{M}_{\boldsymbol{uu}}^{-1}\boldsymbol{\Gamma}_{\boldsymbol{su}}\right) , \tag{4.99}$$

where it considers the computed control signal on the *controlled* DOF taking into account the influence of the transformed control signal of the *non-controlled* DOF. This can be interpreted like the partial feedback linearization proposed by Spong (1996).

To corroborate the benefits of the controller proposed, two experiments have been made with the two-wheeled self-vehicle illustrated in Fig. 4.10. The parameters of the vehicle are presented in Table 4.5.

The weighting parameters of the proposed nonlinear $\mathscr{H}_\infty$ have been adjusted with the following values: $\omega_{1s} = 1$, $\omega_{1c} = 3$, $\omega_{2c} = 11$, $\omega_{3c} = 0$, $\omega_{us} = 0.6$, $\omega_{uc} = 0.8$, $\gamma = 1.5$.

The first experimental result has been obtained with the vehicle at a static initial inclination angle $\theta \approx 56°$, as is shown in Figs. 4.21a and 4.21b. These results show the capacity of the controller to stabilize the system around the equilibrium point $\theta_{eq} = 0°$, with angular velocity of wheels zero. It can be observed that the vehicle is quickly stabilized and remains around the operation point, without causing saturation of the control signal.

In the second experiment, to confirm the good features and the robustness of the control law, the vehicle has been initialized in a hard initial condition and has been affected by external disturbances.

The experimental results are showed in Figs. 4.22a and 4.22b. In Fig 4.22a, it can be observed trough the angular position graph that the proposed controller is able to bring up the self-balanced vehicle from a static initial approximated position of $-65°$ to the upper vertical position. This is achieved in a small set-

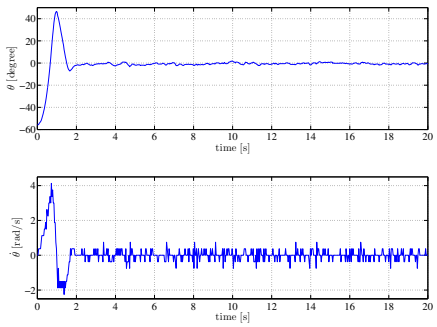

(a) Two-wheeled vehicle angular position, θ, and angular rate, $\dot{\theta}$.

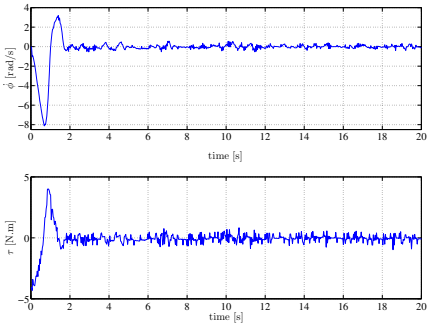

(b) Motors axle angular rate, $\dot{\phi}$, and the applied torque, τ.

Figure 4.21: First experimental result with the two-wheeled self-balanced vehicle.

tling time, and the pendulum is maintained stabilized around the operation point. On the other hand, external disturbances like impulses have been applied in three different instants of time, being the controller capable to reject all of them even when the disturbances led the angular position of the pendulum to -71° approximately. After the transient caused by the disturbances, the pendulum has been stabilized again around the upper vertical position with null angular velocity $\dot{\phi}$ in steady-state.

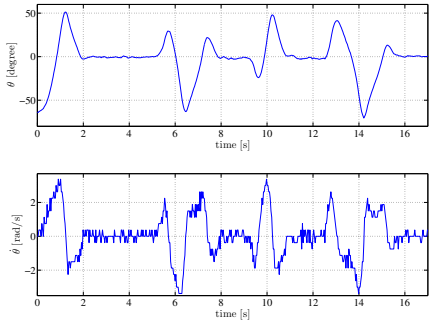

(a) Two-wheeled vehicle angular position, θ, and angular rate, $\dot{\theta}$.

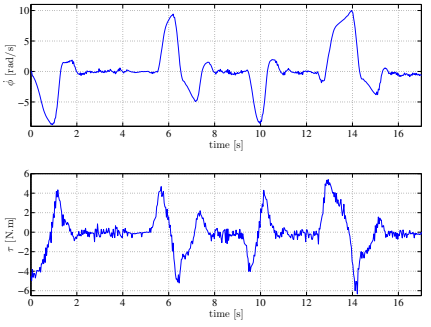

(b) Motors axle angular rate, $\dot{\phi}$, and the applied torque, τ.

Figure 4.22: Second experimental result with the two-wheeled self-balanced vehicle.

4.5 Conclusions

In this chapter, two new approaches of nonlinear $\mathscr{H}_\infty$ controllers to deal with underactuated mechanical systems have been proposed.

Firstly, an underactuated nonlinear $\mathscr{H}_\infty$ control law, based on the reduced subsystem, has been developed. This controller is an improvement of the one proposed by Siqueira and Terra (2004b), where an integral term has been added allowing to obtain null steady-state error when persistent disturbances are acting on the system. The proposed controller has been applied to three different systems, the *QuadRotor* helicopter, the pendulum on a cart and the two-wheeled self-balanced vehicle. It computes the applied control actions on the *QuadRotor* helicopter, and is based on the six DOF *QuadRotor* helicopter model that provides a control law with knowledge of both the *active* degrees of freedom and the *passive* ones. This feature is an advantage when compared to the most common strategy presented in the literature, where two controllers considering separately the translational and rotational movements are designed. Besides, in this kind of strategy, the coupling between both dynamics are addressed as a system disturbed. To solve the path tracking problem, an outer-loop controller has been implemented which is used as a track generator. That is, using a previously known path reference, an MPC based on the *xy* motion error model is designed to generate the necessary ϕ and θ reference angles. Moreover, because of the predictive controller features, a good and smooth performance in the *xy* plane reference tracking is achieved.

The robust performance provided by the inner-outer control strategy has been tested by simulation. The simulation model of the helicopter is more accurate than the one used for control synthesis purposes, which introduces structural uncertainty in the problem. Besides, an amount of 40% of uncertainty has been considered in several mechanical parameters of the vehicle, and some sustained disturbances on all the degrees of freedom have been applied during the simulations. Despite these facts, an excellent tracking performance has been achieved with the proposed control structure.

Simulation results on the *PPCar* model have also been presented using the controller based on the reduced underactuated system. Several tests were carried out taking into account the differences between the model used for controller synthesis and the one implemented on the simulator. Moreover, this controller has been implemented in a real two-wheeled self-balanced vehicle. The proposed controller has been used to control an underactuated mechanical system under input coupling. Experimental results on the two-wheeled self-balanced vehicle have

been shown. From these results, it can be observed that the nonlinear $\mathscr{H}_\infty$ controller is able to guide the vehicle from extreme initial conditions to the operating point in a short response time with a small overshoot. Furthermore, the controller is capable to reject external disturbances affecting the system and leads the error to zero at steady-state.

On the other hand, a new approach of the nonlinear $\mathscr{H}_\infty$ control design for a class of underactuated mechanical system under input coupling has been presented. To derive the proposed controller, a normalization of the equations of motion of the system has been used, which allows to consider the dynamic of the *remaining* DOF in the $\mathscr{H}_\infty$ control design. Besides, it enables to weigh the velocity error of the DOF through different criteria, which is an improvement of the works proposed by Chen et al. (1994), Feng and Postlethwaite (1994), Siqueira and Terra (2004b), Ortega et al. (2005) and others.

Furthermore, to apply this controller to the *QuadRotor* helicopter, a modified model has been used, which adds coupling between the translational and rotational movements. This coupling avoids the necessity to use cascade control strategies, or to consider an augmented state vector through a double integrator. The proposed controller have been corroborated by simulation results to solve the path tracking problem for the *QuadRotor* helicopter, when sustained disturbances were acting on the six degrees of freedom, and structural and parametric uncertainties have been considered.

Finally, this second nonlinear $\mathscr{H}_\infty$ controller has also been applied to the two-wheeled self-balanced vehicle. The proposed control law ensures the stability of the *non-controlled* DOF and guides the *controlled* ones to some equilibrium points. Experimental results have been carried out with this vehicle, which showed the capacity of the controller to bring up the vehicle from extreme initial conditions to the upper vertical position.

CHAPTER 5

Robustifying Nonlinear $\mathscr{H}_\infty$ Controller

Contents

5.1 Introduction

Despite the robustness of the methodology used throughout the thesis to design nonlinear $\mathscr{H}_\infty$ control laws, its formulation is properly indicated to deal with disturbance rejection, assuming a perfect knowledge of the model. This assumption implies to include in the same term, $\boldsymbol{\delta}(\boldsymbol{q}, \dot{\boldsymbol{q}}, \ddot{\boldsymbol{q}}, \boldsymbol{\Gamma_d})$ (see equation (2.40)), uncertainties of the system associated to an imperfect knowledge of the physical parameters that characterize the system, modeling errors, unmodeled dynamics of the actuators, sensors or structural mechanical vibrations, friction phenomena, electrical noise signals, computational errors and exogenous disturbances.

Since this hypothesis is not very realistic, to counterattack this problem, in this chapter a solution to robustify the nonlinear $\mathscr{H}_\infty$ control law designed for mechanical systems is presented, where an additional control signal is computed to cope with modeling errors. This solution is based on the known method of saturation functions. In Sage et al. (1999) a survey about robust control of robot manipulators is presented, where different ways to implement the saturation function method based on dynamic equations of linear system's error are discussed.

In Spong and Vidyasagar (1989) and Spong et al. (2006) this method is used to robustify the control technique of inverse dynamics, also known as the so-called computed-torque-like controller, which is a particular case of the feedback linearization technique. This strategy results in a linear closed-loop system when no uncertainties are considered. The procedure used in both Spong and Vidyasagar (1989) and Spong et al. (2006) consists in designing a PD-like or PID-like controller, or with a pole placement procedure, that ensures that the linear error dynamic in closed-loop is stable, assuming no uncertainties. Thus, a matrix $\boldsymbol{P}$ is found to be a solution of the Lyapunov equation of the closed-loop system, and the saturation function method follows.

As stated in Lewis et al. (2004), there is a class of mechanical system controllers (generally, nonlinear control laws) that are not obtained through the inverse dynamics technique. These controllers, including the nonlinear $\mathscr{H}_\infty$ control, are computed based directly on the equations of motion of mechanical systems without using the feedback linearization procedure. They are often designed taking into account the properties of mechanical systems such as those described in Chapter 2 for Euler-Lagrange systems. However, as could be observed in the nonlinear $\mathscr{H}_\infty$ control laws presented in Chapters 3 and 4, usually, this class of controllers can be posed as a totally or partially feedback linearization with an external, nonlinear control law. This nonlinear term considers the coupling between all the degrees of freedom.

Based on this idea, the robust inverse dynamics control with the saturation function method is extended to nonlinear systems in Ortega et al. (2005) in order to robustify the nonlinear state feedback $\mathscr{H}_\infty$ controller designed for robot manipulators. The authors used the same procedure presented in Spong and Vidyasagar (1989) to obtain the additional control signal, but they have taken into account the nonlinear gain matrices with a PID shape obtained from the solution of the HJBI equation formulated for the nonlinear $\mathscr{H}_\infty$ problem. By the resulting controller in a feedback linearization form with the nonlinear PID term, the nonlinear error dynamics in closed-loop was obtained. From this system, a Hamilton-Jacobi equation for the closed-loop stability analysis was computed. However, the authors did not provide any analytical expression to solve this HJ equation. To overcome this, they used a quadratic approximated solution, $\boldsymbol{x}'\boldsymbol{P}(t)\boldsymbol{x}$, of the proposed PDE. Thus, matrix $\boldsymbol{P}(t)$ was obtained as the solution of a Lyapunov equation making use of the successive linearization procedure of the closed-loop system. The stability of the closed-loop system was assumed guaranteed under the Aizerman's conjecture.

However, taking into account that the Aizerman's conjecture is not true in

general (Vidyasagar, 2002), in this chapter, one analytical solution to the proposed PDE in Ortega et al. (2005) is presented.

In what follows, a brief explanation about the saturation function method applied to the inverse dynamics control is exposed, followed by its extension to nonlinear systems. Some preliminary simulation results will be presented with the nonlinear $\mathscr{H}_\infty$ controllers proposed throughout the thesis.

5.2 Inverse Dynamics Control with Saturation Function Method

Consider the following dynamic model of a mechanical system obtained from the Euler-Lagrange formulation:

$$\boldsymbol{M}(\boldsymbol{q})\ddot{\boldsymbol{q}} + \boldsymbol{C}(\boldsymbol{q},\dot{\boldsymbol{q}})\dot{\boldsymbol{q}} + \boldsymbol{G}(\boldsymbol{q}) = \boldsymbol{B}(\boldsymbol{q})\boldsymbol{\Gamma} + \boldsymbol{\Gamma}_{\boldsymbol{d}}\,, \tag{5.1}$$

where $\boldsymbol{\Gamma}_{\boldsymbol{d}}$ are bounded external torque disturbances. Since the real dynamic of the mechanical system cannot be known exactly, the matrices and vectors of the system, $\boldsymbol{M}(\boldsymbol{q})$, $\boldsymbol{C}(\boldsymbol{q},\dot{\boldsymbol{q}})$ and $\boldsymbol{G}(\boldsymbol{q})$, may be partitioned in a nominal part, $\widehat{\boldsymbol{M}}(\boldsymbol{q})$, $\widehat{\boldsymbol{C}}(\boldsymbol{q},\dot{\boldsymbol{q}})$ and $\widehat{\boldsymbol{G}}(\boldsymbol{q})$, and in an uncertain one, $\Delta\boldsymbol{M}(\boldsymbol{q})$, $\Delta\boldsymbol{C}(\boldsymbol{q},\dot{\boldsymbol{q}})$ and $\Delta\boldsymbol{G}(\boldsymbol{q})$, where:

$$\begin{aligned}
\Delta\boldsymbol{M}(\boldsymbol{q}) &:= \widehat{\boldsymbol{M}}(\boldsymbol{q}) - \boldsymbol{M}(\boldsymbol{q})\,,\\
\Delta\boldsymbol{C}(\boldsymbol{q},\dot{\boldsymbol{q}}) &:= \widehat{\boldsymbol{C}}(\boldsymbol{q},\dot{\boldsymbol{q}}) - \boldsymbol{C}(\boldsymbol{q},\dot{\boldsymbol{q}})\,,\\
\Delta\boldsymbol{G}(\boldsymbol{q}) &:= \widehat{\boldsymbol{G}}(\boldsymbol{q}) - \boldsymbol{G}(\boldsymbol{q})\,.
\end{aligned}$$

Therefore, differences between the supposed real matrices and the estimated ones will always exist. As presented in Spong et al. (2006), by the inverse dynamics method, a control law based on the nominal model can be obtained:

$$\boldsymbol{\Gamma} = \boldsymbol{B}(\boldsymbol{q})^{-1}\left(\widehat{\boldsymbol{M}}(\boldsymbol{q})\boldsymbol{v} + \widehat{\boldsymbol{C}}(\boldsymbol{q},\dot{\boldsymbol{q}})\dot{\boldsymbol{q}} + \widehat{\boldsymbol{G}}(\boldsymbol{q})\right), \tag{5.2}$$

such is replaced into (5.1), resulting on the following dynamic equation of the system error:

$$\ddot{\boldsymbol{q}} = \boldsymbol{v} + \boldsymbol{M}(\boldsymbol{q})^{-1}\left(\Delta\boldsymbol{M}(\boldsymbol{q})\boldsymbol{v} + \Delta\boldsymbol{C}(\boldsymbol{q},\dot{\boldsymbol{q}})\dot{\boldsymbol{q}} + \Delta\boldsymbol{G}(\boldsymbol{q}) + \boldsymbol{\Gamma}_{\boldsymbol{d}}\right),$$

or in a compact form:

$$\ddot{\boldsymbol{q}} = \boldsymbol{v} + \pi(\boldsymbol{q}, \dot{\boldsymbol{q}}, \boldsymbol{v}, \boldsymbol{\Gamma_d}), \tag{5.3}$$

where $\boldsymbol{v}$ is the *control acceleration*. Since $\pi(\cdot)$ is a nonlinear function of $\boldsymbol{q}$ and $\boldsymbol{v}$, it cannot be treated only as external disturbances. Thus, the saturation function method can be used to generate an additional control signal considering estimated errors of model matrices and assuming that is possible to obtain upper bounds of such uncertainties.

By defining $\boldsymbol{E}(\boldsymbol{q}) := \boldsymbol{M}(\boldsymbol{q})^{-1}\Delta\boldsymbol{M}(\boldsymbol{q}) := \boldsymbol{M}(\boldsymbol{q})^{-1}\widehat{\boldsymbol{M}}(\boldsymbol{q}) - \mathbb{1}$, the function $\pi(\cdot)$ in equation (5.3) can be written as follows:

$$\pi(\boldsymbol{q}, \dot{\boldsymbol{q}}, \boldsymbol{v}, \boldsymbol{\Gamma_d}) = \boldsymbol{E}(\boldsymbol{q})\boldsymbol{v} + \boldsymbol{M}(\boldsymbol{q})^{-1}\left(\Delta\boldsymbol{C}(\boldsymbol{q}, \dot{\boldsymbol{q}})\dot{\boldsymbol{q}} + \Delta\boldsymbol{G}(\boldsymbol{q}) + \boldsymbol{\Gamma_d}\right), \tag{5.4}$$

which represents an internal disturbance of the linearized error dynamics caused by modeling uncertainties, parameter variations, external disturbances, friction terms, and noise measurements (Lewis et al., 2004). Note that the definition of $\boldsymbol{E}(\boldsymbol{q})$ corresponds to the multiplicative uncertainty of the matrix $\boldsymbol{M}(\boldsymbol{q})$, so that if the estimation of this matrix was perfect ($\boldsymbol{M}(\boldsymbol{q}) = \widehat{\boldsymbol{M}}(\boldsymbol{q})$), the value of $\boldsymbol{E}(\boldsymbol{q})$ would be null.

Accordingly, the following assumptions are made:

- $\sup_{t\geq 0}\|\ddot{\boldsymbol{q}}_{\boldsymbol{r}}\| < \boldsymbol{Q}_{max} < \infty$: this hypothesis assumes that the trajectory generator does not provide an infinity acceleration reference.

- $\|\boldsymbol{E}(\boldsymbol{q})\| := \|\boldsymbol{M}(\boldsymbol{q})^{-1}\widehat{\boldsymbol{M}}(\boldsymbol{q}) - \mathbb{1}\| \leq \alpha \leq 1$ for some value of α. This is the hardest condition. Consequently, the inertia of the system must be well estimated to make α as small as possible. However, it is always possible to find a matrix $\widehat{\boldsymbol{M}}(\boldsymbol{q})$ that meets this condition. As commented in Section 2.4, due to the positive definiteness of $\boldsymbol{M}(\boldsymbol{q})$, it is always possible to find positive scalars m_{min} and m_{max}, such that:

$$\frac{1}{m_{max}} \leq \left\|\boldsymbol{M}(\boldsymbol{q})^{-1}\right\| \leq \frac{1}{m_{min}}, \quad m_{min}, m_{max} \neq 0, \quad \forall \quad \boldsymbol{q} \in \mathbb{Q}.$$

  Thus, by designing $\widehat{\boldsymbol{M}}(\boldsymbol{q}) = \dfrac{m_{min} + m_{max}}{2}\mathbb{1}$ yields to:

$$\|\boldsymbol{E}(\boldsymbol{q})\| := \|\boldsymbol{M}(\boldsymbol{q})^{-1}\widehat{\boldsymbol{M}}(\boldsymbol{q}) - \mathbb{1}\| \leq \frac{m_{max} - m_{min}}{m_{max} + m_{min}} \leq \alpha \leq 1.$$

- $\|\Delta\boldsymbol{N}(\boldsymbol{q}, \dot{\boldsymbol{q}})\| := \|\Delta\boldsymbol{C}(\boldsymbol{q}, \dot{\boldsymbol{q}})\dot{\boldsymbol{q}} + \Delta\boldsymbol{G}(\boldsymbol{q}) + \boldsymbol{\Gamma_d}\| \leq \phi(\boldsymbol{x}, t)$ for some function $\phi(\boldsymbol{x}, t)$

bounded on time, where $\boldsymbol{x}$ is the tracking error vector defined in many cases throughout the thesis. Hence, through the triangle inequality, and the properties of the gravitational force, Coriolis and centrifugal terms and exogenous disturbances (Lewis et al., 2004), $\phi(\boldsymbol{x},t)$ can be defined as follows:

$$\begin{aligned} \|\Delta \boldsymbol{C}(\boldsymbol{q},\dot{\boldsymbol{q}})\dot{\boldsymbol{q}} + \Delta \boldsymbol{G}(\boldsymbol{q}) + \boldsymbol{\Gamma_d}\| &\leq \|\Delta \boldsymbol{C}(\boldsymbol{q},\dot{\boldsymbol{q}})\dot{\boldsymbol{q}}\| + \|\Delta \boldsymbol{G}(\boldsymbol{q})\| + \|\boldsymbol{\Gamma_d}\| \\ &\leq \gamma_c \|\dot{\tilde{\boldsymbol{q}}}\|^2 + \gamma_g + \gamma_d \\ \phi(\boldsymbol{x},t) &:= \gamma_c \|\dot{\tilde{\boldsymbol{q}}}\|^2 + \gamma_g + \gamma_d \,, \end{aligned}$$

with γ_c, γ_g and γ_d nonnegative finite constants which depend on the size of the uncertainties.

The saturation function technique provides a robust controller due to the fact that it is designed based on uncertainty bounds rather than on the actual values of the parameters (Lewis et al., 2004). Once the bound values are obtained, this method proposes to use a control structure like computed torque, where through feedback linearization attempts to linearize the estimated matrices. If the estimation were perfect and if a linear external controller were used, like PD and PID, for example, the error dynamic of the linearized system in closed-loop would be defined as follows:

$$\dot{\boldsymbol{x}}(t) = \bar{\boldsymbol{A}}\boldsymbol{x}(t) = (\boldsymbol{A} - \boldsymbol{B}\boldsymbol{K})\boldsymbol{x}(t)\,, \tag{5.5}$$

where $\boldsymbol{A}$ and $\boldsymbol{B}$ are constant matrices of the system, and $\boldsymbol{K}$ is the constant gain matrix of a linear state feedback control law. In this case, only the matrix $\boldsymbol{K}$ is needed to be computed to specify the error dynamic, which makes that the matrix $\bar{\boldsymbol{A}}$ has the desired eigenvalues.

However, since it is not possible to obtain a perfect estimation of the system, through the saturation function method, the following algorithm is proposed to compute an additional control signal $\Delta \boldsymbol{v}$ applied to the linearized system:

1. Design an external control law as follows:

$$\boldsymbol{v}(t) = \ddot{\boldsymbol{q}}_{\boldsymbol{r}}(t) - \boldsymbol{K}\boldsymbol{x}(t) + \Delta \boldsymbol{v}(t)\,, \tag{5.6}$$

where $\boldsymbol{K}$ is the controller matrix designed before and $\Delta \boldsymbol{v}(t)$ is an increment of the control signal that attenuates the effects of the estimated uncertainties of the system. Thus, the control objective is to compute the additional control law $\Delta \boldsymbol{v}(t)$ to achieve the desired tracking performance under the

unknown uncertainties π.

Note that the dynamic equation of the closed-loop error obtained from the linearized estimated matrices and the linear external controller presents the following expression:

$$\dot{\boldsymbol{x}} = \bar{\boldsymbol{A}}\boldsymbol{x} + \boldsymbol{B}(\boldsymbol{\Delta v} + \pi)\,, \tag{5.7}$$

where $\bar{\boldsymbol{A}}$ is Hurwitz and, by replacing (5.6) into (5.4) yields to:

$$\pi = \boldsymbol{E}\boldsymbol{\Delta v} + \boldsymbol{E}(\ddot{\boldsymbol{q}}_{\boldsymbol{r}} - \boldsymbol{K}\boldsymbol{x}) + \boldsymbol{M}^{-1}\boldsymbol{\Delta N}\,. \tag{5.8}$$

Equation (5.7) shows that in the case of null uncertainty, the additional control law $\boldsymbol{\Delta v}$ must also be null to obtain the dynamic equation of error (5.5).

2. Once the dynamic equation of the system error is obtained from the previous step, where $\bar{\boldsymbol{A}}$ is Hurwitz, it is assumed that it is possible to find a continuous scalar function $\rho(\boldsymbol{x},t)$ bounded over time such that the following inequalities are satisfied:

$$\|\pi\| \leq \rho(\boldsymbol{x},t)\,, \tag{5.9}$$

$$\|\boldsymbol{\Delta v}\| \leq \rho(\boldsymbol{x},t)\,. \tag{5.10}$$

Note that, from (5.9) the uncertainty of the system can be upper bounded. In such case, function $\rho(\boldsymbol{x},t)$ can be implicitly defined. Thus, taking into account the three previously assumptions, the following is obtained:

$$\begin{aligned} \|\pi\| &= \|\boldsymbol{E}\boldsymbol{\Delta v} + \boldsymbol{E}(\ddot{\boldsymbol{q}}_{\boldsymbol{r}} - \boldsymbol{K}\boldsymbol{x}) + \boldsymbol{M}^{-1}\boldsymbol{\Delta N}\| \\ &\leq \alpha\rho(\boldsymbol{x},t) + \alpha\boldsymbol{Q}_{max} + \alpha\|\boldsymbol{K}\|\|\boldsymbol{x}\| + \frac{1}{m_{min}}\phi(\boldsymbol{x},t) \qquad (5.11) \\ &:= \rho(\boldsymbol{x},t)\,. \end{aligned}$$

Since $\alpha < 1$, by isolating $\rho(\boldsymbol{x},t)$ yields to:

$$\rho(\boldsymbol{x},t) = \frac{1}{1-\alpha}\left(\alpha\boldsymbol{Q}_{max} + \alpha\|\boldsymbol{K}\|\|\boldsymbol{x}\| + \frac{1}{m_{min}}\phi(\boldsymbol{x},t)\right). \tag{5.12}$$

3. Therefore, by the assumption that $\boldsymbol{K}$ is chosen for the dynamic error matrix $\bar{\boldsymbol{A}} = (\boldsymbol{A} - \boldsymbol{B}\boldsymbol{K})$ be Hurwitz, select a symmetric, positive definite matrix $\boldsymbol{Q}$ and find the unique symmetric, positive definite solution $\boldsymbol{P}$ of the following

Lyapunov equation:

$$\bar{\boldsymbol{A}}'\boldsymbol{P} + \boldsymbol{P}\bar{\boldsymbol{A}} + \boldsymbol{Q} = \mathbb{0}\,. \tag{5.13}$$

4. Compute the additional control signal $\boldsymbol{\Delta v}(t)$ as follows:

$$\boldsymbol{\Delta v}(t) = \begin{cases} -\rho(\boldsymbol{x},t)\dfrac{\boldsymbol{B}'\boldsymbol{P}\boldsymbol{x}}{\|\boldsymbol{B}'\boldsymbol{P}\boldsymbol{x}\|} & \text{if} \quad \|\boldsymbol{B}'\boldsymbol{P}\boldsymbol{x}\| \geq \varepsilon \\ \\ -\dfrac{\rho(\boldsymbol{x},t)}{\varepsilon}\boldsymbol{B}'\boldsymbol{P}\boldsymbol{x} & \text{if} \quad \|\boldsymbol{B}'\boldsymbol{P}\boldsymbol{x}\| < \varepsilon \end{cases} \tag{5.14}$$

where $\varepsilon \ll 1$. It must be noticed to avoid the chattering effect this control law assumes values of $\|\boldsymbol{B}'\boldsymbol{P}\boldsymbol{x}\|$ lower than ε.

This controller guarantee uniform ultimate boundedness of $\tilde{\boldsymbol{q}}$ and $\dot{\tilde{\boldsymbol{q}}}$, and uniform boundedness if $\tilde{\boldsymbol{q}}(0) = \dot{\tilde{\boldsymbol{q}}}(0) = 0$. See (Spong and Vidyasagar, 1989, Chapter 8) and (Lewis et al., 2004, Chapter 5) for the demonstration of this controller.

Other approaches to design the additional control signal, $\boldsymbol{\Delta v}$, can also be find in Khalil (2002); Lewis et al. (2004) and Spong et al. (2006).

5.3 Robustifying Nonlinear $\mathscr{H}_\infty$ Controller via Saturation Functions

This section deals with an analytical solution for the algorithm presented in Ortega et al. (2005), which improves the robustness of the nonlinear $\mathscr{H}_\infty$ control design. Although the controllers obtained by nonlinear $\mathscr{H}_\infty$ theory already possess robustness properties, they are designed based on knowledge of the system model (nominal model) and assuming uncertainties such as external disturbances. However, as stated at the beginning of the chapter, uncertainties arise from a number of different sources and, to increase the desired tracking performance, they must be considered separately. Therefore, in the case of mechanical systems, the nonlinear $\mathscr{H}_\infty$ controller can be in charge only of external forces and torques in the $\mathscr{L}_2$ space, while an additional control law can be designed to cope with parametric uncertainties and unmodeled dynamics.

The proposed idea in Ortega et al. (2005) was to extend the saturation function method to the nonlinear $\mathscr{H}_\infty$ control law designed for fully actuated robot manipulators. In this chapter, this method is also applied to the designed controllers for underactuated mechanical systems, apart from applying it to fully actuated

mechanical systems. Due to the similar shape of these controllers with the inverse dynamics control presented in Section 5.2, the same procedure to obtain the additional control law can be carried out here. Some considerations about the stabilizing controller must be taken into account since it is a nonlinear control law, which leads to the following remarks:

Remark 5.1. *The dynamic equation of the system error in the method used in Spong et al. (2006) is a linear time-invariant system. However, in the case of the nonlinear $\mathscr{H}_\infty$ controllers, the dynamic equation of the system error is a time-variant nonlinear differential equation (e.g. see equations (3.40) with the gain matrices (3.52)).*

Remark 5.2. *The Lyapunov function for the nominal closed-loop system obtained with the nonlinear state feedback $\mathscr{H}_\infty$ control law is known. Since, as demonstrated in Theorem 3.3.2, it is the solution of the HJ equation (3.34). Besides, uniformly asymptotically stability of the origin is guaranteed when no external disturbances affecting the system. Therefore, for the design of the additional control law, it is more appropriate to use the procedure called Lyapunov redesign, presented in Khalil (2002), instead of the robust inverse dynamics method presented in Spong and Vidyasagar (1989). Although both procedures result in similar controllers, the approaches are slight different.*

Nonetheless, a methodology for the nonlinear case can be proposed under the same assumptions about the bounds on the Euler-Lagrange model made for the method described above. This method will be presented based on the nonlinear $\mathscr{H}_\infty$ controller designed in Section 3.3.2, being maintained the same notation. The additional control laws for the underactuated nonlinear $\mathscr{H}_\infty$ controllers developed in Chapter 4 are derived directly.

To start, the closed-loop nonlinear dynamic equation of the system error (3.40) obtained by applying the nonlinear $\mathscr{H}_\infty$ control law (3.48) is written as follows:

$$\dot{\boldsymbol{x}}_{\boldsymbol{\eta}} = \hat{f}(\boldsymbol{x}_{\boldsymbol{\eta}}, t) + k(\boldsymbol{x}_{\boldsymbol{\eta}}, t)\boldsymbol{d}$$

$$\dot{\boldsymbol{x}}_{\boldsymbol{\eta}} = \begin{bmatrix} -\boldsymbol{K_D} & -\boldsymbol{K_P} & -\boldsymbol{K_I} \\ \mathbb{1} & \mathbb{0} & \mathbb{0} \\ \mathbb{0} & \mathbb{1} & \mathbb{0} \end{bmatrix} \boldsymbol{x}_{\boldsymbol{\eta}} + \boldsymbol{T_o}^{-1} \begin{bmatrix} \widehat{\mathscr{J}}(\boldsymbol{\eta})^{-1} \\ \mathbb{0} \\ \mathbb{0} \end{bmatrix} \boldsymbol{d}, \tag{5.15}$$

where $\boldsymbol{K_D}$, $\boldsymbol{K_P}$ and $\boldsymbol{K_I}$ are the nonlinear gain matrices obtained by equation (3.50), $\widehat{\mathscr{J}}(\boldsymbol{\eta})$ is the nominal inertia matrix of the rotational subsystem, $\boldsymbol{T_o}$ is defined in (3.38) and $\boldsymbol{x}_{\boldsymbol{\eta}}$ represents the tracking error vector given by (3.36). The disturbance signal vector $\boldsymbol{d}$ is obtained by (3.41).

Recalling Theorem 3.3.2, for $\boldsymbol{d} = 0$, the equilibrium $(\dot{\tilde{\boldsymbol{\eta}}}, \tilde{\boldsymbol{\eta}}, \int \tilde{\boldsymbol{\eta}}) = (0,0,0)$ of the closed-loop (5.15) is uniformly asymptotically stable by (3.46), and if $\boldsymbol{d} \neq 0$, the origin $\boldsymbol{x_\eta} = 0$ is uniformly bounded. As discussed in Chapter 4, for the rotational subsystem, the trajectory reference needs to be constant to maintain the *QuadRotor* helicopter stabilized. Thus, in the case of the bounded-energy disturbance is $\boldsymbol{d} \neq 0$, this gives the new equilibrium point $(\dot{\tilde{\boldsymbol{\eta}}}, \tilde{\boldsymbol{\eta}}, \int \tilde{\boldsymbol{\eta}}) = (0, 0, \boldsymbol{K_I}^{-1}\boldsymbol{T_1}^{-1}\widehat{\mathscr{J}(\boldsymbol{\eta})}^{-1}\boldsymbol{d})$ if the reference is constant. Thus, performing the following change of variable $\overline{\int \tilde{\boldsymbol{\eta}}} = \int \tilde{\boldsymbol{\eta}} - \boldsymbol{K_I}^{-1}\boldsymbol{T_1}^{-1}\widehat{\mathscr{J}(\boldsymbol{\eta})}^{-1}\boldsymbol{d}$ yields:

$$\begin{bmatrix} \ddot{\tilde{\boldsymbol{\eta}}} \\ \dot{\tilde{\boldsymbol{\eta}}} \\ \overline{\tilde{\boldsymbol{\eta}}} \end{bmatrix} = \begin{bmatrix} -\boldsymbol{K_D} & -\boldsymbol{K_P} & -\boldsymbol{K_I} \\ \mathbb{1} & \mathbb{0} & \mathbb{0} \\ \mathbb{0} & \mathbb{1} & \mathbb{0} \end{bmatrix} \begin{bmatrix} \dot{\tilde{\boldsymbol{\eta}}} \\ \tilde{\boldsymbol{\eta}} \\ \overline{\int \tilde{\boldsymbol{\eta}}} \end{bmatrix}, \tag{5.16}$$

which is the same as (5.15) for $\boldsymbol{d} = 0$. Therefore, the following theorem can be stated:

Theorem 5.3.1. *The equilibrium* $(\dot{\tilde{\boldsymbol{\eta}}}, \tilde{\boldsymbol{\eta}}, \int \tilde{\boldsymbol{\eta}}) = (0,0,\boldsymbol{K_I}^{-1}\boldsymbol{T_1}^{-1}\widehat{\mathscr{J}(\boldsymbol{\eta})}^{-1}\boldsymbol{d})$ *of the closed-loop dynamic equation of system error (5.15) is uniformly asymptotically stable for any constant disturbance* $\boldsymbol{d}$ *by Theorem 3.3.2. That is, the nonlinear* $\mathscr{H}_\infty$ *controller presented in Section 3.3.2 with the integral action guarantees zero tracking error for the rotational subsystem.*

Proof: Considering the definition of the gain matrix $\boldsymbol{K_I}$ given in (3.50), the equilibrium point of the closed-loop system (5.15), when $\boldsymbol{d} \neq 0$, has two components $\dot{\tilde{\boldsymbol{\eta}}}$ and $\tilde{\boldsymbol{\eta}}$ that are clearly nulls. For the third component, $\int \tilde{\boldsymbol{\eta}}$, it is obtained as follows:

$$0 = -\boldsymbol{T_1}^{-1}\widehat{\mathscr{J}(\boldsymbol{\eta})}^{-1}\left(\boldsymbol{C}(\boldsymbol{\eta},\dot{\boldsymbol{\eta}})\boldsymbol{T_3} + \boldsymbol{R}^{-1}\left(\boldsymbol{S_3'} + \boldsymbol{T_3}\right)\right)\int \tilde{\boldsymbol{\eta}} + \boldsymbol{T_1}^{-1}\widehat{\mathscr{J}(\boldsymbol{\eta})}^{-1}\boldsymbol{d}$$

$$\int \tilde{\boldsymbol{\eta}} = \boldsymbol{R}^{-1}\left(\boldsymbol{S_3'} + \boldsymbol{T_3}\right)\boldsymbol{d},$$

with a constant reference trajectory.

Thus, through the change of variable over $\int \tilde{\boldsymbol{\eta}}$, the new (constant) equilibrium point for the rotational subsystem is obtained:

$$(\dot{\tilde{\boldsymbol{\eta}}}, \tilde{\boldsymbol{\eta}}, \int \tilde{\boldsymbol{\eta}}) = (0,0,\boldsymbol{R}^{-1}\left(\boldsymbol{S_3'} + \boldsymbol{T_3}\right)\boldsymbol{d}), \tag{5.17}$$

which is uniformly asymptotically stable for the rotational subsystem from the Theorem 3.3.2 ■

Remark 5.3. *The Theorem 5.3.1 holds only whether the reference trajectory and*

the disturbance are constants. Since the uncertainty term $\boldsymbol{d}$ does not depend only on external disturbances and parametric uncertainties, for a more generalized formulation, it is desired to assume the uniformly bounded condition of the Theorem 3.3.2.

Thus, considering that $\boldsymbol{d}$ includes a large variety of disturbances sources, it can be split up into two parts: the first one is compound by exogenous disturbances in the $\mathscr{L}_2$-space, and the second part is due to model simplification and parametric uncertainty. Notice that only external perturbations in the $\mathscr{L}_2$-space are assumed, being the nonlinear $\mathscr{H}_\infty$ controller in charge of them.

Taking into account that $\boldsymbol{d}$ is a transformation of the uncertainty $\boldsymbol{\delta_\eta}$ given by (3.41), the closed-loop system (5.15) can be rewritten as follows:

$$\begin{aligned}
\dot{\boldsymbol{x}}_{\boldsymbol{\eta}} &= \begin{bmatrix} -\boldsymbol{K_D} & -\boldsymbol{K_P} & -\boldsymbol{K_I} \\ \mathbb{1} & \mathbb{0} & \mathbb{0} \\ \mathbb{0} & \mathbb{1} & \mathbb{0} \end{bmatrix} \boldsymbol{x}_{\boldsymbol{\eta}} + \boldsymbol{T_o}^{-1} \begin{bmatrix} \widehat{\mathscr{J}}(\boldsymbol{\eta})^{-1} \\ \mathbb{0} \\ \mathbb{0} \end{bmatrix} \widehat{\mathscr{J}}(\boldsymbol{\eta}) \boldsymbol{T_1} \mathscr{J}^{-1}(\boldsymbol{\eta}) \boldsymbol{\delta_\eta} \\
&= \begin{bmatrix} -\boldsymbol{K_D} & -\boldsymbol{K_P} & -\boldsymbol{K_I} \\ \mathbb{1} & \mathbb{0} & \mathbb{0} \\ \mathbb{0} & \mathbb{1} & \mathbb{0} \end{bmatrix} \boldsymbol{x}_{\boldsymbol{\eta}} + \boldsymbol{T_o}^{-1} \begin{bmatrix} \widehat{\mathscr{J}}(\boldsymbol{\eta})^{-1} \\ \mathbb{0} \\ \mathbb{0} \end{bmatrix} \widehat{\mathscr{J}}(\boldsymbol{\eta}) \boldsymbol{T_1} \mathscr{J}^{-1}(\boldsymbol{\eta}) \boldsymbol{\tau_{\eta_d}} \\
&\quad + \boldsymbol{T_o}^{-1} \begin{bmatrix} \widehat{\mathscr{J}}(\boldsymbol{\eta})^{-1} \\ \mathbb{0} \\ \mathbb{0} \end{bmatrix} \widehat{\mathscr{J}}(\boldsymbol{\eta}) \boldsymbol{T_1} \mathscr{J}^{-1}(\boldsymbol{\eta}) \boldsymbol{\Xi_\eta}(\boldsymbol{\eta}, \dot{\boldsymbol{\eta}}, \ddot{\boldsymbol{\eta}}) \\
&= \begin{bmatrix} -\boldsymbol{K_D} & -\boldsymbol{K_P} & -\boldsymbol{K_I} \\ \mathbb{1} & \mathbb{0} & \mathbb{0} \\ \mathbb{0} & \mathbb{1} & \mathbb{0} \end{bmatrix} \boldsymbol{x}_{\boldsymbol{\eta}} + \boldsymbol{T_o}^{-1} \begin{bmatrix} \widehat{\mathscr{J}}(\boldsymbol{\eta})^{-1} \\ \mathbb{0} \\ \mathbb{0} \end{bmatrix} \boldsymbol{d_\tau} \\
&\quad + \begin{bmatrix} \mathbb{1} \\ \mathbb{0} \\ \mathbb{0} \end{bmatrix} \mathscr{J}^{-1}(\boldsymbol{\eta}) \boldsymbol{\Xi_\eta}(\boldsymbol{\eta}, \dot{\boldsymbol{\eta}}, \ddot{\boldsymbol{\eta}}, t),
\end{aligned} \tag{5.18}$$

or in a compact form:

$$\dot{\boldsymbol{x}}_{\boldsymbol{\eta}} = \hat{f}(\boldsymbol{x}_{\boldsymbol{\eta}}, t) + k(\boldsymbol{x}_{\boldsymbol{\eta}}, t) \boldsymbol{d_\tau} + \boldsymbol{B} \pi(\boldsymbol{\eta}, \dot{\boldsymbol{\eta}}, \ddot{\boldsymbol{\eta}}, t), \tag{5.19}$$

where:

$$\begin{aligned}\pi(\boldsymbol{\eta},\dot{\boldsymbol{\eta}},\ddot{\boldsymbol{\eta}},t) &= \mathscr{J}^{-1}(\boldsymbol{\eta})\boldsymbol{\Xi}_{\boldsymbol{\eta}}(\boldsymbol{\eta},\dot{\boldsymbol{\eta}},\ddot{\boldsymbol{\eta}},t)\\ &= \mathscr{J}^{-1}(\boldsymbol{\eta})\boldsymbol{\Delta}\mathscr{J}(\boldsymbol{\eta})\ddot{\boldsymbol{\eta}} + \mathscr{J}^{-1}(\boldsymbol{\eta})\left(\boldsymbol{\Delta C}(\boldsymbol{\eta},\dot{\boldsymbol{\eta}})\dot{\boldsymbol{\eta}} + \boldsymbol{\Delta G}(\boldsymbol{\eta})\right)\\ &= \boldsymbol{E}(\boldsymbol{\eta})\ddot{\boldsymbol{\eta}} + \mathscr{J}^{-1}(\boldsymbol{\eta})\left(\boldsymbol{\Delta C}(\boldsymbol{\eta},\dot{\boldsymbol{\eta}})\dot{\boldsymbol{\eta}} + \boldsymbol{\Delta G}(\boldsymbol{\eta})\right),\end{aligned} \tag{5.20}$$

with $\boldsymbol{E}(\boldsymbol{\eta}) := \mathscr{J}^{-1}(\boldsymbol{\eta})\boldsymbol{\Delta}\mathscr{J}(\boldsymbol{\eta}) := \mathscr{J}^{-1}(\boldsymbol{\eta})\widehat{\mathscr{J}}(\boldsymbol{\eta}) - \mathbb{1}$, and:

$$\ddot{\boldsymbol{\eta}} = \ddot{\boldsymbol{\eta}}_r - \boldsymbol{K_D}\dot{\tilde{\boldsymbol{\eta}}} - \boldsymbol{K_P}\tilde{\boldsymbol{\eta}} - \boldsymbol{K_I}\int \tilde{\boldsymbol{\eta}}dt\,.$$

By assuming that the nonlinear $\mathscr{H}_\infty$ control law is able to reject exogenous disturbances included in vector $\boldsymbol{d}$, the control design purposes here is to robustify the closed-loop when at least the knowledge of bounds on the dynamic model are available. Hence, the external disturbance vector $\boldsymbol{d_\tau}$ in the system (5.19) will be assumed null, assuming it has already been treated by the stabilizing controller. Then, an additional control law is included to the closed-loop to deal with the parametric uncertainties and unmodeled dynamics represented by function $\pi(\cdot)$.

Accordingly, the external control law is reformulated as in (5.6), where matrix $\boldsymbol{K}$ is compound by the gain matrices (3.50), which is given for the rotational subsystem by:

$$\ddot{\boldsymbol{\eta}} = \ddot{\boldsymbol{\eta}}_r - \boldsymbol{K_D}\dot{\tilde{\boldsymbol{\eta}}} - \boldsymbol{K_P}\tilde{\boldsymbol{\eta}} - \boldsymbol{K_I}\int \tilde{\boldsymbol{\eta}}dt + \boldsymbol{\Delta v}(t)\,. \tag{5.21}$$

Thus, the dynamic equation of the closed-loop system error (5.19), with $\boldsymbol{d_\tau} = 0$, is rewritten as follows:

$$\dot{\boldsymbol{x}}_{\boldsymbol{\eta}} = \hat{f}(\boldsymbol{x}_{\boldsymbol{\eta}},t) + \boldsymbol{B}(\boldsymbol{\Delta v} + \pi)$$

$$\dot{\boldsymbol{x}}_{\boldsymbol{\eta}} = \begin{bmatrix} -\boldsymbol{K_D} & -\boldsymbol{K_P} & -\boldsymbol{K_I} \\ \mathbb{1} & \mathbb{0} & \mathbb{0} \\ \mathbb{0} & \mathbb{1} & \mathbb{0} \end{bmatrix}\boldsymbol{x}_{\boldsymbol{\eta}} + \begin{bmatrix} \mathbb{1} \\ \mathbb{0} \\ \mathbb{0} \end{bmatrix}(\boldsymbol{\Delta v} + \pi)\,, \tag{5.22}$$

In the next step, to obtain the additional control law, a scalar function $\rho(\boldsymbol{x}_{\boldsymbol{\eta}},t)$ is computed through the expression (5.12), where the inequalities (5.9) and (5.10) are assumed to be satisfied. Note that, from (5.9) only the model uncertainties are bounded, which are independent of the method used.

Since the matrix $\boldsymbol{K}$ is obtained for the nominal model, i.e., with null parametric uncertainties, the dynamic of the error in closed-loop is uniform asymptotically stable with the nonlinear $\mathscr{H}_\infty$ control law via state feedback when no external disturbances affect the system (see Theorem 3.3.2). Thus, the same solution of the HJBI equation is a candidate Lyapunov function and the following holds:

$$\frac{\partial V(\boldsymbol{x_\eta},t)}{\partial t}+\frac{\partial' V(\boldsymbol{x_\eta},t)}{\partial \boldsymbol{x_\eta}}\cdot\hat{f}(\boldsymbol{x_\eta},t)<0 \quad \forall \boldsymbol{x_\eta}\neq 0\,, \tag{5.23}$$

where $\dot{\boldsymbol{x_\eta}}=\hat{f}(\boldsymbol{x},t)$ with $\pi=0$.

Finally, to complete the control law (5.21), the additional term $\boldsymbol{\Delta v}$ is computed by the following equation:

$$\boldsymbol{\Delta v}(t)=\begin{cases} -\rho(\boldsymbol{x_\eta},t)\dfrac{B'\dfrac{\partial V(\boldsymbol{x_\eta},t)}{\partial \boldsymbol{x_\eta}}}{\left\|B'\dfrac{\partial V(\boldsymbol{x_\eta},t)}{\partial \boldsymbol{x_\eta}}\right\|} & \text{if} \quad \left\|B'\dfrac{\partial V(\boldsymbol{x_\eta},t)}{\partial \boldsymbol{x_\eta}}\right\|\geq\varepsilon \\ -\dfrac{\rho(\boldsymbol{x_\eta},t)}{\varepsilon}B'\dfrac{\partial V(\boldsymbol{x_\eta},t)}{\partial \boldsymbol{x_\eta}} & \text{if} \quad \left\|B'\dfrac{\partial V(\boldsymbol{x_\eta},t)}{\partial \boldsymbol{x_\eta}}\right\|<\varepsilon \end{cases} \tag{5.24}$$

where $V(\boldsymbol{x_\eta},t)$ is given by (3.46) and its gradient with respect to $\boldsymbol{x_\eta}$ is computed as follows:

$$\frac{\partial' V(\boldsymbol{x_\eta},t)}{\partial \boldsymbol{x_\eta}}=\frac{1}{2}\boldsymbol{x_\eta'}\boldsymbol{T_o'}\begin{bmatrix}\widehat{\mathscr{J}}(\boldsymbol{\eta}) & \mathbb{0} & \mathbb{0}\\ \mathbb{0} & \boldsymbol{Y} & \boldsymbol{X-Y}\\ \mathbb{0} & \boldsymbol{X-Y} & \boldsymbol{Z+Y}\end{bmatrix}\boldsymbol{T_o}+\frac{1}{2}\left[\mathbb{0},\boldsymbol{\Omega},\mathbb{0}\right],$$

with:

$$\boldsymbol{\Omega}=\left(\boldsymbol{x_\eta'}\boldsymbol{T_o'}\begin{bmatrix}\dfrac{\partial'\widehat{\mathscr{J}}(\boldsymbol{\eta})}{\partial\tilde{\boldsymbol{q}}_1} & \mathbb{0} & \mathbb{0}\\ \mathbb{0} & \mathbb{0} & \mathbb{0}\\ \mathbb{0} & \mathbb{0} & \mathbb{0}\end{bmatrix}\boldsymbol{T_o}\boldsymbol{x_\eta},\cdots,\frac{1}{2}\boldsymbol{x_\eta'}\boldsymbol{T_o'}\begin{bmatrix}\dfrac{\partial'\widehat{\mathscr{J}}(\boldsymbol{\eta})}{\partial\tilde{\boldsymbol{q}}_n} & \mathbb{0} & \mathbb{0}\\ \mathbb{0} & \mathbb{0} & \mathbb{0}\\ \mathbb{0} & \mathbb{0} & \mathbb{0}\end{bmatrix}\boldsymbol{T_o}\boldsymbol{x_\eta}\right)$$

Therefore, the term $B'(\partial V(\boldsymbol{x_\eta},t)/\partial \boldsymbol{x_\eta})$ is obtained by:

$$B'\frac{\partial V(\boldsymbol{x_\eta},t)}{\partial \boldsymbol{x_\eta}} = \begin{bmatrix} \mathbb{1} \\ \mathbb{0} \\ \mathbb{0} \end{bmatrix}' \left(\boldsymbol{T_o}' \begin{bmatrix} \widehat{\mathscr{J}}(\boldsymbol{\eta}) & \mathbb{0} & \mathbb{0} \\ \mathbb{0} & \boldsymbol{Y} & \boldsymbol{X}-\boldsymbol{Y} \\ \mathbb{0} & \boldsymbol{X}-\boldsymbol{Y} & \boldsymbol{Z}+\boldsymbol{Y} \end{bmatrix} \boldsymbol{T_o}\boldsymbol{x_\eta} + \frac{1}{2}[\mathbb{0}, \boldsymbol{\Omega}, \mathbb{0}]' \right)$$

$$= \begin{bmatrix} \mathbb{1} \\ \mathbb{0} \\ \mathbb{0} \end{bmatrix}' \boldsymbol{T_o}' \begin{bmatrix} \widehat{\mathscr{J}}(\boldsymbol{\eta}) & \mathbb{0} & \mathbb{0} \\ \mathbb{0} & \boldsymbol{Y} & \boldsymbol{X}-\boldsymbol{Y} \\ \mathbb{0} & \boldsymbol{X}-\boldsymbol{Y} & \boldsymbol{Z}+\boldsymbol{Y} \end{bmatrix} \boldsymbol{T_o}\boldsymbol{x_\eta},$$

where $\boldsymbol{X}$, $\boldsymbol{Y}$ and $\boldsymbol{Z}$ are obtained by solving some Riccati algebraic equations that compose the expression (3.47).

For the particular case given by the weighting matrices (3.51), the following matrices are obtained:

$$\boldsymbol{T_1} = \rho\mathbb{1} = \frac{\gamma\omega_u\omega_1}{\sqrt{\gamma^2-\omega_u^2}}\mathbb{1}, \qquad \boldsymbol{T_3} = \mu\mathbb{1} = \frac{\gamma\omega_u\omega_3}{\sqrt{\gamma^2-\omega_u^2}}\mathbb{1},$$

$$\boldsymbol{T_2} = \kappa\mathbb{1} = \frac{\gamma\omega_u\sqrt{\omega_2^2+2\omega_1\omega_3}}{\sqrt{\gamma^2-\omega_u^2}}\mathbb{1}, \qquad \boldsymbol{X} = \omega_1\omega_3\mathbb{1},$$

$$\boldsymbol{Y} = \omega_1\sqrt{\omega_2^2+2\omega_1\omega_3}\mathbb{1}, \qquad \boldsymbol{Z} = \omega_3\sqrt{\omega_2^2+2\omega_1\omega_3}\mathbb{1}-2\omega_1\omega_3\mathbb{1}.$$

The stability proof of the resulting system applying the additional control law (5.24) can be performed through the Lyapunov second method. Thus, assuming that the scalar function $V(\boldsymbol{x_\eta},t)>0$ satisfies the equation (5.23), its time derivative is given by:

$$\frac{dV(\boldsymbol{x_\eta},t)}{dt} = \frac{\partial V(\boldsymbol{x_\eta},t)}{\partial t} + \frac{\partial' V(\boldsymbol{x_\eta},t)}{\partial \boldsymbol{x_\eta}} \cdot \dot{\boldsymbol{x}}_{\boldsymbol{\eta}}.$$

Replacing the closed-loop dynamic equation of the system error (5.22), where has been assumed no external disturbances, i.e. $\boldsymbol{d_\tau}=0$, into the time derivative of the

Lyapunov candidate function yields to:

$$\begin{aligned}\frac{dV(\boldsymbol{x_\eta},t)}{dt} &= \frac{\partial V(\boldsymbol{x_\eta},t)}{\partial t}+\frac{\partial' V(\boldsymbol{x_\eta},t)}{\partial \boldsymbol{x_\eta}}\cdot(\hat{f}(\boldsymbol{x_\eta},t)+B(\boldsymbol{\Delta v}+\pi))\\ &= \frac{\partial' V(\boldsymbol{x_\eta},t)}{\partial \boldsymbol{x_\eta}}\cdot B(\boldsymbol{\Delta v}+\pi),\end{aligned}$$

where the inequality (5.23) has been used.

To ensure that the time derivative of $V(\boldsymbol{x_\eta},t)$ is negative, the following must also be:

$$\frac{\partial' V(\boldsymbol{x_\eta},t)}{\partial \boldsymbol{x_\eta}}\cdot B(\boldsymbol{\Delta v}+\pi)\leq 0,$$

from which the additional control signal $\boldsymbol{\Delta v}$ can be selected:

$$\frac{\partial' V(\boldsymbol{x_\eta},t)}{\partial \boldsymbol{x_\eta}}B\boldsymbol{\Delta v}\leq \frac{\partial' V(\boldsymbol{x_\eta},t)}{\partial \boldsymbol{x_\eta}}B\pi.$$

Thus, taking into account that the norm of π is bounded by the function $\rho(\boldsymbol{x_\eta},t)$ and assuming the worst-case, where the vectors $B'\frac{\partial V(\boldsymbol{x_\eta},t)}{\partial \boldsymbol{x_\eta}}$ and π have the same direction, $\boldsymbol{\Delta v}$ is selected to have opposite direction to $\frac{\partial' V(\boldsymbol{x_\eta},t)}{\partial \boldsymbol{x_\eta}}B$ and modulus $\rho(\boldsymbol{x_\eta},t)$, that is:

$$\boldsymbol{\Delta v}(t)=-\rho(\boldsymbol{x_\eta},t)\frac{B'\dfrac{\partial' V(\boldsymbol{x_\eta},t)}{\partial \boldsymbol{x_\eta}}}{\left\|B'\dfrac{\partial' V(\boldsymbol{x_\eta},t)}{\partial \boldsymbol{x_\eta}}\right\|},$$

which is the expression in (5.24).

Therefore, for the closed-loop system (5.22) with the additional control law (5.24), there exists a solution $\boldsymbol{x_\eta}(t)$, with initial condition $\boldsymbol{x_\eta}(t_0)=\boldsymbol{x_{\eta_0}}$, that is uniformly ultimately bounded. The demonstration of this result follows the same steps as in Spong and Vidyasagar (1989, Chapter 8).

If external disturbances are considered, by substituting the system (5.19) with the additional control law (5.24) into the time derivative of the Lyapunov candid-

ate function, results in:

$$\begin{aligned}\frac{dV(\boldsymbol{x_\eta},t)}{dt} &= \frac{\partial V(\boldsymbol{x_\eta},t)}{\partial t}+\frac{\partial' V(\boldsymbol{x_\eta},t)}{\partial \boldsymbol{x_\eta}}\cdot(\hat{f}(\boldsymbol{x_\eta},t)+k(\boldsymbol{x_\eta},t)\boldsymbol{d_\tau}+B(\boldsymbol{\Delta v}+\pi))\\ &= -\frac{1}{2\gamma^2}\boldsymbol{x'_\eta}\boldsymbol{T'}\boldsymbol{T}\boldsymbol{x_\eta}-\frac{1}{2}\|\boldsymbol{\zeta}\|^2+\boldsymbol{x'_\eta}\boldsymbol{T'}\boldsymbol{d_\tau}+\frac{\partial' V(\boldsymbol{x_\eta},t)}{\partial \boldsymbol{x_\eta}}\cdot B(\boldsymbol{\Delta v}+\pi).\end{aligned}$$

Thus, if $\boldsymbol{d_\tau}=0$ and $\pi=0$, according to the Theorem 3.3.2, $\dot{V}(\boldsymbol{x_\eta},t)\leq 0$ and the closed-loop system is uniformly asymptotically stable. If $\boldsymbol{d_\tau}=0$ and $\pi\neq 0$, the result above follows. Finally, if $\boldsymbol{d_\tau}\neq 0$ and $\pi\neq 0$, only the uniformly bounded condition can be considered.

Notice that the previous adjustment of the nonlinear $\mathscr{H}_\infty$ controller considers in the same vector $\boldsymbol{d}$ external disturbances and model uncertainties. After the design of the additional control law based on the bounds of the Euler-Lagrange model, the nonlinear $\mathscr{H}_\infty$ controller can be tuned again to improve the performance with external disturbance rejection.

The additional control law designed in this section can also be implemented with both reduced and entire underactuated nonlinear $\mathscr{H}_\infty$ controllers developed in Section 4. For the controller presented in Section 4.3, only the boundaries of the *controlled* degrees of freedom dynamic equation must be considered, while for the closed-loop obtained with the underactuated nonlinear $\mathscr{H}_\infty$ controller assuming the entire dynamic model, the bounds must be computed for the whole system.

Some simulation results with the *QuadRotor* helicopter will be presented in the next section in order to show the robustness improvement of some of the nonlinear $\mathscr{H}_\infty$ controllers designed in this thesis.

5.4 Simulation Results

In this section simulation results have been carried out using the proposed method based on saturation functions to improve the robustness of nonlinear $\mathscr{H}_\infty$ controllers. Two control strategies have been chosen to test the benefits provided by this method. First, the cascade control strategy presented in Section 3.4.3, which combines the integral backstepping controller with the nonlinear $\mathscr{H}_\infty$ controller for fully actuated mechanical systems, has been performed. The second simulation collection has been executed with the nonlinear $\mathscr{H}_\infty$ controller for entire underactuated mechanical systems presented in Section 4.4. Both control strategies

have been conducted to solve the path tracking problem for the *QuadRotor* helicopter.

The second reference trajectory (Fig. 3.3) presented in the *Simulation Protocol* has been used to analyze the robustness improvement provided by the proposed method. Moreover, a quantitative comparative through the performance indexes ISE and IADU has been performed. The same comparison conditions used throughout the thesis have been also implemented here, where an amount of $+40\%$ of uncertainty in the elements of the mass and the moment of inertia tensor has been assumed. However, the *QuadRotor* helicopter was initially placed in the same position of the reference trajectory. This initial condition is due to the assumption that the nonlinear $\mathscr{H}_\infty$ controllers have already stabilized the vehicle on the track. Therefore, the robustness improvement provided by the additional control law designed in this chapter can be verified when model uncertainties are present on the system.

In what follows, the simulation comparison between some of the control strategies presented in Chapters 3 and 4 are shown.

IntBS-NL$\mathscr{H}_\infty$ Cascade Control Strategy

This control strategy has been synthesized with the same parameters presented in Section 3.4.3.2, while the bounds of the rotational subsystem needed to achieve the function $\rho(\boldsymbol{x_\eta},t)$ of the additional control signal have been designed as follows:

- Since the values of the references of the pitch and roll angles are not known previously, the bound of the reference acceleration of the Euler angles has been defined by observing the necessary accelerations without considering the saturation function method in previous simulation results, which led to the following value, $\boldsymbol{Q}_{max} = 50$.
- The bound of the inertia matrix uncertainty, α, has been computed numerically through the error between the inertia matrix considering cross terms and the inertia one with only the diagonal terms. This bound has been obtained for different values of angles and taking into account an uncertainty of $\pm 40\%$ in the parameters. The computed value of this bound han been $\alpha = 0.3327$.
- The design of function $\phi(\boldsymbol{x},t)$ is based on the bounds of the gravitational, friction and Coriolis and centrifugal forces. As presented in Chapter 2,

the rotational equations of motion do not present neither gravitational nor friction terms. Thus, only the upper bound of the Coriolis and centrifugal forces has been calculated. This bound has been achieved in a more conservativeness way, assuming that the magnitudes of *sin* and *cos* functions are bounded by 1. The value of the γ_c parameter was achieved equal to 0.18.

- The maximum and minimum bounds of the inertia matrix have been achieved numerically, by means of the inequalities (2.34), for different values of the Euler angles and considering the uncertainty interval into $\pm 40\%$ of the moment of inertia tensor terms. The values of these parameters are: $m_{min} = 0.0369$ and $m_{max} = 0.1077$.

- The term $\|\boldsymbol{K}\|\|\boldsymbol{x}\|$, in equation (5.12), that bounds the control law, has been computed less conservative, where the norm of the nonlinear $\mathscr{H}_\infty$ control law has been obtained computing in each sampling time of the inner loop the following term: $\|\boldsymbol{K}\boldsymbol{x}\|$.

- The value of the parameter ε has been chosen in order to avoid chattering in the control signal. For this requirement, its value was defined as $\varepsilon = 2 \cdot 10^{-5}$.

Figs. 5.1 to 5.6 illustrate the path tracking of the *QuadRotor* helicopter using the cascade control strategy IntBS-NL$\mathscr{H}_\infty$ with and without the the additional control signal obtained by saturation functions.

In these figures it can be observed that both control structures present a very similar performance. Since the saturation function method is applied to improve the robustness of the nonlinear $\mathscr{H}_\infty$ controller for the rotational subsystem of the *QuadRotor* helicopter, through Fig. 5.5, the enhance obtained with the proposed method is clearly appreciated. In this figure, it can be observed that the tracking error of the rotational subsystem is reduced by using the additional control law $\boldsymbol{\Delta v}$, which compensates the inexact cancellation caused by the applied nonlinear $\mathscr{H}_\infty$ control law (3.49) designed assuming nominal parameters.

Thus, analyzing Fig. 5.6 and the ISE and IADU performance index tables, it can be noticed an increase in performance, reflected by the ISE index. On the other hand, the control effort obtained with the use of the saturation function method is higher.

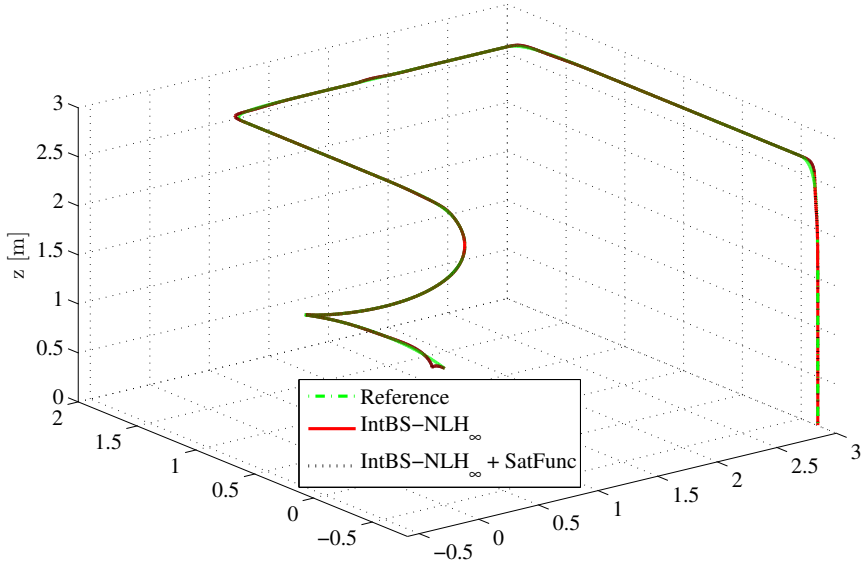

Figure 5.1: Path tracking.

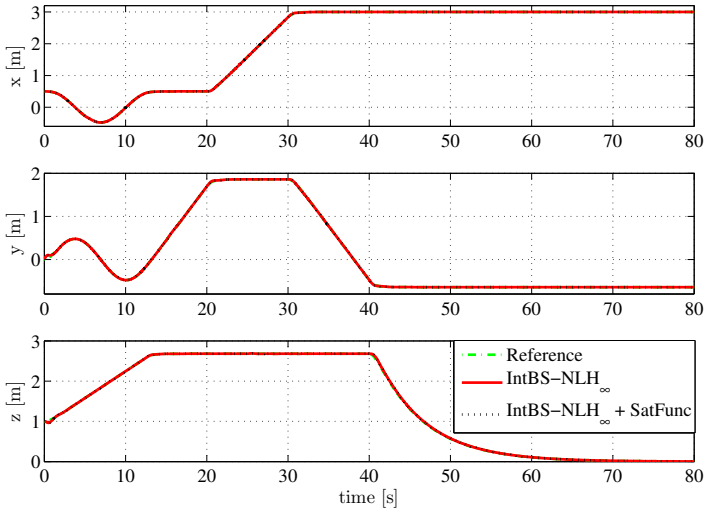

Figure 5.2: Position (x, y, z).

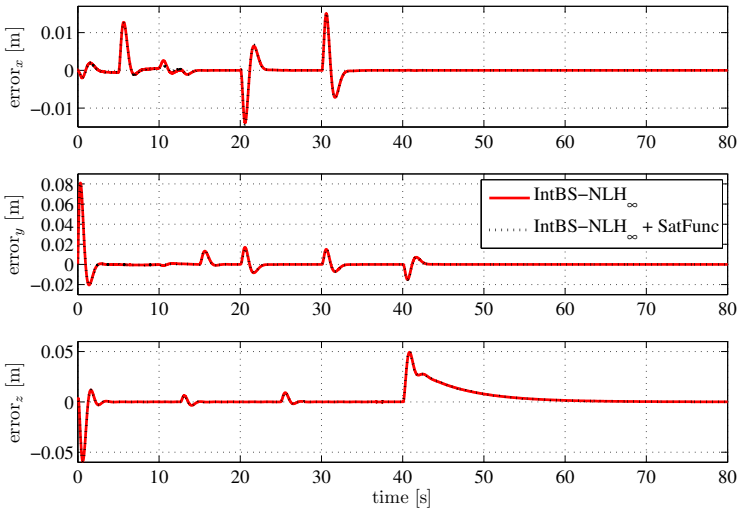

Figure 5.3: Position error (x, y, z).

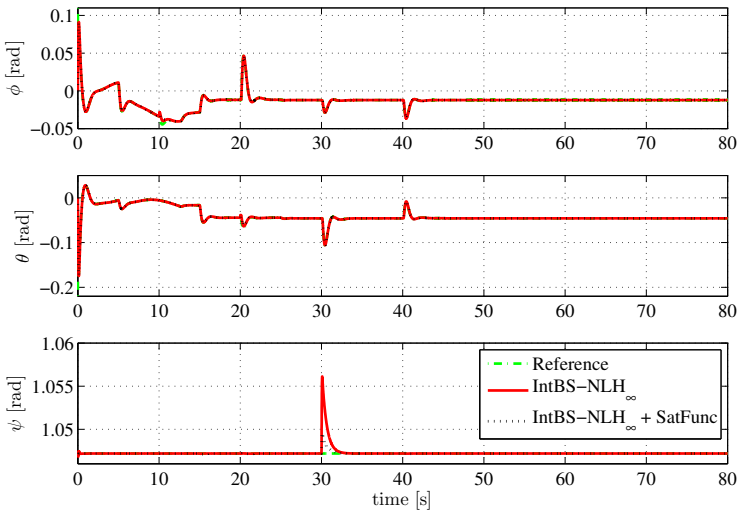

Figure 5.4: Orientation (ϕ, θ, ψ).

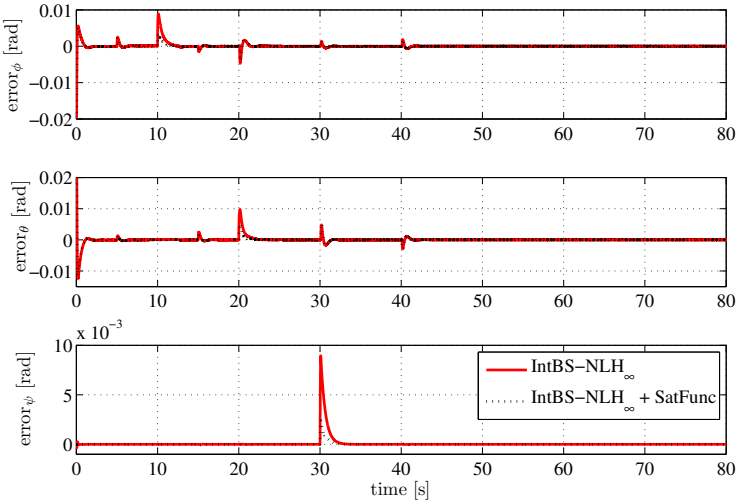

Figure 5.5: Orientation error(ϕ, θ, ψ).

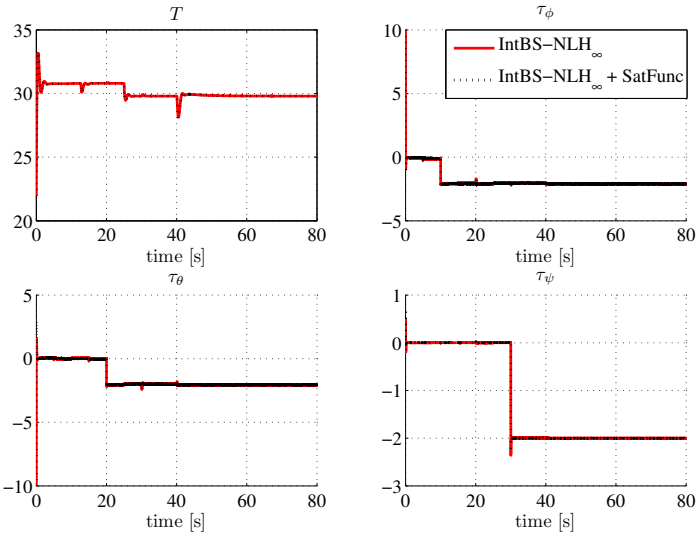

Figure 5.6: Control inputs $(U_1, \tau_{\phi_a}, \tau_{\theta_a}, \tau_{\psi_a})$.

Table 5.1: ISE Index Performance Analysis.

States [Unit Symbol]	IntBs-NL$\mathscr{H}_\infty$	IntBs-NL$\mathscr{H}_\infty$-SatFunc
$x\ [m^2 \cdot s]$	0.0718	0.0693
$y\ [m^2 \cdot s]$	0.6811	0.6215
$z\ [m^2 \cdot s]$	1.3228	1.2489
$\phi\ [rad^2 \cdot s]$	0.1193	0.1095
$\theta\ [rad^2 \cdot s]$	0.5840	0.5689
$\psi\ [rad^2 \cdot s]$	0.0052	0.0003

Table 5.2: IADU Index Performance Analysis.

Control Signals [Unit Symbol]	IntBS-NL$\mathscr{H}_\infty$	IntBS-NL$\mathscr{H}_\infty$-SatFunc
$T\ [N]$	24.0267	24.0244
$\tau_{\phi_a}\ [N \cdot m]$	207.3646	215.4339
$\tau_{\theta_a}\ [N \cdot m]$	213.7419	211.3500
$\tau_{\psi_a}\ [N \cdot m]$	14.4524	15.6005

Entire UActNL$\mathscr{H}_\infty$ Cascade Control Strategy

As in the previous case, this control strategy has been adjusted with the same parameters used in Section 4.4.1. The bounds of the dynamic model of the *QuadRotor* helicopter have been obtained following the same procedure described above:

- The upper bound of the reference acceleration is defined by analyzing the necessary acceleration of the six degrees of freedom, which value has been determined for the second path presented in the *Simulation Protocol*. The value of the parameter $\boldsymbol{Q}_{max}$ was obtained equal to 80.

- The bound of the inertia matrix uncertainty, α, has been computed again numerically through the error between the inertia matrix considering cross terms and the center of mass displaced from the center of rotation, and the inertia matrix used to design the controller with only the diagonal terms and the center of mass and the rotation one assumed congruent. This bound has been obtained for different values of angles and taking into account an uncertainty of $\pm 40\%$ in the parameters. The computed value of this bound han been $\alpha = 0.3442$.

- The design of function $\phi(\boldsymbol{x},t)$ is based on the bounds of the gravitational and Coriolis and centrifugal forces. The upper bound of the gravitational forces has been obtained numerically, which value γ_g was calculated equal to 30.78. The value of the parameter γ_c was achieved equal to 0.18.
- The maximum and minimum bounds of the inertia matrix have also been achieved numerically, by means of the inequalities (2.34), for different values of the Euler angles and considering the uncertainty interval into $\pm 40\%$ of the mass and the moment of inertia tensor terms. The values of these parameters are: $m_{min} = 1.3453$ and $m_{max} = 3.1423$.
- The value of the parameter ε has been chosen in order to avoid chattering in the control signal, resulting, in this case, in $\varepsilon = 15$.

The results obtained when the saturation function method has been applied to improve the robustness of the underactuated nonlinear $\mathscr{H}_\infty$ controller for the entire system are presented in Figs. 5.7 to 5.12.

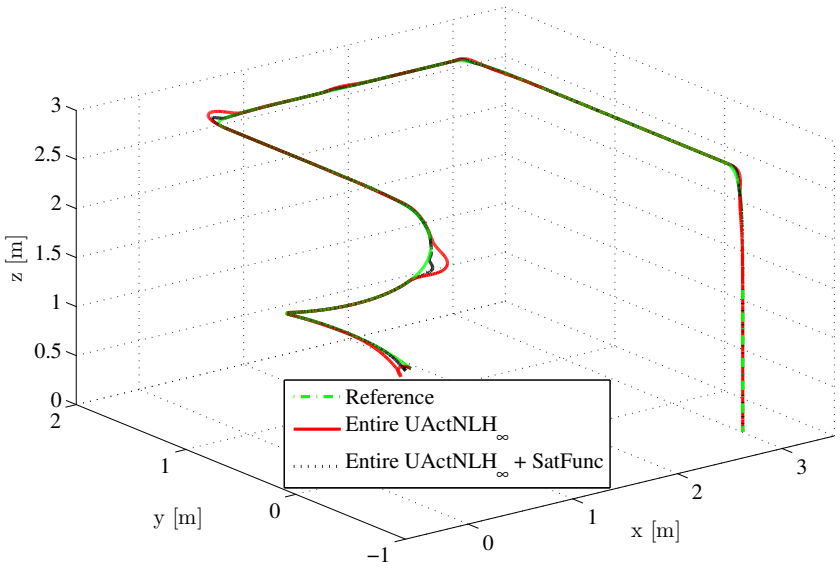

Figure 5.7: Path tracking.

As it can be observed in these simulation results, the path tracking for the *QuadRotor* helicopter performed by the Entire UActNL$\mathscr{H}_\infty$ has been improved

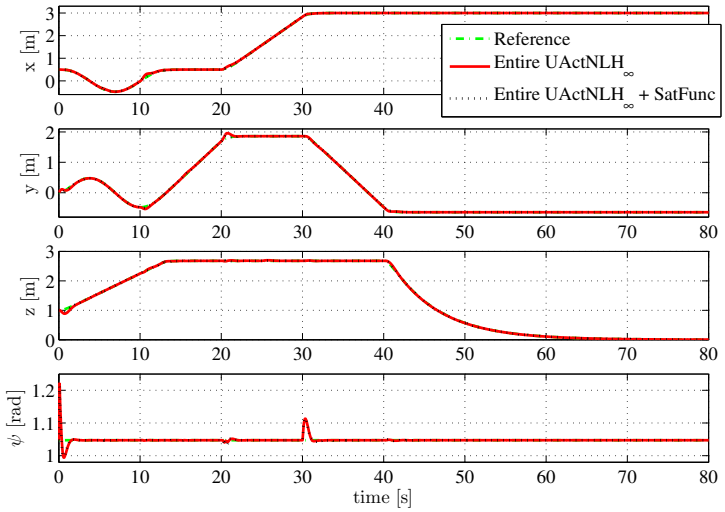

Figure 5.8: Position of the *controlled* DOF (x, y, z, ψ).

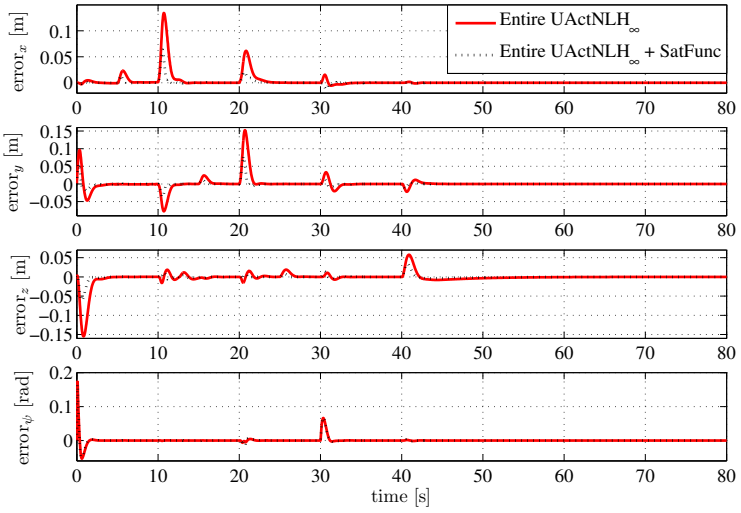

Figure 5.9: Position error of the *controlled* DOF (x, y, z, ψ).

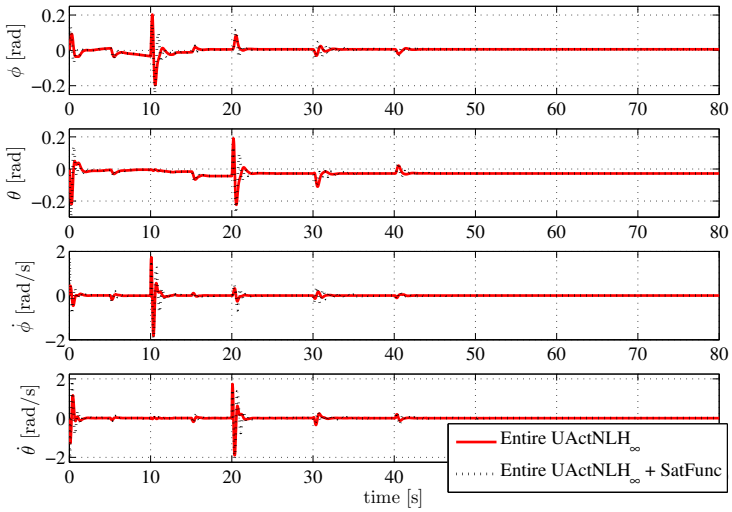

Figure 5.10: Position and velocity of the *remaining* DOF $(\phi, \theta, \dot{\phi}, \dot{\theta})$.

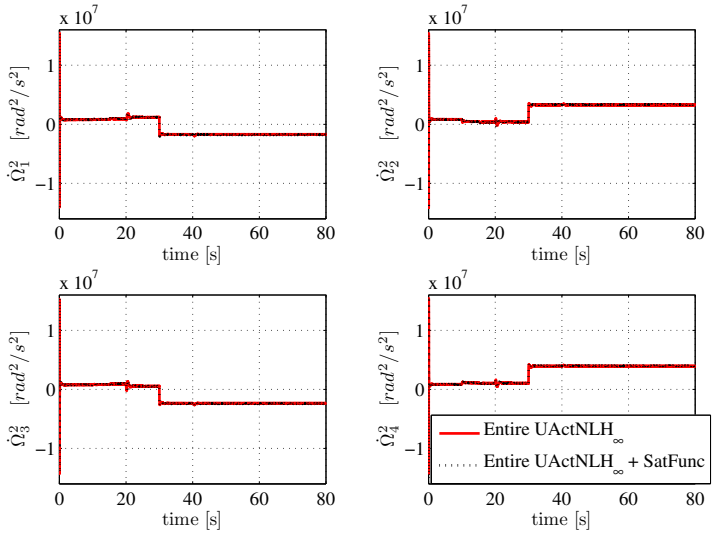

Figure 5.11: Squared Angular velocities of the rotors.

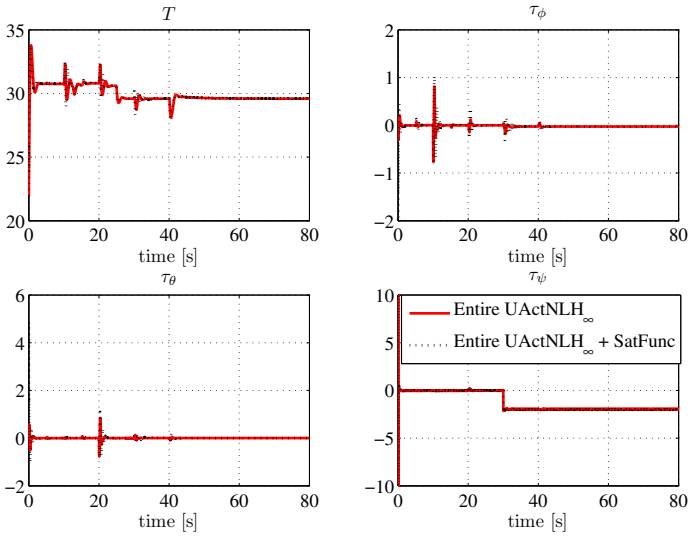

Figure 5.12: Control actions (T, τ_ϕ τ_θ τ_ψ).

by using the robustifying additional control law. The benefits of the saturation function method can be observed when abrupt changes on the trajectory occur or external disturbances affect the system. In these cases, the helicopter has been capable to recover the reference trajectory faster than using only the nonlinear $\mathscr{H}_\infty$ control law, as can be seen in Fig. 5.9. Moreover, the tracking errors of the *controlled* DOF have been reduced.

To make a deeper analysis, the ISE and IADU performance indexes have been used again, allowing to confirm the performance illustrated by the graphs. The accumulative errors of the *xyz*-motion and yaw angle have been decreased considerably, which justify the use of the proposed method. However, by analyzing the IADU performance index, it can be noticed that the control effort needed by the nonlinear $\mathscr{H}_\infty$ controller with the additional control law has been increased. This increment on the control effort is due to the fact the additional controller uses saturation functions in its formulation, leading to a more aggressive control signal.

Some reasons can explain the similar performances of the yaw angle and the improved behavior of the *xyz*-motion, for example, since the complete dynamic model of the helicopter considers both translational and rotational dynamics, it must be scaled to obtain bound values with same magnitudes. This feature can be observed by the maximum and minimum bounds obtained only for the rotational

Table 5.3: ISE Index Performance Analysis.

States [Unit Symbol]	**Entire UActNL$\mathscr{H}_\infty$**	**Entire UActNL$\mathscr{H}_\infty$-SatFunc**
$x\ [m^2 \cdot s]$	0.6215	0.0794
$y\ [m^2 \cdot s]$	0.9984	0.1699
$z\ [m^2 \cdot s]$	0.9238	0.1313
$\psi\ [rad^2 \cdot s]$	0.4259	0.4018

Table 5.4: IADU Index Performance Analysis.

Control Signals [Unit Symbol]	**Entire UActNL$\mathscr{H}_\infty$**	**Entire UActNL$\mathscr{H}_\infty$-SatFunc**
$T\ [N]$	38.4747	70.8024
$\tau_{\phi_a}\ [N \cdot m]$	7.2683	21.1510
$\tau_{\theta_a}\ [N \cdot m]$	7.8432	25.3203
$\tau_{\psi_a}\ [N \cdot m]$	88.0007	88.3142

inertia matrix ($m_{min} = 0.0369$ and $m_{max} = 0.1077$) and for the complete dynamic model ($m_{min} = 1.3453$ and $m_{max} = 3.1423$), where the mass magnitude is predominant in their computation. Besides, the desired control objective for both dynamics is different, since the translational motion must track a varying reference trajectory, the rotational one must be stabilized at the origin. This results in different bound values of the acceleration reference.

5.5 Conclusions

In this chapter, an analytical expression for the algorithm presented in Ortega et al. (2005), to improve the robustness of the nonlinear $\mathscr{H}_\infty$ controller for mechanical systems, has been proposed. The algorithm is based on the saturation function method, which allows to separate parametric uncertainties from external disturbances at the control design stage.

The proposed expression makes use of the solution of the HJBI equation formulated for the nonlinear $\mathscr{H}_\infty$ problem, overcoming the necessity to use a quadratic approximated solution and the successive linearization procedure of the closed-loop system.

Furthermore, the stability demonstration follows from the one of the nonli-

near $\mathscr{H}_\infty$ problem, which ensures the uniformly ultimately bounded condition for the closed-loop system when only parametric uncertainties are assumed. On the other hand, if external disturbances also affect the system the uniformly bounded condition can be considered.

Preliminary simulation results have been presented with the nonlinear $\mathscr{H}_\infty$ controller for fully actuated mechanical systems described in Chapter 3, and with the nonlinear $\mathscr{H}_\infty$ controller for underactuated mechanical systems considering the entire dynamic model proposed in Section 4.4. Both control strategies have been applied to solve the path tracking problem for the *QuadRotor* helicopter.

The results obtained with both IntBS-NL$\mathscr{H}_\infty$ and Entire UActNL$\mathscr{H}_\infty$ control strategies have presented a decrease of the tracking error of the *controlled* DOF in presence of parametric uncertainties. Therefore, the objective of improve the robustness of the nonlinear $\mathscr{H}_\infty$ controllers was achieved. It must be noticed that due to the use of saturation functions in the additional control law, the control effort in both control strategies has been increased. Moreover, to analyze the benefits of the method, the *QuadRotor* helicopter has been initially placed on the track in both simulation collections.

Despite the good results obtained in this chapter, it can be stated that to improve the results achieved with the proposed nonlinear $\mathscr{H}_\infty$ controller for underactuated mechanical systems, a study of the scaling of the complete dynamic model must be performed.

CHAPTER 6

Conclusions

Contents

6.1 Thesis contributions and conclusions

This thesis has dealt with the development of robust control strategies to solve the path tracking problem for autonomous aerial vehicles, focusing efforts on the *QuadRotor* helicopter on a small scale. Such strategies have been designed taking into account sustained external disturbances affecting the whole system, unmodeled dynamics, and structural and parametric uncertainties. Moreover, this kind of UAV is an underactuated mechanical system, since it has six degrees of freedom and only four actuators. Therefore, both cascade control structures and single controllers have also been developed considering this feature to achieve the desired performance.

Usually, an accuracy dynamic model of the system must be obtained to design advanced control strategies, taking in mind a tradeoff between complexity and realism. Therefore, in **Chapter 2**, initially, the *QuadRotor* helicopter operation have been described, in which the relationship between the applied forces/torques to the vehicle and the velocities of the four rotors have been stated. Moreover, the rotational and translational motions, assuming a point in the space, were deduced, which allowed to obtain the kinematic equations of a rigid body moving in a three-dimensional space. The rotational movement has been described by means of three successive rotations using the so-called Tayt-Bryan angles, which are also known as the nautical angles or the ZYX Euler angles.

The dynamic equations of the helicopter based on two approaches have been computed from the rotation matrix and kinematic equations. First, the Euler-

Lagrange formulation have been used to obtain the equations of motion of the *QuadRotor* helicopter, which consider the center of mass of the vehicle is displaced from the origin of the rotation body-fixed frame by a position $\boldsymbol{r}$. This assumption results in a highly-coupled nonlinear dynamic model. To overcome that, a simplified model of the *QuadRotor* helicopter has been deduced for control design purposes, where the center of mass and the center of rotation were assumed congruent. This simplified model results in a decentralized system allowing designing controllers separately for both translational and rotational motions. The second approach used to obtain the equations of motion of the helicopter was based on the Newton-Euler formulation. Both complete and simplified models have also been presented. However, this formulation has been used only to illustrate the relationship between the forces/torques obtained by using the Euler angles and their time derivative, and by using the angular rates, which allowed to obtain the applied forces/torques to the vehicle.

Since the *QuadRotor* helicopter is an underactuated mechanical system, a common way to perform path tracking of UAV's is using cascade control strategies. Therefore, most of the contributions of this thesis with respect to this kind of control structure have been presented in **Chapter 3**, where different control techniques have been used to control both the rotational and translational movements. The controllers have been designed to attain robustness against parametric and structural uncertainties, and to reject sustained disturbances acting on the six degrees of freedom of the helicopter. The contributions of **Chapter 3** are summarized in what follows:

- A nonlinear $\mathscr{H}_\infty$ controller has been used to perform the stabilization of the *QuadRotor* helicopter. This controller is able to reject sustained external disturbances due to the inclusion of the integral action in the tracking error vector. The control law has been designed for fully actuated mechanical systems. Hence, the Euler angles are controlled through the applied roll, pitch and yaw moments.

- The first translational controller has been designed using a linear state feedback $\mathscr{H}_\infty$ controller based on the error model, considering parametric uncertainties. The synthesis method used was based on LMIs. The cascade strategy, which combines this controller with the nonlinear $\mathscr{H}_\infty$ one used to stabilize the vehicle, have allowed to reject sustained external disturbances affecting the whole system. The translational controller has been performed taking into account an augmented state vector, where the integral of the translational position error was considered.

- In a second approach, designing the translational controller, an MPC algorithm has been used, while the nonlinear $\mathscr{H}_\infty$ controller for the helicopter stabilization was maintained in the inner loop. The main reason to use the MPC is due to its predictive features. Since the reference trajectory is usually known, the MPC can provide a smooth path tracking. The integral of the position error has also been considered for this controller, in order to maintain the good performance of the linear $\mathscr{H}_\infty$ controller to reject sustained disturbances that act on the translational movements.

  The linear MPC algorithm used considers that the real vehicle follows a *virtual* reference helicopter over the desired path, originating the error model, which is discrete and time-varying.

- The third control law applied to the translational subsystem has been developed based on the backstepping technique improving robustness in presence of model uncertainties. Again, the nonlinear $\mathscr{H}_\infty$ controller for the rotational subsystem has been combined in the cascade control structure with the integral backstepping controller. This translational controller considers the integral term in the second step of the backstepping procedure, presenting better results when compared with a controller that uses this term in the first step.

- Simulation results have been carried out to corroborate the good performance of the proposed cascade control strategies for the path tracking, when uncertainties of the mass and the moment of the inertia tensor were considered and in presence of sustained external disturbances. Comparison results have also been performed, where the ISE and IADU indexes have been used to make a quantitative analysis.

  From the comparison analysis, it can be observed that both MPC-NL$\mathscr{H}_\infty$ and IntBs-NL$\mathscr{H}_\infty$ control strategies have presented smaller accumulative error along the trajectories. However, when the control effort has been analyzed by means of the IADU index, the IntBs-NL$\mathscr{H}_\infty$ control strategy has presented smoother control signals. Therefore, despite all cascade control strategies, proposed in **Chapter 3**, have been solved the path tracking problem, only the IntBs-NL$\mathscr{H}_\infty$ control structure has attained the objective to perform the path tracking for the *QuadRotor* helicopter with a fast time response and a smooth control signal.

In **Chapter 4**, nonlinear $\mathscr{H}_\infty$ control structures for underactuated mechanical systems have been proposed. The contributions of this chapter are detailed as

follows:

- Firstly, an underactuated nonlinear $\mathscr{H}_\infty$ controller based on a reduced model has been designed, only taking into account the *controlled* degrees of freedom. The control structure allows considering the overall behavior of the system at the moment to compute the applied control signals. The controller has been applied to three different underactuated mechanical systems. In the case of the *QuadRotor* helicopter, this controller has been used to control the *active* degrees of freedom. Unlike the controllers used in Chapter 3, this proposed controller uses the information of the *passive* DOF dynamic to generate the control law, instead of assuming it as external disturbances. Since the *passive* degrees of freedom of the *QuadRotor* helicopter are unstable, a cascade control strategy has also been performed, where the MPC algorithm used in Chapter 3 for the *xy*-motion has been used to generate the roll and pitch reference angles. Simulations results and a quantitative analysis have been performed, which has demonstrated that using the proposed underactuated controller the accumulative error of the *active* DOF has been decreased with smoother control signals.

  The nonlinear $\mathscr{H}_\infty$ controller using the reduced model has also been implemented to control two vehicles based on the inverted pendulum concept, where the *controlled* DOF have been chosen as the *passive* ones. Experimental results have been obtained with a two-wheeled self-balanced vehicle.

  Additionally, an approach of the nonlinear $\mathscr{H}_\infty$ controller for mechanical systems has been proposed allowing to weight different dynamics of the system.

- A nonlinear $\mathscr{H}_\infty$ control strategy for underactuated mechanical systems with input coupling has been provided to avoid the use of cascade control structures and augmented state vector. This controller considers the entire dynamic of the underactuated mechanical system allowing regulates the *controlled* degrees of freedom while the *remaining* ones are stabilized. Moreover, it has guaranteed robustness for the path tracking of the *QuadRotor* helicopter without the necessity of an outer controller. The good performance attained by this control strategy has been corroborated by simulation results, which has improved the ISE and IADU performances indexes of all control input and *controlled* DOF. Experimental results have also been obtained with a two-wheeled self-balanced vehicle.

Normally, the controllers designed for mechanical system are based on nominal models. However, as it is well known, these models involve both structural and parametric uncertainties. Moreover, the nonlinear $\mathscr{H}_\infty$ controllers presented in Chapters 3 and 4 have been developed under the assumption that all uncertainties affecting the system are external disturbances. Nevertheless, this hypothesis is not very realistic. Therefore, in **Chapter 5**, a solution for the algorithm presented in Ortega et al. (2005) has been proposed to improve the robustness of the nonlinear $\mathscr{H}_\infty$ controllers designed for mechanical systems, where an additional control signal has been computed by means of the saturation functions technique to deal with modeling errors. Preliminary simulation results have been obtained with two control strategies presented in the thesis to solve the path tracking problem for the *QuadRotor* helicopter: the IntBS-NL$\mathscr{H}_\infty$ and the Entire UActNL$\mathscr{H}_\infty$. Both simulation collections have presented a reduction of the tracking error of the *controlled* DOF, corroborating the method by using the proposed solution. Despite the good results obtained in Chapter 5, it can be stated that to improve the results achieved with the proposed nonlinear $\mathscr{H}_\infty$ controller for underactuated mechanical systems, the scaling of the complete dynamic model must be performed when different dynamics are considered by the controller.

6.2 Future Works

In this section are described some possible directions for future researches in continuation of this work, including some already started

- *Implementation of the proposed control strategies.* As commented in Chapter 2, a *QuadRotor* helicopter is being constructed in the Automation, Control and Robotic Group, Department of Systems Engineering and Automation at the University of Seville. Therefore, an immediately goal is the implementation of the control strategies presented in this thesis to the real vehicle.

- *Guaranteed state estimation.* One drawback when designing controllers for UAV is whether all states are accessible, and if they are not, how to estimate state vector to perform a feasible path tracking. Moreover, usually the available sensors provide measures with bounded errors. An approach to estimate the state vector through these inaccuracy measures is by means of set-membership methods. For example, if the *QuadRotor* helicopter is equipped with a GPS, the measurement error can be in a range of $\pm 2m$, or more, as well as to feedback the controller at least every second. However,

the translational dynamic for this kind of vehicle can be of the order of milliseconds. Thus, between each GPS sampling time, the translational state vector must be estimated and guaranteed to be into a feasible set, and after a measured data is received, it must be updated.

- *Nonlinear $\mathscr{H}_\infty$ control for underactuated mechanical systems via output feedback.* Following the research line presented above, to extend the nonlinear $\mathscr{H}_\infty$ controllers for underactuated mechanical systems, presented in Chapter 4, to the control law design via output feedback.

- *Study of the boundary layers to ensure stability of the cascade control strategies.* The cascade control structures presented in this thesis are composed by inner and outer loop controllers, which are designed to obtain stability for each loop separately. However, when both controllers are combined no analysis has been made. By simulation results, it can be observed that the complete closed-loop system is stable, but it must also be demonstrated analytically. To perform this analysis, a suitable choice is the singular perturbation methods, where the outer loop is the slow dynamic, while the inner loop is the fast one.

- *Consideration of the rotor's closed-loop dynamics.* Taking into account that the *QuadRotor* helicopter in a small scale is powered by electrical batteries, in the course of time the batteries are discharged. This leads to a loss of thrust generated by the propellers, whose are not able to maintain the same velocity required by the rotational and translational controllers. Therefore, a rotor speed controller is required to ensure a regular performance throughout the flight. This control system results in having to consider a third closed-loop dynamic in the cascade control analysis. Hence, the three dynamics to be considered are: the translational motion (slow dynamic), the rotational motion (fast dynamic) and the rotor speed control loop (ultra-fast dynamic).

- *Visual feedback control of the QuadRotor helicopter.* Implementation of visual tracking and visual servoing techniques to estimate the position and attitude of the helicopter, and also to perform visual feedback control. Alternatively, it can be integrated both features in techniques as one proposed by Malis and Benhimane (2005).

- *Networked control system.* In the case that the UAV is controlled from a ground station, there is the possibility of losing data packages, both in sending control signals and the reception of signals measured. The information

loss caused by encoding and decoding of the transmitted signals must be added to this problem, as well as the data transmission rate. These problems are particularly interesting to this kind of systems when considering their unstable behavior.

- *Extension of the nonlinear $\mathscr{H}_\infty$ controllers to time-delay systems.* Some of the most common dynamic phenomena that appear in engineering applications are time-delays between the input and output variables. An emerging research line is how to treat the time-delay systems trough the nonlinear control theory. Recently works try to extend the predictor feedback idea to nonlinear systems, systems modeled by partial differential equations, systems with uncertain or totally unknown time-delay in the input-output channel, etc. The approach based on PDEs or DDEs (Delay Differential Equations) generates Lyapunov-Krasovskii functionals that allow a constructive control design and the stability analysis. Moreover, this approach based on PDEs allows an extension of predictor feedback design to nonlinear systems and to the robust and adaptive control of systems with unknown time-delay.

  Following this research line and through the nonlinear $\mathscr{H}_\infty$ controllers designed for fully and underactuated mechanical systems presented in this thesis, one objective is to extend these controllers to time-delay systems. Thus, the control of remote autonomous vehicles can be performed, for example, underwater autonomous vehicles in offshore petrol exploration and aerospace robotics.

APPENDIX A

Introducción

Contents

A.1 Motivación

El desarrollo de vehículos aéreos no tripulados (en inglés conocidos como UAV's - *Unmanned Aerial Vehicles*) ha despertado un gran interés en el área de control automático en las últimas décadas. Varios campos del control y de la robótica, como por ejemplo la fusión de sensores, técnicas de visión por computador, estimadores de estado y metodologías de control, han sido investigados para mejorar el comportamiento de estos sistemas. Los UAV's han sido utilizados tanto en el ámbito militar como en el civil, centrándose en las tareas de búsqueda y rescate, exploración de edificios, seguridad, inspección y cinematografía aérea, así como para maniobras acrobáticas (Pallet and Ahmad, 1991). Es de destacar, además, que los UAV's son muy útiles, sobre todo, cuando estas tareas son ejecutadas en entornos peligrosos e inaccesibles.

Hasta hace poco tiempo, desarrollar un vehículo aéreo en escala miniatura y controlado de manera autónoma era un desafío para muchos investigadores, lo cual estaba limitado por las restricciones impuestas por el *hardware*, hasta

entonces existente. Lo que hizo posible la construcción exitosa de vehículos aéreos autónomos fueron los avances tecnológicos en actuadores y sensores en escala reducida, los llamados *MicroElectroMechanical Systems* (MEMS), así como en el almacenamientos de energía y en el procesamiento de datos.

Por otra parte, el desarrollo de sistemas de control para este tipo de vehículos no es trivial. Los UAV's tienen un comportamiento altamente no lineal y variante en el tiempo y están constantemente afectados por perturbaciones aerodinámicas. Además, suelen estar sujetos a dinámicas no modeladas e incertidumbres paramétricas. Esto significa que las leyes clásicas de control lineal y monovariables pueden presentar una cierta limitación con respecto a su cuenca de atracción, provocando inestabilidades cuando el sistema está funcionando en condiciones lejanas del equilibrio. Por lo tanto, son necesarias estrategias avanzadas de control para hallar un buen desempeño durante vuelos totalmente autónomos, o por lo menos, para ayudar el pilotaje del vehículo, con alta maniobrabilidad y robustez con respecto a las perturbaciones externas.

En relación a esto, se debe tener en cuenta que, debido al diseño electromecánico de los vehículos aéreos, gran parte de estos vehículos son sistemas mecánicos subactuados (esto es, poseen menos entradas de control que grados de libertad). Generalmente, el diseño electromecánico se realiza con el fin de buscar una reducción de la masa y del coste del vehículo. Sin embargo, los sistemas subactuados conllevan una mayor complejidad y un desafío adicional al área de control. Las técnicas desarrolladas para robots totalmente actuados tampoco se pueden aplicar directamente a este tipo de sistemas mecánicos, ya que la mayoría de los sistemas subactuados no son totalmente linealizables por realimentación y presentan restricciones no holónomas (Fantoni and Lozano, 2002; Aguiar, 2002). De ahí que las técnicas de modelado no lineal y la teoría de control no lineal moderna son normalmente empleadas para alcanzar un alto desempeño en vuelos autónomos y en condiciones de vuelo específicas, tales como: vuelo estacionario, aterrizaje y despegue, etc (Frazzoli et al., 2000; Isidori et al., 2003; Castillo et al., 2005b).

Los objetivos de un sistema de control de vuelo pueden clasificarse en tres fases, en función de la autonomía que alcance el sistema:

- *Sistemas de estabilización* (del inglés SAS: *Stability Augmentation Systems*): Este tipo de sistemas persigue ayudar al pilotaje del vehículo, estabilizando el sistema con un control de bajo nivel. Así se evita que el piloto deba actuar en base al comportamiento dinámico de un sistema, que una vez alejado de cierto punto de equilibrio, deja de ser intuitivo para el razonamiento humano.

- *Sistemas de control* (del inglés CAS: *Control Augmentation Systems*): Estos sistemas están en un nivel jerárquico superior a los SAS. Así, además de estabilizar al vehículo, estos sistemas deben ser capaces de proporcionar una respuesta con ciertas prestaciones a referencias que proporcione el piloto, como por ejemplo, el seguimiento del ángulo de cabeceo.

- *Sistemas de pilotaje automático* (del inglés *Autopilots*): Constituyen el nivel de control jerárquicamente superior. Son sistemas de control totalmente automáticos que son capaces de realizar por sí solos ciertos tipos de maniobras, como por ejemplo, el despegue, el aterrizaje, o vuelo estacionario a cierta altura.

En el área de control de vuelo, los sistemas más estudiados han sido los aviones y helicópteros convencionales (es decir, helicópteros con rotores principal y de cola). Sin embargo, en los últimos años, UAV's en la configuración *QuadRotor* han destacado en una gran cantidad de trabajos producidos con ellos, los cuales presentan algunas características ventajosas en comparación con el helicóptero convencional, tales como:

- El helicóptero *QuadRotor* está propulsado por cuatro rotores, lo que hace posible reducir el tamaño de cada rotor y mantener o aumentar la capacidad de carga total, en comparación con la de un helicóptero con un rotor principal.

- Estos vehículos no requieren accionamientos mecánicos para actuar en las hélices. Esto reduce el diseño, mantenimiento y coste del vehículo (Hoffmann et al., 2007).

- La sencillez del diseño mecánico permite el control de movimiento a través de accionamiento directo de los rotores variando sus velocidades. En un helicóptero convencional, la velocidad de giro de las hélices suele ser constante, controlando el movimiento mediante la variación de los ángulos de ataque de las palas (cíclico y colectivo). Esto requiere transmisiones entre los rotores, bien como dispositivos mecánicos de precisión para poder variar los mencionados ángulos.

- Estos helicópteros son interesantes para el uso en el interior de edificios debido a la utilización de motores eléctricos en lugar de los de combustión, ya que no contaminan el aire con carburantes.

- Se basan en el concepto VTOL (en inglés *Vertical Take-Off and Landing*) que normalmente se utiliza para desarrollar leyes de control. El *QuadRotor* intenta lograr un vuelo estable y estacionario a través del balance de las fuerzas producidas por los cuatro rotores (Castillo et al., 2005b).

- Las ventajas anteriores sumadas a su alta maniobrabilidad, permite despegues y aterrizajes, así como vuelo en entornos complicados.

El principal inconveniente de este tipo de UAV es que presenta un aumento de peso y de consumo de energía debido a los motores adicionales.

Desde el punto de vista del control, la construcción de este tipo de helicóptero en miniatura está lejos de simplificar el problema, más bien sucede lo contrario. Esto se debe a los pares y fuerzas necesarios para controlar el sistema son aplicados no sólo a través de los efectos aerodinámicos, sino también a través del efecto de acoplamiento que aparece entre la dinámica de los rotores y la del cuerpo del helicóptero. Este efecto de acoplamiento se debe al principio de acción y reacción originado en la aceleración y desaceleración de las hélices (efecto que no sucede en el control con velocidad de hélices constante).

A pesar de los efectos de acoplamiento mencionados anteriormente, la falta de acoplamiento entre las entradas tiene algunas implicaciones para el diseño de control de la dinámica del *QuadRotor*. Tal desacoplamiento surge de la suposición de que el helicóptero está en una configuración coplanaria, es decir, las cuatro hélices son paralelas entre sí, generando el vector de fuerza con elementos sólo en el eje vertical. Por lo tanto, si se consideran como salidas a controlar la posición de traslación y el ángulo de guiñada, una linealización por realimentación estática de la dinámica completa del helicóptero *QuadRotor* da lugar a una matriz singular haciendo que el desacoplamiento entrada-salida sea inviable. Por lo tanto, esta técnica de control no se puede utilizar directamente (Mistler et al., 2001). Este hecho, unido con el acoplamiento entre las dinámicas de los rotores y el cuerpo del helicóptero, así como incertidumbres del modelo, especialmente en el rango de alta frecuencia, hacen que el sistema sea incluso más difícil de controlar que un helicóptero convencional, al menos empleando técnicas básicas de control.

A.2 Estado del Arte

Muchos esfuerzos han sido realizados para controlar helicópteros basados en cuatro rotores y varias estrategias han sido desarrolladas para hacer frente al problema

de seguimiento de trayectorias para este tipo de sistema. En general, se utilizan dos tipos de estrategias para realizar el seguimiento de trayectorias del helicóptero *QuadRotor*. Por un lado, gran parte de las estructuras utilizan estrategias de control en cascada, las cuales usan un bucle de control interno para el subsistema de rotación, o en algunos casos para los grados de libertad actuados, combinado con un bucle de control externo para controlar los movimientos de traslación. Sistemas de control que utilizan esta estrategia pueden ser encontrados en Chen and Huzmezan (2003) y Bouabdallah and Siegwart (2007). Por otro lado, otras estructuras de control usan un espacio de estados aumentado (Mistler et al., 2001; Mokhtari et al., 2006b), donde se considera un doble integrador en el empuje, la entrada de control de altura, que genera acoplamiento entre los movimientos de traslación y rotación, permitiendo utilizar técnicas de linealización por realimentación.

En Mistler et al. (2001) se utilizó un modelo no lineal que representa tanto la cinemática como la dinámica del vehículo, y a través de las Leyes de Newton se obtuvieron las ecuaciones dinámicas para el helicóptero *QuadRotor*. En este modelo se consideraron las fuerzas y momentos aerodinámicos actuantes en el sistema. Para realizar la tarea de seguimiento de trayectorias se demostró que no se pueden desacoplar las salidas deseadas por linealización por realimentación estática, y se propuso un controlador con desacoplamiento entrada-salida y linealización exacta por realimentación dinámica.

En Bouabdallah et al. (2004a) se diseñó un controlador basado en una función de control de Lyapunov para estabilizar el subsistema de rotación, y usando la misma técnica de control, el control de la altura fue implementado en cascada. En Bouabdallah et al. (2004b), se obtuvieron las ecuaciones del movimiento del helicóptero *QuadRotor* a través de la formulación de Euler-Lagrange, considerando además las dinámicas de los rotores. En este trabajo se realizó una comparación entre dos técnicas de control, un PID y un Regulador Cuadrático Lineal, donde se ha considerado un modelo linealizado para diseñar el controlador PID. El desarrollo del control LQ fue basado en un modelo variante con el tiempo. En Castillo et al. (2005a, 2007) se han diseñado controladores no lineales para estabilizar el *QuadRotor* basado en el análisis de Lyapunov y en técnicas de saturaciones anidadas. En Park et al. (2005) se ha usado un algoritmo para la compensación de la dinámica del vehículo para controlar el sistema. En Lara et al. (2006) se han presentado nuevos resultados para calcular el margen de robustez del sistema de control para un helicóptero *QuadRotor* utilizando un PID multivariable para estabilizar la posición del vehículo. En Das et al. (2009b) se ha considerado una

estrategia con dos bucles utilizando linealización entrada-salida para diseñar un controlador no lineal con dinámica inversa del bucle interno y un bucle externo para estabilización de la dinámica interna. En Önkol and Efe (2009) cuatro técnicas de control fueron comparadas para resolver el problema de seguimiento de trayectorias: esquema de control PID, control de modos deslizantes, *backstepping* y linealización por realimentación.

En Mederreg et al. (2004) se mostraron resultados de simulación para un control basado en técnicas de *backstepping* combinado con un observador del estado, mientras que en Mahony and Hamel (2004) se combinó esta técnica con un control basado en Lyapunov. En Bouabdallah and Siegwart (2005) el modelo dinámico del helicóptero *QuadRotor* fue dividido en dos subsistemas: de rotación angular y de traslación lineal. Se presentaron dos técnicas de control: *backstepping* y modos deslizantes. En varios trabajos se ha utilizado la técnica de *backstepping* para realizar tanto el seguimiento de trayectorias cuanto la estabilización helicóptero *QuadRotor*. Controladores *backstepping* aplicados al helicóptero pueden ser encontrados en Madani and Benellegue (2006a,b); Madani and Benallegue (2007); Zemalache et al. (2007) y Guenard et al. (2008).

Aunque varias estrategias de control han sido probadas en el helicóptero *QuadRotor*, gran parte de ellas no considera perturbaciones externas en los seis grados de libertad, dinámicas no modeladas e incertidumbres paramétricas en todo el modelo. Por ejemplo, en Bouabdallah and Siegwart (2005), Castillo et al. (2005a) y Zemalache et al. (2007), los controladores propuestos no son capaces de rechazar perturbaciones mantenidas y en Mistler et al. (2001) apenas se consideran perturbaciones en los movimientos de traslación.

Sin embargo, en los últimos años, algunos investigadores han empezado a considerar estos efectos en la etapa de diseño de control y, por ejemplo, han sido desarrolladas técnicas robustas de modos deslizantes y *backstepping* también, además de como observadores de las perturbaciones. En Mokhtari et al. (2006b) se ha diseñado un controlador basado en linealización por realimentación combinado con un observador basado en la técnica de modos deslizantes para el helicóptero *QuadRotor*. Un observador adptativo se ha añadido al sistema de control para estimar el efecto de las perturbaciones externas. En Xu and Özgüner (2006), se sintetizó un controlador basado en modos deslizantes, mientras que Xu and Özgüner (2008) propusieron un abordaje usando un controlador de modos deslizantes para sistemas mecánicos subactuados para estabilizar un helicóptero *QuadRotor* cuando se considera un 30% de incertidumbre en cada parámetro del modelo. En Lee et al. (2009), los resultados obtenidos con un controlador usando

linealización por realimentación fueran comparados con los obtenidos con un control de modos deslizantes adaptativo usando un vector de entrada aumentado para hacer frente a propiedades de sistemas subactuados, incertidumbre paramétrica y ruido de sensores. En Kim et al. (2010) se propuso un controlador basado en observador de perturbación usando el modelo dinámico para control robusto en vuelo estacionario, que es un compensador del bucle interno.

En Bouabdallah and Siegwart (2007) se abordó la técnica *backstepping* utilizando acción integral para mejorar el desempeño del seguimiento de trayectorias para el helicóptero *QuadRotor* cuando vientos mantenidos perturban todo el sistema. En Das et al. (2009a), un controlador basado en la técnica *backstepping* fue usado para controlar el helicóptero *QuadRotor*, aplicando el procedimiento del *backstepping* a la forma Lagrangiana de la dinámica. Además, se han introducido redes neuronales para estimar las componentes aerodinámicas.

El uso de la acción integral en la técnica de *backstepping* fue propuesto inicialmente por Kanellakopoulos and Krein (1993). La manera más común de incluir la acción integral en este enfoque es usando adaptación paramétrica (Krstic et al., 1995). Un análisis de diferentes técnicas usando la acción integral en el control *backstepping* se llevó a cabo en Skjetne and Fossen (2004), donde se presentaron otros dos métodos que consisten en aumentar la dinámica del sistema con la acción integral como un estado.

En algunos trabajos el helicóptero *QuadRotor* ha sido controlado usando un controlador $\mathscr{H}_\infty$ lineal basado en modelos linealizados. En Chen and Huzmezan (2003), se presentó un modelo no lineal simplificado para el movimiento del UAV. El problema de seguimiento de trayectorias se dividió en dos partes, en primer lugar se buscó la estabilización de las velocidades angulares y de la velocidad vertical a través de un controlador $\mathscr{H}_\infty$ de 2DOF utilizando la técnica de *loop shaping*. La misma técnica se ha utilizado para controlar, en un bucle externo las velocidades longitudinal y lateral, el ángulo de guiñada y la altura. En la segunda parte, para resolver el problema de seguimiento de trayectorias se diseñó un controlador predictivo basado en un modelo incluyendo los bucles internos y el modelo del helicóptero. En Mokhtari et al. (2005, 2006a) se ha aplicado una linealización por realimentación robusta con un controlador $\mathscr{H}_\infty$ lineal para tratar el problema de seguimiento con incertidumbre paramétrica y perturbaciones externas.

Adicionalmente al control inercial, el helicóptero *QuadRotor* ha sido también controlado mediante realimentación por visión artificial. En Altug et al. (2002), se ha usado una cámara en tierra para estimar la posición y orientación del heli-

cóptero, mientras en Tournier et al. (2006) se ha utilizado una cámara montada sobre el vehículo utilizando patrones de Moiré para obtener una estimación de los seis grados de libertad. En Altug et al. (2005) se usaron dos cámaras para estimar los seis grados de libertad del helicóptero, una de ellas montada sobre el *QuadRotor*, mientras que la otra cámara estaba localizada en el suelo. Para conseguir un helicóptero autónomo, dos métodos de control fueron utilizados: un controlador *backstepping* y un controlador con linealización por realimentación. En Metni et al. (2005), se consideró un modelo dinámico mecánico general del UAV apto para realizar vuelos estacionarios. La estimación de la posición y orientación se realizó a través de visión utilizando una técnica de control servo visual basada en homografía. Así, se dedujo una ley de control basada en *Backstepping* que fuerza la trayectoria a seguir a través de una secuencia de imágenes pregrabadas. La trayectoria deseada se obtiene a través de un operador que enseña cada paso preliminarmente, siendo comparadas la imagen actual y la imagen deseada a una imagen de referencia por las matrices homográficas en cada paso. Para determinar el vector de traslación se estima la información de la profundidad de referencia usando una ley de control adaptativa.

Además, hay dos cuestiones que vale la pena señalar. Por un lado, muchas de estas aplicaciones de control asumen que los valores calculados nunca alcanzarán los limites de saturación de los actuadores, aunque en la práctica esto es posible. Por ejemplo, cuando el vehículo está muy lejos de su destino, las señales de control generadas son normalmente más altas que las admisibles. Sin embargo, los vehículos están dotados de partes mecánicas y electrónicas, las cuales están sujetas a limitaciones físicas del sistema.

Cuando estas restricciones deben ser consideradas, los algoritmos de MPC se presentan como una interesante elección. El objetivo del MPC es calcular acciones de control para un determinado horizonte de tiempo futuro, de tal manera que la predicción de la salida de la planta siga cerca de la referencia, minimizando una determinada función de coste multiobjetivo respecto a acciones de control futuro. Para hacer esto, los valores de las salidas predichas son calculadas como una función de valores pasados de las entradas y salidas, y de señales de control futuras, haciendo uso de un modelo explícito del proceso y sustituyéndolo en la función de coste, obteniendo una expresión cuya minimización conduce a los valores deseados. Se puede obtener una solución analítica para una función de coste cuadrática, si el modelo es lineal y no existen restricciones; en caso contrario se deben usar métodos iterativos de optimización (Camacho and Bordons, 1998; Mayne et al., 2000; Rawlings and Mayne, 2009).

Además, la formulación del MPC genera (implícitamente) una ley de control no-suave (discontinua). Dado que las trayectorias son normalmente conocidas y usando una adecuada instrumentación en el vehículo que informe sobre su desplazamiento y localización, o bien con información del entorno donde se encuentra (usando, por ejemplo, GPS, mapas digitales, etc), el controlador predictivo se presenta como una técnica muy apropiada para esta tarea. Además de conducir el vehículo suavemente, esta técnica permite mejorar la autonomía del mismo, aparte de ser fácilmente extendido a sistemas multivariables. Como desventaja se puede considerar el elevado coste computacional introducido, que puede hacer que sea imposible realizar aplicaciones reales.

Por otro lado, es bastante común asumir que todos los estados están accesibles para los controladores. En general, esto puede resultar en dificultades para las aplicaciones prácticas. Para evitar estos problemas prácticos, en algunos trabajos se han propuesto observadores de estado para estimar la velocidad lineal del helicóptero *QuadRotor*. En Benzemrane et al. (2007) un estimador no lineal adaptativo fue propuesto para mejorar la robustez de la estimación de velocidad cuando sólo se dispone de medidas de la aceleración lineal, de los ángulos y de la velocidad angular. En Benzemrane et al. (2008) la estimación de velocidad se observó a través de un filtro de Kalman y de un observador adaptativo, siendo corroborado con medidas de aceleración lineal exactas y ruidosas. Al mismo tiempo, hay una gran variedad de sensores disponibles que proporcionan las medidas necesarias. Por ejemplo, los ángulos de Euler y las velocidades angulares pueden ser obtenidas a través de una Unidad de Medición Inercial (del inglés *Inertial Measurement Systems* - IMU). Además, si esto se combina con GPS (o GPS diferencial), la posición lineal y velocidad lineal también pueden ser medidas. En esta etapa es necesario tener en cuenta los objetivos de la aplicación, como, por ejemplo, si el UAV debe volar en interiores o al aire libre, o si la precisión del GPS es admisible. Otros tipos de sensores también pueden ser utilizados para estimar la posición y orientación del UAV, como los sistemas de ultrasonido en un entorno estructurado (Roberts et al., 2007), sistemas de visión (Altug et al., 2002; Metni et al., 2005; Tournier et al., 2006; Guenard et al., 2008) y sistemas de seguimiento 3D (POLHEMUS) (Castillo et al., 2005a; Guisser et al., 2006).

Aparte de lo mencionado, las investigaciones sobre la coordinación de múltiples UAV's usando helicópteros en la configuración *QuadRotor* han generado un gran interés en los últimos años , sobre todo en la comunidad de robótica. Algunos trabajos en este campo pueden ser citados, tales como Hoffmann et al. (2006); Bethke et al. (2007); Michael et al. (2010b,a).

En esta tesis, será abordado el problema de seguimiento de trayectorias para un único helicóptero *QuadRotor*, donde el objetivo principal es mejorar la robustez de las estrategias de control cuando el vehículo está volando en presencia de perturbaciones externas, dinámicas no modeladas e incertidumbres paramétricas.

A.2.1 Control $\mathscr{H}_\infty$ No Lineal para Sistemas Mecánicos

Como se puede deducir de lo presentado anteriormente, muchas estrategias de control han sido aplicadas al helicóptero *QuadRotor*, pero la mayoría no considera incertidumbres paramétricas ni perturbaciones externas. Sin embargo, los UAV's están constantemente afectados por incertidumbres del modelo y ráfagas de viento, que pueden fácilmente desestabilizar el vehículo.

Una selección adecuada para rechazar estas perturbaciones es la teoría de control $\mathscr{H}_\infty$ no lineal. Los primeros esfuerzos para extender el problema de control $\mathscr{H}_\infty$ a sistemas no lineales se hizo en los años ochenta. En Ball et al. (1987a,b) se formuló el problema no lineal para sistemas en tiempo discreto y, utilizando Series de Volterra, se encontraron soluciones aceptables. La solución para sistemas no lineales continuos en el tiempo fue proporcionada por van der Schaft en van der Schaft (1991) y van der Schaft (1992).

El objetivo de la teoría $\mathscr{H}_\infty$ es hallar un relación acotada entre la energía de las señales de error y la energía de las señales de perturbación. En general, el abordaje no lineal de esta teoría considera una ecuación en derivadas parciales de Hamilton-Jacobi (EDP HJ), que reemplaza la ecuación de Riccati en el caso de la formulación de control $\mathscr{H}_\infty$ lineal. La solución del problema de control $\mathscr{H}_\infty$ no lineal se puede obtener a través de dos enfoques: teoría de juegos diferenciales (Doyle et al., 1989; Basar and Bernhard, 2008) y teoría de sistemas disipativos (van der Schaft, 2000). El principal problema en el caso no lineal es la falta de un método general para resolver esta EDP HJ. Por lo tanto, se deben resolver soluciones analíticas para cada caso particular.

Debido a la dificultad de obtener soluciones analíticas, algunos trabajos proponen métodos numéricos que permiten integrar tales ecuaciones, por ejemplo, métodos de Galerkin y Series de Taylor (Beard et al., 1997; Beard and McLain, 1998; Beard et al., 1998; Hardt et al., 2000).

Dado que el interés principal de esta tesis es trabajar con modelos de sistemas mecánicos obtenidos a través de la formulación de Euler-Lagrange, las soluciones del control $\mathscr{H}_\infty$ no lineal se pueden encontrar minimizando las fuerzas que rea-

lizan trabajo sobre el sistema, como fue expuesto en Johansson (1990). En este artículo, el autor propuso una solución para el problema de control óptimo $\mathscr{H}_2$ no lineal para sistemas mecánicos totalmente actuados. A partir de este trabajo pionero, una enorme cantidad de modificaciones han sido realizadas para formular controladores no lineales $\mathscr{H}_2$, $\mathscr{H}_\infty$ y $\mathscr{H}_2/\mathscr{H}_\infty$ para sistemas mecánicos (Chen et al., 1994; Feng and Postlethwaite, 1994; Astolfi and Lanari, 1994; Kang, 1995; Chen et al., 1997; Postlethwaite and Bartoszewicz, 1998). En Sage et al. (1999) se presentó un estudio de control robusto de robots manipuladores, donde se puede encontrar un breve resumen del control $\mathscr{H}_\infty$ no lineal aplicado a sistemas mecánicos.

Una solución parametrizada global y explícita para el problema óptimo $\mathscr{H}_\infty$ a través de realimentación de estados, formulada como un juego *min-max*, fue desarrollada en Chen et al. (1994). Esta solución trata el caso particular de sistemas mecánicos totalmente actuados formulados via ecuaciones de Euler-Lagrange, utilizando la ecuación de estados del error de seguimiento propuesta por Johansson (1990) y propiedades de sistemas mecánicos. En el mismo año, Feng and Postlethwaite (1994) propusieran una formulación similar al controlador $\mathscr{H}_\infty$ no lineal con realimentación de estados para sistemas robóticos, donde la variable de coste considera el acoplamiento entre las variables controladas y la ley de control por realimentación de estados, proporcionando más grados de libertad para el diseño de control. Además, se presentó una ley de control $\mathscr{H}_\infty$ no lineal con un enfoque adaptativo para mejorar la robustez del sistema completo.

En Ortega et al. (2005) se propuso una estrategia para controlar sistemas mecánicos totalmente actuados considerando la ecuación dinámica del error de seguimiento, donde se agregó la integral del error de posición al vector del error. En tal estrategia se aplica un control $\mathscr{H}_\infty$ no lineal formulado vía teoría de juegos, la cual provee, a través de una solución analítica, una ley de control variante con el tiempo que es altamente dependiente del modelo y es similar a los resultados obtenidos con procedimientos de linealización por realimentación. Se han establecido condiciones para formular el controlador en la forma de un PID no lineal, donde la señal de control puede ser penalizada, así como las señales del error, sus integrales y sus derivadas.

Algunos trabajos utilizando controladores no lineales $\mathscr{H}_2$, $\mathscr{H}_\infty$ y $\mathscr{H}_2/\mathscr{H}_\infty$ han sido publicados en el área de la aeronáutica. En Yang and Chen (2001), se utilizó la teoría de control $\mathscr{H}_\infty$ no lineal para diseñar una ley de control para guiar misiles en el espacio tridimensional. En Chen et al. (2002), maniobras de persecución de misiles tácticos en el espacio tridimensional fue resuelto usando una ley de control

$\mathscr{H}_\infty$ no lineal basado en un modelo borroso. In Chen et al. (2003), se propuso un control lateral mixto $\mathscr{H}_2/\mathscr{H}_\infty$ adaptativo borroso de sistemas de misiles no lineales con perturbaciones desconocidas. En López-Martínez et al. (2007) se ha controlado un helicóptero de laboratorio con dos rotores usando un controlador $\mathscr{L}_2$ no lineal basado en un modelo de orden reducido de los rotores.

A.2.2 Sistemas Mecánicos Subactuados

Como se ha comentado anteriormente, los UAV's son sistemas mecánicos subactuados, y el helicóptero *QuadRotor* no es diferente, ya que cuenta con seis grados de libertad y sólo cuatro acciones de control, los cuatro rotores. Los sistemas mecánicos subactuados aparecen en varias aplicaciones, tales como robots aeroespaciales y subacuáticos, sistema móviles, sistema flexibles, robots caminantes, braquiadores y gimnastas. De acuerdo con Olfati-Saber (2001), la propiedad de subactuación de sistemas subactuados se debe a cuatro razones: la dinámica del sistema, el diseño para la reducción de coste o algunos fines prácticos, el fallo de actuadores y la imposición artificial para crear sistemas no lineales complejos de orden reducido con el fin de ampliar el conocimiento sobre el control de sistemas subactuados de orden superior.

En el área de control de sistemas mecánicos subactuados, una importante contribución se ha presentado en Spong (1994), donde los autores usan la linealización por realimentación parcial propuesta por Isidori (1989) para linealizar los grados de libertad no actuados.

El control de movimiento de sistemas mecánicos subactuados es frecuentemente difícil debido a las restricciones no holónomas en la aceleración generada por la subactuación, que resulta en la imposibilidad de regular todos los grados de libertad del sistema en el mismo instante de tiempo en un posición deseada. En Wichlund et al. (1995) se han estudiado propiedades de control de las dinámicas de vehículos subactuados (esto es, vehículos subacuáticos, helicópteros, aviones, etc). Una interesante propiedad de este tipo de sistemas fue presentada, la cual dice que los sistemas mecánicos subactuados con campo gravitacional $\boldsymbol{G}(\boldsymbol{q})$ donde las componentes de $\boldsymbol{G}$ correspondientes a las dinámicas no actuadas son nulas, no son C^1 asintóticamente estabilizables en un punto de equilibrio. Olfati-Saber (2001) reescribió esta propiedad diciendo que si la energía potencial $\mathscr{U}(\boldsymbol{q})$ es independiente de la variable externa $\boldsymbol{q_x}$, o sea, $\partial\mathscr{U}(\boldsymbol{q_x},\boldsymbol{q_s})/\partial\boldsymbol{q_x} = 0$, entonces $\boldsymbol{g_r} = 0$ (donde, $\boldsymbol{g_r}$ es el término gravitacional del subsistema restante) y el momento generalizado p_r es una cantidad conservada. Por lo tanto, el sistema

mecánico subactuado no es controlable o estabilizable en ningún punto de equilibrio para condiciones iniciales con $p_r(0) \neq 0$. El hecho de que el sistema no actuado es un sistema Lagrangiano simple sin ninguna fuerza de entrada significa que el sistema debe ser controlado a través de la fuerza potencial que es parametrizada por $\boldsymbol{q_s}$. Por lo tanto, el vector de coordenadas *moldeadas* $\boldsymbol{q_s}$ juega el papel de la entrada de control para la dinámica del sistema restante. Además, en Reyhanoglu et al. (1996, 1999) se derivan propiedades de controlabilidad y estabilizabilidad de sistemas mecánicos subactuados con restricciones no holónomas de segundo orden. Un interesante estudio sobre sistemas mecánicos subactuados puede ser encontrado en Spong (1998).

El seguimiento de posición de sistemas mecánicos subactuados se ha realizado en varios trabajos utilizando controladores $\mathscr{L}_2$ no lineal. En Toussaint et al. (2000) se controló un modelo no lineal de un barco subactuado a través de una ley de control $\mathscr{H}_\infty$ con realimentación de estados para seguimiento en presencia de perturbaciones y medidas ruidosas de los estados. En Siqueira and Terra (2004a) se presentó un control $\mathscr{H}_\infty$ no lineal para manipuladores subactuados, como una extensión del controlador propuesto por Chen et al. (1994). Los mismos autores realizaron una comparativa de un controlador $\mathscr{H}_\infty$ no lineal basado en la teoría de juegos con uno obtenido a través de una representación casi-lineal con parámetros variantes (del inglés *quasi-linear parameter varying* - quasi-LPV) en Siqueira and Terra (2004b), para controlar la posición de manipuladores subactuados. En este trabajo, además, se ha desarrollado un controlador $\mathscr{H}_\infty$ Markoviano para cuando el manipulador subactuado esté sujeto a cambios bruscos en la configuración. En Siqueira et al. (2006) se han aplicado controladores no lineales obtenidos a través de los problemas de optimización $\mathscr{H}_2$, $\mathscr{H}_\infty$ y $\mathscr{H}_2/\mathscr{H}_\infty$ usando la teoría de juegos a manipuladores subactuados a través de actuación redundante. En He and Han (2008) una ley de control con realimentación de la aceleración fue propuesta, tanto para vehículos autónomos totalmente actuados, como para los subactuados, usando la teoría $\mathscr{H}_\infty$. Además, se han presentado resultados de simulación del seguimiento de trayectorias para un helicóptero.

A.3 Objetivos

El objetivo principal de esta tesis es contribuir para el desarrollo y aplicación de estrategias de control robusto para resolver el problema de seguimiento de trayectorias para vehículos aéreos autónomos. El UAV que será utilizado es un helicóptero *QuadRotor* en escala reducida, que se caracteriza por ser un sistema

mecánico subactuado. Asimismo, se busca el diseño de controladores $\mathscr{H}_\infty$ no lineales para una clase de sistemas mecánicos subactuados. En la Fig. A.1 se ilustra el diagrama de flujo utilizado para desarrollar esta tesis.

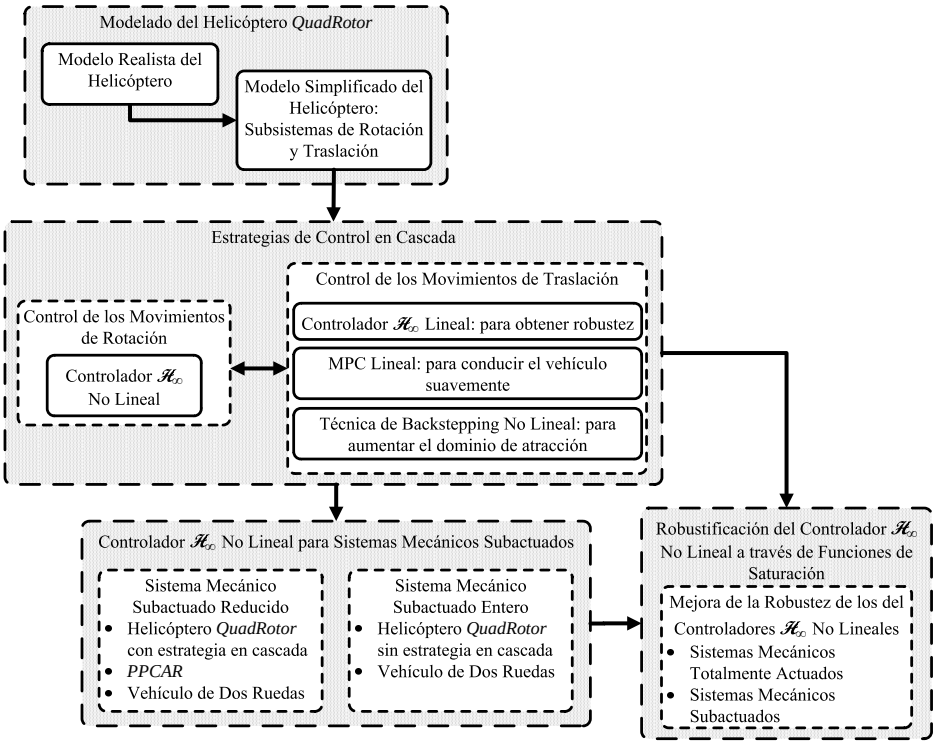

Figure A.1: Diagrama de flujo de la tesis.

Normalmente, para el diseño de estrategias de control avanzado se necesita un modelo dinámico preciso del sistema. Siendo así, el primer objetivo planteado en esta tesis es la obtención de un modelo dinámico adecuado del helicóptero *QuadRotor* con fines de diseño de control, teniendo en cuenta un equilibrio entre complejidad y realismo. El sistema se basará en leyes físicas para obtener un modelo que represente el comportamiento del vehículo en presencia de diversas fuentes de incertidumbres y que sea apropiado al prototipo utilizado en este trabajo.

Dado que el helicóptero *QuadRotor* es un sistema mecánico subactuado, una manera común para realizar el seguimiento de trayectorias de UAV's es utilizando estrategias de control en cascada. Por lo tanto, se proponen estructuras en cascada para controlar dos subsistemas: el de rotación y el de traslación. Las técnicas de control utilizadas en cada bucle se basarán en la teoría de control $\mathscr{H}_\infty$ lineal y no

lineal, en técnicas de *backstepping* y metodologías de control predictivo. Estas técnicas serán combinadas para obtener un sistema de control robusto en bucle cerrado en presencia de perturbaciones externas, incertidumbres paramétricas y dinámicas no modeladas. Además, se requiere un seguimiento de trayectorias suave.

Sin embargo, se debe enfatizar que las estrategias de control en cascada poseen un inconveniente. Aunque en los resultados de simulación, el sistema completo en bucle cerrado presente un comportamiento estable, se requiere que esto sea demostrable. Para evitar el uso de estructuras en cascada, se desarrollarán estrategias de control basadas en técnicas de control $\mathscr{H}_\infty$ no lineal aplicadas a sistemas mecánicos subactuados. El objetivo es obtener una ley de control que garantice robustez para el problema de seguimiento de trayectorias del helicóptero *QuadRotor* sin la necesidad de estrategias en cascada. Adicionalmente, un enfoque del controlador $\mathscr{H}_\infty$ no lineal para sistemas mecánicos será presentado, permitiendo ponderar diferentes dinámicas del sistema.

Otra cuestión a ser abordada es la mejora de la robustez del controlador $\mathscr{H}_\infty$ no lineal diseñado para sistemas mecánicos. Esta ley de control es calculada teniendo en cuenta que todas las incertidumbres que afectan al sistema son perturbaciones externas. Sin embargo, esta hipótesis no es muy realista. Por lo tanto, para contraatacar este problema, será presentada una solución para robustificar la ley de control $\mathscr{H}_\infty$ no lineal, donde se calculará una señal de control adicional a través de la técnica de funciones de saturación para hacer frente a errores de modelado.

En general, esta tesis presenta un desarrollo teórico de estrategias de control robusto para resolver el problema de seguimiento de trayectorias para vehículos aéreos no tripulados, centrándose en sistemas mecánicos subactuados.

A.4 Organización del Trabajo

Esta tesis está organizada como sigue:

- El **Capítulo 2** presenta el modelado del helicóptero *QuadRotor*. Se proporciona una descripción del funcionamiento del vehículo, así como las características estáticas de los grupos motor-hélice. Las ecuaciones del movimiento de un UAV son obtenidas a través de dos formulaciones: Euler-Lagrange y Newton-Euler. Además, se proporcionan los parámetros del vehículo aéreo no tripulado *QuadRotor* utilizados en esta tesis. En este capítulo se presentan algunas propiedades útiles de sistemas mecánicos.

- El **Capítulo 3** trata de estrategias de control en cascada para realizar el seguimiento de trayectorias del vehículo, donde se destaca la búsqueda de una continua mejoría del desempeño. En este capítulo se divide el modelo dinámico en dos subsistemas: el de rotación y el de traslación. El control del subsistema de rotación se realiza mediante un controlador $\mathscr{H}_\infty$ no lineal a fin de estabilizar el helicóptero. Para el subsistema de translación se han aplicado tres técnicas para seguir la trayectoria deseada. Primero, se calcula un controlador $\mathscr{H}_\infty$ lineal con realimentación de estados basado en el modelo del error utilizando el métodos de síntesis a través de LMIs, que asegura propiedades de robustez. Después de esto, se utiliza un controlador predictivo en espacio de estados con acción integral basado en el modelo del error variante con el tiempo para seguir suavemente la trayectoria de traslación deseada. El último controlador de traslación utilizado se basa en una técnica de control *backstepping* con acción integral para aumentar la robustez en presencia de incertidumbres en el modelo y aumenta el espacio de trabajo de los movimientos de traslación cuando comparado con los controladores anteriores del bucle externo. Se presentan resultados de simulación para corroborar las buenas características de las estrategias de control propuestas

- El **Capítulo 4** proporciona dos novedosos controladores $\mathscr{H}_\infty$ no lineales para sistemas mecánicos subactuados. El primer controlador se basa en un modelo reducido, donde solamente se consideran los grados de libertad controlados. Este controlador es aplicado en una estrategia en cascada al helicóptero *QuadRotor*, además, utilizado para controlar los grados de libertad pasivos de dos vehículos basados en el concepto del péndulo invertido. El segundo controlador considera toda la dinámica del los sistemas mecánicos subactuados, permitiendo regular los grados de libertad controlados mientras los grados de libertad restantes son estabilizados. El helicóptero *QuadRotor* es controlado sin la necesidad de estrategias en cascada ni el uso del espacio de estados aumentado. Asimismo, resultados experimentales son obtenidos con un vehículo de dos ruedas auto-balanceado.

- El **Capítulo 5** trata con un método de robustificación del controlador $\mathscr{H}_\infty$ no lineal diseñado para sistemas mecánicos. Se presenta una nueva solución para el algoritmo propuesto en Ortega et al. (2005). Este método se basa en la técnica de funciones de saturación. Resultados de simulación son llevados a cabo con algunos de los controladores presentados en los Capítulos 3 y 4.

- El **Capítulo 6** resume las contribuciones y resultados presentados en esta tesis y se sugieren posibles líneas de investigación futuras.

A.5 Lista de Publicaciones

Los siguientes artículos han sido publicados o enviados para su publicación durante la elaboración de esta tesis:

Capítulos de libro:

1. (Raffo and Normey-Rico, 2011) G. V. Raffo and J. E. Normey-Rico. *Robótica Móvel, Ed. R. A. F. Romero, F. Osorio, E. Prestes and D. Wolf*, capítulo *Controle de Robôs Móveis para Seguimento de Trajetórias*. Springer-Verlag, São Paulo, Brasil, 2011. Aceptado para publicación.

Artículos en Revista:

1. (Raffo et al., 2011a) G. V. Raffo, M. G. Ortega, F. R. Rubio, *Path Tracking of a UAV via an Underactuated $\mathscr{H}_\infty$ Control Strategy*. European Journal of Control, 17(2), 2011. In press.

2. (Raffo et al., 2010d) G. V. Raffo, M. G. Ortega, F. R. Rubio, *Robust Backstepping/Nonlinear $\mathscr{H}_\infty$ control for path tracking of a quadRotor unmanned aerial vehicle*. IET Control Theory & Applications, 2010. Enviado para publicación con estado de la revisión preliminar: potencialmente publicable.

3. (Raffo et al., 2010c) G. V. Raffo, M. G. Ortega, F. R. Rubio, *An integral predictive/nonlinear $\mathscr{H}_\infty$ control structure for a quadrotor helicopter*. Automatica (Oxford), 46(1), p. 29-39, 2010.

4. (Raffo et al., 2009a) G. V. Raffo, G. K. Gomes, J. E. Normey-Rico, C. R. Kelber, and L. B. Becker. *A predictive controller for autonomous vehicle path tracking*. IEEE Transactions on Intelligent Transportation Systems, 10 (1):92–102, 2009.

5. (Raffo et al., 2009b) G. V. Raffo, J. E. Normey-Rico, F. R. Rubio, and C. R. Kelber. *Control predictivo en cascada de un vehículo autónomo*. Revista Iberoamericana de Informática y Automática (RIAI), 6(1):63–74, 2009.

Artículos en Congreso:

1. (Raffo et al., 2011b) G. V. Raffo, M. G. Ortega, F. R. Rubio, *Nonlinear $\mathscr{H}_\infty$ Controller for the Quad-Rotor Helicopter with Input Coupling*, Aceptado para el 18th IFAC World Congress, IFAC'2011, Milan, Italy.

2. (Raffo et al., 2010b) G. V. Raffo, V. M. Madero, M. G. Ortega, *Un Controlador $\mathscr{H}_\infty$ No Lineal para Sistemas Mecánicos Subactuados con Acoplamiento en la Entrada - Una Aplicación a un Vehículo Auto-Balanceado con Dos Ruedas*, Actas de las XXXI Jornadas de Automática, 2010, Jaén, Spain.

3. (Raffo et al., 2010a) G. V. Raffo, V. M. Madero, M. G. Ortega, *An Application of the Underactuated Nonlinear $\mathscr{H}_\infty$ Controller to Two-Wheeled Self-Balanced Vehicles*. In Proc. of the 15th IEEE International Conference on Emerging Technologies and Factory Automation. ETFA'2010, Bilbao, Spain, September 2010.

4. (Raffo et al., 2009c) G. V. Raffo, M. G. Ortega, F. R. Rubio, *An Underactuated $\mathscr{H}_\infty$ Control Strategy for a QuadRotor Helicopter*. In Proc. of the European Control Conference 2009 - ECC2009, pages 3845-3850, Budapest, Hungary, August 2009.

5. (Raffo et al., 2008d) G. V. Raffo, M. G. Ortega, F. R. Rubio, *Plataforma de Pruebas para un Vehículo Aéreo No Tripulado Utilizando LabView*, 2008, Actas de las XXIX Jornadas de Automática, 2008, Tarragona, Spain.

6. (Raffo et al., 2008b) G. V. Raffo, M. G. Ortega, F. R. Rubio, *MPC with Nonlinear $\mathscr{H}_\infty$ Control for Path Tracking of a Quad-Rotor Helicopter*. In Proc. of the 17th IFAC World Congress 2008 - IFAC'08, pages 8564-8569, Seoul, Korea, July 2008.

7. (Raffo et al., 2008c) G. V. Raffo, M. G. Ortega, F. R. Rubio, *Robust $\mathscr{H}_\infty$ Control Strategy for a 6 DOF Quad-Rotor Helicopter*. In Proc. of the 8th Portuguese Conference on Automatic Control - CONTROLO'08, pages 402-407, Vila Real, Portugal, July 2008.

8. (Raffo et al., 2008a) G. V. Raffo, M. G. Ortega, F. R. Rubio, *Backstepping/Nonlinear $\mathscr{H}_\infty$ Control for Path Tracking of a QuadRotor Unmanned Aerial Vehicle*. In Proc. of the 2008 American Control Conference-ACC08, pages 3356-3361, Seattle, USA, June 2008.

9. (Raffo et al., 2007b) G. V. Raffo, M. G. Ortega, F. R. Rubio, *Nonlinear $\mathscr{H}_\infty$ Control Applied to the Personal Pendulum Car*. In Proc. of the European Control Conference. ECC'07, Kos, Greece, July 2007.

10. (Raffo et al., 2007a) G. V. Raffo, M. G. Ortega, F. R. Rubio, *Control Predictivo de la Dinámica de un Vehículo Autónomo*, 2007, Actas de las XXVIII Jornadas de Automática, 2007, Huelva, Spain.

11. (Raffo et al., 2006b) G. V. Raffo, M. G. Ortega, F. R. Rubio, *Control $\mathscr{H}_\infty$ Multivariable de un Modelo de Helicóptero*, 2006, Actas de las XXVII Jornadas de Automática, 2006. p. 854-859, Almería, Spain.

12. (Raffo et al., 2006a) G. V. Raffo, G. K. Gomes, J. E. Normey-Rico, L. B. Becker, and C. R. Kelber. *Seguimento de Trajetória de um Veículo Mini-Baja com CPBM*. Atas do XVI Congresso Brasileiro de Automática, Salvador, Brasil, 2006.

APPENDIX B

Conclusiones

Contents

B.1 Aportaciones y Conclusiones de la Tesis

Esta tesis ha abordado el desarrollo de estrategias de control robusto para resolver el problema de seguimiento de trayectorias para vehículos aéreos autónomos, centrándose en el helicóptero *QuadRotor* a pequeña escala. Estas estrategias han sido diseñadas teniendo en cuenta perturbaciones externas sostenidas que afectan al sistema completo, dinámicas no modeladas, e incertidumbres estructurales y paramétricas. Además, este tipo de UAV es un sistema mecánico subactuado, ya que tiene seis grados de libertad y sólo cuatro actuadores. Por lo tanto, se han desarrollado también estructuras de control en cascada y controladores únicos, considerando esta característica para conseguir el comportamiento deseado.

Normalmente, para diseñar estrategias de control avanzado es necesario obtener un modelo dinámico del sistema preciso, teniendo en cuenta el compromiso entre complejidad y realismo. De este modo, en el **Capítulo 2**, se ha descrito inicialmente el funcionamiento del helicóptero *QuadRotor*, donde se ha expuesto la relación entre las fuerzas y pares aplicados al vehículo y las velocidades de los cuatro rotores. Además, se han deducido los movimientos rotacionales y traslacionales, asumiendo un punto en el espacio, lo que permite obtener las ecuaciones cinemáticas de un sólido rígido que se mueve en el espacio tridimensional. El movimiento rotacional se describe mediante tres rotaciones sucesivas, usando los llamados ángulos de Tayt-Bryan, los cuales son también conocidos como ángulos náuticos o ángulos de Euler ZYX.

A partir de la matriz de rotación y de las ecuaciones cinemáticas se han calculado las ecuaciones dinámicas del helicóptero, basadas en dos enfoques. Primero, se ha usado la formulación de Euler-Lagrange para obtener las ecuaciones de movimiento del helicóptero *QuadRotor*, en las cuales se ha considerado que el centro de masas del vehículo está desplazado del origen del sistema de coordenadas de rotación por una distancia $\boldsymbol{r}$. Con esta suposición se obtiene un modelo dinámico no linear altamente acoplado. Para superar esto, se ha obtenido un modelo simplificado del helicóptero *QuadRotor* para el diseño de controladores, donde se asume que el centro de masas y el centro de rotación coinciden. Este modelo simplificado es un sistema descentralizado que permite separar el diseño de controladores para los movimientos traslacionales y los rotacionales. El segundo enfoque usado para la obtención de las ecuaciones de movimiento del helicóptero está basada en la formulación de Newton-Euler. Se han presentado también tanto el modelo completo como el simplificado. De todas formas, esta formulación se ha usado sólo para ilustrar la relación entre las fuerzas y pares obtenidas usando los ángulos de Euler y su derivada temporal, y usando las velocidades angulares, las cuales permiten obtener las fuerzas/pares aplicados al vehículo.

Como el helicóptero *QuadRotor* es un sistema mecánico subactuado, una manera común de realizar el seguimiento de trayectorias de UAV's es usar estrategias de control en cascada. Así, la mayoría de las contribuciones de esta tesis con respecto a este tipo de estructuras de control han sido presentadas en el **Capítulo 3**, donde se han usado diferentes técnicas de control para controlar tanto los movimientos rotacionales como los traslacionales. Los controladores han sido diseñados para conseguir robustez frente a incertidumbres paramétricas y estructurales, y para rechazar perturbaciones mantenidas que actúen sobre los seis grados de libertad del helicóptero. Las contribuciones del **Capítulo 3** se resumen a continuación:

- Para conseguir la estabilización del helicóptero *QuadRotor*, se ha usado un controlador $\mathscr{H}_\infty$ no lineal, el cual es capaz de rechazar perturbaciones externas mantenidas debido a que se ha incluido una acción integral en el vector de errores de seguimiento. La ley de control se ha diseñado para sistemas mecánicos totalmente actuados. De ahí que los ángulos de Euler se controlen mediante los momentos *roll*, *pitch* y *yaw* aplicados.

- El primer controlador traslacional se ha diseñado usando un controlador $\mathscr{H}_\infty$ lineal por realimentación de estados, basado en el error del modelo, donde se han considerado incertidumbres paramétricas. El método de síntesis usado se ha basado en LMIs. La estrategia del control en cascada, combin-

ando este controlador con el $\mathscr{H}_\infty$ no lineal usado para estabilizar el vehículo, ha permitido rechazar perturbaciones externas mantenidas que afectan al sistema completo. El controlador traslacional ha sido obtenido teniendo en cuenta un vector de estados aumentado, donde se ha considerado la integral del error de posición de traslación.

- Un segundo enfoque para diseñar el controlador traslacional ha sido usar un algoritmo MPC, a la vez que se mantiene el controlador $\mathscr{H}_\infty$ no lineal para la estabilización del helicóptero en el bucle interior. La razón principal para el uso del MPC es que tiene características predictivas. Como la trayectoria de referencia es conocida normalmente, el MPC puede proporcionar un seguimiento suave. Para mantener el buen comportamiento del controlador $\mathscr{H}_\infty$ lineal para el rechazo de las perturbaciones mantenidas que actúan en los movimientos traslacionales, se ha considerado la integral del error en posición también para este controlador.

  El algoritmo MPC lineal que se usa considera que el vehículo real sigue un helicóptero *virtual* de referencia que está sobre el camino deseado, originando el modelo del error, que es discreto y variante con el tiempo.

- La tercera ley de control aplicada al subsistema de traslación se ha desarrollado en base a la técnica de *backstepping*, mejorando la robustez en presencia de incertidumbres en el modelo. De nuevo, se ha combinado el controlador $\mathscr{H}_\infty$ no lineal para el subsistema de rotación, en la estructura del control en cascada, con el controlador *backstepping* con acción integral. Este controlador traslacional considera el término integral en el segundo paso del procedimiento del *backstepping*, presentando así mejores resultados que con un controlador que usa este término en el primer paso.

- Los resultados en simulación se han realizado para corroborar el buen funcionamiento de las estrategias propuestas de control en cascada para seguimiento de trayectorias, cuando se consideran incertidumbres en la masa y en el momento del tensor de inercia, y en presencia de perturbaciones externas mantenidas. Se ha realizado también una comparación de los resultados, donde se han usado los índices ISE y IADU para hacer un análisis cualitativo.

  Del análisis comparativo se puede observar que las estrategias de control MPC-NL$\mathscr{H}_\infty$ y IntBs-NL$\mathscr{H}_\infty$ presentan menores errores acumulativos a lo largo de las trayectorias. Sin embargo, cuando se analiza el esfuerzo de control mediante el índice IADU, la estrategia de control IntBs-NL$\mathscr{H}_\infty$ ha

presentado señales de control más suaves. Además, a pesar de que todas las estrategias de control en cascada propuestas en el **Capítulo 3** han resuelto el problema de seguimiento de trayectorias, sólo la estructura de control IntBs-NL$\mathscr{H}_\infty$ ha conseguido el objetivo de realizar el seguimiento de trayectorias para el helicóptero *QuadRotor* con una respuesta rápida y una señal de control suave.

En el **Capítulo 4**, se han propuesto estructuras de control $\mathscr{H}_\infty$ no lineal para sistemas mecánicos subactuados. Las contribuciones de este capítulo se detallan a continuación:

- Primero, se ha diseñado un controlador $\mathscr{H}_\infty$ no lineal subactuado basado en un modelo reducido, donde sólo se han considerado los grados de libertad controlados. La estructura de control permite considerar el comportamiento global del sistema en el momento para calcular las señales de control aplicadas. Se ha aplicado el controlador a tres sistemas mecánicos subactuados diferentes. En el caso del helicóptero *QuadRotor*, este controlador se ha usado para controlar los grados de libertad activos. Pero, a diferencia de los controladores usados en el Capítulo 3, el controlador propuesto usa la información de la dinámica de los GDL pasivos para generar la ley de control, en vez de asumirlas como perturbaciones externas. Como los grados de libertad pasivos del helicóptero *QuadRotor* son inestables, se ha realizado también una estrategia de control en cascada, donde el algoritmo MPC usado en el Capítulo 3 para el movimiento *xy* ha sido usado para generar los ángulos de referencia *roll* y *pitch*. Se han obtenido resultados en simulación y un análisis cuantitativo, el cual ha demostrado que, usando el controlador subactuado propuesto, el error acumulativo de los GDL *activos* decrece con señales de control suaves.

  El controlador $\mathscr{H}_\infty$ no lineal usando el modelo reducido se ha implementado también para controlar dos vehículos basados en el concepto del péndulo invertido, donde se han elegido los GDL pasivos para seren controlados. Se han obtenido resultados experimentales con un vehículo de dos ruedas auto-balanceado.

  Adicionalmente, se ha propuesto un enfoque de un controlador $\mathscr{H}_\infty$ no lineal para sistemas mecánicos, que permite ponderar dinámicas distintas del sistema.

- Para evitar el uso de estructuras de control en cascada y vectores de estado aumentado, se ha proporcionado una estrategia de control $\mathscr{H}_\infty$ no lineal para

sistemas mecánicos subactuados con acoplamiento en las entradas. Este controlador considera la dinámica completa del sistema mecánico subactuado permitiendo regular los grados de libertad controlados mientras que los que queden son estabilizados. Además, se ha garantizado robustez para el seguimiento de trayectorias del helicóptero *QuadRotor* sin necesidad de un controlador externo. Por medio de resultados de simulación, se ha corroborado el buen funcionamiento de esta estrategia de control, la cual ha mejorado los índices de comportamiento ISE y IADU para todas las entradas de control y GDL controlados. Se han obtenidos también resultados experimentales con un vehículo de dos ruedas auto-balanceado.

Normalmente, los controladores diseñados para sistemas mecánicos están basados en modelos nominales. No obstante, como es bien sabido, estos modelos implican incertidumbres tanto estructurales como paramétricas. Además, los controladores $\mathscr{H}_\infty$ no lineales presentados en los Capítulos 3 y 4 han sido desarrollados bajo la suposición de que todas las incertidumbres que afectan al sistema son perturbaciones externas. Sin embargo, esta hipótesis no es muy realista. Por tanto, en el **Capítulo 5**, se ha propuesto una solución para el algoritmo presentado en Ortega et al. (2005) para mejorar la robustez de los controladores $\mathscr{H}_\infty$ no lineales diseñados para sistemas mecánicos, donde se ha calculado una señal de control adicional por medio de la técnica de funciones de saturación para tratar con errores de modelado. Se han obtenido resultados de simulación preliminares para dos estrategias de control presentadas en la tesis para resolver el problema de seguimiento de trayectorias para el helicóptero *QuadRotor*: IntBS-NL$\mathscr{H}_\infty$ y *Entire* UActNL$\mathscr{H}_\infty$. En ambos resultados de simulación se ha observado una reducción del error de seguimiento de los GDL controlados, corroborando el método mediante el uso de la solución propuesta. A pesar de los buenos resultados obtenidos en el Capítulo 5, para mejorar los resultados obtenidos con el controlador $\mathscr{H}_\infty$ no lineal propuesto para sistemas mecánicos subactuados, se debe realizar un escalado del modelo dinámico cuando diferentes dinámicas son consideradas por el controlador.

B.2 Trabajos Futuros

En esta sección se describen algunas posibles líneas de investigaciones futuras que continúen este trabajo, incluyendo algunas que ya se han empezado:

- *Implementación de las estrategias de control propuestas.* Como se comentó

en el Capítulo 2, se está construyendo un helicóptero *QuadRotor* en el Grupo de Automática, Control y Robótica, Departamento de Ingeniería, Sistemas y Automática en la Universidad de Sevilla. Por lo tanto, un objetivo inmediato es la implementación de las estrategias de control presentadas en esta tesis en el vehículo real.

- *Estimación garantista de estados.* Un inconveniente cuando se diseñan controladores para UAV es que, o todos los estados son accesibles, o si no, cómo estimar el vector de estado para conseguir que sea posible el seguimiento de trayectorias. Además, normalmente los sensores disponibles proporcionan medidas con errores acotados. Un enfoque para estimar el vector de estado con estas medidas inexactas es por medio de métodos basados en el error acotado. Por ejemplo, si el helicóptero *QuadRotor* está equipado con un GPS, el error de medida puede estar en un rango de $\pm 2m$, o más, además de realimentar el controlador cada segundo como mínimo. Así, entre cada tiempo de muestreo del GPS, el vector de estado traslacional debe ser estimado y garantizar que se encuentra dentro de un conjunto admisible, y cuando se reciba un dato medido, se debe actualizar.

- *Control $\mathscr{H}_\infty$ no lineal para sistemas mecánicos subactuados por medio de realimentación de la salida.* Siguiendo la línea de investigación presentada, extender los controladores $\mathscr{H}_\infty$ no lineales para sistemas mecánicos subactuados, presentados en el Capítulo 4, al diseño de una ley de control por medio de realimentación de la salida.

- *Estudio de las regiones fronteras para asegurar la estabilidad de las estrategias del control en cascada.* Las estructuras de control en cascada presentadas en esta tesis se componen de controladores de bucle interno y externo, los cuales se han diseñado para obtener la estabilidad de cada bucle de forma separada. Sin embargo, no se ha hecho ningún análisis cuando se combinan ambos controladores. Con los resultados de las simulaciones, se puede observar que el sistema completo en bucle cerrado es estable, pero esto debe ser demostrado también analíticamente. Para realizar este análisis, una buena opción son los métodos de perturbaciones singulares, donde el bucle externo es de dinámica lenta, mientras que el lazo interno es de dinámica rápida.

- *Consideración de las dinámicas del bucle cerrado del rotor.* Teniendo en cuenta que el helicóptero *QuadRotor* en pequeña escala funciona con baterías eléctricas, con el paso del tiempo las baterías se descargan. Esto lleva

a una pérdida del empuje generado por las hélices, que no son capaces de mantener la misma velocidad requerida por los controladores rotacionales y traslacionales. Por lo tanto, se requiere un controlador de la velocidad del rotor para asegurar un funcionamiento regular durante el vuelo. Este sistema de control resulta en tener que considerar una tercera dinámica en bucle cerrado en el análisis del control en cascada. Por lo tanto, las tres dinámicas a considerar son: el movimiento traslacional (dinámica lenta), el movimiento rotacional (dinámica rápida) y el bucle de control de la velocidad del rotor (dinámica ultra-rápida).

- *Control por realimentación visual del helicóptero* QuadRotor. Implementación de seguimiento visual y técnicas de control servo visual para estimar la posición y postura del helicóptero, y para realizar un control por realimentación visual también. Alternativamente, se pueden integrar ambas características en técnicas como la propuesta en Malis and Benhimane (2005).

- *Control a través de red.* En el caso en que el UAV se controle desde una estación en tierra, existe la posibilidad de perder paquetes de datos, tanto en el envío de las señales de control como en la recepción de las señales medidas. A este problema, se le añade la pérdida de información causada por la codificación y la descodificación de las señales transmitidas, así como la velocidad de transmisión de datos. Estos problemas son particularmente interesantes para estos tipos de sistemas teniendo en cuenta su comportamiento inestable.

- *Extensión de controladores $\mathscr{H}_\infty$ no lineales a sistemas con retrasos.* Algunos de los fenómenos dinámicos más comunes que aparecen en las aplicaciones en ingeniería son los retrasos entre las variables de entrada y las de salida. Una línea de investigación emergente es cómo tratar los sistemas con retrasos con la teoría de control no lineal. Recientes trabajos tratan de extender la idea del predictor realimentado a los sistemas no lineales, sistemas modelados por ecuaciones diferenciales parciales, sistemas con retrasos con incertidumbre o totalmente desconocido en el canal entrada-salida, etc. El enfoque basado en EDPs o EDRs (*Ecuaciones Diferenciales con Retraso*) genera funcionales de Lyapunov-Krasovskii que permiten un diseño de un control constructivo y el análisis de estabilidad. Y lo que es más importante, este enfoque basado en EDPs permite una extensión del diseño del predictor realimentado a sistemas no lineales y a control robusto y adaptativo de sistemas con retrasos desconocidos.

Siguiendo esta línea de investigación y con el diseño de controladores $\mathscr{H}_\infty$ no lineales, para sistemas mecánicos completamente actuados y subactuados, presentados en esta tesis, un objetivo es extender estos controladores a los sistemas con retrasos. De este modo, se puede realizar el control de vehículos autónomos remotos, como vehículos autónomos submarinos en exploraciones de petróleo submarinas, y robótica aeroespacial.

Bibliography

T. Álamo, J. E. Normey-Rico, M. R. Arahal, D. L. Marruedo, and E. F. Camacho. Introducing Linear Matrix Inequalities in a Control Course. In *Proc. of the 7th IFAC Symposium on Advances in Control Education (ACE 2006)*, Madrid, Spain, 2006.

J. A. Acosta. *Control no lineal de sistemas subactuados*. PhD thesis, Universidad de Sevilla, Departamento de Ingeniería de Sistemas y Automática, Sevilla, España, 2004. in spanish.

J. A. Acosta, J. Aracil, and F. Gordillo. Nonlinear control strategies for the furuta pendulum. *Control and Intelligent Systems*, 29(3):101 – 107, 2002.

A. P. R. Aguiar. *Nonlinear Motion Control of Nonholonomic and Underactuated Systems*. PhD thesis, Instituto Superior Técnico, Universidade Técnica de Lisboa, 2002.

E. Altug, J. P. Ostrowski, and R. Mahony. Control of a Quadrotor Helicopter Using Visual Feedback. In *Proc. of the 2002 IEEE International Conference on Robotics and Automation*, pages 72–77, Washington, DC, 2002.

E. Altug, J. P. Ostrowski, and C. J. Taylor. Control of a quadrotor helicopter using dual camera visual feedback. *The International Journal of Robotics Research*, 24(5):329–341, 2005.

J. Aracil and F. Gordillo. Apuntes de Control Óptimo. Technical report, Departamento de Ingeniería de Sistemas y Automática, Universidad de Sevilla, Sevilla, 2004.

A. Astolfi and L. Lanari. Disturbance attenuation and set-point regulation of rigid robots via $\mathscr{H}_\infty$ control. In *Decision and Control, 1994., Proceedings of the 33rd IEEE Conference on*, volume 3, pages 2578–2583, 1994.

K. Aström and K. Furuta. Swinging up a pendulum by energy control. *Automatica*, 36(2):287 – 295, 2000.

J. Ball, C. Foias, J. W. Helton, and A. Tannenbaum. On a local nonlinear commutant lifting theorem. *Journal of Mathematics*, 37:693–709, 1987a.

J. Ball, C. Foias, J. W. Helton, and A. Tannenbaum. *Modelling, Robustness, and Sensitivity Reduction in Control Systems*, chapter Nonlinear interpolation in $\mathscr{H}_\infty$, pages 31–47. Springer-Verlag, 1987b.

T. Basar and P. Bernhard. *$\mathscr{H}^\infty$ Optimal Control and Related Minimax Design Problems: A Dynamic Game Approach*. Birkhäuser, Boston, 2008. 2nd Ed.

R. Beard, G. Saridis, and J. Wen. Approximate solutions to the time-invariant hamilton-jacobi-bellman equation. *Journal of Optimization Theory and Applications*, 96:589–626, 1998.

R. W. Beard and T. W. McLain. Successive Galerkin approximation algorithms for nonlinear optimal and robust control. *Int. J. Control*, 71(5):717–743, 1998.

R. W. Beard, G. N. Saridis, and J. T. Wen. Galerkin approximations of the generalized hamilton-jacobi-bellman equation. *Automatica*, 33(12):2159 – 2177, 1997.

K. Benzemrane, G. L. Santosuosso, and G. Damm. Unmanned aerial vehicle speed estimation via nonlinear adaptive observers. In *Proc. of the 2007 American Control Conference - ACC'2007*, pages 985–990, New York City, USA, July 11-13 2007.

K. Benzemrane, G. Damm, and G. L. Santosuosso. Adaptive observer and kalman filtering. In *Proc. of the 17th World Congress IFAC'08*, pages 3865–3870, Seoul, Lorea, July 06-11 2008.

B. Bethke, M. Valenti, and J. How. Cooperative vision based estimation and tracking using multiple uavs. In P. Pardalos, R. Murphey, D. Grundel, and M. Hirsch, editors, *Advances in Cooperative Control and Optimization*, volume 369 of *Lecture Notes in Control and Information Sciences*, pages 179–189. Springer Berlin / Heidelberg, 2007.

S. P. Bhattacharyya, A. Datta, and L. H. Keel. *Linear Control Theory: Structure, Robustness, and Optimization*. CRC Press, Boston, 2009.

S. Bouabdallah and R. Siegwart. Backstepping and Sliding-mode Techniques Applied to an Indoor Micro Quadrotor. In *Proc. IEEE Int. Conf. on Robot. and Automat.*, pages 2259–2264, Barcelona, Spain, 2005.

S. Bouabdallah and R. Siegwart. Full control of a quadrotor. In *Proc. of the Intelligent Robots and Systems. IROS 2007*, pages 153–158, San Diego, USA, 2007.

S. Bouabdallah, P. Murrieri, and R. Siegwart. Design and Control of an Indoor Micro Quadrotor. In *Proc. IEEE Int. Conf. on Rob. and Automat.*, volume 5, pages 4393–4398, New Orleans, USA, 2004a.

S. Bouabdallah, A. Noth, and R. Siegwart. PID vs LQ Control Techniques Applied to an Indoor Micro Quadrotor. In *Proc. IEEE Int. Conf. on Intelligent Robots and Systems*, volume 3, pages 2451–2456, Sendai, Japan, 2004b.

S. Bouabdallah, A. Noth, and R. Siegwart. Dynamic Modelling of UAVs. Technical Report Version 2.0, Autonomous Systems Laboratory - EPFL, May 2006.

E. Camacho and C. Bordons. *Model Predictive Control*. Springer-Verlag, New York, 1998.

P. Castillo, R. Lozano, and A. Dzul. Stabilization of a Mini Rotorcraft with Four Rotors. *IEEE Control Systems Magazine*, 22(6):45–55, Dec. 2005a.

P. Castillo, R. Lozano, and A. E. Dzul. *Modelling and Control of Mini-Flying Machines*. Springer-Verlag, London, UK, 2005b.

P. Castillo, P. García, R. Lozano, and P. Albertos. Modelado y Estabilización de un Helicóptero con Cuatro Rotores. *RIAI Revista Iberoamericana de Automática e Informática Industrial*, 4(1):41–57, Jan 2007.

B. S. Chen, T. S. Lee, and J. H. Feng. A nonlinear $\mathscr{H}_\infty$ control design in robotic systems under parameter perturbation and external disturbance. *Int. J. Control*, 59(2):439–461, 1994.

B.-S. Chen, Y.-C. Chang, and T.-C. Lee. Adaptive control in robotic systems with $\mathscr{H}_\infty$ tracking performance. *Automatica*, 33(2):227 – 234, 1997.

B.-S. Chen, Y.-Y. Chen, and C.-L. Lin. Nonlinear fuzzy $\mathscr{H}_\infty$ guidance law with saturation of actuators against maneuvering targets. *Control Systems Technology, IEEE Transactions on*, 10(6):769 – 779, 2002.

M. Chen and M. Huzmezan. A Combined MBPC / 2DOF $\mathscr{H}_\infty$ Controller for a Quad Rotor UAV. In *Proc. AIAA Guidance, Navigation, and Control Conference and Exhibit*, pages –, Texas, USA, 2003.

Y.-Y. Chen, B.-S. Chen, and C.-S. Tseng. Adaptive fuzzy mixed $\mathscr{H}_2/\mathscr{H}_\infty$ lateral control of nonlinear missile systems. In *Fuzzy Systems, 2003. FUZZ '03. The 12th IEEE International Conference on*, volume 1, pages 512–516, 2003.

J. J. Craig. *Introduction to Robotics - Mechanics and Control*. Addison-Wesley Publishing Company, Inc., USA, 2nd edn edition, 1989.

A. Das, F. Lewis, and K. Subbarao. Backstepping Approach for Controlling a Quadrotor Using Lagrange Form Dynamics. *Journal of Intelligent & Robotic Systems*, 56(1-2):127–151, September 2009a.

A. Das, K. Subbarao, and F. Lewis. Dynamic inversion with zero-dynamics stabilisation for quadrotor control. *IET Control Theory and Applications*, 3(3): 303–314, 2009b.

J. Doyle, K. Glover, P. Khargonekar, and B. Francis. State-space solutions to standard $\mathscr{H}_2$ and $\mathscr{H}_\infty$; control problems. *Automatic Control, IEEE Transactions on*, 34(8):831 –847, aug. 1989.

S. Esteban. Control Nolineal en Tres Escalas de Tiempo de un Helicóptero de Radio/Control sobre una Plataforma. Technical report, Universidad de Sevilla, Sevilla, ES, 2005.

I. Fantoni and R. Lozano. *Non-linear Control for Underactuated Mechanical Systems*. Springer-Verlag, London, UK, 2002.

W. Feng and I. Postlethwaite. Robust Nonlinear H_∞/Adaptative Control of Robot Manipulator Motion. *Proc. Instn. Mech. Engrs.*, 208:221–230, 1994.

M. Fiacchini, A. Viguria, R. Cano, A. Prieto, F. R. Rubio, J. Aracil, and C. C. de Wit. Design and experimentation of a personal pendulum vehicle. In *Proc. Controle, 7th Portuguese Conference on Automatic Control*, Lisboa, Portugal, Sept. 2006.

E. Frazzoli, M. Dahleh, and E. Feron. Trajectory tracking control design for autonomous helicopters using a backstepping algorithm. In *Proc. of the American Control Conference*, volume 6, pages 4102–4107, 2000.

F. Gómez-Stern. *Control de sistemas no lineales basado en la estructura hamiltoniana*. PhD thesis, Universidad de Sevilla, Departamento de Ingeniería de Sistemas y Automática, Sevilla, España, 2002. in spanish.

F. Gordillo and J. Aracil. A new controller for the inverted pendulum on a cart. *International Journal of Robust and Nonlinear Control*, 18(17):1607 – 1621, 2008.

N. Guenard, T. Hamel, and R. Mahony. A practical visual servo control for an unmanned aerial vehicle. *IEEE Transactions on Robotics*, 24(2):331–340, 2008.

M. Guisser, H. Medromi, H. Ifassiouen, J. Saadi, and N. Radhy. A coupled nonlinear discrete-time controller and observer designs for underactuated autonomous vehicles with application to a quadrotor aerial robot. In *Proc. of the 33th IEEE-IECON06*, pages 1–6, Paris, France, 2006.

M. Hardt, J. W. Helton, and K. Kreutz-Delgado. Numerical solution of nonlinear $\mathscr{H}_2$ and $\mathscr{H}_\infty$ control problems with application to jet engine compressors. *Control Systems Technology, IEEE Transactions on*, 8(1):98 –111, 2000.

Y.-Q. He and J.-D. Han. Acceleration feedback enhanced $\mathscr{H}_\infty$ disturbance attenuation control for a class of nonlinear underactuated vehicle systems. *Acta Automatica Sinica*, 34(5):558–564, 2008.

J. W. Helton and M. R. James. *Extending H^∞ Control to Nonlinear Systems*. Siam, Philadelphia, USA, 1999.

G. Hoffmann, S. Waslander, and C. Tomlin. Distributed cooperative search using information-theoretic costs for particle filters, with quadrotor applications. In *Proceedings of the AIAA Guidance, Navigation, and Control Conference and Exhibit*, pages 1–21, Keystone, USA, August 21-24 2006.

G. M. Hoffmann, H. Huang, S. L. Waslander, and C. J. Tomlin. Quadrotor helicopter flight dynamics and control: Theory and experiment. In *Proc. of the AIAA Guidance, Navigation and Control Conference and Exhibit*, pages 1–20, South Carolina, USA, 2007.

A. Isidori. *Nonlinear Control Systems*. Springer-Verlag, Berlim, 1989. 2nd Ed.

A. Isidori, L. Marconi, and A. Serrani. *Robust Autonomous Guidance*. Springer-Verlag New York, Secaucus, NJ, USA, 2003.

R. Johansson. Quadratic optimization of motion coordination and control. *IEEE Transactions in Automatic Control*, 35(11):1197–1208, Nov. 1990.

I. Kanellakopoulos and P. Krein. Integral-action nonlinear control of induction motors. In *Proc. of the 12th IFAC World Congress*, pages –, Sidney, Australia, 1993.

W. Kang. Nonlinear $\mathscr{H}_\infty$ control and its application to rigid spacecraft. *Automatic Control, IEEE Transactions on*, 40(7):1281 –1285, 1995.

R. Kelly, V. Santibáñez, and A. Loría. *Control of Robot Manipulators in Joint Space*. Springer-Verlag, Germany, 2005.

H. K. Khalil. *Nonlinear systems*. Prentice Hall, New Jersey, USA, 3nd edn edition, 2002.

J. Kim, M. Kang, and S. Park. Accurate modeling and robust hovering control for a quad-rotor vtol aircraft. *Journal of Intelligent & Robotic Systems*, 57:9 –26, 2010.

M. Krstic, P. V. Kokotovic, and I. Kanellakopoulos. *Nonlinear and Adaptive Control Design*. John Wiley & Sons, Inc., New York, USA, 1995.

D. Lara, G. Romero, A. Sanchez, and R. Lozano. Parametric Robust Stability Analysis for Attitude Control of a Four-rotor mini-rotorcraft. In *Proc. of 45th IEEE Conference on Decision and Control, 2006*, pages 4957–4962, San Diego, CA, 2006.

D. Lee, H. J. Kim, and S. Sastry. Feedback linearization vs. adaptive sliding mode control for a quadrotor helicopter. *International Journal of Control, Automation and Systems*, 7(3):419–428, June 2009.

F. L. Lewis, D. M. Dawson, and C. T. Abdallah. *Robot Manipulator Control - Theory and Practice*. Marcel Dekker, Inc, USA, 2004.

M. López-Martínez, M. G. Ortega, and F. R. Rubio. Nonlinear L_2 control of a laboratory helicopter with variable speed rotors. *Automatica*, 43(4):655–661, 2007.

T. Madani and A. Benallegue. Sliding mode observer and backstepping control for a quadrotor unmanned aerial vehicles. In *Proc. of American Control Conference, 2007. ACC '07*, pages 5887–5892, New York, USA, July 2007.

T. Madani and A. Benellegue. Backstepping Control for a Quadrotor Helicopter. In *Proc. of the IEEE/RSJ International Conference on Intelligent Robots and Systems, 2006*, pages 3255–3260, 2006a.

T. Madani and A. Benellegue. Control of a Quadrotor Mini-Helicopter via Full State Backstepping. In *Proc. of 45th IEEE Conference on Decision and Control, 2006*, pages 1515–1520, San Diego, CA, 2006b.

V. Madero, J. Aracil, and F. Gordillo. A nonlinear control law for two-wheeled self-balanced vehicles. In *Proc. of the 15th IEEE Mediterranean Electrotechnical Conference, MELECON'2010*, Valleta, Malta, 2010.

R. Mahony and T. Hamel. Robust trajectory tracking for a scale model autonomous helicopter. *International journal of robust and nonlinear control*, 14, 2004.

E. Malis and S. Benhimane. A unified approach to visual tracking and servoing. *Robotics and Autonomous Systems*, 52(1):39–52, 2005.

D. Q. Mayne, J. B. Rawlings, C. V. Rao, and P. O. M. Scokaert. Constrained model predictive control: Stability and optimality. *Automatica*, 36(6):789 – 814, 2000.

F. Mazenc and S. Bowong. Tracking trajectories of the cart-pendulum system. *Automatica*, 39(4):677 – 684, 2003.

L. Mederreg, F. Diaz, and N. K. M'Sirdi. Nonlinear Backstepping Control with Observer Design for a 4 Rotors Helicopter. In *Proc. of the IFAC International Conference on Advances in Vehicle Control and Safety (AVXS'04)*, pages –, 2004.

N. Metni, T. Hamel, and F. Derkx. Visual Tracking Control of Aerial Robotic Systems with Adptive Depth Estimation. In *Proc. of the CDC/ECC*, pages 6078–6084, Seville, Spain, 2005.

N. Michael, J. Fink, and V. Kumar. Cooperative manipulation and transportation with aerial robots. *Autonomous Robots*, pages 1–14, 2010a.

N. Michael, D. Mellinger, Q. Lindsey, and V. Kumar. The grasp multiple micro-uav testbed. *Robotics Automation Magazine, IEEE*, 17(3):56 –65, 2010b.

V. Mistler, A. Benallegue, and N. K. M'Sirdi. Exact linearization and noninteracting control of a 4 rotors helicopter via dynamic feedback. In *Proc. IEEE Int. Workshop on Robot and Human Inter. Communic.*, pages –, 2001.

A. Mokhtari, A. Benallegue, and B. Daachi. Robust Feedback Linearization and $G\mathscr{H}_\infty$ Controller for a Quadrotor Unmanned Aerial Vehicle. In *Proc. of the IEEE/RSJ International Conference on Intelligent Robots and Systems, 2005. (IROS 2005)*, pages 1009–1014, 2005.

A. Mokhtari, A. Benallegue, and B. Daachi. Robust Feedback Linearization and $\mathscr{G}H_\infty$ Controller for a Quadrotor Unmanned Aerial Vehicle. *Journal of Electrical Engineering*, 57(1):20–27, 2006a.

A. Mokhtari, A. Benallegue, and Y. Orlov. Exact Linearization and Sliding Mode Observer for a Quadrotor Unmanned Aerial Vehicle. *International Journal of Robotics and Automation*, 21(1):39–49, 2006b.

R. M. Murray, Z. Li, and S. S. Sastry. *A Mathematical Introduction to Robotic Manipulation*. CRC Press, Berkeley, USA, 1994.

M. Önkol and M. Efe. Experimental model based attitude control algorithms for a quadrotor unmanned vehicle. In *Proc. of the 2nd International Symposium on Unmanned Aerial Vehicles*, pages 1–6, Nevada, USA, June 8-10 2009.

R. Olfati-Saber. *Nonlinear Control of Underactuated Mechanical Systems with Application to Robotics and Aerospace Vehicles*. PhD thesis, Massachusetts Institute of Technology, 2001.

M. G. Ortega. *Aportaciones al Control $\mathscr{H}_\infty$ de Sistemas Multivariables*. PhD thesis, Universidad de Sevilla, Departamento de Ingeniería de Sistemas y Automática, Sevilla, España, 2001. in spanish.

M. G. Ortega and F. R. Rubio. Systematic design of weighting matrices for the H_∞ mixed sensitivity problem. *Journal of Process of Control*, 14:89–98, 2004.

M. G. Ortega, M. Vargas, C. Vivas, and F. R. Rubio. Robustness Improvement of a Nonlinear H_∞ Controller for Robot Manipulators via Saturation Functions. *Journal of Robotic Systems*, 22(8):421–437, 2005.

M. G. Ortega, M. Vargas, F. Castaño, and F. R. Rubio. Improved Design of the Weighting Matrices for the *S/KS/T* Mixed Sensitivity Problem - Application to a Multivariable Thermodynamic System. *IEEE Transactions on Control Systems Technology*, 14(1):82–90, 2006.

T. J. Pallet and S. Ahmad. Real-Time Helicopter Flight Control: Modelling and Control by Linearization and Neural Networks. Technical Report TR-EE 91-35, School of Electrical Engineering - Purdue University, West Lafayette, Indiana, August 1991.

S. Park, D. H. Won, M. S. Kang, T. J. Kim, H. Lee, and S. J. Kwon. RIC(Robust Internal-loop Compensator) Based Flight Control of a Quad-Rotor Type UAV.

In *Proc. of the IEEE/RSJ International Conference on Intelligent Robots and Systems, 2005. (IROS 2005)*, pages 3542–3547, 2005.

K. Pathak, J. Franch, and S. Agrawal. Velocity and position control of a wheeled inverted pendulum by partial feedback linearization. *Robotics, IEEE Transactions on*, 21(3):505 – 513, June 2005.

I. Postlethwaite and A. Bartoszewicz. Application of nonlinear $\mathscr{H}_\infty$ control to the tetrabot robot manipulator. In *Proc. Inst. Mech. Eng. Part I: J. Syst. Contr. Eng.*, volume 212, pages 459–465, 1998.

G. Raffo, G. Gomes, J. Normey-Rico, L. B. Becker, and C. R. Kelber. Seguimento de Trajetória de um Veículo Mini-Baja com CPBM. In *Atas do XVI Congresso Brasileiro de Automática*, Salvador, Brasil, 2006a.

G. V. Raffo and J. E. Normey-Rico. *Robótica Móvel, Ed. R. A. F. Romero, F. Osorio, E. Prestes and D. Wolf*, chapter Controle de Robôs Móveis para Seguimento de Trajetórias. Springer-Verlag, São Paulo, Brasil, 2011. Accepted for publication.

G. V. Raffo, M. G. Ortega, and F. R. Rubio. Control $\mathscr{H}_\infty$ Multivariable de un Modelo de Helicóptero. In *Acta XXVIII Jornadas de Automática, JAL06*, pages 854–859, Almería, Spain, Sept. 2006b.

G. V. Raffo, J. E. Normey-Rico, and F. R. Rubio. Control Predictivo de la Dinámica de un Vehículo Autónomo. In *Actas de las XXVIII Jornadas de Automática - University of Huelva*, Huelva, Spain, Sep 2007a.

G. V. Raffo, M. G. Ortega, and F. R. Rubio. Nonlinear $\mathscr{H}_\infty$ Control Applied to the Personal Pendulum Car. In *Proc. of the European Control Conference. ECC'07*, pages 2065–2070, Kos, Greece, July 2007b.

G. V. Raffo, M. G. Ortega, and F. R. Rubio. Backstepping/Nonlinear $\mathscr{H}_\infty$ Control for Path Tracking of a QuadRotor Unmanned Aerial Vehicle. In *Proc. of the 2008 American Control Conference - ACC2008*, pages 3356–3361, Seattle, USA, June 2008a.

G. V. Raffo, M. G. Ortega, and F. R. Rubio. MPC with Nonlinear $\mathscr{H}_\infty$ Control for Path Tracking of a Quad-Rotor Helicopter. In *Proc. of the 17th IFAC World Congress 2008 - IFAC'08*, pages 8564–8569, Seoul, Korea, July 2008b.

G. V. Raffo, M. G. Ortega, and F. R. Rubio. Robust $\mathscr{H}_\infty$ Control Strategy for a 6 DOF Quad-Rotor Helicopter. In *Proc. of the 8th Portuguese Conference on Automatic Control - CONTROLO'08*, pages 402–407, Vila Real, Portugal, July 2008c.

G. V. Raffo, M. G. Ortega, and F. R. Rubio. Plataforma de Pruebas para un Vehículo Aéreo No Tripulado Utilizando LabView. In *Actas de las XXIX Jornadas de Automática, JA2008*, Tarragona, Spain, September 2008d.

G. V. Raffo, G. K. Gomes, J. E. Normey-Rico, C. R. Kelber, and L. B. Becker. A predictive controller for autonomous vehicle path tracking. *IEEE Transactions on Intelligent Transportation Systems*, 10(1):92–102, 2009a.

G. V. Raffo, J. E. Normey-Rico, F. R. Rubio, and C. R. Kelber. Control predictivo en cascada de un vehículo autónomo. *Revista Iberoamericana de Informática y Automática (RIAI)*, 6(1):63–74, 2009b.

G. V. Raffo, M. G. Ortega, and F. R. Rubio. An Underactuated $\mathscr{H}_\infty$ Control Strategy for a QuadRotor Helicopter. In *Proc. of the European Control Conference 2009 - ECC2009*, pages 3845–3850, Budapest, Hungary, August 2009c.

G. V. Raffo, V. Madero, and M. G. Ortega. An Application of the Underactuated Nonlinear $\mathscr{H}_\infty$ Controller to Two-Wheeled Self-Balanced Vehicles. In *Proc. of the 15th IEEE International Conference on Emerging Technologies and Factory Automation. ETFA'2010*, Bilbao, Spain, September 2010a.

G. V. Raffo, V. Madero, and M. G. Ortega. Un Controlador $\mathscr{H}_\infty$ No Lineal para Sistemas Mecánicos Subactuados con Acoplamiento en la Entrada - Una Aplicación a un Vehículo Auto-Balanceado con Dos Ruedas. In *Acta de las XXXI Jornadas de Automática, JA2010*, Jaén, Spain, September 2010b.

G. V. Raffo, M. G. Ortega, and F. R. Rubio. An integral predictive/nonlinear $\mathscr{H}_\infty$ control structure for a quadrotor helicopter. *Automatica*, 46:29–39, 2010c.

G. V. Raffo, M. G. Ortega, and F. R. Rubio. Robust Backstepping/Nonlinear $\mathscr{H}_\infty$ control for path tracking of a quadRotor unmanned aerial vehicle. *IET Control Theory & Applications*, 2010d. Submitted for publication with preliminary review status: potentially publishable.

G. V. Raffo, M. G. Ortega, and F. R. Rubio. Path Tracking of a UAV via an Underactuated $\mathscr{H}_\infty$ Control Strategy. *European Journal of Control*, 17(2), 2011a. In press.

G. V. Raffo, M. G. Ortega, and F. R. Rubio. Nonlinear $\mathscr{H}_\infty$ Controller for the Quad-Rotor Helicopter with Input Coupling. In *18th World Congress, IFAC 2011*, Milano, Italy, August 2011b. Accepted for publication.

J. B. Rawlings and D. Q. Mayne. *Model Predictive Control: Theory and Design*. Nob Hill Publishing, Madison, 2009.

M. Reyhanoglu, A. van der Schaft, N. McClamroch, and I. Kolmanovsky. Nonlinear control of a class of underactuated systems. In *Decision and Control, 1996., Proceedings of the 35th IEEE*, volume 2, pages 1682–1687, Dec. 1996.

M. Reyhanoglu, A. van der Schaft, N. Mcclamroch, and I. Kolmanovsky. Dynamics and control of a class of underactuated mechanical systems. *Automatic Control, IEEE Transactions on*, 44(9):1663 –1671, Sept. 1999.

J. Roberts, T. Stirling, J. Zufferey, and D. Floreano. Sensing For Autonomous Indoor Flight. In *Proc. of the European Micro Air Vehicle Conference and Flight Competition (EMAV)*, 2007.

J. A. Rossiter. *Model-Based Predictive Control: A Practical Approach*. CRC Press, New York, 2003.

H. Sage, M. De Mathelin, and E. Ostertag. Robust control of robot manipulators: a survey. *International Journal of Control*, 72(16):1498–1522, 1999.

R. S. Sánchez-Peña and M. Sznaier. *Robust Systems - Theory and Applications*. Wiley Interscience, New York, USA, 1998.

A. A. G. Siqueira. *Controle $\mathscr{H}_\infty$ Não Linear de Robôs Manipuladores Subatuados*. PhD thesis, Universidade de São Paulo, Escola de Engenharia de São Carlos, São Carlos, Brasil, 2004. in portuguese.

A. A. G. Siqueira and M. H. Terra. Nonlinear $\mathscr{H}_\infty$ control for underactuated manipulators with robustness tests. *Revista de Controle & Automação*, 15(3): 339–350, 2004a.

A. A. G. Siqueira and M. H. Terra. Nonlinear and Markovian $\mathscr{H}_\infty$ Controls of Underactuated Manipulators. *IEEE Transactions on Control Systems Technology*, 12(6):811–826, 2004b.

A. A. G. Siqueira, M. H. Terra, and B. C. O. Maciel. Nonlinear mixed $\mathscr{H}_2/\mathscr{H}_\infty$ control applied to manipulators via actuation redundancy. *Control Engineering Practice*, 14:327–335, 2006.

R. Skjetne and T. I. Fossen. On integral control in backstepping: Analysis of different techniques. In *Proc. of the 45th IEEE Conf. on Decision and Control*, pages 1899–1904, Boston, USA, 2004.

S. Skogestad and I. Postlethwaite. *Multivariable Feedback Control: Analysis and design*. John Wiley & Sons, Chicester, UK, 2005.

E. Sontag. *Mathematical Control Theory. Deterministic Finite-Dimensional Systems*. Springer-Verlag, New York, USA, 1998. 2nd Ed.

M. Spong. Partial feedback linearization of underactuated mechanical systems. In *Intelligent Robots and Systems '94. 'Advanced Robotic Systems and the Real World', IROS '94. Proceedings of the IEEE/RSJ/GI International Conference on*, volume 1, pages 314–321, 1994.

M. Spong. Underactuated mechanical systems. In B. Siciliano and K. Valavanis, editors, *Control Problems in Robotics and Automation*, volume 230 of *Lecture Notes in Control and Information Sciences*, pages 135–150. Springer Berlin / Heidelberg, 1998.

M. W. Spong. Energy based control of a class of underactuated mechanical systems. In *IFAC World Congress*, pages 431–435, 1996.

M. W. Spong and M. Vidyasagar. *Robot Dynamics and Control*. John Wiley & Sons, Inc, USA, 1989.

M. W. Spong, S. Hutchinson, and M. Vidyasagar. *Robot Modeling and Control*. John Wiley & Sons, Inc, USA, 2006.

S. Sun. Designing Approach on Trajectory-Tracking Control of Mobile Robot. *Robotics and Computer-Integrated Manufacturing*, 21(1):81–85, 2005.

G. P. Tournier, M. Valenti, J. P. How, and E. Feron. Estimation and Control of a Quadrotor Vehicle Using Monocular Vision and Moiré Patterns. In *Proc. of the AIAA Guidance, Navigation, and Control Conference and Exhibit*, August 2006.

G. Toussaint, T. Basar, and F. Bullo. $\mathscr{H}_\infty$-optimal tracking control techniques for nonlinear underactuated systems. In *Decision and Control, 2000. Proceedings of the 39th IEEE Conference on*, volume 3, pages 2078–2083, 2000.

A. van der Schaft. *L_2-Gain and Passivity Techniques in Nonlinear Control*. Springer-Verlag, New York, 2000. 2nd Ed.

A. van der Schaft. L_2-Gain Analysis of Nonlinear Systems and Nonlinear State Feedback Control. *IEEE Trans. Automat. Control*, 37(6):770–784, 1992.

A. J. van der Schaft. On a state space approach to nonlinear h[infinity] control. *Systems & Control Letters*, 16(1):1 – 8, 1991.

M. Vidyasagar. *Nonlinear System Analysis*. SIAM, Philadelphia, USA, 2002. 2nd Ed.

C. Vivas. *Control Óptimo y Robusto $\mathscr{H}_\infty$ de Sistemas No Lineales. Aplicaciones a Sistemas Electromecánicos*. PhD thesis, Universidad de Sevilla, Departamento de Ingeniería de Sistemas y Automática, Sevilla, España, 2004. in spanish.

K. Wichlund, O. Sordalen, and O. Egeland. Control properties of underactuated vehicles. In *Robotics and Automation, 1995. Proceedings., 1995 IEEE International Conference on*, volume 2, pages 2009–2014, 1995.

R. Xu and U. Özgüner. Sliding Mode Control of a Quadrotor Helicopter. In *Proc. of 45th IEEE Conference on Decision and Control, 2006*, pages 4957–4962, San Diego, CA, 2006.

R. Xu and U. Özgüner. Sliding mode control of a class of underactuated systems. *Automatica*, 44:233–241, 2008.

C.-D. Yang and H.-Y. Chen. Three-dimensional nonlinear $\mathscr{H}_\infty$ guidance law. *International Journal of Robust and Nonlinear Control*, 11(2):109–129, 2001.

K. M. Zemalache, L. Beji, and H. Maaref. Two inertial models of x4-flyers dynamics, motion planning and control. *Integrated Computer-Aided Engineering*, 14(2):107–119, 2007.